

---

Saksnummer:  
24-081980TVI-TOSL/04

---

Oslo, 28.06.2024  
2024-0459

## Tilsvar til Oslo tingrett

**Saksøker:** WWF Verdens Naturfond  
Postboks 6784 St. Olavs plass  
0130 Oslo

Prosessfullmektig: Advokat Jenny Sandvig  
Advokatfirmaet Simonsen Vogt Wiig AS  
Postboks 2043 Vika  
0125 Oslo

**Saksøkt:** Staten v/Energidepartementet  
Postboks 8148 Dep  
0033 Oslo

Prosessfullmektig: Regjeringsadvokaten  
v/advokat Karen Mellingsen  
Postboks 8012 Dep  
0030 OSLO

## 1 INNLEDNING

Det vises til stevning 23. mai, forkynt for staten 24. mai, med tilsvarsfrist 28. juni. Saken gjelder gyldigheten av beslutning av 12. april 2024 fra Kongen i statsråd om åpning av område på norsk kontinentalsokkel for mineralvirksomhet. Etter statens syn hefter det ingen feil ved åpningsbeslutningen som kan lede til ugyldighet. Staten vil derfor legge ned påstand om frifinnelse og at staten tilkjennes sakskostnader.

Krav om ugyldighet av beslutninger om «åpning» av områder fattet etter lover som gir anvisning på åpningsprosesser er, så vidt staten kan se, tidligere ikke reist. Beslutningen er ikke vedtak etter forvaltningsloven § 2 bokstav a til c, og spørsmålet om kravet omfattes av søksmålsadgangen i tvisteloven §§ 1-3 og 1-4 er kommentert nedenfor i punkt 4.2.

## 2 SAKENS BAKGRUNN OG KONTEKST

### 2.1 Oversikt over konsesjonssystemet i havbunnsmineralloven

Lov 22. mars 2019 nr. 7 om mineralvirksomhet på kontinentalsokkelen (havbunnsmineralloven) regulerer mineralvirksomhet på havbunnen innenfor norsk jurisdiksjon. Med «mineralvirksomhet» menes all virksomhet knyttet til undersøkelse og utvinning av mineralforekomster på havbunnen og grunnen under havbunnen, jf. lovens § 1-5 bokstav a, jf. § 1-2 første ledd.

Havbunnsmineralloven § 1-1 fastslår at lovens formål er å legge til rette for undersøkelse og utvinning av mineralforekomster på kontinentalsokkelen i samsvar med samfunnsmessige målsettinger, slik at hensynet til verdiskaping, miljø, sikkerhet ved virksomheten, øvrig næringsvirksomhet og andre interesser blir ivarettatt. I loven § 1-7 om krav til forsvarlig virksomhet fremgår det at mineralvirksomhet skal foregå på en forsvarlig måte og ivareta hensynet til sikkerhet for personell, miljø og de økonomiske verdiene innretninger og fartøyer representerer.

Havbunnsmineralloven bygger på en suksessiv beslutningsprosess etter modell fra petroleumsloven. Systemet kjennetegnes ved at viktige beslutninger ikke tas før det er nødvendig: Vilkårene for fremtidig virksomhet utformes innen rammen av tidligere beslutninger, men slik at valg som kan utstå, utsettes, se Knut Kaasen, «Petroleumsretten» i *Knophs oversikt over Norges rett*, Harald Irgens-Jensen (red.), 15. utgave, Universitetsforlaget 2019, s. 373.

Første skritt er at områder må åpnes for havbunnsmineralvirksomhet. Det gjøres ved at det fattes en beslutning av Kongen i statsråd om å åpne et nærmere avgrenset område på norsk kontinentalsokkel for mineralvirksomhet, jf. havbunnsmineralloven § 2-1 første ledd. Før et område kan åpnes, skal departementet gjennomføre en konsekvensutredning, jf. § 2-1 andre ledd, jf. § 2-2 første ledd. Konsekvensutredningen skal bidra til å belyse de ulike interessene som gjør seg gjeldende på det aktuelle området. Videre skal konsekvensutredningen belyse hvilke virkninger en eventuell åpning kan få for miljøet og antatte næringsrelaterte, økonomiske og sosiale virkninger, jf. § 2-2 andre ledd. Konsekvensutredningen skal sendes på høring sammen med et utkast til beslutning om åpning. I forarbeidene er det lagt til grunn at det avhengig av blant annet størrelsen på området som åpnes vil kunne være



naturlig å forelegge saken for Stortinget før Kongen i statsråd tar beslutning om åpning, jf. Prop. 106 L (2017–2018) s. 36. Åpningsbeslutningen er ikke bestemmende for rettigheter eller plikter til private, jf. forvaltningsloven § 2 første ledd bokstav a, og er derfor ikke et vedtak i forvaltningslovens forstand, se til sammenligning HR-2020-2472-P avsnitt 180.

Åpning av områder betyr ikke at mineralvirksomhet kan settes i gang. Før et område åpnes, er det kun staten som kan drive mineralvirksomhet, herunder gjennomføre undersøkelser etter mineraler, jf. havbunnsmineralloven § 1-6. Åpning innebærer at myndighetene kan tildele kvalifiserte søkere tillatelse til mineralvirksomhet innenfor det området åpningsbeslutningen omfatter, jf. havbunnsmineralloven § 2-3 første ledd. For å lete etter mineraler må selskapene først søke om undersøkelsestillatelse (§ 3-1) eller utvinningstillatelse (§ 4-2). Etter søknad kan hhv. departementet og Kongen i statsråd tildele tillatelse (§§ 3-1 og 4-1). For utvinningstillatelser kan myndighetene sette vilkår om et arbeidsprogram som rettighetshaver skal gjennomføre frem til innsendelse av plan for utvinning, jf. havbunnsmineralloven § 4-3. Tildeling av undersøkelses- og utvinningstillatelser er enkeltvedtak etter forvaltningsloven.

Tildeling av utvinningstillatelse gir ingen ubetinget rett til å sette i gang med å utvinne mineraler. Før utvinning iverksettes må rettighetshaver forelegge for departementet til godkjenning en plan for utvinning av mineralforekomsten, jf. havbunnsmineralloven § 4-4. Utvinningsplanen skal bl.a. inneholde en prosjektspesifikk konsekvensutredning, jf. andre ledd. Både forslag til utredningsprogram og konsekvensutredningen sendes på offentlig høring. Departementet skal i et eget dokument redegjøre for og begrunne vedtaket om å godkjenne eller ikke godkjenne en plan for utvinning, jf. syvende ledd. De første planene for utvinning skal forelegges Stortinget før en eventuell godkjenning, se nærmere i punkt 3.6 og 3.7.

## 2.2 Etterspørselen etter mineraler

Befolkningsvekst, velstandsøkning, økt digitalisering og overgangen til et lavutslippssamfunn er forventet å føre til en betydelig økning i etterspørselen etter mineraler og metaller. Blant annet vil fornybar energiproduksjon og økende grad av elektrifisering kreve ulike metalliske grunnstoff. Det internasjonale energibyrådet (International Energy Agency, IEA) la i mai frem deres årlige rapport for markedet for kritiske mineraler, «Global Critical Minerals Outlook 2024». Ifølge byrådet vil det økende tempoet i det grønne skiftet og overgangen til fornybare energikilder føre til en betydelig økning i mineraletterspørsel. Byrådet har vurdert fremtidig mineraletterspørsel i tre ulike scenarier for fremtidig politikkutvikling. I to av scenarioene vil etterspørselen etter mineraler i lavutslippsteknologier doubles mellom i dag og 2030, mens den vokser nesten tre ganger i det tredje scenarioet. Ser man til 2050 vil etterspørselen tredobles eller vokse over 3.5 ganger i to av scenarioene. Spesielt øker etterspørselen som følge av voksende utrulling av el-biler og behov for batterier og lagring. Kobber, grafitt, nikkel, mangan og litium er de mineralene som spesielt trekkes frem. På tvers av mineralene er det ifølge rapporten lavutslippsteknologier som vil være den største bidragsyteren i den betydelig økte etterspørselen sammenlignet med dagens nivå.

**Bilag 1:** Global Critical Minerals Outlook 2024, International Energy Agency.

Utvinning av havbunnsmineraler har derfor potensial til å bli en ny og viktig havnæring i Norge som kan bidra til verdiskaping og sysselsetting, og samtidig være med på å sikre forsyningen av viktige mineraler i fremtiden.

Produksjonskjedene for flere sentrale mineraler og metaller er i dag dominert av land utenfor Vesten. Høy grad av geografisk konsentrasjon blant produsentland kan gi utfordringer for forsyningssikkerheten. Samtidig vil som påpekt blant annet overgangen til et lavutslippssamfunn føre til en betydelig økning i etterspørselen etter mineraler og metaller.

### 2.3 Kort om mineralvirksomhet på havbunnen i dag

Som nevnt i punkt 3.2 i stevningen, foregår det ikke kommersiell utvinning av havbunnsmineraler på dypt vann i verden i dag. Mineralvirksomhet i form av leting etter mineraler på havbunnen har imidlertid pågått i lang tid. Dette er nærmere omtalt i Meld. St. 25 (2022–2023) s. 16–19 (**stevningen bilag 41**).

I Norge har staten v/Sokkeldirektoratet siden 2011 gjennomført datainnsamling i dyphavsområdene i Norskehavet og Grønlandshavet, og i de senere år kartlagt ressurspotensialet for havbunnsmineraler på norsk kontinentalsokkel (**stevningen bilag 41**, s. 19). Andre stater som Japan, Kina, Papua Ny-Guinea og USA har også gjennomført leteaktiviteter og kartlagt områder innenfor nasjonal jurisdiksjon. Ulike prosjekter for testing av utvinningsteknologi er også gjennomført. Cookøyene i Stillehavet har i tillegg åpnet for kommersiell leteaktivitet innenfor sine områder, og tildelte i februar 2022 tre letetillatelser. Leting etter havbunnsmineraler foregår også utenfor nasjonal jurisdiksjon i både statlig og privat regi (**stevningen bilag 41**, s. 16–19).

Utenfor nasjonal jurisdiksjon er det under FNs havrettskonvensjon opprettet en internasjonal havbunnsmyndighet (The International Seabed Authority (ISA)) for å regulere mineralvirksomhet utenfor nasjonal jurisdiksjon, det såkalte «Området». I konsekvensutredningen på s. 21 (**stevningens bilag 20**) er aktiviteten i ISA oppsummert slik:

*«Det er så langt utarbeidet et regelverk for undersøkelsesaktivitet. Det er tildelt om lag 30 kontrakter (tillatelser) for leting i Området, og innsamling av data foretatt av kontraktørene har pågått i over tyve år. Det pågår nå et arbeid i ISA for å utvikle et regelverk for utvinning av havbunnsmineraler i Området.»*

For å få en letekontrakt må søkeren ha formell støtte fra en stat som garanterer at søkeren er under effektiv kontroll av denne staten (omtalt som «sponsorstat»). De fleste kontraktørene som driver aktivitet innenfor Området, er statsinstitusjoner og statseide selskap, mens mindretallet er private selskap. Land som Frankrike, Tyskland, Storbritannia, Belgia, India, Brasil, Polen, Russland, Kina, Sør-Korea, Nauru, Tonga, Kiribati, Singapore, Cookøyene og Jamaica er sponsorstater (**stevningen bilag 41**, s. 17).

### 2.4 Kort om området som er åpnet for mineralvirksomhet og ressurspotensialet

Området på norsk kontinentalsokkel som er besluttet åpnet for mineralvirksomhet er beskrevet i punkt 5 i kongelig resolusjon 12. april 2024 (**stevningen bilag 1**), og omtalt i

stevningen punkt 3.1. Det er tale om et område på 281 200 kvadratkilometer i Norskehavet og Grønlandshavet. Som påpekt i punkt 3.1 i stevningen overlapper deler av åpningsområdet med områder definert som særlig verdifulle og sårbare områder (SVO-områder). SVO-områder har ikke direkte virkninger i form av begrensninger for næringsvirksomhet, men signaliserer viktigheten av å vise særlig aktsomhet i disse områdene, jf. Meld. St. 21 (2023–2024) (**stevningen bilag 4**, s. 50). Forholdet til SVOene ble omtalt i konsekvensutredningen (**stevningen bilag 20**, s. 72).

Det er påvist flermetalliske manganskorper og sulfider i åpningsområdet. Analyser viser at mineralprøver som er samlet inn inneholder metaller som bl.a. kobber, sink og kobolt. I ressursvurderingen av 27. januar 2023 vurderer Sokkeldirektoratet (tidligere Oljedirektoratet) at forventede tilstedeværende ressurser på norsk kontinentalsokkel er betydelige (s. 3).

#### **Bilag 2:** Ressursvurdering havbunnsmineraler av 27. januar 2023

Mineralvirksomhet på havbunnen kan på sikt bidra til å diversifisere og sikre forsyningen av viktige mineraler og metaller. Selv om omfanget av disse ressursene foreløpig i begrenset grad er kartlagt, er det potensielt tale om betydelige verdier. Det forventes derfor økt interesse for undersøkelse etter og utvinning av mineralforekomster til havs både globalt og på norsk kontinentalsokkel.

### **3 SAKENS FAKTISKE SIDE**

#### **3.1 Innledning**

Åpningsprosessen ble satt i gang i 2020 av daværende Olje- og energidepartementet (nå Energidepartementet), og er sammensatt av to hoveddeler; en konsekvensvurdering av 27. oktober 2022 og en ressursvurdering av 27. januar 2023. I stevningen punkt 4 er det redegjort for åpningsprosessen med fokus på konsekvensutredningen. Staten er enig i kronologien i saksøkers redegjørelse. Etter statens syn gir imidlertid redegjørelsen et misvisende og skjevt bilde av selve prosessen. Den kan derfor ikke legges til grunn som omforent. I det følgende redegjøres det for statens syn på de faktiske forholdene.

Det bemerkes innledningsvis at havbunnsmineralloven ikke har egne bestemmelser om prosessen for konsekvensutredning på åpningsstadiet. Lovens § 2-2 tredje ledd gir hjemmel til å regulere dette nærmere i forskrift. Forskriftshjemmelen er foreløpig ikke benyttet. I konsekvensutredningsprosessen har departementet derfor sett hen til mer detaljerte regler for konsekvensutredning ved åpning av nye områder for andre havnæringer, som reglene i petroleumsforskriften kapittel 2a. Forskriften gjennomfører konsekvensutredningsreglene i EUs plandirektiv (2001/42/EF), som departementet også har sett hen til. Dette fremgår av konsekvensutredningen (**stevningen bilag 20**, s. 27).

Energidepartementet var ansvarlig for å gjennomføre konsekvensutredningen. Departementet ba daværende Oljedirektoratet (nå Sokkeldirektoratet) om å bistå i gjennomføringen av konsekvensutredningsprosessen, herunder koordinere det faglige utredningsarbeidet. Sokkeldirektoratet konsulterte øvrige relevante statlige etater, herunder

Miljødirektoratet, angående definisjon av relevante utredningstema og vurdering av utredninger innenfor deres ansvarsområde (**stevningen bilag 20**, s. 28).

## 3.2 Forslag til program for konsekvensutredning

Første steg i konsekvensutredningsprosessen er å utarbeide et forslag til program for konsekvensutredningen. Departementet utarbeidet med bistand fra Søkeldirektoratet et forslag til konsekvensutredningsprogram som ble sendt på offentlig høring 12. januar 2021 med en høringsfrist på tre måneder (**stevningen bilag 5**). Som påpekt ovenfor i punkt 3.1 var også Miljødirektoratet involvert i utarbeidelsen. Programforslaget ble sendt til om lag 150 mottakere fordelt på departementer og statlige etater, fylkeskommuner, statsforvaltere, forskningsinstitusjoner, selskaper og interesseorganisasjoner.

Forslaget til konsekvensutredningsprogram inneholdt blant annet forslag til utredningsområde og problemstillinger og temaer for konsekvensutredningen. Formålet var å invitere til tidlig involvering av interesserte aktører og berørte myndigheter for å sikre at konsekvensutredningen dekker de forhold som er relevante for spørsmålet om åpning av områder for mineralvirksomhet på havbunnen (**stevningen bilag 5**, s. 6).

Departementet mottok til sammen 53 høringsinnspill til programforslaget fra ulike høringsinstanser, herunder både støtte og kritikk. Departementet vurderte innkomne høringsinnspill i et eget dokument som ble lagt ut på regjeringens nettsider (**stevningen bilag 8**, uriktig kalt «Oljedirektoratets gjennomgang» i stevningen). Departementets vurdering av høringsuttalelsene var basert på daværende Oljedirektoratets faglige gjennomgang av høringsuttalelsene.

Høringsinnspill av mer prinsipiell karakter og med lignende innhold fra flere høringsinstanser ble behandlet samlet innledningsvis i dokumentet. Blant disse var innspill knyttet til mangel på kunnskap om miljøforhold i foreslått utredningsområde, behov for mer kartlegging og at tidsplanen var for stram for å samle inn tilstrekkelig kunnskap. I tillegg ble de detaljerte kommentarene i samtlige høringsinnspill behandlet enkeltvis.

På basis av høringsforslaget og innkomne høringsinnspill ble programmet for konsekvensutredningen fastsatt av departementet 10. september 2021 (**stevningen bilag 9**). Det fastsatte programmet bestod av forslaget til utredningsprogram og departementets vurdering av innkomne høringsinnspill. Fastsatt program ble sendt til dem som hadde avgitt uttalelse til forslaget til program.

**Bilag 3:** Brev fra departementet 13. september 2023 om fastsetting av konsekvensutredningsprogram for mineralvirksomhet på norsk kontinentalsokkel

## 3.3 Konsekvensutredningen, inkludert underlagsrapporter

Konsekvensutredningen ble gjennomført på basis av det fastsatte utredningsprogrammet (**stevningen bilag 20**). Utredningsområdet som dannet grunnlaget for konsekvensutredningen, dekket et område på ca. 592 500 kvadratkilometer mellom

yttergrensen for kontinentalsokkelen/avtalt avgrensningslinje sør og sørøst for Jan Mayen og Svalbard og omfatter områder fra 100 til 4000 meters havdyp.

Konsekvensutredningen gir et oppdatert og sammenstilt kunnskapsgrunnlag basert på eksisterende kunnskap knyttet til eventuell fremtidig havbunnsmineralaktivitet på norsk kontinentalsokkel. Kunnskapen er fremskaffet gjennom faglige grunnlagsstudier og virkningsstudier utarbeidet av aktuelle fagmiljøer, herunder statlige etater og institutter, universiteter og andre kompetansemiljøer. Det ble utarbeidet totalt ni grunnlags- og virkningsrapporter for å sammenfatte kunnskap om relevante forhold og utrede mulige virkninger av havbunnsmineralvirksomhet.

Det er i tråd med havbunnsmineralloven § 2-2 og i henhold til utredningsprogrammet ikke gjort vurderinger av spesifikke prosjekter eller scenarier. Vurderingene er gjennomført tematisk og overordnet for å kunne avdekke hvilke typer av virkninger som er de mest vesentlige og hvilke som eventuelt har mindre virkningspotensial. Dette dekker alle de tema som er angitt i konsekvensutredningsprogrammet. Tilgjengelig kunnskap er lagt til grunn og kunnskapsmangler er påpekt.

Konsekvensutredningen inneholder heller ikke detaljerte vurderinger knyttet til mulige, fremtidige konkrete utvinningsprosjekter, og dette er heller ikke et krav verken etter EUs plandirektiv eller etter havbunnsmineralloven. I henhold til havbunnsmineralloven vil utredning av alle relevante forhold ved slike prosjekter skje i tilknytning til eventuelle fremtidige søknader fra industriaktører om godkjenning av en plan for utvinning av konkrete mineralforekomster, jf. havbunnsmineralloven § 4-4.

Åpningsprosessen omhandler en ny næring med liten grad av teknologisk modenhet, særlig når det gjelder utvinningsteknologier. Det er ingen faktisk kunnskap eller erfaring fra tilsvarende virksomhet. Vurderingen av virkninger er derfor, i tillegg til den kunnskap som finnes fra relevant internasjonal forskning og annen sammenlignbar virksomhet, basert på ulike faglige forutsetninger og antagelser, inkludert modelleringer og målinger fra tester. Formålet har vært å gi et konservativt, men mest mulig riktig, overordnet bilde av type av virkninger og omfang av disse generelt og eksemplifisert for ett prosjekt av hver ressurstype. Konsekvensutredningen peker på ulike teknologier som kan være aktuelle og identifiserer forhold som kan kreve avbøtende tiltak for å tilfredsstille krav til en miljømessig forsvarlig aktivitet.

Som del av utredningsarbeidet bestilte direktoratet flere grunnlags- og virkningsstudier. Det ble innhentet totalt seks grunnlagsstudier, og tre virkningsstudier for å avklare virkningene av undersøkelse og utvinning av havbunnsmineralvirksomhet, inkludert virkninger for miljø (**stevningen bilag 20**, s. 29–30). Rapportene sammenstiller all den kunnskap som er opparbeidet gjennom mange tiår, med henvisning til at biologiske undersøkelser i norske havområder går tilbake helt til 1870-tallet. Denne kunnskapen er langt fra fullstendig, men er samtidig grunnleggende for forståelsen av områdene og har vært sentral for konsekvensutredningen.

Det er riktig som påpekt av saksøkerne at grunnlagsstudiene påpekte kunnskapsmangel. Å beskrive kunnskapsmangler var en del av utredningsprogrammet (**stevningen bilag 5**, s. 30). For de relevante grunnlagsstudiene ba departementet i tillegg spesifikt om at

kunnskapsmangler påpekes og beskrives. Det fremgår av bestillingen til Havforskningsinstituttet at:

*«Det er viktig at det tydelig kommer fram hva vi har kunnskap om og hva vi ikke har kunnskap om innenfor utredningsområdet, og i hvilke geografiske områder vi har kunnskap og hvor vi evt. mangler kunnskap. Rapporten skal derfor angi en vurdering av kvaliteten på tilgjengelig kunnskap (både hos HI og basert på gjennomgang av litteratur) og, som relevant, beskrive ytterligere kunnskap som vurderes som nyttig knyttet til eventuelle fremtidige prosjekter for utvinning av havbunnsmineraler i området.»*

**Bilag 4:** Arbeidsbeskrivelse for grunnlagsstudie om pelagisk økosystem, Havforskningsinstituttet

Tilsvarende tok også Universitetet i Bergen sikte på å adressere usikkerhet og kunnskapshull i sin grunnlagsstudie:

*«Beskrivelse av usikkerhet og kunnskapshull vil utgjøre en viktig del av faktagrunnlaget. Dette vil bli fremhevet under hvert tema, og det vil også bli behandlet overordnet som et eget tema. En gjennomgang av metodikken vil også være en viktig del av faktagrunnlaget.»*

**Bilag 5:** Forslag til utredning i regi av Universitetet i Bergen om landskapstrekk, naturtyper og bentiske økosystemer.

Også arbeidsbeskrivelsen til grunnlagsstudien om sjøfugl ber om at kunnskapsmangler adresseres:

*«Vurdering av virkninger på naturressurser og miljø krever kunnskap om miljøtilstand og naturforhold innenfor område med mulig virksomhet og tilhørende influensområde. I tillegg er det viktig å ha oversikt over mangler og usikkerhet i kunnskapsgrunnlaget og fremtidig kunnskapsbehov.»*

**Bilag 6:** Arbeidsbeskrivelse for grunnlagsstudie om sjøfugl, Norsk polarinstitutt i samarbeid med NINA og Akvaplan-NIVA.

Når det gjelder grunnlagsstudien til Fiskeridirektoratet som påpekte begrenset kunnskap om internasjonale fiskeriaktiviteter i området, gjøres det oppmerksom på at rapporten kun beskrev norsk og utenlandsk fiskeriaktivitet i de deler av utredningsområdet som er underlagt norsk fiskerijurisdiksjon. Utenlandsk aktivitet i de delene av utredningsområdet som er internasjonalt farvann og som forvaltes av kyststatene via NEAFC<sup>1</sup> ble ikke beskrevet da Fiskeridirektoratet ikke hadde oversikt over denne aktiviteten. Senere ble det derfor sendt en forespørsel via ICES<sup>2</sup> om utlevering av sammenholdte sporingsdata og fangstatistikk for utenlandske fartøy i delene av utredningsområdet som er internasjonalt farvann.

---

<sup>1</sup> Den Nordøstatlantiske fiskerikommisjonen (North East Atlantic Fisheries Commission).

<sup>2</sup> International Council for the Exploration of the Sea.

Fiskeridirektoratet fikk oversendt data for perioden 2013–2019 i slutten av 2022 og utarbeidet et vedlegg til grunnlagsrapporten som ble publisert på regjeringens nettsider.

**Bilag 7:** Rapportvedlegg til grunnlagsrapport om fiskeriaktiviteten i utredningsområdet, Fiskeridirektoratet

Departementet innhentet også en miljøvirkningsstudie fra Akvaplan-niva og IKM Acona. Det er riktig at det i rapporten ble lagt til grunn antakelser om tilstedeværelse av miljøverdier og sårbarhet. Staten vil imidlertid fremheve at det nettopp på grunn av begrenset kunnskap ble lagt til grunn *konservative* antakelser<sup>3</sup>:

*«Siden utredninger er gjort på generelt grunnlag for et stort utredningsområde, der bunnfauna i stor grad ikke er kartlagt, er det lagt til grunn konservative antakelser om tilstedeværelse av typisk sårbar fauna ved sjøfjell og aktive sulfidforekomster.» (stevningen bilag 17, s. 61)*

Videre fremgår det av rapporten at:

*«Det innebærer at vurderingene er konservative og at prosjektspesifikke konsekvensvurderinger senere kan konkludere med lavere konsekvensnivå basert på stedsspesifikke kartlegginger og registreringer.» (stevningen bilag 17, s. 22)*

For ytterligere beskrivelse av metodikken vises det til rapporten s. 17–22.

I stevningen punkt 4.3 hevder saksøker at vurderingen i rapporten om at leteaktivitet har liten miljøpåvirkning ikke støttes av uavhengige forskningsmiljøer. Dette er ikke riktig. Staten viser til Senter for dyphavsforskning ved Universitetet i Bergen sitt høringsinnspill til konsekvensutredningen der det uttales:

*«Slik vi ser det, er dagens faktagrunnlag tilstrekkelig til å starte en letefase under et juridisk rammeverk (se spesifikke kommentarer nedenfor). Vi deler utredningens vurdering av at leteaktivitet vil ha liten miljøpåvirkning, forutsatt at den baserer seg på metodikk tilsvarende den som har vært benyttet i forbindelse med forskning og offentlig utredningsarbeid.» (stevningen bilag 27, s. 1)*

Som saksøker påpeker ga Nærings- og fiskeridepartementet (NFD) Havforskningsinstituttet en frist på to og en halv virkedag (som senere ble utvidet til omtrent tre virkedager) til gjennomgang av rapporten fra Akvaplan-Niva og IKM Acona. Isolert sett kan det fremstå som en svært kort frist. Her er det imidlertid viktig å fremheve at denne gjennomgangen ikke var ment å være en fullstendig kvalitetssikring av rapporten. Formålet med denne gjennomgangen var utelukkende å se om det var noe i utkastet til konsekvensutredning (kalt sammenstillingsrapporten i bestillingen) «som avviker fra omtalen i fagrapportene som sammenstillingsrapporten bygger på» (stevningen bilag 18).

---

<sup>3</sup> «Konservativt» innebærer i denne sammenhengen at det benyttes sikkerhetsmargin når det gjelder vurderingen av miljøkonsekvenser av aktivitet.



Henvendelsen fra NFD til Havforskningsinstituttet hvor det ble anmodet om innspill var for øvrig ikke en del av den ordinære høringsprosessen av konsekvensutredningen, men noe Nærings- og fiskeridepartementet valgte å gjøre som del av regjeringens interne behandling av konsekvensutredningen og forberedelse til høringen av denne. Da konsekvensutredningen etter denne interne behandlingen i regjeringen ble sendt på høring, var Havforskningsinstituttet på ordinært vis en høringsinstans, og kom med sine innspill til underlagsrapportene og konsekvensutredningen i den forbindelse. Foreleggelsen til instituttet i forkant av høringsrunden var altså ikke en saksbehandling som var påkrevd etter loven, men et ledd i en intern arbeidsprosess mellom Nærings- og fiskeridepartementet og Havforskningsinstituttet som departementets underliggende etat.

I god tid før fristen utløp ga Havforskningsinstituttet overordnede kommentarer der instituttet særlig understreker behovet for mer kunnskap om naturforhold i utredningsområdet for å vurdere miljøverdiens sårbarhet for påvirkning fra mineralutvinning. Staten viser her til redegjørelsen nedenfor i punkt 3.6 der regjeringens strategi for videre kunnskapsinnhenting omtales.

I tilbakemeldingen til NFD pekte Havforskningsinstituttet også på mangel på kunnskap om strømforhold i området og at konsekvensene av dette ikke blir reflektert tilstrekkelig i det videre arbeidet i rapporten. På basis av innspill fra Havforskningsinstituttet har regjeringen lagt en plan for innsamling av denne type data, jf. Meld. St. 25 (2022-2023) der det fremkommer at regjeringen vil:

«[G]i Havforskningsinstituttet eit oppdrag om å auke kunnskapen om regionale og lokale havstraumar i dei ulike djupa i Norskehavet og Grønlandshavet.» (**stevningen bilag 41**, s. 9)

I punkt 4.4 i stevningen hevdes det at konsekvensutredningen i det vesentligste var basert på rapporten fra Akvaplan-niva og IKM Acona. Til dette vil staten påpeke at konsekvensutredningen var basert på samtlige grunnlagsstudier og virkningsrapporter. Det er summen av faggrunnlaget som oppsummeres i konsekvensutredningen.

### **3.4 Høringsinnspill til konsekvensutredningen**

Sammen med et utkast til beslutning om å åpne et område for mineralvirksomhet, ble konsekvensutredningen sendt på offentlig høring 27. oktober 2022 med tre måneders høringsfrist til 27. januar 2023. Utkast til beslutning med forslag til åpningsområde fulgte som vedlegg til høringsbrevet. Det foreslåtte åpningsområdet var betydelig redusert sammenlignet med utredningsområdet.

**Bilag 8:** Kart over forslag til åpningsområde.

En rekke høringsinstanser, hovedsakelig bestående av næringsaktører og lokale og regionale myndigheter, uttrykte støtte til konsekvensutredningen og den foreslåtte prosessen med åpning av areal. Faktorer som vektlegges av de som støtter åpning er blant annet mulighet for verdiskaping og teknologioverføring fra eksisterende industrier. Kommuner peker på muligheter for ringvirkninger på land i form av tilgjengelige baser, verft, prosesseringsanlegg etc. Det vises til betydelig fremtidig mineraletterpørsel. Havbunnsmineraler som en mulig



ny forsyningskilde fremheves som positivt for å styrke forsynings sikkerheten. Sirkulærøkonomien fremheves som viktig, men med bred enighet om at det ikke er en tilstrekkelig kilde til mineraler. Det vises til departementets gjennomgang av innkomne høringsinnspill i Meld. St. 25 (2022–2023) punkt 4.3.8.1 (**stevningen bilag 41**, s. 70).

Andre høringsinstanser kritiserte konsekvensutredningen, blant annet på grunn av begrenset kunnskap om dyphavet. Som nevnt ble innspillene, inkludert Miljødirektoratets, vurdert i Meld. St. 25 (2022–2023) punkt 4.3 (**stevningen bilag 41**, s. 54–71). Til de høringsinnspillene som saksøker fremhever i stevningen punkt 4.5 vil staten påpeke følgende:

- NGU skriver i sin høringsuttalelse at de er enig i behovet for en konsekvensutredning og enig i at private aktører bør få utføre kartlegging, leting og undersøkelser av mineralressurser på havbunnen. Uttalelsen om at konsekvensutredningen vurderes som «misvisende og tendensiøs» knytter seg til ressursgrunnlaget, og ikke til vurderingene av miljøvirkninger (**stevningen bilag 26**). Staten viser her til at NGUs merknad er basert på omtalen av ressursgrunnlaget i konsekvensutredningen, og ikke Sjøkulturdirektoratets ressursvurdering som ble lagt frem i januar 2023. Flere forhold som NGU påpeker i høringsuttalelsen er utdypet og forklart i ressursrapporten.
- Fiskeridirektoratet ga ikke uttrykk for bekymring i sin høringsuttalelse slik saksøker påstår. I høringsuttalelsen har ikke Fiskeridirektoratet innvendinger til funnet i konsekvensutredningen om at havbunnsmineralvirksomhet har «ingen/ubetydelige» konsekvenser for fiskeriene. Direktoratet viser bl.a. til at reglene som forbyr fiske med bunnberørende redskap i store deler av utredningsområdet gjør området mindre interessant for store deler av flåten (**stevningen bilag 29**).
- Når det gjelder høringsuttalelsen fra Senter for dyphavsforskning ved Universitetet i Bergen (**stevningen bilag 27**), støtter den som alt nevnt vurderingen i konsekvensutredningen om at leteaktivitet har små miljøpåvirkninger, jf. ovenfor i punkt 3.3.

### 3.5 Høringsinnspill fra notifiserte naboland

Siden havbunnsmineralvirksomhet er en ny næring og området som ble sendt på høring grenset opp til andre lands kontinentalsokler, sendte Energidepartementet forslaget til beslutning om åpning av område på norsk kontinentalsokkel for mineralvirksomhet og konsekvensutredningen til Island og Danmark. Island svarte i form av note (**stevningen bilag 40**). Danmark oversendte sine innspill til konsekvensutredningen (**stevningen bilag 39**) og ga uttrykk for at de behandlet dette som en høring under Espoo-konvensjonen. Reelt sett er kravene i Espoo-konvensjonen derfor tilfredsstillende.

### 3.6 Meld. St. 25 (2022–2023) med forslag om åpning av område for mineralvirksomhet

På bakgrunn av ressursvurderingen, konsekvensutredningen og innkomne høringsinnspill utarbeidet departementet en stortingsmelding med forslag om åpning av område på norsk

kontinentalsokkel for mineralvirksomhet. Meld. St. 25 (2022–2023) ble fremmet i statsråd 20. juni 2023 (**stevningen bilag 41**).

Regjeringen vurderte på bakgrunn av kunnskapsgrunnlaget som ble fremskaffet gjennom åpningsprosessen at det var grunnlag for å anbefale åpning av det området som ble sendt på høring i utkastet til åpningsbeslutning (se ovenfor i punkt 3.3), med unntak av et område i sør som ble tatt ut av hensyn til fiskeriaktiviteten som pågår i området. Området som ble foreslått åpnet i stortingsmeldingen var på 281 200 kvadratkilometer og 53 prosent mindre enn utredningsområdet (**stevningen bilag 41**, s. 75).

Basert på funnene i konsekvensutredningen og innkomne høringsinnspill fant departementet behov for å beskytte aktive hydrotermale strukturer. Dette er strukturer som kjennes igjen ved at de er assosiert med utstrømming av varm væske, oppreiste skorsteiner og ofte kolonisert av biosamfunn som er avhengig av hydrotermale væsker, se konsekvensutredningen (**stevningen bilag 20**, s. 23). I stortingsmeldingen satte derfor regjeringen som vilkår for åpning at utvinning av aktive hydrotermale strukturer ikke skal være tillatt, og at slike strukturer skal beskyttes slik at de heller ikke blir skadet av virksomhet i tilgrensende områder. En utvinningsplan vil bare bli godkjent dersom det kan godtgjøres at utvinning kan gjennomføres slik at det ikke medfører vesentlige negative virkninger for naturmangfoldet knyttet til de aktive strukturene (**stevningen bilag 41**, s. 73 og 77).

I stortingsmeldingen pekes det på begrenset kunnskap om miljøforhold i dyphavet og at det må samles inn mer kunnskap før utvinning kan settes i verk. Det ble vektlagt at en åpning er nødvendig for at private aktører skal kunne bidra til kartlegging av ressurspotensialet og miljøverdiene, og til å øke kunnskapen om miljøvirkningene av en eventuell framtidig havbunnsmineralvirksomhet. Aktivitet knyttet til leting er i konsekvensutredningen generelt funnet å gi små miljømessige virkninger. I utvinningstillatelsene vil det bli fastsatt et arbeidsprogram, jf. havbunnsmineralloven § 4-3, som forplikter rettighetshaverne til å samle inn ressurs- og miljødata i området for tillatelsen. Slike data skal deles med myndighetene. Dette sikrer at det bygges mer kunnskap om både våre havbunnsmineralressurser og om naturmiljøet på dyphavet. Samtidig vil videre kunnskapsinnhenting i statlig regi fortsette. Havbunnsminerallovens skrittvis system innebærer at utvinning ikke settes i verk før det kan godtgjøres at det kan skje på en bærekraftig og forsvarlig måte. Sammen med regjeringens strategi for å øke kunnskapen om dyphavet og mineralressursene på norsk sokkel, sikrer dette at beslutningene som treffes, tillatelsene som tildeles og aktivitetene som utøves hele tiden er tilpasset kunnskapsgrunnlaget.

Meldingen ble behandlet i Stortingets energi- og miljøkomite som ga sin innstilling 19. desember 2023 (**stevningen bilag 44**). Komiteens flertall ga med noen tilleggsmerknader sin tilslutning til regjeringens forslag om åpningsområde og regjeringens strategi for forvaltningen av havbunnsmineraler, herunder forutsetningen om ikke å tillate utvinning av aktive hydrotermale strukturer.

I lys av den begrensede kunnskapen om natur- og miljøforhold i dyphavet som ble identifisert i åpningsprosessen, fremmet komiteens flertall forslag om at de første planene for utvinning av havbunnsmineraler forelegges for Stortinget som proposisjon før departementet godkjenner utvinningsplanen etter havbunnsmineralloven § 4-4. Videre foreslo flertallet å tydeliggjøre at hensynet til nasjonal sikkerhet vil være et kriterium ved tildeling av utvinningstillatelser. I tillegg foreslo flertallet at Sjøkeldirektoratet skal innhente

innspill fra øvrige berørte statlige etater, herunder Miljødirektoratet og Havforskningsinstituttet, i forbindelse med utarbeidelse av sitt forslag til arbeidsprogram til departementet.

Et mindretall i komiteen ga ikke sin tilslutning og fremmet forslag om at stortingsmeldingen sendes tilbake til regjeringen for mer kunnskapsinnhenting.

Stortinget behandlet regjeringens forslag 9. januar 2024. Et flertall på 79 mot 20 stemmer sluttet seg til komitéflertallets innstilling. Stortingsmeldingen ble deretter vedlagt protokollen.

### 3.7 Åpningsbeslutningen

Den 12. april 2024 besluttet Kongen i statsråd å åpne et område på norsk kontinentalsokkel for mineralvirksomhet i tråd med stortingsbehandlingen av Meld. St. 25 (2022–2023) (**stevningen bilag 1**). Beslutningen betyr ikke at utvinning kan settes i verk slik saksøker antyder i stevningen punkt 4.9. Det vises til redegjørelsen ovenfor i punkt 2.1.

Området som er åpnet er redusert med 53 prosent sammenlignet med utredningsområdet. Beslutningen legger til grunn regjeringens strategi for videre kunnskapsinnhenting som beskrevet i stortingsmeldingen, og som Stortinget har sluttet seg til. Utvinningstillatelser vil bli gitt med et konkret arbeidsprogram som stiller krav om gjennomføring av leteaktivitet som første steg. Gjennom de arbeidsprogrammene som blir fastsatt, og den tilhørende leteaktiviteten, vil myndighetene få mer datainnsamling og mer omfattende kunnskapsinnhenting, både om ressurser og miljøforhold. Dette vil bidra til viktig kunnskapsoppbygging. Parallelt vil videre kunnskapsinnhenting i statlig regi fortsette.

Videre fremgår det av beslutningen av myndighetene kun vil godkjenne en utvinningsplan dersom planen med tilhørende konsekvensutredning godtgjør at utvinningen kan skje på bærekraftig og forsvarlig vis, slik at hensynet til miljø, sikkerhet og sameksistensen med ev. fiskeri- og annen virksomhet til havs i det aktuelle området er godt ivaretatt. I tråd med føringene fra stortingsbehandlingen av Meld. St. 25 (2022–2023) vil departementet før godkjenning av de første utvinningsplanene forelegge dem for Stortinget.

### 3.8 Høring av arealforslag til første konsesjonsrunde

For fullstendighetens skyld kommenteres her også prosessen som etterfølger åpningsbeslutningen.

Energidepartementet sendte 26. juni 2024 forslag til områder for første konsesjonsrunde for havbunnsmineraler på offentlig høring. Høringsfristen er satt til 26. september 2024. I forslaget foreslås det å lyse ut deler av åpningsområdet for søknader om utvinningstillatelser. Et utarbeidet kart viser områdene som foreslås utlyst.

#### **Bilag 9:** Kart: Første konsesjonsrunde – forslag til utlysning

Høringsrunden er en del av første konsesjonsrunde for mineralvirksomhet på norsk kontinentalsokkel. Etter høringen vil departementet gjennomgå høringsinnspillene. Deretter

vil konsesjonsrunden bli utlyst. Utlysningen vil blant annet inneholde en søknadsfrist for selskapene, og opplysninger om krav og vilkår som vil pålegges søkere knyttet til blant annet miljø. Som en del av søknadene, vil selskapene også bli bedt om å inkludere et forslag til arbeidsprogram for arealet de søker på. Den enkelte utvinningstillatelse som tildeles vil omfatte et geografisk avgrenset område innenfor arealet som er utlyst. En ev. senere utvinningsplan vil igjen gjelde for et enda snevrere område innenfor den aktuelle utvinningstillatelsen.

**Bilag 10:** Høring av arealforslag – Utlysning av områder for mineralvirksomhet på havbunnen. Høringsbrev datert 26. juni 2024

**Bilag 11:** Pressemeldingen «Høring av første konsesjonsrunde for havbunnsmineraler», datert 26. juni 2024

## 4 STATENS SYN PÅ SAKEN

### 4.1 Overordnet om statens syn

Det anføres i stevningen at åpningsbeslutningen lider av saksbehandlingsfeil som følge av at konsekvensutredningsplikten er brutt. Anførelsen synes å være konsekvensutredningen er for overordnet og generell og bygger på et for svakt kunnskapsgrunnlag til å oppfylle innholdsmessige minstekrav etter havbunnsmineralloven § 2-2, lest i lys av Grunnloven § 112 andre ledd og Norges folkerettslige forpliktelser. Videre anføres det at beslutningen bygger på faktiske feil.

Denne side vil anføre at Kongen i statsråds beslutning 12. april 2024 er gyldig. Etter statens syn hefter det ingen saksbehandlingsfeil på ovennevnte grunnlag som kan lede til at åpningsbeslutningen er ugyldig. Etter statens syn er saksøkers anførsler lite konkrete. Med unntak av noen få forhold (se nedenfor i punkt 4.5 og 4.6), fremkommer det ikke klart av stevningen hvilke ytterligere utredninger saksøker mener er påkrevd for å oppfylle lovens krav.

### 4.2 Søksmålsadgangen

Inngangsvilkåret for søksmål er at saken gjelder et «rettskrav», jf. tvisteloven § 1-3 første ledd. Dette gjelder også ved søksmål anlagt av organisasjoner etter tvl § 1-4. Spørsmålet her blir først og fremst hvorvidt et krav om at en beslutning om åpning er ugyldig er et «rettskrav». Spørsmålet skal avgjøres av domstolene ex officio.

Åpningsbeslutninger er ikke «vedtak» etter forvaltningsloven § 2 bokstav a, jf. HR-2020-2472-P avsnitt 180. Dette trekker i retning av at krav om ugyldighet av avgjørelsen heller ikke er et «rettskrav».

Domstolene løser konkrete tvister, men det finnes samtidig noen spredte eksempler på at også søksmål av mer generell karakter fremmes etter en helhetsvurdering. I HR-2021-417-P Acer heter det om dette fra flertallet i avsnitt 172:

*"Ved den helhetsvurderingen som må foretas, vil en rekke momenter kunne inngå, avhengig av de nærmere omstendighetene. Blant disse nevner jeg: Reiser søksmålet uavklarte rettsspørsmål av prinsipiell rekkevidde? Er det vanskelig eller klart uhensiktsmessig å få grunnlovsspørsmålet prøvd på en mer konkret måte? Vil spørsmålet bli godt nok opplyst ved å tillate søksmålet nå og i denne formen, eller vil domstolene få et bedre grunnlag for å avgjøre saken dersom den fremmes i en mindre generell form? Hvor generelt er det kravet som gjøres gjeldende – knytter det seg til et konkret og avgrenset faktum?"*

Saksøkers innsigelser til beslutningens gyldighet er lite konkrete, og det er av den grunn vanskelig å konkludere etter en helhetsvurdering. Det er eksempelvis varslet vitneførsel fra marinbiologer om dyphavet, men det er vanskelig å se om partene har en konkret faktisk uenighet om biologien i åpningsområdet. Åpningsbeslutninger er politiske og prosessledende beslutninger som ikke reiser uavklarte rettsspørsmål. Prosessuelle krav kan prøves når og hvis det fattes konkrete vedtak, slik det ble gjort i klimasaken i HR-2020-2472-P. Slike vedtak vil gjelde langt mindre geografiske områder, og søksmål vil da ha mer preg av konkret rettstvist enn hva tilfellet er i saken her.

Lignende hjemler for åpning som i havbunnsmineralloven finnes i petroleumsloven og havenergilova. Så vidt staten er kjent med er det tidligere ikke reist søksmål om «åpning». Kommer retten til at ugyldighetskravet ikke kan anses som «rettskrav» og/eller at saken mangler aktuell interesse, skal søksmålet avvises. Staten har ikke innvendinger til at rettens vurdering av spørsmålet om søksmålsadgang i denne saken behandles og avgjøres som ledd i hovedforhandlingen, jf. tvl § 9-6 (3) annen setning.

### 4.3 Domstolskontroll

I stevningen på s. 10 anføres det at «Domstolskontrollen skal i dette tilfellet være inngående», og det vises til at «Åpningsvedtaket har utvilsomt store konsekvenser». Etter statens syn er det ikke grunnlag for å oppstille plikt til en særlig streng kontroll fra domstolenes side.

Domstolenes kontroll må her som ellers ta utgangspunkt i lovgivningen. Havbunnsmineralloven § 2-2 fastsetter at konsekvensutredningen skal «belyse» interesser og virkninger. Prop.106 L (2017–2018) s. 36 benytter begrep som «en viss oversikt over [...] de miljømessige forholdene, mulige farer for forurensing, samt antatte [...] virkninger.» Loven legger mao. ikke opp til at konsekvensutredningen skal «avklare» interesser og virkninger, og etter statens syn er det da ikke grunnlag for noen særlig inngående kontroll.

Premisset om at beslutningen om åpning «har utvilsomt store konsekvenser», er ikke treffende. I havbunnsminerallovens system er funksjonen til beslutning om «åpning» at myndighetene gis adgang til å tillate leting i regi av kommersielle aktører, slik at andre enn staten kan bidra med videre kunnskapsinnhenting ved siden av slik innhenting i offentlig regi. Konsekvensen av «åpning» er ikke at drift nødvendigvis vil bli igangsatt. En eventuell drift vil under enhver omstendighet ligge lenger frem i tid.

#### 4.4 Konsekvensutredningen er utarbeidet i samsvar med krav stilt i norsk rett

##### 4.4.1 *Kravene til konsekvensutredningens innhold, jf. havbunnsmineralloven § 2-2 andre ledd*

Kravene til konsekvensutredningens innhold på åpningsstadiet er gitt i havbunnsmineralloven § 2-2 andre ledd, som lyder:

*«Konsekvensutredningen skal bidra til å belyse de ulike interessene som gjør seg gjeldende på det aktuelle området, slik at dette kan ligge til grunn når det skal tas stilling til om, og eventuelt på hvilke vilkår, området kan åpnes for mineralvirksomhet. Konsekvensutredningen skal belyse hvilke virkninger en eventuell åpning kan få for miljøet og antatte næringsrelaterte, økonomiske og sosiale virkninger.» (uth. her)*

Bestemmelsen angir hvilke temaer konsekvensutredningen skal belyse. Det følger av forarbeidene at det nærmere innholdet i konsekvensutredningsprogrammet må besluttes konkret for det enkelte området, jf. Prop. 106 L (2017–2018) s. 35, der det fremgår at:

*«Typiske elementer vil være å belyse de ulike interessene som gjør seg gjeldende på det aktuelle området, en viss oversikt over hvilke mineralressurser som kan være aktuelle og hvor de befinner seg, de miljømessige forholdene, mulige farer for forurensing, samt antatte næringsmessige, økonomiske og sosiale virkninger. Konsekvensutredningsprogrammet kan også vise behov for ytterligere vitenskapelige studier i området som må iverksettes før konsekvensutredningen kan avsluttes og eventuell åpning besluttes.» (uth. her)*

Lest i sammenheng med forarbeidene stilles det krav om en konsekvensutredning som på overordnet nivå belyser de angitte temaene i havbunnsmineralloven § 2-2 andre ledd, jf. uttrykket «en viss oversikt» i forarbeidene. At det er virkningene en eventuell åpning «kan få» som skal belyses tyder på at vurderingene kan være usikre. Etter statens syn gir verken lovens ordlyd eller forarbeidene støtte for de krav til kunnskapsgrunnlag som saksøker oppstiller. Uttalelsen i forarbeidene om behov for ytterligere vitenskapelige studier er et eksempel på hva et konsekvensutredningsprogram kan inneholde. Uttalelsen gir ikke grunnlag for et forbud mot åpning når konsekvensutredningen identifiserer og drøfter begrensninger i kunnskapsgrunnlaget, slik saksøker synes å anføre i stevningen punkt 5.2.1.1. Saksøker har heller ikke angitt hvilke «ytterligere vitenskapelige studier» som departementet skulle sørget for gjennomføring av før åpning kunne vært besluttet.

I denne saken er det utarbeidet en konsekvensutredning som belyser de ulike interessene i utredningsområdet og hvilke virkninger en åpning kan få for miljøet og antatte næringsrelaterte, økonomiske og sosiale virkninger. For temaer og spørsmål der det er identifisert begrenset kunnskap eller er usikkerhet knyttet til vurderingene, er dette opplyst om i konsekvensvurderingen og tatt i betraktning i interesseavveiningen ved beslutning om åpning. Regjeringen vurderte kunnskapsgrunnlaget som tilstrekkelig til å anbefale åpning – med de virkninger selve åpningsbeslutningen vil ha, jf. over og Meld. St. 25 (2022–2023) (**stevningen bilag 41**, s. 75). Stortinget behandlet stortingsmeldingen 9. januar 2024 og støttet regjeringens anbefaling med noen tilleggspunkter, se ovenfor i punkt 3.7. I tråd med havbunnsminerallovens skrittvis system er det lagt en strategi for videre kunnskapsinnhenting.

#### 4.4.2 *Grunnloven § 112 stiller ikke ytterligere krav*

Grunnloven § 112 andre ledd gir borgerne «rett til kunnskap om naturmiljøets tilstand og om virkningene av planlagte og iverksatte inngrep i naturen», for at de skal kunne ivareta sin rett etter første ledd til «et miljø som sikrer helsen, og til en natur der produksjonsevne og mangfold bevares». Det er uklart for staten om saksøker hevder bestemmelsen oppstiller utredningskrav ut over det som følger av havbunnsminerallovens ordlyd. Staten vil uansett påpeke at bestemmelsen ikke legger konkrete føringer for hvordan myndighetene innhenter og tilgjengeliggjør miljøinformasjon, men overlater til myndighetene å treffe de tiltak som er nødvendige, jf. § 112 tredje ledd. I praksis ivaretas retten til informasjon om miljøet gjennom saksbehandlingskrav på det enkelte område. I denne saken er det havbunnsmineralloven.

Staten kan heller ikke se at HR-2020-2472-P gir holdepunkter for å anta at konsekvensutredningsplikten er brutt. Saksøkers anførsel om at det ikke er foretatt en «grundig» avklaring av fordelene og ulempene ved åpning, jf. HR-2020-2472-P avsnitt 184, er ikke nærmere underbygget.

Det tilføyes at passusen i avsnitt 184 i plenumsdommen om «fordelene og ulempene ved åpninga» (uth. her), må leses i lys av dommen for øvrig, særlig avsnitt 217-223. «Åpning» etter havbunnsmineralloven gir ikke kommersielle aktører rettskrav på utvinning av ev. drivverdige funn. Konsekvensene av åpning er i første omgang kun at det åpnes for ytterligere undersøkelser, som igjen har som konsekvens at kunnskapsgrunnlaget øker.

#### 4.4.3 *Prinsippene i naturmangfoldloven § 7, jf. §§ 8–10 er hensyntatt*

Staten bestrider at prinsippene i naturmangfoldloven § 7, jf. §§ 8–10 er brutt. Saksøkers anførsler knyttet til disse bestemmelsene synes å bygge på en forutsetning om at åpningsbeslutningen i seg selv har store konsekvenser, jf. også stevningen punkt 5.1. Det medfører ikke riktighet. Åpning betyr ikke at mineralvirksomhet kan iverksettes, men beslutningen innebærer at konsesjonsmyndighetene kan sette i gang en prosess for tildeling av tillatelser i området som er åpnet. I første omgang gir tillatelser rett til leting, jf. ovenfor i punkt 2.1. Ved anvendelsen av prinsippene i naturmangfoldloven §§ 8–10 må det tas utgangspunkt i den konkrete beslutningen som er gjenstand for gyldighetskontroll, jf. også HR-2020-2472-P avsnitt 148.

Det fremgår av Meld. St. 25 (2022–2023) at prinsippene i naturmangfoldloven § 7, jf. §§ 8-10 er lagt til grunn som retningslinjer for åpningsprosessen (**stevningen bilag 41**, s. 57). Gjennom konsekvensutredningen er det utarbeidet et oppdatert og sammenstilt kunnskapsgrunnlag basert på eksisterende kunnskap knyttet til eventuell fremtidig havbunnsmineralaktivitet på norsk kontinentalsokkelen. Kunnskapen er fremskaffet gjennom faglige grunnlagsstudier og virkningsstudier utarbeidet av aktuelle fagmiljøer, herunder statlige etater og institutter, universiteter og andre kompetansemiljøer. Tilgjengelig kunnskap er lagt til grunn og kunnskapsmangler er påpekt. På denne måten er det best mulige kunnskapsgrunnlaget fremskaffet, slik naturmangfoldloven § 8 foreskriver.

Det er ikke riktig som saksøker hevder i stevningen punkt 5.2.2 at konsekvensutredningen avstår fra å vurdere samlet belastning. Dette er vurdert i punkt 8.5 i konsekvensutredningen i tråd med naturmangfoldloven § 10:



«Basert på vurderinger av konsekvensene for ulike påvirkninger som er aktuelle i utredningsområdet, er det gjort en vurdering av samlede forventede påvirkninger på økosystemene i utredningsområdet fra en ev. havbunnsmineralvirksomhet, andre relevante sektorer i området og globale virkninger som klimaendringer (temperaturrendringer, forsuring, endring i strømmønster, osv.) og forurensninger (se f.eks. Faglig Forum, 2019).» (**stevningen bilag 20**, s. 110)

Som følge av åpningen kan private selskaper tildeles tillatelse til å lete etter mineraler på havbunnen. I konsekvensutredningen er leteaktivitet vurdert å ha små miljøvirkninger. I en utvinningsfase er konsekvensene i dag lite kjent fordi det hittil ikke har vært noen slik aktivitet. Selskaper med utvinningstillatelse vil derfor bli pålagt å samle inn data om miljøforhold i de områdene de undersøker i tillatelsens første fase. Denne kunnskapen vil sammen med ytterligere kunnskap som erverves fra myndighetenes side bli lagt til grunn ved behandling av eventuelle utvinningsplaner. Dette, sammen med en skrittvis tilnærming til aktivitet i området som åpnes, vil sørge for en føre-var-tilnærming, jf. naturmangfoldloven § 9.

Når det gjelder høyesterettsavgjørelsen fra New Zealand som saksøker viser til i stevningen punkt 5.2.1.5, fremstår ikke den som relevant for spørsmålene i denne saken. Avgjørelsen fra New Zealand gjaldt gyldigheten av en tillatelse til å utvinne mineraler på havbunnen. Saksforholdet er dermed ikke sammenlignbart. Det tilføyes at det i norsk rett ikke kan iverksettes utvinning uten godkjent plan for utvinning, som også skal inneholde en prosjektspesifikk konsekvensutredning, jf. havbunnsmineralloven § 4-4.

#### **4.5 Konsekvensutredningen oppfyller folkerettslige krav**

Konsekvensutredningen er utarbeidet og gjennomført i samsvar med gjeldende folkerettslige krav. Saksøker har i stevningen vist til seks folkerettslige kilder med til dels overlappende krav om konsekvensutredning og anført generelt at:

«Konsekvensutredningen identifiserer, beskriver eller evaluerer ikke potensielle miljøvirkninger. Konsekvensutredningen er overordnet, og bærer preg av omfattende mangel på kunnskap om de miljømessige virkningene av åpning for mineralvirksomhet på havbunnen.» (stevningen punkt 5.3.2)

Staten kan ikke se at anførselen er nærmere underbygget i stevningen. Det er ikke konkretisert hvilke miljøvurderinger konsekvensutredningen mangler. Anførselen om at konsekvensutredningen er for overordnet og generell savner rettslig forankring, da det heller ikke er konkretisert hvilke spesifikke utredningskrav som eventuelt skulle følge av folkerettslige forpliktelser.

Hva gjelder plandirektivet, viser staten til redegjørelsen ovenfor i punkt 3.1 der det fremgår at det generelt har blitt sett hen til direktivets krav i åpningsprosessen.

For EMK artikkel 2 og 8 har saksøker konkretisert anførselene til manglende utredning av konsekvenser for klima og havforsuring ved potensiell oppvirvling av karbon fra havbunnen og påvirkning av karbonsyklusen i dyphavet.



Det er riktig at dette ikke er utredet i konsekvensutredningen. Spørsmålet er ikke ansett som relevant for havbunnsmineralvirksomhet på norsk kontinentalsokkel, fordi mengden karbon i sedimentene er for små til å ha negative konsekvenser for klima og havforsuring. Organisk karbon avsatt i dyphavet har sitt opphav i de øverste 200m av vannsøylen. Herfra "regner" algerester og mikrofauna som beiter på algerester, nedover i vannsøylen og blir til en komponent av «marin snø». Mesteparten av organisk karbon er allerede oksydert til karbondioksid før partiklene når havbunnen (Passow & Weber 2023, s. 2–4 og 11).

**Bilag 12:** Passow, U. & Weber, T., The biological carbon pump, i Treatise on Geochemistry, 3. utgave, Elsevier, 2023.

Dette er en av grunnene til at dyphavssedimenter inneholder lite karbon og få næringsstoffer. Derfor er dyphavssedimenter preget av lavt arts mangfold. Målinger av organisk karbon i områder som er aktuelle for mineralutvinning bekrefter at det organiske karboninnholdet (TOC) i sedimentene er svært lavt, som oftest mellom 0,1 og 1 prosent, med medianverdi = 0,4 prosent (Jørgensen, S.L. et al. 2012).

**Bilag 13:** Jørgensen, S.L., Hannisdal, B., Lanzén, A., Baumberger, T., Flesland, K., Fonseca, R., Øvreås, L., Steen, H.A., Thorseth, I.H., Pedersen, R.B., & Schleper, C. Correlating microbial community profiles with geochemical data in highly stratified sediments from the Arctic Mid-Ocean Ridge. Proceedings of the National Academy of Sciences. Vol. 109, No. 42 (2012).

I tillegg er sedimentlagene tynne i de aktuelle områdene. Dette indikerer at oppvirvling av karbon fra havbunnen ikke vil ha negative konsekvenser for klima og havforsuring.

Staten er derfor ikke enig med saksøkerne i at det utgjør en saksbehandlingsfeil som leder til ugyldighet at potensiell oppvirvling av karbon fra havbunnen og påvirkning på karbonsyklusen i dyphavet ikke er vurdert i konsekvensutredningen.

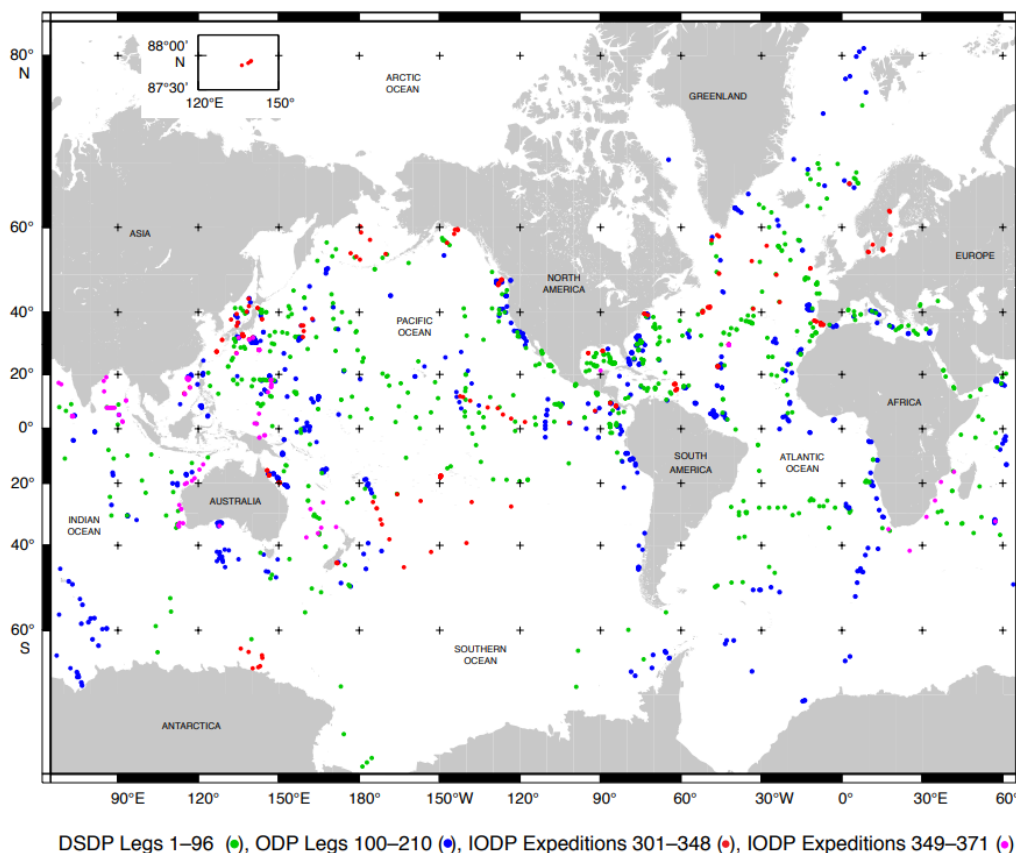
#### **4.6 Beslutningen bygger ikke på mangelfull konsekvensutredning eller uriktige faktiske antakelser om virkningene av leting**

Det bestrides at åpningsbeslutningen bygger på mangelfull konsekvensutredning eller uriktige faktiske antakelser om virkningene av leteaktivitet.

Leting etter mineraler på havbunnen foregår ved innsamling av data fra overflatefartøy og/eller undervannsfarkoster (passive undersøkelser), samt innsamling av geologiske prøver på og under havbunnen (aktiv prøvetaking). Teknologien for leting og kartlegging kan ikke anses som umoden slik saksøker hevder. Det vises til at Sokkeldirektoratet har samlet inn dyphavsdata i over 25 år (**bilag 2**, s. 13–21), og at det internasjonale vitenskapelige konsortiumet International Ocean Discovery Program (IODP, tidligere DSDP og ODP) i mer enn 50 år har utført store boreoperasjoner i dyphavet i alle verdenshav. Flere tusen borehull er boret, og boreoperasjonene har tilført mye kunnskap om undergrunnen i dyphavet og nærliggende miljø.

**Bilag 14:** Utskrift fra [Om IODPs historie](#) (nettside)

Bildet nedenfor viser boreoperasjoner foretatt av IODP:



Kilde: [Combined IODP2 \(pink\), IODP \(red\), ODP \(blue\), and DSDP \(green\) drill sites \(tamuedu\)](http://tamuedu.com)

Ifølge saksøker bygger konsekvensutredningen på en uriktig faktisk antakelse når den finner at leteaktivitet vil ha små miljøvirkninger grunnet kort varighet og lite berørt område. Denne side kan ikke se at det i stevningen fremkommer opplysninger som tilsier at konsekvensutredningens funn er uriktig. Saksøker støtter anførselen på NGUs høringsuttalelse til konsekvensutredningen, som lyder:

*«Leting og undersøkelser er ikke kortvarige, men har begrenset lokal påvirkning.»  
(stevningen bilag 26)*

NGU er altså enig i at leting og undersøkelser har begrenset lokal påvirkning (lite berørt område). Uttalelsen om varighet må antas å sikte til aktivitet over lengre tid. Aktivitetene som inngår i letefasen vil gjerne spres på flere, ofte sesongavhengige, tokt. De enkelte aktivitetene vil derfor hver for seg være kortvarige og medføre små fysiske inngrep, selv om aktivitetene samlet sett kan foregå over noen år.

I stevningen anføres det videre at vurderingen i konsekvensutredningen om at omfanget av kjerneboring under leting vil være begrenset i forhold til utvinning, er uriktig. I de relevante avsnittene i konsekvensutredningen heter det om dette:

*«Undervannsfarkostene vil ha ulike typer utstyr for passiv undersøkelse eller aktiv prøvetaking, herunder ulike former for sonar og ekkolodd samt spesifikt tilpassende sensorer, kamera, osv. Fysiske prøver (stein) kan bli tatt med gripeklo som mindre kjerneboringsprøver eller skjæres ved motorsaglignende verktøy. Slike inngrep er generelt av lite omfang.*

*For bedre å avgrense utstrekningen av en påvist forekomst, kan mer omfattende kjerneboring være aktuelt. Omfangsmessig vil dette være begrenset i forhold til utvinning.» (stevningen bilag 20, s. 46)*

Ifølge saksøker er vurderingen i siste avsnitt tilbakevist av NGU, som i sin høringsuttalelse skriver:

*«Dette må bero på en misforståelse. Å påvise, avgrense og karakterisere en mineralforekomst er finansielt krevende og en utfordring for de fleste landbaserte lete- og utviklingsprosjekter. Det stilles krav til hvordan av forekomster dokumenteres, og børsnoterte selskap må benytte rigide rutiner definert ved ulike CRIRSCO-systemer som JORC, PERC, NI43-101 når de oppgir ressurser og reserver. Karakterisering og avgrensning krever omfattende boring og tillater ikke ekstrapolasjon. På dette punktet vil ikke havbunnsmineraler stå i en særstilling i forhold til landbaserte forekomster.» (stevningen bilag 26)*

Slik staten forstår høringsuttalelsen, viser NGU her til at fastsetting av en mineralforekomsts ressurser og reserver for innrapportering til børsen vil kunne kreve et omfattende boreprogram, og synes å mene at dette er det viktigste i letingen etter havbunnsmineraler. Det er det ikke. Det viktigste er å finne forekomstene først og vektlegge de aktivitetene dette omfatter. Som vist til i konsekvensutredningen består disse aktivitetene av passive undersøkelser og aktiv prøvetaking med ROV og begrenset kjerneboring. Slik kjerneboring vil bli foretatt med små borerigger på havbunnen (stevningen bilag 20, s. 46–48).

At leteaktivitet vil ha liten miljøpåvirkning støttes også av uavhengige forskningsmiljøer. Senter for dyphavsforskning ved Universitetet i Bergen skriver i sin høringsuttalelse til konsekvensutredningen at de anser dagens faktagrunnlag som tilstrekkelig til å starte en letefase og at de «delar utredningens vurdering av at leteaktivitet vil ha liten miljøpåvirkning, forutsatt at den baserer seg på metodikk tilsvarende den som har vært benyttet i forbindelse med forskning og offentlig utredningsarbeid» (stevningen bilag 27, s. 1).

Saksøker knytter anførselen om mangelfull utredning til 1) virkningene av støy, vibrasjon og kunstig lys under leting, samt 2) risikoen for å innføre fremmede arter i økosystemene tilknyttet hydrotermale strukturer under henvisning til lite kontakt (konnektivitet) mellom ulike lokaliteter. Staten viser til at begge forholdene er utredet som ledd i konsekvensutredningsprosessen.

Virkinger av lyd, vibrasjoner og kunstig lys er behandlet i punkt 8.2.5 i konsekvensutredningen (stevningen bilag 20) og punkt 3.7 i virkningsstudien fra Akvaplan-Niva og IKM Acona, som inngikk i utredningsarbeidet og ble vedlagt konsekvensutredningen (stevningen bilag 17). Generelt kunnskapsnivå om påvirkning for marine organismer er gjennomgått og presentert i studien. Konsekvenser for fisk, marine pattedyr og sjøfugl er vurdert særskilt. Studien konkluderer ut fra de nivåene som forventes

av støy og lys fra havbunnsmineralutvinning at dette vil medføre et konsekvensnivå fra «ingen» til «liten» konsekvens for fisk, sjøfugl eller hval i utredningsområdet (**stevningen bilag 17**, s. 51). Vurderingen gjelder også for leting, der alle miljøpåvirkninger er vurdert til konsekvensnivå «liten» i konsekvensutredningen (**stevningen bilag 20**, s. 104).

Risiko for innføring av fremmede arter er behandlet på side 104 i konsekvensutredningen, med utgangspunkt i vurderingen i punkt 3.8 i virkningsstudien fra Akvaplan-niva og IKM Acona. Konsekvensen av å innføre fremmede arter er vurdert som betydelig. Utstyr som benyttes på havbunnen vil imidlertid tas til overflaten etter bruk og eventuelle fastsittende organismer ventes ikke å overleve transport, eksponering mot luft og utsetting på ny lokalitet. Sannsynligheten for introduksjon av fremmede arter via ballastvann eller påvekst på skip/utstyr som benyttes i havbunnsmineralvirksomhet i Norskehavet vurderes som svært liten, og risikoen for slik etablering er vurdert som lav (**stevningen bilag 20**, s. 104).

Spørsmålet om konnektivet (i vannmasser og langs havbunnen) er dessuten behandlet flere steder i kapittel 8 i konsekvensutredningen. I denne sammenheng vil staten fremheve at de kjente, aktive hydrotermale strukturene i spredningsgrøften langs Mohnsryggen og Knipovitsryggen allerede er studert av akademia ved gjentatte besøk og fysiske undersøkelser, uten at det er rapportert om innføring av arter mellom disse lokalitetene.

Staten kan på denne bakgrunn ikke se at det fremkommer opplysninger i stevningen som underbygger saksøkers anførsler om mangelfull utredning og uriktige faktiske antakelser. Det bemerkes for øvrig at anførselen om mangelfull utredning er lite konkret. Det er uklart for staten hvilke utredninger saksøker mener er påkrevd.

#### **4.7 Eventuelle feil medfører uansett ikke ugyldighet**

Denne side vil anføre at mangler ved konsekvensutredningen uansett ikke har virket inn på åpningsbeslutningens innhold, jf. prinsippet i forvaltningsloven § 41 om gyldigheten av enkeltvedtak. Forslag til utredningsprogram og konsekvensutredningen har vært på høring der samtlige av svakhetene saksøker anfører ble påpekt. Begrensningene i kunnskapsgrunlaget og høringsinnspillene er også gjort rede for i Meld. St. 25 (2022–2023). Regjeringen og Stortinget var godt kjent med dette og andre kritiske merknader da de fattet sine beslutninger om åpning. Et bredt stortingsflertall sluttet seg til regjeringens åpningsforslag, med 79 mot 20 stemmer.

Etter statens syn tilsier ikke konstitusjonelle og folkerettslige føringer en strengere norm som leder til ugyldighet i dette tilfellet. Plandirektivet gjelder i utgangspunktet ikke på sokkelen, men departementet valgte å se hen til direktivets mer detaljerte krav som er vedtatt gjennom petroleumsforskriften. Uansett er det etter EU-domstolens praksis ingen automatikk i at ethvert brudd på konsekvensutredningsplikten leder til ugyldighet. For tilfeller der det er identifisert mangler ved en gjennomført konsekvensutredning, åpner praksisen for en vurdering av feilens innvirkning på avgjørelsen innhold, der også feilens grovhet hensyntas, jf. for eksempel sakene C-72/12 avsnitt 49–54 og C-137/14 avsnitt 59–61. Det vises også til Commission Notice on access to justice in environmental matters (2017/C 275/01), avsnitt 4.2. Åpningsbeslutningen vil etter en slik vurdering uansett være gyldig.

## 5 ANNET

Etter statens syn er det behov for avklaring av hvilke innsigelser saksøker har til konsekvensutredningen med underlagsrapporter. Selve utredningen (**stevningens bilag 20**) er et omfattende og grundig arbeid, og det stemmer ikke at utredningen verken «identifiserer, beskriver eller evaluerer» potensielle miljøvirkninger slik saksøker anfører i punkt 5.3.2. Bare utredningen, uten underlag, er på 115 sider hvor store deler er knyttet til miljø og miljøvirkninger av mineralaktivitet. **Det bes opplyst:**

- 1) Hva i konsekvensutredningen, eventuelt underlagene, anfører saksøker at er uriktig?
- 2) Er det andre tema enn karbon og havforsuring saksøker mener skulle vært inkludert i utredningen, men som er utelatt?
- 3) Hvilke tilleggsundersøkelser er det saksøker mener skulle vært foretatt før åpningsbeslutningen for å redusere kunnskapsmangel?

Staten vil komme tilbake til vitner det er aktuelt å føre.

Som representanter fra staten v/Energidepartementet møter førstekonsulent Sebastian Mydland Langbakk og fagsjef Cecilie Myklatun.

Saken er berammet til 5 rettsdager, noe som etter statens vurdering fremstår som tilstrekkelig.

## 6 PÅSTAND

1. *Staten v/Energidepartementet frifinnes.*
2. *Staten v/Energidepartementet tilkjennes sakskostnader.*

• • •

Oslo, 28.06.2024

REGJERINGSADVOKATEN

Karen Mellingen  
advokat



# Global Critical Minerals Outlook 2024



# INTERNATIONAL ENERGY AGENCY

---

The IEA examines the full spectrum of energy issues including oil, gas and coal supply and demand, renewable energy technologies, electricity markets, energy efficiency, access to energy, demand side management and much more. Through its work, the IEA advocates policies that will enhance the reliability, affordability and sustainability of energy in its 31 member countries, 13 association countries and beyond.

This publication and any map included herein are without prejudice to the status of or sovereignty over any territory, to the delimitation of international frontiers and boundaries and to the name of any territory, city or area.

Source: IEA.  
International Energy Agency  
Website: [www.iea.org](http://www.iea.org)

## **IEA member countries:**

Australia  
Austria  
Belgium  
Canada  
Czech Republic  
Denmark  
Estonia  
Finland  
France  
Germany  
Greece  
Hungary  
Ireland  
Italy  
Japan  
Korea  
Lithuania  
Luxembourg  
Mexico  
Netherlands  
New Zealand  
Norway  
Poland  
Portugal  
Slovak Republic

Spain  
Sweden  
Switzerland  
Republic of Türkiye  
United Kingdom  
United States

The European Commission also participates in the work of the IEA

## **IEA association countries:**

Argentina  
Brazil  
China  
Egypt  
India  
Indonesia  
Kenya  
Morocco  
Senegal  
Singapore  
South Africa  
Thailand  
Ukraine

## Abstract

Critical minerals, which are essential for a range of clean energy technologies, have risen up the policy agenda in recent years due to increasing demand, volatile price movements, supply chain bottlenecks and geopolitical concerns. The dynamic nature of the market necessitates greater transparency and reliable information to facilitate informed decision-making, as underscored by the request from [Group of Seven \(G7\) ministers](#) for the IEA to produce medium- and long-term outlooks for critical minerals.

The Global Critical Minerals Outlook 2024 follows the IEA's [inaugural review](#) of the market last year. It provides a snapshot of industry developments in 2023 and early 2024 and offers medium- and long-term outlooks for the demand and supply of key energy transition minerals based on the latest technology and policy trends.

The report also assesses key risks to the reliability, sustainability and diversity of critical mineral supply chains and analyses the consequences for policy and industry stakeholders. It will be accompanied by an updated version of the [Critical Minerals Data Explorer](#), an interactive online tool that allows users to explore the latest IEA projections.



## Table of contents

|  |     |  |     |
|--|-----|--|-----|
| Executive summary.....   | 5   | Clean energy transition risk assessments.....      | 202 |
| Introduction.....  | 11  | Implications.....                                  | 222 |
| Market review.....   | 16  | Investment in diversified supply.....              | 224 |
| Clean energy deployment trends.....                                    | 17  | Recycling, innovation, and behavioural change..... | 233 |
| Market trends for critical minerals.....                               | 34  | Market transparency.....                           | 243 |
| Short-term market developments for key energy transition minerals..... | 45  | Sustainable and responsible supplies.....          | 250 |
| Investment trends.....   | 54  | Annex.....   | 253 |
| Latest policy developments.....  | 67  |  |     |
| ESG performance tracking.....  | 74  |  |     |
| Demand and supply outlook for key materials.....                       | 80  |  |     |
| Mineral demand for clean energy technologies.....                      | 83  |  |     |
| Overview of the projections for key energy transition minerals.....    | 95  |  |     |
| Outlook for copper.....  | 107 |  |     |
| Outlook for lithium.....   | 124 |  |     |
| Outlook for nickel.....  | 136 |  |     |
| Outlook for cobalt.....  | 154 |  |     |
| Outlook for graphite.....  | 167 |  |     |
| Outlook for rare earth elements.....                                   | 177 |  |     |
| Brief review of other key materials.....                               | 193 |  |     |

---

# Executive summary

---

## Executive summary

**Fast-growing critical minerals markets remain turbulent, with prices falling sharply in 2023 following two years of dramatic increases.** Battery materials saw particularly large declines with lithium spot prices plummeting by 75% and cobalt, nickel, and graphite prices dropping by 30-45%. The IEA Energy Transition Mineral Price Index, which tracks a basket price of copper, major battery metals and rare earth elements, tripled in the two years following January 2020, but relinquished most of the increase by the end of 2023 – although copper prices remained at elevated levels.

**Demand growth has remained robust.** Demand for critical minerals experienced strong growth in 2023, with lithium demand rising by 30%, while demand for nickel, cobalt, graphite and rare earth elements all saw increases ranging from 8% to 15%. Clean energy applications have become the main driver of demand growth for a range of critical minerals. Electric vehicles (EVs) consolidated their position as the largest-consuming segment for lithium, and increased their share considerably in the demand for nickel, cobalt and graphite.

**The main reason for price declines has been a strong increase in supply and ample inventories of technologies made with critical minerals.** From Africa to Indonesia and the People's Republic of China (hereafter "China"), the ramp-up of new supply outpaced demand growth over the past two years. Together with an inventory overhang in the downstream sector (e.g. battery cells,

cathodes) and a correction of overly steep price rises in 2021-2022, this produced downward pressure on prices.

**Clean energy deployment continues to advance in all our scenarios for the future, including a strong growth story for EVs.**

Following the 75% growth in deployment in 2023, solar PV and wind account for the majority of capacity additions in every region in all IEA scenarios. This is accompanied by a substantial expansion of electricity networks, pushing up demand for copper and aluminium. Electric car sales [neared 14 million](#) in 2023, a 35% year-on-year increase, and continued growth is projected as major markets progress and adoption increases in emerging economies. In a scenario that limits global warming to 1.5 °C (the Net Zero Emissions by 2050 [NZE] Scenario), the sales share of electric cars rises from 18% today to 65% in 2030, pushing up demand for batteries by a factor of seven to 6 TWh in 2030. Electric cars are the major source of demand for batteries, but battery storage for the power sector exhibits faster growth.

**Today's well-supplied market may not be a good guide for the future, as demand for critical minerals continues to rise.** Just as clean energy deployment expands, so too does demand for critical minerals. Mineral demand for clean energy technologies doubles between today and 2030 in a scenario that reflects today's policy settings, the Stated Policies Scenario (STEPS). It is even higher in a

scenario that meets all national energy and climate goals in full, the Announced Pledges Scenario (APS), and it almost triples by 2030 and quadruples by 2040 in the NZE Scenario, reaching nearly 40 Mt. Lithium sees the most rapid growth in demand, due to rising EV battery needs. In the NZE Scenario, for example, it increases by a factor of nine to 2040. In terms of production volume, copper – which connects a more electrified energy system – has by far the largest increase. Graphite demand almost quadruples by 2040 in the NZE Scenario, while demand for nickel, cobalt and rare earth elements doubles.

**Strong growth in demand produces a major uptick in the overall value of critical minerals markets.** The combined market value of key energy transition minerals – copper, lithium, nickel, cobalt, graphite and rare earth elements – more than doubles to reach USD 770 billion by 2040 in the NZE Scenario. At around USD 325 billion, today's aggregate market value of key energy transition minerals aligns broadly with that of iron ore. By 2040, copper on its own attains that scale.

**The benefits of market expansion are shared across different regions, especially for mining.** Latin America captures the largest amount of market value for mined output with around USD 120 billion by 2030. Indonesia sees the fastest growth, doubling its market value by 2030 due to its burgeoning nickel production. Africa witnesses a 65% increase in market value by 2030. Nearly 50% of the market value from refining is concentrated in China by 2030. China also sees

a rise in market value for mined materials with its growing copper and lithium production.

**The recent fall in prices has affected investments in new mineral supply, but they are still growing.** Increases in 2023 were smaller than those seen in 2022, but investment in critical mineral mining nonetheless grew by 10%. Investment by lithium specialists saw a sharp rise of 60%, despite weak prices. Exploration spending also rose by 15%, driven by Canada and Australia. Venture capital spending increased by 30%, with significant growth in battery recycling offsetting reduced investment in mining and refining start-ups. China's spending on and acquisition of overseas mines has grown significantly in the past ten years reaching record levels of [USD 10 billion](#) in the first half of 2023 with a particular focus on battery metals such as lithium, nickel and cobalt.

**Our projections show a mixed picture for future supply-demand balances.** Based on a detailed review of all announced projects, we have constructed two supply scenarios. The base case includes production from existing assets and those under construction, along with projects that have a high chance of moving ahead. The high production case adds in projects, which are at a reasonably advanced stage of development, seeking financing and/or permits. Using the APS as a benchmark, the situation in 2035 looks as follows:

- There is a significant gap between prospective supply and demand for copper and lithium: Anticipated mine supply from

announced projects meets only 70% of copper and 50% of lithium requirements.

- Balances for nickel and cobalt look tight relative to confirmed projects, but better if prospective projects are included (our high production case).
- Graphite and rare earth elements may not face supply volume issues but are among the most problematic in terms of market concentration: over 90% of battery-grade graphite and 77% of refined rare earths in 2030 originate from China.

The NZE Scenario necessitates further project developments across most minerals.

**Our analysis of announced projects shows limited progress in diversifying supply.** The geographical concentration of mining operations is set to rise further or remain high over the projection period in the base case. The situation improves somewhat in the high production case, indicating that many potential projects being developed in geographically diverse regions are not among the front-runners for development. For refined materials, the shares of the top three producing nations have all increased since 2020, with the trend most pronounced for nickel and cobalt. Announced projects indicate that refined material production is set to remain highly concentrated in a few countries. Between now and 2030, some 70-75% of projected supply growth for refined lithium, nickel, cobalt and rare earth elements comes from today's top three producers. For battery-

grade spherical and synthetic graphite, almost 95% of growth comes from China. These high levels of supply concentration represent a risk for the speed of energy transitions, as it makes supply chains and routes more vulnerable to disruption, whether from extreme weather, trade disputes or geopolitics.

**Analysis based on asset ownership reveals a slightly different picture.** The concentration in the mining sector looks different if viewed through the lens of asset ownership, with US and European companies playing a major role for copper and lithium supplies whereas Chinese companies have a greater role for nickel and cobalt production, despite these minerals being mined elsewhere (e.g. Indonesia for nickel and the Democratic Republic of the Congo for cobalt).

**High market concentration means there is a risk of significant shortfalls in supply if, for any reason, supply from the largest producing country is interrupted.** This “N-1” analysis is a typical measure of the resilience of any system and reveals significant vulnerabilities. If the largest supplier and its demand is excluded, then available “N-1” supply of all key energy transition minerals would fall significantly below material requirements. The situation is most pronounced for graphite where the available “N-1” supply covers only 10% of the N-1 material requirements – significantly below the minimum non-single-origin threshold of 35% proposed in the EU Critical Raw Materials Act. This indicates that without urgent efforts

to expedite the development of projects, achieving announced diversification goals will be highly challenging.

**Today's price declines are a double-edged sword – a boon for clean energy deployment but a bane for critical mineral investment and diversification.** Lower prices have been good news for consumers and for affordability, bringing clean technology costs back on a downward trajectory, including the 14% reduction in battery prices in 2023. However, falling prices also make spending to ensure reliable and diversified supply less appealing to investors. This price effect has had the biggest consequences in new and emerging resource holders; in the case of nickel, three-quarters of operating or potential projects that are at risk are outside the top three producers.

**Our first-of-its-kind risk assessment reveals potential areas of weakness for each mineral in supporting energy transition goals.** The *Outlook* includes a new risk assessment framework for key energy transition minerals, across four major dimensions – supply risks, geopolitical risks, barriers to respond to supply disruptions, and exposure to environmental, social and governance (ESG) and climate risks. Overall, lithium and graphite show the highest risk scores. Lithium and copper are more exposed to supply and volume risks whereas graphite, cobalt, rare earths and nickel face more substantial geopolitical risks. Most minerals are exposed to high environmental risks. For example, today's refining operations occur in places where grids tend to have a higher carbon intensity, relying mostly on coal-based electricity.

**Some USD 800 billion of investment in mining is required to get on track for a 1.5 °C scenario to 2040.** In the APS, approximately USD 590 billion is required over the same period. These increases need to be made in a way that fosters a more diversified array of supply sources in the future. Financing diversified critical mineral supply chains faces numerous challenges, such as cost inflation, long-term price uncertainty and limited value placed on diversification by consumers. This requires specific policy measures to reinforce the investment case for supply chain diversification. Enhancing market transparency can also help, from pricing – with benefits to be drawn from efficient price discovery mechanisms and financial tools to hedge risks – to information, with a strong need for increasing the availability of reliable data on consumption, supply and trade.

**Stepping up efforts to recycle, innovate and encourage behavioural change is vital to ease potential strains on supply.** In the case of lithium, the combination of right sizing EV batteries, alternative chemistries and recycling could reduce demand by 25% in 2030 in the NZE Scenario, saving an amount roughly equivalent to today's production. Recycling rates for many materials have exhibited limited growth in the past. In the NZE Scenario, however, this needs to change, with growing policy attention to stepping up rates of collection and reprocessing. Recycled quantities of copper and cobalt could reduce 2040 primary supply requirements by 30%, and 15% for lithium and nickel. Without the uptake of recycling and reuse, mining capital requirements would need to be one-third higher.

**New supplies must not come at the cost of local communities or the environment.** Our systematic ESG performance tracking paints a mixed picture. The industry is making progress on worker safety, gender balance, community investment and renewable energy uses, but the same cannot be said for waste generation, emissions and water consumption and discharge, suggesting ample scope for

improvement. The benefits associated with mineral production, such as revenue and jobs, have to be felt by producer countries and communities. Voluntary sustainability standards can help actors improve ESG performance, but greater transparency, due diligence, harmonised approaches to credibility and [appropriate incentives](#) are needed to tap their full potential.

---

# Introduction

---



## Introduction

After the relentless surge in prices since 2021, the critical minerals market underwent another tumultuous year in 2023. Prices for most materials experienced a significant decline, relinquishing most of the increases accumulated over the past two years. Prices for battery metals saw particularly steep reductions due to an inventory overhang in the downstream sector, a slight easing in the pace of demand growth and an increase in overall supply.

While immediate concerns appear to have eased, the risks of market tightness and price volatility remain ever-present as countries pursue decarbonisation goals. Moreover, the geopolitical context is increasingly complex, highlighted by a series of trade restriction measures in 2023, including gallium, germanium, graphite and technologies related to rare earth elements. Low material prices helped to put the costs of clean energy technologies back on a downward trajectory, but they present a challenge for efforts to diversify supply, given the financial difficulties that they pose for new and emerging producers. The imperative to bolster the diversity and resilience of critical mineral supplies remains at the top of the policy agenda.

In line with new [mandates](#) approved by the 2024 Ministerial meeting, the IEA has been working together with countries and industry to address these emerging challenges and ensure reliable and

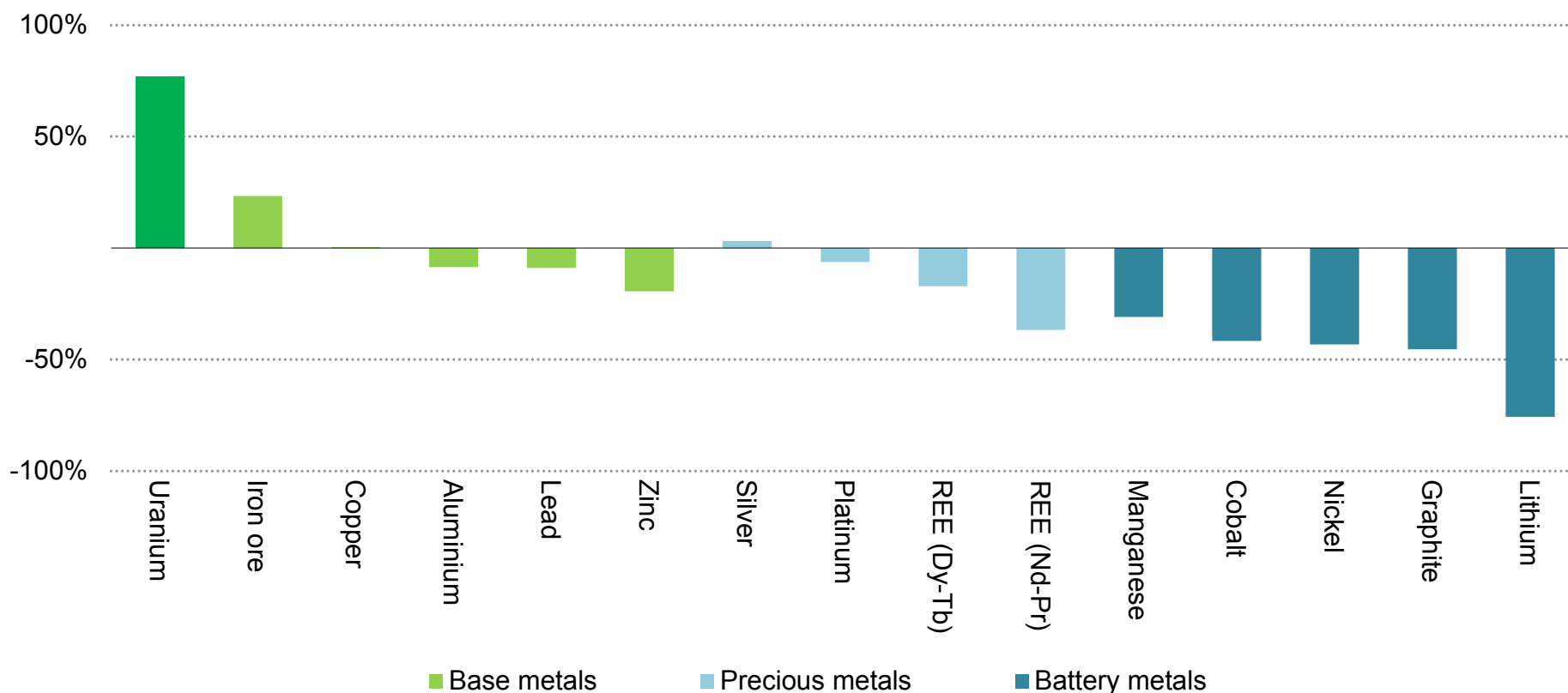
sustainable supplies of critical minerals. On 28 September 2023, the IEA hosted the first-ever [Critical Minerals and Clean Energy Summit](#) at the IEA headquarters in Paris. Almost 50 countries, including key producing and consuming nations around the world, came together with around 40 business leaders, investors, heads of international organisations and civil society organisations to share their experiences and discuss effective courses of action to ensure rapid and secure energy transitions. Chief among various desired actions was the need for robust market monitoring and outlooks that can help bring a clear understanding of today's market situation and anticipate potential risks in the medium to long term.

Earlier in 2023, the Group of Seven (G7) ministers asked the IEA to play a strengthened role in safeguarding minerals security in its [G7 Five-Point Plan](#), through producing medium- and long-term outlooks for critical minerals and introducing the IEA Voluntary Critical Minerals Security Programme.

This report, following the inaugural [Critical Minerals Market Review 2023](#), responds to these growing needs for enhanced market transparency by reviewing latest market movements, examining the prospects for future mineral demand and supply, and assessing potential risks along the supply chain of key commodities.

## Prices for minerals and metals experienced a widespread decline in 2023, with battery metals experiencing particularly sharp reductions

Change in selected commodity prices in 2023



IEA. CC BY 4.0.

Notes: REE = rare earth elements; Dy-Tb = dysprosium and terbium; Nd-Pr = neodymium and praseodymium. Change in prices between December 2022 and December 2023.

Sources: IEA analysis based on Bloomberg and S&P Global.

## Scope of the analyses and scenarios

The report considers a wide range of “critical minerals” that play a vital role in clean energy applications, as indicated in the Annex. The main focus is on “key energy transition minerals” (also referred to as “focus minerals”) such as **copper, lithium, nickel, cobalt, graphite and rare earth elements**. However, the report also discusses trends for other important materials such as aluminium, manganese, phosphate, platinum group metals and uranium as relevant.

Our assessment of mineral demand in the clean energy sector includes demand for low-emissions power generation (solar PV, wind, hydro, nuclear and other renewables), electric vehicle batteries and battery storage, grid networks (transmission, distribution and transformer), and hydrogen (fuel cells and electrolyser) technologies.

Our forward-looking analysis is based on the three main IEA scenarios included in the [World Energy Outlook 2023](#), updated for the latest data points.

- The **Stated Policies Scenario (STEPS)** provides a sense of the prevailing direction of travel for the energy system, based today’s policy settings. The STEPS is associated with a temperature rise of 2.4 °C in 2100 (with a 50% probability).
- The **Announced Pledges Scenario (APS)** assumes that governments will meet, in full and on time, all of the climate-

related commitments that they have announced, including longer term net zero emissions targets and pledges in nationally determined contributions (NDCs). The APS is associated with a temperature rise of 1.7 °C in 2100 (with a 50% probability).

- The **Net Zero Emissions by 2050 (NZE) Scenario** charts a pathway for the global energy sector to achieve net zero CO<sub>2</sub> emissions by 2050 and limit the global temperature rise to 1.5 °C above pre-industrial levels in 2100 (with at least a 50% probability) with limited overshoot. The NZE Scenario also meets the key energy-related UN Sustainable Development Goals (SDGs) such as universal access to reliable modern energy services and major improvements in air quality.

Alongside the main scenarios, we explore some alternative cases reflecting key technological and behavioural uncertainties that could affect future material demand (see Annex).

**Chapter 1 (Market review)** offers a snapshot of industry developments in 2023 and early 2024. It describes the trends of clean energy technology deployment that drives the demand growth for critical minerals and reviews major production, investment and price trends. The chapter also discusses the latest policy developments and insights based on systematic

tracking of the industry's environmental, social and governance (ESG) performance.

**Chapter 2 (Demand and supply outlook for key energy transition minerals)** provides an outlook for demand and supply of key individual minerals and related market and policy issues. Following a brief review of mineral demand for clean energy technologies, the chapter provides projections for focus minerals including copper, lithium, nickel, cobalt, graphite and rare earth elements. It also reviews key trends for other important materials.

**Chapter 3 (Clean energy transition risk assessment)** contains structured “clean energy transition risk assessments” for the six

focus minerals that cover supply risks, geopolitical risks, barriers to respond to disruptions, and exposure to ESG and climate risks.

**Chapter 4 (Implications)** presents the strategic implications of the scenario projections for policy and industry stakeholders seeking to promote reliable, sustainable and diversified supplies of critical minerals. The chapter considers four major issues such as i) investment in diversified supply; ii) recycling, innovation and behavioural change; iii) market transparency; and iv) sustainable and responsible supplies.

---

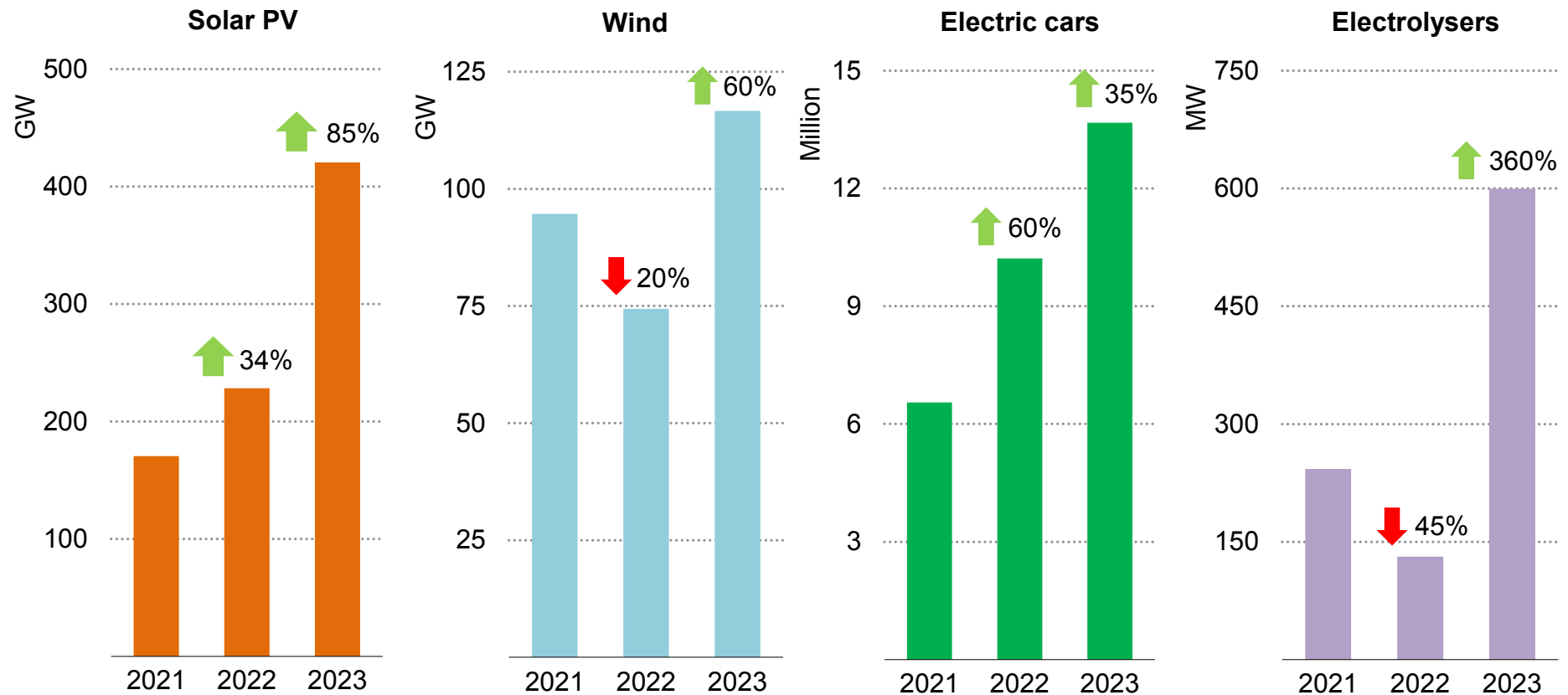
# 1. Market review

---

## Clean energy deployment trends

## Global clean energy deployment climbed to new heights in 2023

Annual capacity additions for selected clean energy technologies



IEA. CC BY 4.0.

Sources: IEA (2024), [Clean Energy Market Monitor – March 2024](#), and IEA (2024), [Global EV Outlook 2024](#).



## Clean energy deployment continues to soar, with China the main driving force

Global clean energy deployment scaled new heights in 2023, with annual additions of [solar PV growing 85% and wind turbines growing 60%](#). The growth in clean energy deployment, however, remains concentrated in advanced economies and the People's Republic of China (hereafter "China"), with most developing economies lagging behind.

### Solar PV

Global solar PV capacity additions for electricity generation broke a new record, reaching 420 GW in 2023. Solar PV alone accounted for [three-quarters of renewable capacity additions](#) worldwide. China alone accounted for 62% of the increase in global solar PV capacity. Despite the phase out of central government subsidies, the country commissioned as much solar PV in 2023 as the entire world did in 2022.

In the European Union (EU), annual solar PV additions rose by a quarter and reached a record level 52 GW in 2023. Following the Russian Federation's (hereafter "Russia") invasion of Ukraine, the EU member states improved the policy environment to accelerate renewables deployment, in part to help bring down natural gas consumption. This has led annual solar PV additions to double since 2021. In the United States (US), solar PV capacity additions increased 50% year-on-year following the easing of supply chain

issues that slowed deployment in 2022. Federal tax incentives and state-level support have continued to drive both utility-scale and rooftop solar PV applications. India added only 12 GW of solar PV in 2023, one-third lower than in 2022. Nevertheless, in 2023 the government unveiled an objective to conduct [annual auctions for 50 GW](#) of renewable energy capacity that promises to accelerate deployment significantly.

### Wind

Global wind capacity additions jumped by 60% in 2023 to break the record seen in 2020. Onshore wind projects accounted for over 85% of global wind deployment in 2023. China accounted for more than 60% of global wind expansion as the country almost doubled its additions compared with 2022.

In the European Union, wind additions increased by less than 10% in 2023, with onshore wind deployment slowing down. Developers have been facing multiple challenges, including rising equipment costs, inflation, and supply chain constraints, which have made them less eager to participate in competitive auctions. Most countries in Europe have introduced policies to address the challenges posed by slow and complex permitting procedures for wind projects. However, the impact of these policies will take time to be visible in deployment trends. In the United States, wind additions declined by more than a

quarter in 2023. This was mainly due to prior uncertainty over the future of tax credits, prior to the adoption of the Inflation Reduction Act (IRA). Wind capacity additions are expected to increase significantly in the coming years thanks to the policy visibility provided by the IRA. In India, a larger number of projects awarded in previous years led annual deployment to increase by almost 50% in 2023.

Offshore wind growth has recovered from a major drop seen in annual additions in 2022. However, the offshore industry outside of China is facing challenges with investment costs today more than 20% higher than a few years ago. In 2023, developers cancelled or postponed 15 GW of offshore wind projects in the United States and the United Kingdom because pricing for previously awarded capacity no longer reflected prevailing project development costs.

Overall, the world is poised for a significant acceleration in renewable capacity in the coming years driven by supportive policies in [more than 130 countries](#). Renewables are expected to surpass coal to become the largest source of electricity generation by the mid-2020s. Substantial demand for materials such as copper, silicon and rare earth elements will be required to support the rapid deployment of renewable generation capacity. However, challenges such as high interest rates and low profitability persist. Policymakers need to address issues related to permitting and grid expansion to achieve the target of [tripling global renewable capacity](#) by 2030 that was agreed at the 28th Conference of the Parties (COP28).

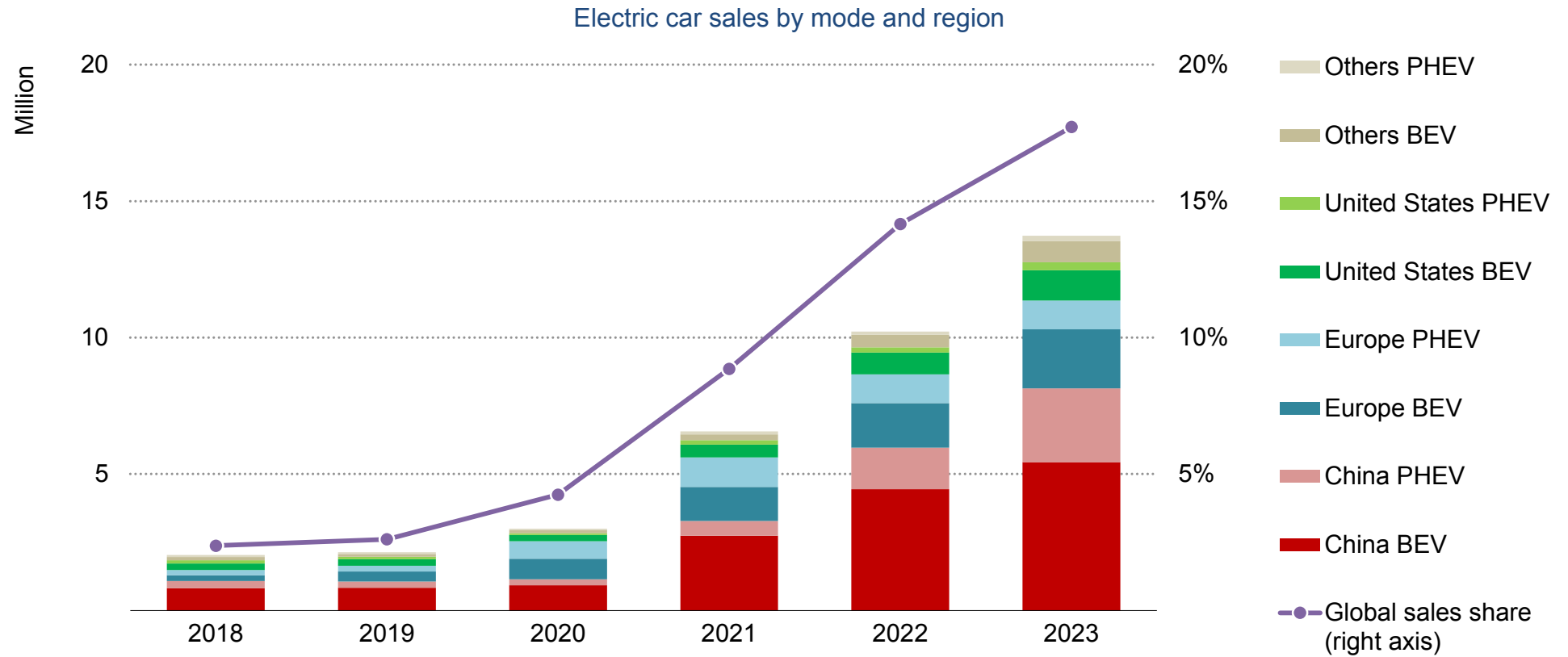
## Electrolysers

The growing markets for electrolysers could push up demand for nickel, platinum group metals, zirconium and other minerals depending on the specific technology deployed. In 2023, global installed capacity of electrolysers for hydrogen production [reached 1.3 GW](#), underpinned by a surge in annual additions to 600 MW. However, this is still far from the annual multi-gigawatt additions required to keep global climate goals within reach.

From less than 10% of global installed capacity in 2020, China has emerged as the leading region since 2021, reaching an installed capacity of more than 650 MW by the end of 2023. China now represents close to half of the global installed capacity. This transformation has been fuelled by the scaling up of project sizes by Chinese developers, with several projects now exceeding 100 MW in capacity. Consequently, China now hosts six of the world's largest operational electrolysis projects. The European Union accounted for around a third of global installed capacity in 2020, but has now ceded its leading position, with additions of around 70 MW in 2023. The United States emerged as the third-largest market, with additions exceeding 30 MW.

Demand uncertainty and lack of regulatory clarity, coupled with recent challenges such as inflation and slow implementation of support mechanisms are hindering faster adoption of electrolysers in other regions.

## The growth story continued in 2023 for EVs



IEA. CC BY 4.0.

Note: BEV = Battery electric vehicle; PHEV = Plug-in hybrid electric vehicle.

Source: IEA (2024), [Global EV Outlook 2024](#).

## Growth in electric car sales remains robust as major markets progress and emerging economies ramp up

Electric car sales neared 14 million in 2023, a 35% year-on-year increase, and more than six times higher than five years earlier in 2018. Electric cars accounted for 18% of all car sales in 2023 up from 14% in 2022 and only 2% five years earlier, and nearly 95% of all sales were in China, Europe and the United States. These trends demonstrate robust growth in electric car markets as they become more mature, even if the growth in global electric car sales slowed somewhat compared with the 60% seen in 2022.

China is the world's largest electric car market with 8.1 million electric car sales and 60% of the global total in 2023, a share that has been increasing, up from 50% five years earlier in 2018. In 2023 more than one in three new car registrations in China was electric. The growth rate of electric car sales in China more than halved in 2023 to 35% from 80% in 2022. One of the critical reasons for this is that 2023 was the first year that the government provided no purchase subsidies for electric cars, with their [phase-out in 2022](#). Therefore, a slowdown of electric car sales was expected. This is also coupled with relatively weak consumer sentiment. As the Chinese market matures, the industry is entering a phase of price competition and consolidation. To mitigate lower domestic demand, China exported 1.2 million electric vehicles (EVs) in 2023, an 80% increase from the previous year, with primary export markets being Europe and the Asia Pacific

region including Thailand and Australia. In April, China [removed down payment requirements](#) for new car loans in an effort to stimulate consumer demand. In the first quarter of 2024 the year-on-year electric car sales growth rate in China increased to 36% compared with 27% in the same period last year. It is estimated that around 45% of all cars sold in China in 2024 could be electric.

Europe is the second-largest electric car market with almost 25% of global sales in 2023, reaching 3.2 million electric car sales. This year more than one in five cars sold in Europe was electric. Unlike China, Europe did not experience a slowdown as the growth rate of electric car sales slightly accelerated in 2023 to 20%, up from 15% in 2022. However, sales trends differed by country. In Germany the electric car sales share fell from 30% in 2022 to 25% in 2023 due to the sudden [end of all EV subsidies](#) in 2023, which were originally intended to apply until the end of 2024. Nevertheless, in the rest of Europe electric car sales shares increased, with the Netherlands reaching 30%, the United Kingdom and France 25%, and Sweden 60%.

In the United States electric car sales grew to 1.4 million in 2023, increasing by 40% compared with 2022, the fastest growth rate of the three largest regions, though the sales share of electric cars reached only 10%. The United States experienced a slight slowdown

compared with the 55% rise in 2022, but growth in sales remained strong, with the IRA having supported sales despite some concerns about domestic component requirements hindering deployment. The revision of eligibility criteria for IRA tax credits in 2023 meant several popular vehicles were covered, and the Tesla Model Y increased its sales by 50% year-on-year. In 2024 [new guidance](#) significantly reduced the number of eligible vehicles for tax credits.

In the rest of the world, total electric car sales grew by 70% and sales almost reached 1 million electric cars. India experienced 70% year-on-year growth, with sales of 80 000 vehicles, compared with just 10% growth for total car sales. In Thailand electric car sales increased more than fourfold, reaching 90 000 vehicles and a 10% market share, a particularly impressive achievement given that total car sales decreased from 2022 to 2023. Subsidies in both regions have facilitated demand growth though India is anticipated to [reduce subsidy levels](#) in 2024.

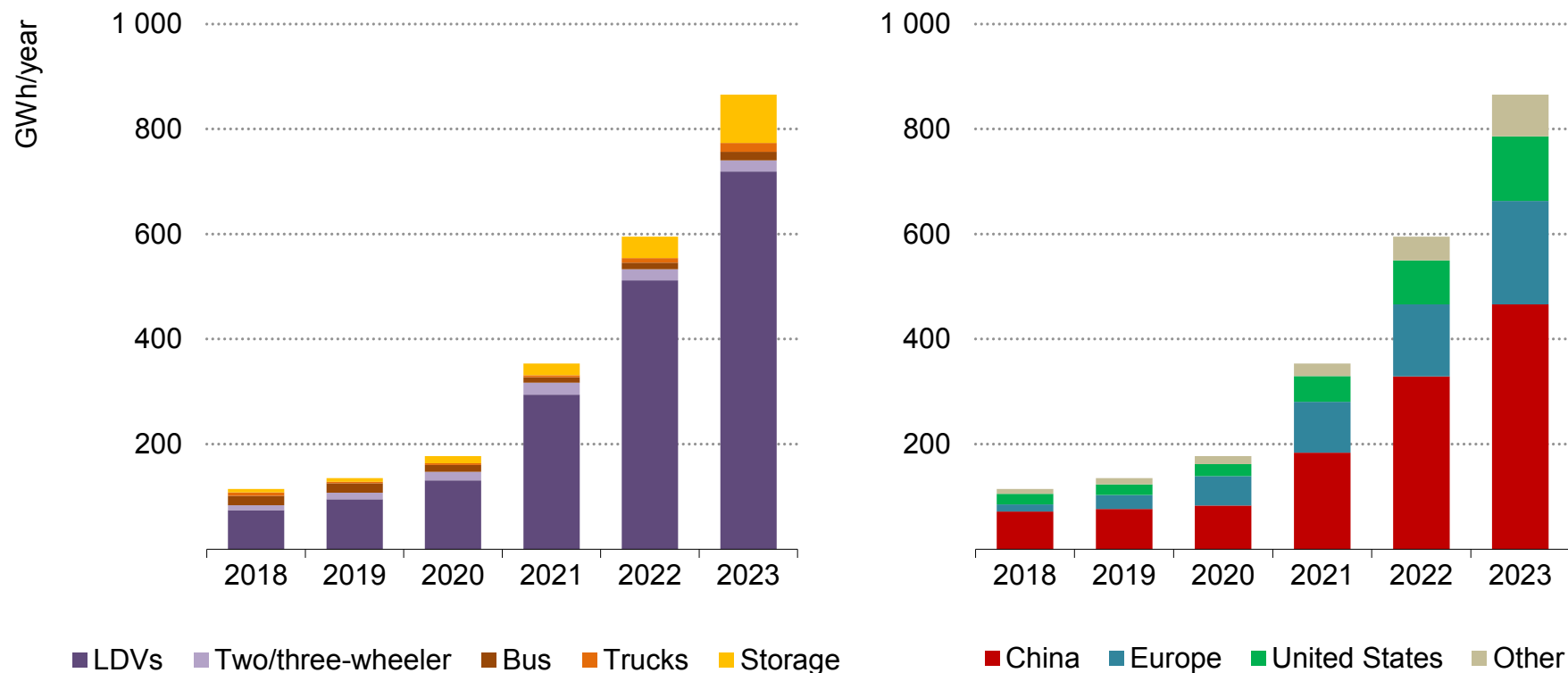
In both China and the United States, sales of plug-in hybrid electric vehicles (PHEVs) grew significantly faster than battery electric vehicles (BEVs) (55% against 40% for the United States and a remarkable 80% against 20% in China). As a result, the share of PHEVs in EV sales reached 33% in China, up from 25% in 2022, and 20% in the United States. Concerns about driving range and lack of sufficient charging infrastructure for BEVs appear to be the driving

force. In China, this surge in PHEV demand suggest that the growing middle-class appear to be more concerned about range going forward, marking a break from the past where relatively low-range BEVs were popular. The average battery size for PHEVs in China is around 50% higher than in Europe. A recent trend in China has been towards [extended-range EVs \(EREVs\)](#), which have an electric powertrain but also have a combustion engine able to recharge the battery. EREVs have a battery around twice the size of a typical PHEV, enabling real-world electric range of around 150 km, more than double that of conventional PHEVs. In 2023 EREVs accounted for a quarter of Chinese PHEV sales, a 10% increase from 2022, although EREVs have a negligible sale share outside of China. Europe, however, saw significantly higher growth in BEV sales with over 30% growth year-on-year compared with a small drop in PHEV sales in 2023.

Although growth rates in EV sales are slowing, early signs from 2024 indicated that sales remain generally strong. As the market matures and subsidies are phased out, growth rates may decrease somewhat. However, robust growth in EV sales is still expected to continue in the near and long term, supported by ongoing policy momentum, major increases in manufacturing capacity, cost declines and expanded adoption in developing economies.

## Battery demand is dominated by electric cars, although storage is the fastest growing source of demand

EV and storage battery demand by mode and region, 2018-2023

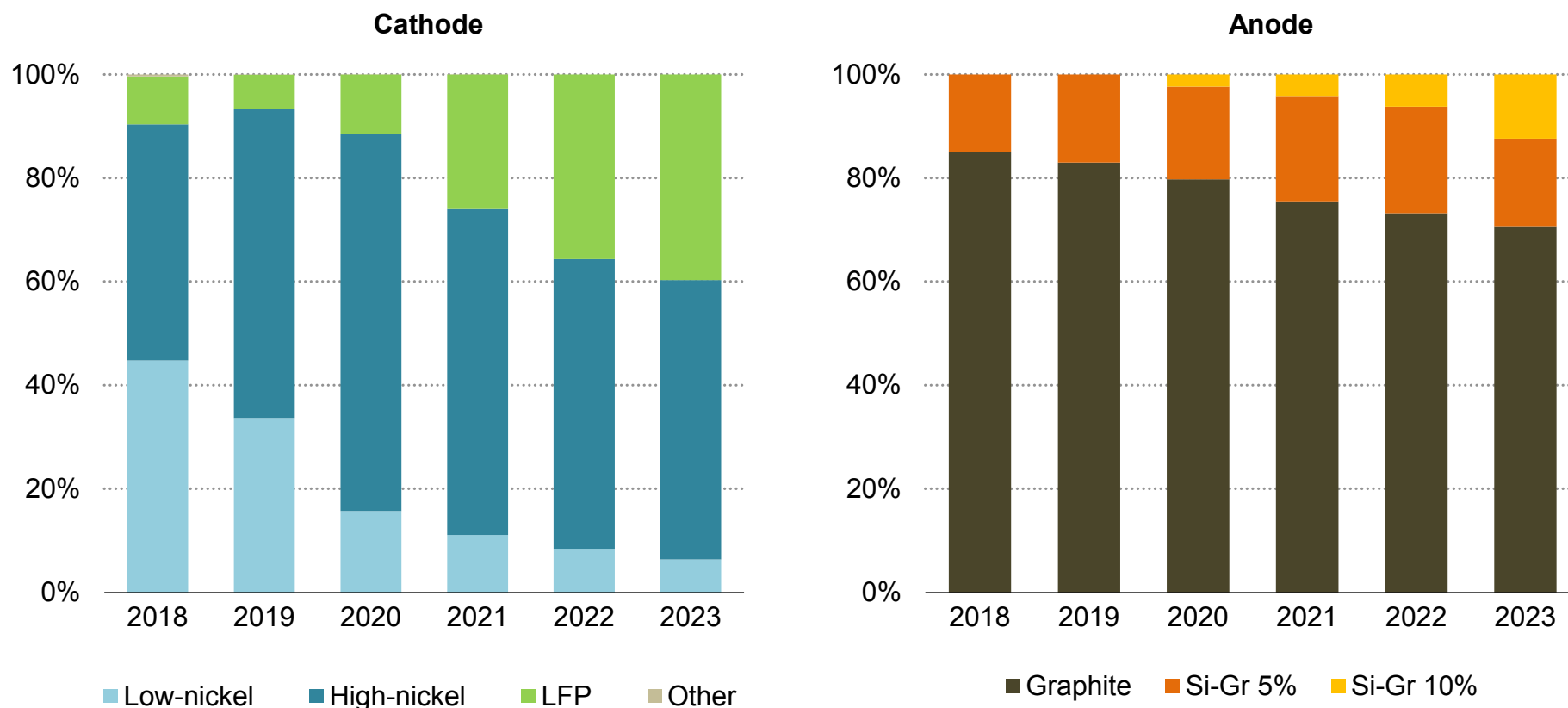


IEA. CC BY 4.0.

Note: LDVs = light-duty vehicles.  
Source: IEA analysis based on EV Volumes.

## The market share of LFP chemistries rose to 40% of electric car sales while silicon is gaining ground in graphite anodes

Electric car battery cathode and anode chemistries sales share, 2018-2023



IEA. CC BY 4.0.

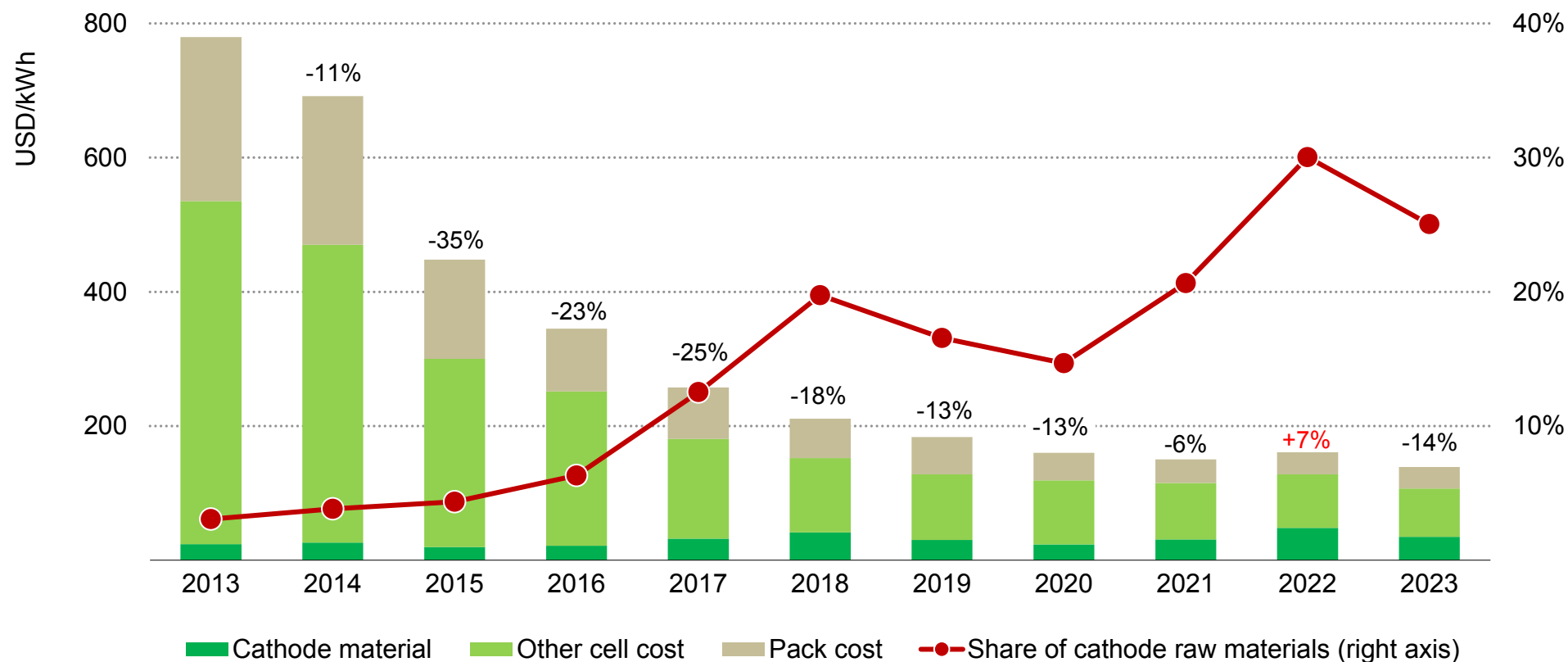
Notes: NMC = lithium nickel manganese cobalt oxide. Low-nickel includes: NMC333 and NMC532. High-nickel includes: NMC622, NMC721, NMC811, NCA and NMCA. LFP = lithium iron phosphate; Si-Gr = Silicon-doped graphite with % of silicon content. Sales share is based on capacity.

Source: IEA analysis based on EV Volumes and BloombergNEF.



## Battery pack prices have dropped with falling critical minerals prices

Average lithium-ion battery pack price and share of cathode raw material cost, 2013-2023



IEA. CC BY 4.0.

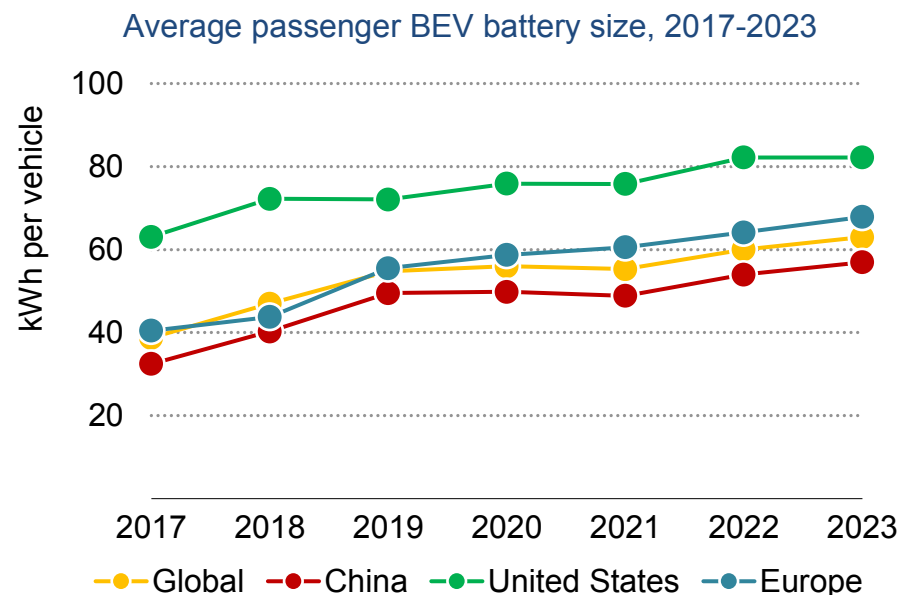
Notes: Cathode material costs include lithium, nickel, cobalt and manganese. Other cell costs include costs for anode, electrolytes, separator and other components as well as costs associated with labour, manufacturing and capital depreciation. Percentages on bars show year-on-year total pack price change. Analysis includes all cathode chemistries and global chemistry sales shares.

Source: IEA analysis based on BloombergNEF (2024).

## Batteries: The rise and rise of LFP

In 2023, global battery demand from EVs and storage reached 865 GWh in 2023, a 45% year-on-year increase. This was primarily driven by sales of electric cars, which were responsible for 85% of global demand. The annual growth rate for battery demand from electric cars, buses and trucks slowed in 2023 to 40%, compared with 75% in 2022, in line with broader sales trends, although annual demand growth from two- or three-wheelers increased. Battery storage demand experienced the most impressive rise, more than doubling from the 2022 level, bringing its share in total EV and storage demand up to 10%. Given that growth rates for battery storage had almost doubled in 2021, this represents a remarkable surge in utility-scale and behind-the-metre storage deployment.

China was the largest source of battery demand in 2023 with 55% of the global total, followed by Europe with around a quarter and the United States with 15%, in each case dominated by EV sales. Battery demand in China grew by over 40% in 2023; this was half the rate seen in 2023 despite a threefold rise in demand for storage deployment. Battery demand in Europe and the United States both grew by 45%, a higher rate than for electric car sales due to a combination of larger vehicle and battery sizes and higher rates of storage deployment.



IEA. CC BY 4.0.

Alongside sales, the rise in battery sizes for EVs is a critical driver of growth in demand for batteries and for critical minerals. In most regions the average battery size for passenger BEVs has been increasing year-on-year, with the global average increasing more than 60% since 2017. The trend towards an increasing share of sport utility vehicles (SUVs) found in conventional car markets is being replicated in the EV market. Automakers are focusing on larger vehicles, which are typically more profitable, and consumers appear to have a strong

appetite for larger vehicles and ranges, even if they are often beyond their requirements. All regions follow the same overall trend for increased battery sizes, but there are significant regional variations in absolute values. The average battery size in the United States is 30% larger than the global average, Europe is 10% larger while China is 10% smaller. This mirrors size trends in conventional vehicle sectors, and also shows the greater preference from consumers in the United States and Europe for higher range EVs.

### Battery pack price trends

In 2023 average battery pack prices dropped 14% to a [record low of USD 139/kWh](#). This was the largest price decrease since 2018, driven primarily by the fall in critical minerals prices, in combination with a surge in battery production capacity and slightly weaker demand than expected. This reinstates the trend of declining battery prices that was temporarily reversed in 2022 due to the exceptionally high prices of battery critical minerals. Cells now account for 80% of the total pack price, an increasing ratio partly due to the cell-to-pack (CTP) design innovation reducing dead weight in the pack and pack costs.

With decreasing manufacturing costs from economies of scale and innovation, critical minerals have been a growing share of the battery pack cost, leaving the battery pack price more susceptible to mineral price volatility. This was seen clearly in 2022 when cathode raw materials peaked at 30% of the total pack price before falling back to 25% in 2023.

### Battery chemistry trends

One of the most remarkable developments in the global battery sector in the last five years has been the resurgence of the lithium iron phosphate (LFP) cathode chemistry. With a lower energy density but more stable and lower-cost chemistry compared to the nickel-based chemistries, LFP was being phased out in favour of the significantly higher energy density nickel-based cathode chemistries. However, there has been a remarkable reversal of fortune since 2019. The fact that LFP contains no nickel or cobalt became an important asset that helped reduced exposure to high commodity prices. In addition, the emergence of CTP technology eliminated dead weight in the battery pack and enhanced the energy density of LFP. CTP was pioneered by [BYD with the Blade battery](#). LFP has now become a major chemistry in 2023 with around 40% of electric car battery sales by capacity. Due to favourable patent agreements China had been the only country producing LFP batteries after 2010. However, the patents [expired in 2022](#), which kick-started production plans outside China. Nevertheless, there are still major regional differences, less than 10% of total EV sales by capacity in the United States and Europe are LFP while two-thirds are LFP in China.

Another major recent innovation was the first [fast charging LFP battery](#). Shenxing developed by CATL, capable of delivering 400km of range from a ten-minute charge. This is achieved through a new electrolyte and graded anode porosities among other innovations. The novel fast charging LFP battery will be utilised in EV vehicles this year, significantly increasing the attractiveness of LFP chemistries.

The other significant recent LFP innovation is the development and commercialisation of lithium manganese iron phosphate (LMFP), the upgraded version of LFP including manganese which increases its energy density. With CATL's M3P battery confirmed for use in [six Chinese EV models](#) and undergoing [validation by Tesla](#) for its Chinese Model 3, it is anticipated that LMFP will continue to take market share from nickel-based chemistries due to its increased range.

In terms of the anode, silicon-doped graphite anodes are increasing in market share with almost a third of electric car anode capacity market share. Higher fractions of silicon are also being used with 10% silicon graphite anodes doubling in market share in 2023 to 12%. Silicon doping increases the energy density of the graphite anode, and increased doping and higher quantities of silicon are expected in the near future.

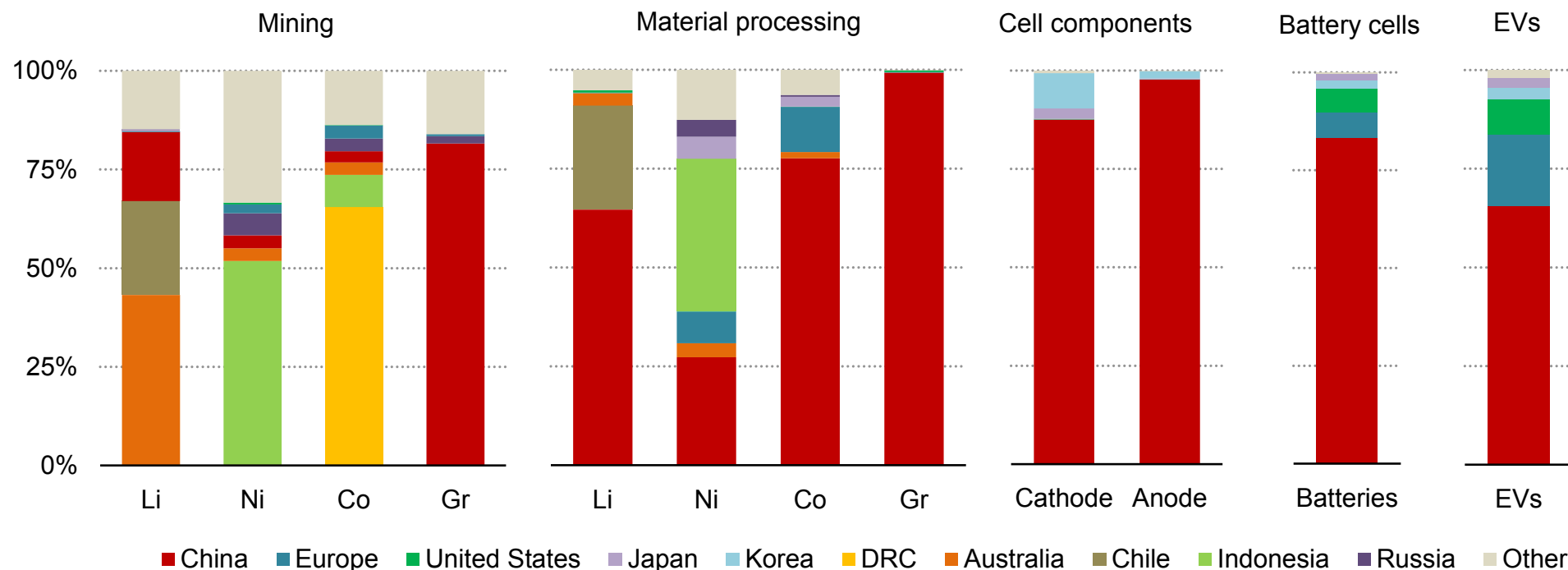
Looking beyond lithium-ion chemistries, sodium-ion (Na-ion) batteries have experienced a surge of development in recent years, especially while lithium prices were high. As the name suggests, this chemistry contains no lithium and also requires less critical minerals than lithium-ion batteries. Leading battery makers including [CATL](#), [Northvolt](#) and many others announced their sodium-ion cells.

However, the fall in lithium prices has diminished the advantage of sodium-ion chemistries and major ramping up plans have stalled or been delayed. The progress of sodium-ion batteries hinges on their price advantage over lithium-ion, with major influence of the lithium price.

All solid-state batteries (ASSBs) are the anticipated step-change technology for battery energy density and safety. There has been widespread industrial research and development in recent years, yet major technical challenges remain such as the typically high pressures required to ensure good electrode contact or relying on difficult-to-scale, expensive production processes. Progress has been made utilising hybrid solid-liquid electrolyte batteries, for instance from [CATL](#) and [Quantumscape](#); however, the use of an organic liquid electrolyte diminishes any safety advantage and may even have higher risks than conventional lithium-ion batteries due to the use of lithium metal. Progress is also being made with ASSBs, with Samsung, an industry leader in solid-state, recently announcing plans [for mass production in 2027](#). CATL also expects to produce [small-scale production](#) in the same year. Though ASSBs hold potential in the future, they are not expected to have significant impact until after 2030.

## China dominates the downstream and midstream global EV battery supply chain

Geographical distribution of the global EV battery supply chain, 2023



IEA. CC BY 4.0.

Notes: Li = lithium; Ni = nickel; Co = cobalt; Gr = graphite; DRC = Democratic Republic of the Congo. Geographical breakdown refers to the country where the production occurs. Mining is based on production data. Material processing is based on refining production data. Cell component production is based on cathode and anode material production capacity data. Battery cells are based on battery cell production capacity data. EVs is based on electric cars production data. For all minerals mining and refining shows total production not only that used in EVs. Graphite refining refers to spherical graphite production only.

Sources: IEA analysis based on EV Volumes; Benchmark Mineral Intelligence; BloombergNEF.

## Growth in China's manufacturing capacity has strong implications for EV battery supply chains

One of the most critical considerations in the global battery outlook is the strength of manufacturing capacity in China. China dominates the downstream battery supply chain, including processing of the battery minerals, cathode and anode material production, and battery cell and EV production. China holds 85% of battery cell production capacity and 90% of cathode and 98% of anode material production capacity globally. Over half of global processing for lithium and cobalt occurs in China. The country dominates the entire graphite anode supply chain end-to-end. China also produces two-thirds of the world's EVs. In almost all stages of the midstream and downstream supply chain, China has increased its [market share since 2021](#).

China has been building battery plants and cathode and anode production capacity at a speed that [exceeds projected demand](#). In 2023 China's maximum cell production capacity was more than double the amount needed to meet the country's battery cell demand. For cathode active materials, the [manufacturing capacity anticipated in 2030](#) is about two times greater than the projected battery cell manufacturing capacity in the same year. In the case of anode active materials, this ratio increases to five times greater, raising doubts about whether all cathode and anode material manufacturers will be able to remain competitive in the face of such a surplus. There are several reasons for China's strong manufacturing position. The fruits of China's industrial strategy have been seen already in many sectors

including [solar, aluminium and steel](#). Years of government support, alongside a large and growing domestic market, have meant that the EV and battery industries in China have thrived and gained global market share. This has now set the stage for considerable price competition and consolidation. [High-technology manufacturing](#) is now a pivotal element of China's strategy for growth.

Ample manufacturing capacity across the battery supply chain is a double-edged sword. If excess production is pushed on to export markets, battery prices and EV prices may fall, which may be good for consumers and thus support progress towards climate goals. However, it could make difficult for producers globally to compete, increasing the level of supply concentration and exposing the supply chains to various physical and geopolitical risks.

For manufacturers in China in the coming years, the primary challenge will be to identify a sufficiently large export market to absorb their output and to improve low margins. Conversely, there is strong pressure on manufacturers in other regions such as the European Union and the United States to improve their cost competitiveness. The quality, cost and characteristics of cells and components provided by various suppliers, alongside local regulatory requirements and environmental, social and governance standards, will be crucial in determining how these markets develop.

## The battery storage market is continuing its upward march

The battery storage market continued its remarkable growth in 2023, with installed capacity reaching over 85 GW. [Almost half of this capacity, over 40 GW, was added in 2023 alone, another record year that saw additions doubling from 2022.](#) A large part of the capacity growth has come from utility-scale systems, with behind-the-metre (BTM) battery storage responsible for about 35% of the annual additions on average. The strong increase in capacity additions over the last few years has been driven almost entirely by China, the European Union and the United States, which collectively accounted for nearly 90% of the capacity added in 2023.

The past two years have seen China rise above the United States to become the leading market for battery storage, with its share in annual global additions rising from around 20% in 2019 to 55% in 2023. In China, about two-thirds of the additional capacity was utility-scale, driven mainly by province-level mandates that encourage the pairing of new solar PV or wind projects with energy storage. BTM storage capacity grew strongly as well, with larger-scale commercial rather than residential users driving the uptake, underpinned by subsidies and a rising proliferation of time-of-use electricity tariffs.

The United States remains the second-largest battery storage market. Utility-scale projects accounted for nearly 90% of the additional capacity, with California, Texas and other states in the Southwest leading deployments. Falling costs have allowed batteries

to make inroads into ancillary service markets and they are increasingly tapped to provide balancing services and secure capacity in states with high shares of variable renewables.

Installed battery storage capacity in the European Union grew 1.7 times in 2023, with annual additions rising to nearly 6 GW. Nearly 90% of the capacity growth was associated with BTM storage, mostly in Germany and Italy, where incentives such as tax breaks and low-interest loans, as well as high retail electricity prices support the pairing of rooftop solar with storage. In 2023, around 80% of the rooftop solar installed in Germany and Italy came with storage.

Capacity additions in Australia jumped to 1.3 GW in 2023, more than doubling last year's deployment levels, thanks in part to financial incentives that encourage the pairing of residential PV systems with batteries. Utility-scale battery storage capacity additions in Japan and Korea increased substantially in 2023, jumping to 400 MW in Japan and 300 MW in Korea. Chile, meanwhile, added nearly 250 MW of utility-scale storage in 2023, making it the first country in Latin America to deploy battery storage at scale.

In other regions, capacity additions have so far been limited. However, in addition to further rapid acceleration in today's core markets, capacity growth is expected to broaden over the next few years. Energy storage targets and financial support mean that India



in particular has significant potential to emerge as another large market for battery storage.

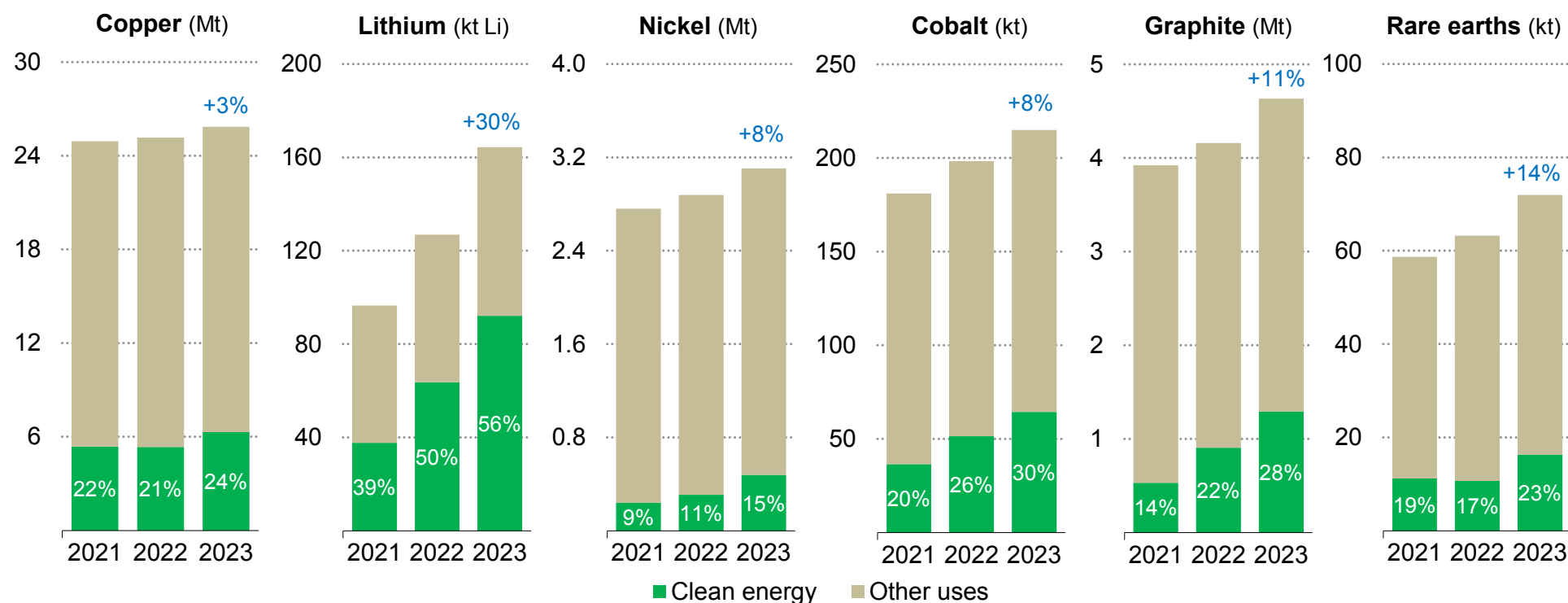
Lithium-ion batteries dominate the battery storage market today, accounting for more than 90% of the market. The chemistries available for lithium-ion batteries used in storage applications are the same as the ones available for the EV market. However, storage applications have different technical needs than EVs, and characteristics such as cost, capacity to charge/discharge frequently, and lifetime are prioritised over energy density. [This has led to a shift](#)

[towards LFP batteries, which accounted for about 80% of the total battery storage market in 2023, up from about 65% in 2022.](#) The growing battery market, together with the resurgence of LFP batteries for EV applications, is leading non-Chinese battery manufacturers to develop their own LFP batteries, which today are almost exclusively produced in China. Lithium-ion battery technology is set to remain a key part of short-duration (eight hours or less) storage, but alternative technologies (such as vanadium flow batteries) are being developed either to compete or to complement it.

## Market trends for critical minerals

## Demand for key energy transition minerals continued to grow strongly in 2023, propelled by the expansion of clean energy technologies

Demand outlook for selected minerals, 2021-2023

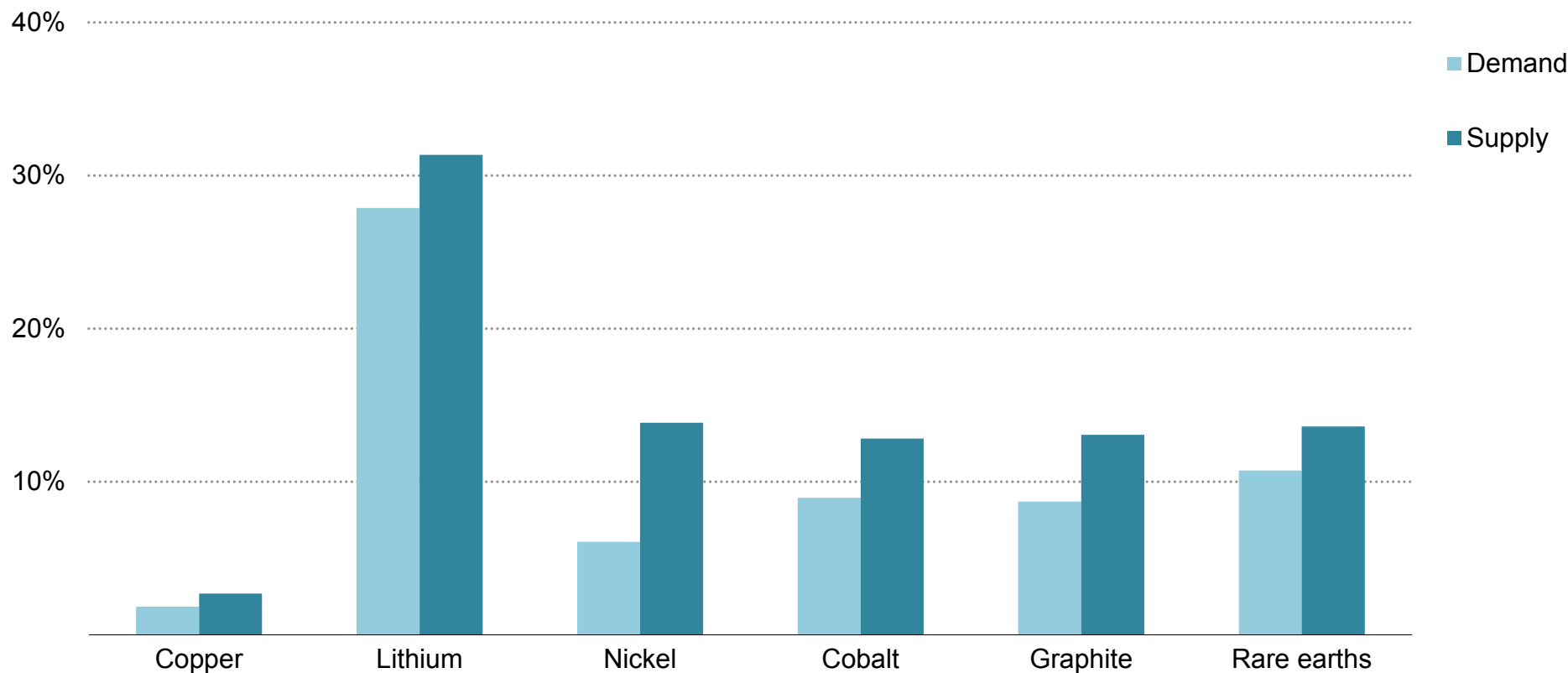


IEA. CC BY 4.0.

Notes: Rare earths include the four magnet elements: neodymium, praseodymium, dysprosium and terbium. Demand for clean energy applications includes consumption for low-emissions power generation, EV and battery storage, grid networks and hydrogen technologies.

## However, supply has expanded at a faster rate than demand, resulting in downward pressure on prices

Annual average demand and supply growth rates between 2021 and 2023 for selected minerals

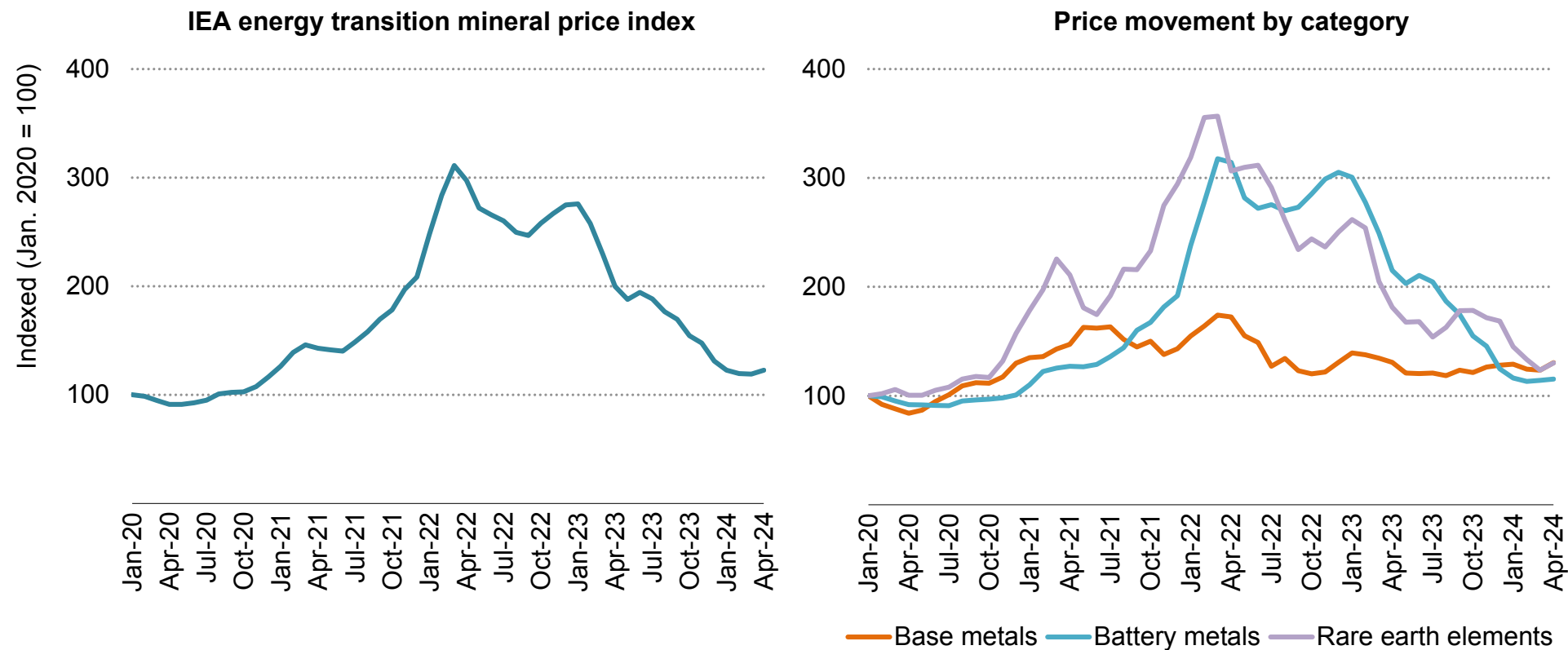


IEA. CC BY 4.0.

Notes: Supply growth rates are based on refined output. The figure for graphite includes both natural and synthetic graphite.

## Prices for key minerals have returned to pre-pandemic levels

Mineral price developments



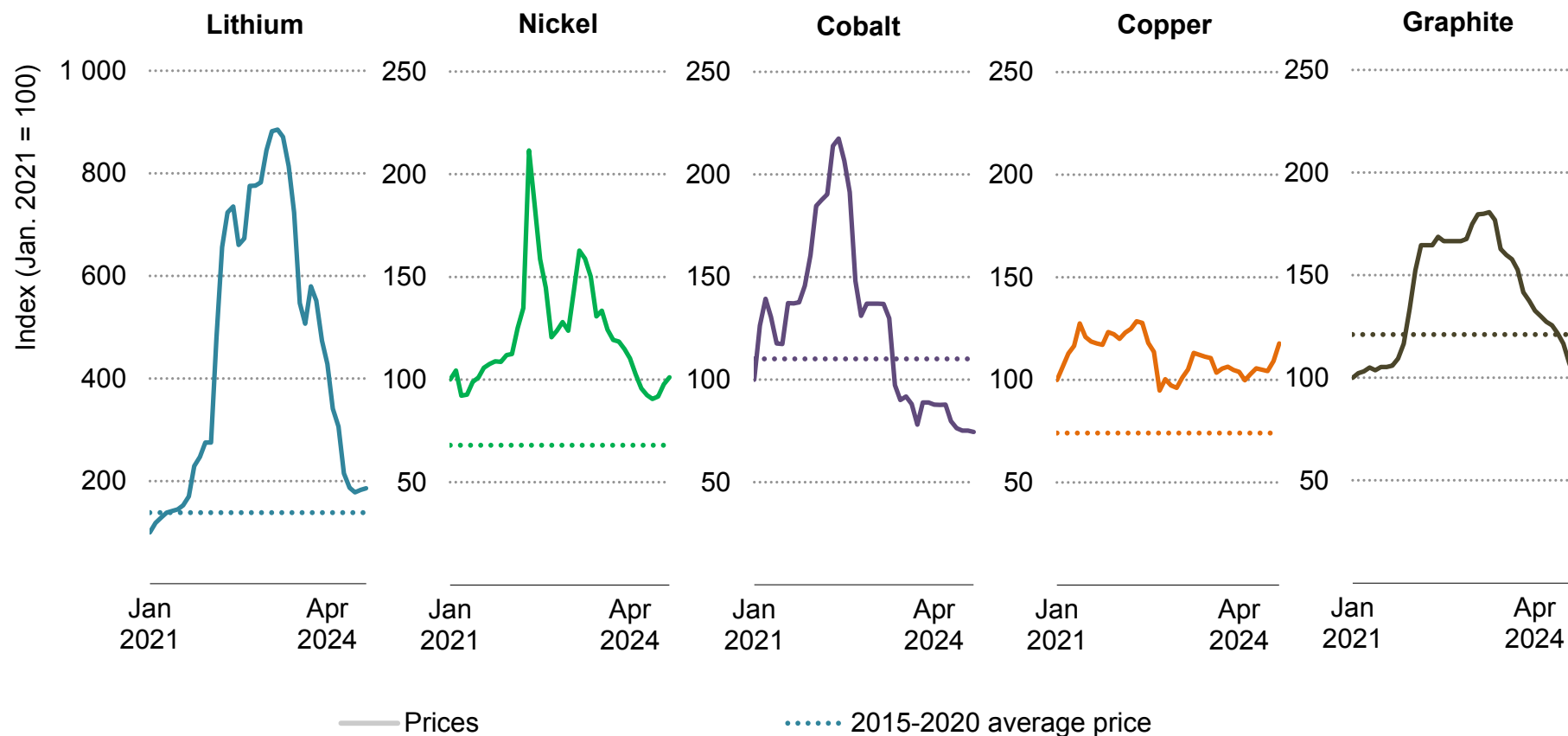
IEA. CC BY 4.0.

Notes: IEA Energy Transition Minerals price index is a basket price of copper, lithium, nickel, cobalt, graphite, manganese and neodymium. On the right-hand chart, base metals include iron, aluminium, zinc and copper. Battery metals include lithium, nickel, cobalt, graphite and manganese. Rare earth elements include neodymium, praseodymium, dysprosium and terbium.

Sources: IEA analysis based on Bloomberg and S&P Global.

## Battery critical minerals have seen the greatest volatility

Critical minerals prices, 2021-2024



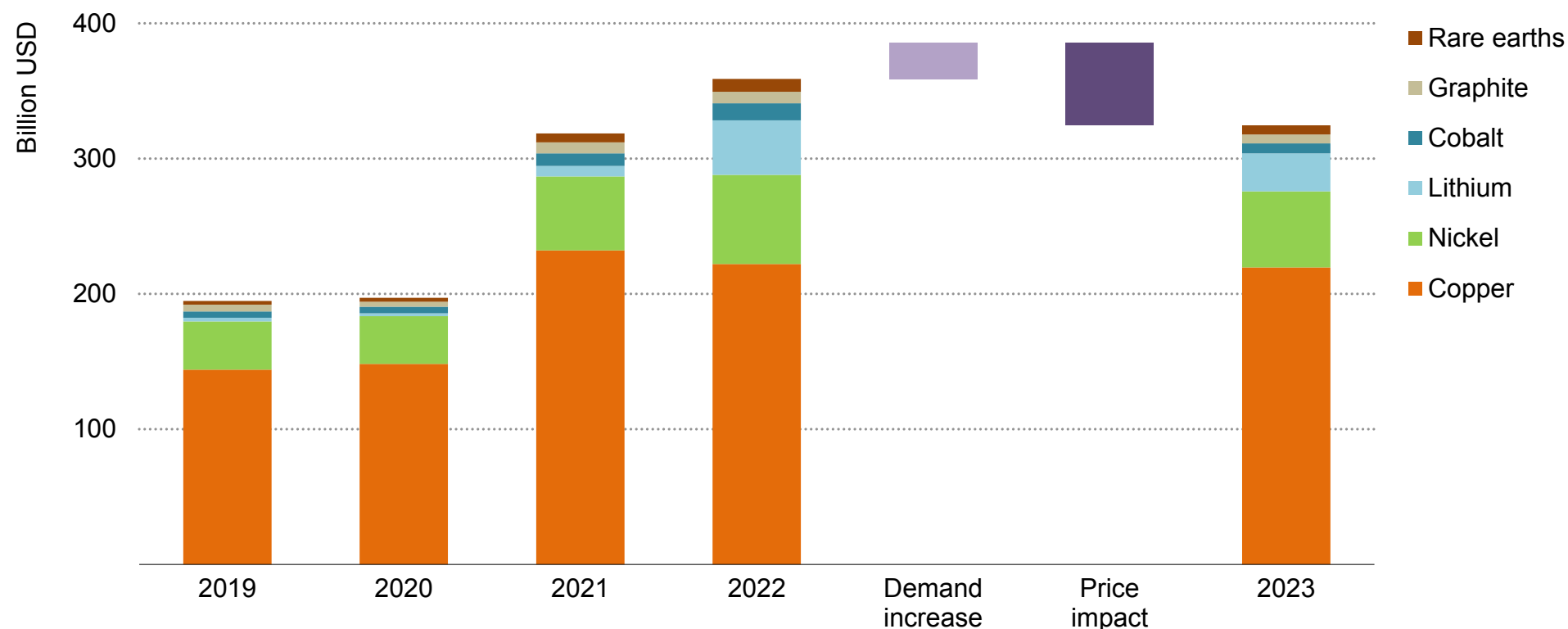
IEA. CC BY 4.0.

Notes: Graphite historical average from 2016-2020. Assessment based on the London Metal Exchange (LME) Lithium Carbonate Global Average, LME Nickel Cash, LME Cobalt Cash and LME Copper Grade A Cash prices and China flake graphite – 194 free on board. Nominal prices.

Source: IEA analysis based on S&P Global and Bloomberg.

## Due to falling prices, the market size for key energy transition minerals contracted by 10% to USD 325 billion in 2023, despite demand growth

Market size for key energy transition minerals, 2019-2023



IEA. CC BY 4.0.

Notes: The market size for rare earth elements is based on the aggregate size of four magnet materials. In this year's assessment, rare earth elements and refined copper based on secondary scrap were included in the calculation, which raised the 2022 market size to USD 360 billion (up from USD 320 billion in the [Critical Minerals Market Review 2023](#)).



## The widespread decline in critical mineral prices in 2023

The critical minerals market had a turbulent year in 2023 and the main story of the year was falling prices. Battery minerals saw particularly large declines with lithium spot prices plummeting by 75% and other key materials such as nickel, cobalt, manganese, and graphite seeing declines of 30-45%. The IEA Energy Transition Mineral Price Index, which tracks a basket price of copper, major battery metals and rare earth elements, tripled in just two years starting in January 2020, but it began to slide from the beginning of 2023, returning to pre-pandemic levels. However, except for cobalt and graphite, prices remain higher than the historical averages observed in the 2010s. In contrast, prices for copper stayed relatively resilient. While expectations for a strong post-pandemic demand recovery did not materialise at scale, actual output fell short of anticipated supply, leading to tighter market conditions, particularly for copper concentrates.

Several factors contributed to the drop in prices. The slowing growth rate of EV battery sales, coupled with large-scale cell and cathode production, has led to a substantial accumulation of downstream products in inventory. China's expansion of battery plants, as well as cathode and anode production capacity, has far outpaced demand. This expansion has been a key driver behind the considerable build-up of inventory throughout the supply chain, resulting in reduced purchases of new materials. Furthermore, amid record high prices in

2022, many downstream consumers also made efforts to secure ample volumes to ensure business continuity.

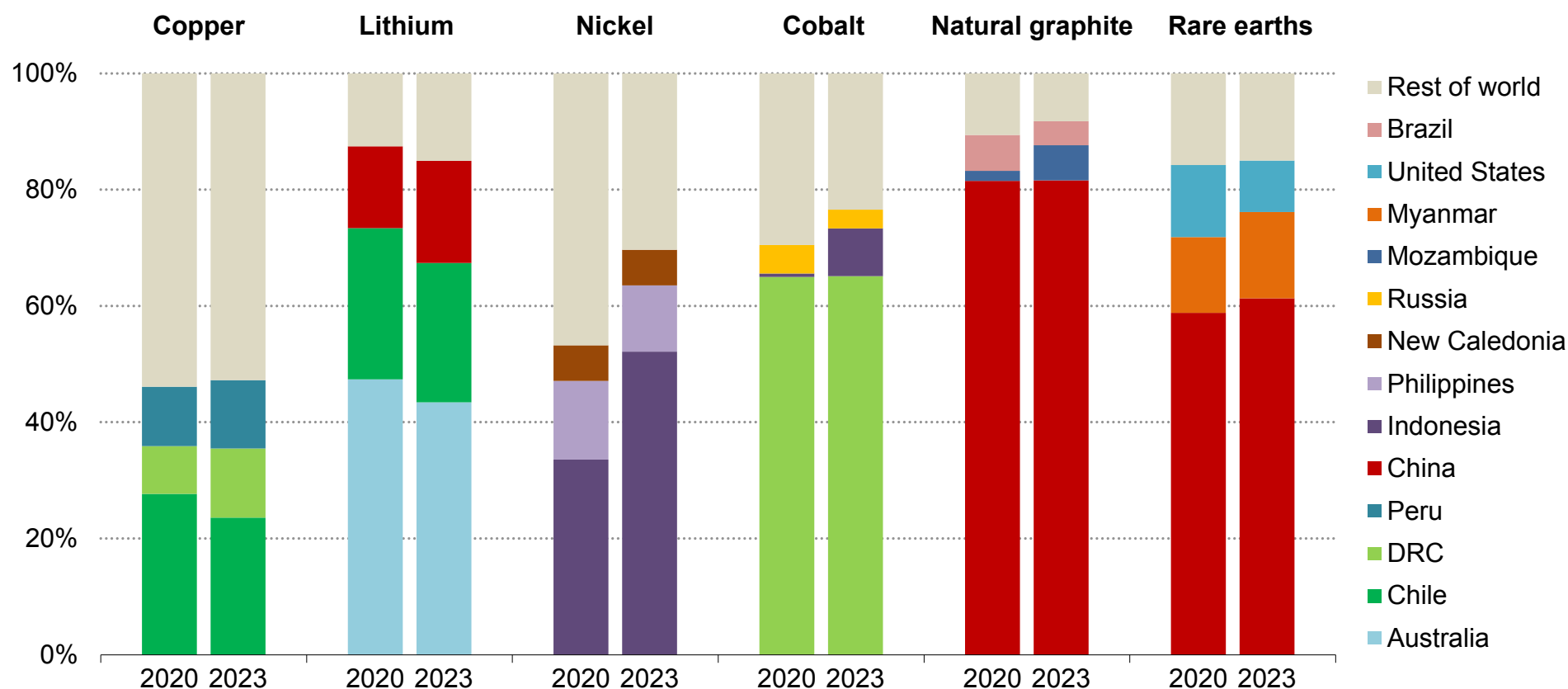
The rate of demand growth remained robust in 2023, with lithium demand rising by 30% and demand for nickel, cobalt, graphite and rare earths expanding by 8-15%. Clean energy applications were one of the primary contributors to this demand growth. Across all key minerals, the share of clean energy technologies has risen consistently. EVs cemented their position as the largest-consuming segment for lithium, and increased their share considerably in the demand for nickel, cobalt and graphite.

Nonetheless, the ramp-up of new supply outpaced demand growth in the past two years. From Africa to Indonesia, and to China, new projects came online relatively quickly, adding sizeable volumes to the supply pool. The remarkable increase in nickel supply from Indonesia is a notable example.

Overall, a combination of demand and supply-side trends, alongside a correction of overly steep price rises in 2021-22 contributed to the lower price environment, which is likely to continue in 2024. As a result, despite demand growth, the market size for energy transition minerals contracted by 10% to USD 325 billion in 2023. It would have been 20% higher if prices had remained at 2022 levels.

## Production growth has been accompanied by rising levels of geographical concentration, with the trends particularly pronounced for nickel and cobalt

Share of mined or raw material production by country

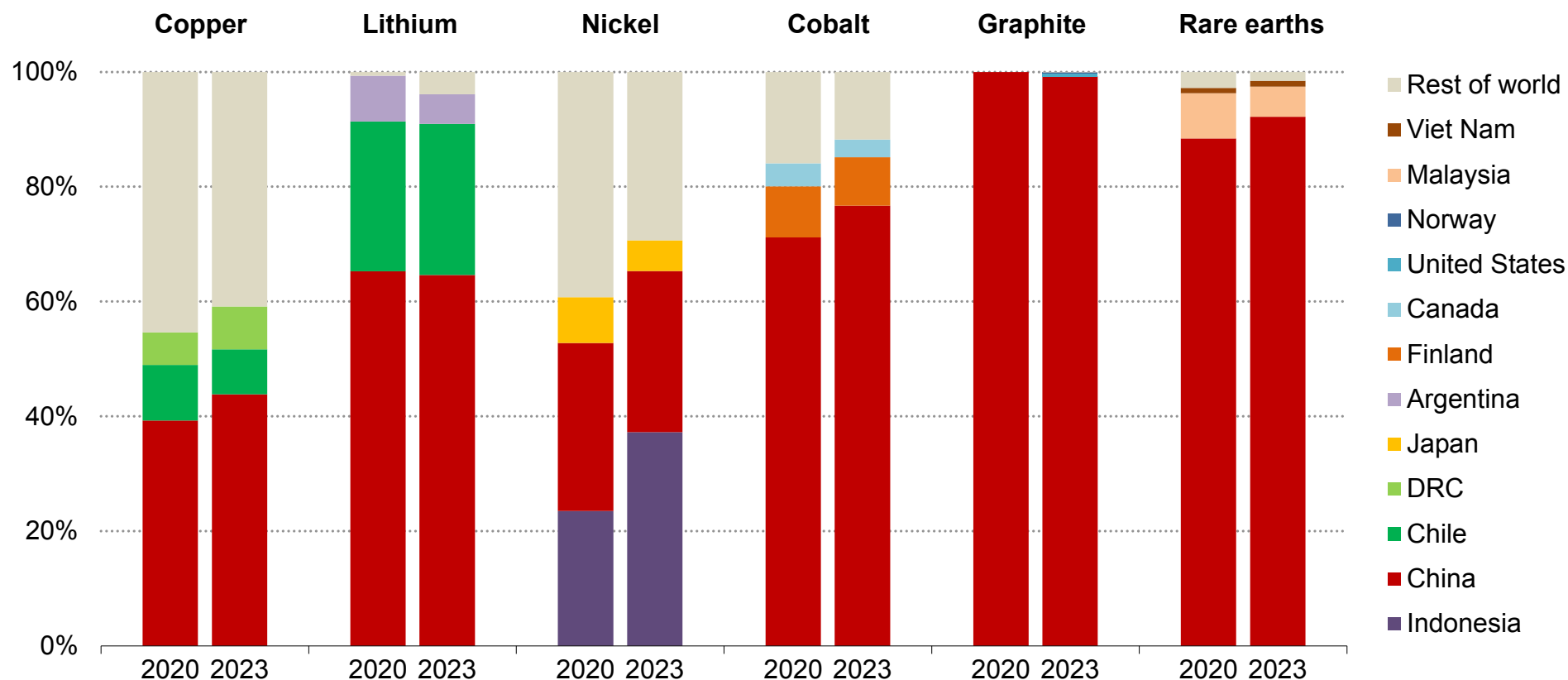


IEA. CC BY 4.0.

Notes: DRC = Democratic Republic of the Congo. Graphite extraction is for natural flake graphite. Rare earths are magnet rare earths only.

## The level of geographical concentration for refined products has increased in recent years

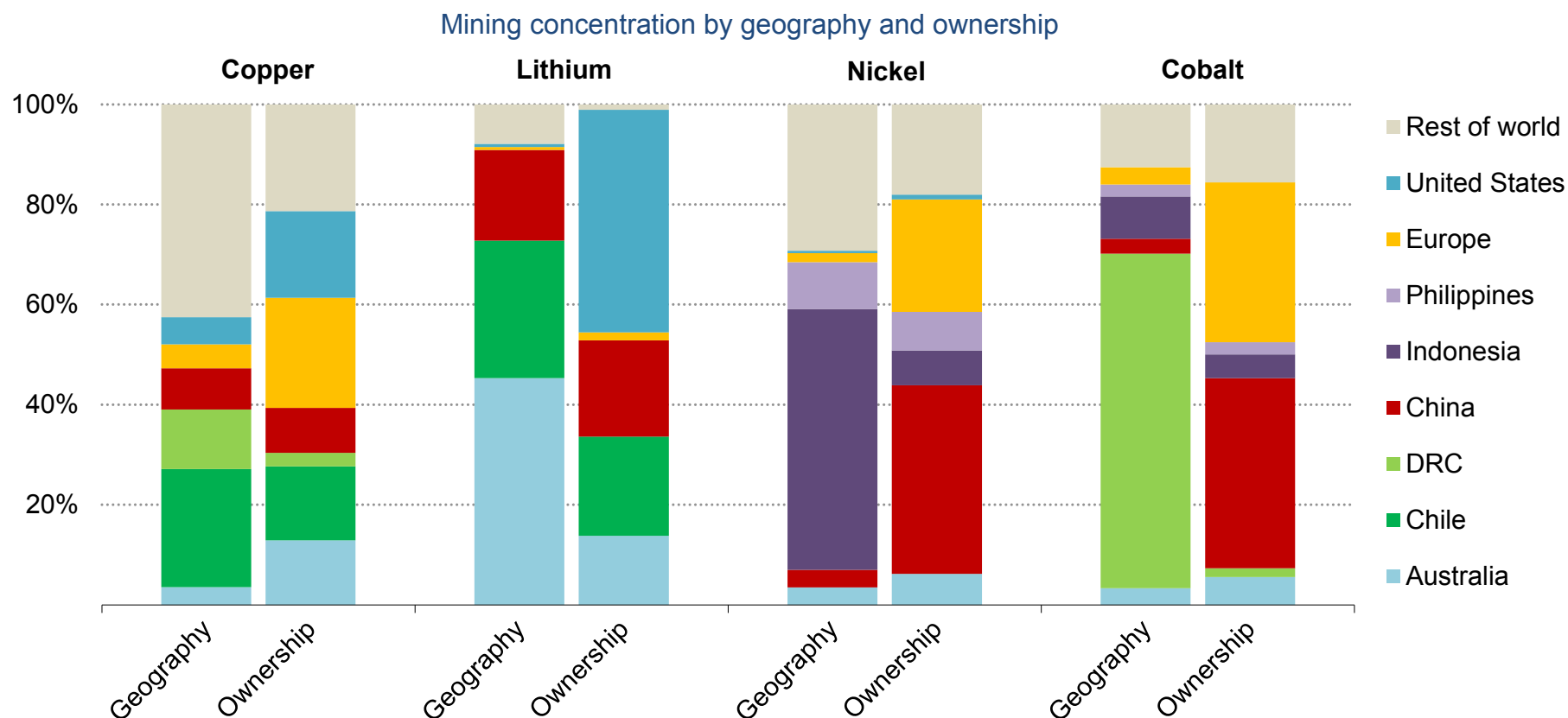
Share of refined material production by country



IEA. CC BY 4.0.

Note: Graphite is based on spherical graphite for battery grade. Rare earths are magnet rare earths only.

## Mining concentration looks different if viewed through the lens of asset ownership, with US and European companies playing a greater role



IEA. CC BY 4.0.

Notes: Ownership based on company headquarters location. For projects run by multiple companies, production is assigned to the company with the largest share. For copper, data are on the top 20 mining companies in 2023 representing 57% of production. For lithium, data cover 100% of production in 2023; for nickel, 93% of production; and for cobalt 97% of production.

Sources: IEA analysis based on S&P Global and Wood Mackenzie.

## New and more diversified supply sources remain vital, especially for refined materials

Production of key energy transition minerals has expanded substantially over the past several years, easing concerns about near-term supply shortages. However, as underscored already in the IEA's first [Critical Minerals Market Review](#) in 2023, this growth has come with increasing levels of geographical concentration. While high levels of supply concentration are well-known in the critical mineral space, the issue has been exacerbated by further production increases from today's dominant suppliers.

In the case of refined materials, the share of the top three producing nations have all increased since 2020, except for lithium. This trend is most pronounced for nickel and cobalt, where the rise of Indonesia has significantly boosted the level of supply concentration. Between 2020 and 2023, Indonesia's share of mined nickel production increased from 34% to 52% and its share of refined nickel increased from 23% to 37%. Meanwhile, 2023 also witnessed a proliferation of trade restriction measures, including increased Chinese controls over exports of gallium, germanium, graphite and technologies for processing rare earth elements.

For mining, however, assessing production by ownership (based on the leading owner company's headquarter location) shows a very different picture compared with the geographical mine location. Companies in the United States and Europe play a much greater role

in the supply of all critical minerals than what the geographical location of mines may suggest. Much of this is from some of the largest multi-national mining majors such as Glencore and Rio Tinto.

Although the majority of copper production occurs in Chile, European companies are the leading copper producers with over 10% of production, with Glencore, Rio Tinto and Anglo American playing major roles, and US companies controlling the second-largest amount of production. For lithium, Australia and Chile are the primary locations of raw material production, whereas US companies such as Abermarle are a major shareholder of over 40% of producing mines.

Both nickel and cobalt also show stark differences between the geographical location of mines compared with the ownership. Although Indonesia is the leading location of nickel mining, Indonesian companies hold less than 10% of production. Chinese companies are the major nickel mine owners, accounting for around 40% of production. European companies also have a sizeable share with over 20% of supply, predominantly due to operations in Indonesia owned by Eramet. For cobalt, the majority of mines are located in the Democratic Republic of the Congo (DRC), whereas European companies such as Glencore and Chinese companies such as CMOC own a third each of the supply. Notably, DRC-owned companies account for less than 5% of production.

## Short-term market developments for key energy transition minerals

## Short-term market developments for key energy transition minerals

### Copper

Demand for refined copper increased by 2.7% in 2023, up from 0.9% in 2022, almost entirely driven by growing consumption in China and India. Demand in other regions registered a modest decline. The growth in China was predominantly underpinned by copper uses in construction and electricity networks, a trend expected to persist in the coming years. Indications from China's 'Two Sessions' meeting in March 2024 signal a continued emphasis on expanding copper usage, particularly in renewable energy and grid expansion.

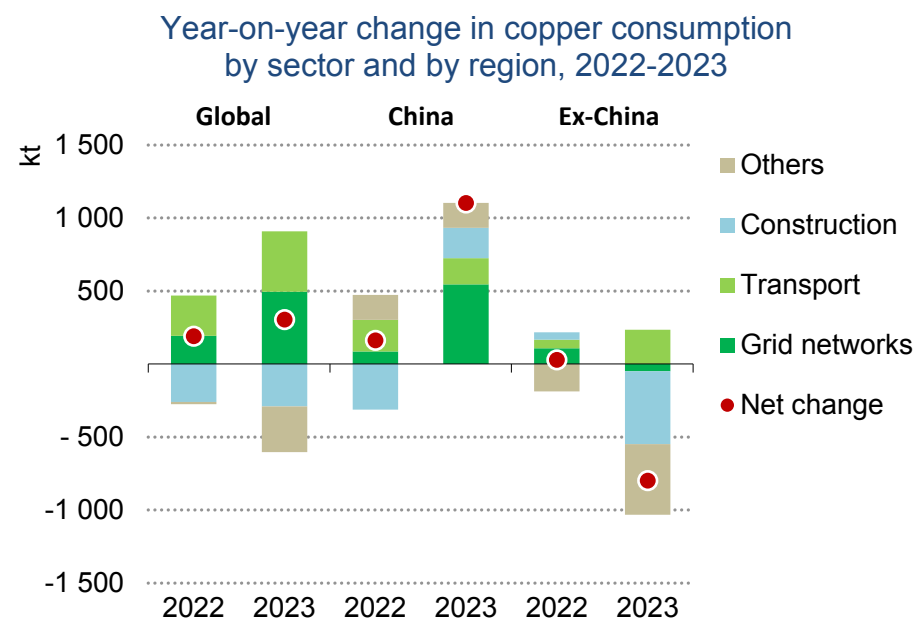
Mined copper output saw an increase of less than 2% in 2023, with notable growth in the Democratic Republic of the Congo (DRC) and Peru offset by declines in Chile and elsewhere. Refined copper supply expanded by 4% in 2023, primarily driven by increased production in China, with some contributions from the DRC.

In early 2024, copper prices saw a strong increase as lower-than-anticipated mined output tipped the concentrate market balance toward a slight deficit, contrary to earlier expectations of surpluses. The closure of the [Cobre Panama mine](#) and downgraded production guidance by Anglo American, Vale and Southern Copper contributed to this result. Several supply disruptions are continuing in 2024, for example, production at the [Radomiro Tomic mine](#) in Chile was halted due to a worker strike in March. As many smelters sought to secure

copper concentrates, the spot treatment and refining charges (TC/RC) plummeted by 80% between October 2023 and February 2024. In response, Chinese smelters agreed on several measures to limit the decline in TC/RCs, including replacing concentrate usage with scrap, bringing forward the schedule for maintenance, reducing utilisation rates for unprofitable facilities and postponing new projects.

The tightness in the concentrate markets extended to the scrap market as many smelters sought to increase their usage of scrap to complement concentrates. Over recent months, there has been a noticeable uptick in China's scrap imports, with repercussions in the global scrap market.

Limited growth in mined supply is anticipated for 2024. However, in 2025 and 2026, several new projects and expansion plans are expected to ramp up, such as Tenke Fungurume (DRC), Quebrada Blanca Phase 2 (Chile) and Udokan (Russia). These would bring additional volumes to the market but risks remain if these projects fail to meet expected growth targets or experience slower ramp-ups. Possible sanctions on Russian copper may not materially affect the market as many European companies have already diversified their supplies and a large portion of Russian volumes currently flow to China and Türkiye.



IEA. CC BY 4.0.

Note: Includes direct use of scrap.

## Lithium

In 2023, lithium demand rose by around 30%, maintaining the level of growth seen in 2022. Raw material supply increased by 30% with traditional producers such as Australia and Chile being joined by new players such as Argentina and Zimbabwe. Lithium chemical production experienced even greater expansion by 40%, primarily driven by China.

Lithium was a notable beneficiary during the price rally in 2021 and early 2022, but in 2023 it was the commodity that was most affected

by price downturns. The substantial build-up of inventories in the downstream battery value chain (e.g. battery cells, cathodes) progressively dampened purchasing activity in 2023. Meanwhile new supplies from Australia, Argentina and China continued to increase throughout the year, further pressuring prices. Lithium prices fell by over 75% during the course of 2023, returning to pre-pandemic levels. This steep decline prompted various actions by producers to reduce output and scale back expansion plans. Core Lithium decided to [suspend mining operations](#) at its Finniss mine to focus on processing stockpiled ore. Albemarle outlined plans to [reduce capital expenditures for 2024](#) while implementing cost-cutting measures. Talison announced a production reduction plan in response to market conditions.

Lithium prices saw a slight uptick in March-April 2024, supported by production cuts and expectations for the end of the destocking cycle. The revival of downstream activities may provide some upside for prices. However, a significant price surge in the near term is difficult to envision. Several potential supply sources stand ready to ramp up production, which could cap the potential for a substantial price increase. For example, it is estimated that lepidolite assets in China currently runs at 40% utilisation rates but could return to the market if prices were to rise substantially in the short term. Additionally, spodumene assets in China, Canada, Brazil and Africa are also positioned for robust growth. On the chemical front, numerous lithium refineries are scheduled to commence operations and expand capacity in 2024 and 2025, primarily in Argentina, Australia and



China. Most of the recently announced supply reductions or postponements have been associated with hard rock lithium, not chemicals.

While investment and exploration activities in the lithium sector remained strong in 2023, the enduring low prices may dampen investment appetite for new greenfield projects, thereby impacting medium-to-long-term market balances.

## Nickel

Nickel was another material that experienced significant price declines, with prices falling more than 40% in 2023. Several factors, including a downstream inventory overhang, the accelerated adoption of LFP chemistries, and subdued stainless steel demand, particularly in advanced economies, contributed to this downturn. However, the primary driver was oversupply, driven by a surge in output from Indonesia.

While demand for nickel grew by 4% in 2022 and 8% in 2023, mined nickel supply increased by 19% in 2022 and 9% in 2023. In 2023, Indonesia's production growth was greater than global output growth, implying reduced output from other producers. Refined nickel production expanded by 14% in 2022 and 2023 each, again led by Indonesia and China.

The delivery of high-pressure acid leaching (HPAL) projects in Indonesia, aimed at producing high-purity nickel products from

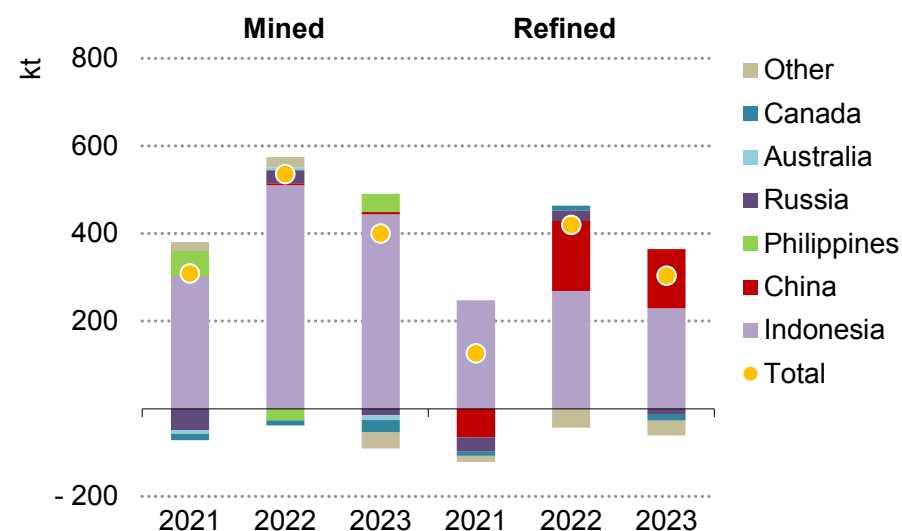
laterite resources, exceeded initial projections in terms of speed. Indonesia's HPAL projects yielded 180 kt of nickel in 2023, a significant rise from 88 kt in 2022. The development of a process to convert nickel pig iron (NPI) to nickel matte further contributed to notable output growth in the country.

In recent years, the proliferation of methods to convert low-purity Class II products and intermediates has blurred the traditional boundary between Class I and Class II products, contributing to a decline in nickel prices on the London Metal Exchange (LME) where high-purity Class I products are traded. With the notable discounts of nickel sulphate and NPI to the LME price, several producers in China (and Tsingshan in Indonesia) have begun producing higher-grade nickel cathodes suitable for delivery on both the LME and Shanghai Future Exchange (SHFE). In July 2023, [Huayou's nickel products were accepted by the LME](#), and other nickel sulphate producers such as China's GEM and CNGR are following suit. Overall, the oversupply of Class II and intermediates in Indonesia and China and mechanisms to bring the surplus of Class II products to the Class I market coincided with weak demand, causing a sharp correction in prices.

These market conditions have taken a heavy toll on many higher-cost producers, prompting them to temporarily suspend production or, in some cases, cease operations. Panoramic Resources made the decision to [halt operations](#) at its Savannah nickel mine in West Australia. BHP is reassessing its [Nickel West operations](#) and planned investments for the West Musgrave project in Australia. This has

sparked discussions about price premiums for nickel products with high environmental and social performance. However, there are limited indications thus far that consumers favour products with lower environmental and social impacts (see the nickel section in Chapter 2).

Change in nickel supply by country, 2021-2023



IEA. CC BY 4.0.

In 2023, the nickel market saw a surplus equivalent to around 8% of annual consumption. While the magnitude of this surplus may diminish in 2024 due to growing demand and production cuts, prices could remain suppressed given the numerous projects in the pipeline, particularly those slated to come online in Indonesia in 2024 and beyond. Indonesia's share of global nickel supply has risen significantly, climbing from 34% in 2020 to 52% in 2023 for mined output and from 23% in 2020 to 37% in 2023 for refined

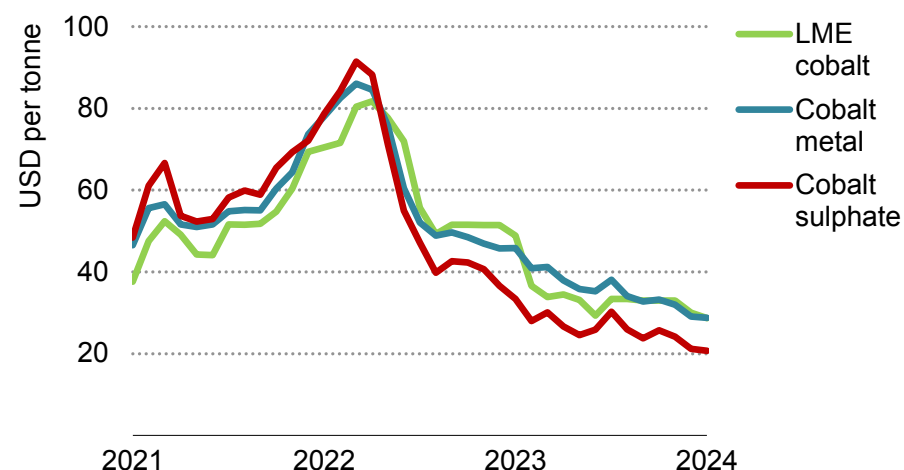
output. The persistent low-price environment may further bolster this share in the years ahead.

## Cobalt

Cobalt prices remained subdued throughout 2023 due to a combination of production growth from the DRC and Indonesia coinciding with weak demand. Over the past two years, demand for cobalt has increased by 8-10% annually, while mined cobalt supply expanded by an average of 16% and refined cobalt supply by 13%. In 2023, prices for cobalt metal performed better than those for cobalt sulphate, signalling weaker demand in the battery sector compared with demand for alloys and magnets.

The DRC, the largest supplier with a 65% market share, delivered the largest increase in production in 2023. The ramp-up of CMOC's Kisanfu mine in the DRC exceeded expectations from the industry, and [the resolution of the dispute](#) between DRC's state-owned mining company Gécamines and China's CMOC allowed the Tenke Fungurume mine to resume exports. Consequently, CMOC surpassed Glencore as the largest supplier of mined cobalt to the global market. Indonesia rapidly ascended to become the second-largest producer, driven by the burgeoning production of mixed-hydroxide precipitate (MHP) from its HPAL facilities. For refined cobalt, China has dominated production volume growth over the past few years, with virtually no growth observed in other regions.

Price developments for cobalt, 2021-2024



IEA. CC BY 4.0.

Notes: Cobalt metal is based on China Cobalt Metal 99.8%. Cobalt sulphate is based on Cobalt sulphate 20.5% China. Quality adjusted.

Sources: IEA analysis based on S&P Global and Bloomberg.

Subdued prices prompted many producers to [stockpile](#) cobalt hydroxide or metal in an effort to bolster future profitability, though the effectiveness of these measures hinges on the evolution of near-term market balances. Cobalt prices are expected to remain subdued in 2024 as supply growth continues to outpace demand growth. While overall battery deployment continues to increase, the trend in battery chemistry choices is shifting towards those using less cobalt. Although the pace of supply growth is anticipated to slow in 2024, significant price support in the near term is unlikely, although logistical bottlenecks or unexpected supply disruptions of large mines could trigger a brief price rally.

## Graphite

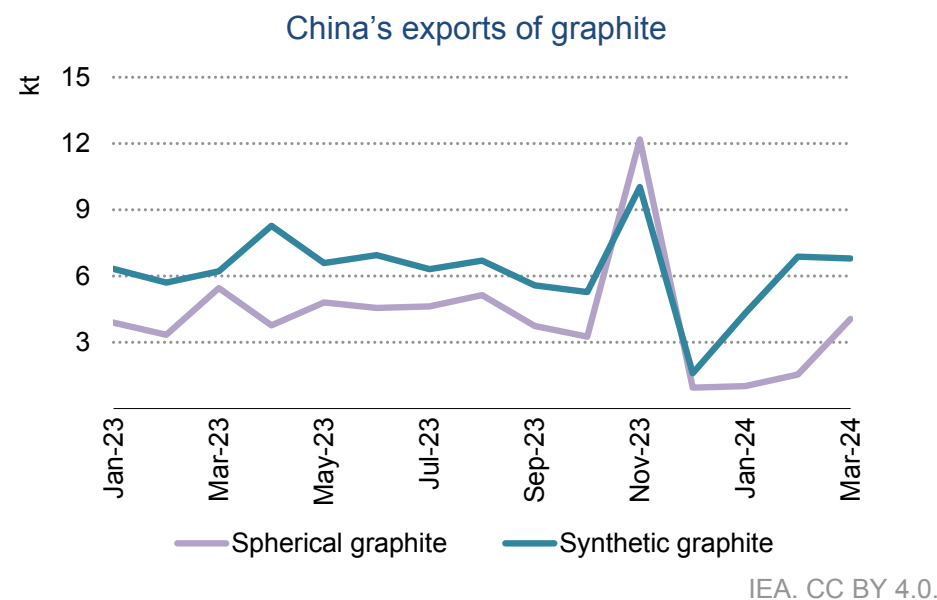
In 2023, graphite consumption grew by 11% to 4.6 Mt, with battery-related demand growing by 40% to 1.5 Mt. Mining production of natural graphite has been stable, while synthetic production continued to ramp up, allowing total graphite supply to grow by 10.5% and reach 5.5 Mt.

Production is ramping up in more diversified areas, such as the Lac-des-Îles mine coming back [online](#) in Quebec, and production [starting](#) in Madagascar's Molo mine. New developments are taking place with more integrated models, with anode producers building increasingly integrated supply chains – such as Korea's POSCO [securing](#) supply of 24 kt per year from the Balama mine in Mozambique, whose owner is also developing anode material [production](#) in Louisiana.

As for other key battery metals, graphite prices experienced a significant drop in prices over the course of 2023 with prices for natural flake graphite falling by 30% and spherical graphite by 45%.

One of the most significant developments for graphite this year is that since December 2023, natural and refined battery-grade graphite are subject to [export controls from China](#). These are not the first set of Chinese export controls for critical minerals, with restrictive measures taken for rare earth elements in the early 2010s and for gallium and germanium since July 2023, but it is the first time these happened for a critical input of the EV supply chain. In January and February 2024, exports to Japan and Korea – key EV anode producers outside of

China – were significantly below average although they returned to normal levels in March. In parallel, new US IRA guidance is creating [incentives](#) for a number of battery manufacturers to source graphite from outside of China. While the market is well supplied for the moment, this raises an important question about the availability of graphite that is compliant with a range of policy measures aimed at promoting supply chain diversification. It remains to be seen whether market fragmentation creates divergent regional price dynamics going forward.



Source: IEA analysis based on Wood Mackenzie.

## Rare earth elements

The rare earth elements (REE) industry is still bearing the legacy of concerns around risk and volatility which emerged during the 2010-2011 price spike. Over several decades, China has built its position in the REE market with the long-term goal of growing its downstream industry and has become the leader in refined rare earth technologies (see the rare earth elements section in Chapter 2). The REE market is fundamentally driven by developments in China, which is the single-largest source of mined rare earths from two principal areas. The largest source of light rare earths (LREE) - including neodymium and praseodymium, is a by-product supply from the [Bayan Obo iron mine in Inner Mongolia](#). But China also hosts vast quantities of heavy rare earths (HREE) - including dysprosium and terbium, in ionic adsorption clay deposits in southern China. With additional mine supply spread across the country, China is the largest producer of mined REEs.

The supply chain for REEs and permanent magnets is complex, regionally concentrated and marked by a lack of transparent pricing. In 2023, the REE markets saw an oversupply from China and a lower-than-expected downstream demand. Chinese production quotas for [LREEs increased modestly](#) in the second half of 2023, raising the availability of materials in the market. Neodymium prices are estimated to have fallen by 45% over the course of 2023. Net profit for the China Northern Rare Earth Group, one of the largest global producers, was estimated to be in the range of CNY 2.17 billion (Yuan renminbi) (USD 303 million) to CNY 2.33 billion in 2023, a [decline of around 60%](#) from CNY 5.98 billion (USD 934 million) in 2022.

As China imports HREE feedstock from Myanmar and Laos for domestic processing, Myanmar's decision to close its borders raised concerns about the reliable supply of HREEs. However, the latest data indicates that the closures had little impact on trade flows. REE mining activity mainly occurs in Kachin state, which has significant autonomy. Meanwhile, there was an increasing volume of HREE feedstock from Lao PDR to China, which also contributed to alleviating concerns about material availability.

While the markets appear to be well-supplied to meet near-term demand, the current low-price environments could delay projects planned outside China, further pushing back already lengthy lead time projects intended to boost diversification. Another area of concern could be tightened supply of HREEs in the medium term. While a lot of attention was paid in the last decade to LREEs used in EV motor magnets (neodymium and praseodymium), HREEs such as dysprosium and terbium are also key components, but their relative supply from the main rare earth deposits is not in sync with their use. Avoiding this would require all currently announced projects to secure funding and scale up rapidly.

Concerns surrounding transparent reporting in rare earth markets also need to be addressed to avoid situations such as the [recent legal action against major players in Viet Nam](#), which could put expected supplies at risk or create barriers for diversification.

## Will uranium be a bottleneck for a nuclear comeback?

After a decade of slow deployment, a changing policy landscape is creating opportunities for a nuclear comeback. Nuclear power capacity increases from 420 GW in 2023 to 500 GW by 2030 and 770 GW by 2050 in the Announced Pledges Scenario (APS), with growth mainly in China and other developing economies, while advanced economies carry out lifetime extensions and look to build new projects to offset retirements. Large-scale reactors remain the dominant form, but growing interest in small modular reactors increases the potential for nuclear power in the long run.

After climbing steadily for a couple of years, spot prices for uranium oxide spiked in the second half of 2023, reaching over USD 100 per pound in February 2024, the highest price seen in over 15 years, before falling again to just under USD 90 in March. Amid ongoing uncertainty over the possibility of import restrictions from the United States and European countries on supplies from Russia, news in 2023 of a coup in Niger and a sulphuric acid shortage in Kazakhstan put pressure on supplies of uranium oxides. While the current price spikes are not entirely supported by market fundamentals given that many countries have sizeable stockpiles for nuclear fuels and it will take many years for planned nuclear capacities to come online, the recent price rally highlights a growing concern around uranium supplies to support the growth of nuclear power.

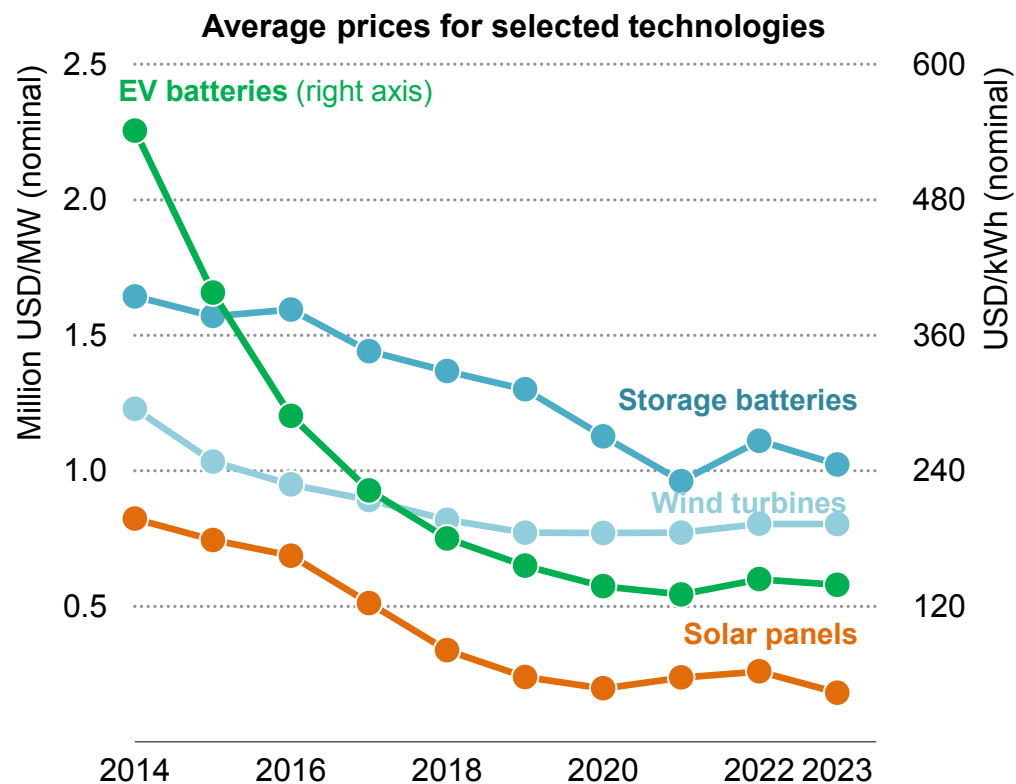
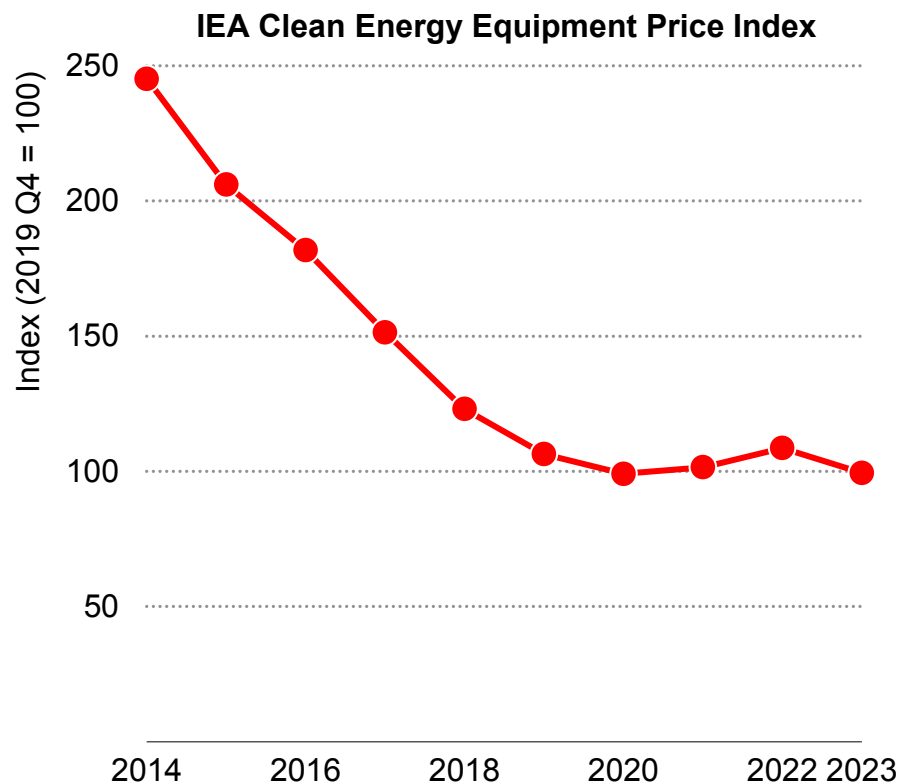
Following the invasion of Ukraine, Western governments have become increasingly concerned about Russia's role in the nuclear fuel supply chain. In recent years, Russia has accounted for [a third of all conversion and 40% of enrichment services](#) globally. Russia is also the [only commercial supplier](#) of high-assay low-enriched uranium (HALEU) necessary for certain advanced reactor designs.

Several governments have recently announced moves to reduce dependence on Russia. In January 2023, the US Department of Energy announced [awards to the conversion industry](#) to develop its strategic uranium reserve. In April 2023, Canada, France, Japan, the United Kingdom and the United States announced an agreement to support the stable supply of nuclear fuel and “undermine Russia's grip” on nuclear fuel supply chains. Since then, the [United Kingdom](#) and the [United States](#) have announced moves to encourage the development of HALEU enrichment capacity.

Nonetheless, it is too early to tell if high prices and supply supports seen in 2023 will be sufficient to encourage Western suppliers to expand production. US domestic production of uranium in [2023 remained at historically low levels](#). However, some producers in [Canada](#) and the [United States](#) have announced that they will restart production in 2024 at previously mothballed facilities.

## Investment trends

## Reduced material prices and increased manufacturing capacity underpinned major cost reductions for clean energy technologies, with solar PV and batteries reaching record lows



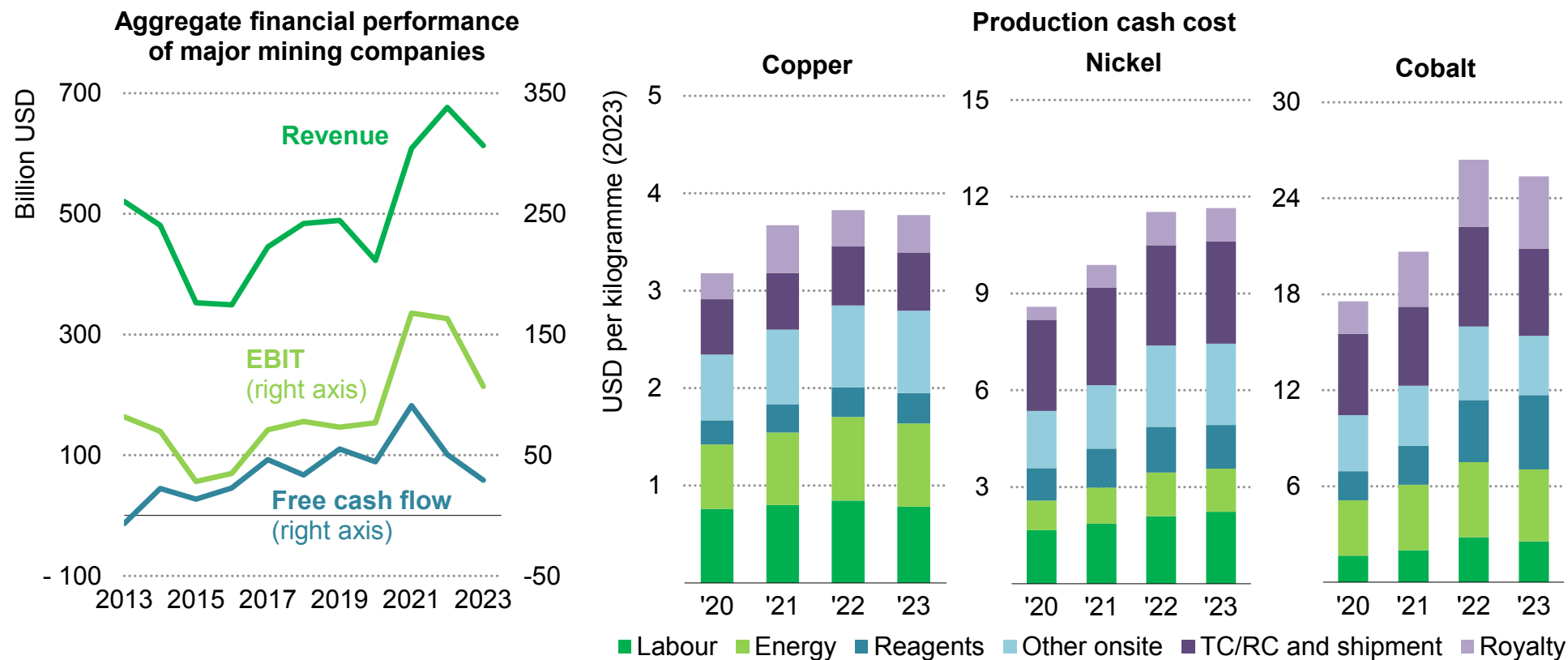
IEA. CC BY 4.0.

Notes: The IEA Clean Energy Equipment Price Index tracks price movements of a fixed basket of solar PV panels, wind turbines and lithium-ion batteries (for EVs and energy storage). Prices are weighted based on the shares of global average annual investment.

Sources: IEA analysis based on company financial reports and BloombergNEF.



However, low prices resulted in a decline in industry profits by a third in 2023, exacerbated by recent increases in production costs

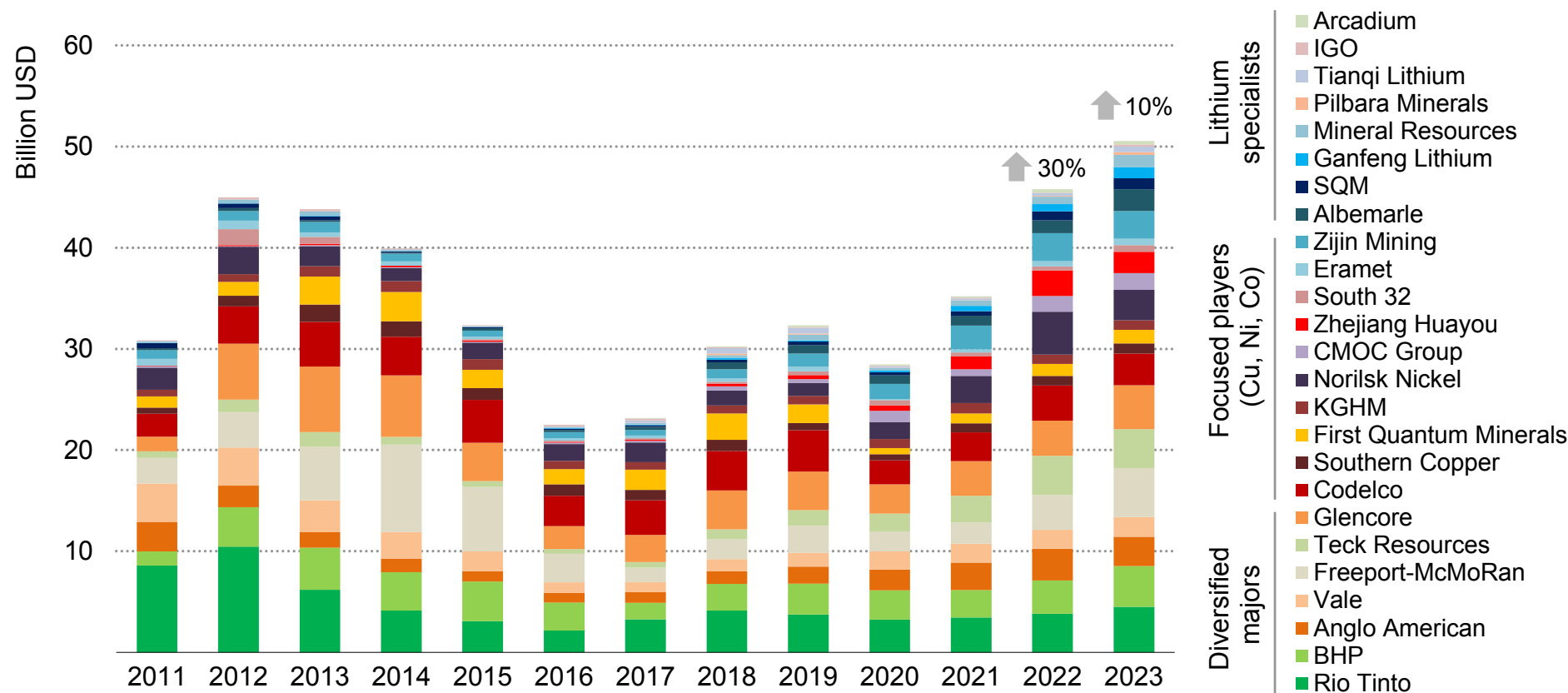


IEA. CC BY 4.0.

Notes: EBIT = earnings before interest and taxes. Production case cost is based on the weighted average value for the assets in the 75<sup>th</sup> quartile.  
Sources: IEA analysis based on company financial reports and S&P Global.

## Investment in critical mineral mining grew by 10% in 2023, a smaller increase than seen in 2022, as price declines placed pressure on producers' financial capacity

Capital expenditure on nonferrous metal production by major mining companies, 2011-2023



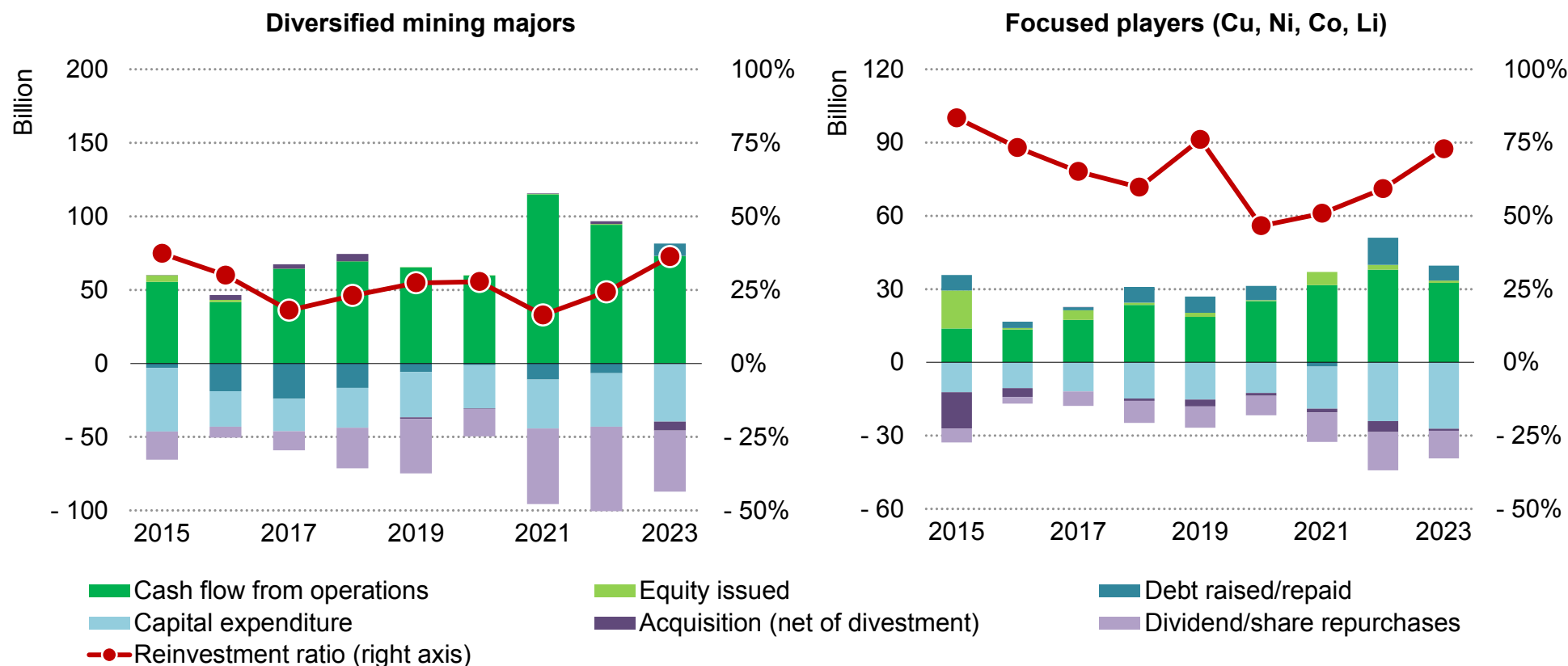
IEA. CC BY 4.0.

Notes: Co = cobalt; Cu = copper; Ni = nickel. For diversified majors, capex on the production of iron ore, gold, coal and other energy products was excluded. Nominal values. The results for Arcadium start from 2016.

Source: IEA analysis based on company annual reports and S&P Global.

## Diversified mining majors are taking a measured approach to investment; specialist players are taking on more risks in pursuit of future growth, albeit with reduced new debt issuances

Cash generation and disposition trends by major mining companies, 2015-2023



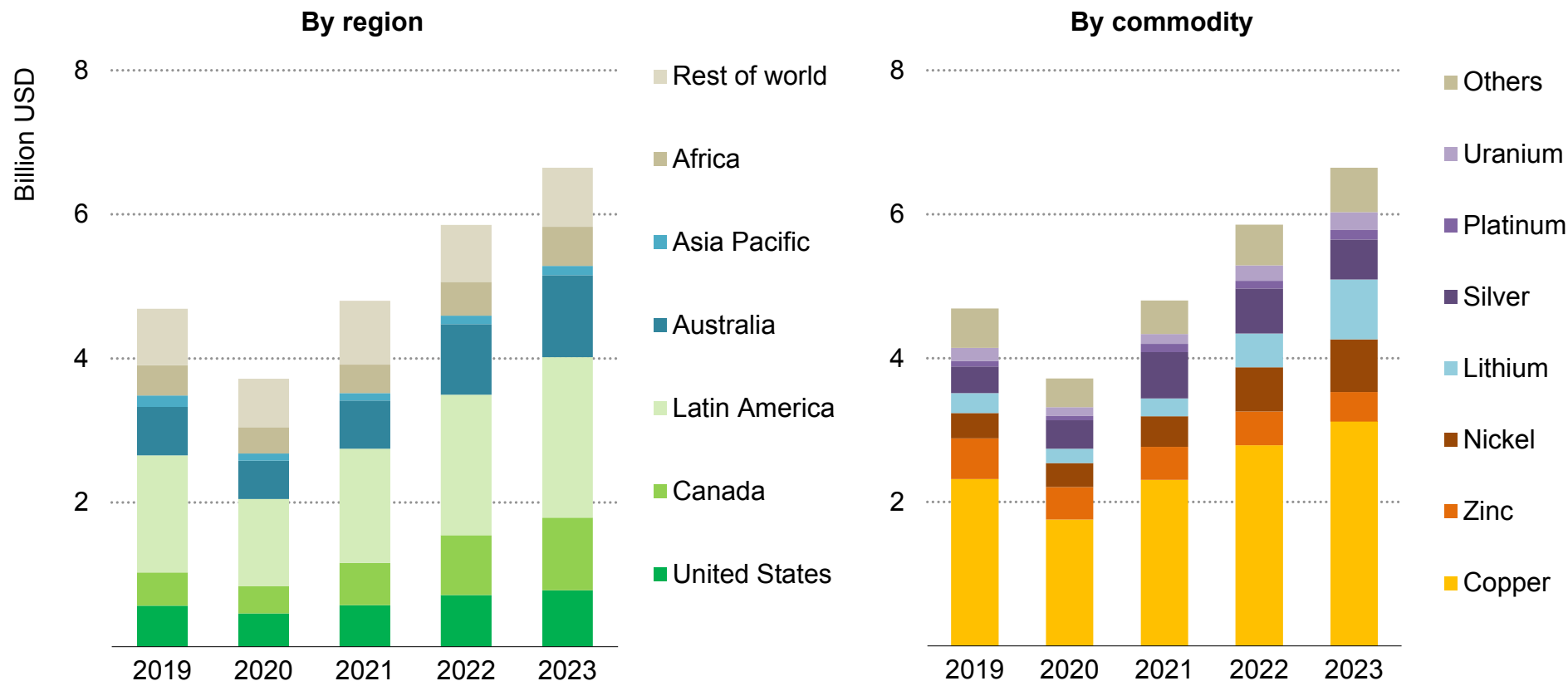
IEA. CC BY 4.0.

Notes: Excludes investment in marketable securities and others. Capital expenditure covers all commodities, including nonferrous metals. Reinvestment ratio investment = capital expenditure in nonferrous metal production as a percentage of operating cash flow.

Sources: IEA analysis based on company annual reports and S&P Global.

## Exploration spending increased by 15% in 2023, driven by Canada and Australia; despite headwinds from falling prices, lithium exploration spending continued to surge by nearly 80%

Exploration spending for selected nonferrous mineral resources, 2019-2023

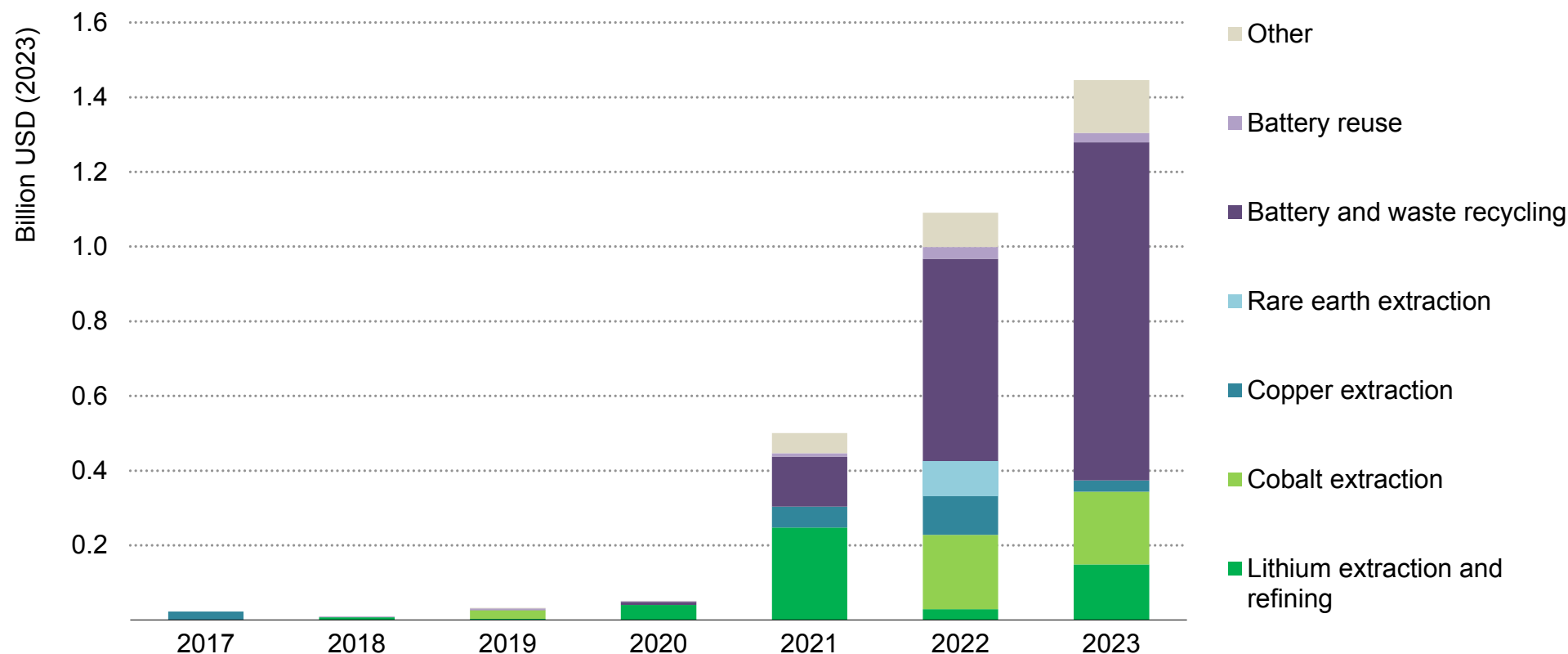


IEA. CC BY 4.0.

Notes: Excludes budgets for iron ore, coal, aluminium, gold and diamonds. Others comprise rare earth elements, potash/phosphate and many other minor metals.  
Sources: IEA analysis based on S&P Global.

## Venture capital investment in the critical mineral sector continued to rise in 2023, with significant growth in battery recycling offsetting reductions in mining and refining start-ups

Early- and growth-stage venture capital investment into critical mineral start-ups, 2017-2023



IEA. CC BY 4.0.

Note: The USD 450 million deal for Energy Exploration Technologies was excluded from the 2022 records as it was subject to the initial public offering process in 2024. This adjustment resulted in a lower 2022 figure compared with the previous year's [Critical Minerals Market Review 2023](#).

Source: IEA analysis based on Cleantech Group i3 database.

## Two sides of price declines: A boon for clean energy deployment but a bane for investment and diversification?

Lower prices have contributed to cost reductions for a number of clean energy technologies, although they were not the only factor. Substantial increases in manufacturing capacity, especially in China, have also driven a decrease in prices of clean energy equipment in 2023.

Following two years of rise, IEA's global [Clean Energy Equipment Price Index \(CEEPI\)](#) reveals that prices eased considerably during 2023, with the fourth quarter of 2023 reaching the index's lowest level. The CEEPI tracks price movements in a global basket of solar PV modules, wind turbines, lithium-ion batteries for EVs and battery storage, weighted by shares of investment. Solar PV module prices saw a strong decline as Chinese exports of cells and modules reached 255 GW in 2023, over three times the 2019 level. Price pressures in the wind turbine industry have somewhat eased although prices remain high for non-Chinese producers. After an increase in prices in 2022, battery pack prices also dropped by 14% in 2023. The main driver was a major reduction in prices of critical minerals, as well as an increase in production capacity.

While the low-price environment may foster additional deployment of clean energy technologies in the medium term, it currently presents challenges for producers' financial performance. Industry revenues declined by 10% in 2023 while operating profits plummeted by 34%.

Free cash flow also decreased by over 40%, constraining the industry's ability to allocate significant capital for future growth. These challenges have been exacerbated by increases in production costs in recent years. Since 2020, production cash costs for copper, nickel, and cobalt have all trended upwards, with marginal declines in 2023. Between 2020 and 2023, production costs increased by 6% per year for copper, 11% for nickel and 13% for cobalt. Royalties were the largest contributor for copper and nickel, and costs related to energy and reagents were the main driver across the materials.

This triggered a flurry of announcements to put capacity into maintenance and suspend operations (suspension does not mean a permanent closure). While many high-cost producers and new entrants are feeling the impact of the price crash, numerous established assets are still profitable in the current price environment. This suggests that, while prices may rebound as the destocking cycle ends, significant increases could be restrained by growing supplies in the near term. Consequently, this could lead to further geographical concentration of production, as today's dominant suppliers typically operate at the lower end of the cost curve.

Against this backdrop, we have assessed the combined investment levels of 25 major mining companies with substantial involvement in developing minerals essential for the energy transition. These

companies encompass diversified mining majors and specialised developers focused on specific energy transition minerals such as copper, nickel, cobalt, and lithium.

Our assessment suggests that investment in critical minerals mining grew by 10% in 2023 (6% when adjusted for inflation), a smaller increase compared with the 30% growth in 2022. While investment spending by diversified majors increased by 15%, investment by lithium specialists saw a sharp rise by 60%, despite headwinds from weak prices.

Exploration spending grew by 15% in 2023, with Canada and Australia registering the largest increases, followed closely by Africa. Spending for lithium exhibited an impressive 80% increase despite challenging market conditions, followed by platinum and nickel.

In 2023, companies allocated approximately 50% of the generated cash to investment, while the remainder flowed back to shareholders and lenders through dividends, share buybacks and debt repayment. Diversified mining majors appear to take a more measured approach to investment, whereas specialist players focusing on specific

minerals allocated a greater portion to growth investment, although noticeable reductions in new debt issuances were observed.

As venture capital (VC) investors look for new opportunities across EV supply chains, battery recycling and critical mineral extraction and refining continued to gain momentum. VC investment in the battery recycling space expanded significantly in 2023, notably driven by a [USD 540 million](#) round of growth equity funding to United States-based Ascend Elements. Investment in mining and refining start-ups contracted by 12% to USD 375 million in 2023. Cobalt extraction attracted nearly USD 200 million in 2023. Lithium extraction and refining attracted USD 150 million, much higher than the dip of 2022 but still below the record year of 2021.

Notable critical mineral deals in 2023 included [USD 50 million](#) series A investment by Canada-based Summit Nanotech to scale its more sustainable lithium extraction technology. In the United States, Kobold Metals raised [USD 195 million](#) in growth equity to expand cobalt extraction, Energy Exploration Technologies raised [USD 50 million](#) for direct lithium extraction from GM Ventures, and Atlas Materials raised [USD 27 million](#) in seed money to develop nickel extraction technologies.

## China's approach to mineral investment and security

China is the dominant global refiner for critical minerals, processing over half of all lithium, cobalt, graphite and rare earth elements. However, with the exception of graphite and rare earth elements, China is not a major mining centre for these minerals. Therefore, China relies on imports of concentrates and feedstock to supply its refining and subsequent manufacturing operations. The security of supply of these minerals is of a critical concern to China as well.

The importance of these minerals has driven an acceleration of Chinese investment into the mining sector, both domestically and internationally. In 2023 Chinese investment in the metals and mining sector related to the Belt and Road Initiative [reached USD 19.4 billion](#), the highest level in a decade, and a remarkable 160% increase from 2022. China's investment in and acquisition of overseas mines has grown significantly in the past ten years, reaching record levels of [USD 10 billion](#) in the first half of 2023 with a particular focus on battery metals such as lithium, nickel and cobalt. Out of the seven lithium assets in Africa that are expected to start production by 2027, [five have at least 50% equity ownership by Chinese companies](#). One of the most significant investments was the Arcadia project in Zimbabwe (by Zhejiang Huayou Cobalt). In Latin America, a consortium led by CATL won a bid in 2023 for a USD 1.4 billion investment to develop [Bolivia's resources of lithium](#). In addition, the Chinese mining major Zijin Mining acquired Canada's

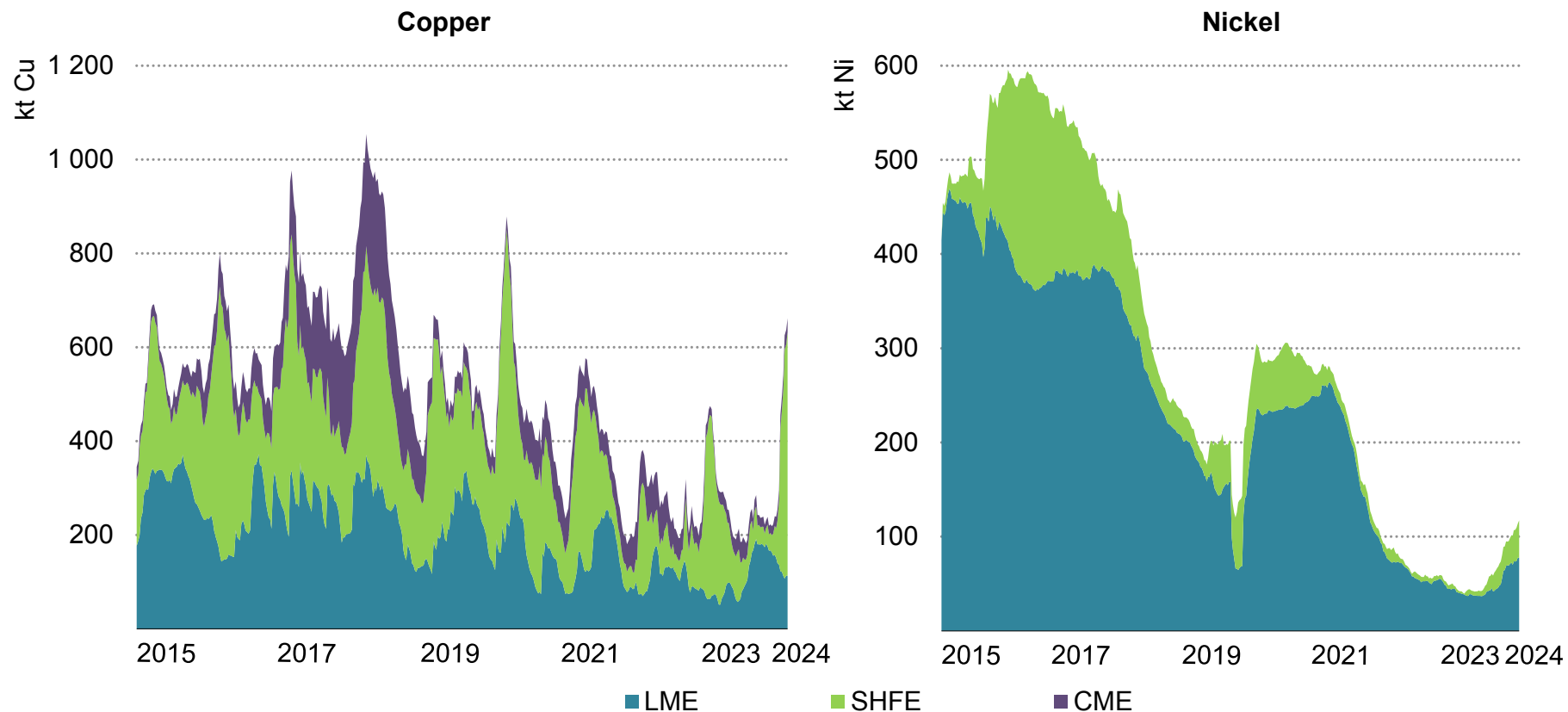
Neo Lithium for [USD 770 million](#) in 2021 to access the Tres Quebradas lithium project in Argentina. China accounted for 44% of global lithium M&A investments (by value) over the past three years and most of these deals were related to projects in the initial stage of development (initial exploration, feasibility, development). Chinese companies also dominate nickel mining in Indonesia, the largest global supplier of nickel, with a surge of investment over recent years since the complete ore export ban in 2020, including in supporting infrastructure from the [Belt and Road initiative](#). In 2024, majority Chinese-owned producers supply [over 80% of Indonesia's battery nickel output](#). Domestically, China has also ramped up its mining activity, being the third-largest lithium producer. The Xiangyuan lepidolite project (Hunan) is expected to bring 60 kt to 70 kt of lithium carbonates equivalent per year to the domestic market.

Another critical measure from China is the accumulation of national stockpiles, particularly during times of low commodity prices. China's [State Reserves Bureau](#) took advantage of the global financial crisis and metal price slump to build up inventories and stockpiles of critical materials, acting as a buffer for the industry against short-term disruption which can also be used as market-balancing volumes to influence prices. In the current lower price and oversupply environment, there is anticipation that China may continue to increase supply, taking market share from other players.



## Inventories of key energy transition minerals at major metals exchanges have been trending downwards

Historical stock levels of copper and nickel at major metals exchanges, 2015-2024

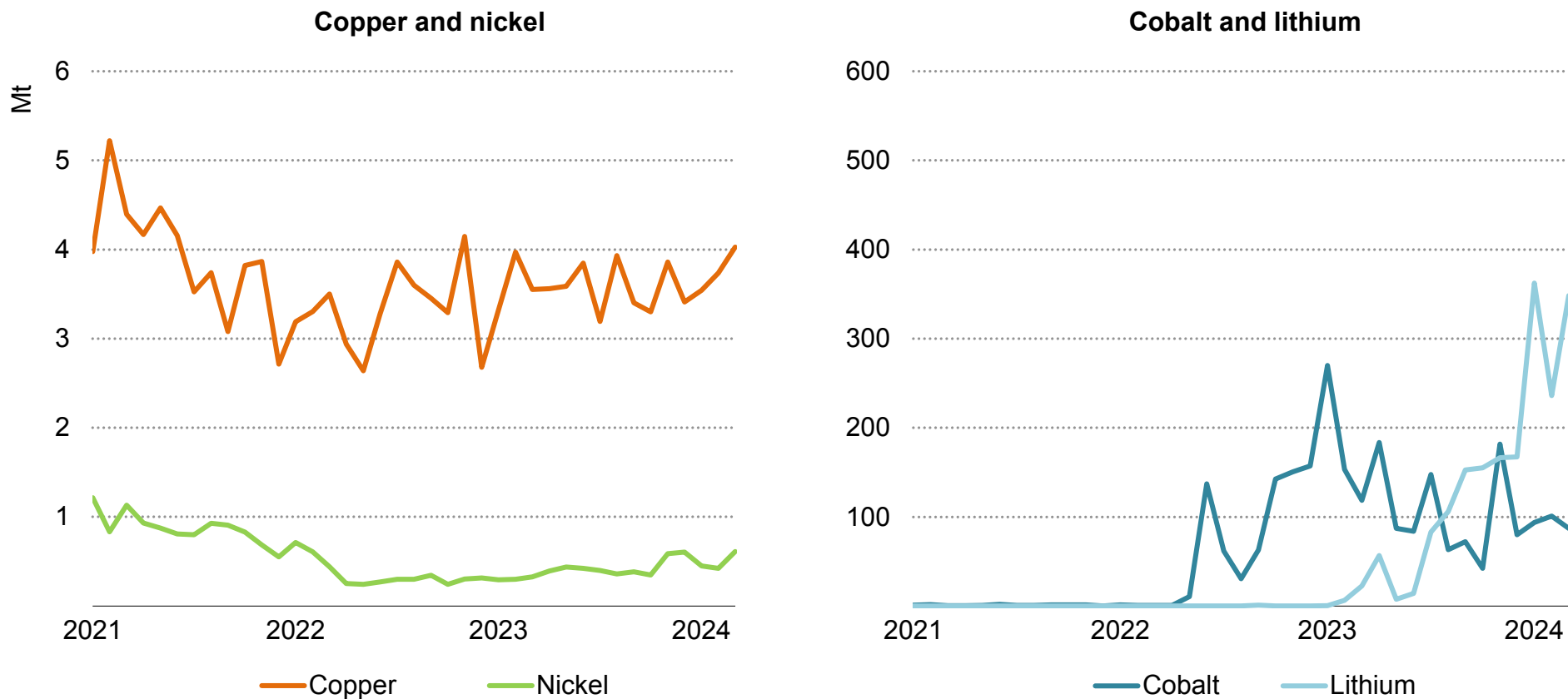


IEA. CC BY 4.0.

Notes: CME = Chicago Mercantile Exchange. Copper (LME, SHFE, CME); nickel (LME, SHFE). Metals stock is an aggregate volume of deliverables and on warrant. Source: IEA analysis based on Bloomberg.

## Trading volumes for copper and nickel have been declining, while those for cobalt and lithium rise but from much lower levels

Daily trade volume for key battery metals at major exchanges



IEA. CC BY 4.0.

Notes: Trading liquidity indicates monthly average of daily traded volumes in major metal exchanges. Copper (LME, SHFE, CME); nickel (LME, SHFE); cobalt (LME, CME); lithium (LME, CME).

Source: IEA analysis based on Bloomberg.

## Inventories and trading liquidity at major exchanges remain subdued

Inventories and trading volumes of critical minerals at major metals future exchanges provide an indicator on the liquidity. Copper and nickel have been traded for long and more actively in London Metal Exchange (LME), Shanghai Futures Exchange (SHFE), or Chicago Mercantile Exchange (CME) due to their longstanding consumption in industries. With the rising demand for clean energy technologies, cobalt and lithium have been making notable appearances in major metal exchanges in recent years.

### Stock

With LME and CME stocks combined, copper stocks have been dwindling to historic lows although there has been a recent surge in SHFE stocks. In recent months, copper stock in the SHFE saw the strongest increase since 2020, reflecting China's high imports to fill up the low inventory from last year and meet demand growth in manufacturing. This high level may subside in the near term, however, as consumption picks up with China's stronger-than-expected manufacturing activity and higher business confidence. While visible stocks at exchanges represent only a fraction of total stocks, their decline suggests a tightening market and limited capacity to absorb supply shocks.

Inventories for nickel, despite the SHFE recording a four-year high in recent months, still dwindles from its historical high level in aggregate

terms. The LME saw a rise earlier in 2024 due to the addition of Russian and Chinese nickel. However, [a ban on Russian-origin metal introduced in April 2024](#) may impact this growth going forward.

### Trading volume

Trading volumes of copper and nickel on major metals exchanges indicate them as the most liquid among key energy transition minerals due to their longer history of consumption in industries. Liquidity of nickel has yet to recover from the level prior to the LME's contract suspension in March 2022, which created a ripple effect on the SHFE to also suspend nickel contract for a day.

Cobalt and lithium have seen notable growth in trading volumes in the LME and CME over the last two years as their demand trends upwards. As expected cobalt demand rises, trading activity increased on the CME cobalt contract with producers and consumers responding to the narrative. Lithium contracts soared last year with growing hedging activity from traders and industry after its price dropped in 2023. Growing demand for lithium has led market players to hedge from increasing exposure to the volatile commodities market. However, the trading liquidity of battery metals still lags significantly behind that of other bulk materials, despite recent improvements. As it stands, daily traded volume as a percentage of annual production represents less than 1% for lithium and cobalt.

## Latest policy developments

## Producing countries intensify efforts to secure economic benefits; consumer nations enact significant laws and regulations to ensure an adequate and responsible supply

Laws, regulations, and high-level policies are being reformed and issued globally, given the latest surge in interest for critical minerals projects. From policies included in the 2023 update of the [Critical Minerals Policy Tracker](#), it is clear that producing countries and consumer countries often have different policy objectives. ESG regulations and co-operation agreements are more apparent in developed producer economies and in consumer countries, with some endowed with resources also focusing on financing project development. On the other hand, jurisdictions on the supply side have focused on ensuring economic benefits from their own resources. To boost supply resilience, countries are increasingly working together – both multilaterally and bilaterally – to identify priority projects and strengthen co-operative ties.

### Producer policies

While some producing countries already have high-level critical minerals strategies, such as [Australia](#) and [Canada](#), more critical minerals strategies are now under development, particularly by new market entrants. For example, the [African Minerals Development Centre](#) (ADMC) is developing an [African Green Minerals Strategy](#) which will aim to guide African countries as they consider how to exploit their raw materials. Individual countries are also in the process

of developing strategies, such as [Zambia](#), which is intending to release a critical minerals strategy in 2024.

Some mineral-producing jurisdictions have created public strategic minerals investment funds. In February 2024, [Brazil](#) announced a USD 200 million fund to support both exploration and improvements in ESG practices. In October 2023, [Australia](#) expanded its Critical Minerals Facility with a USD 1.3 billion investment, financing extraction and processing projects. [Canada](#)'s CAD 1.5 billion (Canadian dollars) Strategic Innovation Fund, as part of the CAD 2.8 billion Critical Minerals Strategy, aims to prioritise innovative critical minerals manufacturing, processing and recycling projects.

In Latin America, both Mexico and Chile enacted policies to develop their domestic lithium mining industries. Mexico followed its 2022 [Mining Reform](#) with [legislative amendments in 2023](#) that streamlined the mining permitting process and strengthened environmental and social protections. Pertinent amendments include: (i) cancelling concessions for environmental and safety risks; (ii) creating new mining offenses; (iii) empowering the water authority to reduce the industrial water concession for mining operations to ensure enough water for local consumption; (iv) prohibiting mining operations in protected areas; and (v) placing the liability for mining and metallurgical waste on concession holders.

Chile also followed its 2023 [National Lithium Strategy](#) with an update to its [Mining Royalty Law](#) in 2023. The law established a mining royalty for the exploitation of copper and lithium to distribute economic benefits across the country, along with a legal body to administer it. Included in the law are increases to the tax burden on mining activities specifically for mining operators whose annual sales are predominantly derived from copper and exceed an equivalent value of 50 000 metric tonnes of fine copper, but with a maximum potential tax burden of 45.5% for those with 80 000 metric tonnes and 46.5% for the rest. Revenue from the law (estimated to be [USD 450 million](#)) will be distributed to funds such as: (i) a fund to compensate mining communities that have been directly affected by the negative externalities of mining activities (USD 55 million); (ii) a fund for the most vulnerable communities in the country; and (iii) a fund to leverage productive infrastructure investments in the northern regions.

The United States and European Union have proposed reforms to permitting processes to increase domestic mining production and reduce dependency on imports. The [Permitting Action Plan](#) outlines key actions, including better internal coordination, tracking of review progress, enhancing outreach and providing technical assistance to affected stakeholders. The [Inflation Reduction Act](#) provides funding to various government agencies to hire new personnel and develop tools and guidance [to strengthen and accelerate environmental reviews](#).

Separately, the proposed [Critical Raw Materials Act](#) (CRMA) would allow certain projects to be designated as “strategic” that would have a streamlined permitting process. The act lays out criteria for a project to be designated as “strategic,” including whether the project would be implemented sustainably and responsibly. Besides permitting processes, the CRMA would also create a monitoring mechanism to mitigate the risk of supply chain bottlenecks.

In order to meet the policy goal of increasing the amount of local value addition, some producing countries are turning to export restrictions on raw or unprocessed ores. In 2020, [Indonesia](#) announced that it would restrict the export of unprocessed nickel. While the World Trade Organization (WTO) [ruled against Indonesia’s restrictions](#) following the [European Union’s challenge](#), the lack of a quorum at the WTO Appellate Body has delayed the appeal process indefinitely. In the meantime, Indonesia implemented similar restrictions [on bauxite ore in June 2023](#) and announced restrictions on [copper ore](#) expected to be in force in June 2024. Other countries have adopted or are considering adopting similar measures, including [Namibia](#), which banned the export of lithium ore in mid-2023, and [Zimbabwe](#), which banned raw lithium exports in 2023 to attempt to secure value addition.

Other countries in Asia have enacted export restrictions designed to encourage supply and safeguard national interest. China issued export controls last year, such as the [export control of gallium- and germanium-related items](#) (in force August 2023) and the [export](#)

[control for graphite-related items](#) (in force December 2023), through which businesses are required to seek export licences from the government.

## Consumer policies

At the same time, consumer countries have developed laws and regulations targeting sufficient supplies of responsible critical minerals. This has been particularly true in countries with large downstream manufacturing industries, which rely on a supply of these minerals. Japan announced a [policy on initiatives for ensuring stable supply of critical minerals](#) in 2023, which aims to secure supplies for its battery manufacturing goals and provides subsidies for exploration, feasibility studies, mine development, smelting and research and development to develop supplies. [Korea](#) announced a list of 33 critical minerals and 10 strategic critical minerals, of which the latter will be prioritised to stabilise the supply chain of high-tech industries such as semi-conductors and secondary batteries. The country is also seeking to deepen co-operation with [30 identified resource-rich countries](#) to secure mineral deals.

As a next step to minerals lists, strategic plans have been issued over the last year which focus on specific needs based on countries' priority minerals. Japan released a [Resource Diplomacy Guidance](#), which outlines the country's approach to minerals and producing countries and specifies the priority minerals and countries from which it intends to source.

Some countries also make financing support available for overseas projects through direct equity investments or sovereign wealth funds, such as in [Japan](#), [Saudi Arabia](#) and [China](#). The United Kingdom also pledged [USD 1 million](#) to identify bankable projects in processing and midstream value addition in 14 African countries. In the European Union, [France set up a critical minerals and metals equity fund](#) managed by InfraVia and backed by up to USD 500 million in government funds. The fund will function as a minority shareholder of industrial and mining stakeholders across the value chain, and is focused on securing offtake contracts to support French and European industries, with a commitment to adhere to high social and environmental standards in collaboration with various financing partners.

In the last year, consumer countries have also made significant strides to integrate policies targeting the sourcing of responsibly produced minerals. In the European Union, the [Corporate Sustainability Reporting Directive](#) (CSRD) and the [Corporate Sustainability Due Diligence Directive](#) (CSDDD) enhance corporate accountability regarding ESG performance. The CSRD will make it mandatory for all large European companies and companies listed on EU-regulated markets to report on selected ESG metrics by 1 January 2024. The CSRD is working to release sector-specific requirements, including for the mining sector. Complementary to the CSRD, the CSDDD imposes mandatory human rights and environmental due diligence requirements on large companies, compelling them to identify, prevent, and mitigate adverse impacts in

their operations and entire value chain. This includes obligations for companies to establish and update a climate transition plan aimed at aligning business strategies with the Paris Agreement and the European Union's 2050 climate neutrality target.

## International co-operation

A number of countries work through the [Minerals Security Partnership \(MSP\)](#) to collaboratively strengthen security of supply. In 2024, the MSP [welcomed Estonia](#) as its newest member, bringing participation to 14 countries plus the European Union. This effort is focused on supporting the development of strategic projects. In late 2023 and early 2024, the MSP countries announced progress in raising financing or securing offtake agreements for a number of projects including ones targeting manganese, nickel, and graphite.

There has been a growing trend of countries announcing bilateral or multilateral strategic partnerships focused on critical minerals, some of which integrate strong ESG standards. Recent examples include a Statement of Intent between [Australia and the United Kingdom](#) and [the United Kingdom and South Africa](#) partnership on minerals for future clean energy technologies, Strategic Partnerships between the European Union and [Chile](#), the [Democratic Republic of the Congo](#) and [Zambia](#), and a [memoranda of understanding between Canada and Korea](#). The specific content of these partnerships varies, but they generally are aimed at strengthening bilateral ties and providing vehicles for countries to support individual projects. That said, the

specific impact of individual partnerships depend on how they are implemented, which is difficult to gauge in many cases as [many partnership arrangements are not made public](#).

In the next year, we expect to see more bilateral agreements and strategic partnerships emerge with a focus on either securing or developing critical minerals supplies. The [European Union](#) is looking to expand its network of Sustainable Investment Facilitation Agreements of Free Trade Agreements. Emerging producer countries are also expected to continue signing agreements to boost investment into critical minerals projects in their countries. In 2023, economic ministers from France, Germany, and Italy aligned to [enhance the sustainable supply chain of critical raw materials](#) by setting specific targets for extraction, processing, and recycling, and by expanding the list of strategic materials to include aluminium. They committed to enforcing stringent ESG criteria and established a dedicated working group to ensure effective implementation of these initiatives.

## Recycling policies

Strategic plans have incorporated measures aimed at boosting rates of battery recycling, and 2023 saw a notable uptick in policies aimed at increasing the recycling of clean energy technologies to secure critical minerals from both consumer and producer countries. The European Union's [Critical Raw Materials Act](#) will require member states to identify, adopt and implement measures to improve the



collection and recycling of critical mineral-rich waste, as well as investigate the potential for recovery of critical raw materials from extractive waste in active and historic mining sites. [Norway](#)'s Mineral Strategy, released in June 2023, also includes focus on a circular economy, requiring new mineral projects to present a circular business plan.

Specific measures to increase recycling have come in the form of investment into research and development and waste collection, such as the [United States](#)' USD 192 million of funding for increasing recycling rates and research and development into battery recycling technologies from consumer products. There has also been project-specific funding, with the European Commission providing battery producer [BASF with a USD 110 million grant](#) to support a battery recycling project in Spain.

## Example of harmonisation of ESG standards: Consolidated Mining Standard Initiative

In recent years, there has been a growing chorus of calls for greater harmonisation or convergence of existing ESG standards and sustainability initiatives. Against this backdrop, the International Council on Mining and Metals (ICMM), The Copper Mark, the Mining Association of Canada and the World Gold Council announced in [November 2023](#) that they will seek to consolidate their individual standards into one global responsible mining standard with a multi-stakeholder oversight system. The [collaboration aims](#) to simplify the landscape of standards and sustainability initiatives and drive performance improvements at scale.

The organisations have expressed their expectation that the consolidation process will combine the best attributes of each individual standard and be implementable by any mine operator at site-level with a commitment to mine responsibly, with substantive prescriptive performance requirements, robust independent assurance and a multi-stakeholder governance model. The consolidated standard will cover more than 20 performance areas grouped under Ethical Business Practices, Worker and Social Safeguards, Social Performance, and Environmental Stewardship. The organisations have announced that they will collect input from all interested stakeholders, including affected communities,

Indigenous peoples, civil society organisations, industry, investors, downstream customers and government.

With the proposal expected to go out for public consultation in mid-2024, the goal is to release the standard during 2025. Once finalised and launched, the consolidated mining standard would be expected to be adopted by members of the organisations – around 80 mining companies with 700 operations spanning 60 countries.

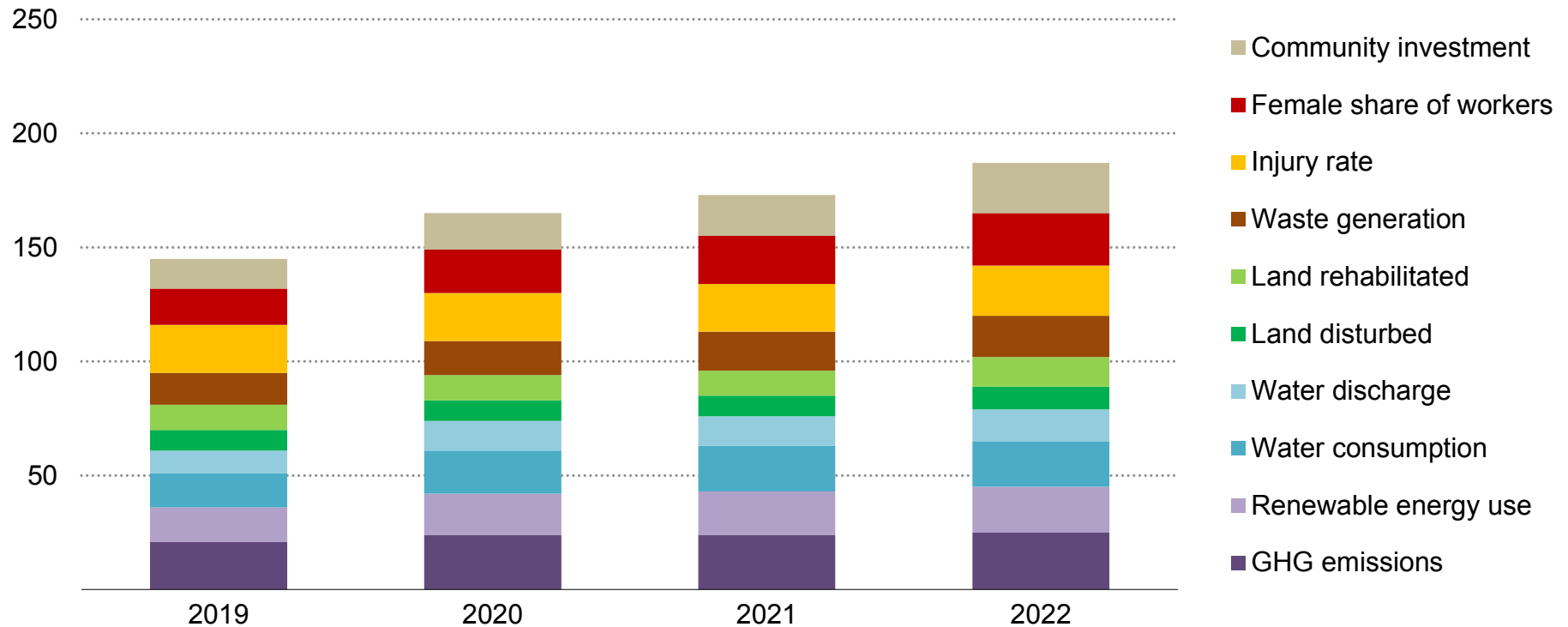
While harmonising standards provisions may facilitate practical application, addressing key issues remains essential. Firstly, ensuring credibility necessitates a robust multi-stakeholder governance model. Secondly, ensuring comparability requires a transparent, uniform reporting structure. Thirdly, harmonised standards must remain aligned with relevant international frameworks and avoid a “lowest common denominator” outcome.

A combined standard may also be a step towards comparable data that governments and civil society organisations can easily track to assess the mining industry’s ESG performance. However, high ESG performance should still be contingent on the jurisdiction of mining operation as well as the importing country.

## ESG performance tracking

## The industry is making progress on ESG reporting

Number of companies with a strong presence in energy transition minerals reporting selected ESG indicators



IEA. CC BY 4.0.

Note: GHG emissions considers reporting on total scope 1 and 2 greenhouse gas emissions; water use considers water consumption. Data from 25 major companies were reviewed, so the maximum value for each of the ten selected ESG indicators and commitments is 25, with a potential overall total of 250.  
 Source: IEA analysis based on the latest sustainability reports of Albemarle, Allkem and Livent (Arcadium Lithium), Anglo American, BHP, CMOC Group, Codelco, Eramet, First Quantum, Freeport Mc-MoRan, Ganfeng Lithium, Glencore, IGO, KGHM, Mineral Resources, NorNickel, Pilbara Minerals, Rio Tinto, South32, Southern Copper, SQM, Teck Resources, Tianqi Lithium, Vale, Zhejiang Huayou, and Zijin Mining Group Co. Ltd.

## Current company reporting does not allow for an industry-wide assessment of progress towards sustainable and responsible supply, but ESG performance is slowly becoming clearer

Critical mineral supply chains cannot be truly secure, reliable and resilient unless they are also sustainable and responsible. The mining industry does not have the best track record managing ESG impacts, but many players are aiming to change that. Our assessment of company progress across various ESG dimensions – based on the public sustainability reports and commitments published by 25 major companies that have a strong presence in critical minerals supply chains – shows progress in reporting and growing commitments.

All of these companies report efforts to improve their ESG performance, but goals vary starkly. About 20 have pledged to achieve net zero emissions by or before 2050, with the remaining yet to establish a firm long-term emissions target. Most net zero targets apply only to emissions from direct operations (scope 1) or purchased energy and heat (scope 2), leaving out other emissions from the industry's value chains (scope 3). Around five companies have established targets to reduce absolute emissions by 35% or more by 2030 or earlier. Many companies refer to a reduction in emissions intensities to 2030 or have established reduction targets only for 2035. Several industry players have also committed to other ESG goals, such as causing no net loss of biodiversity or limiting the amount of freshwater used in mining.

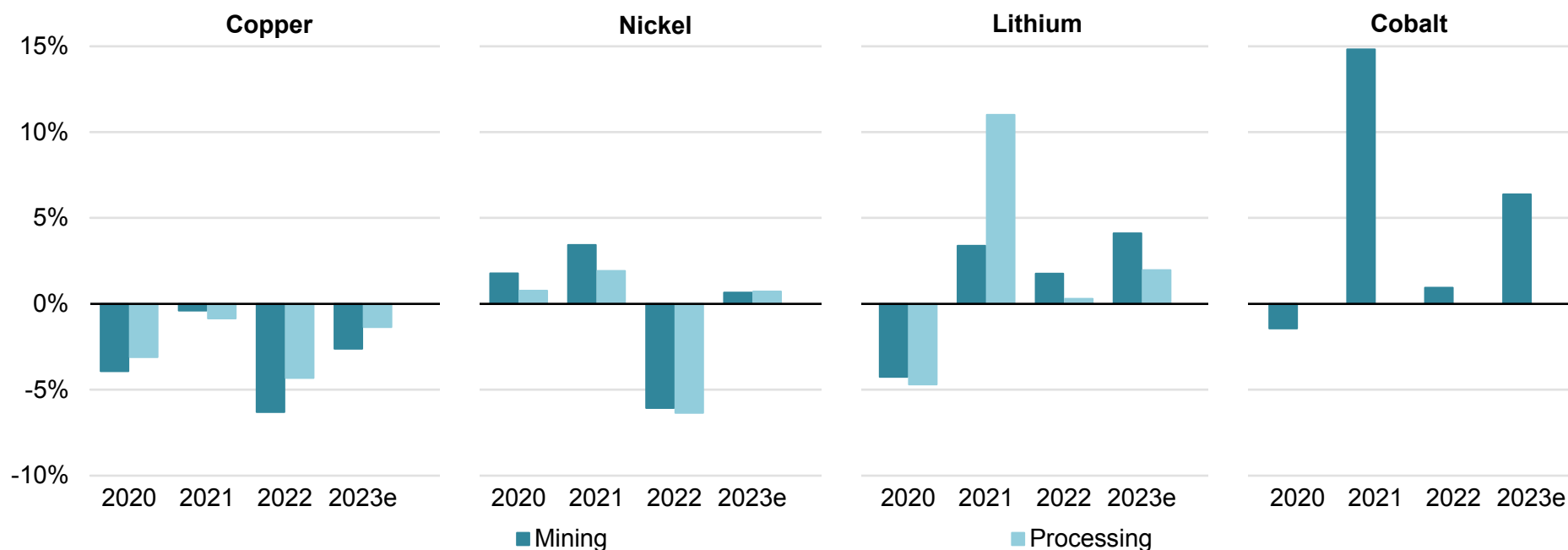
These commitments are being followed by better reporting of ESG practices. Our assessment revealed an increase in the availability of data for the latest years, indicating the industry is putting more effort into tracking its performance. The number of companies reporting investment in communities, female share of workers and water discharge increased by 40% or more during this period. All players now report GHG emissions and nearly 90% report share of female workers, injury rates and community investment.

Nevertheless, an industry-wide assessment of progress on ESG still faces many challenges. Only around ten companies published data on land area disturbed and rehabilitated, and less than five reported on involuntary resettlement. Few operators detail risks related to their supply chains, such as potential child labour, or provide clear information on contract disclosure.

ESG reporting varies substantially in both consistency and breadth. Most companies aggregate their reported data in some form or another, often at the company level, making it difficult to compare performance for specific minerals or regions. Less than five companies disclosed site-level data consistently in their reports; positive examples include Aracidium Lithium, Codelco, and First Quantum. Units and scope of reporting also vary, sometimes even within the same report (e.g. for different operational units).

## Climate pledges are driving decarbonisation measures, particularly in copper supply, but overall performance on emissions is still far from showing robust reductions

Annual changes in GHG intensities for selected minerals



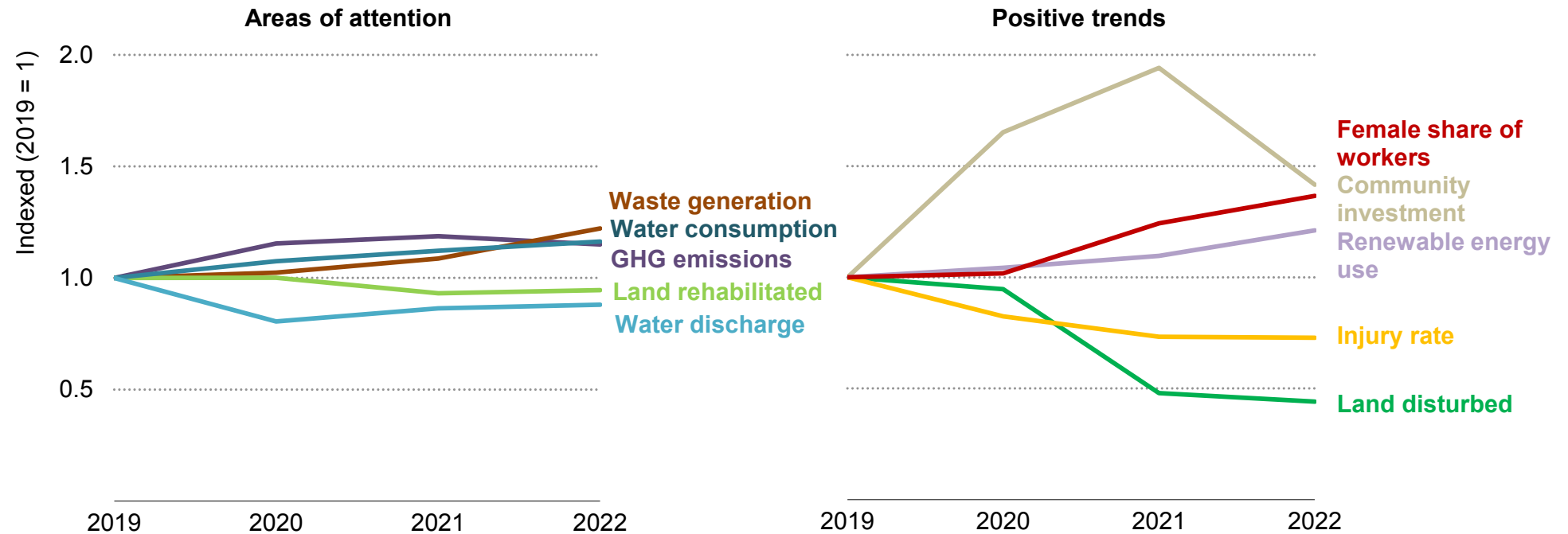
IEA. CC BY 4.0.

Notes: 2023e = estimated values for 2023. Mining covers scope 1 and 2 greenhouse gas emissions intensity (measured in tonnes of CO<sub>2</sub>-equivalent per tonne of mineral). Processing covers scope 1, 2 and 3 greenhouse gas emissions intensities, usually up to refined metal or first saleable product. No data available for cobalt processing.

Source: Data provided by Skarn Associates.

## Sustainability reporting paints a mixed ESG picture, with substantial room for improvement

Selected ESG indicators, 2019-2022



IEA. CC BY 4.0.

Notes: Aggregated data for 25 major companies that have a strong presence in critical minerals supply chain. Considers reported data for all operations. Indicators are calculated per tonne of mineral produced – except for injury rate, water recycling and female share of workers – which reflect the weighted average by production.

Source: IEA analysis based on the latest sustainability reports of Albemarle, Alkerm and Livent (Arcadium Lithium), Anglo American, BHP, CMOC Group, Codelco, Eramet, First Quantum, Freeport-McMoRan, Ganfeng Lithium, Glencore, IGO, KGHM, Mineral Resources, NorNickel, Pilbara Minerals, Rio Tinto, South32, Southern Copper, SQM, Teck Resources, Tianqi Lithium, Vale, Zhejiang Huayou, and Zijin Mining Group Co. Ltd.

## Key ESG challenges and trends

The sustainable and responsible supply of critical minerals depends on a myriad of interrelated practices, from water stewardship to emissions management, engaging with communities and ensuring safe labour standards, a fair share of benefits, protecting biodiversity, reducing waste, and much more. The industry is making progress on several of these fronts. From 2019 to 2022, reported injury rates decreased by nearly 30%, investments in communities surged from USD 0.3 billion to USD 1 billion, and the average share of female workers went from just over 15% to 20%. Data are more sparse for other indicators, but available information suggests improvements in the amount of waste being recovered through reprocessing and reuse and the share of water that is being recycled or re-used in industry facilities. These positive trends do not hold for all companies, but reflect widespread industry efforts.

On the other hand, there are many areas where progress has been limited and some even show negative trends. The amount of waste generated per unit of mineral produced increased by over 20% from 2019 to 2022, potentially due to the development of lower-grade resources. Reported water consumption increased by around 25% during this period even in the face of high supply risks related to droughts for copper and other minerals. Similarly, indicators related to land rehabilitation, effluent discharge and GHG emissions did not exhibit visible improvements despite growing ESG commitments.

Voluntary sustainability standards can help actors improve performance and earn ESG credentials. These include the [ICMM's Mining Principles](#) and performance expectations, the [Initiative for Responsible Mining Assurance's](#) Standard for Responsible Mining, Canada's [Towards Sustainable Mining](#), the [Responsible Minerals Initiative](#) and the [Copper Mark's](#) Risk Readiness Assessment Criteria Guide. While these standards can all lead to increased transparency and sustainability performance, there are [major differences](#) between the overall stringency of requirements, the scope of their application, the approach to compliance and reporting, uptake, and in oversight and assurance systems. Greater transparency, due diligence, harmonised approaches to credibility and [appropriate incentives](#) are needed to untap their full potential.

Material traceability services are also on the rise. This involves working with suppliers to track sources and related impacts up to the point of incorporation into an end product. It can allow an assessment of risks and ESG performance along the supply chain, contributing to increased mineral security. Policymakers and companies, however, should be aware of the limitations of end-to-end product traceability. Due to the nature of both aggregation and blending in mineral supply chains, particularly at the smelting and refinery stage, traceability is not always possible or practical. Traceability mechanisms can be paired with a risk mitigation approach for better ESG due diligence.



---

## 2. Demand and supply outlook for critical minerals

---

## Introduction

The world is on a journey towards achieving net zero emissions, and has declared its ambition to limit global warming to 1.5 °C, which would mean completing this journey already by 2050. Whichever pathway this journey eventually takes, it will require a massive expansion of clean energy technology deployment, along with reliable supplies of critical minerals. While short-term market dynamics are crucial, medium- to long-term perspectives on critical minerals demand and supply are equally important to ensure that clean energy transitions are not hindered by supply chain bottlenecks. There are numerous questions that need to be addressed. How fast might demand for critical minerals grow under different assumptions about the strength of climate action? Can we ensure sufficient volumes of critical minerals to support the acceleration of energy transitions? What are the key risk areas that policymakers need to monitor, and how do prospects vary by mineral? Where are today's project developments leading us in 2030 and beyond, in terms of diversified supplies? What role do environmental, social, and governance (ESG) considerations play in shaping future market developments?

This chapter addresses these crucial questions by providing a comprehensive outlook for demand and supply for key energy transition minerals, namely copper, lithium, nickel, cobalt, graphite and rare earth elements. Additionally, we also briefly discuss key

issues around aluminium, manganese, silicon, phosphate and platinum group metals (PGMs).

Demand projections encompass both clean energy applications and other uses, focusing on the three IEA scenarios – the Stated Policies Scenario (STEPS), the Announced Pledges Scenario (APS) and the Net Zero Emissions by 2050 (NZE) Scenario – with a particular focus on the latter two climate-driven scenarios in which national and/or global climate goals are achieved (see “Introduction” for scenario descriptions). More details on the methodology can be found in the Annex.

Supply projections are based on a detailed review of all announced projects. We have constructed two supply scenarios – a base case and a high production case. The **base case** includes production from existing assets and those under construction, along with projects that have a high chance of moving ahead as they have obtained all necessary permits, secured financing, and/or established offtake contracts. The **high production case** additionally considers projects at a reasonably advanced stage of development, seeking financing and/or permits. In many instances, these projects are in the process of conducting feasibility studies, and in some cases these assessments are already complete.

Neither case considers projects that are in very early stages of development, or includes theoretical projects for which resources might be adequate but which have not been proposed. For these reasons, our focus on the supply side is on the period to 2040.

Based on these two supply scenarios, we assess how today's geographical concentration evolves over time, for both mining and refining, and how expected supply compares with primary supply requirements in climate-driven scenarios (total demand net of expected contributions from secondary supply and reuse). In some cases, we highlight potential gaps between expected supplies and material requirements in climate-driven scenarios.

We do not attempt to close these gaps by introducing additional projects beyond those already underway or being considered. Climate-driven scenarios, the NZE Scenario in particular, reflect many demand-side measures such as higher recycling rates, some behavioural changes (e.g. wider use of public transport in relation to private transport, policies to promote optimal sizing of cars), but we recognise that there is a possibility of additional demand-side measures or technological innovation which could contribute to reducing demand further.

The aim of the exercise is to provide a framework for assessing progress towards achieving global energy security and climate goals and risks that may arise along the way.

There remain considerable uncertainties over how market balances evolve in practice. On the demand side, it should be noted that the world is not yet on track for the outcomes in the APS or the NZE Scenario; doing so will require significant additional efforts by policymakers and industries alike.

Where gaps are identified between future demand and supply, these may potentially be closed by developing additional projects, scaling up recycling further, and promoting a range of material efficiency measures beyond what are already assumed. The results should not be interpreted to mean that energy transition goals are unattainable due to material constraints.

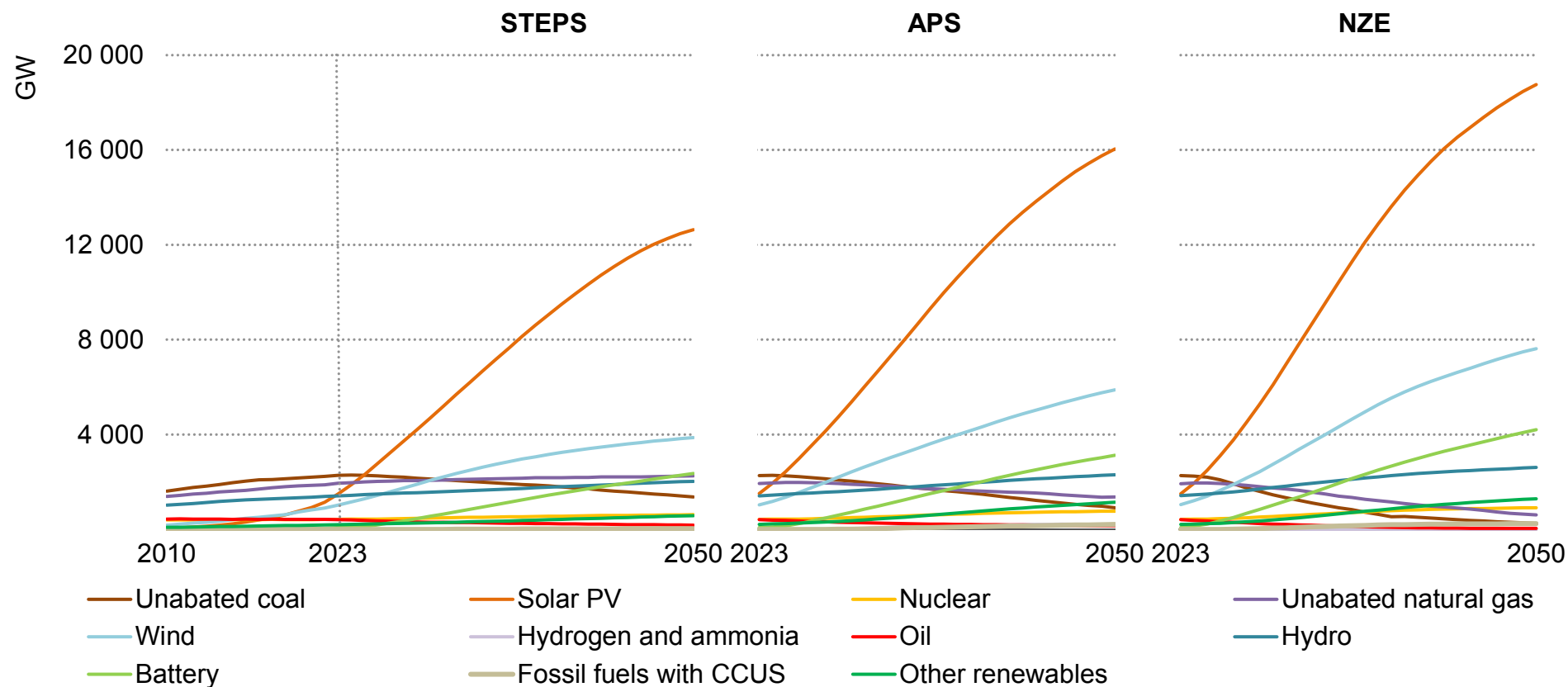
This chapter starts a brief review of projected mineral demand in the clean energy sector and presents overall findings of the detailed outlook for key energy transition minerals. Each mineral section then presents demand and supply projection results and discusses key issues underpinning long-term market developments.

The analysis in this chapter is complemented by the assessment in Chapter 3, which provides structured “clean energy transitions risk assessments” across four major dimensions – supply risks, geopolitical risks, barriers to respond to supply disruptions, and exposure to ESG and climate risks. These assessments aim to help policymakers identify potential areas of weakness for each material in supporting their energy transition goals.

## Mineral demand for clean energy technologies

## Solar PV and wind capacity surge ahead, moving well beyond any other source; renewables account for the majority of capacity additions in every region in all scenarios

Global installed electricity capacity by source and scenario

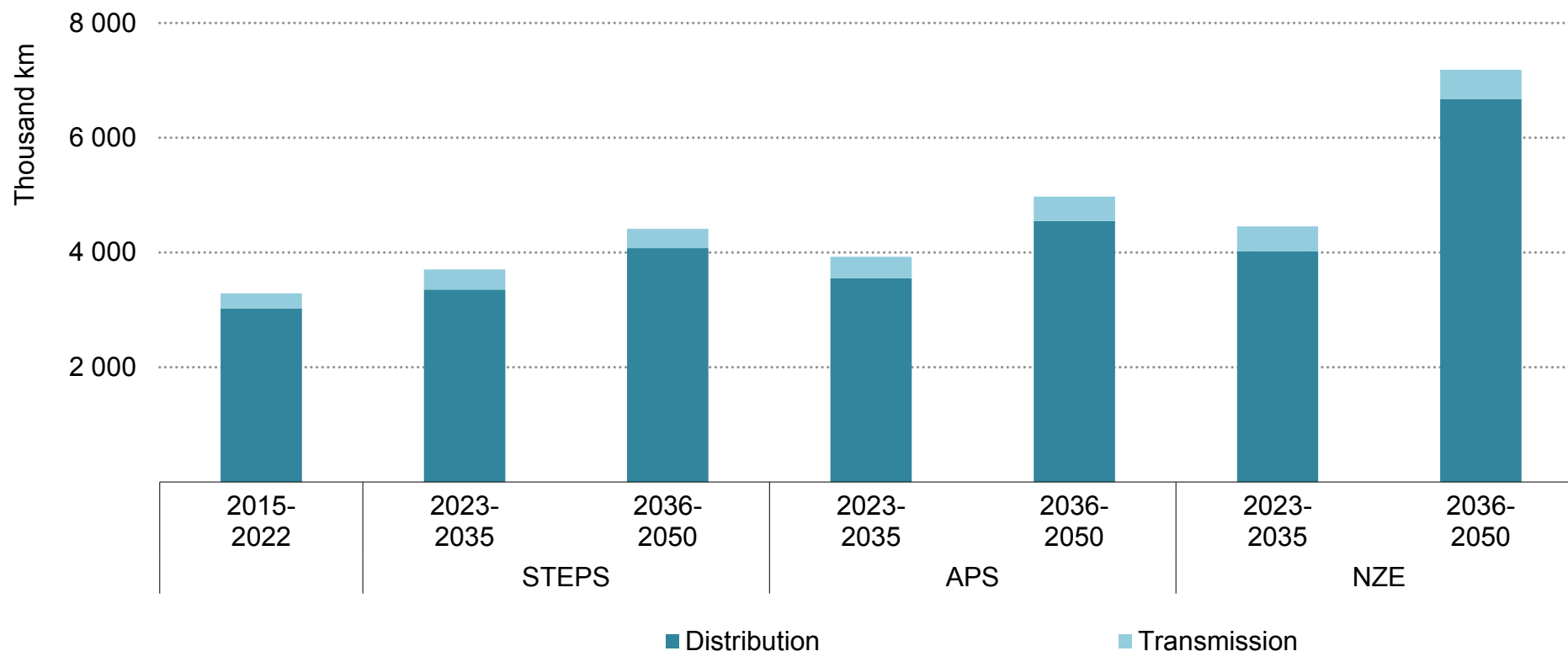


IEA. CC BY 4.0.

Note: CCUS = carbon capture, utilisation and storage.

## The acceleration of renewable energy deployment necessitates a substantial expansion of transmission and distribution networks, pushing up demand for copper and aluminium

Average annual grid line additions by scenario



IEA. CC BY 4.0.

Note: Includes both new additions and replacements.

## Rising deployment of renewables and grids is set to raise demand for critical minerals

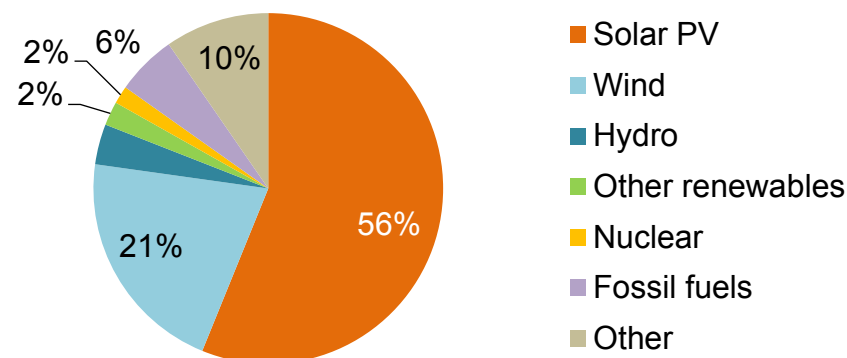
The growth of power generation capacity from low-emissions sources accelerates in all three scenarios. Renewables account for the majority of capacity additions in every region over the outlook period. By far, wind and solar PV are the largest contributors to this development, and total installed solar PV capacity in particular far outstrips that of any other source in all scenarios.

By 2026, solar PV becomes the largest contributor to installed electrical capacity in the STEPS, followed by wind. This growth trajectory would see global renewable capacity increase to 2.5 times its current level by 2030, a major expansion but one that falls short of the tripling goal agreed at COP28. Government actions to facilitate grid connections, and resolve permitting, policy and financing issues, are needed to accelerate growth. In the APS, low-emissions power sources account for almost 80% of total power capacity additions in 2030, with solar PV making up 55% and wind 20%. Annual solar PV and wind capacity additions grow by two times to 2050 in the APS and by over two and a half times in the NZE Scenario.

The acceleration of renewable energy deployment calls for modernising distribution grids and establishing new transmission corridors to connect renewable resources that are far from demand centres such as cities and industrial areas. Around 3 000 GW of renewable power projects are [waiting in grid connection queues](#) – equivalent to five times the amount of solar PV and wind capacity

added in 2022. Due to aged infrastructure and a high share of variable renewables in the system across the globe, reaching national goals also means adding or refurbishing a total of [over 80 million km of grids](#) by 2040, the equivalent of the entire existing global grid. This would underpin significant growth of copper and aluminium demand for cables. Grid investment growth in the past decade has occurred mainly in the People’s Republic of China (hereafter “China”) and advanced economies. China alone accounted for over one-third of the world’s transmission grid expansion in the past decade, connecting, among other places, the eastern load centres to the renewable energy-rich provinces.

Share of cumulative power capacity addition by source in the APS, 2024-2030

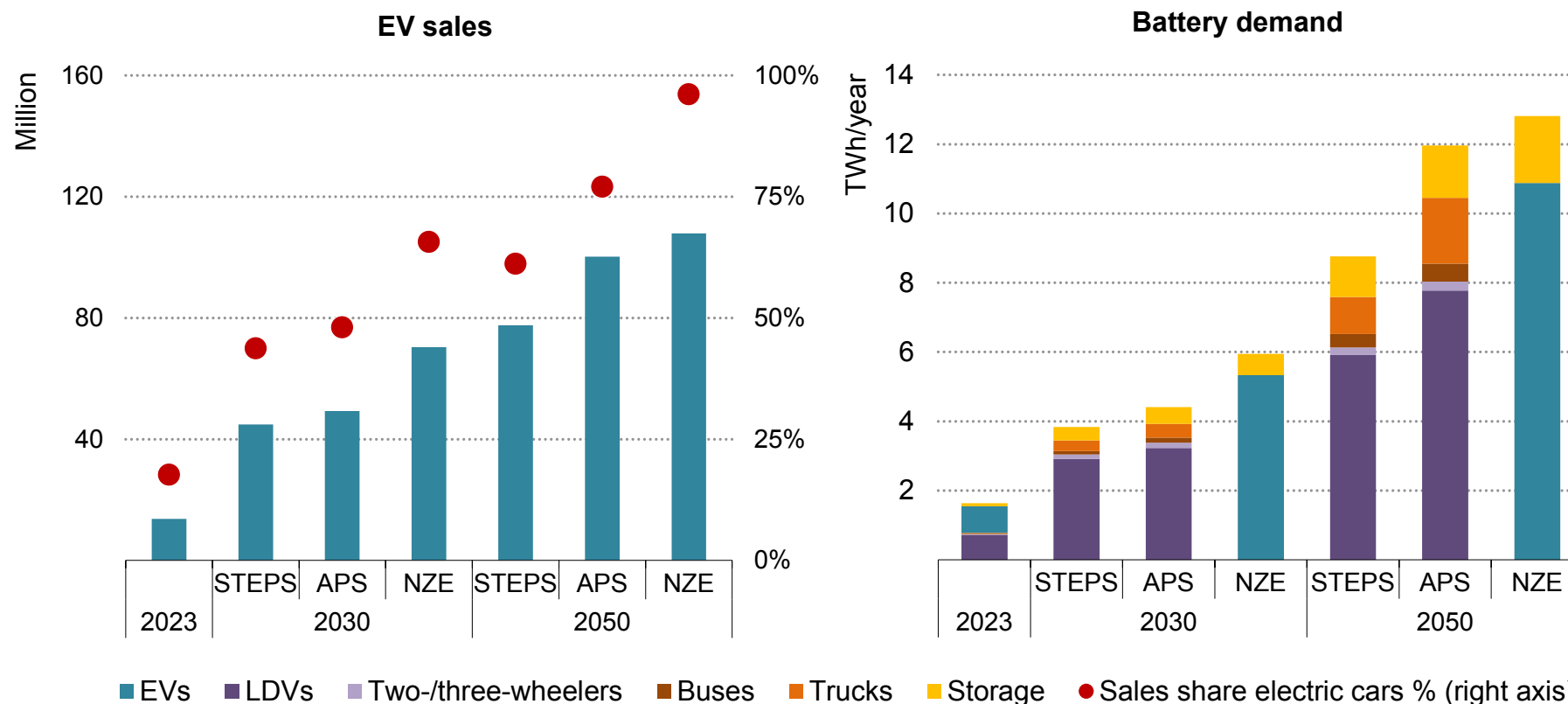


IEA. CC BY 4.0.

Note: Other include batteries, hydrogen and ammonia.

## Battery demand increases fivefold to 2030 and fourteen-fold to 2050 to meet climate pledges driven by EV sales and growth in deployment of electric trucks

EV sales and battery demand growth by scenario

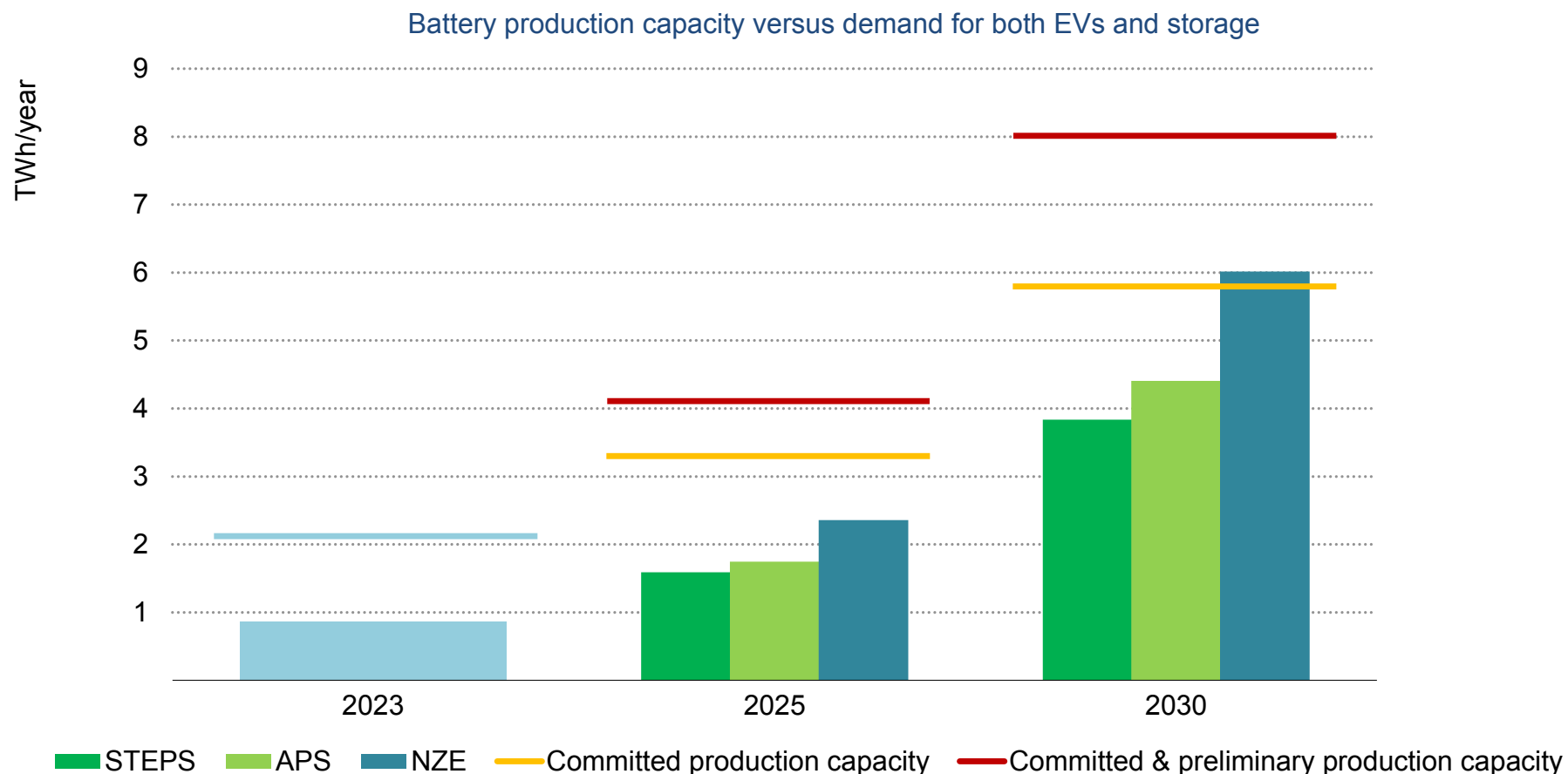


IEA. CC BY 4.0.

Notes: EV = electric vehicle; LDV = light-duty vehicle. EV sales numbers exclude two-/three-wheelers. EV battery demand in the NZE Scenario includes all modes.



## Manufacturing capacity for batteries is already running ahead of projected demand



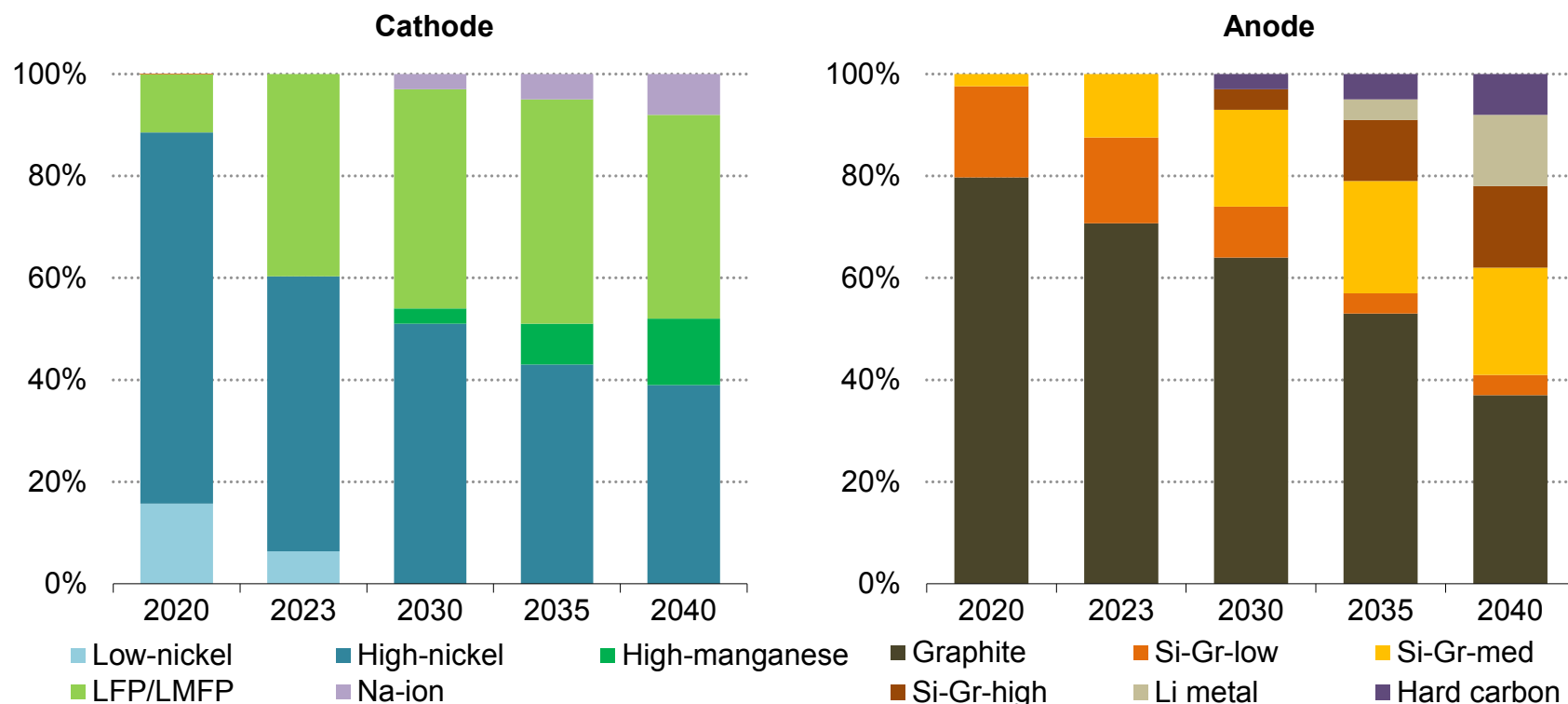
IEA. CC BY 4.0.

Notes: Demand and capacity include both EVs and storage. Committed refers to current capacity and gigafactories that have reached a final investment decision and are starting or have already started construction, and preliminary refers to gigafactories that have been announced but are not yet being built. Preliminary and committed production capacity assumes a utilisation rate of 85%.

Sources: IEA analysis based on BloombergNEF and Benchmark Mineral Intelligence.

## LFP cathodes continue growing in share, and manganese-rich chemistries are set to play a bigger role, while silicon doping of graphite anodes increases significantly

Electric car battery chemistry share development



IEA. CC BY 4.0.

Notes: LFP = lithium iron phosphate; LMFP = lithium manganese iron phosphate; Na-ion = sodium-ion; NMC = lithium nickel manganese cobalt oxide. NCA = lithium nickel cobalt aluminium oxide. NMCA = lithium nickel manganese cobalt aluminium oxide. LNO = lithium nickel oxide. Low-nickel includes: NMC333 and NMC532. High-nickel includes: NMC622, NMC721, NMC811, NCA, NMCA, LNO. High-manganese includes lithium nickel manganese oxide (LNMO) and lithium-manganese-rich NMC (LMR-NMC). Si-Gr = silicon-doped graphite. Si-Gr-low refers to 5% silicon content, Si-Gr-med = 5-50% and Si-Gr-high > 50%.

## The adoption of EVs and battery storage is set to accelerate rapidly over the coming decades, driving a fourteen-fold increase in battery demand by 2050 in the APS

With ongoing policy support, improving economics, and an expanding number of models available, global EV sales (excluding two-/three-wheelers) are set to grow strongly, more than tripling by 2030 in the STEPS and APS to almost 45 million and 50 million vehicles, respectively, and increasing more than fivefold to 70 million in the NZE Scenario. This is primarily driven by the sales of electric cars, where a global sales share of 18% in 2023 increases to 45% in the STEPS and almost 50% in the APS by 2030, while reaching two-thirds of all sales in the NZE Scenario. This rapid sales growth continues to accelerate to 2050 with sales growing more than fivefold in the STEPS and over sevenfold in the APS. Sales grow almost eightfold in the NZE Scenario by 2050 reaching 110 million vehicles. The share of electric cars in total car sales continues to surge, reaching 60% in the STEPS, over three-quarters in the APS and over 95% in the NZE Scenario by 2050.

This exceptional growth in EV sales drives a dramatic growth in battery demand. From almost 1 TWh in 2023, demand more than quadruples by 2030 in the STEPS to 3.8 TWh and reaches 4.4 TWh in the APS, while increasing sevenfold to 6 TWh by 2030 in the NZE Scenario. The growth rates in battery demand outpace growth in EV sales due to additional demand growth of battery storage, which surpasses the rates of demand growth for light-duty vehicles in both the STEPS and APS by 2030 and by 2050. There is also significant

growth in battery demand for electric trucks, which increases eighteen-fold in the STEPS and twenty-three-fold in the APS by 2030. In the NZE Scenario, EV battery demand grows sevenfold. By 2050 global battery demand reaches 9 TWh in the STEPS and 12 TWh in the APS, growing tenfold and fourteen-fold from 2023 demand, respectively. In the APS, demand from electric trucks becomes larger than global storage demand in 2050. In the NZE Scenario demand reaches 13 TWh, a fifteen-fold increase.

### Manufacturing capacity

In 2023 battery production capacity (at 85% utilisation rates) is two and half times battery demand. Looking forward, our analysis of committed production capacity includes gigafactories that are starting or under construction or have reached final investment decision. In 2025 committed production is double both STEPS and APS demand, while being 40% higher than demand in the NZE Scenario. By 2030, rapid demand growth narrows this gap, such that committed production is only 30% higher than APS demand and close to the requirements in the NZE Scenario. However, if preliminary announcements are included, meaning gigafactories that have been announced but not yet reached final investment decision, anticipated manufacturing capacity takes another leap ahead. When preliminary announcements are included, production capacity exceeds APS

demand by 80% and is 40% greater than demand in the NZE Scenario. Of all new committed capacity additions from 2023, 55% are in China by 2030. These projections imply intense price competition among producers, with significant implications for global battery supply chains.

### Chemistry development

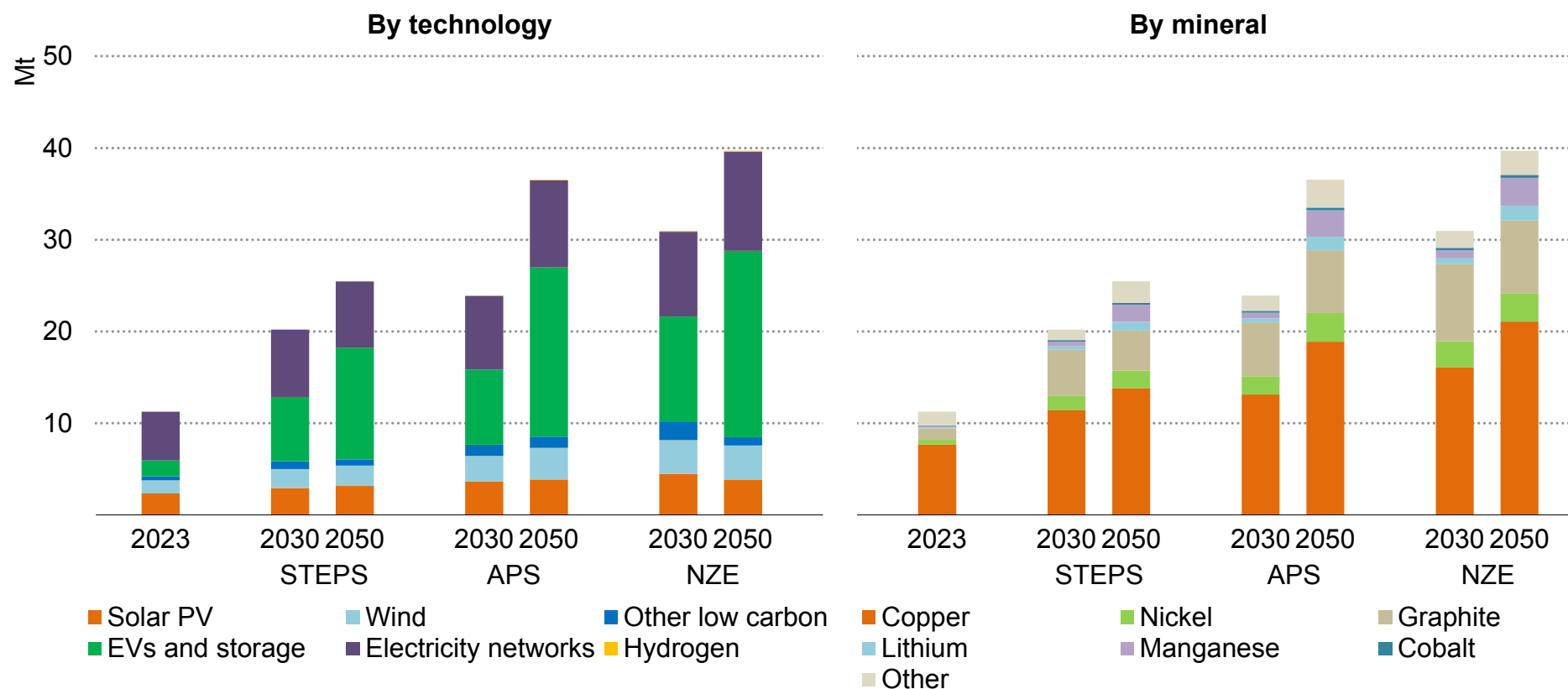
In terms of electric car cathode chemistries, lithium iron phosphate (LFP) and lithium manganese iron phosphate (LMFP) are set to become the leading chemistries by share from 2035. The LFP variant LMFP looks likely to be increasingly utilised, taking share from LFP and also from the high-nickel chemistries due to its higher energy density than conventional LFP. Low-nickel high-cobalt chemistries such as the nickel manganese cobalt (NMC) 333 are assumed to be phased out by 2030, with the trend of reducing cobalt content in favour of higher nickel contents continuing. Manganese-rich chemistries including lithium-manganese-rich NMC (LMR-NMC) and lithium nickel manganese oxide (LNMO) start to take increasing shares of the high-nickel and LFP market. LNMO are anticipated to take a small share of the mid-range market, being higher energy density than LFP but not near the levels of the high-nickel chemistries. LMR-NMC enables significantly higher energy densities due to its ability to store higher concentrations of lithium, and therefore is expected to take increasing shares of the long-range high-energy-density market at the expense of high-nickel chemistries. High-nickel chemistries continue to play a major role in

the long-range market with higher nickel contents being utilised including the 96% Ni NMC. However, their share of the EV market is expected to decrease from 55% in 2023 to around 40% in 2040, as manganese-rich chemistries and LFP/LMFP continue to displace them. This is a remarkable change from 2020 when high-nickel chemistries dominated the EV battery market. Finally, sodium-ion batteries are anticipated to play an increasingly significant role after 2030, reaching a global market share of almost 10% in 2040, displacing some LFP in the low-range EV market, particularly if lithium prices rise and if there are phosphorous supply issues for LFP. Our analysis suggest that LFP remains the preferred solution for the battery storage market, with a growing longer-term role for sodium-ion.

Looking at anodes, current trends indicate a growing share of silicon-doped graphite anodes and a shift towards higher silicon contents. This trend continues to displace conventional graphite anodes, eventually reaching high silicon contents above 50% and ultimately silicon anodes for long-range premium markets. Lithium metal anodes are anticipated to eventually play a greater role after 2035 with ASSBs, hybrid liquid-solid-state batteries and advanced liquid electrolytes, starting with the most premium long-range vehicles. However, the speed of deployment is highly uncertain and dependent on considerable technical and scaling challenges to be solved. Finally, with the increasing adoption of sodium-ion batteries, hard carbon, anode material for sodium-ion batteries takes a greater share of the electric car anode market.

## Mineral demand for clean energy technologies doubles between today and 2030 in the STEPS and APS and grows by almost three times in the NZE Scenario

Mineral requirements for clean energy technologies by scenario



IEA. CC BY 4.0.

Note: Includes most of the minerals used in various clean energy technologies but does not include steel and aluminium.

## The energy transition continues to drive mineral demand in all scenarios

The accelerating pace of energy transitions is set to significantly boost mineral demand across all the three scenarios. In the STEPS, demand doubles to 2030 with continued growth thereafter. In the APS, demand more than doubles by 2030 and triples by 2050. In the NZE Scenario, the swifter adoption of clean energy technologies implies an even more pronounced surge in demand for critical minerals, nearly tripling by 2030 and growing to over 3.5 times the current levels by 2050, reaching nearly 40 Mt.

Our latest mineral demand projections have been updated from those in the [Critical Minerals Market Review 2023](#), reflecting several new technological and policy developments:

- Projected demand in the STEPS has been revised upwards due to faster clean energy deployments, notably in solar PV installations and EV sales, driven by strengthened policy measures and improved economics for these technologies.
- Although they face some short-term headwinds, EV sales have also been revised slightly upwards in the long-term, driven by improving economics and policy efforts in major markets.
- LFP shares have increased considerably over the last years, and its rapidly growing global share has been reflected in the updated chemistry projections. Manganese-based chemistries also take a

larger share in the future in the revised assumptions. Alongside assessments of other emerging technologies such as sodium-ion batteries, solid-state batteries and silicon-based anodes, near- and long-term battery chemistry assumptions have been adjusted, affecting demand projections for nickel, cobalt, manganese, and other materials.

- The projected deployment of battery storage has been revised upward to account for the rapid pace of deployment in recent years and the increasing need for power system flexibility, resulting in increased demand for battery metals, lithium in particular.
- Material intensity assumptions have been updated based on the latest literature review and industry consultations.
- Graphite material requirements have been revised upwards in all scenarios, reflecting a more detailed representation of the amount of silicon required in anodes.

Each factor influences projected mineral requirements differently, resulting in slightly higher aggregated mineral demand across all three scenarios by 2050 compared with the previous outlook, with the STEPS seeing the largest overall upwards revision.

Demand for each mineral is affected in different ways from these revisions and updates. Nickel sees the largest downwards revisions in both the APS and the NZE Scenario, largely due to the increased prominence of LFP, whereas graphite sees large upwards revisions in all scenarios.

However, despite these adjustments in projected mineral demand, demand in climate-driven scenarios remains multiple times higher than current levels, underscoring the pivotal role of clean energy technologies in propelling total mineral demand growth. From copper to lithium and to cobalt, clean energy technologies emerge as the predominant consuming segment, significantly elevating their share in total demand compared with present levels.

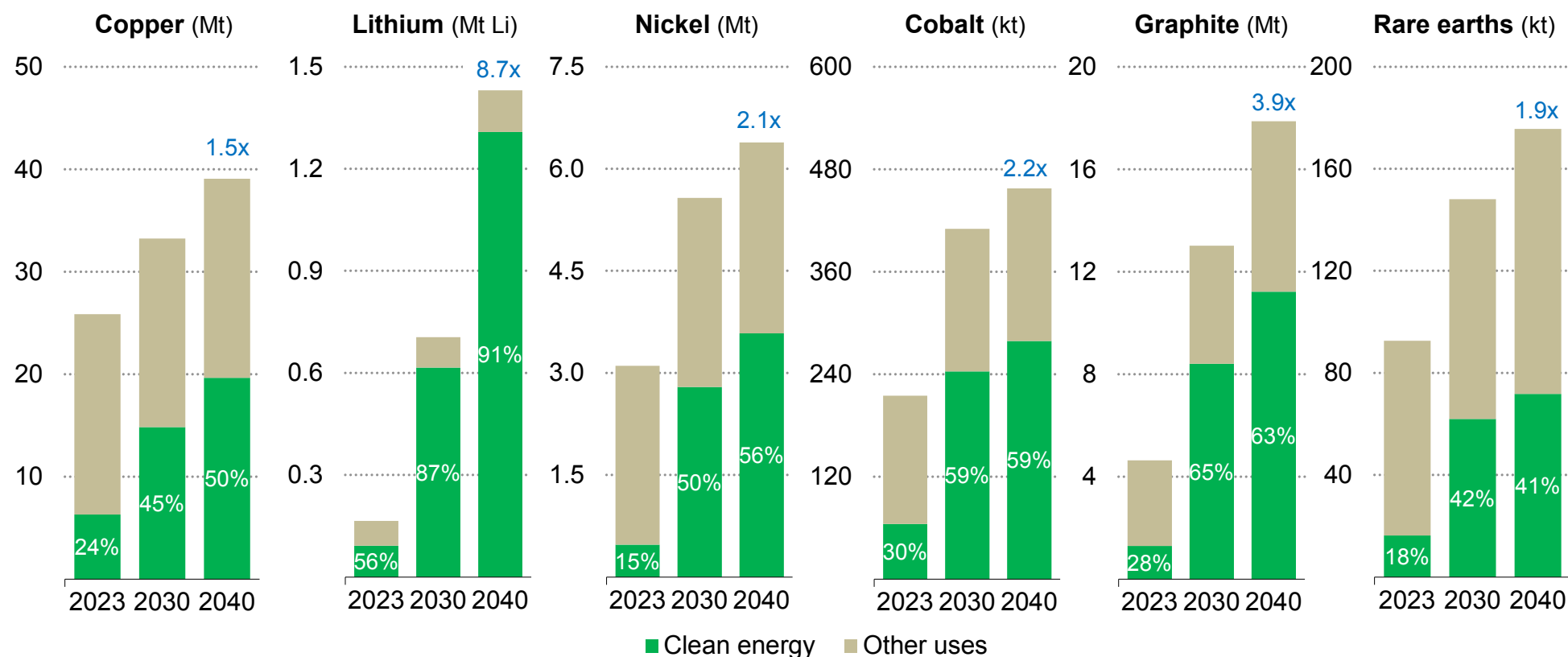
It is important to note that demand projections are subject to large variations, influenced not only by broader policy considerations (reflected in our energy scenarios) but also by technology costs and innovations, as well as behavioural factors. To address this complexity, the IEA has developed more than ten alternative cases to assess the impacts of different consumer preferences and technology advancements on future mineral requirements. The findings of these cases are available through the updated [IEA Critical Minerals Data Explorer](#), an accompanying online data tool designed to allow users to easily access and navigate the projection results (see Annex).

## Overview of the projections for key energy transition minerals



## Limiting global warming to 1.5 °C, as in the NZE Scenario, means very rapid growth in demand for key minerals

Global critical minerals demand in the NZE Scenario

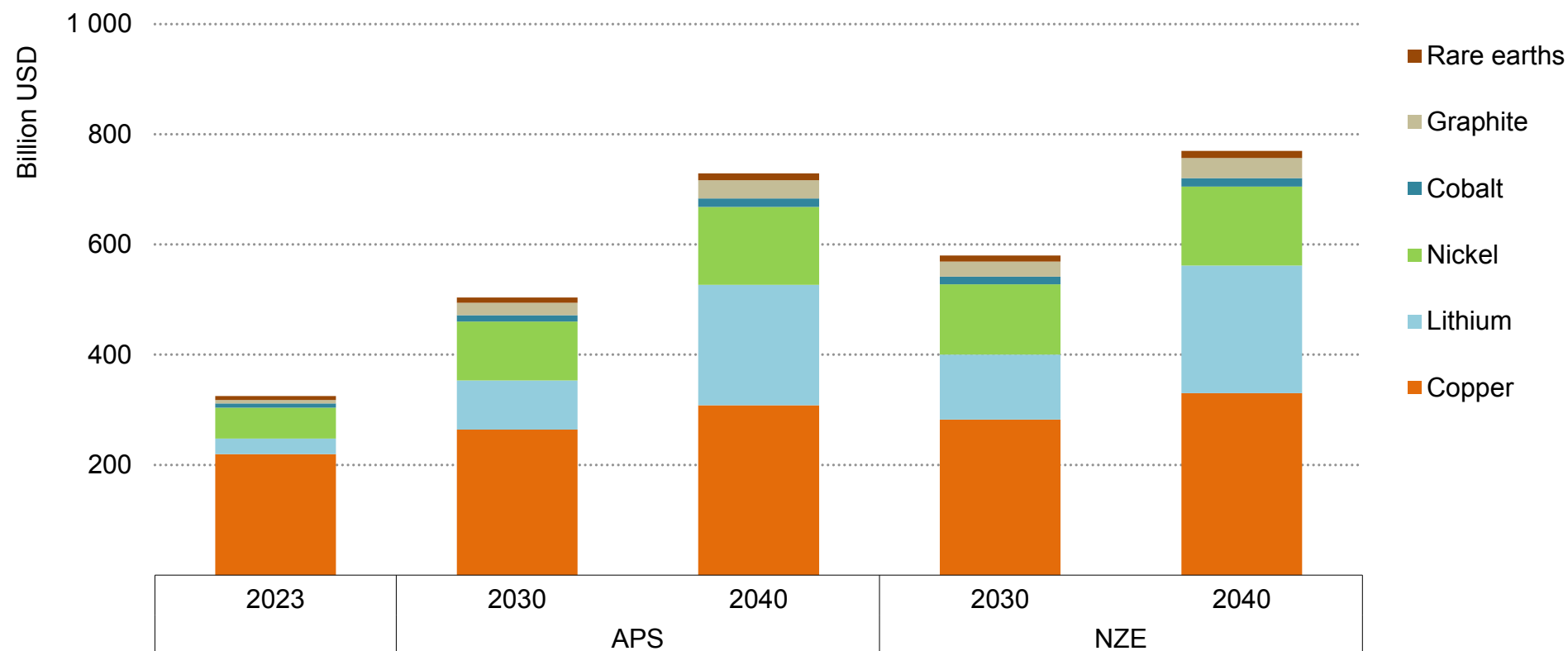


IEA. CC BY 4.0.

Notes: The figures for copper are based on refined copper. Those for rare earth elements are for magnet rare earth elements only. Growth rates (in blue) are between 2023 and 2040.

## The combined market value of key energy transition minerals more than doubles by 2040 in climate-driven scenarios, reaching USD 770 billion in the NZE Scenario

Market value of key energy transition minerals in the APS and the NZE Scenario

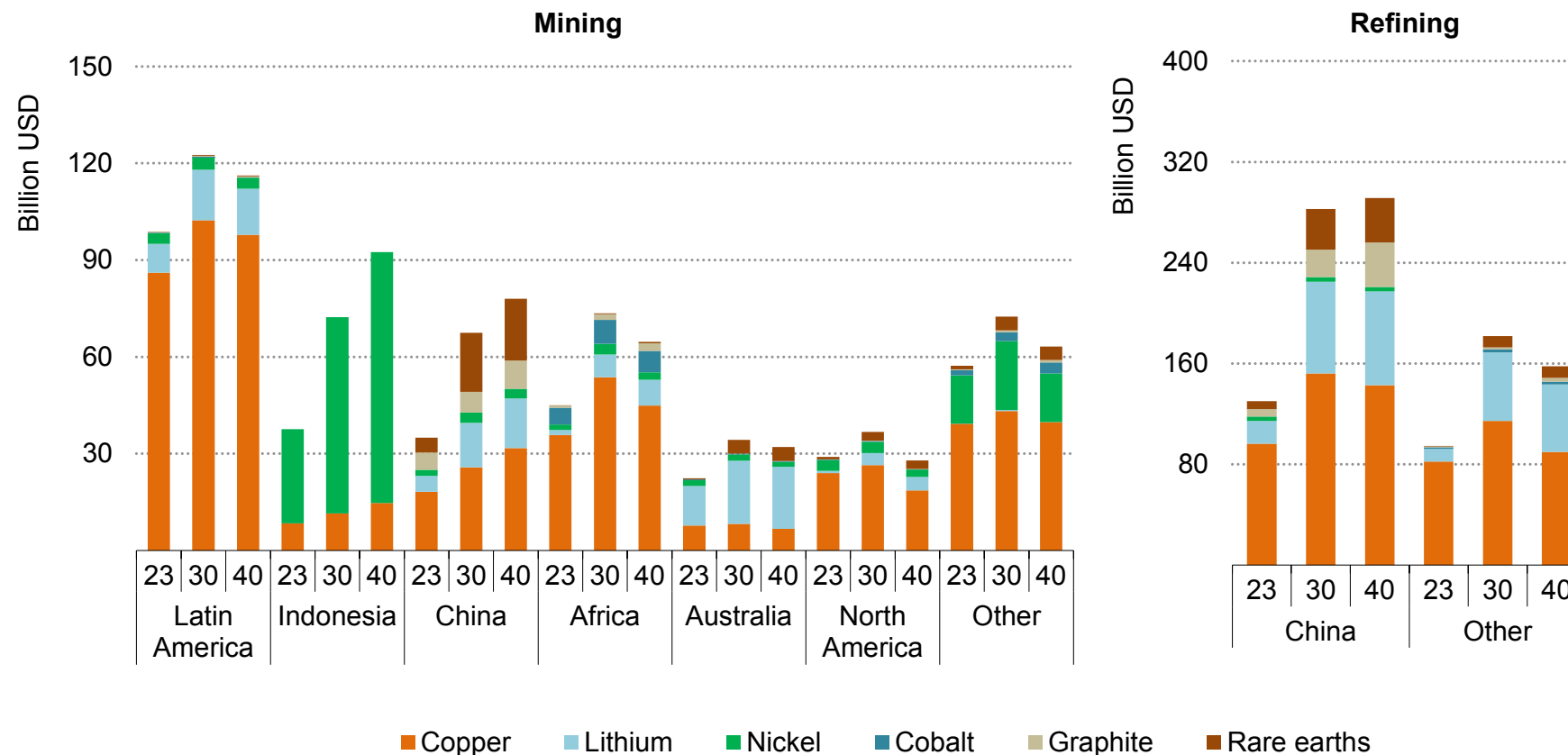


IEA. CC BY 4.0.

Note: 2023 annual average price levels are assumed to estimate the market size for the projection period.

## Latin America, Africa and Indonesia see a growing market value from their mining operations; nearly 50% of the market value from refining is concentrated in China by 2030

Market value of mined and refined materials in select regions in the base case

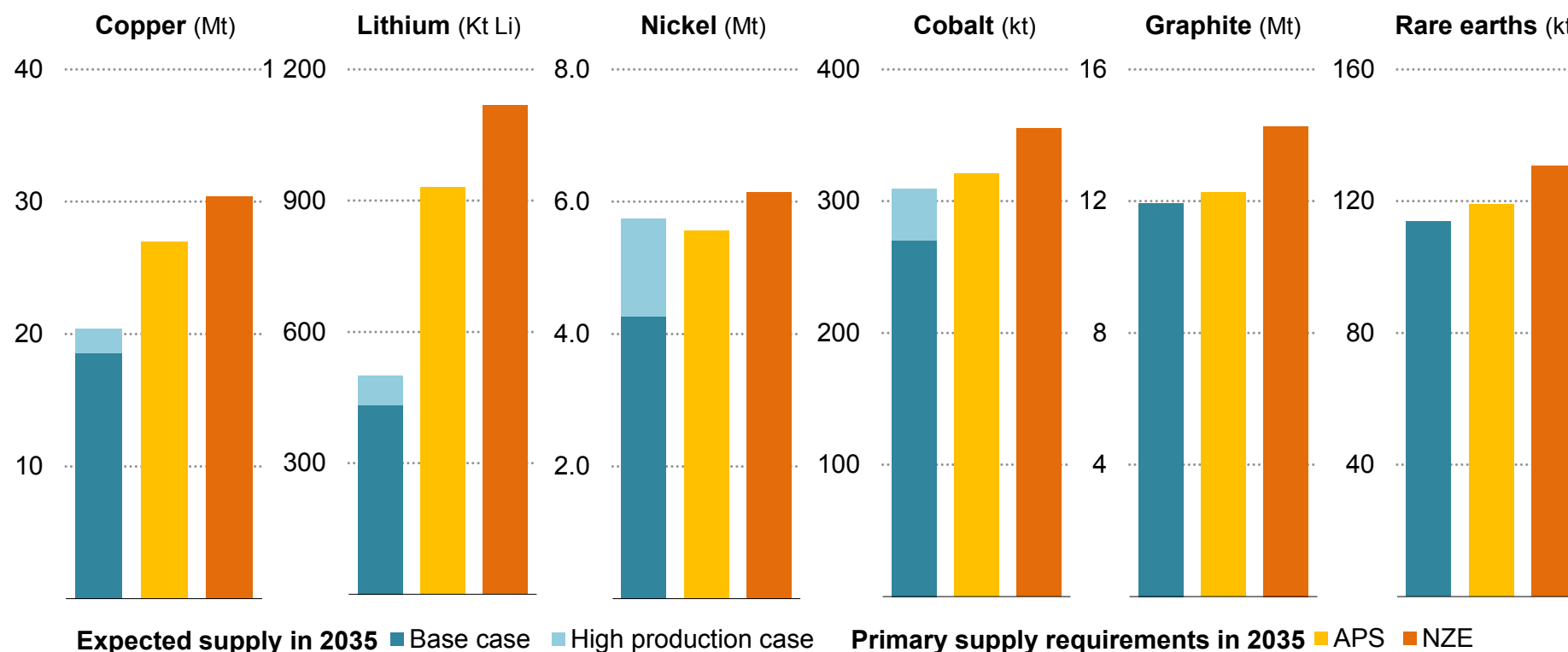


IEA. CC BY 4.0.

Note: Market value was calculated by multiplying each region's production volume in the base case with today's market price for final products.

## Expected supply from announced projects is within range of projected 2035 requirements to reach national and global climate goals, with the major exceptions of copper and lithium

Expected supply from existing and announced projects and 2035 primary supply requirements for focus minerals by scenario

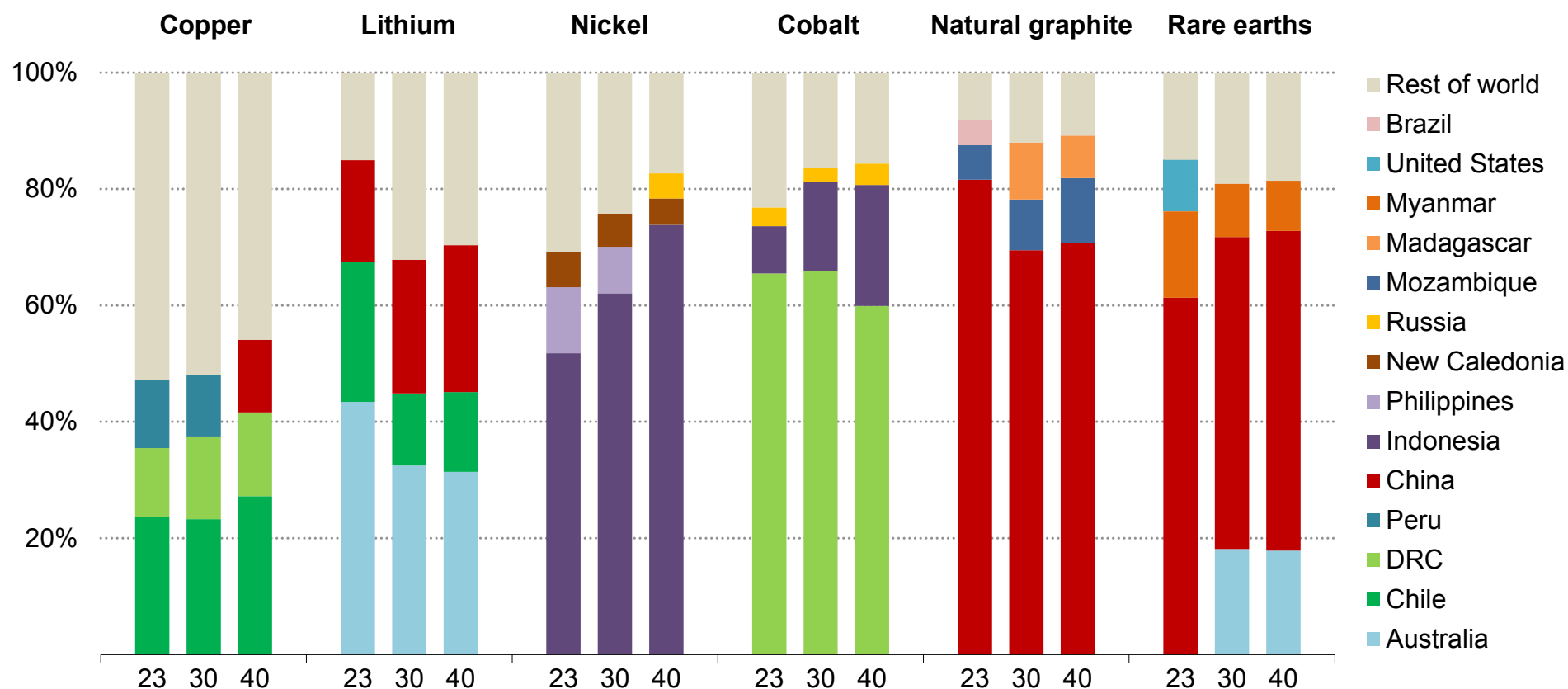


IEA. CC BY 4.0.

Notes: Expected supply is based on mined or raw material output, except for graphite where the figure includes expected spherical graphite and synthetic graphite supplies. Primary supply requirements are calculated as “total demand net of secondary supply”, also accounting for losses during refining operations. The figures for rare earth elements are for magnet rare earth elements only.

## Analysis of project pipelines indicates that the geographical concentration of mining operations is set to rise further or remain high over the projection period

Geographical distribution of mined or raw material production for focus minerals in the base case

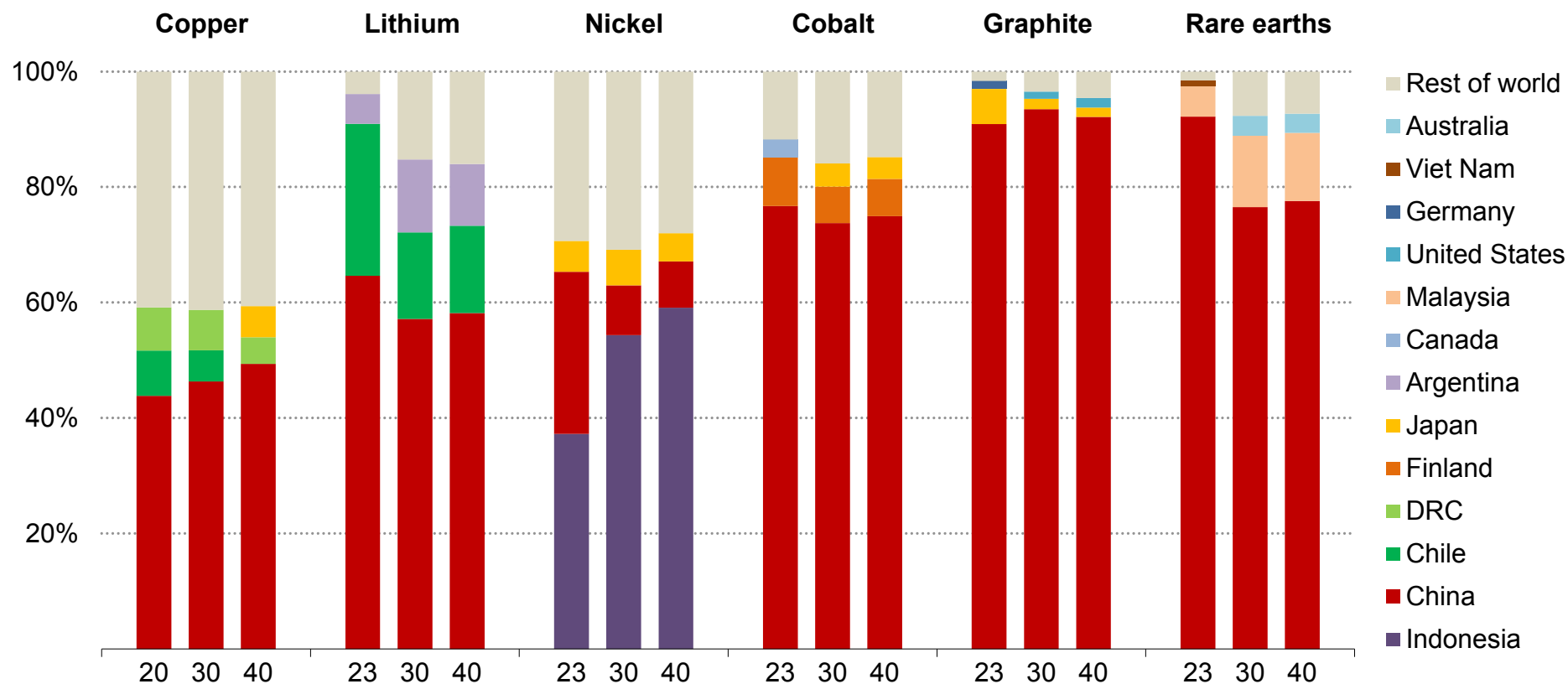


IEA. CC BY 4.0.

Notes: DRC = Democratic Republic of the Congo. Graphite extraction is for natural flake graphite. The figures for rare earth elements are for magnet rare earth elements only. The figure depicts the value of the top three producing countries in a given year.

## As many refining projects are being developed in today's dominant producers, refined material production is also set to remain highly concentrated in a few countries

Geographical distribution of refined material production for key minerals

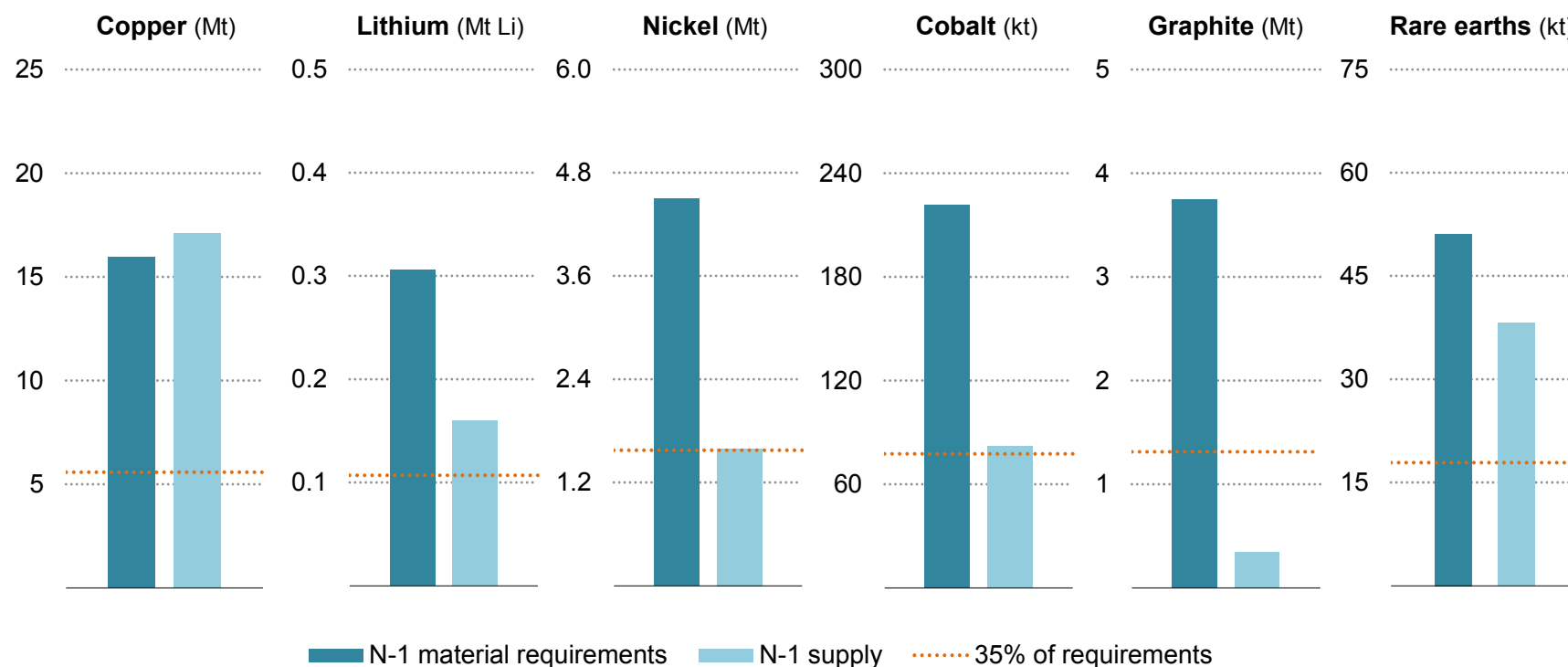


IEA. CC BY 4.0.

Notes: The figures for graphite are based on battery-grade spherical graphite and synthetic graphite supplies. The figures for rare earth elements are for magnet rare earth elements only. The figure depicts the value of the top three producing countries in a given year.

## Major implications for market balances if the largest supplier and their demand is excluded from the equation

N-1 material requirements and N-1 refined material supply in 2030 in the APS

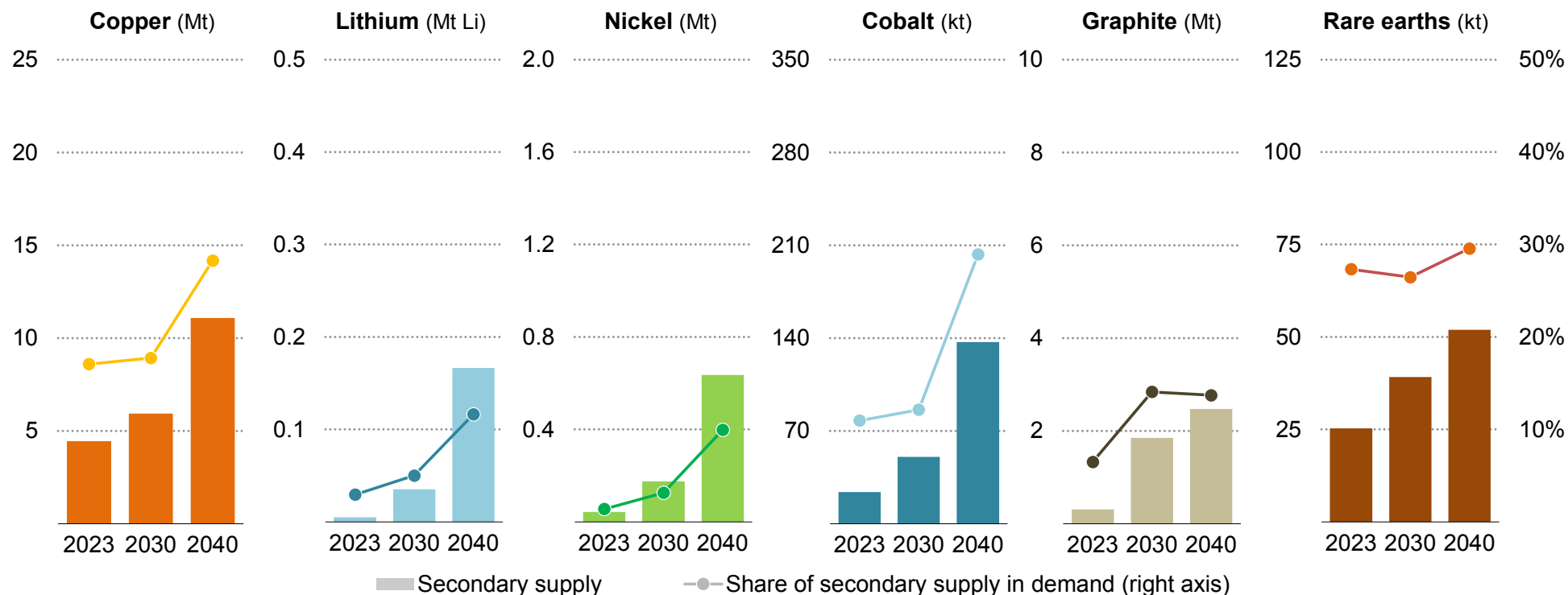


IEA. CC BY 4.0.

Notes: The N-1 supply excludes the production volumes from the largest producer from the total global supply, and N-1 requirements exclude consumption of that country from the total global demand. Graphite considers only battery-grade requirements and battery-grade supply, covering both spherical and synthetic materials. The figures for rare earth elements are for magnet rare earth elements only. For demand in the clean energy sector, the N-1 material requirements were estimated by considering each region's share of clean energy deployment. For demand outside the clean energy sector, the region's current consumption share was applied to the projected global demand in 2030.

## Secondary supply from recycling plays an increasingly crucial role in meeting demand growth in climate-driven scenarios, particularly after 2030

Secondary supply volumes and share of total demand for focus minerals in the NZE Scenario



IEA. CC BY 4.0.

Note: Includes recycled volumes from end-of-life equipment and manufacturing scrap. For copper, direct use of scrap is excluded.



## A complex and varied picture for future supply-demand balances and security of supply

Demand for key energy transition minerals is set to expand significantly across all scenarios, mainly driven by the burgeoning requirements in the clean energy sector. In the STEPS, demand for lithium grows fivefold between today and 2040, while demand for graphite almost doubles over the same period. Demand for nickel, cobalt and rare earth elements also shows robust growth, increasing by 65-80% by 2040.

If the world gets on track to limit global warming to 1.5 °C, as modelled in the NZE Scenario, demand for copper rises by 50% by 2040. In this scenario, demand for nickel, cobalt and rare earth elements doubles over the next two decades, and graphite demand increases by almost four times to 2040, propelled by the substantial increase in battery deployment for EVs and grid storage. Of all the minerals, lithium stands out in this scenario with nearly ninefold growth by 2040, highlighting its crucial role in batteries. Across all materials, the share of clean energy technologies in total demand rises significantly. In most cases, the clean energy sector emerges as the largest consumer of these minerals. In the NZE Scenario, EVs and battery storage are projected to account for over 90% of total lithium demand by 2030. Moreover, batteries are poised to surpass stainless steel as the leading consumer sector for nickel.

As demand expands, the market value of these minerals experiences substantial growth. From around USD 325 billion today, the combined

market value of key energy transition minerals is set to increase by 55% in the APS by 2030 and by 80% in the NZE Scenario. By 2040, the market value more than doubles in climate-driven scenarios, reaching USD 770 billion in the NZE Scenario. In this scenario, copper maintains the largest market value at USD 330 billion, while the lithium market undergoes significant expansion to USD 230 billion by 2040, emerging as the second-largest market, followed by nickel. The graphite market also registers almost sixfold growth over the same period. Today's aggregate market value of key energy transition minerals aligns broadly with that of iron ore. In the NZE Scenario, copper on its own attains that scale by 2040.

In the base case supply scenario, this growth in market value is spread across key regions. For mining, Latin America captures the largest amount with around USD 120 billion by 2030, driven by substantial copper production in the area. Indonesia sees the fastest growth, doubling its market value by 2030 due to its burgeoning nickel mining activities. Africa also witnesses a 65% increase in market value, attributed to the rapid expansion of copper production in the region. However, the market value for refining is notably more concentrated, with China claiming nearly 50% of the market value in 2030. China also sees a rise in market value for mined materials as the country's production of copper, lithium, and rare earth elements undergoes rapid expansion.

The rapidly growing demand for minerals, and the variations seen across different scenarios, raises uncertainties about future market balances, and whether future supplies can match the pace of demand growth in scenarios that meet national and global climate goals.

In recent years, substantial investments have been made in mineral supply, and an increasing number of projects have been announced, indicating an expansion in expected supply volumes in the coming years. In some cases, such as cobalt, nickel and rare earth elements, the expected supply by 2035 from both existing and announced projects look tight, but aligns more closely with the projected demand in the APS, particularly when projects assumed in the high production case come to fruition.

However, the timely delivery of planned projects is far from guaranteed and meeting the requirements in the NZE Scenario necessitates further project developments. A similar trend is observed for graphite, but it should be noted that there is a massive number of announced synthetic anode material projects, primarily located in China. Should natural graphite supply face price spikes or supply constraints, these facilities could offer additional volumes to the supply pool (see “Outlook for graphite”).

The situation differs for copper and lithium. Announced projects indicate that a mined copper supply gap may develop in the current decade in the base case. Even under the high production scenario, the anticipated supply by 2035 falls well short of meeting the APS requirements, indicating a potential necessity for a further increase in

scrap utilisation, demand reduction through material substitution or technological innovation, alongside efforts to foster additional project developments. Lithium presents another significant challenge, exhibiting a sizeable anticipated gap with climate-driven needs, owing to the strong position of lithium-ion batteries in EVs and storage applications. The current downturn in prices may dampen investment appetite for new greenfield projects, which could have profound longer-term implications.

Global mineral supply chains are not well diversified, as highlighted in Chapter 1, and recent progress on diversifying supply sources has been limited. Will this picture change with the multitude of newly announced projects in recent years? Our analysis of project pipelines suggests that the geographical concentration of mining operations is set to remain high in most cases. The situation improves somewhat in the high production case, indicating that many projects being developed in geographically diverse regions are not among the front-runners for development. This pattern mirrors the situation in refining operations, as most refining projects are located in today's dominant producers, thus prolonging high concentration levels in refined material production. Between now and 2030, some 70-75% of projected supply growth for refined lithium, nickel, cobalt and rare earth elements, and almost 95% for battery-grade spherical and synthetic graphite, comes from today's top three producers. These high levels of supply concentration raise risks of potential supply disruptions due to physical accidents, geopolitical events or other

developments in a key producing country, with major potential implications for the speed of energy transitions.

Global demand and supply balances often mask significant regional disparities. From the Inflation Reduction Act (IRA) in the United States (US) to the European Union's (EU) Critical Raw Materials Act (CRMA), a wave of policies is emerging aimed at diversifying sources of supply. The IRA seeks to restrict the utilisation of materials obtained from Foreign Entities of Concern, while the EU CRMA targets that no single country should supply more than 65% of Europe's annual consumption of any key materials (implying that at least 35% should come from non-dominant players). Other major consuming countries are increasingly aligned with the objective to diversify their supply sources.

However, given that the top producing nation is responsible for a large portion of global supply for most minerals, available supply outside the largest producing country may be significantly constrained to achieve these ambitions. We conducted the “N-1 test” to assess how the supply and demand landscape might appear if the largest global supplier were removed from the market. Specifically we assessed N-1 supply and N-1 material requirements in 2030 in the APS, excluding both anticipated supply from the largest supplier and projected demand from that country. In most cases, the N-1 supply falls significantly below the N-1 material requirements (even for minerals where the overall global balance is reasonably well supplied). If the CRMA's non-single-origin minimum threshold (35%)

is applied in a global context, the N-1 nickel and cobalt supply is barely able to meet this minimum threshold. The situation is even more pronounced for graphite. Although there is abundant supply of graphite globally, the expected N-1 supply is entirely insufficient to meet the minimum threshold. This indicates that without efforts to develop additional projects in geographically diverse regions, achieving the goals set by policy legislation would be challenging.

This analysis underscores the need for concerted efforts to expedite the development of promising projects located in geographically diverse regions. Additionally, it highlights the importance of harnessing the potential for value chain expansion in major resource holders in emerging and developing economies, provided such expansion is economically viable and can yield significant economic and social advantages.

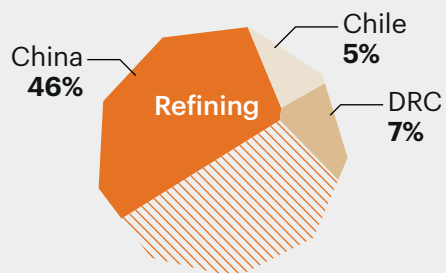
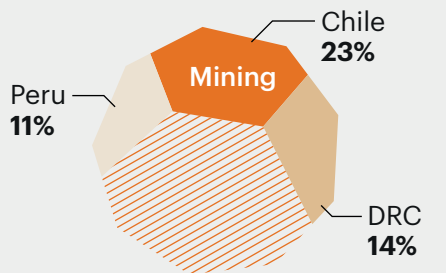
Investment across the supply chain is crucial, yet equally vital is unlocking the potential of recycling, innovation, and behavioural change. A strong emphasis on recycling can not only diminish the magnitude of primary mineral requirements but also yield substantial security benefits for regions dependent on imported materials. While the share of secondary supply from recycling in total demand remains modest for most focus minerals, it experiences significant growth in the NZE Scenario, particularly post-2030, as policy mandates strengthen and a substantial volume of end-of-life EV batteries enters the market (see Chapter 4, “Recycling, innovation and behavioural change” section).

## Outlook for copper

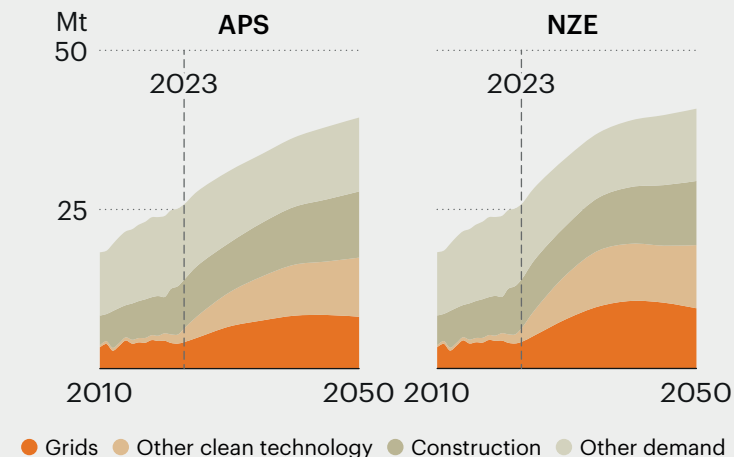
# Copper

## Cu

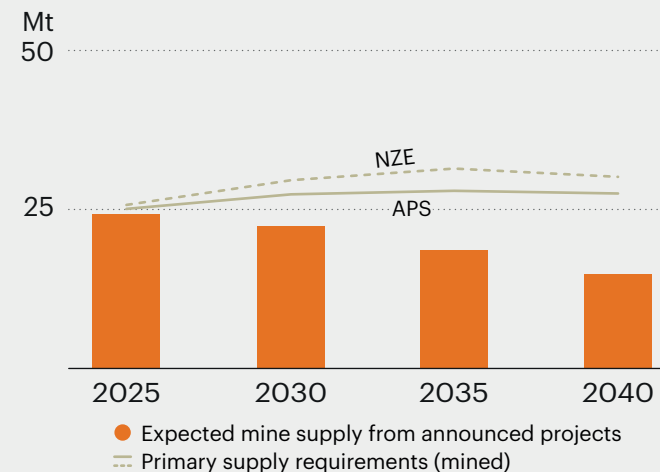
### Top three producers 2030



### Demand outlook

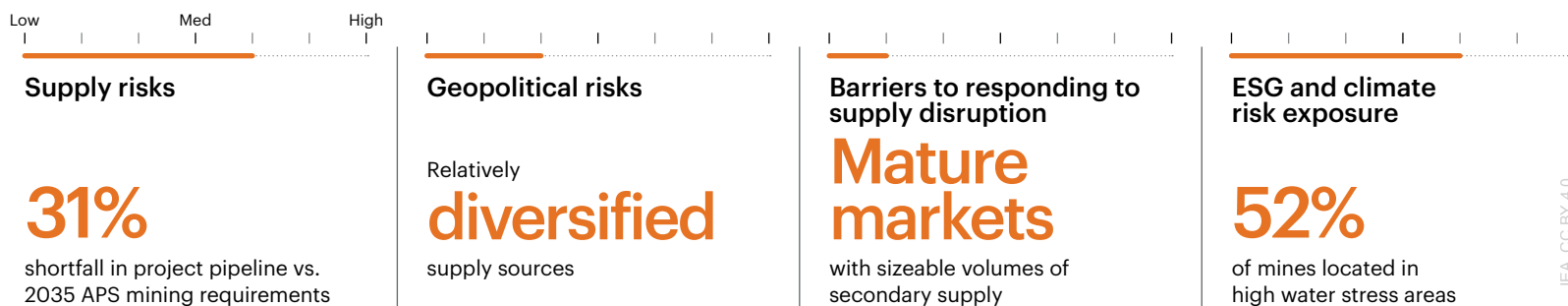


### Mining requirements



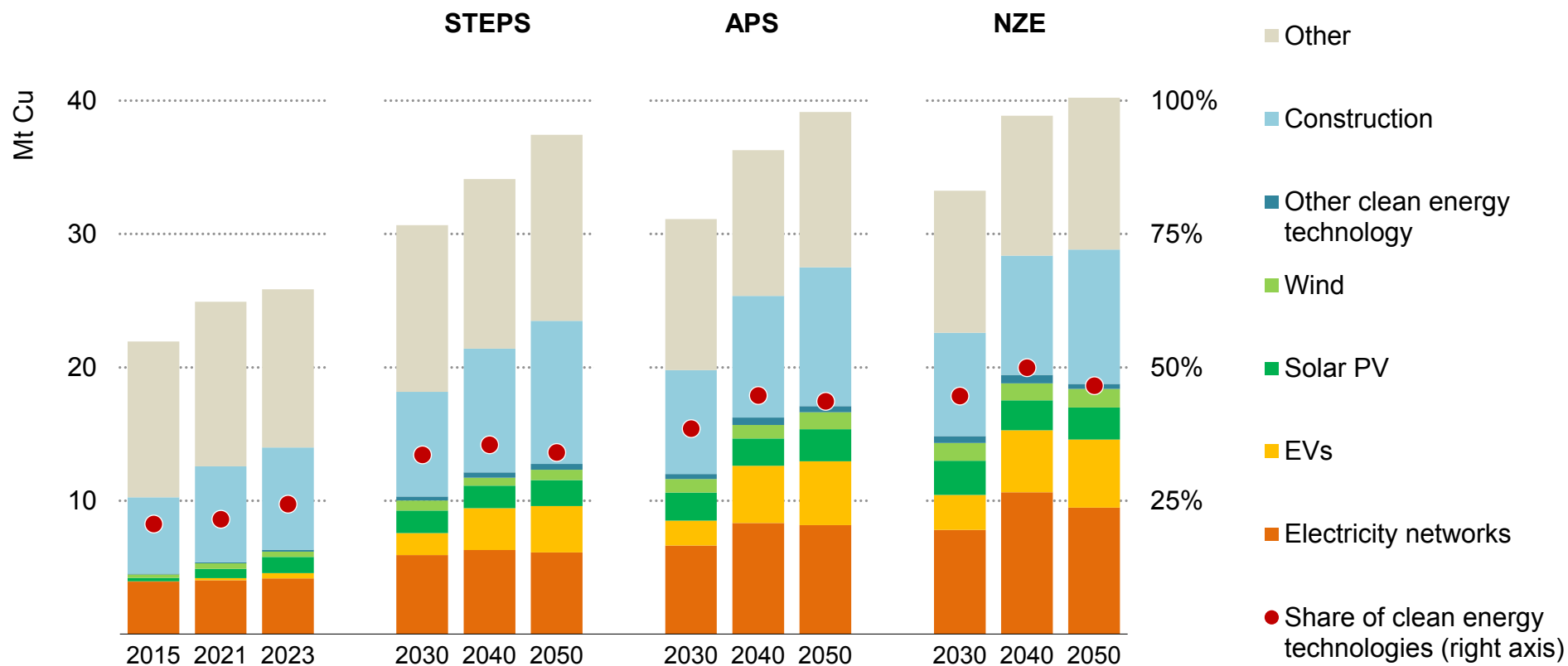
| Milestones (APS)                        | 2021          | 2023          | 2030          | 2040          |
|---|---------------|---------------|---------------|---------------|
| Cleantech demand (kt)                   | 5 380         | 6 311         | 12 001        | 16 343        |
| Other uses (kt)                         | 19 548        | 19 543        | 19 127        | 20 036        |
| <b>Total demand (kt)</b>                | <b>24 928</b> | <b>25 855</b> | <b>31 128</b> | <b>36 379</b> |
| Secondary supply and reuse (kt)         | 4 123         | 4 445         | 5 879         | 11 006        |
| <b>Primary supply requirements (kt)</b> | <b>20 805</b> | <b>21 409</b> | <b>25 249</b> | <b>25 373</b> |
| Share of top three mining countries     | 46%           | 47%           | 48%           | 54%           |
| Share of top three refining countries   | 57%           | 59%           | 59%           | 59%           |

### Clean energy transition risk assessment



## Demand: Clean energy technologies drive substantial growth in copper demand

Copper demand outlook by sector and scenario



Notes: Copper refined demand excluding direct use scrap. EVs demand includes both EV batteries and EV motors demand. Other demand includes: Industrial equipment, other transport, consumer products, cooling, communications, and other electronics.

IEA. CC BY 4.0.

## **Demand:** Copper demand grows rapidly in all scenarios, driven by the rapid deployment of renewables and EVs

Copper is the only critical mineral present in all of the most important clean energy technologies – EVs, solar PV, wind, and electricity networks – due to its unmatched combination of characteristics: electronic conductivity, longevity, ductility and corrosion resistance. Therefore, the security of supply of copper is paramount for the energy transition. Total copper demand is made up of a combination of refined copper demand (including both primary and secondary production, 26 Mt in 2023) plus direct use of scrap (over 6 Mt).

Historically, refined copper demand has been dominated by construction and electricity networks, responsible for 30% and 15% of global demand in 2023, respectively. Other key sources of demand include industrial machinery and equipment (12% of 2023 demand) and the transportation sector (15% of 2023 demand), as copper is used in the manufacture of key components in all modes of transport.

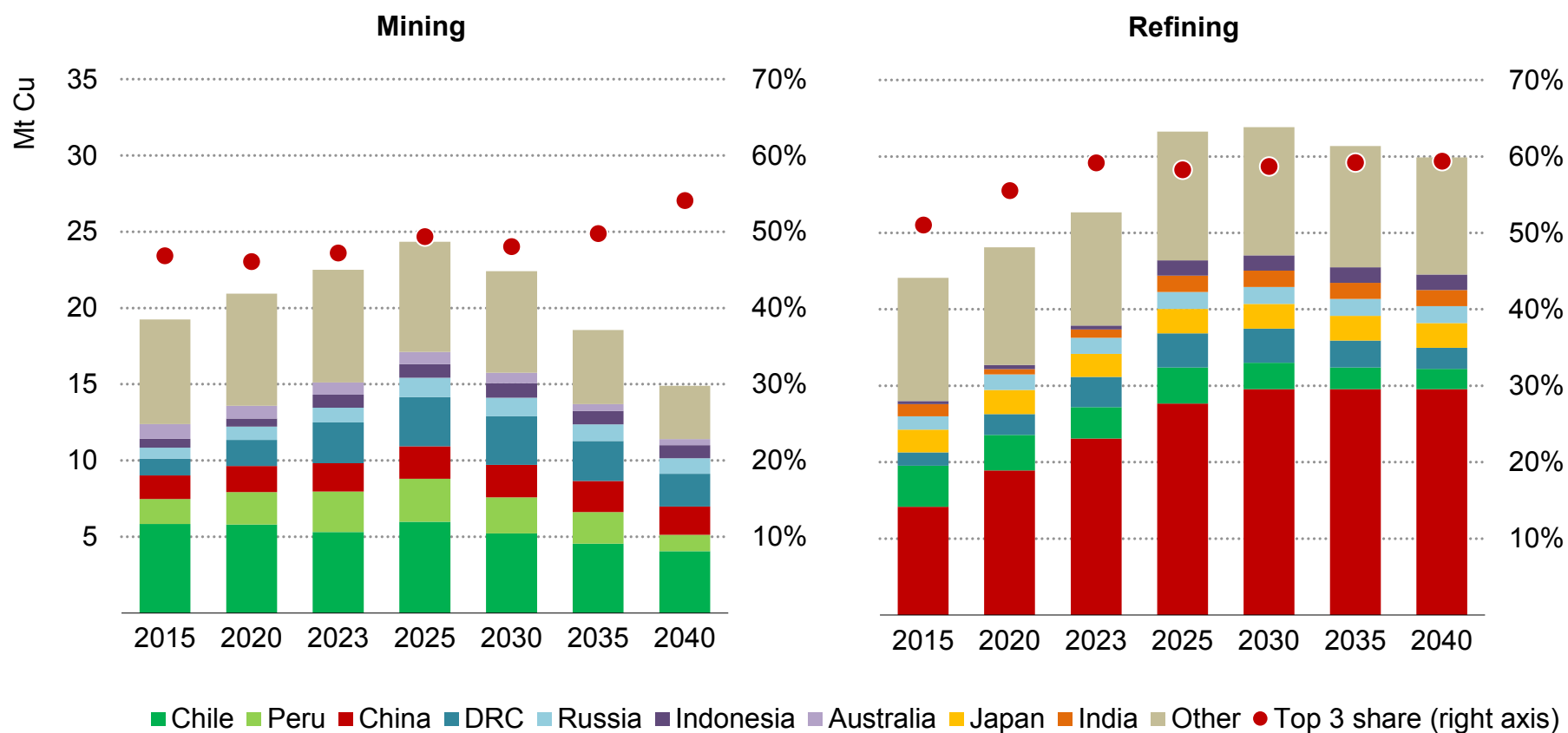
Global refined copper demand grows from 26 Mt in 2023 to 31 Mt in the STEPS and APS and 33 Mt in 2030 in the NZE Scenario. Demand increases further by 20% through to 2050, reaching around 40 Mt in 2050 in the NZE Scenario. This surge in demand is primarily due to the rapid deployment of renewables and EVs, and a significant expansion of electricity networks. Copper is critical for lithium-ion batteries for EVs, being irreplaceable for the anode current collector, as well as being used in wiring in the battery packs and being a key

component of EV motors. Electricity networks remain the second-largest source of demand after construction for the STEPS and APS, but in the NZE Scenario, it becomes the largest source of demand by 2030 before construction again overtakes to be the dominant source after 2040. However, copper demand from EVs experiences the largest growth in demand, increasing more than twelvefold from 2% of demand in 2023 to 12% in 2050 in the APS and 13% in the NZE Scenario. Overall, construction remains the leading source of refined copper demand in climate-driven scenarios although material efficiency measures temper demand in the sector.

The share of clean energy technologies in refined copper demand has grown modestly in recent years from 22% in 2015 to a quarter in 2023; however, this decade the share dramatically increases, reaching a third in STEPS, almost doubling to reach almost 40% in the APS and 45% in the NZE Scenario in 2030 due to the rapid deployment of renewables and EVs. The earlier electrification of end uses and penetration of renewables requires a rapid addition of electricity networks over the period to 2040, after which the pace of expansion decelerates. This leads to a decrease in copper demand for electricity networks between 2040 and 2050, resulting in a slight decrease in the share of clean energy technologies.

## Supply: Chile remains the leading copper miner with the DRC the new second, while China continues to dominate copper refining

Copper production from operating and announced projects in the base case



IEA. CC BY 4.0.

Note: DRC = Democratic Republic of the Congo.



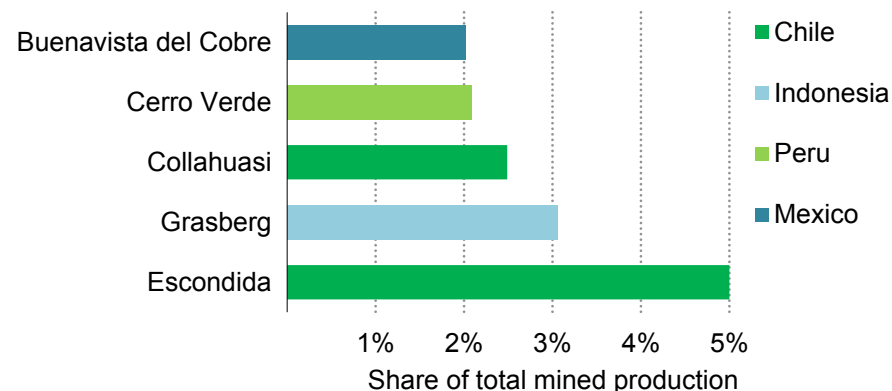
## Supply: Lack of large-scale projects in the pipeline poses challenges for future copper supply

### Mining

Global mined copper supply reached 22.5 Mt in 2023, up 8% from 2020. Today's copper supply is relatively diversified compared with the other key energy transition minerals. The share of the top three producers was 47% in 2023, and it has been at a similar level since 2015. Chile is the world's current largest producer, producing a quarter of global supply. This is down from 30% in 2015 due to declining ore grades, ageing assets and low reinvestment in expansion. Meanwhile, with its remarkable growth of copper output, the DRC has doubled its share of global supply from 6% to 12% over the same period, overtaking Peru as the second-largest supplier. The DRC copper belt is home to some of the highest-grade copper resources in the world, for instance the Kamo-a-Kakula mine is one of the world's highest-grade major copper mines, ten times the global average ([5.5% compared with the global average of 0.6%](#)). This makes capital and production costs, and emissions in the DRC significantly lower than other regions, driving a dramatic growth in supply. China is the fourth-largest producer with 8% of global supply while Russia supplies 5%. Indonesia has seen impressive growth since 2020 doubling its share to 5% in a few years while the share of Australian supply has been decreasing. The top three copper mines in 2023 produced over 10% of global copper production, being Escondida in Chile, PT Freeport Indonesia (Grasberg) in Indonesia and Collahuasi in Chile.

Based on the current project pipeline, mined copper supply reaches around 25 Mt in 2026 then declines thereafter as assets age and grades decline. The top three producer's share in total mine production increases to 55% by 2040 from 47% today. Chile remains the largest producer going forward, contributing around a quarter of global supply through to 2040 while the DRC remains the second-largest producer. China also continues to grow its share of global supply, from 8% in 2023 to 12% in 2040. Russia and Indonesia also continue to grow in supply share, together supplying 13% in 2040. The growing share of supply from these countries displaces a significantly shrinking share from Peru, which drops from 12% today to 7% in 2040 due to a lack of viable projects and ageing assets.

Top five largest copper mines 2023



IEA. CC BY 4.0.

Source: IEA analysis based on Wood Mackenzie.

Beyond the challenges of declining copper ore quality, there are additional pressures coming from local social and environmental opposition, particularly in Latin America. At the end of last year, Cobre Panama, one of the largest copper mines in the world supplying 1.5% of global copper output, was [shut down by the government](#) due to widespread protests regarding environmental damage and corruption concerns. Beyond the loss of one of the largest copper producing assets, the case is expected to deter mining investment in the country. One of Peru's largest copper mines, [Las Bambas, also saw a strike](#) at the end of last year due to workers conditions, having already seen disruptions previously due to indigenous community protests demanding more equitable distribution of mining gains with the local community, as well as other protests. With most of the world's largest mines located in Latin America, if several of these face major opposition, disrupting logistics or shutdowns similar to Cobre Panama, there could be major consequences for global copper supply. The world's largest copper mine Escondida Chile produces 5% of global copper supply alone, while four of today's top five mines are located in the region, emphasising the vulnerability. Efforts to expand mines in other places could reduce this dependency.

## Refining

Copper refining is more concentrated than mining, with a current top three refiner share of 60%, becoming more concentrated since 2015. Refining is much more concentrated in a single country. China is currently the world's dominant copper refiner, with 45% market share,

having rapidly grown from 30% in 2015. Despite Chile being the world's largest copper miner supplying a quarter of global supply in 2023, it produces only 8% of the world's refined copper, and this share has decreased since 2015 when it was 12%. This demonstrates that over half of Chile's mined copper concentrate is exported for refining, with the majority to China. Copper concentrate is the [number one exported](#) product from Chile in terms of value. Since 2012 exports of copper concentrates from Chile have increased 60% mainly to China while exports of refined copper have dropped 20% over the same period. This decline is largely due to the decline in production from solvent extraction electrowinning (SxEw) mines which directly produce refined copper from oxide ore. As the oxide ore supply decreased, with many transitioning from processing oxides to conventional sulphide mining, its export of concentrate increased and refined copper decreased. There are also environmental concerns which have led to the [closing of smelters in Chile](#).

The DRC is now the joint second-largest copper refiner with Chile. While Chile has lost market share since 2015, the DRC has doubled its share in the same time up from 4%. The top three copper refineries in 2023 produced 9% of global refined copper, being Guixi and Jinchuan in China, and Onsan in Korea.



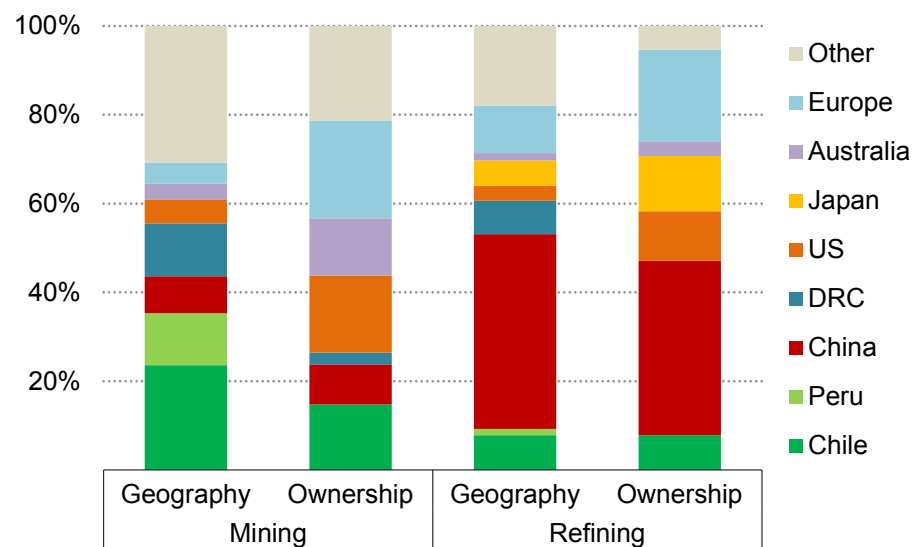
IEA. CC BY 4.0.

Note: LAC = Latin America.  
Source: IEA analysis based on COCHILCO (2023).

Going forward, the share of the top three refiners remains at the same level at around 60%. China, however, continues to increase its dominance of copper processing, supplying around half of global refined copper from 2030 onwards. Little change occurs for the other countries in this period. This again creates a major dependency and vulnerability. Countries in Latin America could prioritise the development of greater domestic processing capability. Not only would this help diversify refined supplies of copper, it would support the countries' economies increasing their share of the value chain. However, cost and environmental concerns are key barriers. Smelting is not a high-margin business, and increasing pressures

from high labour and energy costs have made it challenging to compete with China. Capital requirements to reduce emissions and increase the sustainability of operations add to this pressure. Recently Chile's Codelco [closed its Ventanas smelter](#) due to pollution which resulted in a poisoning incident in the local community.

Copper mining and refining by geography vs. ownership, 2023



IEA. CC BY 4.0.

Notes: Ownership analysis of top 20 mining and refining companies in 2023 representing 57% of mined and 56% of refined copper production. Ownership based on headquarters location.

Source: IEA analysis based on Wood Mackenzie.

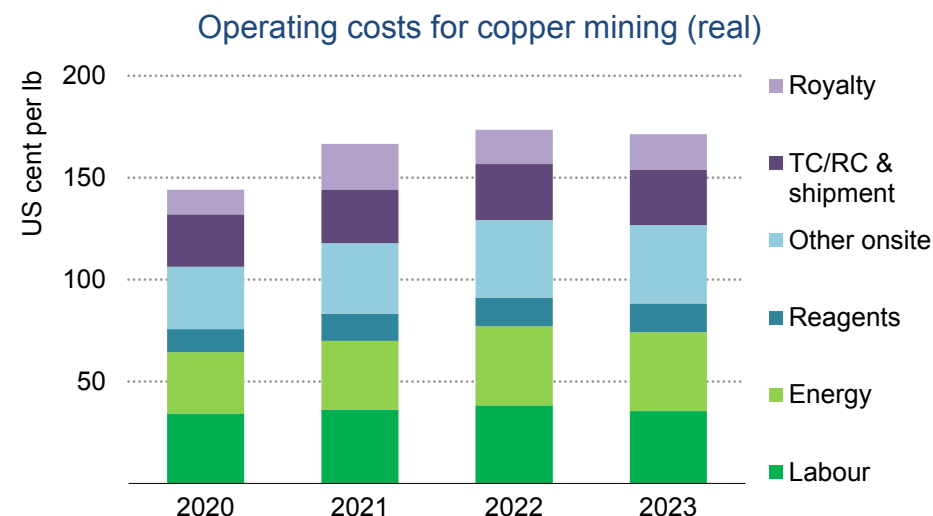
Looking at mining and refining production in 2023 by ownership (defined based on company headquarters location) shows a different

picture from production location. Based on the analysis of top 20 companies, mining appears to be similarly diversified by ownership with a top three country owner share of 45%, the same as production location. European companies are in fact the largest copper producers with over 20% of production. US companies also produce almost 20% of global supply, despite little mining taking place domestically, and this is all from two companies: Freeport-McMoRan and Southern Copper. Companies from Australia and Canada are also major copper producers, together supplying 20% of production despite limited domestic supply. In terms of refining, the picture is similar with Chinese companies dominating with 40% of production. Top three refining countries' share by owner is the same as by location with 60%. European companies are the second-largest refiners with 20% as well as being the second-largest refining location but with only 10% by geography. Japanese companies are the third-largest refiners despite being the fifth-largest refining location. Again US companies play a leading role in copper refining being the fourth-largest refiners.

### Capital and operating costs

Declining ore quality is the most critical issue for copper, resulting in increasing capital and operating costs. Operating costs have increased in most areas in real terms since 2020 with energy, on-site, treatment and refining charges (TC/RCs), shipment costs and reagent cost increases all being major drivers. Capital costs have also increased significantly for new copper projects. Recent brownfield projects have a capital intensity around USD 30 000 per

tonne, whereas in real terms past brownfield projects initiated around 2017 were cheaper at around USD 20 000/tonne. Expansions are costing more due to having to go deeper and the need to mine more waste to maintain production levels from the declining ore quality. Greenfield projects also suffer higher costs due to the lack of high-quality resources, the need to comply with higher ESG standards, challenging geology, and higher labour and equipment costs. The recently commissioned DRC mine Kamoakakula, with one of the highest-grade copper ore in the world, contrasts from current trends with a capital intensity around just USD 7 000/tonne, demonstrating the major cost advantages in the high-grade areas of the DRC, and explaining its rapid rise in supply.



IEA. CC BY 4.0.

Notes: lb = pound. Companies representing 75% of total copper production.  
Source: IEA analysis based on S&P Global.

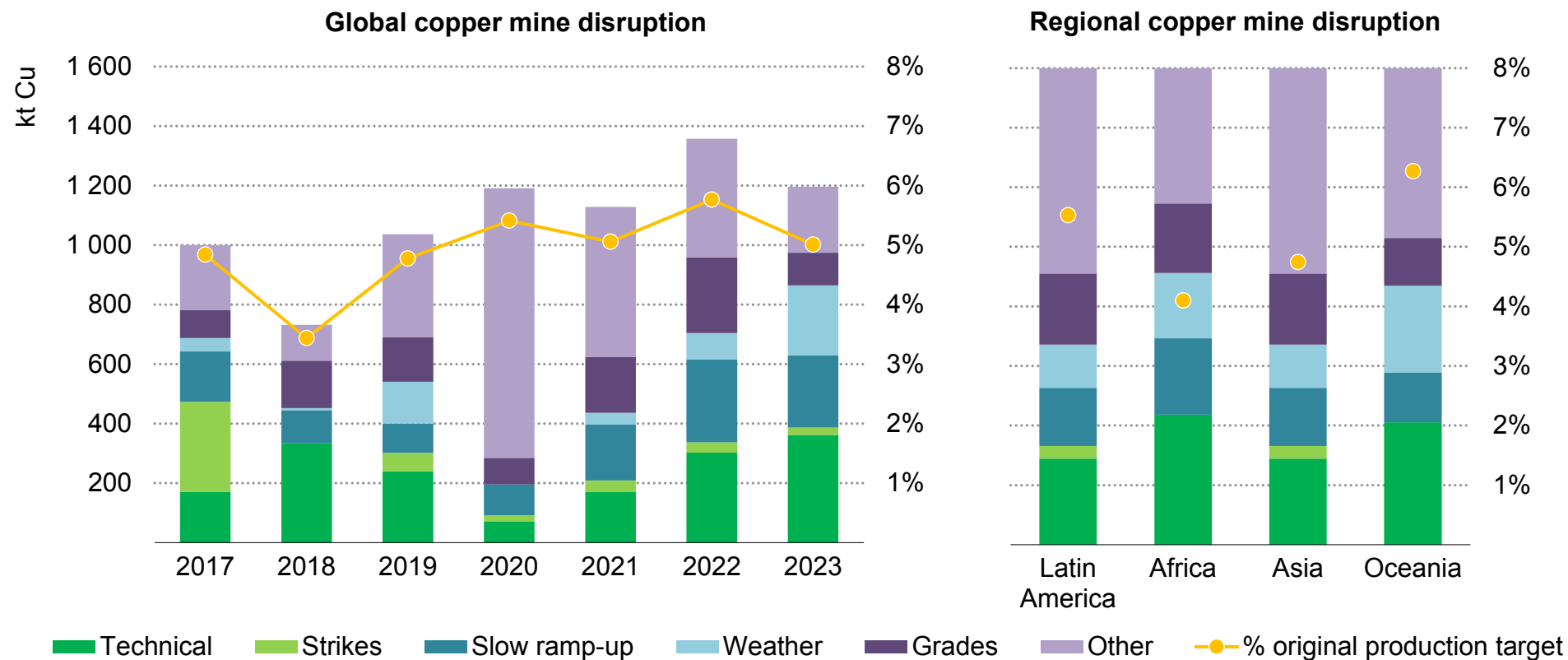
## Copper mining disruptions

Adding to the supply pressures from the declining ore quality are various disruptions to copper supply (assessed as shortfalls relative to expected supply). The global disruption rate in copper supply has been consistent around 5% of the original targeted production. At a global scale, the primary causes vary considerably with the leading causes being technical issues, slow ramp-up, and grades being lower than anticipated. Strikes have been a less critical issue over recent years; however, in 2017 they resulted in exceptional disruption due to [strikes at the world's largest mine Escondida in Chile](#). In 2020,

Covid-19 was the primary cause of supply issues. Regionally, the picture varies considerably. Averaged over the past seven years, Oceania (predominantly Australia but including Papua New Guinea) has the highest apparent disruption rate over 6% of anticipated production, while Africa has had the lowest with 4%. However, in both regions technical disruptions are responsible for a higher share of disruption than the global average. Oceania has also been disproportionately affected by weather-related issues.

## Supply: Oceania and Latin America suffer greater disruptions to mining supply

Copper mining disruptions by cause

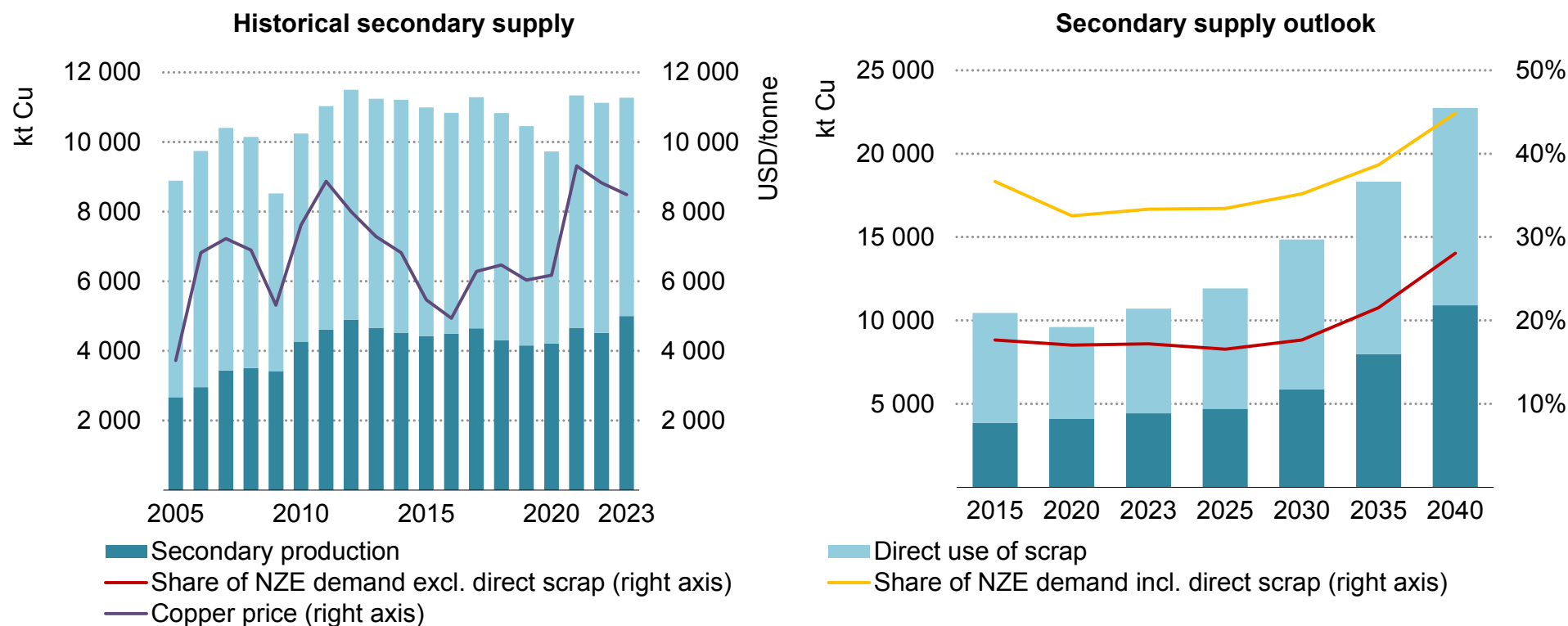


IEA. CC BY 4.0.

Note: Regional mine disruption breakdowns are based on the last seven-year average. Oceania includes Australia and Papua New Guinea  
 Source: IEA analysis based on Wood Mackenzie.

## Secondary supply: Copper recycling and direct use of scrap is set to increase substantially from 2030 providing a major source of supply in the future

Historical and projected secondary copper supply in the NZE Scenario



IEA. CC BY 4.0.

Notes: Direct use of scrap refers to high-grade manufacturing scrap which can be directly used as a source feed. Secondary production refers to end-of life and manufacturing scrap which must be further processed by smelting and/or refining before usage.

Source: IEA analysis based on Wood Mackenzie and S&P Global.

## Secondary supply: Copper scrap plays an important role in cushioning potential market tightness or price shocks

Copper scrap falls under two broad categories. High-grade or No. 1 scrap, known as direct use of scrap, is directly used by semi-manufacturers supplementing their cathode supply as a source feed. There is also lower-grade No. 2 scrap, which contains greater impurities and is used by smelters and refineries. The higher impurities prevent this scrap from being used directly.

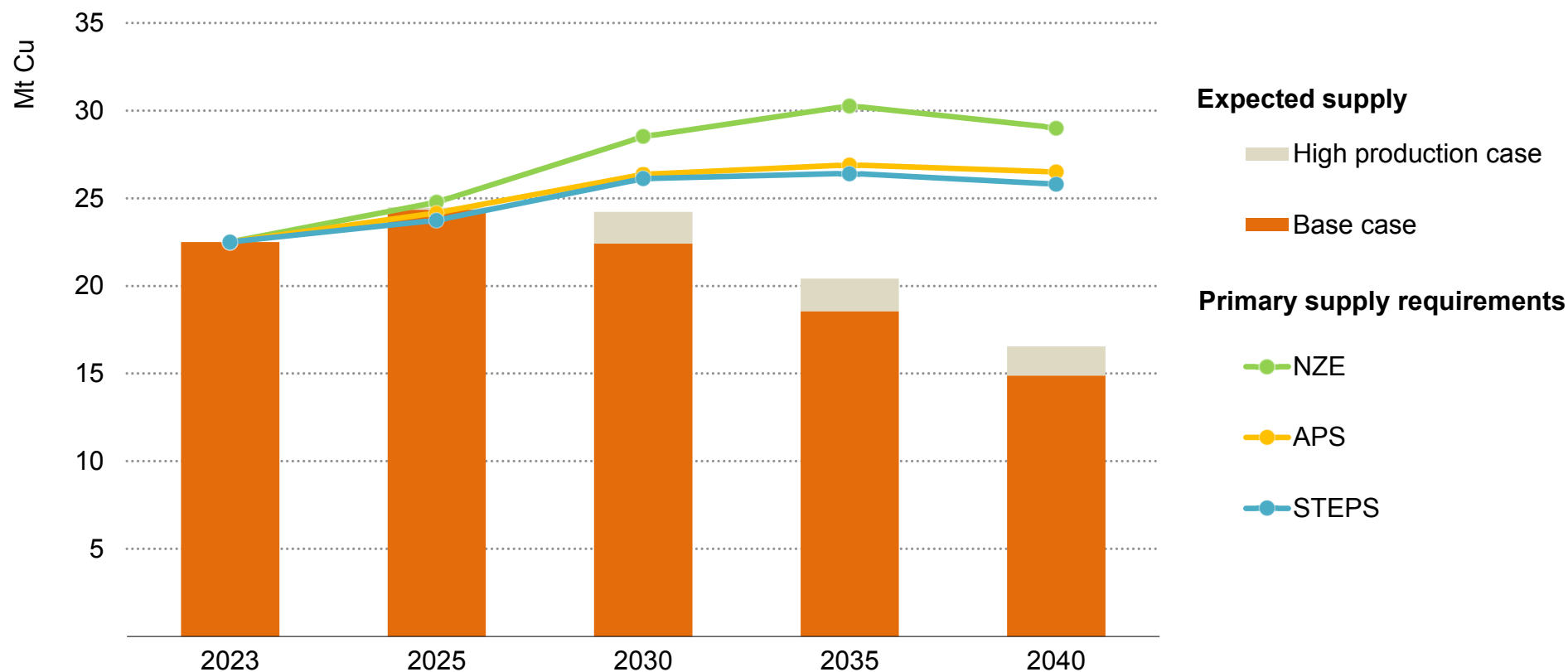
Looking at historical secondary supply correlations with copper price shows they are strongly correlated with little lag, thus the price strongly determines secondary supply, which acts as a market-balancing mechanism. This demonstrates that ramping up secondary supply can happen quickly and reactively with the right incentives. Therefore, secondary supply can be an increasingly important source of copper supply particularly in times of supply shocks and price spikes, if the right policy incentives are in place. However, this also shows the difficulty in sustaining high scrap usage rates in a low-price environment.

Copper scrap use has decreased since 2015 from 18% to 17% of demand excluding direct use of scrap, and more significantly including direct scrap (from 37% to 33%). This is due to a combination of price, scrap trade restrictions from China, higher energy and shipping costs reducing recycling profitability, the impact of Covid-19, and that EU and US policies promoting domestic scrap collection have not yet taken effect. In climate-driven scenarios, however, copper scrap use increases significantly. In the NZE Scenario, the share of secondary supply in total demand rises to 20% by 2030 and 30% in 2040, excluding direct use of scrap. This growth is driven by strong policy efforts to increase collection rates, optimise sorting systems, raise policy mandates for recycling and encourage investment in new processing facilities and smelters. Growing end-of-life volumes from EV batteries also emerge as a major contributor from 2030. In the NZE Scenario, both sources of secondary supply experience strong growth, with direct use of scrap almost doubling from 2023 to 2040 while secondary production scrap increases by 2.5 times in the same period.



## Supply: A major primary copper supply deficit develops after 2025

Expected mined copper supply from existing and announced projects and primary supply requirements by scenario



IEA. CC BY 4.0.

Notes: Based on mined output. Primary supply requirements are calculated as “total demand net of secondary supply”, also accounting for losses during refining operations. See Introduction for definitions of the base and high production cases.

## Implications: A broad combination of supply and demand measures are needed to close the copper supply gap

Our analysis of project pipeline indicates that a copper primary supply shortfall may develop after 2025 in all three scenarios, despite the significant growth in secondary supply. Even in the high production case where almost 2 Mt of extra mined supply is available shows a supply gap of 2.2 Mt (10%) to meet demand required by government climate pledges while there is a 4.5 Mt (20%) shortfall to match demand in the NZE Scenario in 2030. This demonstrates the urgency of financing and approving new supply projects given the long lead times to bring online new production. Beyond 2030 the supply gaps continue to expand as demand grows robustly for all scenarios. By 2040, base case supply would have to increase by 80% to meet APS demand while it would have to double to be on track to meet 1.5° C by 2050. Even in the high production case, supply would have to increase by 60% in the APS and 75% in the NZE Scenario by 2040 to meet demand. This anticipated primary supply deficit presents a growing concern for future clean energy technology deployment.

The most critical risk for copper is this major supply gap from 2030 onwards, being primarily driven by the strong increase in demand from clean energy technology deployment coupled with the declining ore quality in resources. For instance, the average grade of copper concentrate in Chile has [decreased 30% since 2005](#). Although the implied supply gaps do not mean that achieving transition goals are

unattainable, the substantial supply deficit requires a range of solutions to reduce pressure on primary copper supply requirements. This includes considerable supply and demand actions from governments and companies, including investment, substitution, material efficiency and recycling measures. The lack of diversification going forward, particularly in refining is also a key risk for the security of supply of copper.

### Supply measures

First, on the supply side it is essential to stimulate significant investment in new primary supply, including in lower-grade plays. Governments can play a key role in supporting strategic projects financially and in streamlining permitting. However, the problem of declining ore quality poses a considerable challenge on the investment side, as there are few major new resources of high quality to exploit, also as a result of subdued exploration spending over the past decade. The tight supply market is likely to increase prices which could support investment in lower-grade plays, but pose economic pressures on end users. Many projects in the largest supply region, Latin America, which is also the region facing acute water stress challenges, are also facing critical social and environmental opposition, which has already resulted in the shutdown of the Cobre

Panama mine. This underlines the importance of governments and international mining companies working closely with the local community and ensuring benefits are felt to maintain social acceptability.

Recycling is one of the most crucial measures to reduce primary copper supply pressure going forward. Copper is one of few materials that can be recycled repeatedly without any loss of quality. Manufacturing scrap is already reasonably well recycled; however, end-of-life scrap and mining waste have significant potential for improvement. With global copper secondary supply currently 17% of demand (excluding direct use of scrap), but increasing to 30% in 2040 in the NZE Scenario, there is still substantial room for improvement. Given its multitude of applications, the global stock of copper is a critical resource, often referred to as the “urban mine”, and further exploitation of this is crucial. One of the critical issues limiting copper recycling is the [difficulty in economically sorting and separating copper and its alloy types](#) from complex electronic post-consumer scrap, where the value of recovered copper is often not high enough to match the recycling cost. Second, collection infrastructure is often insufficient in many regions, with limited coordination between supply chain actors. This is compounded by insufficient incentives and information for consumers to recycle copper-containing products. Lastly, there is a lack of regulatory mandates on copper recycling and collection.

To address these challenges and enhance copper recycling, several actions are necessary. First, implementing comprehensive regulations is pivotal, including recycling rates and content mandates, bans on metals in landfills, and enforcement of design for recycling standards for new products to ensure a larger pool of products that are economically recyclable. Governments can support copper recycling supply chain coordination, which can reduce costs. Policy measures including China’s “Green Fence” policy, restricting the import of low-quality copper scrap, has inadvertently resulted in scrap oversupplies in Europe and thus [low-quality scrap not being accepted in recent years](#). Therefore, increasing the scrap pool without accompanying investment in processing facilities may be less effective. This reinforces the need for greater global coordination between copper recycling supply chain actors, coupled with improved tracking of global scrap flows. Second, governments can support and scale up collection and sorting infrastructure, including information campaigns and incentives for consumers. Third, support for novel emerging recycling technologies which can efficiently sort and separate copper and its alloys is crucial, for instance [sensor-based scrap sorting](#) such as X-ray fluorescence and laser-induced breakdown spectroscopy. Lastly, supportive trade policies and measures promoting the development of new processing capabilities, along with economic incentives aimed at sustaining higher scrap usage in times of lower prices, are essential.

Novel technologies offer promise for [extracting greater amounts of copper from lower-grade plays](#) and materials currently considered

waste. For instance, primary sulphide leaching, [bioleaching or hydrometallurgy](#) can enable copper recovery from ores below mill head grade, typically considered waste. Advanced separation techniques can also concentrate and upgrade low quality ore. Machine learning has also been used not only to optimise processing operations but also in [identifying new resources](#). Despite their promise, many of these technologies are still emergent and have to be proven at scale.

## Demand measures

On the demand side, there are multiple measures which can be taken to relieve supply pressure. Increasing material efficiency is key to reducing copper demand. For instance setting mandates and standards for copper intensity in products such as construction pipes or wiring can be effective. Providing financial incentives for consumers to purchase high material efficiency products can also help, particularly in appliances. Copper intensity is being reduced in products such as electric motors and solar panels, where price is often a driver.

Substitution of copper where possible is an important measure going forward. Aluminium, though it has 60% of the electronic conductivity

of copper, is the primary substitute option for many copper applications. It is also lower cost and lighter weight providing other potential advantages. There are applications where copper cannot be substituted including lithium-ion anode current collectors, due to lithium alloying with aluminium at low potentials. In networks aluminium's lower electrical conductivity requires thicker cables, while the inferior thermal and mechanical properties necessitates greater maintenance, therefore, [aluminium is less suitable for high-voltage subsea and underground cables](#) (although some OEMs are however starting to consider replacing copper in subsea applications).

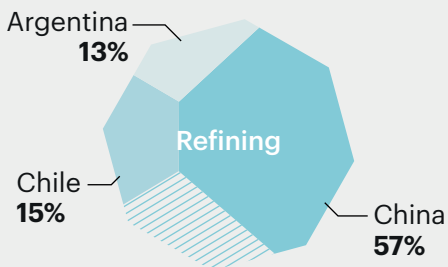
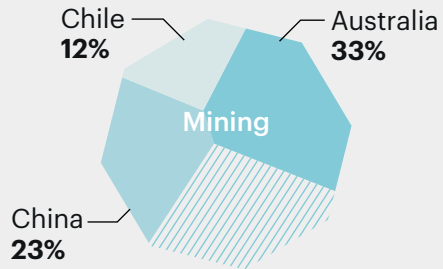
However, in many applications substituting copper is possible with commercial viability with minimal disadvantage. For instance, copper plumbing can often be replaced by plastic pipes such as cross-linked polyethylene (PEX) or high-density polyethylene (HDPE), though they can be difficult to recycle. Aluminium can replace overhead copper distribution cables, as well as copper windings in some motors, generators and transformers. However, it is also important to note aluminium processing is [almost five times more carbon-intensive than copper processing](#); therefore, there are energy-related implications to substituting copper with aluminium.

## Outlook for lithium

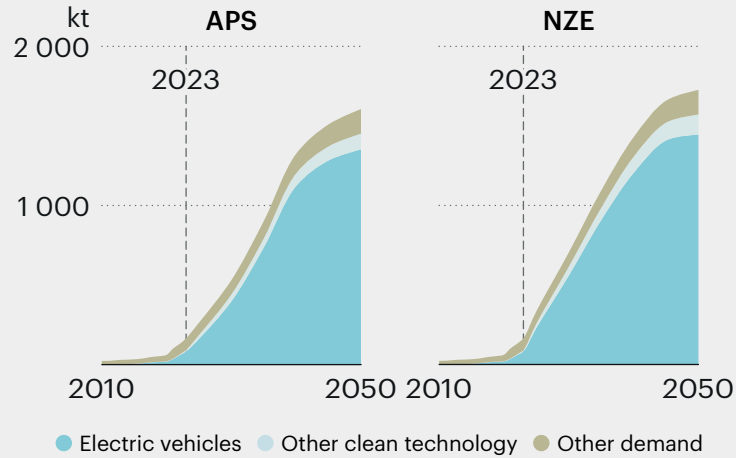
# Lithium

# Li

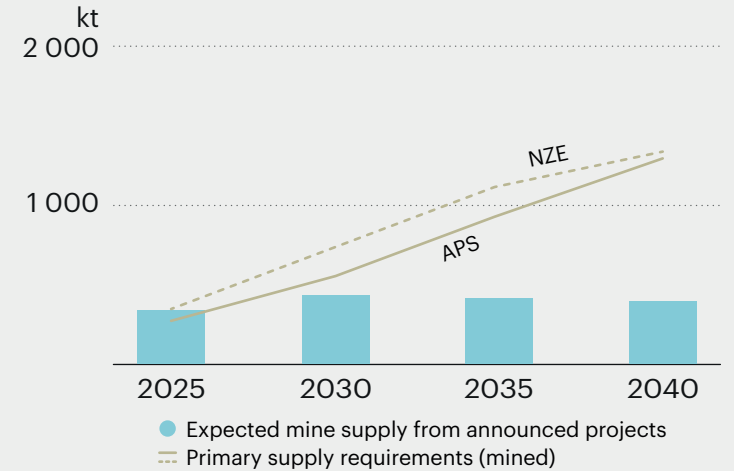
## Top three producers 2030



## Demand outlook



## Mining requirements



### Milestones (APS)

|   | 2021       | 2023       | 2030       | 2040         |
|---|------------|------------|------------|--------------|
| Cleantech demand (kt)                   | 38         | 92         | 442        | 1 203        |
| Other uses (kt)                         | 63         | 73         | 90         | 123          |
| <b>Total demand (kt)</b>                | <b>101</b> | <b>165</b> | <b>531</b> | <b>1 326</b> |
| Secondary supply and reuse (kt)         | 2          | 5          | 28         | 154          |
| <b>Primary supply requirements (kt)</b> | <b>100</b> | <b>160</b> | <b>503</b> | <b>1 172</b> |
| Share of top three mining countries     | 89%        | 85%        | 68%        | 70%          |
| Share of top three refining countries   | 100%       | 96%        | 85%        | 84%          |

## Clean energy transition risk assessment

Low Med High

### Supply risks

**Highest**

price volatility than other focus minerals

### Geopolitical risks

**85%**

of refining by top three countries in 2030

### Barriers to responding to supply disruption

Only **3%**

of lithium sourced from secondary supply today

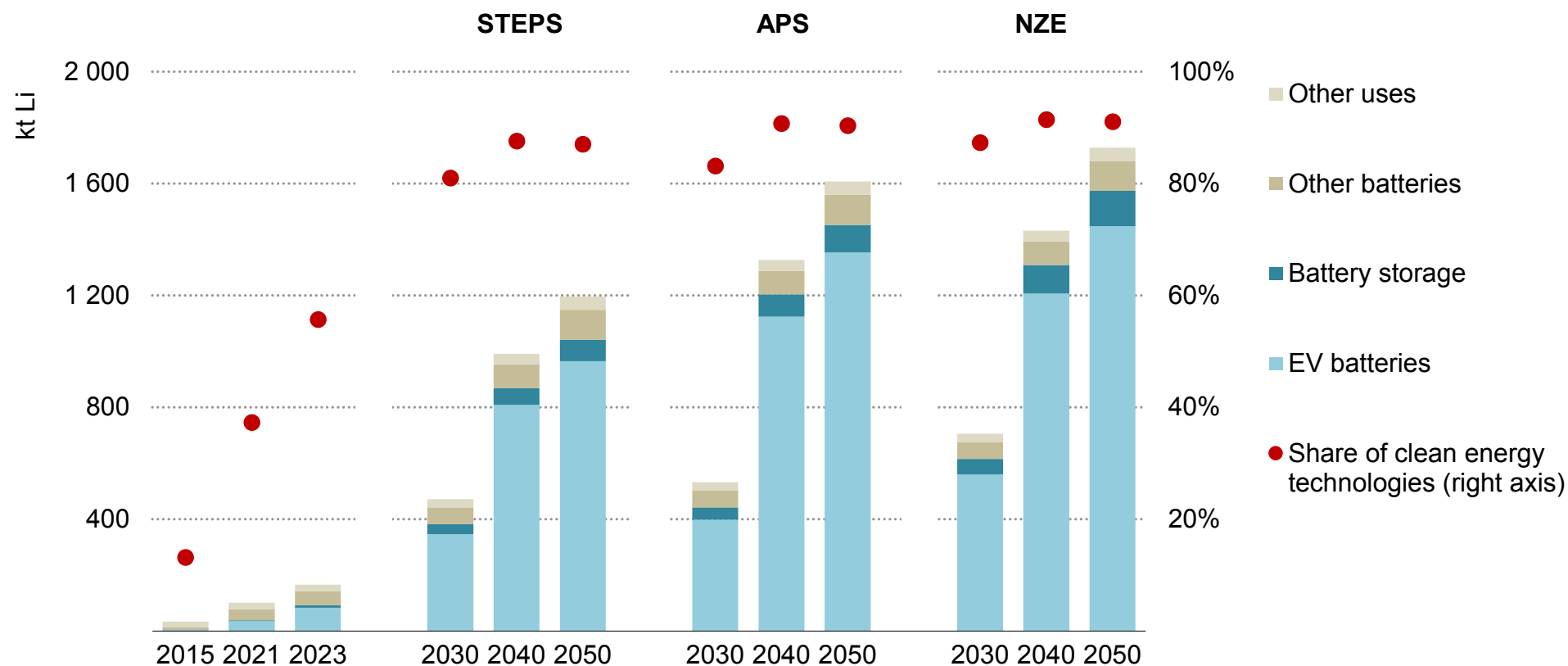
### ESG and climate risk exposure

**50%**

of mines located in high, very high and arid areas

## Demand: In clean energy transitions, lithium is the mineral facing the fastest demand growth

Global lithium demand outlook by sector and scenario



IEA. CC BY 4.0.

## **Demand: Lithium fuels the growth of the EV industry, and its demand grows tenfold to 2050 in the NZE Scenario, propelled by the rapid deployment of EVs**

Lithium is used in a variety of applications such as ceramics or lubricants, as well as in small volumes in pharmaceuticals, but demand structure has deeply transformed over the last ten years, making batteries the dominant driver of global lithium demand growth. Lithium, one of the lightest metals in the periodic table, is the natural candidate for high energy density in batteries due to its superior electrochemical characteristics.

Lithium demand is set to rise almost threefold over this decade in the STEPS, expanding faster than all other focus minerals. By 2050, demand reaches 1 200 kt Li in the STEPS and 1 600 kt Li in the APS. In the NZE Scenario, demand increases to 1 700 kt Li by 2050, a tenfold growth from today's levels, driven by clean energy technologies.

Not only is lithium critical to clean energy transitions, but the lithium industry's ability to ramp up has allowed the EV industry to outpace industry expectations. The EV industry contributes to about 90% of future lithium demand growth between today and 2050 in the APS. Meeting the 1.5 °C climate objective requires particularly rapid growth this decade: in 2030, the EV sector's annual lithium demand is 40% higher in the NZE Scenario than in the APS.

Battery storage is currently a minor consumer of lithium, accounting for about 5% of demand, but its development accelerates by the end of the decade. In the NZE Scenario, lithium demand for battery storage rises to 130 kt Li in 2050, well over ten times the current demand.

Lithium-ion batteries' role in fuelling the growth of the EV industry remains unchallenged in the near term. Alternative technologies such as sodium-ion batteries and vanadium flow batteries begin to take some shares from lithium-ion batteries in low-range vehicles and storage markets, but they do not materially alter the prospects for lithium demand in climate-driven scenarios.

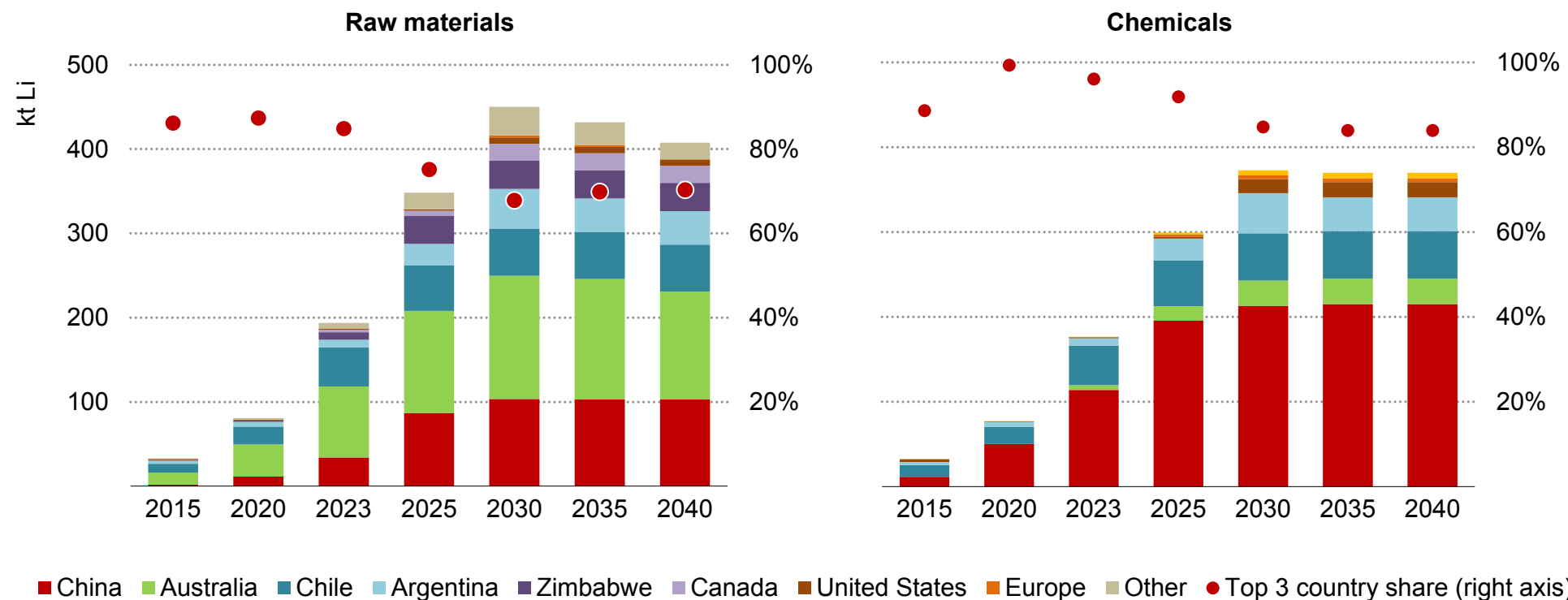
In an alternative case of the NZE Scenario where sodium-ion experiences wider popularity within the EV market, total lithium demand could be reduced by 10% in 2030. Likewise, in the case of an early adoption of vanadium flow technologies, demand for lithium in storage applications could be reduced by 6%.

If technical challenges around their scale-up are overcome, solid-state batteries with lithium metal anodes could create a new market for lithium in metal form (as opposed to chemicals such as carbonates or hydroxides), of 200 kt Li in 2040 and 330 kt Li in 2050 in the NZE Scenario.



## Supply: New lithium players emerge in Argentina and Zimbabwe; China continues to dominate refining of hard rock ore

Lithium raw materials and chemical production from operating and announced projects in the base case



IEA. CC BY 4.0.

Notes: Raw materials cover extraction of lithium from hard rock ore, as well as from clays and brines. Lithium chemicals cover the first production of lithium carbonate, hydroxide, sulphates and chlorides, and excludes reprocessing.

## Supply: New players emerge on the mining side; refining takes different trajectories depending on chemical product

### Mining

Today, annual production of lithium raw materials (from hard rock, brines and clays) amounted to around 190 kt Li in 2023, 70 kt Li from brines and 120 kt Li from hard rock. Lithium production has more than doubled in the past three years. The dominant producer of hard rock lithium is Australia, which produces 84 kt Li in the form of spodumene concentrate, mostly exported to China for refining. Another type of hard rock ore, lepidolite, is being developed, with a boom of production during the high price period of 2021-2023 in China's Jianxi province, providing 12 kt Li to the market in 2023. Brines are extracted in salt lakes of Latin America (46 kt Li for Chile and 9 kt Li for Argentina), but also from high plateaux in western China (14 kt Li).

Analysis of announced projects indicates that lithium raw material supply grows to 450 kt Li around 2030 in the base case, again more than doubling the current production, and reaching five times the production of 2020. In the high production case, an additional 70 kt Li of raw material supply could be made available on the market. If announced projects come online as planned, this volume approaches the requirements in the STEPS as well as in the APS in 2030, but is insufficient to stay on the 1.5 °C pathway. Beyond 2030, all scenarios require a further investment in new supplies to keep pace with the demand growth.

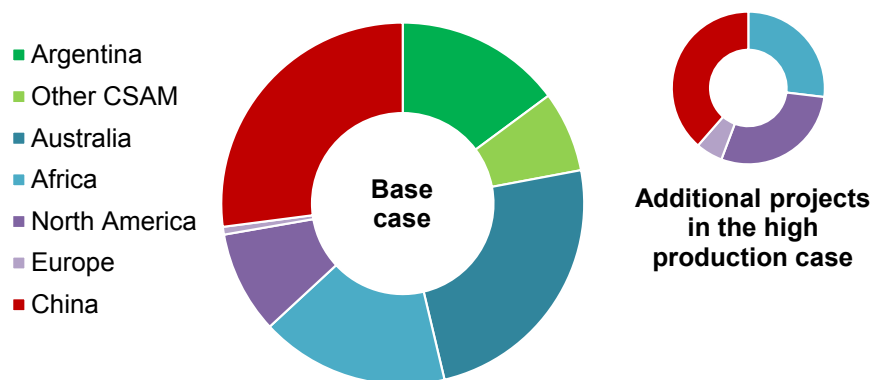
Australia remains a key producer of lithium with its spodumene deposits, through brownfield expansions of its major mines (Pilgongora, Greenbushes, Mount Marion and Wodgina) as well as several new projects, such as the Kathleen Valley and Mount Holland mines. Australia also hosts a first-of-its-kind tailings retreatment facility at Greenbushes, designed to extract further lithium from anterior mining waste. In the base case, Australia remains the largest producer in 2030, accounting for a third of world production.

China is the world's largest consumer of lithium as well as the world's largest refiner, but traditionally sourced lithium feedstock from mines overseas. Significant efforts have been made to develop domestic supplies, with notable investments in domestic mines from downstream manufacturers, such as CATL. The Chinese share of global lithium mining has steadily increased since 2016, from 6% to 17% in 2023. In the base case, it overtakes Chile and becomes the world's second-largest lithium producer in the mid-2020s.

Latin America has traditionally been a major lithium supplier with Chile's Salar de Atacama. Chile remains the continent's largest producer, but there are growing interests in Argentina, with a particularly strong pipeline of brine extraction projects. Based on announced projects, Argentina attracts over 80% of future capital investments for lithium in Latin America, with investors from all

regions, from the United States and Australia, as well as Europe (Eramet), China (Ganfeng, Zijin, Tibet Summit Resources) and Korea (POSCO Chemicals). By 2030, Chile’s base case annual supply grows to 56 kt Li, but Argentina emerges as a close contender, with 47 kt Li of production. Despite significant lithium resources in Bolivia (23 Mt, about a fourth of world known resources), projects have yet to emerge there. The country has signed an [agreement](#) with Russia’s Rosatom and China’s CITIC Guoan Group to develop its lithium resources and recently launched an [international tender](#) for lithium extraction, although significant challenges remain.

Geographical distribution of planned additional lithium mining projects, 2023-2030



IEA. CC BY 4.0.

Note: CSAM = Central and South America.

Lithium mining is a recent phenomenon in Africa, where Zimbabwean production has recently ramped up, with 9 kt Li of lithium exported

every year as concentrates of various hard rock ores (lepidolite, but also other minerals, such as petalite). Some informal artisanal and small-scale (ASM) mining activities have been reported in Nigeria, a phenomenon new to lithium, but frequent for other metals such as cobalt, gold, tin, tungsten and tantalum. Additional industrial capacities are planned in Zimbabwe, but other countries could follow suit, with projects in Ethiopia, Mali, Namibia, and possibly the Democratic Republic of the Congo and Ghana. In 2030, Africa's total lithium production in the base case rises to 53 kt Li, and further to 70 kt Li in the high production case.

There are many projects in the pipeline at their early stages of development, but price volatility may delay the projects coming up, particularly those outside of incumbent country producers, with implications for long-term supply and diversification.

### Refining

Two regions have historically dominated the supply of lithium chemicals, with three distinct business models. Refining of lithium-rich brines of China and Latin America is done locally, and lithium is then exported as a refined chemical – whether carbonate or hydroxide. This process traditionally involved evaporation ponds, making this relatively water-intensive. To reduce water requirements, a diversity of new “direct lithium extraction” technologies are under development, but may involve higher operating costs,

China currently dominates the refining of hard rock ore, from domestic resources, but also by refining the majority of lithium mined from hard rock overseas, notably from African countries and Australia. Lithium is generally mined and then locally processed into an exportable concentrate, but some African facilities, such as in Namibia, were built to directly [ship](#) ore to China.

Some operations focus on conversion of one chemical into another, notably lithium carbonate to hydroxide, covering about 20% of current hydroxide supply, a technology dominated by China.

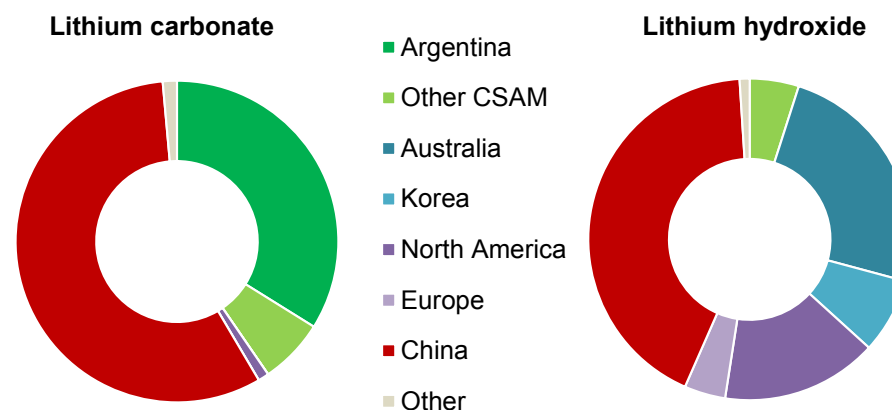
Lithium chemicals can be recycled from secondary resources, typically “black mass” either from end-of-life batteries or manufacturing scrap from gigafactories. Historically, battery recycling facilities focused on higher-value metals, such as nickel and cobalt, and lithium was often not recovered. Depending on prices, the uptake of lithium recycling may require policy incentives. A number of recycling companies are also achieving 90% recycling rates for lithium, and policy makers are strengthening recycling targets significantly, such as with the EU battery [regulation](#), all of which could help scale up secondary supply of lithium. In the APS, the share of secondary lithium supply increases from a low level today to 10% by 2040.

By 2030, lithium carbonate production nearly doubles to 220 kt Li in the base case, and possibly 260 kt Li in the high production case, but the project pipeline leaves little space for diversification. The top three country share remains close to 98%, covered by Argentina and Chile

(refining their domestic brines) as well as China, which remains the major hub both for its domestic extractive activities, but also for the refining of hard rock overseas into carbonates.

Projects being planned in other regions focus on lithium hydroxide, producing 170 kt Li in 2030 in the base case, and 185 kt Li in the high production case, more than twice the current production. The interest that investors take in hydroxide can be attributed to its dominance in North American and European demand, where the recent gigafactory projects almost exclusively focus on high-performance chemistries that require this chemical. The higher value of hydroxide is another aspect weighed by project developers, who anticipated a price premium relative to lithium carbonate.

#### Geographical distribution of planned additional lithium chemical projects, 2023-2030



IEA. CC BY 4.0.

China traditionally dominated refining of lithium from hard rock ore into hydroxide and continues doing so in the base case. It remains the main player with 60% hydroxide market share in 2030. Until recently, Australia was entirely dependent on China for the refining of its lithium ores, but two refineries are currently ramping up to produce lithium hydroxide, producing 30 kt Li by 2030.

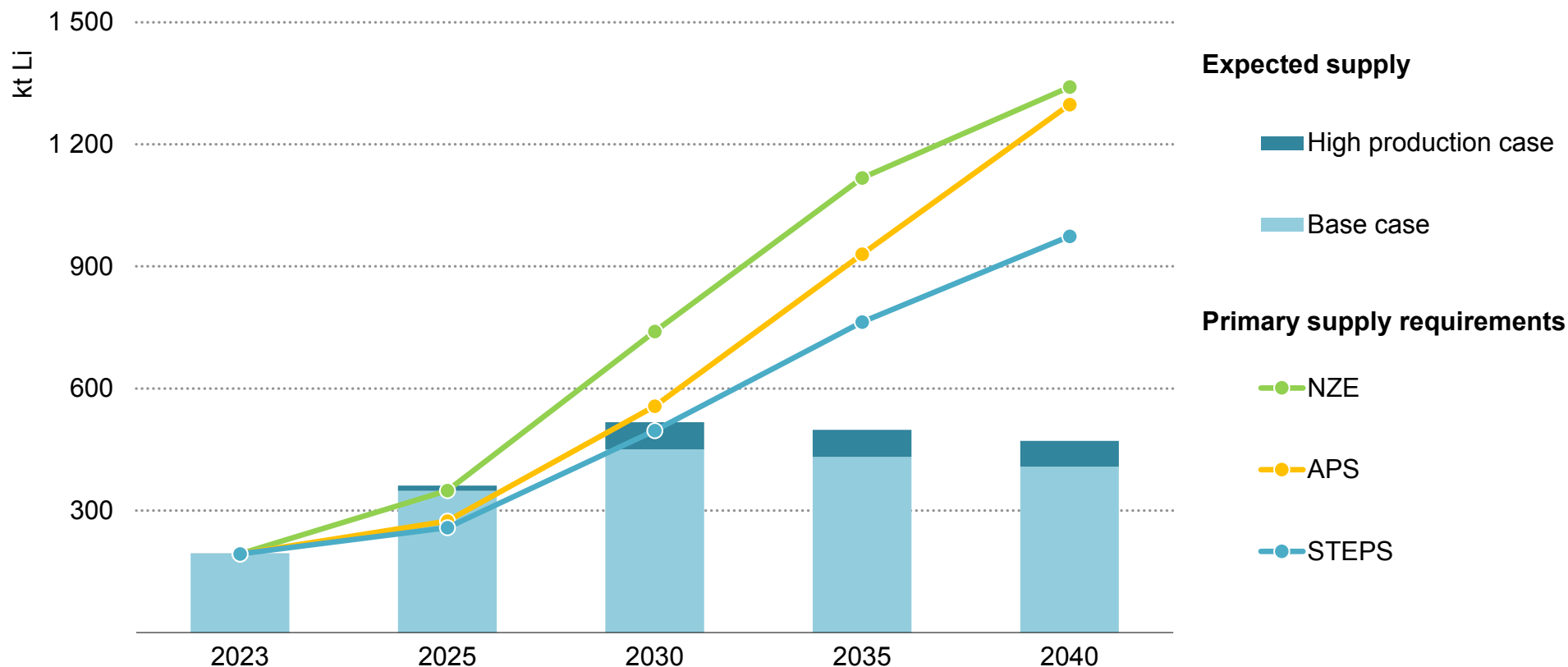
In other advanced economies, investors are also making bets on conversion facilities, importing carbonates and refining them into hydroxide closer to their consumers, with large plants including Albemarle's Megaflex projects, as well as AMG's Bitterfeld plant

inaugurated in 2022 in Germany and POSCO's planned conversion plant in Korea, as well as recycling plants. In North America and Europe, mining projects tend to be integrated, associating a mine with a hydroxide refinery.

Projects are also being considered outside of lithium mining countries. Indonesia's growth in nickel-rich cathode supply chain makes conversion plants likely to emerge there. Three lithium refining projects are also being considered in Saudi Arabia and the United Arab Emirates. However, refining projects have yet to emerge in Africa.

**Implications:** Short-term supply is expected to keep up with demand, but further projects need to come through to serve demand growth in the medium to long term

Expected lithium primary supply from existing and announced projects and primary supply requirements by scenario



IEA. CC BY 4.0.

Notes: Based on raw material output covering extraction of lithium from hard rock ore, clays and brines. Primary supply requirements are calculated as “total demand net of secondary supply”, also accounting for losses during refining operations. See Introduction for definitions of the base and high production cases.

## Implications: Investments are critical to keep pace with strong demand growth, but challenges remain in ensuring sufficient diversification and tailoring to future battery chemistry needs

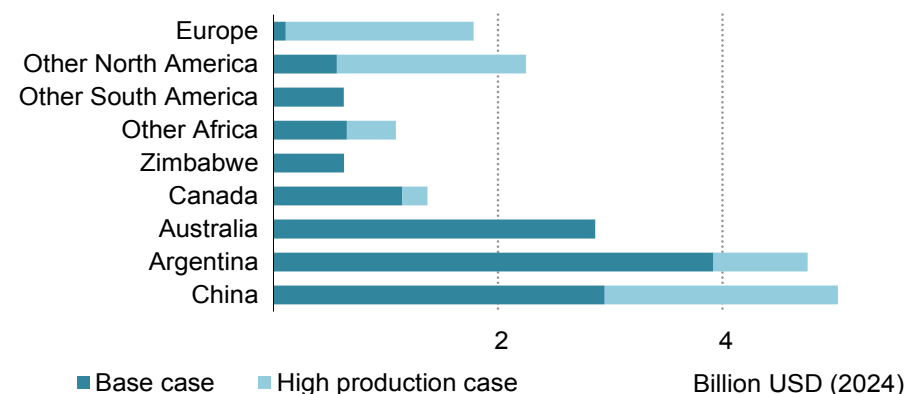
Recent price volatility may lead to short-term supply responses, discouraging investment for new supplies. In February 2024, production in the world's largest mine, Australia's Greenbushes, was [slowed](#), and other lithium producers announced plans to review their operations. Operating cost is one of the major considerations in production suspension decisions, but it is not the only factor. Those with long-term offtake agreements might continue even though their cost profiles are high, which could put additional pressure on prices beyond what supply-and-demand dynamics suggest. Symmetrically, integrated projects are reducing production, despite being on the lower end of the cost curve – such as Australian hard rock players.

There are risks that the current low-price environment may reduce investments in lithium projects, including those offering better ESG performance or outside of incumbent regions, which would affect medium- to long-term supplies. Many recent projects had been planned during periods of higher prices, and their viability may be reassessed if investors' long-term expectations are revised.

While the market is well supplied at the moment, continued investment flows are required to develop projects to serve long-term demand and diversification goals. At 2024 values, the current project pipeline in the base case requires USD 13 billion of investment for

raw material production, with an additional USD 7 billion required for the high production case.

Cumulative capital investment requirements to support the current mining project pipeline in the base case, 2024-2040

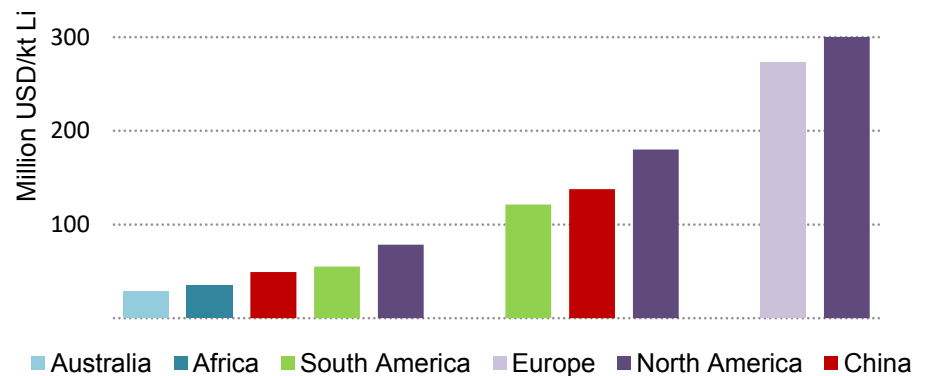


IEA. CC BY 4.0.

Sources: IEA analysis based on company reports, [Battery Materials Review](#).

Analysis of the project pipeline suggests that significant regional disparities exist in the capital costs for developing new projects. In particular, European and American lithium extractive projects generally require higher upfront costs. Business models often compensate for this disadvantage through integrated approaches offering highly refined products, but volatility in the refined chemical markets is putting price assumptions at risk.

### Average capital intensity of lithium mining projects



IEA. CC BY 4.0.

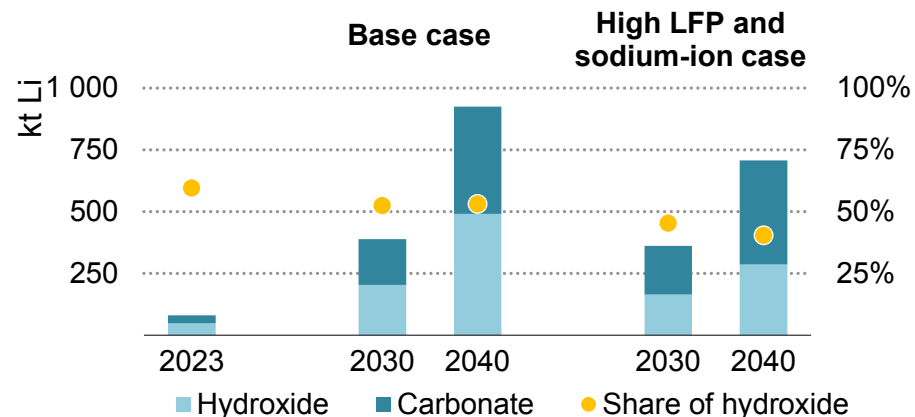
Sources: IEA analysis based on company reports, [Battery Materials Review](#).

In the long term, concerns remain regarding geographical and ownership concentration. Two trends are emerging. First, efforts to increase domestic feedstock supplies from dominant chemical producers – notably progress achieved by China researching new deposits and promoting domestic mining activities, with the financial support of domestic downstream battery manufacturers. Geological considerations put Chinese plays at a competitive disadvantage historically, but new deposits under development may be changing this picture. Notably, miners are developing domestic spodumene projects, the same type of ore as Australia’s lower-cost lithium mines.

The incumbent players’ endeavours to procure resources abroad indicate that sustained supply concentration may exist through

ownership – Chinese enterprises own most domestic ventures as well as major interests in Australian, Argentinian and African ventures.

### Lithium chemical demand by type in the APS



IEA. CC BY 4.0.

Finally, the lithium market structure is sensitive to the respective market shares of different battery chemistries, with growing supply chain segmentation between two chemicals: lithium hydroxide and lithium carbonate. Lithium hydroxide is required for nickel-rich chemistries, while carbonates are used both in the older generation of NMC chemistries and the LFP market. In the APS, EV requirements for carbonate and hydroxide are expected to rise in parallel, with hydroxide being required for 55% of total demand by 2030. In an alternative case where LFP takes a larger share, demand for hydroxide demand would be 25% less, calling for readjustments in regional sourcing strategies and project development planning.

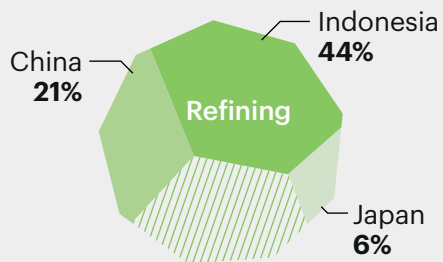
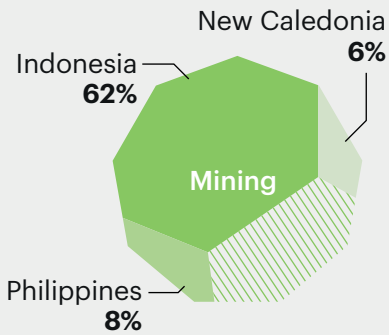


## Outlook for nickel

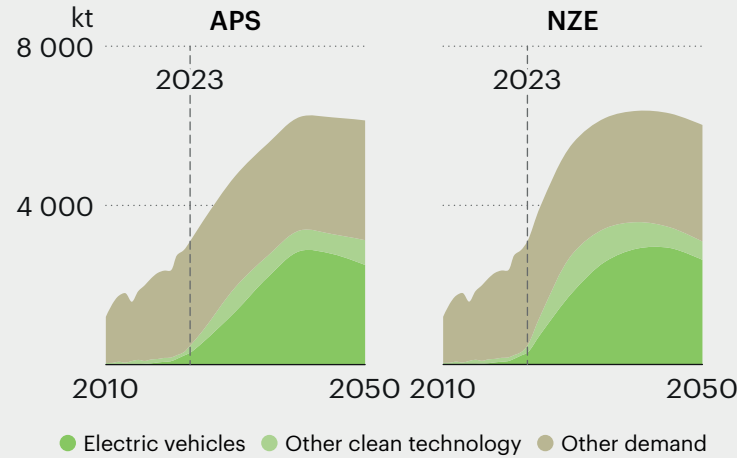
# Nickel

# Ni

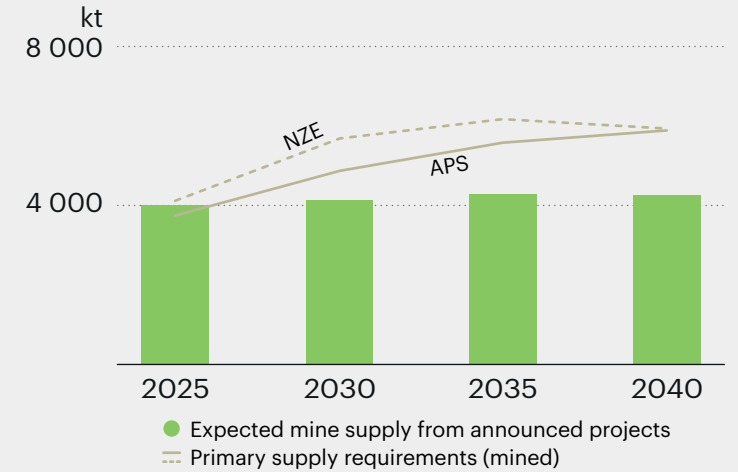
## Top three producers 2030



## Demand outlook

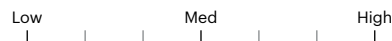


## Mining requirements



| Milestones (APS)                        | 2021         | 2023         | 2030         | 2040         |
|---|--------------|--------------|--------------|--------------|
| Cleantech demand (kt)                   | 240          | 478          | 1 953        | 3 381        |
| Other uses (kt)                         | 2 519        | 2 627        | 2 802        | 2 857        |
| <b>Total demand (kt)</b>                | <b>2 759</b> | <b>3 104</b> | <b>4 754</b> | <b>6 238</b> |
| Secondary supply and reuse (kt)         | 10           | 43           | 139          | 613          |
| <b>Primary supply requirements (kt)</b> | <b>2 749</b> | <b>3 061</b> | <b>4 615</b> | <b>5 625</b> |
| Share of top three mining countries     | 60%          | 69%          | 76%          | 83%          |
| Share of top three refining countries   | 66%          | 71%          | 71%          | 73%          |

## Clean energy transition risk assessment



### Supply risks

**6%**

of battery pack cost in 2023

### Geopolitical risks

**61%**

of mining by one single country in 2030

### Barriers to responding to supply disruption

**1%**

of nickel sourced from secondary supply today

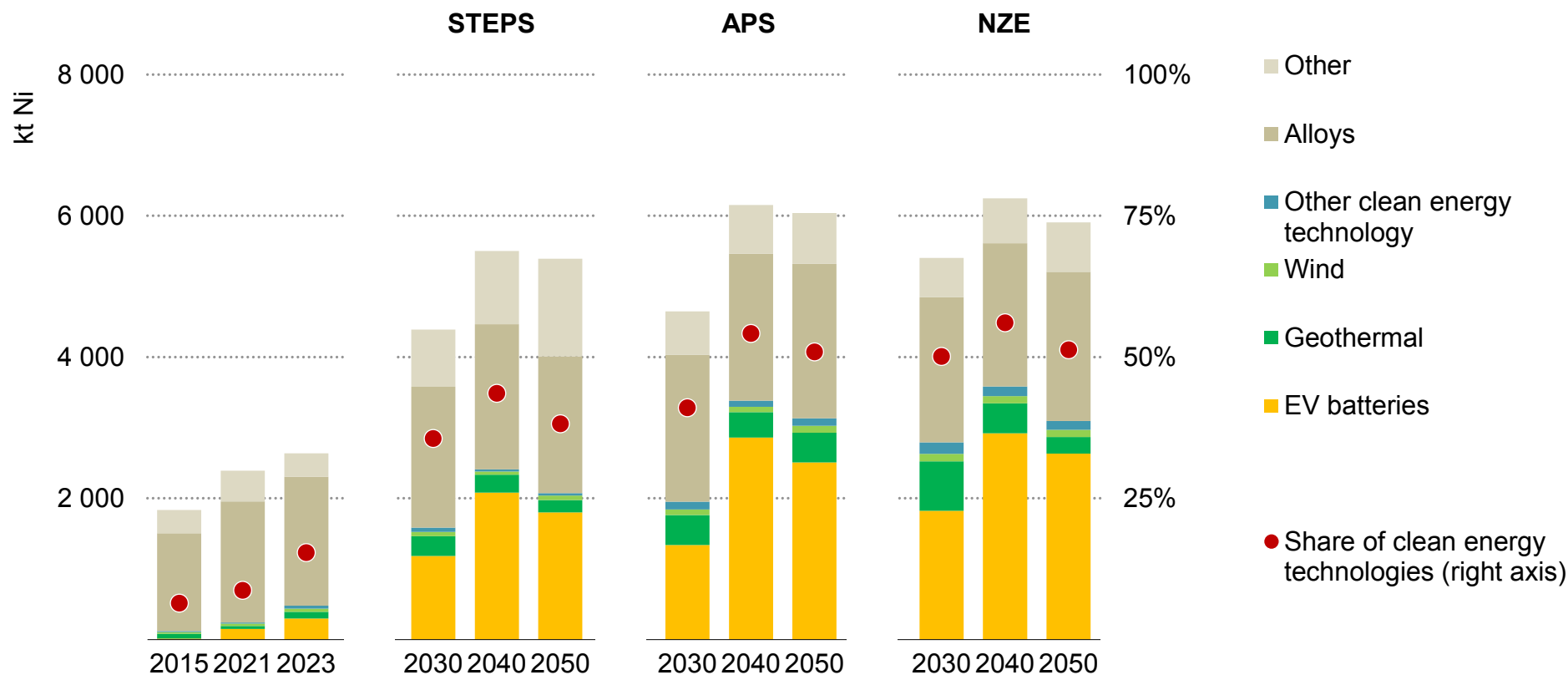
### ESG and climate risk exposure

**603** gCO<sub>2</sub>/kWh

Among the highest average grid carbon intensity for refining

## Demand: Growth in nickel demand is driven by clean energy applications; EVs become the largest-consuming segment in the coming decades in climate-driven scenarios

Global nickel demand outlook by sector and scenario



IEA. CC BY 4.0.

Note: Alloys includes both demand for stainless steel and for non-ferrous applications.

## **Demand: Nickel demand almost doubles over the period to 2050, driven by the rapid deployment of EV batteries**

Nickel is used in a wide range of applications and is important for the broad economy with its use for alloys and stainless steel, as well as in the clean energy sector. The largest applications in the clean energy sector are within EV batteries, but nickel is also used in low-emissions power generation, such as in wind and geothermal energy.

Global nickel demand remained steady between 2018 and 2020 around 2.4 Mt, but then began to increase rapidly, reaching around 3.1 Mt in 2023. Demand is set to grow further in all scenarios, increasing to 4.5 Mt in 2030 in the STEPS. In the APS, demand growth is slightly higher, rising to 4.8 Mt in 2030. In the NZE Scenario, demand increases more rapidly to 5.6 Mt in 2030 as more EVs and low-emissions power generation are deployed. By 2040, demand under the NZE Scenario is slightly higher than the APS, but sees a larger fall to 2050 due to lower demand for uses in stainless steel as secondary supplies increase.

Historically, demand for nickel was primarily for its use in alloys (including stainless steel and non-ferrous applications): in 2015, 75% of nickel's total demand was for alloys. However, from 2020 to 2023 this shifted substantially and demand from the clean energy sector became the main factor behind a 30% increase in overall nickel

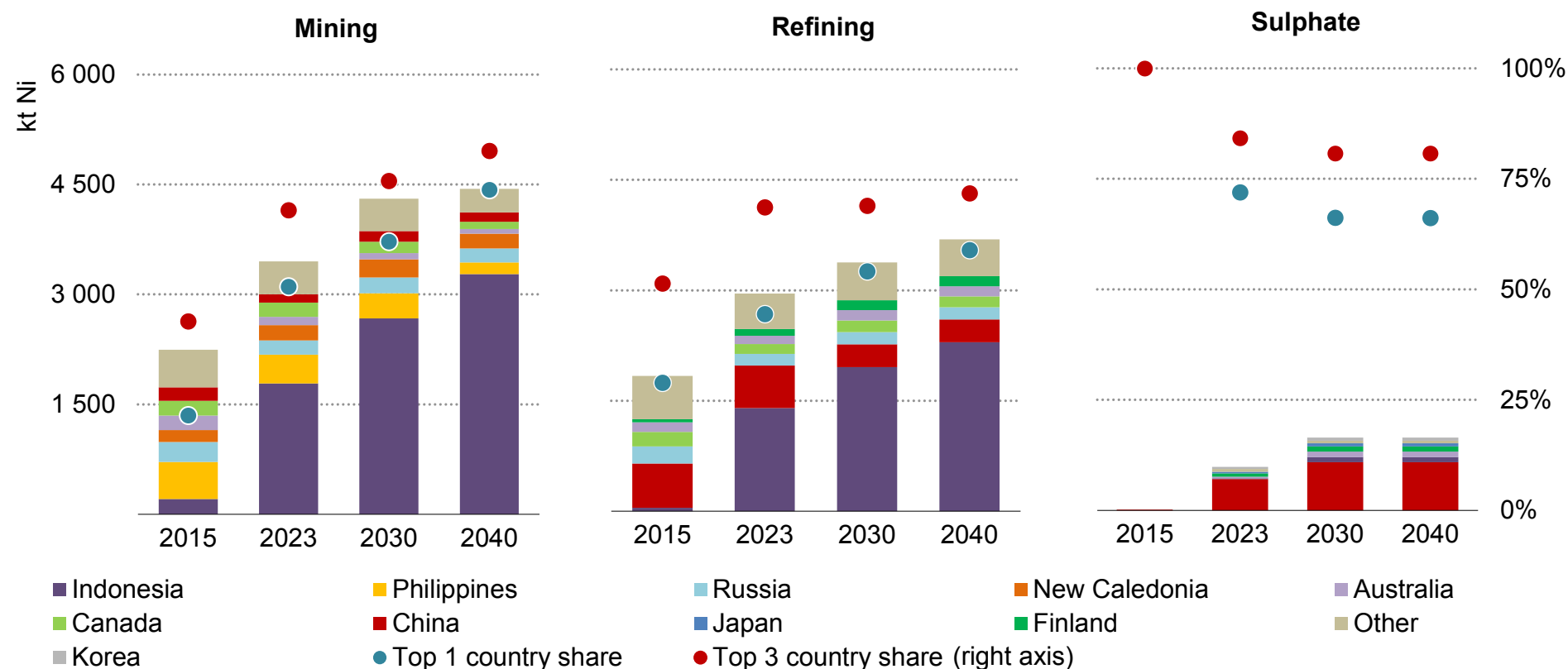
demand over this period. This was primarily due to the increasing use of nickel-rich EV batteries, but was also driven by the use of nickel in low-emissions power. In 2023, the share of clean energy applications in total demand crossed 15%.

Looking to the future, nickel demand for alloys continues to play a large role in overall nickel demand with around 50% of market share in 2050 under the STEPS. In both the APS and NZE Scenario, the market share of nickel in alloys falls to around 35%, in part due to the higher clean energy demand but also due to lower material requirements for steel.

Nickel use in clean energy technologies continues to drive overall growth in nickel demand. In all scenarios, clean energy technology's share in total demand continues to rise, peaking at around 40% in the STEPS and around 55% in the APS and NZE Scenario by 2040 before falling slightly due to lower demand for nickel-rich chemistries. However, the primary driver in nickel's demand growth continues to be EV batteries in all scenarios, whose demand increases by approximately ninefold between today and 2050 in the APS and NZE Scenario.

## Supply: Indonesia remains the largest producer of mined ore and refined primary nickel products to 2040; China dominates sulphate supply

Nickel production from existing and announced projects in the base case



IEA. CC BY 4.0.

Note: Nickel refining includes nickel that is processed into either a metal, oxide, nickel pig iron (NPI), or ferronickel and excludes outputs from intermediate production steps.

## Supply: Intermediates sourced from laterite ores contribute to the largest growth in nickel supply, while conversion of laterite ores to battery-grade nickel continues to grow

### Mining

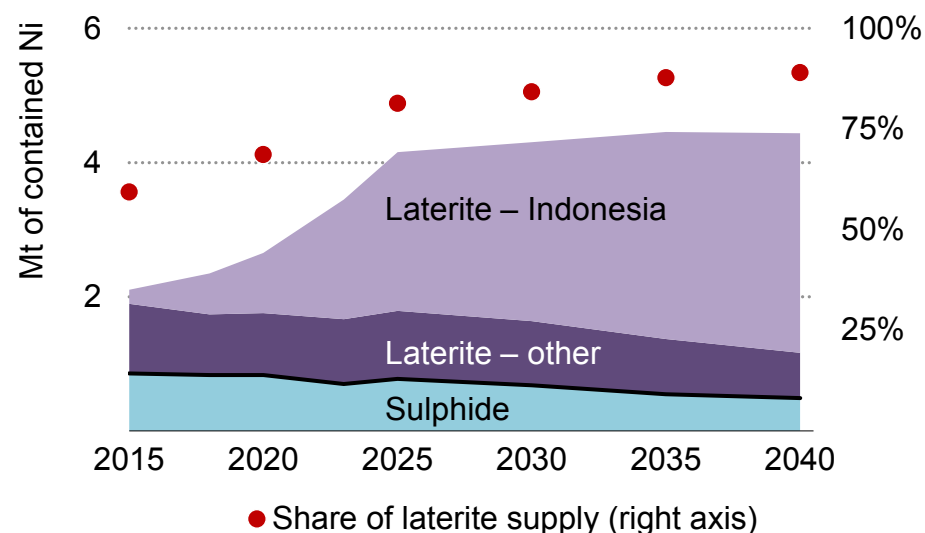
There are two types of nickel ore: laterite and sulphide. Laterite ores are primarily found in Indonesia, New Caledonia, the Philippines, and Australia, and sulphide ores are primarily found in Australia, Canada, Russia, and China.

Over the last five years, nickel mining has experienced significant absolute increases in the amount of material mined, as well as a shift in the type of ore mined. From 2018 to 2023, mined nickel supply increased by almost 1.5 times from 2.4 Mt to 3.5 Mt. This increase was primarily driven by the rapid expansion of mining in Indonesia, which saw a tripling in mined nickel output between 2018 and 2023, rising from just 0.6 Mt in 2018 to 1.8 Mt in 2023. Increases were also seen in Brazil, New Caledonia and Canada.

There has also been an increasing shift in the type of nickel ore, moving away from historically mined nickel sulphide to laterite. From 2018 to 2023, laterite mining nearly doubled from 1.5 Mt to 2.8 Mt, whereas sulphide mining fell slightly from 0.8 Mt to 0.7 Mt. This led to the share of laterites in total supply growing from 65% to 80%. In our base case, this trend is expected to continue until it reaches almost 90% in 2040, primarily driven by the growth in nickel mining in Indonesia, which almost doubles over the same period.

The mined nickel market has been increasingly geographically concentrated since 2018, with Indonesia's share of global production increasing from 25% in 2018 to 52% in 2023.

Mined nickel production by ore type in the base case



IEA. CC BY 4.0.

Looking ahead, in the base case, mined nickel supply is expected to continue growing to 4.4 Mt by 2040, marking a one-third increase from today. As our high production case assumes several early-stage projects come online, mined nickel supply grows to around 6 Mt by 2040, almost doubling. Geographical concentration is set to increase further in the base case, with the top three producing countries' share rising from 70% today to 83% by 2040. However, in the high production case, more projects come online from diversified regions, notably Australia and Brazil, bringing the top three countries' share slightly down to 81% by 2040.

In the near term, there could be some oversupply in the mined nickel market as a result of high investment into nickel developments in the last five years. In the longer term, expected supply from announced projects in the base case may fall short of meeting primary supply requirements in both the STEPS and APS by 2030. Additional projects that are assumed to come online in the high production case will need to materialise in this case. In the NZE Scenario, planned and high-potential projects fall short of primary supply requirements by 2030, requiring new projects to come through.

## Refining

There are two types of primary nickel products: high-purity Class 1 products (containing 99.8% nickel or above) and lower-purity Class 2 products (containing less than 99.8% nickel). Battery cathodes need

nickel sulphate, which has historically been produced from Class 1 products.

There are many stages of the supply chain to produce both Class 1 and Class 2 products. Intermediate products such as mixed-hydroxide precipitate (MHP) or mixed sulphide precipitate (MSP) are produced through hydrometallurgical processes such as bioleaching, and nickel matte is produced through smelting. Primary products such as nickel metals and nickel oxides, nickel pig iron (NPI) and ferronickel are produced through processes such as blast furnaces and electric arc furnaces, which can be used in end-use markets as final products. This section refers to the latter when discussing refined products.

Similar to nickel mining, refined nickel production has significantly increased over the last five years. From 2018 to 2023, refined nickel products grew 1.4fold to 3.1 Mt, primarily driven by growth in Indonesia, which saw an almost fivefold increase in production. Geographical concentration of the top producing country, Indonesia, grew from 30% to 45%, whereas geographical concentration of the top three producers grew from 50% to 70%.

Looking ahead, analysis of the project pipeline indicates that refined nickel production continues to grow in the base case, to 3.9 Mt in 2040. The largest driver of this growth is in NPI and nickel metals, each growing by around a quarter to 2040. This production is primarily driven by Indonesia, which sees an over 1.5-fold increase in refined nickel product production to 2040, primarily in the form of NPI, ferronickel and nickel metals. The top producing country – Indonesia –

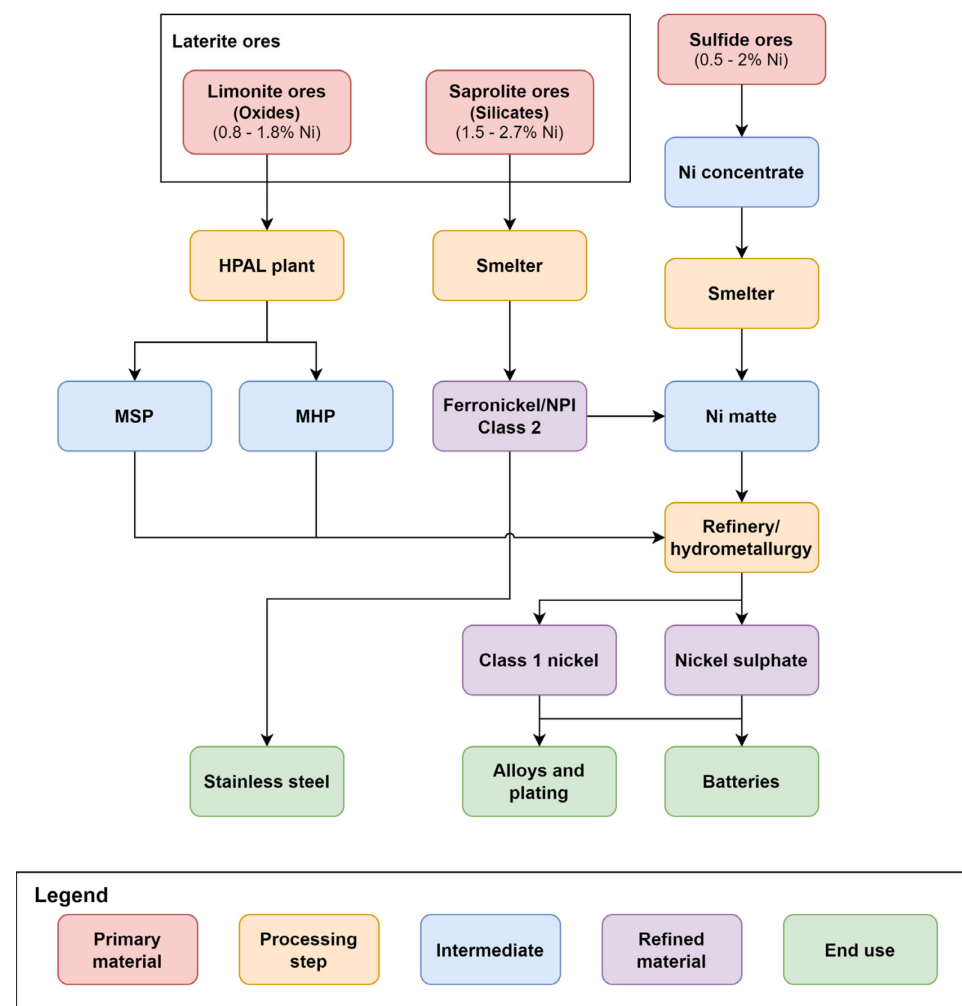
continues to maintain a dominating market share, growing from 45% in 2023 to 59% in 2040. The high production case does not see a much higher refined nickel supply. While there is slightly more production in countries outside of the dominant producer, such as Australia, the level of concentration barely changes compared with the base case.

### Sulphate

For use in EV batteries, nickel needs to be further processed into nickel sulphate, which is then used as input into battery cathodes. Historically, nickel sulphate has been obtained through refining sulphide ores into nickel matte or nickel metals and oxides pellets and then into battery-grade nickel as it requires high-content nickel. Recent nickel market developments, including high prices and Indonesia’s rise in prominence within the supply chain, have led to using MHP and MSP, sourced from laterite ores, as inputs for nickel sulphates. There has also been a rise in converting NPI and ferronickel – typically used in stainless steel applications – into nickel matte, which is then processed into nickel sulphate.

From 2018 to 2023, the most significant increase in inputs for nickel sulphate production was from matte via sulphide ores. Over the same period, there was also a rise in the production of nickel sulphate from matte via laterite ore and the intermediate MHP derived from laterite ore. In the base case, we anticipate this shift towards utilising matte via laterite and intermediates from laterite ores to continue through 2030.

### Nickel supply chain



IEA. CC BY 4.0.

Note: HPAL = high-pressure acid leaching.

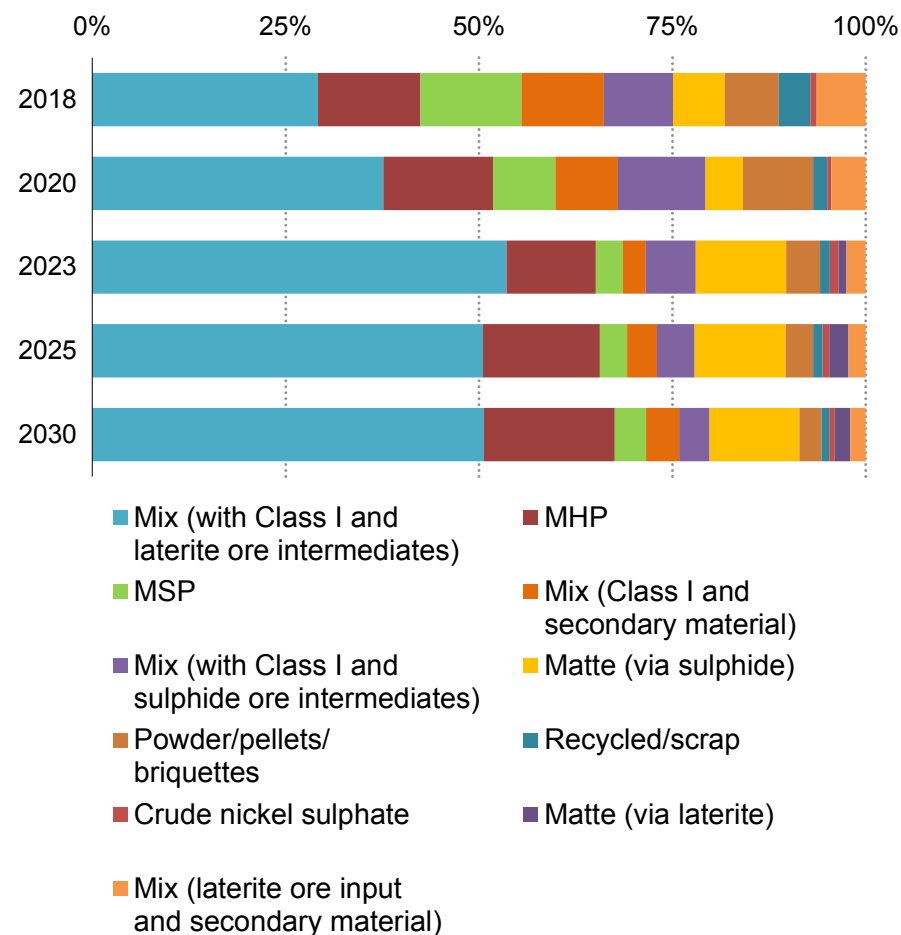


There is also large growth in the utilisation of a mix of inputs into nickel sulphate production, with the largest absolute increase seen in a combination of Class 1 and laterite ore inputs, through either MHP or matte. Mixes combining Class 1 and recycled material or scrap also increase to 2030. In our high production case, while slightly more sulphate projects that utilise matte via sulphide may come online, the primary input drivers are expected to remain as laterite ore inputs.

The surge in processing laterite ore for nickel sulphate production has been chiefly propelled by Indonesia, and the country is poised to maintain its leading role in driving growth in this sector. In the base case, Indonesia sees an over twofold increase in MHP production and an increase of 1.4 times in matte production by 2030.

In the near term, nickel sulphate may be adequately supplied to 2025. However, in both the APS and NZE Scenario, nickel sulphate requirements exceed expected sulphate supply from announced projects by 2030 and beyond, even with increases in sulphate supply from secondary production as more EV batteries are deployed and recycled. However, new sulphate capacity can be introduced relatively quickly – within 18-24 months – and we expect that supply can be relatively responsive to developments within the EV battery industry.

Inputs into nickel sulphate production

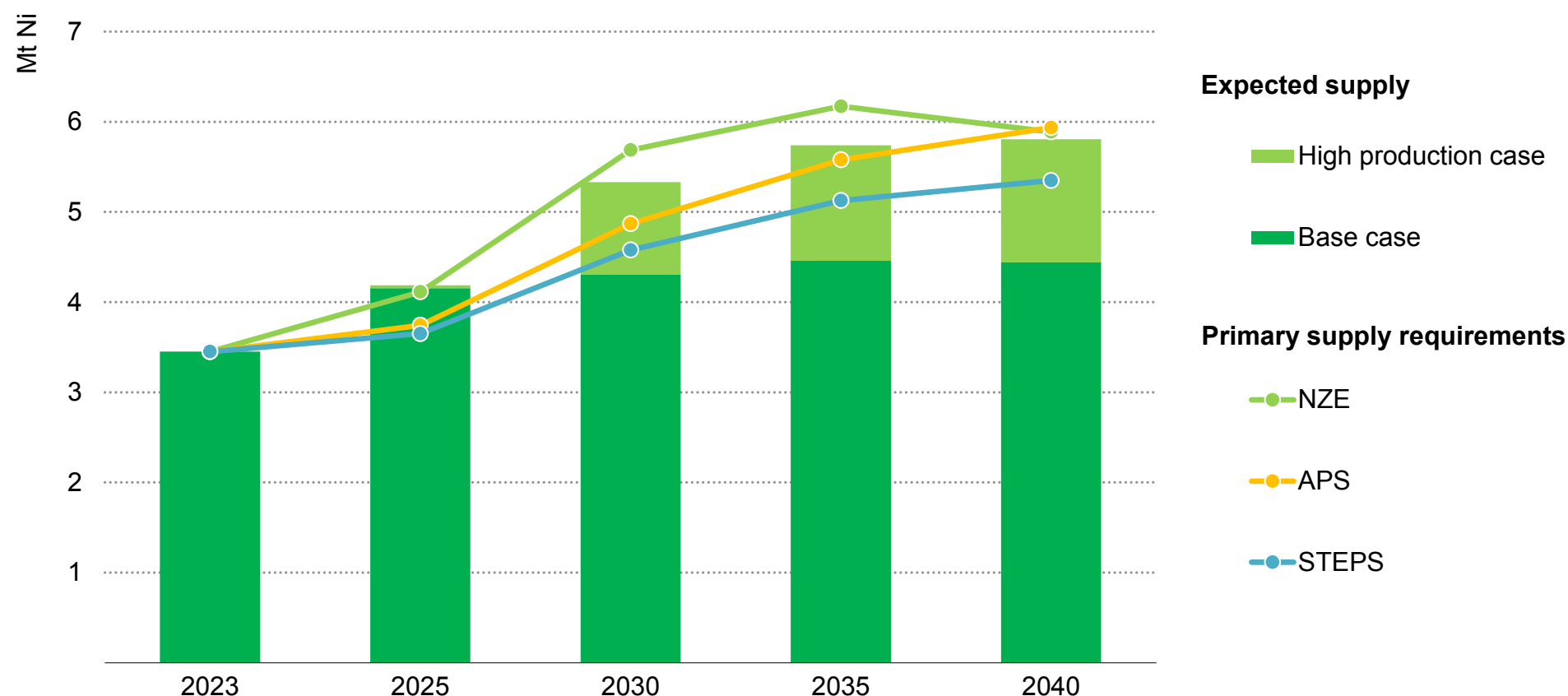


IEA. CC BY 4.0.

Note: Included in Class 1 is power/pellets/briquettes.

**Supply:** The market could be well supplied in the near term, but additional projects need to come through to meet demand in climate-driven scenarios in the medium and long term

Expected mined nickel supply from existing and announced projects and primary supply requirements by scenario

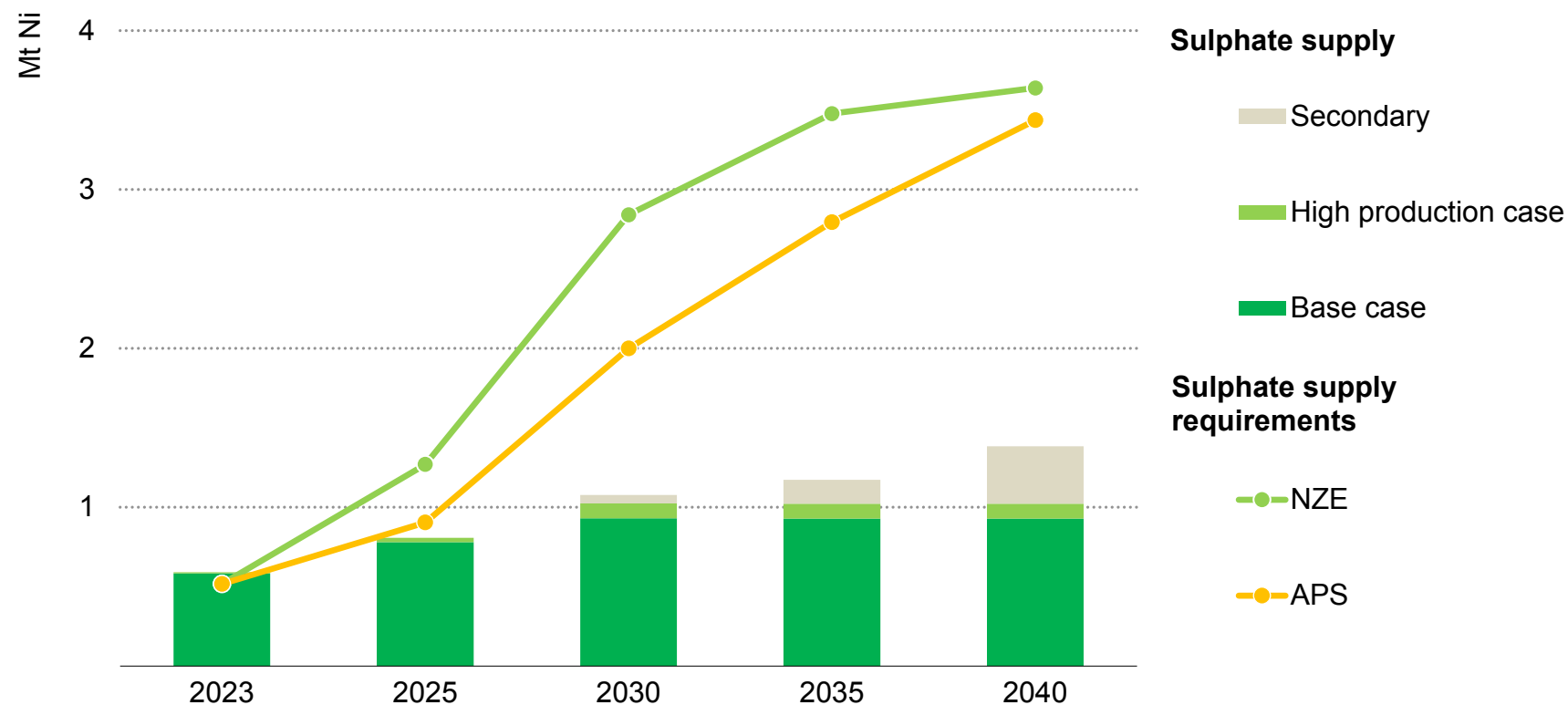


IEA. CC BY 4.0.

Notes: Based on mined output. Primary supply requirements are calculated as “total demand net of secondary supply”, also accounting for losses during refining operations. See Introduction for definitions of the base and high production cases.

**Supply:** Analysis of the current project pipeline indicates that battery-grade nickel may see potential supply gaps in climate-driven scenarios by 2030, even with secondary supply

Nickel sulphate supply and demand balances based on existing and announced projects



IEA. CC BY 4.0.

Notes: Sulphate supply requirements includes nickel demand from EV batteries and demand from non-batteries. Does not include a route where precursor cathode material is directly produced from refining operations.

## Implications: Today's low-price environment creates risks for future nickel supply and for the prospects for greater diversification

The recent low-price environment for nickel prompted several nickel producers to implement cost-cutting measures at existing operations. For instance, [First Quantum's nickel mine](#) announced production cuts, while [BHP's Nickel West operations](#) reduced its workforce. Additionally, other producers, such as [Glencore's Koniambo nickel mine](#), placed their operations into care and maintenance. Consequently, nickel production in 2023 was lower than anticipated, with announced nickel mining production cuts and closures totalling around 80 kt.

While the continuation of low nickel prices supports the growth of the EV market by keeping battery prices low, there is a potential downside: it may lead to further closures of nickel mines or halt ongoing developments. Operations such as BHP's Nickel West are contemplating putting their mines [under care and maintenance](#), while New Caledonia's production faces [the risk of investor loss](#). Reports have surfaced of producers halting project development due to nickel's low price, which threatens the long-term profitability of projects such as [IGO's Cosmos nickel project](#). This risk of closure and development halts is especially pronounced for projects with

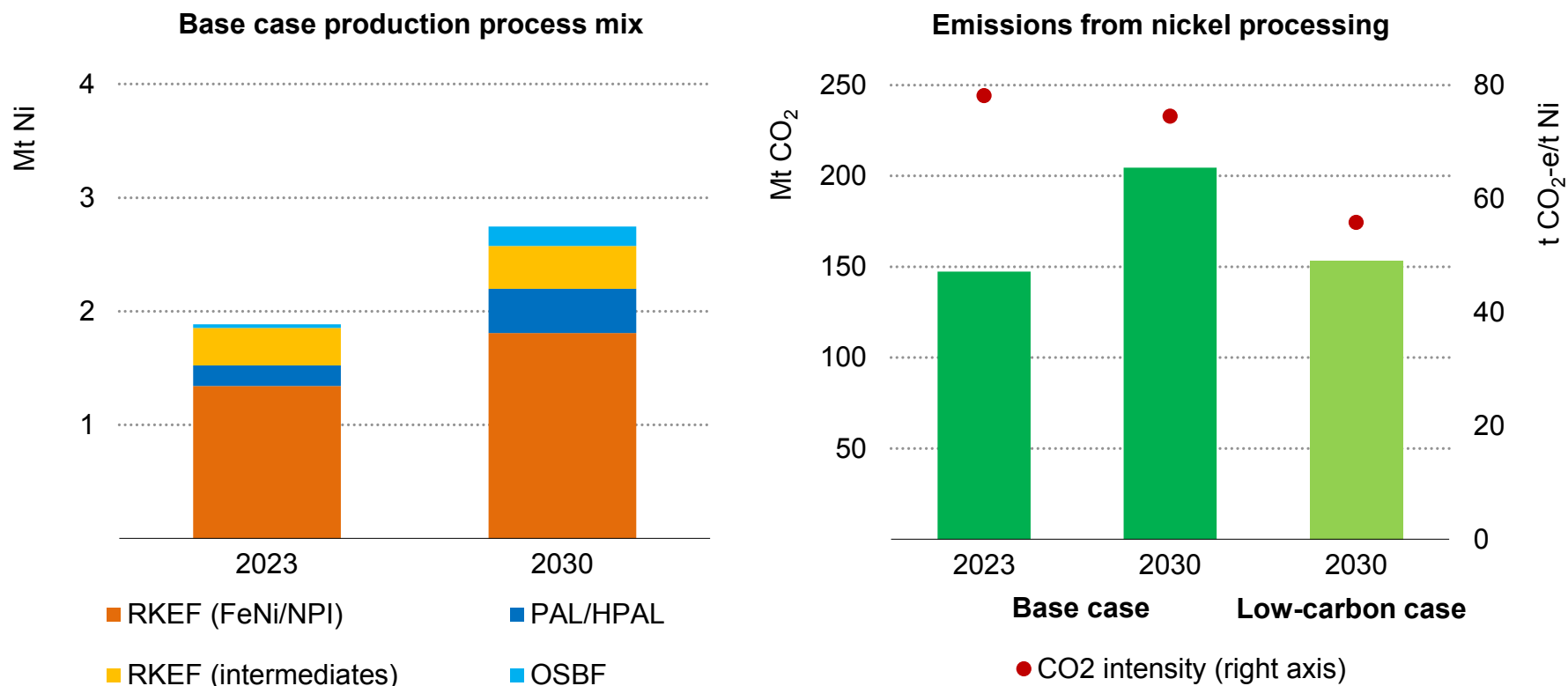
higher costs and lower margins, often located in regions beyond the current dominant producers.

We have identified approximately 25 operating or potential mines that could be at risk if the current low nickel price persists, primarily located in Canada and New Caledonia. While closures of these nickel mines and production cuts may not immediately result in a significant undersupply of mined nickel, given that the market is currently well-supplied, they could lead to a shortfall in supply compared with medium-to-long-term demand in the APS and NZE Scenario. The total supply loss would be around 360 kt of supply in 2030 and 280 kt in 2040, respectively, almost 10% of supply in each year.

The larger concern stemming from the continuation of the current low-price environment is the potential closure of high-cost nickel mines, which would further reduce the diversity of supply in an already geographically concentrated market. If all at-risk nickel mines were to close, this would increase Indonesia's market share — the top nickel mining country — and the top three countries' share by around 6 percentage points in both 2030 and 2040.

**Implications:** Without greater efforts to shift to less energy- and emissions-intensive processes, emissions from Indonesian nickel production are set to increase

Indonesia nickel processing volumes and associated emissions



IEA. CC BY 4.0.

Notes: CO<sub>2</sub>-e = carbon dioxide equivalent; RKEF = rotary kiln electric furnace; OSBF = oxygen-rich side blowing furnace; PAL = pressure acid leaching. The low-carbon case adopts “best case” intensities from the [Minviro paper](#), which assume that processing operations are utilising renewable electricity and, where possible, non-coal thermal energy and reductants.

## Implications: Indonesia has a major role in shaping the global nickel market

In both the base case and high production case, Indonesia's role in the global nickel market continues to expand as the country boosts its mining, refining and nickel sulphate production capacities. Indonesia's laterites ores are converted into nickel ready for conversion to battery-grade nickel by two methods: through processing to MHP or MSP through hydrometallurgical processes such as HPAL or the production of ferronickel or NPI through electric furnaces such as RKEFs, which is then converted into nickel matte.

Emissions per tonne of nickel vary by processing method. Currently, the [emissions intensity of nickel production](#) is estimated to be about 65 t CO<sub>2</sub>-e to 105 t CO<sub>2</sub>-e for RKEF and 10 t CO<sub>2</sub>-e to 60 t CO<sub>2</sub>-e for HPAL depending on the source of electricity and thermal energy or reductant utilised. These variations between processes primarily stem from the higher energy intensity of the laterite-to-NPI via RKEF process, which requires more electricity – around 500 kWh more per tonne of feed – as well as a greater direct use of carbon-intensive chemical reductants and heat energy sources.

In 2023, the primary production route of nickel in Indonesia was RKEF (to produce ferronickel or NPI), which accounts for almost 90% of production, resulting in an estimated 150 Mt CO<sub>2</sub> emissions from nickel production in the country. In both supply cases, operational ramp-ups and new projects in Indonesia lead to a shift in the production mix towards less energy-intensive processes. By 2030,

the share of RKEF production is projected to decrease to around 80%, remaining stable through 2040. Meanwhile, HPAL is expected to increase its share of the production mix to approximately 15% by 2030. Additionally, OSBF processes also see a growing role, rising from 2% of the production mix in 2023 to 6% by 2030 in the base case.

This transition away from RKEF towards less energy-intensive processes could, on its own, lead to a reduction in the overall CO<sub>2</sub> intensity per tonne of refined nickel in Indonesia, from around 80 t CO<sub>2</sub> per tonne to around 75 t CO<sub>2</sub> per tonne by 2030. Despite this decrease in average intensity, if Indonesia's power and thermal energy sources for nickel processing remain dependent on coal, as they do today, absolute CO<sub>2</sub> emissions from nickel refining could be 1.4 higher in 2030 and 1.6 times higher in 2040, compared with 2023.

Indonesia is working to shift its energy mix to cleaner sources, which, in line with a long-term goal of reaching net zero emissions by 2060, could help to reduce the carbon impact of the country's nickel production. There are indications of some near-term progress by industry players. For example, one company is developing [several HPAL projects while exploring replacement of coal](#) with lower-emissions alternatives such as gas and bioenergy.

However, significant work remains to lower the carbon footprint of nickel operations, with measures that address energy demand requirements and emissions from power, chemical and thermal energy processes. As an illustration, if the Indonesian production processes projected in this report's base case were to reduce their CO<sub>2</sub> intensity to the "best case" levels identified in the Minviro paper, which assumes that processing operations utilise renewable electricity and, where possible, non-coal thermal energy and reductants, their average CO<sub>2</sub> intensity would decline by 25% ("low-carbon case"). Absolute CO<sub>2</sub> emissions would be similar to today's levels in 2030 and 20% higher in 2040 than today, despite the almost 65% increase in production.

Moreover, refining and processing operations often cause air, land and water pollution, in addition to significant carbon emissions, and there are trade-offs between the two commonly used processes for converting laterite ores to intermediates for battery-grade nickel. The process of using HPAL results in high waste production but has lower emissions intensity, whereas RKEF results in less waste but extremely high carbon emissions.

There are other environmental issues that could arise from Indonesia's growing role in the nickel market. The shallow, open-pit mining methods used in Indonesian nickel production have led to [significant deforestation and the clearing of farmland](#). Research estimates that the [direct land footprint of nickel mining in Indonesia amounts to 42 m<sup>2</sup> per tonne of nickel](#) contained in ore. Under the base case production, this would equate to around 800 km<sup>2</sup> of additional land use impact between today and 2030.

In addition, tailings management associated with HPAL production is a persistent issue. While initial proposals for [deep-sea tailings placement were dropped over environmental concerns](#), the alternative, [land-based dry tailings stacking](#), still faces technical challenges driven in part by Indonesia's warm and humid climate. Hydrometallurgical waste from HPAL plants can be neutralised, dried and compacted by lining with geotextiles or thick clay layers to prevent waste stream leakage. However, significant investments in drainage and filtration systems are required to mitigate the impacts of high rainfall.

## The use of captive power for nickel in Indonesia

One of the main drivers behind high emissions intensity of Indonesia's nickel is the reliance of the country's power on fossil fuels, especially coal, which make up 81% of the on-grid electricity mix. Approximately [a quarter](#) of current coal-generated power in the country is not grid-connected, known as "captive power", and serves energy-intensive industries, especially minerals processing, which are viewed as important to realising Indonesia's industrial strategy. Coal plants integrated with industries that support value addition in the natural resources sector or have a major contribution to job creation and/or national economic growth are exempted from the moratorium on development in [Perpres No. 112/2022](#).

Over the last ten years, Indonesia has seen an increase in captive coal power capacity, which rose nearly [eightfold from 1.4 GW to 10.8 GW](#). Without a shift in the business plans, technology choices and regulation of such plants, growth is likely to continue, with estimates of the pipeline for new captive coal power ranging from [14.4 GW](#) to [over 20 GW](#) by 2030.

Around two-thirds of existing captive coal plants service the operating nickel smelters in the country, which are located in places that are not well integrated with the grid-connected power system.

Growth in smelter capacity and captive power to support it was driven in part by the country's [export ban of nickel ores in 2020](#). In Central Sulawesi, the location of the Morowali Industrial Park, there is [almost 1 Mt of production capacity and about 2.7 GW of captive coal power](#) in operation, with a further 2.8 GW under construction. The locations of many of the other nickel refining operations in the country – Obi Island and Weda Bay – also have many operating and planned captive power operations.

To prevent a substantial rise in CO<sub>2</sub> emissions as nickel production expands, Indonesia will need to accelerate the uptake of low-emissions alternatives to captive coal power and find ways to phase out existing captive coal plants, as part of an overall strategy to shift Indonesia's nickel sector to a low-emissions pathway. The [Just Energy Transition Partnership](#) plans to develop a study on transitioning the captive power sector, building on Perpres No. 11/2022. Indonesia also released an [Indonesian Taxonomy for Sustainable Finance](#) which incorporates provisions for financing coal plants, aiming to expedite their closure. However, according to the taxonomy, new captive coal plants may be classified as a transition asset, and thus still eligible for finance, if involved in the processing and mining of critical minerals for the energy transition, such as nickel.



## Implications: A price premium for low-emissions nickel?

As low-cost, high-emissions Indonesian nickel has come at scale to the global nickel market, market stakeholders have called on policy makers to support pricing mechanisms that can support the market for more sustainably produced nickel. However, the London Metal Exchange (LME) [rejected calls](#) to create traded contract specifications that would support a price premium for low-emissions or responsible nickel, citing concerns about market liquidity and interest as well as a lack of an agreed definition of “green.”

Instead, the LME has highlighted its [partnership with Metalshub](#), a digital platform for metals procurement and trading, as a way to help market participants assess potential premiums for “cleaner” nickel. Metalshub, in collaboration with a consultancy Minviro, plans to [integrate nickel’s carbon footprint data](#) into the Metalshub procurement platform. While Metalshub does not play an active role in facilitating price determination in the way that an exchange like LME does, its [recent announcement to begin reporting volumes of low carbon Class 1 nickel](#) could contribute to market-based price discovery for a “green premium.” LME and Metalshub have defined “low-carbon” nickel as having a carbon footprint lower than 20 t CO<sub>2</sub>-e.

Similarly, [Fastmarkets](#) and [Benchmark Mineral Intelligence](#), price reporting agencies, have proposed launching price assessments to distinguish cleaner nickel. The Fastmarkets specification would use

self-reported transaction data to identify whether, and at what levels, the market is paying a premium for nickel briquettes with a carbon footprint of less than 18 t CO<sub>2</sub>-e, whereas Benchmark’s assessment considers transaction data for nickel sulphate sourced from companies assessed to be “industry leading” within their proprietary ESG scoring system.

The Fastmarkets and Metalshub emissions thresholds would exclude ferronickel and NPI production due to their relatively high carbon footprints but may still allow some production from HPAL pathways. However, it should be noted that the non-emissions environmental impacts associated with HPAL routes may require a more holistic view of sustainability that goes beyond the carbon footprint alone.

Despite efforts by market participants, it is difficult to imagine a significant premium emerging voluntarily, at least at a level that would support higher-cost producers to restart or maintain production. Processing and manufacturing industries are sensitive to raw material input prices, and voluntarily paying above market price for feedstock is likely to significantly impact their competitiveness. Regulatory intervention may need to play a key role in incentivising the production and consumption of responsibly sourced materials.

Subsidies or tax credits could be used to support the production of responsibly sourced nickel, with those provided under existing provisions such as the [Inflation Reduction Act](#) given only to producers

that source a certain percentage of their nickel supply from “responsibly sourced” supplies or whose upstream greenhouse gas emissions are below a certain threshold. In addition to its [nickel finance assistance programme](#), Australia is considering introducing [nickel production tax credits](#) similar to those in the IRA, which considers giving a production tax credit of 10% to critical minerals producers. Such tax credits might be tied to emissions, giving preferential rates to low-emissions producers.

Pricing differentiation between different sources of nickel could also be established through carbon pricing and trading schemes. The [European Union's Carbon Border Adjustment Mechanism](#) (CBAM), which imposes a carbon tax on imported energy-intensive goods, could be expanded to include other raw materials such as nickel or the embedded emissions in downstream products, such as stainless steel. Disclosure policies, such as the [EU Battery Regulation](#) which by 2025 will mandate battery producers to disclose the complete carbon footprint of EV batteries over their life cycle, could also make it easier for purchasers and consumers to determine the emissions of different nickel sources, which could support voluntary adoption.

At a minimum, all these actions would require policy makers to develop criteria to distinguish between supplies based on ESG performance. Establishing a common understanding of what supplies should be prioritised would require collaboration among industry stakeholders, policy makers and environmental experts to develop a robust and widely accepted framework that takes into account not

only greenhouse gas emissions but also other environmental and social impacts across the supply chain.

All of these policies and industry actions should ensure that producers follow the principle of additionality, ensuring that product emissions are meaningfully reduced over the longer term. Calculations of emissions also need to be meaningful and across the supply chain, avoiding “greenwashing”. Policy makers can support this by creating regulations that mandate reporting and disclosure requirements for emissions. Examples include the US Environmental Protection Agency's [Greenhouse Gas Reporting Program \(GHGRP\)](#) which requires large [metal manufacturing facilities](#) to report their emissions annually under specific methodologies that incorporate those of the Intergovernmental Panel on Climate Change (IPCC).

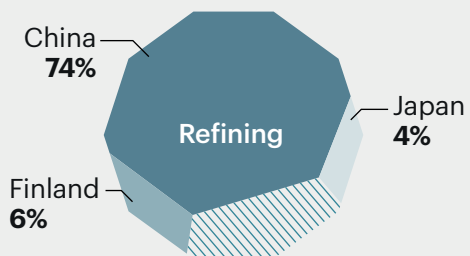
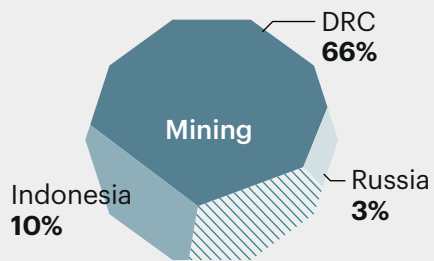
On the demand side, industry can also take actions to start incentivising responsible sourcing. For example, the [First Movers Coalition](#) aims to leverage the collective purchasing power of major market participants to create early markets for low-emissions steel, aluminium, cement, etc. By committing to purchase a proportion of their future supply from low-emissions sources, coalition members aim to send a demand signal to incentivise clean material production at scale. This type of approach could also be taken on a bilateral basis by industry players in the downstream EV market. Some of these players have already showed a preference for low-emissions nickel, such as [Vale's long-term offtake agreement with Tesla](#), which emphasised secure access to low-emissions nickel.

## Outlook for cobalt

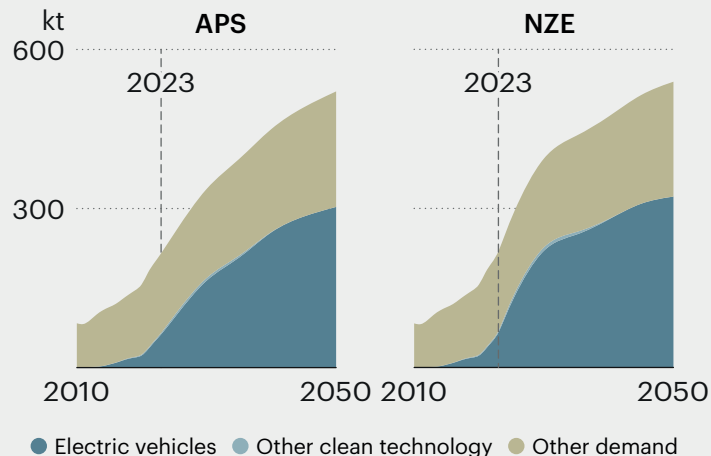
# Cobalt

# Co

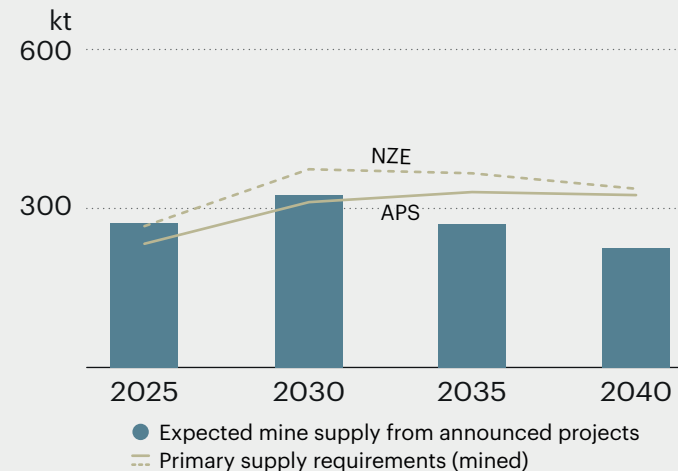
## Top three producers 2030



## Demand outlook



## Mining requirements



### Milestones (APS)

|   | 2021       | 2023       | 2030       | 2040       |
|---|------------|------------|------------|------------|
| Cleantech demand (kt)                   | 36         | 64         | 177        | 260        |
| Other uses (kt)                         | 145        | 150        | 167        | 194        |
| <b>Total demand (kt)</b>                | <b>181</b> | <b>215</b> | <b>344</b> | <b>454</b> |
| Secondary supply and reuse (kt)         | 15         | 24         | 45         | 131        |
| <b>Primary supply requirements (kt)</b> | <b>100</b> | <b>166</b> | <b>299</b> | <b>323</b> |
| Share of top three mining countries     | 75%        | 77%        | 84%        | 84%        |
| Share of top three refining countries   | 86%        | 88%        | 84%        | 85%        |

## Clean energy transition risk assessment

Low Med High

### Supply risks

**16%**

shortfall in project pipeline vs. 2035 APS mining requirements

### Geopolitical risks

**84%**

of mining by one single country in 2030

### Barriers to responding to supply disruption

Growing adoption of

**low-cobalt**

chemistries

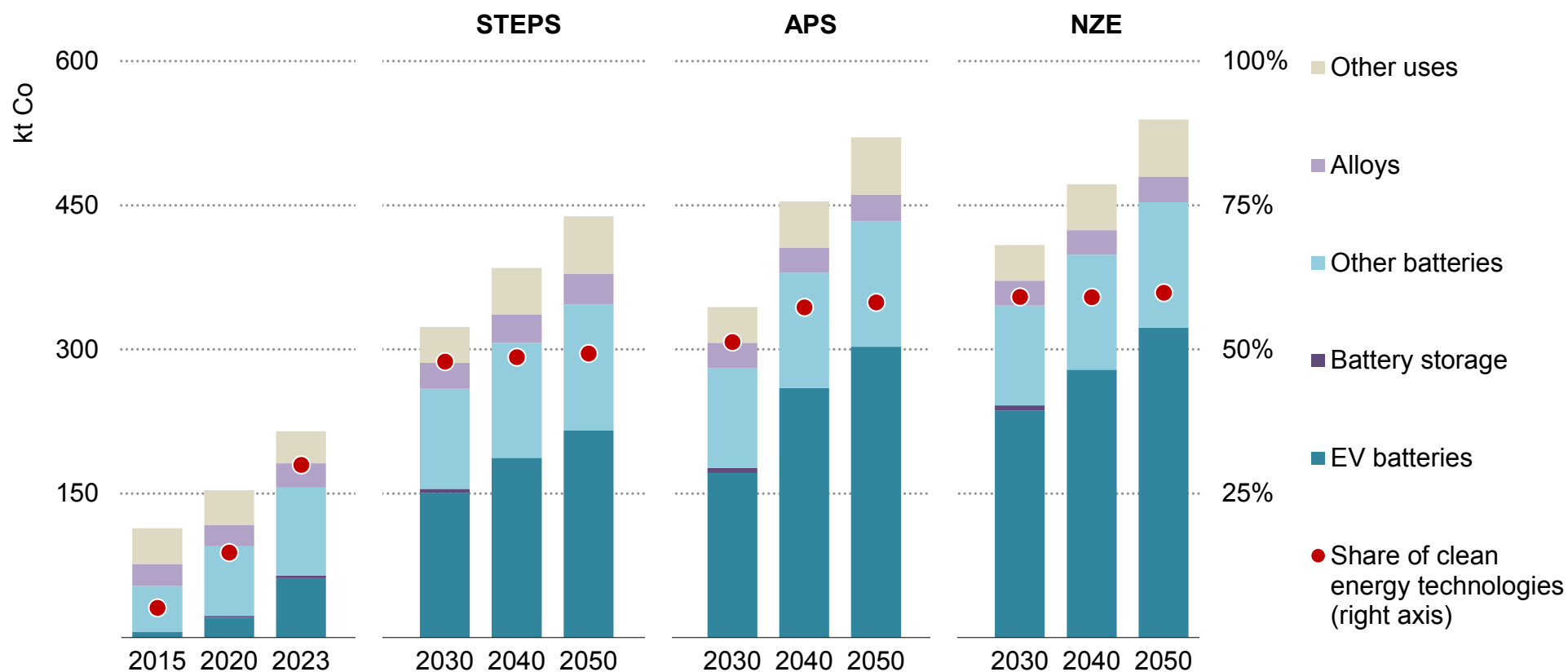
### ESG and climate risk exposure

**Low**

environmental and social performance for mining

**Demand:** Cobalt demand increases robustly with growing EV deployment, but to a lesser extent than other battery metals due to the market preference for low-cobalt or cobalt-free cathodes

Global cobalt demand outlook by sector and scenario



IEA. CC BY 4.0.

## **Demand: EV batteries emerge as the largest segment of cobalt demand, despite the growing trend towards low-cobalt or cobalt-free EV batteries**

Cobalt demand has grown strongly in recent years, with traditional usage supplemented by uses in EV batteries. In 2023, the non-clean energy technology sector accounted for around 70% of total consumption, while EV batteries accounted for the remainder. Within the non-clean energy sector, portable batteries used in electronics represented the largest share. Although absolute demand sees a slight uptick, its proportion of total cobalt demand diminishes to 25% by 2040 in both the APS and NZE Scenario.

Cobalt demand for EVs triples in the STEPS by 2040, grows by more than fourfold by 2040 in the APS and 4.5 times in the NZE Scenario from today. EV batteries take up the largest share of total cobalt consumption by the end of this decade, and their share rises to 60% by 2040 in the NZE Scenario.

While demand for EV batteries continues to rise, the recent trend towards low-cobalt or cobalt-free batteries is slowing the pace of long-term growth compared with other battery metals such as lithium and nickel. In recent years, LFP cathode chemistries have rapidly expanded their market share in the EV industry, reaching a 40% share in 2023. Alternatives to lithium-ion batteries, particularly sodium-ion batteries, are also gaining traction in the EV market. It will take time for this relatively new technology to reach a full commercialisation, but the rise of alternatives implies a smaller piece

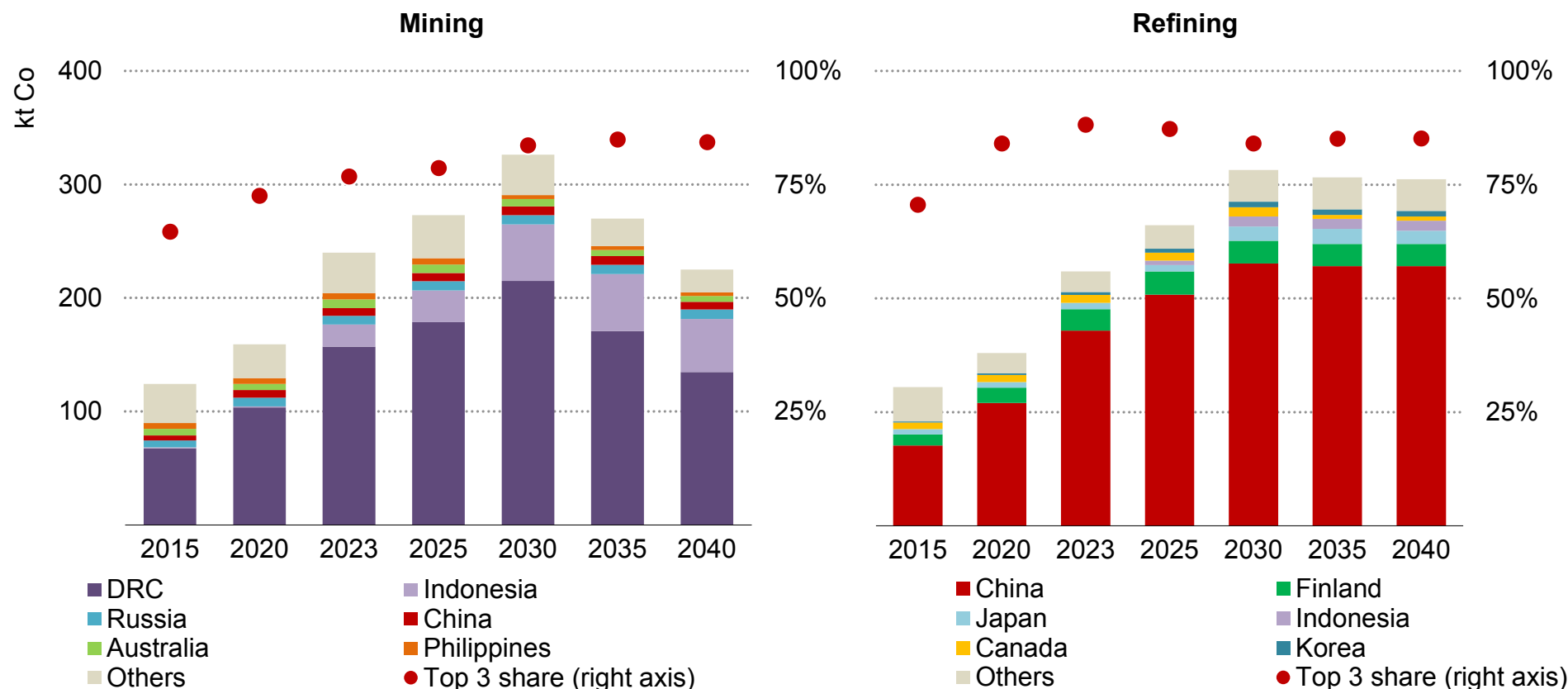
of the EV-battery pie left for cobalt. Even among the traditionally popular NMC chemistries, the market is increasingly favouring chemistries with lower cobalt intensity. However, while alternative batteries with low or no cobalt are gaining traction, the overall size of the EV market continues to expand, supporting continued demand growth in the medium to long term.

Cobalt's role decreases steadily for battery storage, reaching negligible levels by 2050 in both the APS and NZE Scenario. Compared with EVs, storage batteries are not limited by space constraints, so the market is heading towards cheaper alternatives with lower energy density such as LFP cathode chemistries or sodium-ion batteries, neither of which contains cobalt.

Outside of batteries, cobalt was used the most in superalloys integral to the military and aerospace industries due to its pivotal role in providing strong resistance to corrosion, extreme temperature and high pressure. Demand for cobalt in superalloys continues to remain robust. The industries consuming these superalloys are typically less price-sensitive, thus ensuring relatively stable demand, as evidenced by recent price trends where cobalt metal alloys consistently maintained higher prices than cobalt sulphate during periods of price downturns.

## Supply: The already high geographical concentration of both mining and refining processes further intensifies as current dominant players continue to expand their operations

Cobalt production from operating and announced projects in the base case

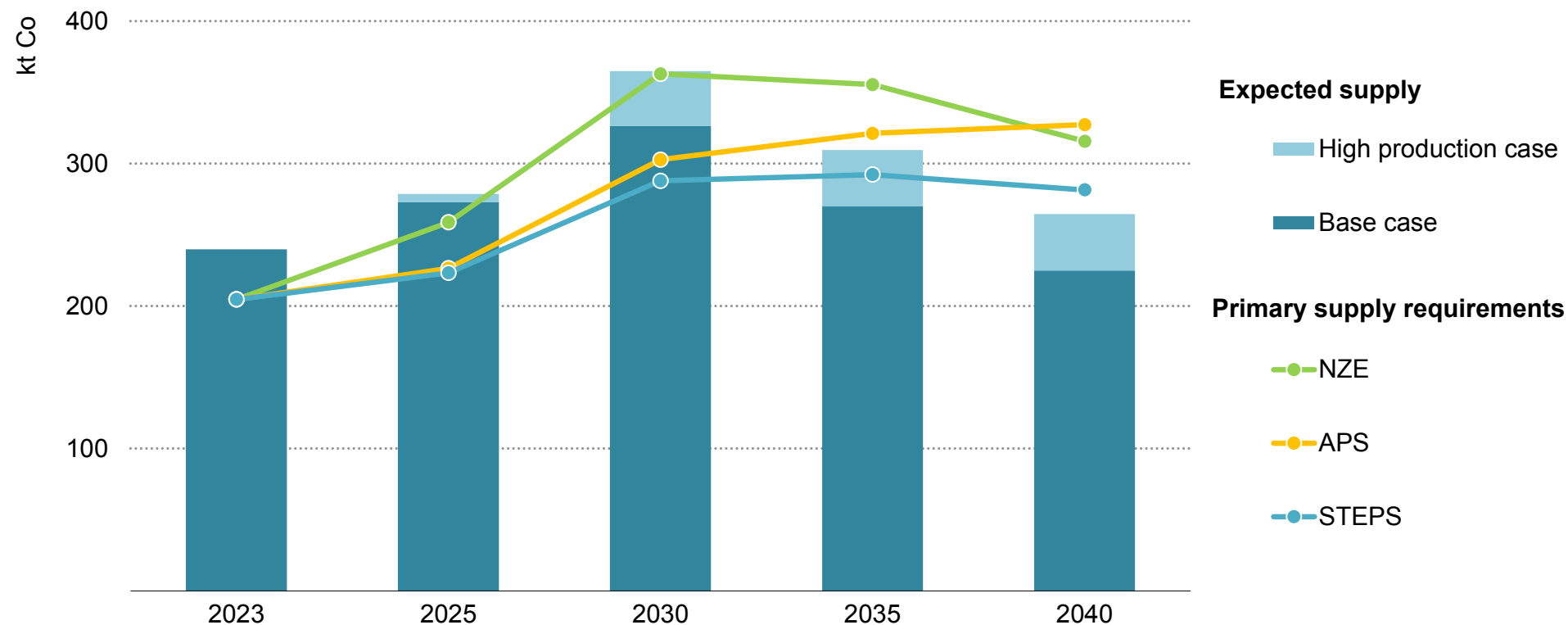


IEA. CC BY 4.0.

Note: DRC = Democratic Republic of the Congo.

## Supply: Analysis of announced projects suggests an increase in cobalt supply to 2030 before falling steadily with declining ore grades

Expected mined cobalt supply from existing and announced projects and primary supply requirements by scenario



IEA. CC BY 4.0.

Notes: Based on mined output. Primary supply requirements are calculated as “total demand net of secondary supply”, also accounting for losses during refining operations. See Introduction for definitions of the base and high production cases.



## Supply: A tale of two suppliers: the DRC and Indonesia

The cobalt market is well supplied today. In the near term, the current oversupply may continue with supplies from new mines and previously stockpiled volumes coming online in the Democratic Republic of the Congo (DRC). In the long-term, global mined supply begins to subside from 2030 as reserves in the DRC deplete although strong growth from Indonesia partly offsets this decline. Future cobalt supply could face major challenges as the current low-price environment makes financing new projects more challenging.

### The DRC, the traditional No. 1 supplier

Mined cobalt production in the DRC is poised for significant growth in the near future as several new mines ramp up their output. China-based CMOC's Tenke Fungurume mine (TFM) resumed exports in April 2023 after resolving a royalty dispute with Gécamines, the DRC state-owned mining company. TFM's second-phase expansion began operations in the second half of 2023, with output estimated to reach 30 kt by 2027. Another major project by CMOC, the [Kisanfu](#) copper-cobalt mine started production in the first half of 2023 and is expected to contribute an average of 30 kt of cobalt per year by 2026 once it reaches full capacity. The Kinsevere copper mine's expansion under the China-based MMG Group, commenced operations in 2023 and is anticipated to produce 5 kt of cobalt annually in the near term. The cobalt output from China-based Jinchuan Group International Resources, which operates an open-pit Ruashi mine and is currently

advancing the underground [Musonoi](#) mine in the DRC, is expected to surge by 75% to 10 kt in 2024. These sizeable new cobalt mines are anticipated to contribute significant volumes to the near-term supply pool, countering the slower production from non-Chinese major cobalt miners.

In the long term, existing mines in the DRC are likely to reduce their supply or close down due to diminishing ore grade and increasing production cost, resulting in a 15% drop in production from today's level by 2040 in the base case. Glencore's Mutanda mine may experience a reduction of up to 15% in annual production due to the depletion of oxide ore deposits on the surface. To sustain production levels, the cobalt-rich DRC would need to explore new deposits, re-evaluate old tailings, or transition its open-pit mines to underground operations. It is important to highlight that the DRC still possesses substantial high-grade resources. However, unlocking this potential necessitates new investments, a task that may pose challenges during periods of weak cobalt prices and ample market supply although robust copper prices could help.

### Indonesia, the fast-rising second place

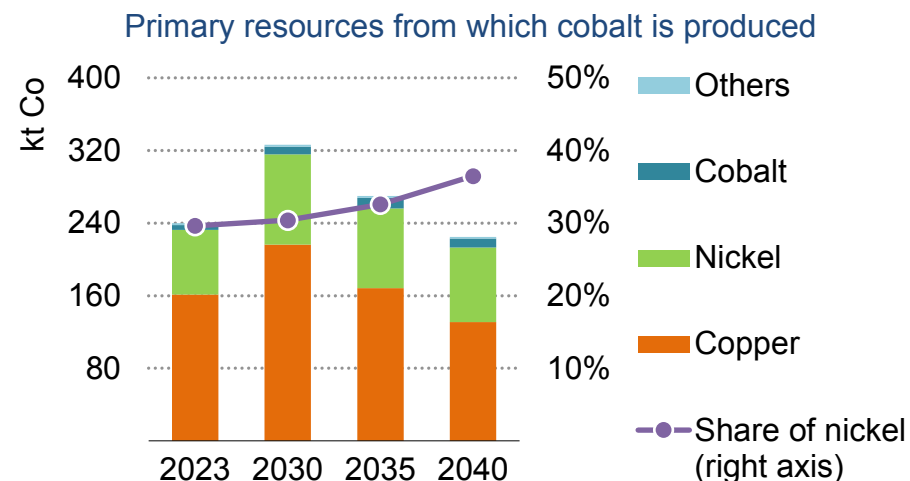
As of 2023, Indonesia had ascended to become the world's second-largest cobalt supplier. Indonesia's cobalt production rose by almost 20 times in the last four years since the Indonesian government

nickel ore export ban drove an influx of investments in domestic nickel-cobalt processing operations including HPAL facilities. In the base case, Indonesia's cobalt production more than doubles to 2030, reaching 50 kt. In the high production case, its supply is estimated to reach 80 kt by 2030, constituting 23% of global cobalt supply, nudging the DRC's production share down from 65% in 2023 to 50% by 2040.

### Cobalt as a by-product

Cobalt is mostly extracted as a by-product of copper ore or nickel ore. Traditionally, the primary mineral from which cobalt is refined as a by-product has been copper due to the abundance of copper-cobalt mines in the DRC. Copper accounts for almost 70% of the primary mineral of cobalt's supply today. However, declining ore quality of existing copper-cobalt mines in the DRC limits its supply post-2030 in the base case, reducing copper's share to below 60% by 2040. Primary cobalt mines continue to take a small part, most of which comes from ASM in the DRC. Its share takes up less than 5% of the total cobalt primary supply throughout 2040 in our base case.

Nickel plays a growing role as a primary mineral for cobalt production with the rise of Indonesia's nickel production. Today, 30% of the primary mineral refined into cobalt has been from nickel plays, and this share rises to almost 40% by 2040 in our base case.



IEA. CC BY 4.0.

Sources: IEA analysis based on Wood Mackenzie and S&P Global.

### Low cobalt price threatens future production

With the weak cobalt prices persisting, mining projects are witnessing delays as project developers are forced to seek additional funding for future production. Trafigura, a commodity trading company, is now forced to seek an additional [USD 200 million to USD 300 million](#) investment, which is worth almost half the initial USD 600 million syndicated financing and marketing deal from 2022 with Chemaf SA, a mining company operating in the DRC. Had the project been completed by the end of 2023 as originally planned, the [Mutoshi mine](#) alone would have become the world's third-largest cobalt mine with capacity reaching 16 kt of annual cobalt hydroxide in its full form.

High inflation has compounded the challenges posed by the low cobalt prices. This caused the suspension of final construction of [Idaho Cobalt Operations](#) in March 2023, which would have been the only primary cobalt mine in the United States with an annual production capacity of 2 kt. The CEO of the project's developer, [Jervois Global](#), argued that prices would have to double or additional government support would be needed to complete the construction.

Despite the unfavourable market conditions, there are some developers willing to finance new projects. Kazakh miner [Eurasian Resources Group](#) announced it would invest USD 800 million to revamp its Comide copper and cobalt mine including the construction of hydrometallurgical plant and drilling programme in October 2023. The plant is set to come online in different phases which would reach up to 15 kt of annual cobalt hydroxide output once its full capacity is met.

The weak prices also triggered actions or considerations to stockpile cobalt. China has notably taken advantage of the low cobalt price. The National Food and Strategic Reserves Administration, the government's stockpiling body, agreed to buy around 5 kt of cobalt in [July 2023](#) and 3 kt in [October](#). As the low price persists, there could be additional stockpiling schemes introduced from the government. The United States also reportedly considered adding cobalt to its stockpiling list. While stockpiling plans of the Defense Logistics Agency ([DLA](#)) that run from October 2023 to September 2024 ultimately did not include cobalt, the United States' efforts to diversify

its cobalt supply sources coupled with low commodity price could lead to new stockpiling activities.

## Smelting and refining

After mining, copper-cobalt or nickel-cobalt concentrates are obtained through mineral processing techniques including crushing, screening, drying, flotation or magnetic separation (though cobalt produced from HPAL facilities does not require significant beneficiation). Then, primary extraction using hydrometallurgical or pyrometallurgical methods take place typically close to the mines. This process produces matte, oxides, nickel-cobalt intermediates, and other co-products, which are then usually shipped overseas for further refining.

Cobalt refining continues to remain geographically concentrated in our base case. Today, China is responsible for more than 75% of the global refined cobalt supply, and its share remains at a similar level to 2040 in the base case. Finland and Japan account for around 9% and 3% of refined cobalt supply in 2023 respectively, and their shares sustain to 2040.

Among many forms of refined chemistries, cobalt sulphate used in EV batteries sees the largest increase in demand. In the base case, cobalt sulphate supply increases by more than 50% by 2030 and more than doubles in the high production case. This helps to meet the sulphate supply requirements in the APS in 2030, helped by growing secondary supply.

## The role of artisanal small-scale mining in cobalt supply

The ASM sector in the DRC has historically made up a significant but variable share of global cobalt supply, accounting for an average 5-15% of the total.

The sector is highly variable depending on the price of cobalt, with higher prices incentivising more ASM activities. Due to lower cobalt prices, in 2023 ASM made up approximately 4 kt of cobalt supply, accounting for only 2% of demand. In our base case, supply from ASM increases to 7 kt in 2030 and almost 10 kt in 2040. However, as global mined supply climbs in response to demand for cobalt for the energy transition, ASM accounts for a smaller share of supply moving forward.

Due to ASM's sensitivity to market fluctuations, the sector has historically played an important role in maintaining market stability: ASM sites take much less time to begin production compared with larger industrial operations, allowing traders and producers to top up supplies during shortages or sell off volumes when other sources are in surplus. This flexibility helps to balance supply and demand, with ASM acting as swing producers. However, as ASM supplies are projected to take up a smaller share of supply moving forward, their role as swing producers may be diminished.

The sector has [historically been associated with human rights abuses](#) due to its unregulated and informal nature. Disengaging entirely from ASM as a strategy [does not constitute responsible sourcing](#) and [may exacerbate the root causes of child labour](#). To varying extents, ASM offers socio-economic advantages; losing these may heighten the local community's vulnerability to other forms of exploitation.

There have been various efforts to formalise the sector over the years. In 2019, the DRC government created the Entreprise Générale du Cobalt (EGC), a state-owned enterprise which is intended to hold the sole right to purchase, treat, transform, sell and export cobalt extracted by artisanal and small-scale miners in the DRC. The entity released a [Responsible Sourcing Standard](#) document in 2021, outlining its steps for formalising the sector. However, the [EGC has not been fully operationalised](#) since it was established.

Formalisation of the sector could mitigate the worst forms of child labour, but could bring some [unintended consequences](#) as well. Addressing poverty at its core is essential for a lasting solution. This requires ongoing collaboration across actors and sustained community engagement.

## Implications: Environmental and logistical bottlenecks mean that reliable cobalt supplies are far from assured

### Environmental consequences from low-quality ores

Cobalt mining practices are becoming more energy-intensive as copper-cobalt mines in the DRC near depletion and HPAL facilities in Indonesia take on a larger role in global cobalt extraction.

As existing DRC mines edge closer to depletion, the country would have to develop new mines or dig wider and deeper in their existing open-pit and underground mines. The process of seeking better quality copper-cobalt ores would involve significant energy uses and emissions.

Moreover, the increasing cobalt extraction from nickel mines in Indonesia is raising concerns on top of the existing environmental challenges. HPAL technology uses sulphuric acid at high pressure and temperature to recover nickel and cobalt separately from low-grade deposits of nickel laterite ore. Additionally, new coal plants have often been added near HPAL facilities to accommodate an increase in power demand and provide affordable source of power to enhance the price competitiveness of mineral supply.

In recent years, there has been a notable increase of the China-backed Indonesia-based HPAL operations such as PT Halmahera Persada Lygend, PT Huayue Nickel Cobalt, PT QMB New Energy Materials and PT Huayou. In the high production case, almost half of

the cobalt supply in 2040 is refined from laterite ore from today's level of less than 30%.

Cobalt mining has traditionally been supported by hydropower in the DRC, which led to relatively lower-emissions intensity associated with production. However, a combination of more energy-intensive operations in the DRC and the rise of Indonesia means that the average emissions intensity associated with cobalt production is set to rise substantially as production grows. This makes a strong case for strengthened regulatory and industry efforts to reduce emissions from cobalt production operations.

### Risks of supply concentration

High concentration of cobalt mining in a single country owned and operated by foreign mining entities has shown the challenge of maintaining a secure supply. As exemplified by the recent disputes between the DRC government and foreign miners, the state's endeavour to gain more control over its mines is forming into royalty disputes and sanctions on some of the largest mines in the world.

Notably, the DRC state-owned [Gécamines had suspended China-based CMOC's TFM](#), the world's second-largest cobalt mine, in July 2022 after an escalation in royalty dispute. CMOC holds an 80%

stake in the TFM copper-cobalt ore project and Gécamines holds 20%. The mine resumed export in April 2023 after CMOC struck a [USD 2 billion deal](#) – a USD 800 million settlement between 2023 and 2028 and at least USD 1.2 billion in dividends.

More recently in April this year, the [DRC suspended nine subcontractors](#) working at mines run by the Kazakhstan-backed Eurasian Resources Group alleging that the firms are not controlled by Congolese nationals as required by law. The sanction affects companies' operations under contracts, including Metalkol, the fourth-largest cobalt supply source in 2023.

Risks of potential supply disruptions from the world's largest cobalt supplying nation persist, amid an ongoing tug of war between the DRC administration and foreign miners over ownership stakes in the region's vast copper and cobalt resources.

### Logistic constraints: Rocky roads from mines to ports

There are also risks associated with logistics due to the fragile transportation infrastructure connecting the copper-cobalt mines in Central Africa located far inland to the nearest ports, the export corridors that would ship raw minerals overseas for refining.

A large portion of DRC production currently relies on trucks to be transported over long distances by road, passing through several borders. Trucks would generally transport minerals from the so-called copper belt to Indian Ocean ports such as Beira in Mozambique, Dar

es Salaam in Tanzania or Durban in South Africa, which take [17, 20 and 25 days](#), respectively. The road networks are inconsistent with large sections in need of significant maintenance and improvement. In rainy seasons, many roads become inoperable.

Truck deliveries have raised concerns for being more costly, slow and unreliable compared with railways. In October 2023, thousands of truckers in the DRC went on strike demanding logistics firms to pay an extra risk allowance of USD 700 per journey. The strike blocked exports of copper and cobalt produced by some of the biggest producers including CMOC's Tenke Fungurume, Glencore's Kamoto, Ivanhoe Mines' Kamoakakula, and Sicomin's Mashamba West until coming to an end in November. These events related to logistics underscore that the possibility of short-term supply disruptions cannot be ruled out, even though overall supply and demand balances may appear stable.

As logistical issues disrupt secure upstream supply, railway transportation via the Lobito Corridor has gained momentum in recent years. The corridor is an agreement to construct railways and supporting infrastructure to connect mines in Central Africa to the Angolan port city of Lobito.

The United States and Europe recently announced significant financing plans for the Lobito Corridor to enhance material shipments via the Atlantic Ocean. In July 2023, the Lobito Atlantic Railway company secured a 30-year concession to provide railway services, contingent on investing USD 100 million in the DRC and [USD 455](#)



[million in Angola](#) through a public-private financing arrangement. In October 2023, the United States, the European Union, the African Development Bank, and the Africa Finance Corporation signed a MoU to co-operate on extending the Lobito Corridor, under the shared vision.

[Initial trial shipments via the Lobito Corridor](#) began in December 2023, loading copper from Kamo-a-Kakula in Kolwezi and reaching the port of Lobito in just eight days. In February 2024, Canada's

[Ivanhoe Mines and Trafigura](#) became the first long-term users of the corridor. Meanwhile, [China](#) proposed a USD 1 billion project to upgrade the Tazara railway connecting Zambia's copper belt to the port of Dar es Salaam in Tanzania. While the extent of the refurbishment plan remains unclear, the revitalisation of railways connecting Central Africa to both the Atlantic and Indian Oceans would help address some of the major logistical issues the region has long suffered from.

## Outlook for graphite

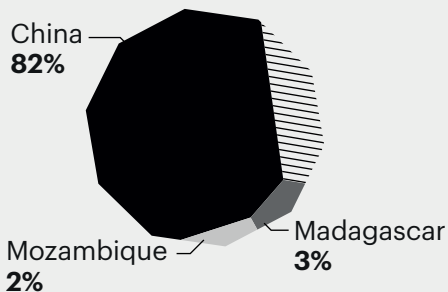


# Graphite

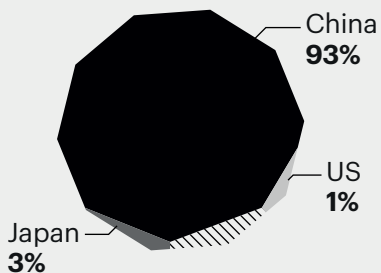
C

## Top three producers 2030

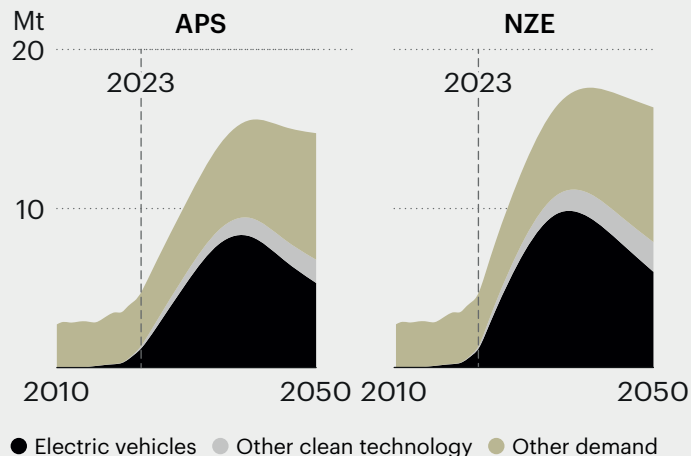
### Total supply (all grades)



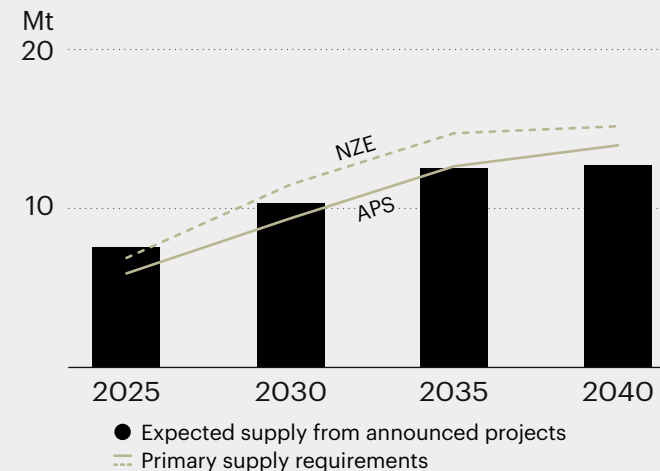
### Battery grade supply



## Demand outlook



## Supply requirements



### Milestones (APS)

|   | 2021         | 2023         | 2030          | 2040          |
|---|--------------|--------------|---------------|---------------|
| Cleantech demand (kt)                   | 532          | 1 292        | 6 013         | 9 839         |
| Other uses (kt)                         | 3 388        | 3 340        | 4 406         | 6 185         |
| <b>Total demand (kt)</b>                | <b>3 920</b> | <b>4 632</b> | <b>10 419</b> | <b>16 023</b> |
| Secondary supply and reuse (kt)         | 149          | 308          | 1 333         | 2 489         |
| <b>Primary supply requirements (kt)</b> | <b>3 771</b> | <b>4 324</b> | <b>9 086</b>  | <b>13 535</b> |
| Share of top three mining countries     | 89%          | 92%          | 88%           | 89%           |
| Share of top three refining countries   | 97%          | 98%          | 97%           | 95%           |

## Clean energy transition risk assessment

Low Med High

### Supply risks

**12%**

annual demand growth in the APS vs. 3% in 2010-19

### Geopolitical risks

**10X higher**

demand than supply outside of top 1 producer in 2030

### Barriers to responding to supply disruption

**Limited**

short-term substitution options

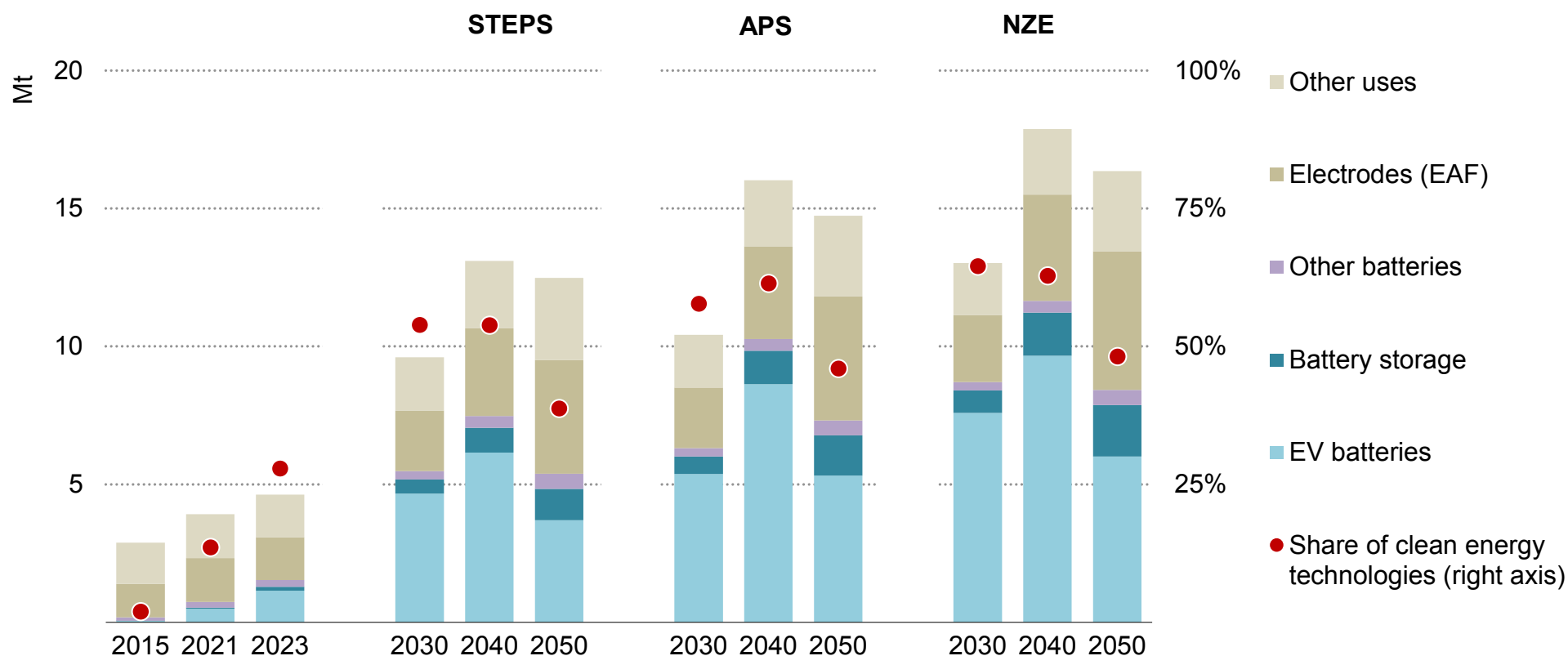
### ESG and climate risk exposure

**Lowest**

average social and governance score for mining

## Demand: Batteries are driving demand growth for graphite to 2040, with demand from electric arc furnaces for steel production also rising fast

Global graphite demand outlook by sector and scenario



IEA. CC BY 4.0.

Notes: EAF = electric arc furnace. Demand is for raw natural flake graphite and synthetic graphite.

## **Demand:** As graphite maintains its dominant position in anodes, its demand is supercharged in climate-driven scenarios by the rapid deployment of EVs and battery storage

Graphite, a form of carbon commonly known for its use in pencil cores, traditionally serves various technical applications: as a lubricant, an electrical conductor, a refractory material or simply as a source of raw carbon. Historically, the metallurgical industry has been the primary consumer of graphite, employing it in crucibles, as an input for steelmaking and as electrodes in electric arc furnaces. However, the battery industry is rapidly emerging as the leading consumer of graphite, with projections indicating it may account for over half of total demand by the late 2020s.

Graphite's expanding role in battery anodes contributes to a robust short-term growth outlook, with global demand projected to double by 2030 in the STEPS. By 2040, total graphite demand reaches 13 Mt in this scenario. Meeting announced climate pledges in the APS pushes up demand further close to 16 Mt by 2040 and to 18 Mt in the NZE Scenario, a fourfold increase from today's levels.

The EV industry emerges as a primary consumer of graphite. In the APS, this sector consumes 5.4 Mt in 2030, higher than current global production levels, representing 60% of total demand. Battery storage is also a significant contributor to demand growth. When considering other battery applications, such as those in electronics, the demand for graphite related to batteries – requiring specific grades and

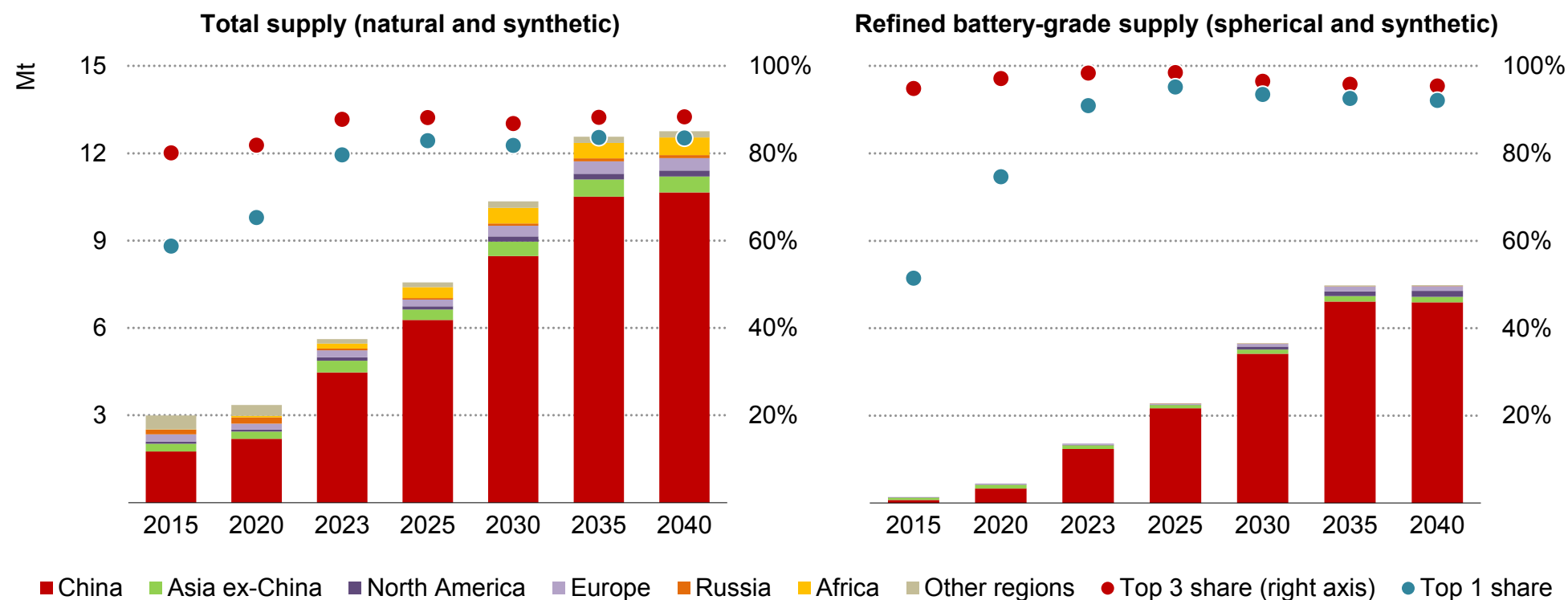
dedicated supply chains – is expected to account for 65% of total demand by 2040, compared with the 33% today.

In EV batteries, while silicon is increasingly being doped in graphite anodes, it is unlikely to challenge graphite's dominant position in the short term. However, we expect a continued shift towards higher silicon contents over time. This trend, coupled with the adoption of alternative anode chemistries such as lithium metal anodes, high silicon anodes (exceeding 50% silicon content) and hard carbon (used in sodium-ion batteries), gradually affects the pace of graphite demand growth in the longer term, leading to a moderate reduction in graphite demand in batteries post-2040. However, the speed of deployment of these alternative chemistries depends on overcoming significant technical and scaling challenges, such as ensuring high cycle life and resisting volume changes.

In both the APS and NZE Scenario, there is a notable shift towards the increased use of electric arc furnaces over traditional blast furnaces, especially in Europe, aiming to decrease emissions associated with steel production. This increases demand for graphite electrodes, primarily based on synthetic graphite. By 2040, graphite demand for metallurgical applications reaches 3.4 Mt in the APS and 3.8 Mt in the NZE Scenario, up from 1.5 Mt today.

### Supply: New natural graphite mining projects emerge in diversified regions, notably in Africa, but the production of battery-grade graphite remains highly concentrated

Total and battery-grade graphite supply from existing and announced projects in the base case



IEA. CC BY 4.0.

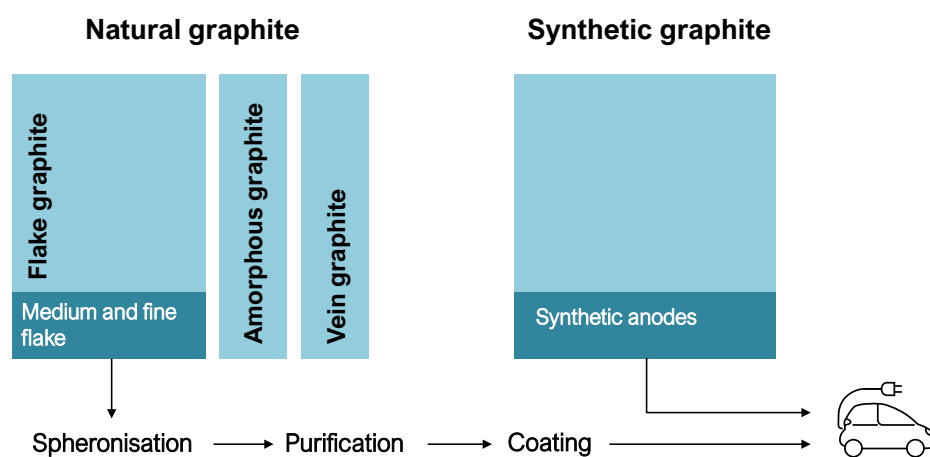
Notes: Total supply includes all grades of mined and synthetic graphite. Refined battery-grade supply includes spherical graphite made from natural flake graphite and synthetic anode production.

## Supply: Options to synthesise graphite allow for sufficient supply volumes, but natural deposits are better able to support cheaper, diversified and less energy-intensive supplies

Graphite is found and extracted from natural geological deposits in various forms (vein, amorphous, flakes). However, since the turn of the 20th century and the discovery of the Acheson process, the mineral can also be synthesised from fossil fuel-based products, such as petroleum coke, with an emissions-intensive process.

Most battery producers globally are heavily reliant on China for graphite anodes. While sizeable natural graphite anode capacities exist outside of China, they depend almost entirely on refined graphite supply from China and exhibit low utilisation rates.

### Battery-grade graphite supply



IEA. CC BY 4.0.

### Mining, a limiting factor to natural anode supply

Currently, natural graphite mining is dominated by China, accounting for 80% of global production. In the base case, mined natural graphite reaches 2.7 Mt in 2030 and 3 Mt by 2040. The share of China declines to 70% in 2030 due to the growth of two emerging producers: Mozambique, notably with the Ancuabe project (60 kt), and Madagascar, with the Molo project (150 kt). Additionally, new players are emerging in Canada, India, Australia and Tanzania (Nachu project, 130 kt), aiming to cater to the growing battery market.

Not all forms of natural graphite are suitable for entry into the battery supply chain. Manufacturers use natural flakes, from medium and fine grades, and their availability emerges as a key limiting factor in scaling up battery-grade anodes based on natural graphite. The production of natural battery anodes involves multiple steps, including spheronisation, a process of reshaping the graphite flakes, involving over 50% material losses. In the base case, the need for natural graphite anode supply reaches 750 kt by 2030, and this requires close to 1 700 kt of fine- and medium-grade flakes. Of the total 2 700 kt of graphite mined in 2030, about 70% is likely to be suitable grades. This brings the battery-grade flake market slightly above equilibrium, limiting the potential for additional natural graphite supply to the battery anode market. Additional mining capacities are

required to meet the necessary volumes of natural graphite anodes post-2030 in climate-driven scenarios.

### Refined natural graphite: A major diversification issue

While some progress has been achieved in diversifying the mining of natural graphite, the production of spherical graphite, a refined form of natural graphite, remains highly concentrated. Currently, China accounts for 99% of the global market for spherical graphite. Although some downstream operations, such as coating and purification, are occasionally conducted overseas, industrial players in these processes become highly dependent on China for their feedstock supplies.

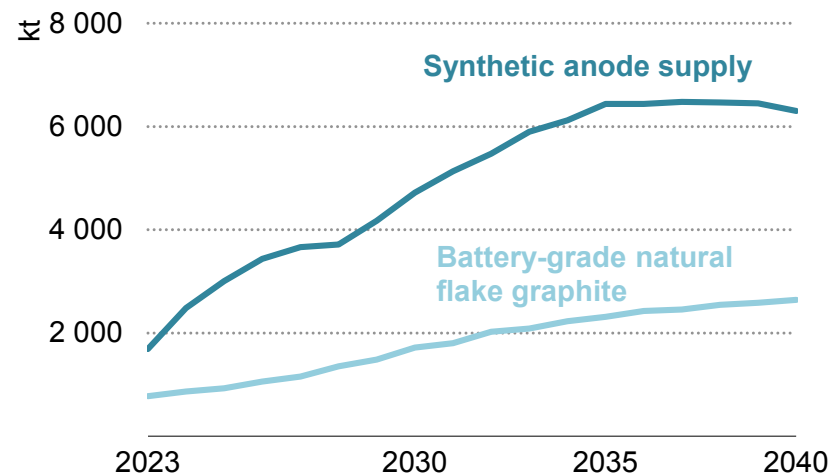
The industry is developing new projects in geographically diverse areas, with a growing number of integrated projects. These include Northern Graphite (80 kt) and Nouveau Monde (32 kt) in Canada, Syrah resources (38 kt) in the United States and several projects in Europe, such as Talga resources of Sweden (12 kt). If these projects come online as planned, the share of China in spherical graphite supply is set to fall to 85% in 2030 and 80% in 2040 in the base case.

### Synthetic supply brings equilibrium to demand, at a cost

Due to constraints on natural graphite supply, synthetic graphite production is increasing its share in batteries although its production is also dominated by a single player, China. Synthetic graphite has been largely used for other applications, notably electrodes, which

required lower-quality products. However, in recent years, battery-related synthetic graphite production has surged from zero to 40% of total synthetic graphite supply, rising to 55% by 2040. Synthetic graphite became a dominant input for battery anodes, commanding an 80% market share.

Use of mined natural and synthetic graphites in batteries

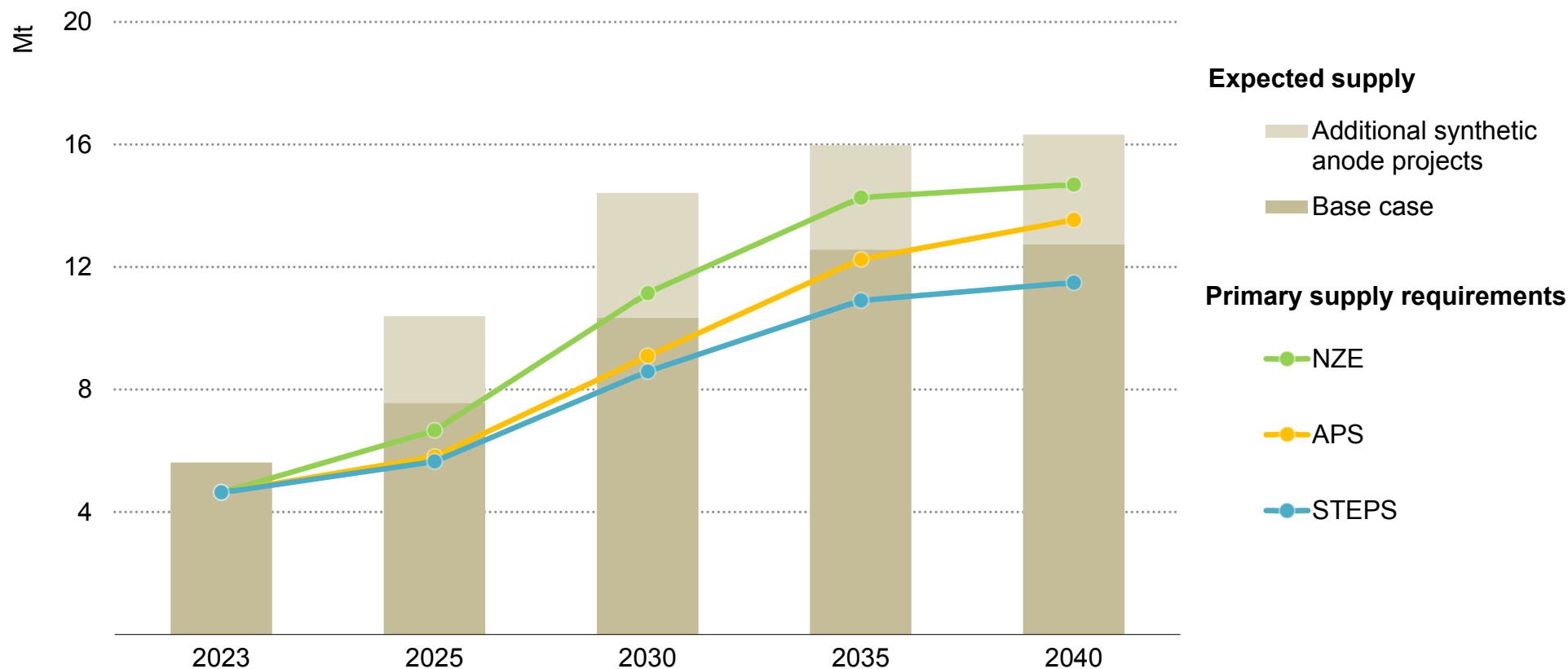


IEA. CC BY 4.0.

Synthesis of graphite requires the supply of needle coke, a co-product from the oil and coal industries. There are surplus capacities to produce needle coke today, mostly in China, meaning that the supply of needle coke is unlikely to be a limiting factor for synthetic graphite supply in the near term, but this may change in the long term in climate-driven scenarios.

**Implications:** The large pipeline of announced synthetic capacities has the potential to balance the market, although this may lead to increased supply concentration and higher emissions

Expected graphite supply from existing and announced projects and primary supply requirements by scenario



IEA. CC BY 4.0.

Notes: Primary supply requirements are calculated as “total demand net of secondary supply”. See Introduction for definition of the base case.

## Implications: Diversification is urgently needed but faces significant challenges

In the base case, the anticipated supply of battery-grade spherical graphite and synthetic graphite is projected to be adequate to meet near-term demand. However, sustaining the long-term demand trajectory will require additional production volumes. The supply of battery-grade natural flake graphite may turn to deficits over the next decade. However, it should be noted that there is a substantial number of announced synthetic anode projects, primarily in China, exceeding the scale required in the NZE Scenario. Many of these projects are likely to experience low utilisation rates or may not come to fruition. However, this implies that any short supply of battery-grade natural graphite could result in a further increase in the share of synthetic graphite to offset the deficit.

However this comes at a cost. The extraction and conversion of synthetic graphite involves significantly higher greenhouse gas emissions compared with its natural equivalent, as it involves an electricity-intensive process relying on fossil resources. Although less energy-intensive graphite synthesis projects and techniques exist, such as lengthwise graphitisation, a higher proportion of synthetic graphite in anodes is expected to result in significantly greater GHG emissions during battery production. Nonetheless, some projects developed in areas with low-emissions power generation sources claim to achieve [significant reductions in emissions](#) compared with current supply chains.

Moreover, China currently accounts for the vast majority of existing and planned synthetic graphite production capacity. Therefore, a further increase in the share of synthetic graphite in batteries would reinforce China's dominance in this sector.

Following germanium, gallium and rare earth elements-related technologies, graphite is now subject to a system of export [licences](#) from China since December 2023. These controls specifically focus on graphite for battery grades (flake graphite, spherical graphite, high-purity products), considered “highly sensitive”, and exclude lower-quality grades, such as electrodes for metallurgical applications.

These controls can have numerous ripple effects. The announcement has placed pressure on anode producers overseas to stockpile significant volumes. As implementation commenced in January 2024, export volumes to key anode producers in Japan and Korea plummeted well below previous monthly averages before returning to normal levels in March. Customers can apply for licences with a six-month validity, a process that requires disclosure of the end user, creating significant rigidity in trade and discouraging risk-averse investors from expanding downstream capacities.

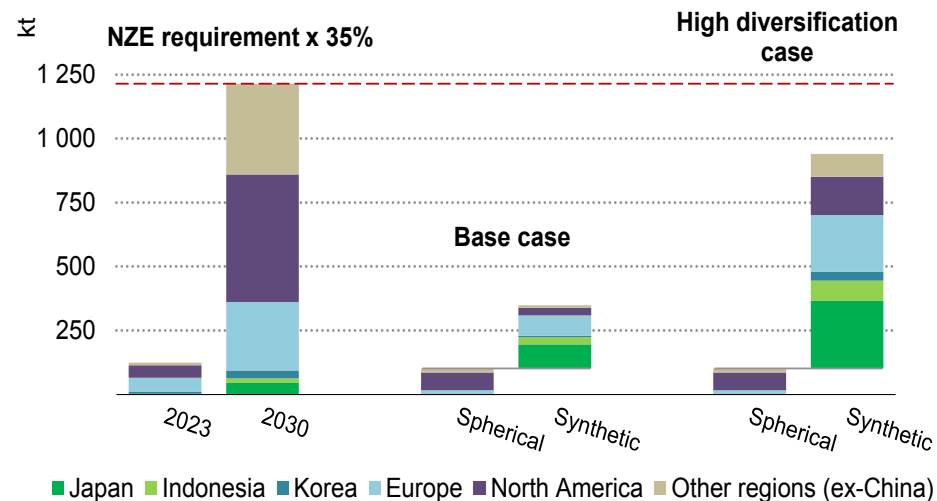
Currently, 45% of EV and storage batteries are sold and installed outside of China, translating into 350 kt of graphite content in their



anodes. By 2030, this implied demand outside of China is set to reach 2.2 Mt in the APS and 3.5 Mt in the NZE Scenario. When the 35% threshold for the share of a single supplier, targeted in the EU Critical Raw Materials Act, is applied, this means that 1.3 Mt needs to come from regions outside of China.

In the base case, the expected supply outside of China falls significantly short of these material requirements. While additional projects in the early stage, not included in the base case, could narrow the gap somewhat — such as those in the United States, Korea, Saudi Arabia, India, Norway and Finland — the anticipated supply may still not be sufficient to meet the requirements. This indicates that achieving the diversification ambitions outlined in recent policy measures would be highly challenging without significant efforts to expedite the development of projects in geographically diverse regions. These projects would, however, need to move ahead amid strong competition from incumbent players and significant announced overcapacities in China, which may require strategic and co-ordinated support from governments.

Ex-China battery-grade graphite requirements and pipeline of probable projects in the NZE Scenario



IEA. CC BY 4.0.

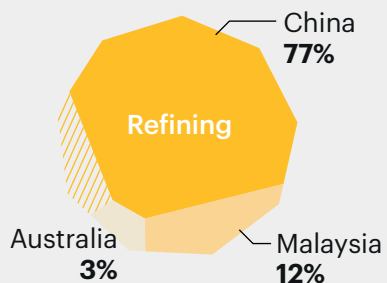
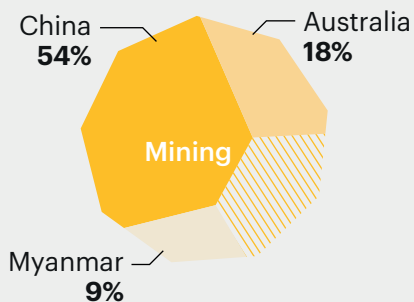
Note: High diversification case assumes that a number of early-stage projects in geographically diverse regions come to fruition.

## Outlook for rare earth elements

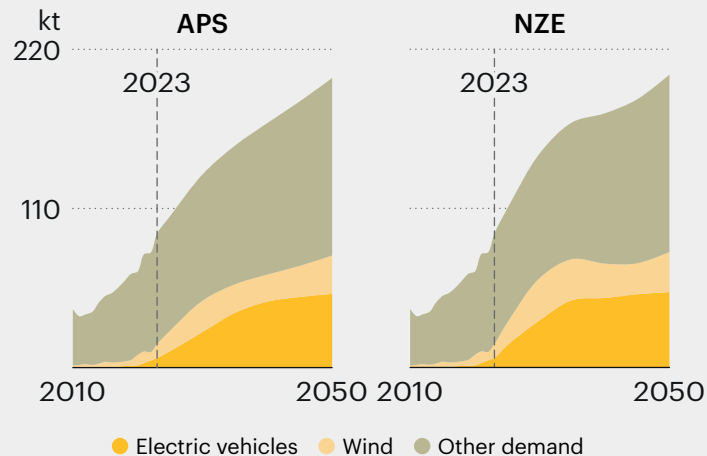
# Rare earth elements

## Nd Pr Dy Tb

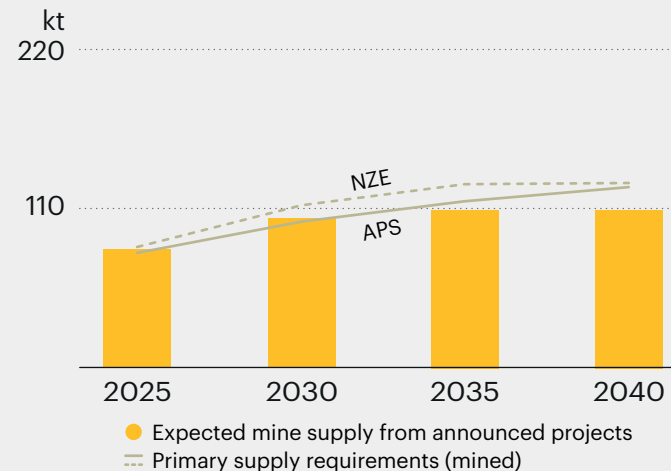
### Top three producers 2030



### Demand outlook



### Mining requirements



### Milestones (APS)

|   | 2021      | 2023      | 2030       | 2040       |
|---|-----------|-----------|------------|------------|
| Cleantech demand (kt)                   | 11        | 16        | 46         | 64         |
| Other uses (kt)                         | 67        | 76        | 87         | 105        |
| <b>Total demand (kt)</b>                | <b>78</b> | <b>93</b> | <b>134</b> | <b>169</b> |
| Secondary supply and reuse (kt)         | 22        | 25        | 36         | 48         |
| <b>Primary supply requirements (kt)</b> | <b>57</b> | <b>67</b> | <b>98</b>  | <b>121</b> |
| Share of top three mining countries     | 81%       | 85%       | 81%        | 81%        |
| Share of top three refining countries   | 98%       | 98%       | 92%        | 93%        |

### Clean energy transition risk assessment

Low Med High

#### Supply risks

**High**

price volatility than other minerals

#### Geopolitical risks

**77%**

of refining by one single country in 2030

#### Barriers to responding to supply disruption

**Low**

transparency of pricing schemes

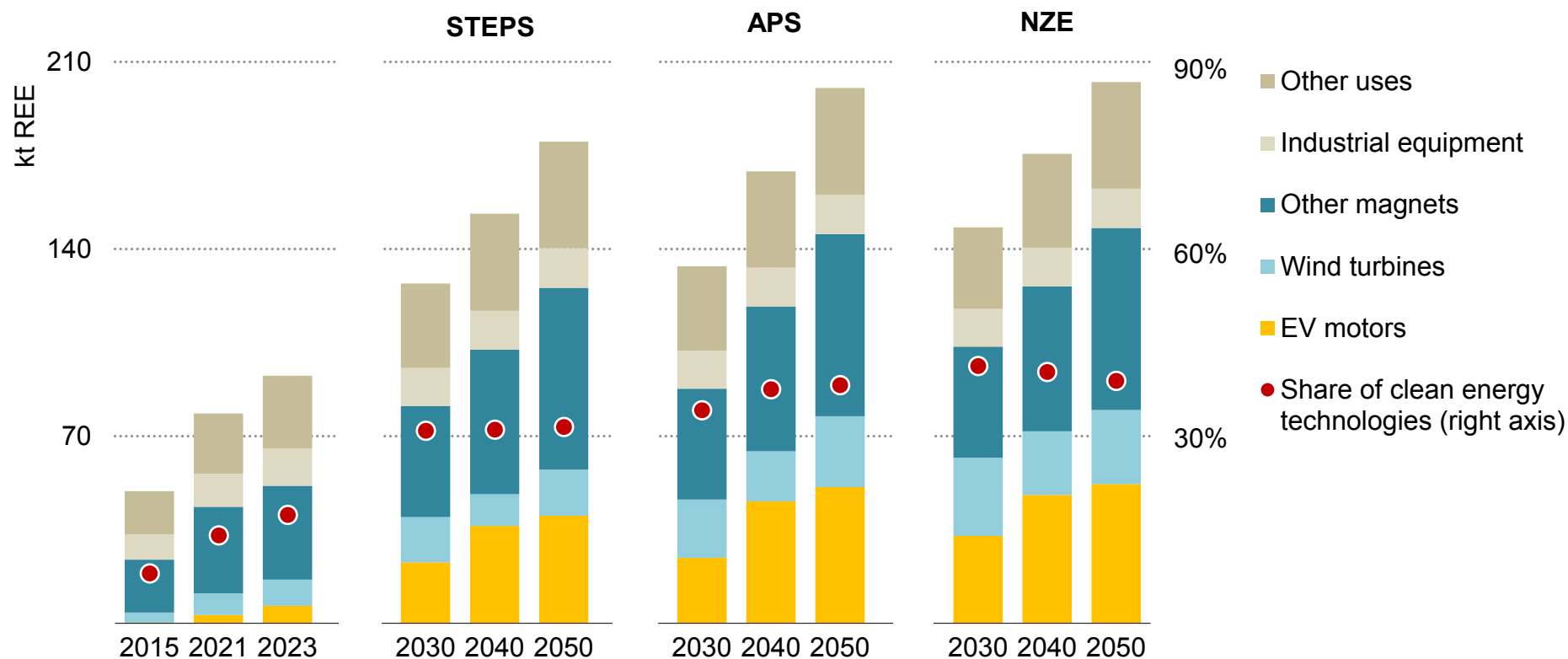
#### ESG and climate risk exposure

**607** gCO<sub>2</sub>/kWh

Among the highest average grid carbon intensity for refining

## Demand: Demand for magnet rare earth elements doubles between today and 2050 in climate-driven scenarios

Global magnet rare earth elements demand outlook by sector and scenario



IEA. CC BY 4.0

Notes: REE = rare earth elements. The figures are for magnet REE only.

## Demand: EV motors and wind turbines drive demand for rare earth elements

Rare earth elements (REE) are a set of 17 nearly indistinguishable silvery-white soft metals. Several of these are often found together in many known deposits. Though relatively plentiful in the entire Earth's crust, they have garnered the label "rare" because of how unusual it is to find them in a pure form. [Rare earth elements are usually classified into](#) light rare earths (LREE) such as lanthanum, cerium, praseodymium, neodymium, samarium and europium; and heavy rare earths (HREE) such as gadolinium, terbium, dysprosium, holmium, erbium, thulium, ytterbium, lutetium, scandium and yttrium. Light rare earths are often used in water purifiers (cerium) and hydrogen absorbers (lanthanum) and as stabilisers in catalytic compounds (lanthanum and cerium). Heavy rare earths are used to produce more energy-efficient phosphors for the displays of computers and phones as well as fluorescent lamps (yttrium and terbium) and in fibre optic cables and repeaters (terbium).

Neodymium and dysprosium can handle a greater saturation magnetisation than more common magnetic elements such as iron, which allows for fabrication of stronger and smaller magnets. Combined with other elements, these magnets (NdFeB magnets) are among the strongest magnets in the industry, able to withstand temperatures as high as 230<sup>o</sup> C. This section presents analysis and insights largely focusing on the four rare earth elements that are commonly used to manufacture modern permanent magnets:

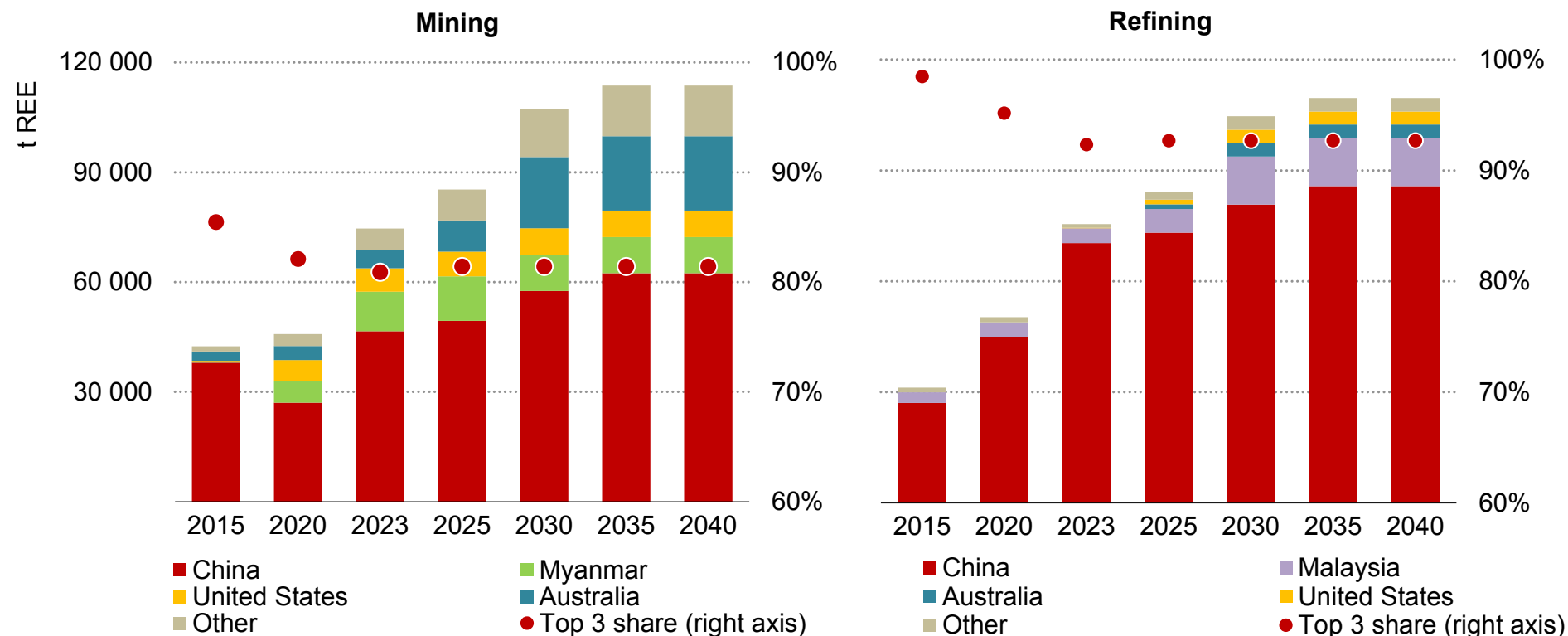
neodymium (Nd) and praseodymium (Pr) are the primary elements, while dysprosium (Dy) and terbium (Tb) are commonly used as additives to enhance the performance of Nd-Pr-based magnets.

Magnets made with these elements play a very important role in clean energy transitions as they are used in automotive traction motors for EVs as well as in wind turbine motors. Electric motors and generators driven by rare earth permanent magnets represent the most energy-efficient devices developed so far, making energy savings of about 20-40% compared with ordinary motors. Moreover, the addition of small quantities (1-2 kg) of these magnet rare earth elements in a motor can dramatically reduce (60-80 kg of lithium, nickel, cobalt) the requirements for other critical minerals needed for an EV.

The global demand for magnet REE nearly doubled between 2015 and 2023 to reach 93 kt, while the share of clean energy technologies, driven by new EV sales and wind turbine deployments to meet climate ambitions, has expanded from just 8% to nearly 18% during the same period. In the APS, we see total magnet REE demand reaching 131 kt by 2030 and further to 181 kt by 2050, with the share of demand from EV motors rising most sharply from 7% in 2023 to nearly 30% in 2050. The NZE Scenario sees a slightly accelerated ramp-up of EV sales and wind turbine deployment between today and 2030 compared with the APS, driving the total demand in this year to be 15 kt higher than in the APS.

## Supply: Magnet rare earths have the highest geographical concentration for refining of all energy transition minerals

Magnet REE production from operating and announced projects in the base case



IEA. CC BY 4.0.

## Supply: Geographical concentration for mining sees some improvements on the horizon, but refining remains in very few hands

The production of rare earth elements is perhaps among the least geographically diversified of all key energy transition minerals. Their high level of geographical concentration is comparable to those of cobalt and natural graphite for mining; at the same time rare earth elements rank as the most concentrated in terms of global refining capacity. The share of the top three producers for mining of magnet REEs in 2023 stood at 85%, of which China alone accounted for 62% of global mined production. When looking at refining, the top three countries controlled the lion's share of the refined output in 2023, with China's dominance being even more pronounced than in mining as it single-handedly represented 92% of the global refined output.

The expected supply of magnet REE from operating and announced mining projects rises by 44% and 52% respectively from today's levels to surpass 107 kt in 2030 and reach 114 kt in 2040. The dominance of the top three countries in global mined supply reduces slightly, falling to around 81% of the total compared with 85% today. The expected refined supply from operating and announced projects rises similarly to 106 kt in 2030 and over 110 kt in 2040, with the share of top three refining countries remaining extremely high, falling marginally from 98% to 92% today. By 2030, China's share of global refined output falls to 77%.

The type of ores that the four magnet REE often come from is heavy sands (monazite sands), which also contain radioactive elements such as uranium and thorium, making their extraction quite challenging. Outside of China, very few countries have the infrastructure and the willingness to build solutions for the storage of these radioactive by-products. Processing a kilogramme of rare earth oxides can produce close to 1 kilobecquerel of uranium-235 (U-235) equivalent of radioactive elements. Proper storage is the only way to prevent this material from entering the environment through waste streams, but studies show that [only 17% of operating rare earth miners align with the Global Industry Standard on Tailings Management \(GISTM\)](#). Appropriate waste management performance will be vital to scaling rare earths supply chains in geographically diverse regions.

In the upstream segment, only a handful of mines are operating at scale outside China and Myanmar (one each in the United States, Australia, Viet Nam and Brazil), and some mines are producing the rare earths as a by-product of manganese or titanium production. In general, newly announced projects have a lead time of eight years on average, making the scaling up of mined production beyond China a challenging proposition. The refining segment of the supply chain outside China is even more nascent than mining, with only a couple

of operating industrial-scale facilities existing in Malaysia and Estonia, some facilities in Australia nearing operation, and some smaller-scale refining units nearing operation in France and the United States.

## Regional mining trends

On mining, a vast majority of total mined REE production as of 2024 comes from China, notably from the Bayan Obo mines in Inner Mongolia. In the rest of the world, Mount Weld in Australia and Mountain Pass in the United States are leading producers. The two fastest growing regions in terms of mined production of magnet REE between 2015 and today have been Myanmar, which grew its share in global production from just 0.2% to 14%, and the United States whose share grew from 1% to 9% in the same period. In the period to 2030, China remains the top mining country for magnet REE supply, but Australia increases its share in the global total to 18% and the United States maintains its share similar to today's levels at 7%.

## REE mining in Myanmar

Most REE mining operations in Myanmar occur close to the Pang War-Tengchong border crossing with China in Kachin State, which is largely controlled by the Kachin Independence Organisation (KIO). As a result of the proximity of these critical resources to China, the vast majority is transported over the border for further processing and refining. While most tin concentrate sourced from Myanmar is

processed in Yunnan Province, China, it should be noted that REEs sourced from Myanmar are far more difficult to trace. This is a result of the multiple REE processing facilities throughout China that often combine raw materials from diverse sources. The resilience of all global supply chains was tested during the pandemic. During this period, the trade of both tin and REEs from Myanmar to China was negatively impacted by major border port closures, notably at the Menglian, Diantan and Menglong ports, resulting from China's zero-Covid policy, exposing the existing fragility of this supply network.

In April 2023, the KIO announced the suspension of REE mining in Kachin state from 4 September 2023, as protests highlighted environmental damage from mining and processing. Despite this, Chinese companies were permitted to gradually halt production in line with necessary steps rather than coming to an abrupt halt. Pressure has been building to comprehensively monitor mining operations in the region following environmental concerns, with the local government announcing inspections of REE mining operations in September 2023 that were expected to last only ten days, equating to one to three weeks of supply. However, after random inspections across more than 300 mining sites, the extended suspension has led to the temporary dismissal of local workers and uncertainty surrounding the resumption of operations as no new notices have been released by authorities.

Chinese imports of REE material spiked significantly in August 2023, increasing by approximately 76% year-on-year, according to Chinese



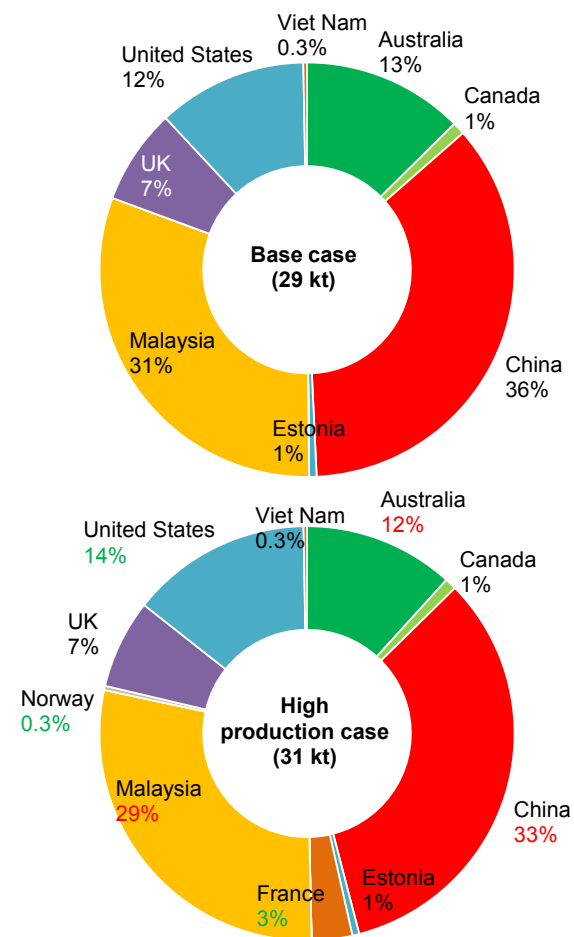
trade data, prior to the implementation of the suspension. Stockpiling of REE material ahead of peak consumption was further driven by environmental inspections that took place in late August in Jiangxi province, a major REE production hub. In early 2022, REE manufacturers in Ganzhou, Jiangxi province, suffered production capacity reductions of at least 25% after border gates between Myanmar and China were shut down at the beginning of the year, illustrating the significance of the current suspension.

While reserves should be sufficient for up to three to six months, any extended suspension of REE mining in Kachin state could be damaging for refineries in China reliant upon feedstock from Myanmar. The government-guided price for REEs in China has remained relatively low to incentivise downstream production, as magnet producers have found it increasingly difficult to pass additional costs to downstream end users, though this has caused poor financial performance for upstream operators.

### Regional refining trends

On refining, Chinese dominance in 2023 remained unchallenged. In the rest of the world, refineries owned by Lynas in Malaysia, Viet Nam Rare Earth JSC (VTRE) in Viet Nam and Neo Performance Materials in Estonia (Silmet) are the few notable industrial-scale producers. The fastest growing region in terms of refined production of magnet REE between today and 2030 is Malaysia, raising its share in global

Additional refined output of magnet REE between 2023 and 2030 in the base and high production cases



IEA. CC BY 4.0.

Notes: The shares in the figure indicate share of additions to 2030 and not the absolute share of the country in global refining capacity. UK= United Kingdom.

refined output from 5% to 12%. While the overall picture for regional distribution of expected refined supply does not change much to 2030, there is an additional 29 kt of refined output between 2023 to 2030 in the base case and 31 kt in the high production case. The majority of additions to 2030 in the base case come from China, Malaysia, the United States and Australia. In the high production case, the emergence of France and Norway as refiners in Europe reduces China's contribution to the total additions to 2030 by 3 percentage points.

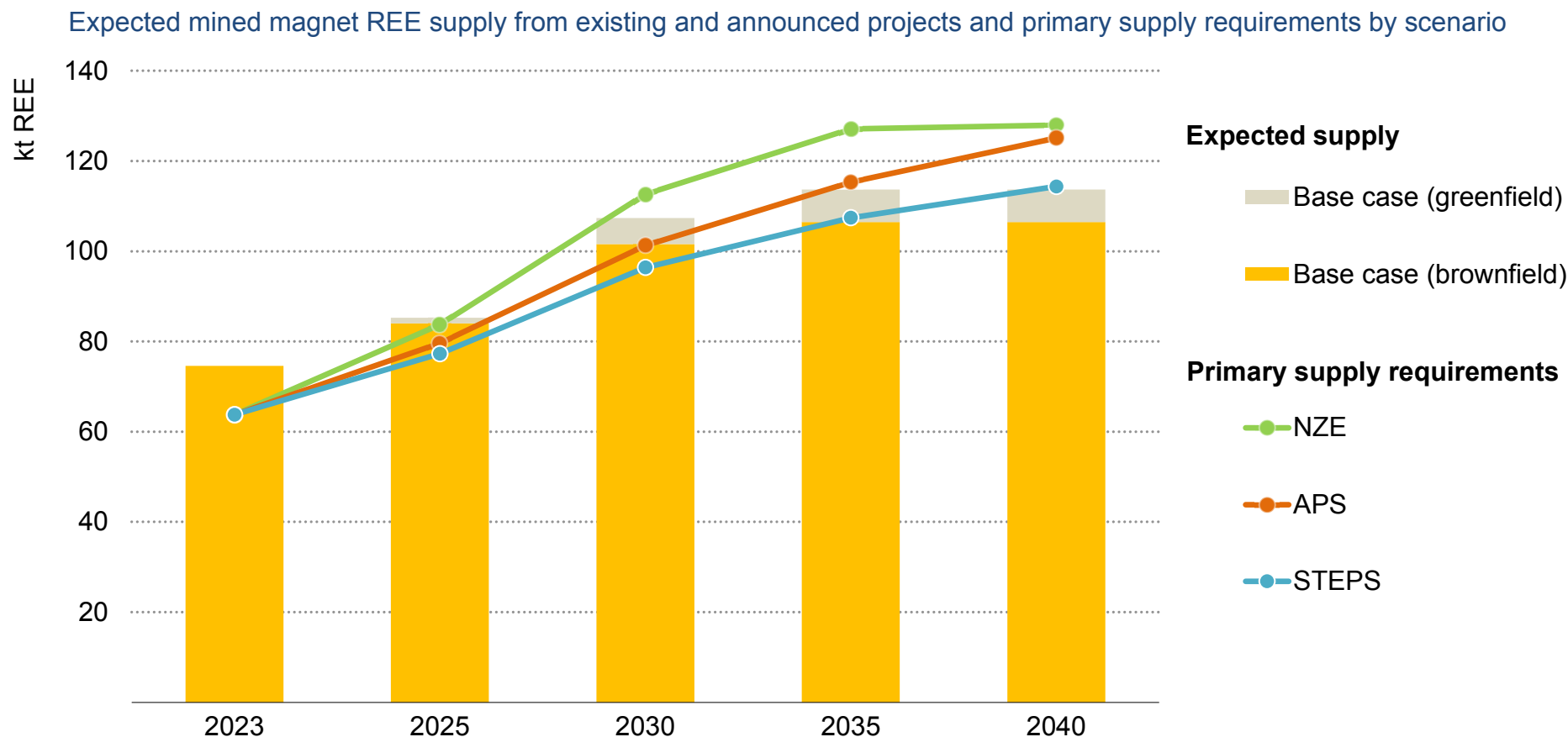
### REE refining in Malaysia

Lynas' operation in Malaysia from 2012 made it the first REE refining plant outside China. After years without steady supply of REEs, Japan started sourcing the materials from Malaysia since 2013 – which has enabled Japan to recover and increase their manufacturing activities since then. Currently, Lynas produces rare

earth oxides, carbonates, oxalates and chlorides in Gebeng, Pahang, with a total capacity of 22 000 tonnes per year.

Recognising the potential of the downstream industry of magnet manufacturing as well as the advantages of having rare earth oxides (REO) production as raw materials in the country, the Malaysian government, through the Malaysian Investment Development Authority (MIDA), has been [promoting the production of advanced materials including rare earth magnets](#) under the Promotion of Investment Act (PIA) 1986. To continuously support this, MIDA announced that it will continue its collaborations with the relevant stakeholders to attract potential investors to develop the industry. The support will focus on downstream manufacturing activities, as well as integrated projects including rare earth metals manufacturing that can convert oxides into metals.

## Supply: Expected supply nearly in line with requirements to 2030, but limited announcements of new projects with long lead times pose risks



IEA. CC BY 4.0.

Notes: Based on mined output. Primary supply requirements are calculated as “total demand net of secondary supply”, also accounting for losses during refining operations. See Introduction for definition of the base case.

## Implications: Supply risks arise from challenges to diversification of production

### Demand-supply balance and secondary supplies

For the four magnet rare earths mentioned above, the supply from today's operating projects is sufficient to meet current demand, and this is broadly likely to be the case in 2025. Between 2025 and 2040, the majority of the supply increases come from operating mines, particularly Bayan Obo in China and Mount Weld in Australia, increasing their expected production (brownfield expansion). The primary supply requirements (total demand net of secondary supply) in the STEPS grow in line with the projected brownfield and greenfield expansion and can be satisfied if additions occur as planned. However, after 2025, for the NZE Scenario and 2035 for the APS, a gap emerges between projected primary supply requirements and supply additions. In the NZE Scenario, there is an implied supply gap of 5 kt in 2030 and 14 kt in 2040. The major concern for magnet REE, however, is not a huge gap between demand and supply like in the case of copper or lithium, but rather an extremely important level of geographical concentration of today's as well as future mining and refining projects that expose this market significantly to supply disruptions.

Primary supply requirements in the medium to long term are also a function of growing interest in recycling manufacturing scrap and end-of-life magnets that will generate secondary supplies. In 2030, around 35 kt and 40 kt of total magnet REE demand may be met using

secondary supplies respectively in the APS and the NZE Scenario. Between 2030 and 2050, the secondary supply expands 1.7-fold in each scenario, to 60 kt and 67 kt respectively. Recycling so far has focused on the traditional "long-loop" recycling, which involves breaking down each element using various techniques to recover them as rare earth oxides that then have to be converted into metals before being cast into alloys and broken down into a fine alloy powder to make the magnets. It is an important but energy-intensive and expensive process. New technologies such as those of [HyProMag](#), a UK-based company with its recycling facility in Birmingham, and [MagREEsources](#), a French start-up that secured [Euro 5 million](#) to open its pilot site in Grenoble, have recently been in the news for their patented Hydrogen Processing of Magnet Scrap (HPMS) technique, [which uses hydrogen as a processing gas](#) to separate magnets from waste streams as a magnet alloy powder, which can be directly compactified into sintered rare earth magnets. This "short-loop" process does not require heat and is relatively quick, and magnets made with these recycled elements have been shown to have significantly [lower environmental footprint \(CO<sub>2</sub> emissions and water consumption\)](#) than those produced in China from mined minerals. Other companies using innovative recycling technologies, such as [ReElement Technologies](#) in the United States and [Ionic Technologies](#) in Northern Ireland, receiving support from major

companies provides further positive signals for increasing contributions from secondary supplies.

### Project funding grows steadily despite price declines

Two major rare earths producers outside China, Australia-based Lynas Rare Earths Limited and US-based MP Materials Corp., are clamping down on costs to offset a sharp drop in prices and weak Chinese demand. Lynas' average selling price for neodymium-praseodymium (Nd-Pr) [fell by 32%](#) per kilogramme year-on-year between July and December 2023, while MP Materials witnessed a [34% price dip](#) to USD 5 622 per metric tonne of rare earth oxide concentrate year-on-year for the December 2023 quarter. This low-price environment in recent months, in part caused by [China producing in excess of demand](#), has created some tensions in the market, but many experts believe that long-term demand beyond 2025 will remain robust. Industry expectations are that export credit agencies will [continue to support rare earth developers outside China](#), despite the challenging price environment at the moment. Moreover, China will continue to be a strong driver of rare earths demand, as evidenced by China's BYD Company Ltd. overtaking Tesla Inc. as the top-selling EV maker in 2023. Under these circumstances, China may prioritise supply for the domestic market, leaving a deficit globally.

Since the last major global discussion about potential disruptions in rare earth elements supply in 2011, almost no new large-scale

facilities have come online. The feasibility of announced projects for these minerals has been very low outside China. Efforts for diversification can be seen from different parts of the world. In September 2023, the Malaysian government stated that it is considering a ban on unprocessed rare earth concentrate in order to boost domestic REE processing. In March 2024, it was further mentioned that the Malay National Mineral Council would assess a proposal to create a [government-linked company for rare earth extraction](#). In the United States, [USA Rare Earth \(USARE\) signed an offtake agreement with ReElement Technologies](#) in March 2024 for supply of rare earth oxides to its magnet manufacturing facility in Oklahoma from 2025, with the goal of expanding to 900 tonnes per year by 2028. Additionally, the US Export-Import Bank sent letters of interest in March 2024 to provide up to [USD 600 million in debt funding](#) to rare earth developers Meteoric Resources and Australian Strategic Minerals. Meteoric Resources is developing the Caldeira project in Brazil targeting ionic adsorption clays, while Australian Strategic Minerals is developing the Dubbo project in Australia and downstream metallisation capabilities in Korea. This announcement from the United States follows a [series of government backed investment in rare earth projects](#), with the US Department of Defense providing additional funding to Lynas Rare Earths for its Texas-based refinery, and the Australian government providing financial support to Hastings Technology Metals, Iluka Resources and Arafura Resources to continue development of their respective rare earth mines and processing facilities.

There are two broad classifications of magnets made from REE: bonded magnets (smaller magnets, mainly used for electronics or small motors) and sintered magnets (most commonly used in traction motors for EVs and wind turbines). Besides China, only two facilities in Japan are known to produce the latter at industrial scale. New project announcements from Neo Performance Materials in Estonia approved by the European Commission and some from the Korean company Star Group funded by POSCO could come online within the next years. Roughly, three-quarters of the unit cost of making

permanent magnets is attributed to the raw materials and about 10% to energy costs, and the rest is labour costs. Labour costs (not labour intensity) are comparable to China in Europe and North America; however, energy costs are significantly lower in China. Today, original equipment manufacturers (OEMs) are hesitant to pay the 30% premium – equivalent to around USD 30 to USD 50 per vehicle – that comes from energy costs and trade taxes for magnets made outside China, creating the biggest challenge for diversification of the industry in the rest of the world.

## New technologies: Innovative extraction processes and new magnet technologies

There is a constant development of new rare earth processing technologies by various industry participants globally, though many of these processes have struggled to make significant advances. This is not always the fault of the technology developer, however, with difficulties in acquiring necessary feedstock at commercially viable prices, as is the case for [REEtec](#) in Norway, also causing delays and setback at processors.

### Will ionic adsorption clay deposits change the game?

Ionic adsorption clay (IAC) is also known as regolith-hosted ionic adsorption deposits (IADs), which contain rare earth elements adsorbed physically to the clay minerals surface, mainly kaolinite and halloysite. Weathering of igneous rock, primarily granite, that contains specific rare earth-bearing minerals results in the formation of IAC. The best environments for this process to occur are warm, humid and [slightly acidic conditions in subtropical regions](#). Important source rocks typically have a relatively high background in rare earths and rare earth-bearing minerals in these rocks will include monazite, xenotime, bastnaesite, allanite, titanite and apatite. The hype surrounding this form of deposit comes from the hope that extracting rare earths that are loosely bonded to the surface of rocks is relatively simpler, less energy-intensive and cheaper than obtaining them from the depths of hard rock formations, and could also avoid the

radioactive by-products that accompany the traditional mining processes for these minerals.

Ore deposits containing physically adsorbed lanthanides are substantially lower-grade than other rare earth deposit types (hard rock); [however, the low mining and processing costs make them economically attractive](#) as sources of rare earths. Global resources of HREE are dominantly sourced from Chinese regolith-hosted IADs or clay deposits in Myanmar and Laos, in which the elements are inferred to be weakly adsorbed onto clay minerals. Similar deposits elsewhere might provide alternative supply for these high-tech metals, but the [adsorption mechanisms remain unclear](#).

Traditional REE projects based on hard rock developments are extremely capital-intensive and can cost [USD 1 billion to USD 2 billion](#) to build, for which most junior miners cannot secure funding. In recent years, focus in the junior miner space has shifted from highly capital-intensive hard rock REE projects to low capital-intensity IAC projects which are enriched in HREE. Despite in-situ grades being lower than most hard rock projects, the mining is easier, leading to substantially lower capital expenditure and operating costs. Most clay operations involve digging or scraping of only the top twenty metres or so of earth, as opposed to blasting hard rock sources which may extend down to hundreds of metres or more. Clay material is soft and requires only breaking up, whereas hard rock



material needs to be crushed and ground, often in large quantities. Then there is the processing. Large-scale high temperature roasting and acid leaching for hard rock projects, compared with heap or vat leaching at atmospheric temperature and pressure for ionic clay projects. Last but not least, clay waste material is generally inert and can be backfilled into the mining area, meaning there is no need for tailings dams or dry stacking.

In regolith deposits, Chinese miners found that weakly acidic ammonium sulphate or sodium chloride solution readily reclaims the rare earths from the ionic bonded clays, allowing the resulting crude solution to be chemically treated to eliminate contaminants for further solvent extraction separation and refining. This processing can be in-situ leaching; heap leaching; or in-tank leaching with increasing cost and all with significant environmental impact. Generally, [Chinese costs for REE reclamation from IAC deposits are low and despite the low recoveries peaking at around 30% to 40%](#) in final products, these projects appear to be economic.

The economic viability of IAC deposits remains uncertain, but they look increasingly attractive from perspectives of capital intensity, ease of working, carbon intensity and radioactive waste management. While China appears to have developed a low-cost method of reclaiming rare earths from IAC deposits, not all REE clay projects are IAC projects and it is important for prospective investors to have sufficient metallurgical testing carried out to establish the

ionic adsorption capacity and suitability for ion exchange within all new clay discoveries.

There has been a steady flow of announcements of IAC discoveries outside southern China and Myanmar in recent years, such as in [Australia](#), [Brazil](#) and [Uganda](#). How quickly these discoveries can be converted to projects operating at scale remains to be seen. In March 2024, [Appia Rare Earths & Uranium](#) announced a maiden mineral resource estimate for its ionic adsorption clay PCH project in Goiás, Brazil.

In addition to the growth in IAC type production, the most significant change in the rare earth space would be the growth of supply from heavy mineral sand (HMS) operations, which are expected to contribute volumes of not only Nd-Pr feedstocks but also provide notable quantities of Dy-Tb to downstream processors. While some HMS producers are looking to integrate production, as is the case with [Iluka](#), [Energy Fuels](#) and [Tronox](#), many producers will continue to supply material into the Chinese market.

### Alternative magnet technologies

On the technology innovation side, the development of alternative magnet technologies such as iron nitride has been a key topic of interest for many stakeholders wanting to understand the potential impact on neodymium iron boron (NdFeB) magnets used in automotive applications. [Niron Magnetics' Clean Earth Magnet](#) has attracted interest from [General Motors](#) in the United States, with



whom Niron has partnered for the development of EV drivetrains, starting with a demonstrator for the Chevrolet Bolt. Further funding for Niron has also come from [Samsung](#) and [Stellantis](#).

One apparent disadvantage of iron nitride magnets is that their coercivity is less than that of neodymium. Coercivity is a measure of the magnet's ability to resist having the polarity of its field reversed when exposed to a strong opposing field. Without coercivity, the

magnetic fields in a motor would rotate without turning the shaft. Initial assessments indicate that iron nitride will struggle to compete with incumbent neodymium iron boron magnets for automotive drivetrains as the importance of high magnetic density, high coercivity and field strength which the latter technologies bring are non-negotiable for compact motor and EV manufacturers.

## Brief review of other key materials

## Aluminium

Aluminium traded within a fairly narrow range of USD 2 100 to USD 2 450 per tonne over the past year, with the strong dollar and slowing industrial activity setting a ceiling on prices. This trend is likely to continue in the near term owing to the persistent slowdown in manufacturing as well as supply-side uncertainty. In the long term, global demand growth is expected to narrow the surplus, driven in large part by increasing utilisation in clean energy applications.

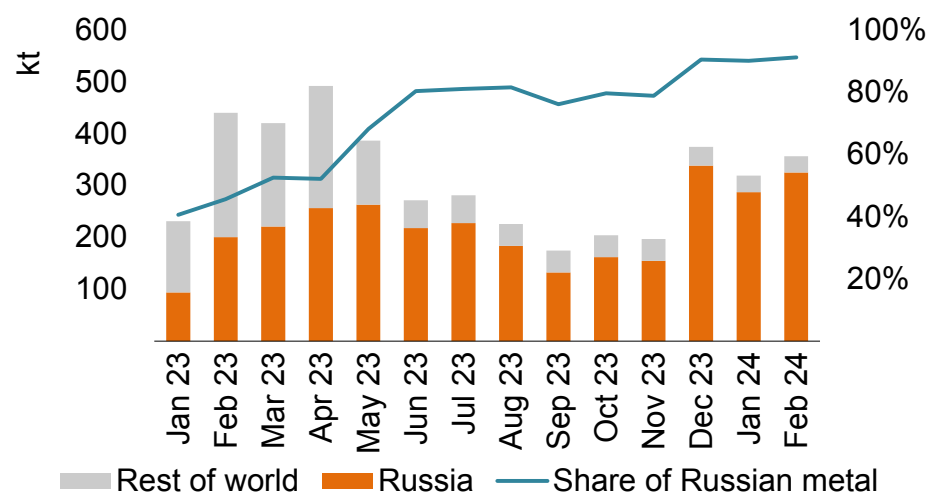
Aluminium's use as a lightweight structural element in solar PV installations and EVs is expected to remain as a primary demand driver. In addition, transmission requirements arising from increased electricity demand and renewable penetration are expected to boost the use of aluminium conductor steel-reinforced cables. Demand growth from traditional demand sectors in construction and manufacturing are likely to remain modest.

On the supply side, [drought risks in the southwestern Chinese province of Yunnan](#) pose significant near-term potential for supply volatility and elevated prices. Hydro-powered Yunnan accounts for about 12% of Chinese aluminium production, but low water levels have resulted in production cuts totalling [more than 1 Mt per annum between November 2023 and February 2024](#).

The proportion of Russian metal within LME stocks has doubled from 45% in February 2023 to over 90% in 2024 amid low overall stock

levels. The LME's April 2024 ban on accepting Russian aluminium, copper and nickel [created opportunities for traders, which further dried up the liquidity](#) for tradeable metal.

Proportion of Russian metal within LME stocks

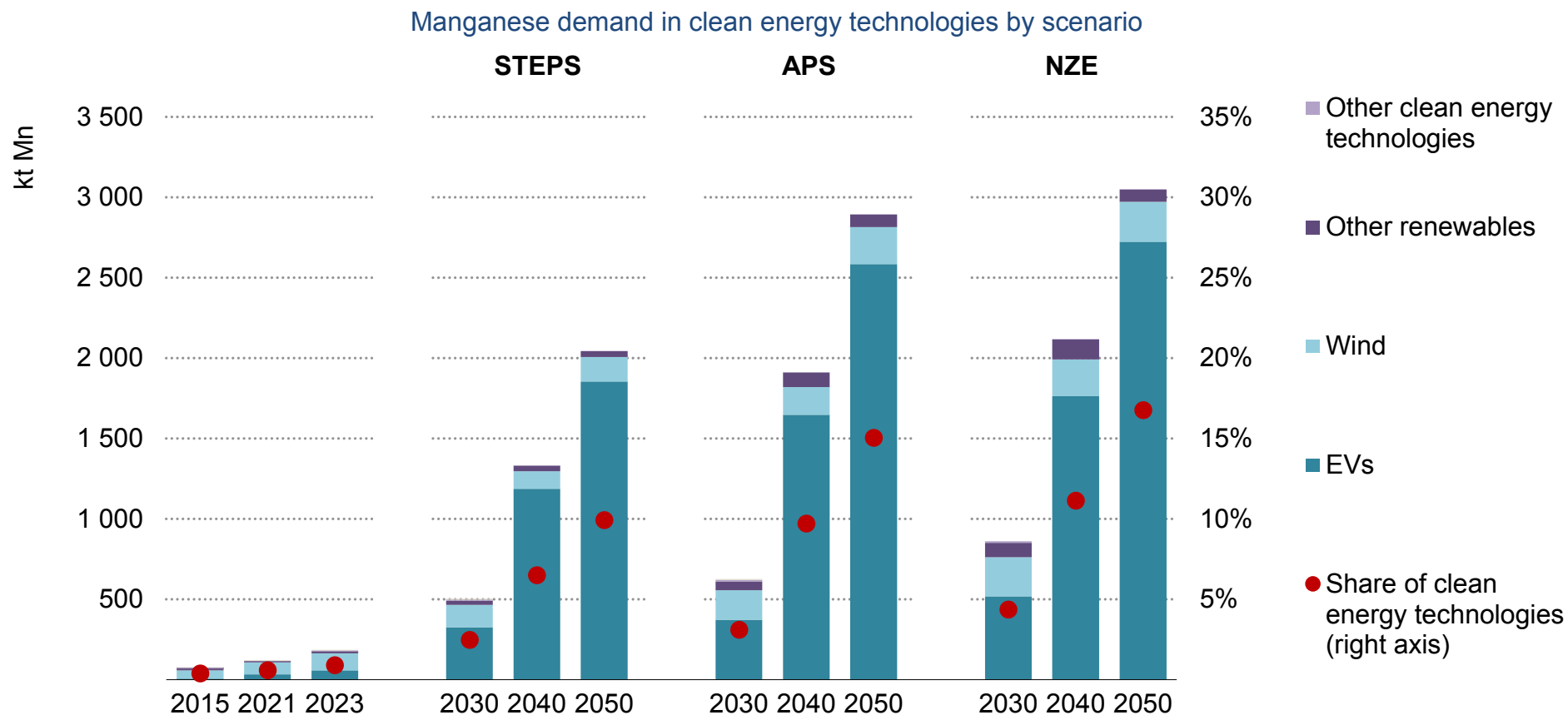


IEA. CC BY 4.0.

Source: IEA analysis based on London Metal Exchange.

Global production levels are expected to be able to serve near-term demand increases. Despite [slowing growth in China](#) as primary production capacity reaches the government-mandated limit of 45 Mt per year, secondary production growth as well as new smelting capacity are expected to support long-term market growth.

## Manganese: Demand surges driven by EV batteries, but significant concerns remain about the future supply of battery-grade manganese sulphate where China dominates supply



IEA. CC BY 4.0.

Source: IEA analysis based on US Geological Survey (2024), [Minerals Commodity Summaries 2024](#).

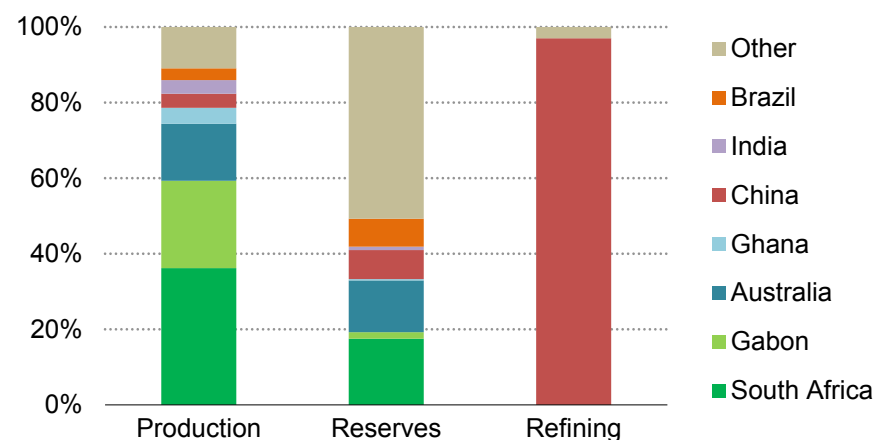
## Manganese

Manganese demand is primarily driven by steel, as it is a key component of steel alloys. Currently, batteries account for a small share of total manganese demand; however, this share is set to increase rapidly due to the surging deployment of EVs. Manganese is a critical component of one of the dominant EV cathode chemistries, NMC, as well as now being utilised in the new variant of the current leading chemistry LFP known as LMFP, where LMFP is set to start taking market share. For instance, CATL's LMFP cells have been confirmed for use in [six models in China](#) and are [undergoing validation by Tesla](#), who are expected to use the cells in the Model 3 made in China. The addition of manganese increases energy density compared with traditional LFP. Other chemistries under development such as lithium nickel manganese oxide (LNMO) also use higher fractions of manganese compared with conventional nickel-rich cathodes. Therefore, this shift towards greater manganese contents in cathode chemistry is expected to drive a surge in demand. Manganese is also a key metal used in wind turbines as a critical part of steel components.

By 2030 manganese demand from clean energy technologies increases almost threefold in the STEPS, over threefold in the APS and almost fivefold in the NZE Scenario. By 2050 manganese demand from clean energy technologies is a remarkable 11 times higher than today in the STEPS, 16 times higher in the APS and 17 times higher

in the NZE Scenario. The rapid growth in EV deployment is responsible for the exceptional increase in manganese demand in clean energy technologies. This results in the share of demand from clean energy technologies increasing from 1% today to 15% in 2050 in the APS and 17% in 2050 in the NZE Scenario. Thus, steel remains the dominant driver of total manganese demand. However, it is critical to note all of this remarkable growth in manganese demand from EV batteries will need to be high-purity manganese sulphate.

### Geographical distribution of manganese production and reserves



IEA. CC BY 4.0.

Note: Refining refers to production of battery-grade manganese sulphate.  
Sources: US Geological Survey (2024), [Minerals Commodity Summaries 2024](#) and IEA (2023), [Critical Minerals Market Review 2023](#).

In terms of supply, mined manganese production is highly concentrated with the top three countries producing three-quarters of global supply. South Africa is the world's largest producer with 35% of production, followed by Gabon with a quarter and Australia with 15%. This concentration already poses significant risks. Exports of manganese ore [from Gabon dropped by 13%](#) from 2022 to 2023 due to [the military coup](#) and [a landslide on key rail infrastructure](#) which required significant maintenance. This increased political instability and risk deters investment and causes concern for future supply disruptions for the key supply region. Gabon also has the [highest grade \(average 45%\)](#) compared with the other two leading producers Australia (42%) and South Africa (38%), thus its critical importance for global manganese supply. Australia's GEMCO mine is the world's second-largest manganese mine but it has suspended exports due to infrastructure damage from Tropical Cyclone Megan in March. Operations and export sales will remain suspended until early 2025. Exports from South Africa also [dropped by 7%](#) following extreme weather, maintenance challenges and insufficient investment [for key rail infrastructure](#) transporting manganese ore.

Nevertheless, there is potential for diversification, seen by comparing current production with reserves (defined as economically extractable resources). In terms of reserves, South Africa is indeed the largest with almost 20%, followed by Australia with 15% of the global total. China and Brazil hold significant reserves with 15% together. There are several qualifications which must also be taken into account when assessing reserves including the resource quality or any above-

ground constraints limiting potential. Also, critically, there is a need for updated geological surveys in emerging and developing economies, where the current surveys are out of date.

However, the critical risk for manganese is the supply of high-purity manganese sulphates required for battery chemistries, a crucial issue given the remarkable growth from EV battery demand. While manganese is abundant, only around [1% of global supply](#) is suitable for batteries. China dominates supply of battery-grade manganese sulphate, producing [97% of global supply](#). There are only two other refineries outside China in operation, in Japan and Belgium, though with several projects in development including in Canada, South Africa, Australia and the United States. With manganese sulphate prices relatively low due to slight surpluses from China, it is difficult for many other regions to compete with China on costs. This is proving [challenging for new ventures](#) to be competitive and secure investment. Some analysts even forecast a deficit in supply of battery-grade manganese sulphate as early as 2027, adding concern for ensuring sufficient supply for EV batteries. Nevertheless, the total dominance of China in the supply of high-purity manganese sulphates today is a major risk alone, making supply highly vulnerable to sudden changes in policy, geopolitics or supply shocks.

## Silicon

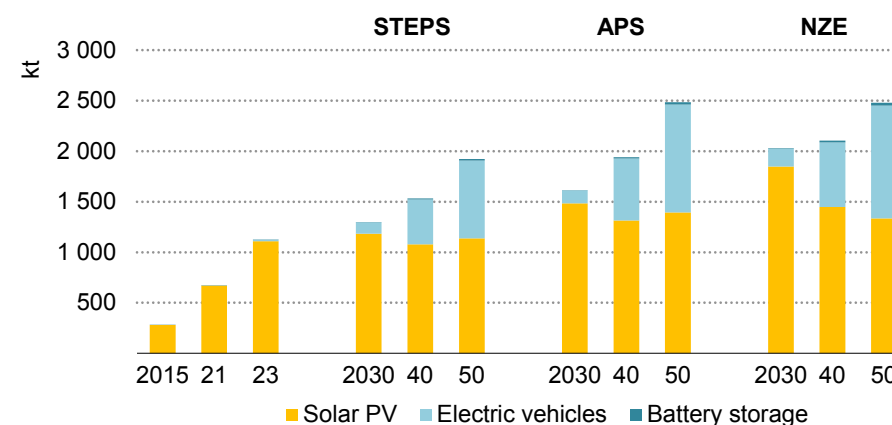
The silicon market is poised to be affected by two waves of demand growth from clean energy technologies. A first phase is related to the ramp-up of solar PV deployment, requiring close to 1.5 Mt in 2030 in the APS, and close to 2 Mt to meet the needs in the NZE Scenario. A second phase corresponds to the growing use of silicon in the battery industry, as a higher-performance substitute for graphite, with related demand reaching over 1 Mt in 2050 in the APS and the NZE Scenario.

Silicon is produced in its metallic and crystalline forms using silica-rich minerals, generally from high-purity quartzite. The existing silicon industry is already mature, supplied by an abundant resource, with a current global production already close to 3.8 Mt, but new demand trends related to clean energy (and also digital transitions) are transforming the supply chain, requiring larger volumes of higher-purity products. Consumption was historically dominated by the aluminium alloy industry and silicone producers (silicon-based polymers, often found in rubber or oil-like products), calling for “metallurgical grade” of 99.99% (4N) purity silicon. Solar PV is known for requiring 99.9999% (6N) while electronic applications can require even higher purity, ranging up to 11N. Both electronic and solar PV uses may increase demand for high-purity products.

Technological gains in efficiency are significantly reducing pressures on silicon resources, with requirements in solar panels declining from

6.8 g/W in 2010 to 2.3 g/W in 2022 and close to 1.5 g/W in the latest generation of solar PV technologies.

Silicon demand related to clean energy technologies by sector and scenario



IEA. CC BY 4.0.

For EV batteries, manufacturers are already adding small volumes of silicon in anodes, but further increasing this share faces significant technological hurdles, such as swelling during the charging cycle. Several start-ups are developing various silicon nanoproductions to reduce these effects, suggesting potential for new specialised silicon supply chains. For stationary storage, silicon uses are expected to remain small, due to lower energy density requirements. Similar to other minerals, the silicon refining industry has demonstrated the capacity to adapt to the rapid growth in demand, albeit at the expense

of increasing concentration and significant price volatility. The supply was initially affected by a glut that began in 2015, followed by a period of supply tightness in 2021. Currently, there is an oversupply situation, with a high volume of capacities developed in China in line with its downstream solar PV capacities. Silicon prices fell by 74% in 2023 to around USD 8 per kilogramme.

China's share of solar-grade silicon grew from 27% in 2010 to over 80% today. The current price context and local energy prices are adding pressure on European solar-grade polysilicon manufacturers, with some capacities closing down. US restrictions on solar PV imports related to concerns of forced labour have increased demand

for supplies outside of China, with some plants being developed in the United States recently.

Recycling silicon remains challenging due to weak economic incentives, driven by the low cost of the material input and the prevailing low-price environment affecting the 6N refined silicon market. Historically, solar PV recycling players have prioritised base materials present in larger volumes (such as copper, aluminium and glass), or precious metals such as silver, rather than silicon. However, some European are [developing](#) plants designed to recycle silicon.



## Phosphoric acid

The success of LFP battery chemistries is creating a market for a new input, iron phosphate, and its precursor – purified phosphoric acid. As LFP cathode production rises, so does demand for this high-purity input, reaching over 2 Mt in the APS by 2030 and close to 4 Mt in the NZE Scenario. Further demand growth for high phosphoric acid comes from next-generation lithium-iron phosphate manganese (LMFP) chemistries, whose higher performance is likely to further popularise EV batteries containing phosphate. In 2040, demand rises to almost 6 Mt in the APS and over 6.5 Mt in the NZE Scenario. In 2050, demand rises to almost 6 Mt in the APS and over 6.5 Mt in the NZE Scenario.

Phosphates are cheaper than the metals they replace from previous battery compositions (cobalt, nickel) and are currently produced in vast quantities for fertiliser applications. About 220 Mt of phosphate rocks are extracted each year, containing about 28 Mt of phosphorus, and enough to produce over 80 Mt of phosphoric acid.

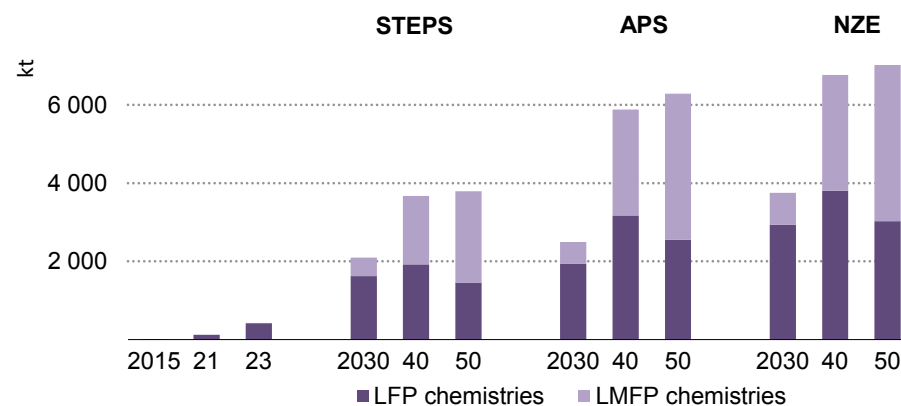
Three challenges could arise from these developments:

- Increased competition with agricultural supply – despite demand in smaller volumes and higher-grade requirements, additional demand from the energy sector could change supply and demand balances in the fertiliser market.
- Geological deposits for phosphate rocks are sufficient, but questions remain regarding mining capacities, particularly the

best deposits for the production of purified phosphoric acid. This process requires high grade and low rates of heavy metals such as cadmium. Some LFP supply chain investments are oriented towards countries with significant phosphate resources, such as Morocco, which also benefits from a number of favourable free trade agreements.

- An ability for new players to access supplies already secured by refining. Once concentrated in China, LFP technologies have gained popularity elsewhere including among North American gigafactories. These new players need to find a channel to source materials reliably.

### Phosphoric acid demand from the EV sector by scenario



IEA. CC BY 4.0.

## Platinum group metals

Prices for platinum group metals (PGMs) remained under pressure for the past year, driven in large part by poor automotive sales. The basket price, defined as the average price of the five PGMs (platinum, palladium, rhodium, iridium and ruthenium) weighted by production, seems unlikely to increase meaningfully in the short term. Although the five PGMs occur together in nature, divergent market outlooks are complicating strategic decision-making for these elements.

In the near term, prices for platinum, iridium and ruthenium are expected to remain stable, with platinum having modest upside potential. Rhodium and palladium are likely to remain under pressure due to lower demand for internal combustion engine (ICE) emissions catalysts, which represents about 90% of demand for rhodium and 80% of demand for palladium. Future increases in platinum demand remain subject to the future of hydrogen fuel cell vehicle sales, along with demand from existing industrial and ICE applications.

Palladium and rhodium demand are likely to decline structurally due to the uptake of EVs. In addition, growing secondary supplies are likely to exert further pressure on producers, especially for [North American mines mining palladium-rich ores](#).

Demand for iridium and ruthenium are likely to increase consistently in the coming years thanks to demand for membrane electrodes, including those used in proton exchange membrane hydrogen electrolyzers. This is likely in spite of continued [technical research and development to reduce the amount of precious metals](#) per unit product. Price volatility in the iridium market is expected to continue, driven by concerns over long-term supply. However, given the relatively small contribution of iridium and ruthenium to the PGM basket, prices for these metals will have to increase significantly to motivate structural increases in supply.

On the supply side, near-term shocks remain possible thanks to persistent [electricity system issues](#) in South Africa and [geopolitical concerns](#) impacting Russian palladium supplies from Norilsk. Since the second half of 2023, South African PGM miners including [Sibanye-Stillwater](#), [Anglo-American Platinum](#) and [Impala Platinum](#) have announced cost-cutting measures to mitigate the impact of low prices. These measures, which include project deferrals and shutting shafts, have not meaningfully boosted prices, which have remained anaemic. If the current price environment continues, further closures might occur, jeopardising long-term primary supply for all five metals.

---

## 3. Clean energy transition risk assessments

---

## IEA’s mineral-specific “clean energy transition risk assessment” framework

|  |  |
|--|--|
| <b>Supply risks</b>                      | Expected pace of demand growth                               |
|  | Short-term supply-demand balances                            |
|  | Long-term market balances in climate-driven scenarios        |
|  | Observed price volatility                                    |
|  | Impacts on clean energy cost                                 |
| <b>Geopolitical risks</b>                | Geographical concentration of mined supply                   |
|  | Geographical concentration of refined supply                 |
|  | N-1 demand and supply balances                               |
|  | Export risks of major suppliers                              |
|  | Hurdles to develop new projects in diversified regions       |
| <b>Barriers to respond to disruption</b> | Visible stock levels   |
|  | Transparency of pricing schemes                              |
|  | Availability of options to moderate demand                   |
|  | Status of secondary supply                                   |
| <b>Exposure to ESG and climate risks</b> | Environmental performance: mining                            |
|  | Environmental performance: refining                          |
|  | Social and governance performance                            |
|  | Exposure to natural hazards and climate risks - water stress |
|  | Exposure to natural hazards and climate risks - earthquake   |

Notes: ESG = environmental, social and governance. “N-1” refers to the case that excludes anticipated supply from the largest supplier and projected demand from that country from global market balances.

## Mineral-specific “clean energy transition risk assessment” framework

Understanding potential risks across the critical mineral supply chain is an essential step to enhance readiness against potential disruptions and devise necessary policy actions. An approach to mineral security may vary depending on each mineral's market context and risk exposure. Conducting structured risk assessments can assist policymakers in identifying vulnerabilities in the supply chain, devising appropriate security measures, and directing policy efforts to where they are most needed.

We have performed “Clean energy transition risk assessments” for the six key energy transition minerals: copper, lithium, nickel, cobalt, graphite, and rare earth elements. These assessments are based on a comprehensive framework that combines both quantitative and qualitative analyses, to understand potential risk areas that could hamper progress towards energy transitions. The framework encompasses four main categories: supply risks, geopolitical risks, barriers to respond to disruptions, and exposure to environmental, social, and governance (ESG) and climate risks (see Annex for detailed evaluation criteria).

The first category (**supply risks**) assesses five dimensions.

- **Pace of demand growth** compares projected annual average demand growth rates in the Announced Pledges Scenario (APS)

between 2023 and 2030 in relation to historical growth rates between 2010 and 2019.

- **Short-term market balances** assesses the near-term balances between expected supply and primary supply requirements.
- **Long-term market balances in climate-driven scenarios** reviews the balances between expected supply and primary supply requirements in 2040 in the APS.
- **Observed price volatility** evaluates historical price volatility based on monthly prices between 2011 and 2023.
- **Impact on clean energy cost** examines the share of a material in the total cost of end-use clean energy technologies to assess how price volatility could affect clean energy deployment.

The second category (**geopolitical risks**) assesses five dimensions.

- **Geographical concentration of mined supply** assesses the expected share of the top three producing countries for mining in 2030 under the base case supply scenario.
- **Geographical concentration of refined supply** assesses the expected share of the top three producing countries for refining in 2030 under the base case supply scenario.

- **N-1 supply and demand balances** reviews market balances excluding the largest supplier by comparing the N-1 supply and material requirements in 2030 in the APS (refined product basis).
- **Export risks of major suppliers** assesses the risks of trade restriction measures by examining the weighted average export restriction risk score of the current production portfolio for both mining and refining, based on the [Organisation for Economic Co-operation and Development's \(OECD's\) inventory of export restrictions on industrial raw materials](#) and announced intentions.
- **Hurdles to develop new projects in diversified regions** conducts qualitative assessments of challenges in building supply chains in geographically diverse regions, such as lead time, capital requirements and technological barriers.

The third category (**barriers to respond to disruptions**) assesses four dimensions.

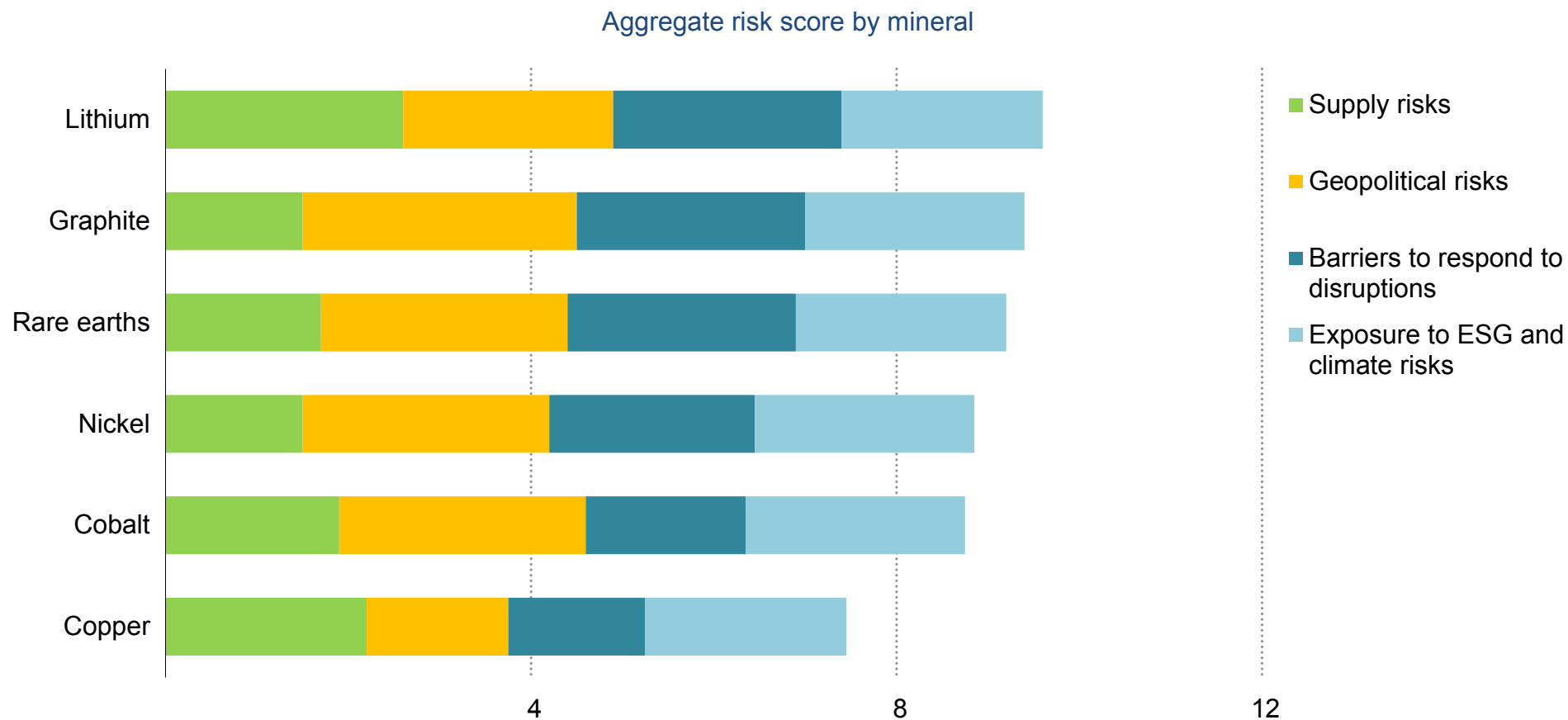
- **Visible stock levels** reviews stock levels at major exchanges. While exchange stocks represent only a fraction of the industry's overall stock levels, they offer a valuable indication of an accessible buffer during disruptions.
- **Transparency of pricing schemes** conducts a qualitative assessment of market liquidity, transparency of pricing schemes and the availability of financial tools to hedge price risks.

- **Availability of options to moderate demand** assesses possible demand-side and technology-switching options to moderate demand growth in the event of supply tightness.
- **Status of secondary supply** assesses the ability of secondary supply to ramp up during market tightness by examining the share of secondary supply in total supply and its potential for growth.

The fourth category (**exposure to ESG and climate risks**) assesses five dimensions.

- **Environmental performance of mining** reviews the weighted average environmental performance score of today's mined production, based on selected indicators in [Yale's Environmental Performance Index](#).
- **Environmental performance of refining** reviews the weighted average grid carbon intensity of the regions refining minerals today, considering that refining operations are highly electricity-intensive.
- **Social and governance performance** assesses the weighted average corruption, human rights and conflict score of today's mined production, based on relevant indicators in the [V-Dem database](#).
- **Exposure to water stress** assesses the share of mine production located in areas with high and extreme high-water stress and arid conditions.
- **Exposure to earthquake risks** assesses the share of mine production located in areas with high earthquake risks.

**Overall:** Lithium and graphite show the highest risk scores, though the specific areas of exposure vary by mineral



IEA. CC BY 4.0.

## Copper: Assessment results

| Area                                       | Score         | Rationale   |
|--|---------------|---|
| <b>Supply risks</b>                        | <b>Medium</b> |   |
| Pace of demand growth                      | Low           | Projected pace of demand growth is in line with historical growth rates   |
| Short-term market balances                 | Medium        | Supply could meet near-term demand, but risks of tightness if disruption occurs beyond usual range  |
| Long-term market balances                  | High          | Expected base case supply falls significantly short of the primary supply requirements in 2040  |
| Observed price volatility                  | Low           | Historical price movement has been less volatile compared with other commodities  |
| Impact on clean energy cost                | High          | Price spikes could significantly affect grid deployment (20% of capital costs). Copper in lithium-ion anode current collector is difficult to be replaced, thus price spikes can have major impacts on battery prices   |
| <b>Geopolitical risks</b>                  | <b>Low</b>    |   |
| Geographical concentration: mining         | Low           | Expected top 3 share in 2030 is around 48% and top 1 share is around 23%  |
| Geographical concentration: refining       | Low           | Expected top 3 share in 2030 is around 60% and top 1 country accounts for less than half of global supply   |
| N-1 supply and demand balances             | Low           | N-1 supply in 2030 able to serve N-1 demand   |
| Export risks of major suppliers            | Medium        | Risk score 2.7 (mining 2.2/refining 3.3)  |
| Hurdles for diversification                | High          | Challenges of declining ore quality, very low global average grade (0.6%), few major resources of high quality to exploit. Capital and operating costs increasing, coupled with long lead times to build new mines  |
| <b>Barrier to respond to disruption</b>    | <b>Low</b>    |   |
| Visible stock levels                       | Medium        | Able to monitor stock levels at major exchanges, but the current exchange stocks at low levels  |
| Transparency of pricing schemes            | Low           | Established regulated market trading with ample liquidity   |
| Availability of options to moderate demand | Medium        | Scope to moderate demand through scaling up recycling and scrap use and substitution for aluminium. However, copper is irreplaceable for many applications (e.g. lithium-ion anode current collectors, subsea cables). The replacement of underground power lines with aluminium requires additional cost |
| Status of secondary supply                 | Low           | Sizeable secondary supply and growing direct use of scrap, which could be tapped in times of price spikes   |
| <b>Exposure to ESG &amp; climate risk</b>  | <b>Medium</b> |   |
| Environmental performance: mining          | Medium        | Weighted average score 47   |
| Environmental performance: refining        | High          | 467 g CO <sub>2</sub> /kWh  |
| Social and governance performance          | Low           | Weighted average score 0.68   |
| Exposure to water stress                   | High          | 52% of mine production located in high-risk areas   |
| Exposure to earthquake risks               | Medium        | 46% of mine production located in high-risk areas   |



## Lithium: Assessment results

| Area                                       | Score         | Rationale   |
|--|---------------|---|
| <b>Supply risks</b>                        | <b>High</b>   |   |
| Pace of demand growth                      | High          | Projected pace of demand growth is materially higher than the rates observed in the last decade                               |
| Short-term market balances                 | Low           | Sufficient supply expected to serve short-term demand   |
| Long-term market balances                  | High          | Expected base case supply meets less than 40% of the primary supply requirements in 2040                                      |
| Observed price volatility                  | High          | High volatile price movements observed in recent years  |
| Impact on clean energy cost                | High          | 20% of battery pack cost. Fluctuation of prices has major impacts on battery prices and deployment                            |
| <b>Geopolitical risks</b>                  | <b>Medium</b> |   |
| Geographical concentration: mining         | Medium        | Expected top 3 share in 2030 is around 68% and top 1 share is around 33%  |
| Geographical concentration: refining       | High          | Expected top 3 share in 2030 is above 80% and top 1 country accounts for more than half of global supply                      |
| N-1 supply and demand balances             | Medium        | Expected ex-China supply could serve around half of APS ex-China material requirements in 2030                                |
| Export risks of major suppliers            | Medium        | Risk score 3.1 (mining 2.4/refining 3.8)  |
| Hurdles for diversification                | Medium        | New capacities do not necessarily involve higher capital, but need to overcome technological barriers                         |
| <b>Barrier to respond to disruption</b>    | <b>High</b>   |   |
| Visible stock levels                       | Medium        | Limited information about visible stock levels, but accumulated industry stocks are expected                                  |
| Transparency of pricing schemes            | Medium        | Early-stage regulated market trading, but liquidity is still lacking  |
| Availability of options to moderate demand | High          | Limited options to reduce demand. Sodium-ion may ease concerns, but has limitations to be adopted in major transport segments |
| Status of secondary supply                 | High          | Limited share of secondary supply as of today, but set to increase in future years  |
| <b>Exposure to ESG &amp; climate risk</b>  | <b>Medium</b> |   |
| Environmental performance: mining          | Medium        | Weighted average score 59   |
| Environmental performance: refining        | High          | 531 g CO <sub>2</sub> /kWh  |
| Social and governance performance          | Low           | Weighted average score 0.78   |
| Exposure to water stress                   | High          | 50% of mine production located in high-risk areas   |
| Exposure to earthquake risks               | Medium        | 26% of mine production located in high-risk areas   |

## Nickel: Assessment results

| Area                                       | Score         | Rationale  |
|--|---------------|--|
| <b>Supply risks</b>                        | <b>Low</b>    |  |
| Pace of demand growth                      | Low           | Projected demand growth rates are in line with historical growth rates   |
| Short-term market balances                 | Low           | Sufficient supply expected to serve short-term demand  |
| Long-term market balances                  | Medium        | Expected base case mine supply meets a large portion of the primary supply requirements in 2040 due to the rise of Indonesian output, but lack of sufficient nickel sulphate capacity remains an issue                   |
| Observed price volatility                  | Low           | Historical price movement has been less volatile compared with other commodities   |
| Impact on clean energy cost                | Medium        | 6% of battery pack cost in 2023. Fluctuation of nickel prices can have major impacts on battery prices   |
| <b>Geopolitical risks</b>                  | <b>High</b>   |  |
| Geographical concentration: mining         | High          | Expected top 3 share in 2030 is around 75% and top 1 share is around 61%   |
| Geographical concentration: refining       | High          | Expected top 3 share in 2030 is around 67% and top 1 country supplies more than half of global output  |
| N-1 supply and demand balances             | Medium        | N-1 supply serves 35% of N-1 requirements in 2030 in the APS   |
| Export risks of major suppliers            | Medium        | Risk score 3.9 (mining 3.8/refining 4.1)   |
| Hurdles for diversification                | High          | Most diversified projects in the pipeline in the base case or high production case are located in higher-cost jurisdictions, posing significant barriers to entry without mechanisms to incentivise high ESG performance |
| <b>Barrier to respond to disruption</b>    | <b>Medium</b> |  |
| Visible stock levels                       | Medium        | Nickel exchange stocks at historically low levels  |
| Transparency of pricing schemes            | Medium        | Established regulated market trading but liquidity has been reduced considerably in recent years   |
| Availability of options to moderate demand | Medium        | Possible to shift more towards lithium iron phosphate (LFP) or lithium manganese iron phosphate (LMFP) at the expense of long-range electric vehicles  |
| Status of secondary supply                 | High          | Limited share of secondary supply as of today, but set to increase in future years   |
| <b>Exposure to ESG &amp; climate risk</b>  | <b>High</b>   |  |
| Environmental performance: mining          | High          | Weighted average score 35.5  |
| Environmental performance: refining        | High          | 603 g CO <sub>2</sub> /kWh, one of the highest   |
| Social and governance performance          | Medium        | Weighted average score 0.65  |
| Exposure to water stress                   | Low           | 12% of mine production located in high-risk areas  |
| Exposure to earthquake risks               | Low           | 19% of mine production located in high-risk areas (Weda Bay / South Sulawesi assessed as low risk)   |

## Cobalt: Assessment results

| Area                                       | Score         | Rationale  |
|--|---------------|--|
| <b>Supply risks</b>                        | <b>Medium</b> |  |
| Pace of demand growth                      | Low           | Projected demand growth rates are in line with historical growth rates   |
| Short-term market balances                 | Low           | Sufficient supply expected to serve short-term demand  |
| Long-term market balances                  | Medium        | Expected base case mine supply meets 70% of the primary supply requirements in 2040  |
| Observed price volatility                  | High          | Highly volatile price movements observed in the past decade  |
| Impact on clean energy cost                | Medium        | 2% of battery pack cost in 2023 with low cobalt prices, but the share was 5-6% in the past, which means cobalt would have modest impacts on battery cost and deployment  |
| <b>Geopolitical risks</b>                  | <b>High</b>   |  |
| Geographical concentration: mining         | High          | Expected top 3 share in 2030 is around 84% and top 1 share is around 66%   |
| Geographical concentration: refining       | High          | Expected top 3 share in 2030 is around 84% and top 1 country supplies three-quarters of global output  |
| N-1 supply and demand balances             | Medium        | N-1 supply serves 37% of N-1 requirements in 2030 in the APS   |
| Export risks of major suppliers            | Medium        | Risk score 3.3 (mining 2.4/refining 4.1)   |
| Hurdles for diversification                | High          | The low-price environment and relatively downbeat demand outlook present challenges in building diversified assets whereas projects continue to be developed in the Democratic Republic of the Congo, Indonesia and the People's Republic of China (hereafter "China") |
| <b>Barrier to respond to disruption</b>    | <b>Medium</b> |  |
| Visible stock levels                       | Medium        | Minimal amount of exchange stocks  |
| Transparency of pricing schemes            | Medium        | Early stage regulated market trading but liquidity is still lacking  |
| Availability of options to moderate demand | Low           | Ongoing efforts to reduce cobalt use in cathode chemistries (e.g. LFP, LMFP)   |
| Status of secondary supply                 | Medium        | Around 10% of secondary supply share, but set to improve in future years   |
| <b>Exposure to ESG &amp; climate risk</b>  | <b>High</b>   |  |
| Environmental performance: mining          | High          | Weighted average score 36  |
| Environmental performance: refining        | High          | 533 g CO <sub>2</sub> /kWh   |
| Social and governance performance          | Medium        | Weighted average score 0.47  |
| Exposure to water stress                   | Low           | 5% of mine production located in high-risk areas   |
| Exposure to earthquake risks               | Low           | 4% of mine production located in high-risk areas   |

## Graphite: Assessment results

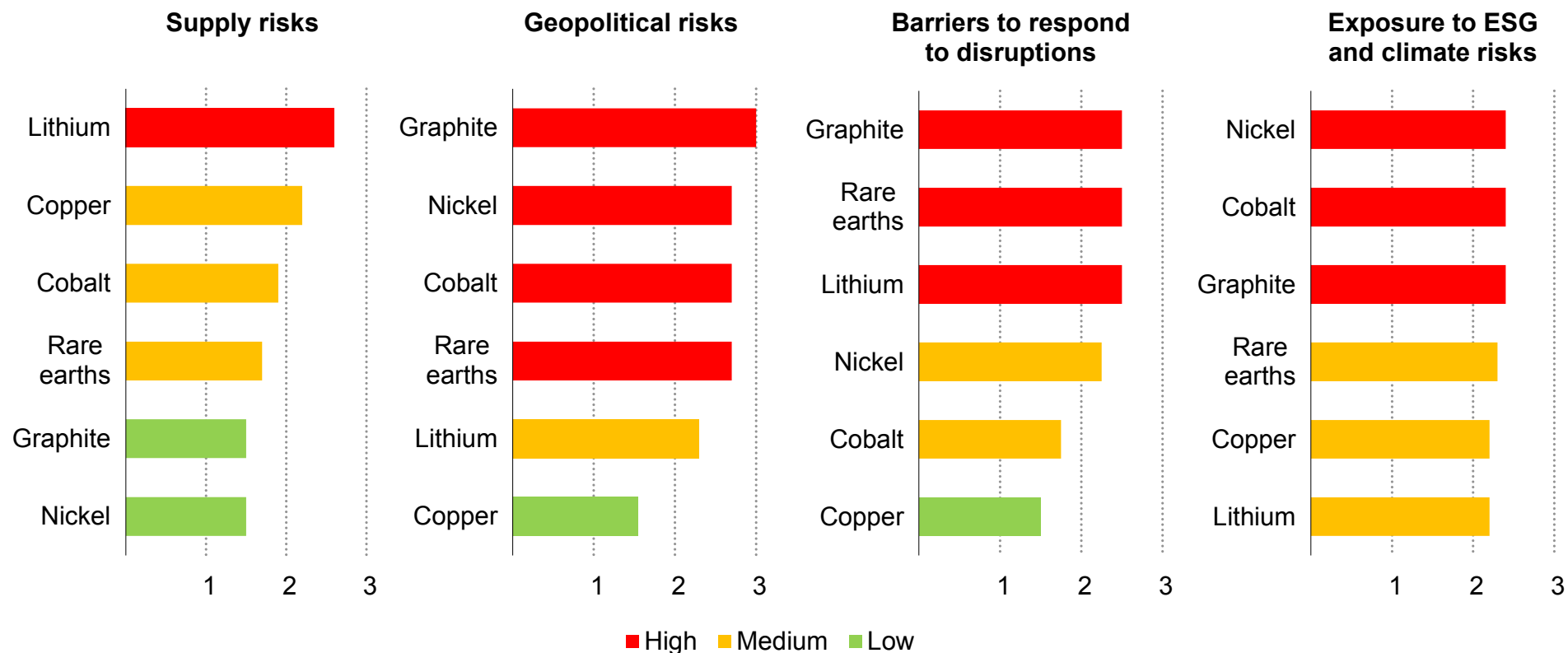
| Area                                       | Score       | Rationale  |
|--|-------------|--|
| <b>Supply risks</b>                        | <b>Low</b>  |  |
| Pace of demand growth                      | High        | Projected pace of future demand growth is significantly higher than the rate observed in the 2010s   |
| Short-term market balances                 | Low         | Sufficient supply expected to serve short-term demand  |
| Long-term market balances                  | Medium      | Expected base case mine supply meets two-thirds of the primary supply requirements in 2040, although synthetic graphite could fill the gap (at cost)                             |
| Observed price volatility                  | Low         | Historical price movement has been less volatile compared with other commodities   |
| Impact on clean energy cost                | Low         | Graphite is not a major part of total battery pack costs   |
| <b>Geopolitical risks</b>                  | <b>High</b> |  |
| Geographical concentration: mining         | High        | Expected top 3 share in 2030 is around 88% and top 1 share is around 69%   |
| Geographical concentration: refining       | High        | Battery-grade supply continues to be dominated by China, with 93% share (down from 100% today)   |
| N-1 supply and demand balances             | High        | Very limited supply potential to serve N-1 battery-grade graphite requirements in 2030   |
| Export risks of major suppliers            | High        | Risk score 4.4 (mining 4.5/refining 4.4)   |
| Hurdles for diversification                | High        | New projects are capital-intensive, requiring up to two times higher capital requirements than Chinese projects. New graphite project developers have limited financial capacity |
| <b>Barrier to respond to disruption</b>    | <b>High</b> |  |
| Visible stock levels                       | Medium      | Limited information about visible stock levels, but accumulated industry stocks are estimated to exist   |
| Transparency of pricing schemes            | High        | Price reporting driven through survey pricing and unregulated platforms with limited liquidity   |
| Availability of options to moderate demand | Medium      | Silicon could take growing shares in anodes, but unlikely to challenge graphite use in the near term   |
| Status of secondary supply                 | High        | Share of secondary supply remains low, with limited ability to scale up secondary supply quickly   |
| <b>Exposure to ESG &amp; climate risk</b>  | <b>High</b> |  |
| Environmental performance: mining          | Medium      | Weighted average score 41  |
| Environmental performance: refining        | High        | 577 g CO <sub>2</sub> /kWh   |
| Social and governance performance          | High        | Weighted average score 0.3   |
| Exposure to water stress                   | Medium      | Many natural graphite mines in Heilongjiang and Inner Mongolia, regions with medium water stress   |
| Exposure to earthquake risks               | Low         | Heilongjiang and Inner Mongolia are not exposed to major earthquake risks  |

## Rare earth elements: Assessment results

| Area                                       | Score         | Rationale  |
|--|---------------|--|
| <b>Supply risks</b>                        | <b>Medium</b> |  |
| Pace of demand growth                      | Low           | Expected demand growth rates are in line with historical growth rates  |
| Short-term market balances                 | Low           | Sufficient supply expected to serve short-term demand  |
| Long-term market balances                  | Medium        | Expected base case mine supply meets 70% of the primary supply requirements in 2040  |
| Observed price volatility                  | High          | Highly volatile price movements observed in recent years   |
| Impact on clean energy cost                | Low           | While crucial for performance, rare earth elements are not a major contributor to final clean energy cost  |
| <b>Geopolitical risks</b>                  | <b>High</b>   |  |
| Geographical concentration: mining         | High          | Expected top 3 share in 2030 is over 80% and top 1 share is around 55%   |
| Geographical concentration: refining       | High          | Expected magnet rare earth supply continues to be dominated by China, with 77% share   |
| N-1 supply and demand balances             | Low           | N-1 supply could serve N-1 requirements in 2030 in the APS   |
| Export risks of major suppliers            | High          | Risk score 4.5 (mining 4.1/refining 4.8)   |
| Hurdles for diversification                | High          | High entry barrier due to extensive resource endowment, accumulated technological know-how in the top producing country. Disadvantaged in terms of scale and costs (energy costs and cross-border trade taxes) |
| <b>Barrier to respond to disruption</b>    | <b>High</b>   |  |
| Visible stock levels                       | High          | Limited information about visible stock levels   |
| Transparency of pricing schemes            | High          | Price reporting driven through survey pricing and unregulated platforms with limited liquidity   |
| Availability of options to moderate demand | Medium        | Alternative new technologies have lower magnetic density and coercivity, and may struggle to compete commercially with the rare earth-based alternatives that produce the strongest known permanent magnets    |
| Status of secondary supply                 | Medium        | Share of secondary supply remains modest but hard to tap in times of price spikes  |
| <b>Exposure to ESG &amp; climate risk</b>  | <b>Medium</b> |  |
| Environmental performance: mining          | Medium        | Weighted average score 40.2  |
| Environmental performance: refining        | High          | 607 g CO <sub>2</sub> /kWh, one of the highest   |
| Social and governance performance          | Medium        | Weighted average score 0.34  |
| Exposure to water stress                   | Medium        | Infrastructure located in Australia and Inner Mongolia (China) are in regions at high risk of water stress   |
| Exposure to earthquake risks               | Medium        | Infrastructure located in Inner Mongolia (China), United States, India and Japan are in regions of medium to high risk of seismic activity   |

**Risk score by category:** Lithium and copper are more exposed to supply and volume risks whereas graphite, cobalt, rare earths and nickel face more substantial geopolitical risks

Risk score by category and mineral



IEA. CC BY 4.0.

Note: High = score above 2.33, Medium = score between 2.33 and 1.67, Low = score less than 1.67.

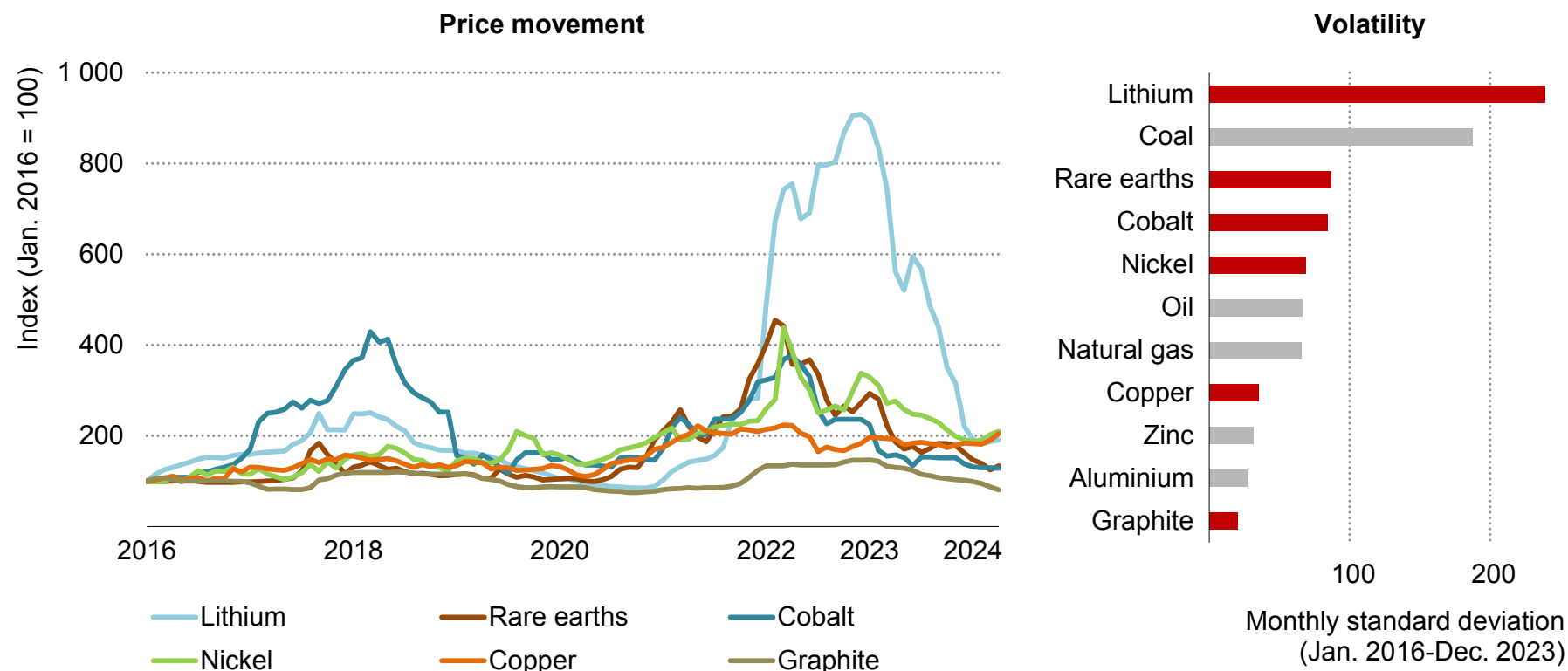
## Supply risks: Lithium and copper are most exposed to supply risks

Risk score for supply risks – aggregate and individual dimensions

| Material            | Overall score | Pace of demand growth | Short-term market balance | Long-term market balance | Observed price volatility | Impact on clean energy cost |
|---------------------|---------------|-----------------------|---------------------------|--------------------------|---------------------------|-----------------------------|
| Lithium             | High (2.6)    | High                  | Low                       | High                     | High                      | High                        |
| Copper              | Medium (2.2)  | Low                   | Medium                    | High                     | Low                       | High                        |
| Cobalt              | Medium (1.9)  | Low                   | Low                       | Medium                   | High                      | Medium                      |
| Rare earth elements | Medium (1.7)  | Low                   | Low                       | Medium                   | High                      | Low                         |
| Graphite            | Low (1.5)     | High                  | Low                       | Medium                   | Low                       | Low                         |
| Nickel              | Low (1.5)     | Low                   | Low                       | Medium                   | Low                       | Medium                      |

## Supply risks: Prices for critical minerals tend to be volatile, often more so than for fossil fuels and base metals

Price movement and volatility of selected commodities



IEA. CC BY 4.0.

Notes: Assessment based on the London Metal Exchange (LME) Lithium Carbonate Global Average, LME Nickel Cash, LME Cobalt Cash, LME Copper Grade A Cash prices, China flake graphite (-194 free on board) and neodymium oxide 99.5-99.9% Min China. Nominal prices.

Sources: IEA analysis based on S&P Global and Bloomberg.



## Geopolitical risks: Most minerals are highly exposed to geopolitical risks

Risk score for geopolitical risks – aggregate and individual dimensions

| Material            | Overall score | Geographical concentration of mining | Geographical concentration of refining | N-1 supply and demand balances | Export risks of major suppliers | Hurdles for diversification |
|---------------------|---------------|--------------------------------------|--|--------------------------------|---------------------------------|-----------------------------|
| Graphite            | High (3.0)    | High                                 | High                                   | High                           | High                            | High                        |
| Nickel              | High (2.7)    | High                                 | High                                   | Medium                         | Medium                          | High                        |
| Cobalt              | High (2.7)    | High                                 | High                                   | Medium                         | Medium                          | High                        |
| Rare earth elements | High (2.7)    | High                                 | High                                   | Low                            | High                            | High                        |
| Lithium             | Medium (2.3)  | Medium                               | High                                   | Medium                         | Medium                          | Medium                      |
| Copper              | Low (1.6)     | Low                                  | Low                                    | Low                            | Medium                          | High                        |

## Barriers to respond to disruptions: Graphite, rare earth elements and lithium have relatively little ability to respond to potential supply disruptions

Risk score for ability to respond to disruptions – aggregate and individual dimensions

| Material            | Overall score | Visible stock levels | Transparency of pricing schemes | Availability of options to moderate demand | Status of secondary supply |
|---------------------|---------------|----------------------|---------------------------------|--|----------------------------|
| Graphite            | High (2.5)    | Medium               | High                            | Medium                                     | High                       |
| Rare earth elements | High (2.5)    | High                 | High                            | Medium                                     | Medium                     |
| Lithium             | High (2.5)    | Medium               | Medium                          | High                                       | High                       |
| Nickel              | Medium (2.3)  | Medium               | Medium                          | Medium                                     | High                       |
| Cobalt              | Medium (1.8)  | Medium               | Medium                          | Low  | Medium                     |
| Copper              | Low (1.5)     | Medium               | Low                             | Medium                                     | Low                        |

IEA. CC BY 4.0.

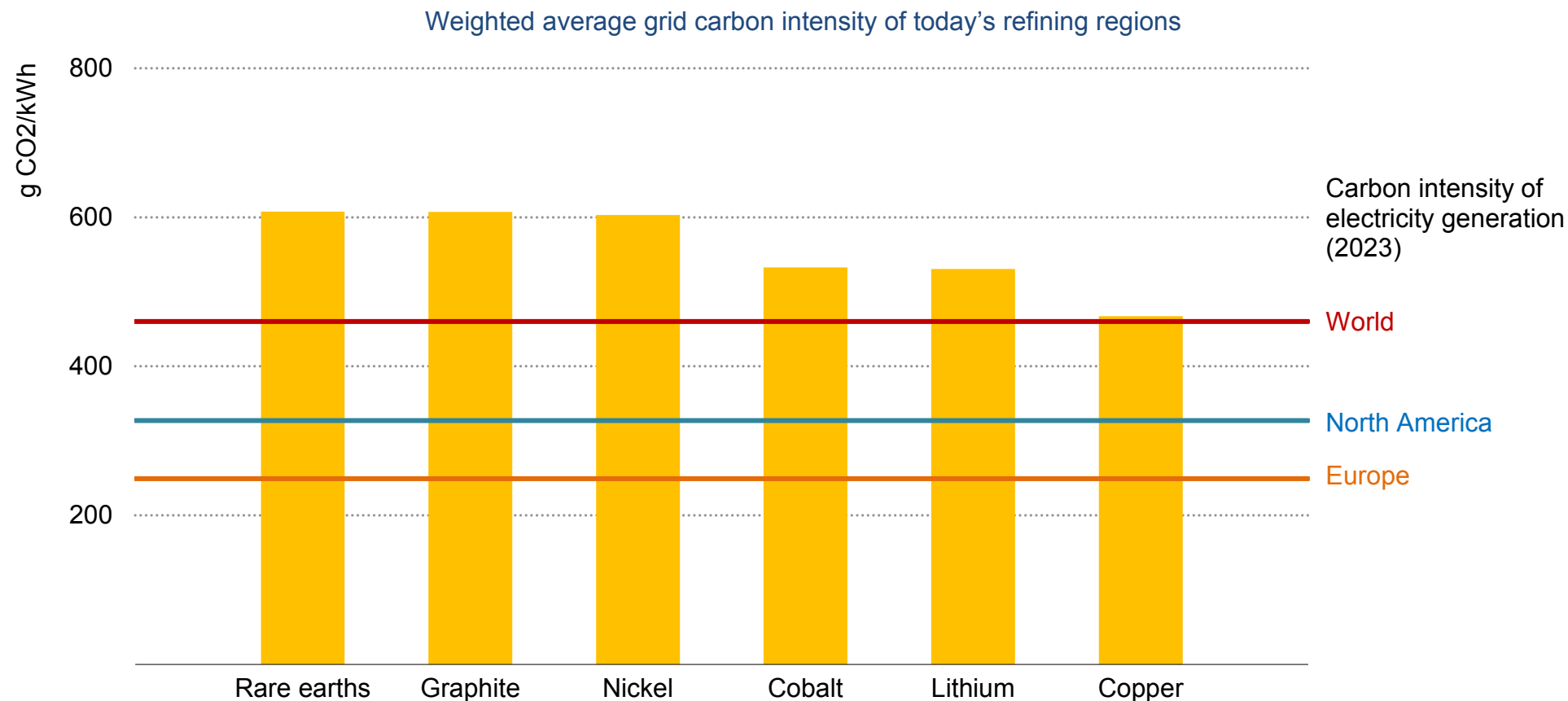
## Exposure to ESG and climate risks: Most minerals are exposed to high environmental risks

Risk score for exposure to ESG and climate risks – aggregate and individual dimensions

| Material            | Overall score | Environmental performance - Mining | Environmental performance - Refining | Social and governance performance | Exposure to water stress | Exposure to earthquake risks |
|---------------------|---------------|------------------------------------|--------------------------------------|-----------------------------------|--------------------------|------------------------------|
| Graphite            | High (2.4)    | Medium                             | High                                 | High                              | Medium                   | Low                          |
| Nickel              | High (2.4)    | High                               | High                                 | Medium                            | Low                      | Low                          |
| Cobalt              | High (2.4)    | High                               | High                                 | Medium                            | Low                      | Low                          |
| Rare earth elements | Medium (2.3)  | Medium                             | High                                 | Medium                            | Medium                   | Medium                       |
| Lithium             | Medium (2.2)  | Medium                             | High                                 | Low                               | High                     | Medium                       |
| Copper              | Medium (2.2)  | Medium                             | High                                 | Low                               | High                     | Medium                       |

IEA. CC BY 4.0.

## Exposure to ESG and climate risks: Today’s refining operations occur in places with higher carbon intensity of the grid, mostly in regions relying on coal-based electricity

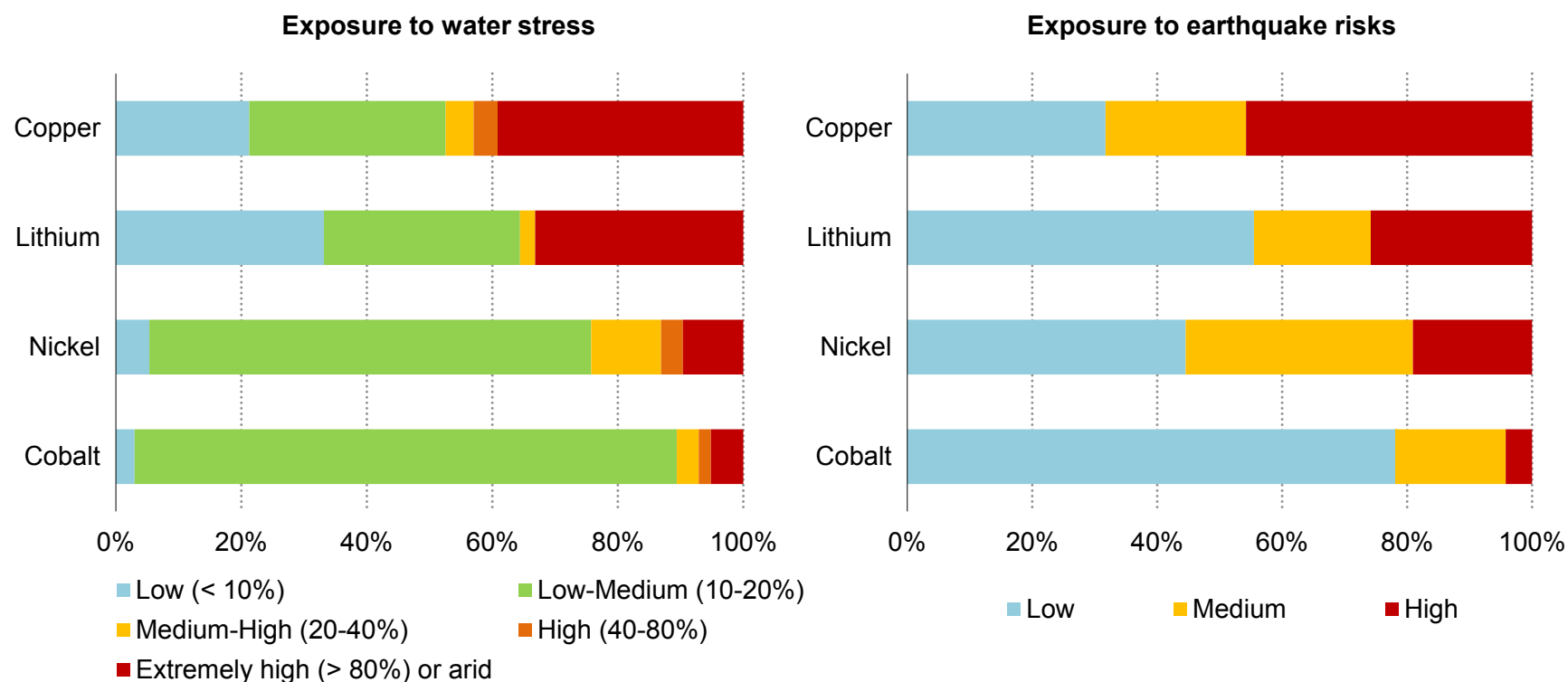


IEA. CC BY 4.0.

Notes: The carbon intensity for natural gas-based power generation is around 427 gCO<sub>2</sub>/kWh. For all minerals, the weighted average carbon intensity of the grid is higher than this, hinting that operations take place in regions relying on coal-based electricity. In some places (e.g. Indonesia), the rise of refining operations is being served mainly by off-grid, which runs entirely based on coal.

## Exposure to ESG and climate risks: Mining assets are exposed to growing water stress and earthquake risks

Share of production volume by water stress and earthquake risk levels for selected minerals, 2023

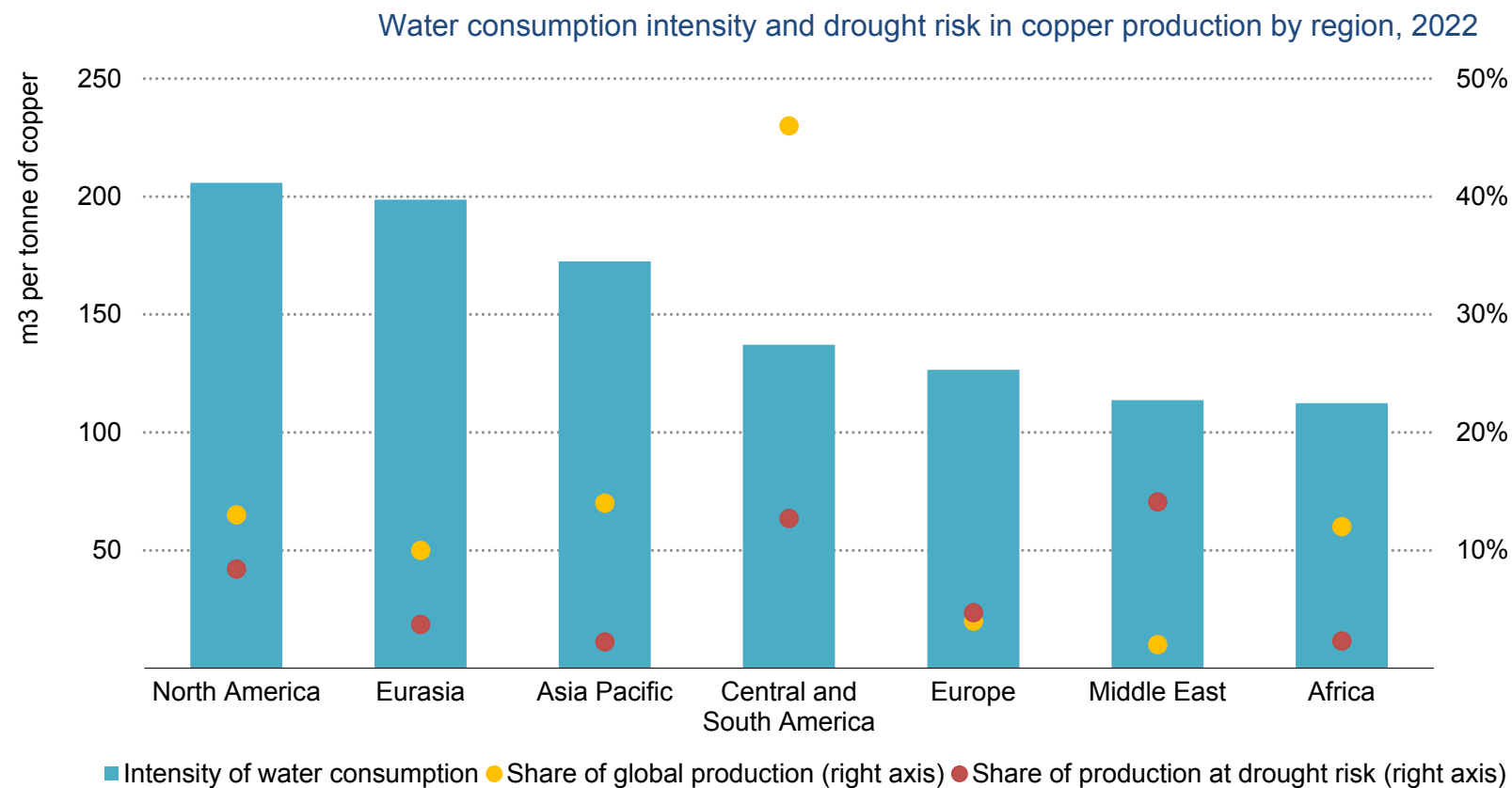


IEA. CC BY 4.0.

Note: Water stress levels are as defined in the [Aqueduct 3.0 dataset](#) according to the ratio of total water withdrawals over the total available surface and groundwater supplies. Earthquake risk levels are as defined in the [GEM Global Seismic Hazard Map \(v2023.1\)](#) based on peak ground acceleration (PGA) with a 10% probability of being exceeded in 50 years.

Sources: IEA analysis based on S&P Global, WRI (2019), [Aqueduct 3.0](#), and GEM (2023), [Global Seismic Hazard Map](#).

## Around 10% of global copper production faces supply risks related to droughts



IEA. CC BY 4.0.

Notes: Production at risk is the exposure percentage of the production at risk due to drought. It reflects the interaction of how water is used on site in the context of identified external climate risks, the operations water source matrix, its water efficiency and operational resilience. Drought risks are based on statistical analysis of monthly precipitation data and trends.

Source: Data provided by Skarn Associates.

---

## 4. Implications

---

## Four focus areas for policy makers, industry, and consumers to promote reliable and sustainable supplies of critical minerals

The picture that emerges from the analysis in previous chapters is a complex one. It shows some commonalities across the critical minerals examined, notably in the combination of rising demand and high concentrations among suppliers. However, it also highlights the specificities of the outlook in each case, with different sources of strain and opportunities for growth and for substitution.

This final chapter reflects on four broad themes that apply, to a greater or lesser extent, to all of the minerals examined. These areas constitute an agenda for future work by policy makers and industry as they seek to ensure reliable and sustainable supplies of critical minerals:

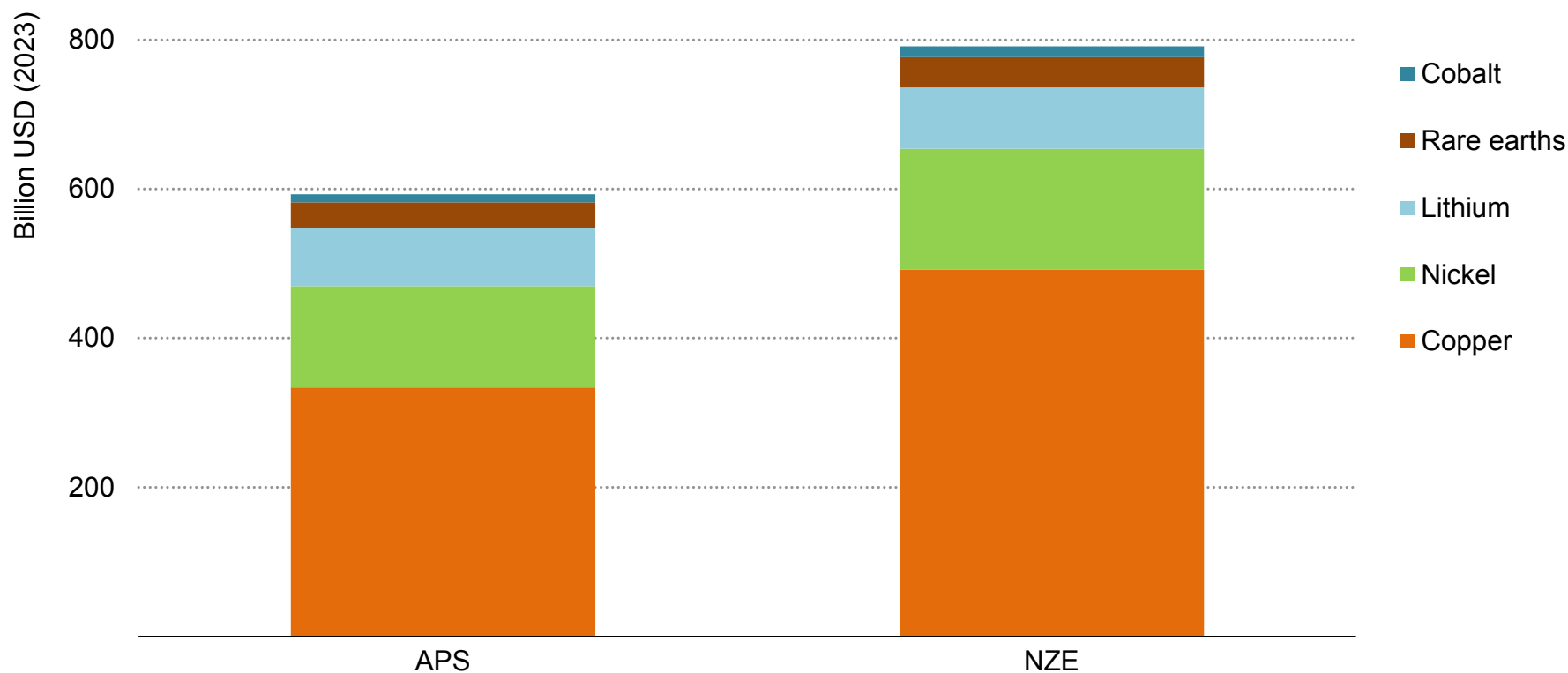
- **Investment in diversified supply.** Long-term security of supply is typically a question of adequate investment, but in the case of critical minerals it is not only the adequacy of supply that matters but also the diversity. It can be very challenging for new entrants to gain a foothold in markets with well-established incumbents. This section looks at the financing options open to governments that are seeking to encourage or de-risk investments in diversified sources of supply.
- **Recycling, innovation, and behavioural change.** Strategies for critical minerals security sometimes have an imbalanced focus on expanding supply, but measures to temper demand are essential. Recycling creates a valuable secondary source of minerals that relieves the pressure on primary supply; technology innovations have proven potential to ease strains on the supply side; and behavioural issues and consumer preferences can have strong implications for vehicle and battery sizes, and therefore on mineral requirements.
- **Market transparency.** Transparency of pricing and market information brings important benefits to all aspects of the supply chain, but for the moment these aspects remain weak for many critical minerals. This section considers options to improve the quality of information available to market participants, including moves towards market-based price discovery.
- **Sustainable and responsible supplies.** As production of critical minerals expands, it will be crucial to ensure that projects do not come at the expense of the people involved or result in local environmental damage. This section discusses how the benefits associated with mineral production, such as revenue and jobs, can be felt by producer countries and communities.



## Investment in diversified supply

## Major capital investment is required across all minerals to meet demand in climate-driven scenarios

Capital requirements for mining to meet 2040 demand in the APS and NZE Scenario



IEA. CC BY 4.0.

Notes: Capital requirements for the APS and NZE Scenario are calculated based on compiled capital intensity by region and production route. The values also assume an increased average capital intensity over today due to declining ore grades.

Source: IEA analysis based on data from S&P Global and company reports.

## The NZE Scenario requires around USD 800 billion of investment in mining between today and 2040

### Capital requirements to meet climate goals

Large amounts of investment will be required to develop new supply sources to meet the required demand for critical minerals in climate-driven scenarios. For mining, we estimate that approximately USD 590 billion is required in new capital investments between now and 2040 in the Announced Pledges Scenario (APS). As the Net Zero Emissions by 2050 (NZE) Scenario sees faster deployment of clean energy technologies, total capital requirements are about 30% higher at USD 790 billion over the same period (excluding sustaining capital expenditure).

The largest investment among the critical minerals is in copper. Capital requirements to 2040 for copper mining are USD 330 billion in the APS and USD 490 billion in the NZE Scenario. These amounts reflect not only the significant levels of demand, but also escalating capital requirements per tonne of ore caused by declining ore quality. Although all minerals face this challenge, it is more acute in mature and established markets such as copper. Nickel sees the second-largest levels of capital spending (USD 160 billion to 2040 in the NZE Scenario), followed by lithium (USD 80 billion). Lower but still significant amounts of investment are also needed for new refining and smelting facilities. Part of these increases in capital investment

need to be made in a way that fosters a more diversified array of supply sources in the future.

### Key financing challenges

Financing diversified critical mineral supply chains faces numerous challenges, primarily stemming from two underlying factors: high input costs and long-term price uncertainty.

Supply-side cost inflation, [driven by rising energy prices and declining resource quality over the past few years](#), have persisted even as commodity prices have dropped in recent years. Rising interest rates have further elevated capital costs for producers. As a result, margins have been reduced across the board, impacting operations at each stage of the value chain. During periods of weak prices, these factors led some producers across many commodities to reduce or defer spending on [mines](#) as well as [midstream assets](#).

Increasingly stringent environmental, social and governance (ESG) requirements have also influenced project costs in some advanced economies, making these assets less competitive compared with those in countries with lower regulatory standards.

Although the volatile, cyclical nature of commodity prices is well understood by market participants, the policy focus on ramping up

the supply of critical minerals for the energy transition has been challenged by record price volatility and persistent supply chain disruptions. Investors and producers have thus been reluctant to commit to large projects without sufficient confidence in the long-term business case for new and more diversified assets.

The lack of transparent pricing for many minerals contributes to this uncertainty. Although price discovery for metals such as nickel and copper takes place on liquid exchanges, pricing of lithium, cobalt and graphite, among other materials, still relies upon bilateral contracts that are surveyed and reported by price reporting agencies (PRAs) (see section on market transparency). Uncertainty over capital costs exacerbates the challenges facing project developers. For instance, in recent years, several lithium raw material development projects experienced a more than 50% increase in estimated capital intensity between pre-feasibility studies or preliminary economic assessments, and definitive feasibility studies.

Diversified refining and processing projects face additional challenges due to their limited pricing power, especially for non-integrated assets, relative to powerful incumbents. Positioned between the raw materials and the downstream value chain, projects are exposed to a cost and revenue squeeze and need to navigate the price volatility between raw material prices and downstream component prices. Price hedging has often proved challenging in relatively small and illiquid markets. Many projects being developed in geographically diverse regions have a higher-cost profile than

those in today's dominant regions: for example, several coated spherical graphite projects under development in advanced economies have more than twice the capital intensity of those in the People's Republic of China (hereafter "China"). Without specific government measures to reinforce the investment case, consumers and investors typically do not assign much value to diversification, so such projects often face major challenges in mobilising the necessary capital. Moreover, many companies that aim to develop new refining and processing projects in diversified regions are small in size with limited track records, making it challenging to mobilise debt financing at affordable rates.

### Government investment vehicles

Governments can intervene in various ways to help finance more diversified value chains. These interventions can come from four main sources: government departments and policy banks, sovereign wealth funds (SWF), development finance institutions (DFI), and export credit/insurance agencies (ECA). These agencies may engage [directly with private sector firms](#), through [state-owned or backed enterprises](#), in a [hybrid fashion](#), or [in partnership with foreign counterparts](#). They have a number of policy options available to them that range from direct debt or equity investments to indirect financial support and de-risking measures that boost competitiveness.

While there are often significant overlaps in the remits and capabilities of many of these institutions, they are differentiated in

their strategic focus, risk tolerance, and the time horizon of their investment decision-making, as outlined in the table at the end of this section. The support they provide can be either in the form of capital expenditure (capex) financing, operating expense (opex) support, and/or risk mitigation.

### Capex financing support

The vast majority of financial support mechanisms for the critical minerals sector have focused on large upfront capital expenditures. These include finance for the construction of mines, refineries and processing plants, and factories. These transactions, like those in the private sector, can contribute to various parts of the capital stack – as loans, equity stakes, or grants.

In the United States, the Department of Energy Loan Programs Office (LPO) has to date authorised more than USD 5 billion in conditional loan commitments for domestic minerals projects. Among these, the [USD 2.26 billion conditional loan](#) for Lithium Americas' Thacker Pass mine is the largest public commitment for a single project.

The French government, through the General Secretariat for Investment (SGPI), invested [EUR 500 million](#) as the anchor investor in a EUR 2 billion critical minerals fund managed by InfraVia, an infrastructure asset manager. In contrast to the approach taken by the US LPO and International Development Finance Corporation (DFC), which has invested directly in specific projects and companies, this investment relies on the external fund manager to

identify the opportunity set and capitalise on them in alignment with French government policy.

### Opex support

In addition to capex support, opex support measures are also adopted in ensuring the long-term bankability of projects given the decades-long investment horizons associated with planning, operating, and decommissioning. By lowering operating costs associated with mineral extraction and processing and helping stabilise long-term cash flows, higher-cost operations can improve economic competitiveness, thus helping the aim of diversification.

One of the most prominent policy initiatives for supply chain diversification is the [Inflation Reduction Act](#) (IRA) in the United States. The use of various tax credits on both the supply and demand sides have led to significant investment in the downstream domestic supply chain as well as the formation of agreements with free-trade agreement-compliant upstream suppliers. In addition to investment support through capital cost tax credits ([48C](#)), there are also production cost credits ([45X](#)) which provide 10% production tax credit for critical mineral processors. These forms of opex support can be effective in improving the business case to stimulate new investment, but require more policy commitment as they incur sustained financial burden over the long term.

Despite the attractiveness and importance of ongoing financial support mechanisms, their long-term nature also makes them more

sensitive to political headwinds. This is in contrast to direct capex financing mechanisms, where committed loans and disbursements cannot easily be clawed back after a change in administration.

### Risk mitigation and ancillary services

A third group of financial measures comprises options that are intended to de-risk investments and crowd in other investors, rather than directly subsidising or financing projects. Common strategies include offering loan guarantees to reduce the financial risk for private investors by providing a sovereign backstop, insuring transactions against counterparty risks that may not be available at a reasonable rate from commercial insurers, and directly lowering the cost of debt by bridging the gap between rates available to public institutions and the firm or project seeking funding.

These services are often offered by ECAs, which typically have expertise in risks associated with complex, multi-jurisdictional projects, in addition to or as an alternative to direct financing options.

For instance, the [Korean Export and Import Bank](#), as part of the government's five-year plan to support battery supply chains, has increased the maximum loan size from 40% of the owner's equity to 50%, in addition to a preferential rate up to 120 basis points (bps) lower. Furthermore, the Korea Trade Insurance Corporation has announced an insurance policy discount of up to 20% in addition to increases in loan guarantees available.

In 2022, Canada's Critical Minerals Strategy introduced the [30% Critical Mineral Exploration Tax Credit \(CMETC\)](#) aimed at helping companies raise equity capital by incentivising investors with tax benefits associated with flow-through shares. This functions by allowing investors to claim a tax deduction equivalent to a portion of exploration expenditures incurred by the company.

The CMETC acts in parallel with, but cannot be claimed in addition to, the existing Mineral Exploration Tax Credit (METC) of 15%. The METC, originally set to expire in March 2024, was [extended to March 2025](#). The Prospectors and Developers Association of Canada estimates that flow-through share financing [contributes over 65% of the funds raised on Canadian stock exchanges](#) for exploration across the country. These tax credits do not subsidise upstream companies directly, but serve to encourage equity investment during the high-risk exploration phase.

### Policy implications

Many of these policy intervention tools (outlined in the table at the end of this section) are intended to support national or regional strategies to decrease the geographic concentration of critical mineral supply chains. This can involve developments in either domestic projects or foreign projects with strategically aligned states.

Government departments and policy banks typically focus their spending on domestic projects and firms. For those without domestic reserves, DFIs and ECAs are the preferred vehicle given their

specific mandate for foreign transactions. SWFs and policy banks with broad investment mandates are not common in advanced economies seeking to diversify their critical minerals supply chains, but there are examples elsewhere. For example, the [Saudi Public Investment Fund](#), which has a wide-ranging mandate to actively invest over the long term to maximise sustainable returns, has taken an active position in global critical mineral supply chains as a financier of domestic and foreign projects.

Financial support from public agencies and institutions not only directly supports investments in projects, but may also serve three important but indirect functions: intergovernmental policy signalling to mitigate potential geopolitical risks, crowding in private capital, and freeing up funds for redeployment.

Given the financial challenges associated with supply chain diversification, there are several aspects to consider when countries introduce policy intervention tools to support financing. First, cross-agency coordination. The multiple risks associated with mineral value chains – geopolitical, financial, environmental, etc. – mean that

the expertise of various departments and agencies is required to ensure that investments meet domestic and international guidelines. Furthermore, investment mandates of agencies such as government policy banks and DFIs often overlap but without a [specific mandate to focus on mineral security](#). Coordination and information sharing between agencies can contribute to strategic alignment, ensuring efficient allocation of resources.

Second, tailored, fit-for-purpose investments. Given the numerous policy options available, investments in critical mineral supply chains should be tailored to meet specific strategic objectives, such as reducing import dependency, improving environmental sustainability, and ensuring the economic viability of domestic resources. A wide range of investment structures should be evaluated for their ability to address the unique risks at each stage of the supply chain.

Finally, financial incentives should aim to be synergistic across the whole value chain, rather than focusing narrowly on one sector. In particular, midstream processing of mined material into intermediate products is often lacking the support seen for end-use sectors.

## While different public agencies and vehicles have distinct strengths and remits, political co-ordination is important in ensuring synergistic efforts

Public institutions and vehicles that play a role in financially supporting critical minerals value chains

|                          | Ministries and programmes  | Sovereign wealth funds  | Development finance institutions   | Export credit and insurance agencies   |
|--------------------------|--|---|--|--|
| Description              | Government departments that develop, implement, and finance policies   | State-owned investment funds designed to manage and invest national wealth  | Organisations that provide financial support and expertise to development projects, often focused on EMDE  | Financial institutions that support national exports and facilitate international trade and investment   |
| Relative risk tolerance  | <b>Low-medium:</b> political questions on public finances lead to greater scrutiny   | <b>Medium-high:</b> asset allocation strategies consider potential for higher returns   | <b>Medium:</b> EMDE investments are associated with higher expected loss rates   | <b>Low:</b> safeguarding domestic export industries is the priority, not returns   |
| Key use case             | <b>Policy alignment and direct financial support:</b> aligning industrial policies with national strategies via broad-based domestic investment, including in non-industry sectors | <b>Long-term investment in strategic assets:</b> investing in domestic and international projects across the value chain as part of a diversified asset portfolio | <b>Achieving co-benefits in the minerals sector:</b> advancing more socially and environmentally responsible supply chains that also contribute to policy priorities | <b>Export facilitation and trade financing:</b> assisting domestic companies in competing internationally, securing supply chains, and accessing new markets |
| Examples of institutions | <a href="#">DOE LPO</a> (US)   | <a href="#">Public Investment Fund</a> (Saudi Arabia), <a href="#">Minerals Income Investment Fund</a> (Ghana)  | <a href="#">KfW</a> (Germany), <a href="#">US DFC</a> , <a href="#">IFC</a>  | <a href="#">Export Finance Australia</a> (Australia), <a href="#">K-Sure</a> (Korea)   |

Note: EMDE = emerging market and developing economies; DOE = Department of Energy; IFC = International Finance Corporation.



## A range of policy options can be deployed to address various financing challenges associated with each segment of the value chain

Financial policy options available for promoting investment in critical mineral supply chains

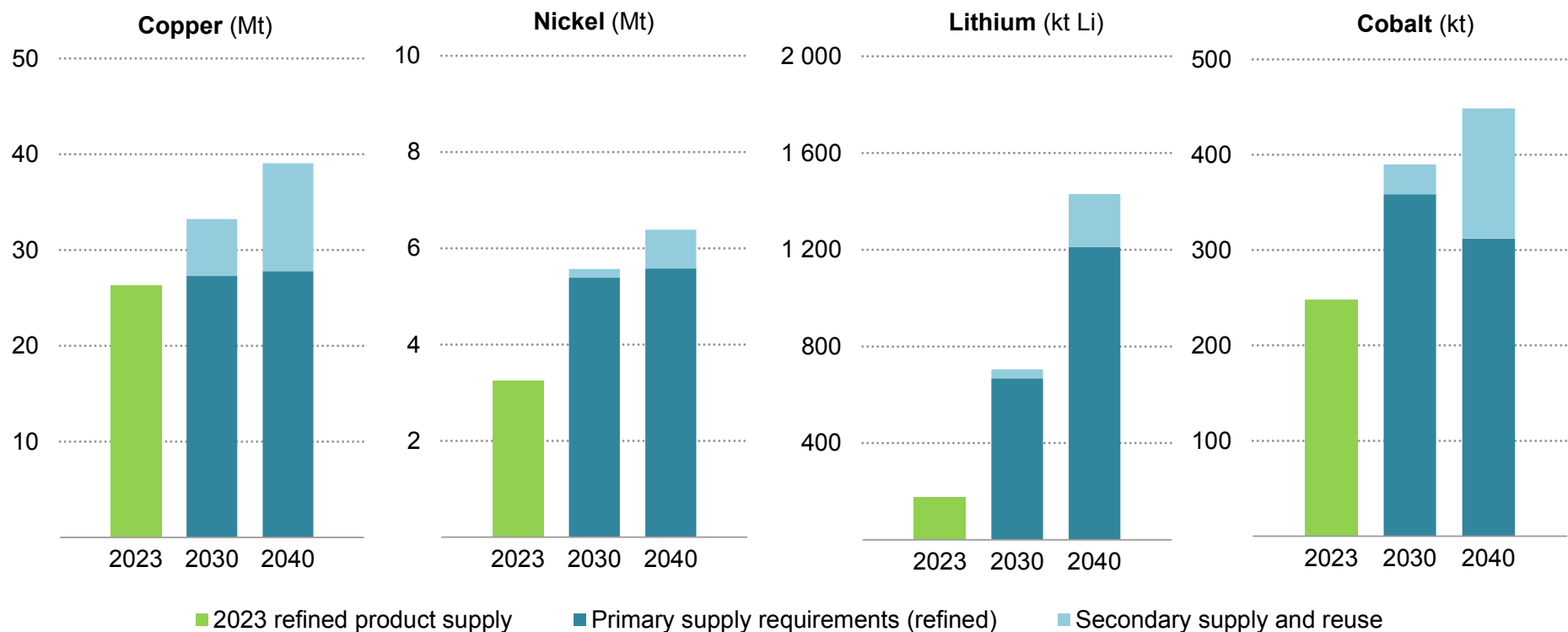
|                 |   | Policy option                  | Description  | Typical size (USD million) | Examples   |
|-----------------|---|--------------------------------|--|----------------------------|--|
| Capex financing | 1 | <b>Grants</b>                  | Non-repayable awards, usually to support capital projects                    | 1-100                      | Australia: <a href="#">International Partnerships in Critical Minerals Grants</a> (AUD 40 million)<br>US: DoD grants to Albermarle for <a href="#">lithium production</a> (USD 90 million) and <a href="#">processing plants</a> (USD 150 million) |
|                 | 2 | <b>Concessional loans</b>      | Loans with favourable rates and/or repayment terms                           | 100-1 000                  | US: <a href="#">DOE LPO loan to Lithium Americas</a> (USD 2.26 billion)  |
|                 | 3 | <b>Equity investments</b>      | Taking stakes in key minerals projects with risk-sharing                     | 10-100                     | France: <a href="#">SGPI investment in equity fund</a> (EUR 500 million)<br>US: <a href="#">DFC stake in TechMet</a> (USD 75 million)<br>Germany: <a href="#">KfW raw materials fund</a> (EUR 1 billion)   |
| Opex support    | 4 | <b>Tax credits</b>             | Reductions in tax liability in exchange for investment or production targets | N/A                        | US: <a href="#">Inflation Reduction Act 45X</a> (10% of production cost)   |
|                 | 5 | <b>Reduced royalties</b>       | Increasing the operating income margin of the asset                          |                            | Australia: <a href="#">Western Australia nickel royalty assistance programme</a> (50% rebate for 18 months)  |
| Risk mitigation | 6 | <b>Loan guarantees</b>         | Sovereign guarantees on private loans to reduce lender risk                  | 10-100                     | Canada: <a href="#">Indigenous loan guarantee programme</a> (CAD 5 billion)  |
|                 | 7 | <b>Insurance products</b>      | Protection against risks that may not be covered by commercial insurers      | 10-100                     | Japan: <a href="#">Loan insurance for procurement and equity investment</a>  |
|                 | 8 | <b>Interest rate reduction</b> | Directly lowering the cost of debt for borrowers                             | N/A                        | Korea: <a href="#">KEXIM to lower rates for strategic industries, including batteries, by up to 120 bps</a>  |

Note: AUD = Australian dollars; DoD = Department of Defense; KEXIM = Korea Export-Import Bank.

## Recycling, innovation, and behavioural change

## Recycled volumes from manufacturing scrap and end-of-life equipment contribute to reducing the requirements for primary supply

Primary supply requirements and projected secondary supply for selected minerals in the NZE Scenario

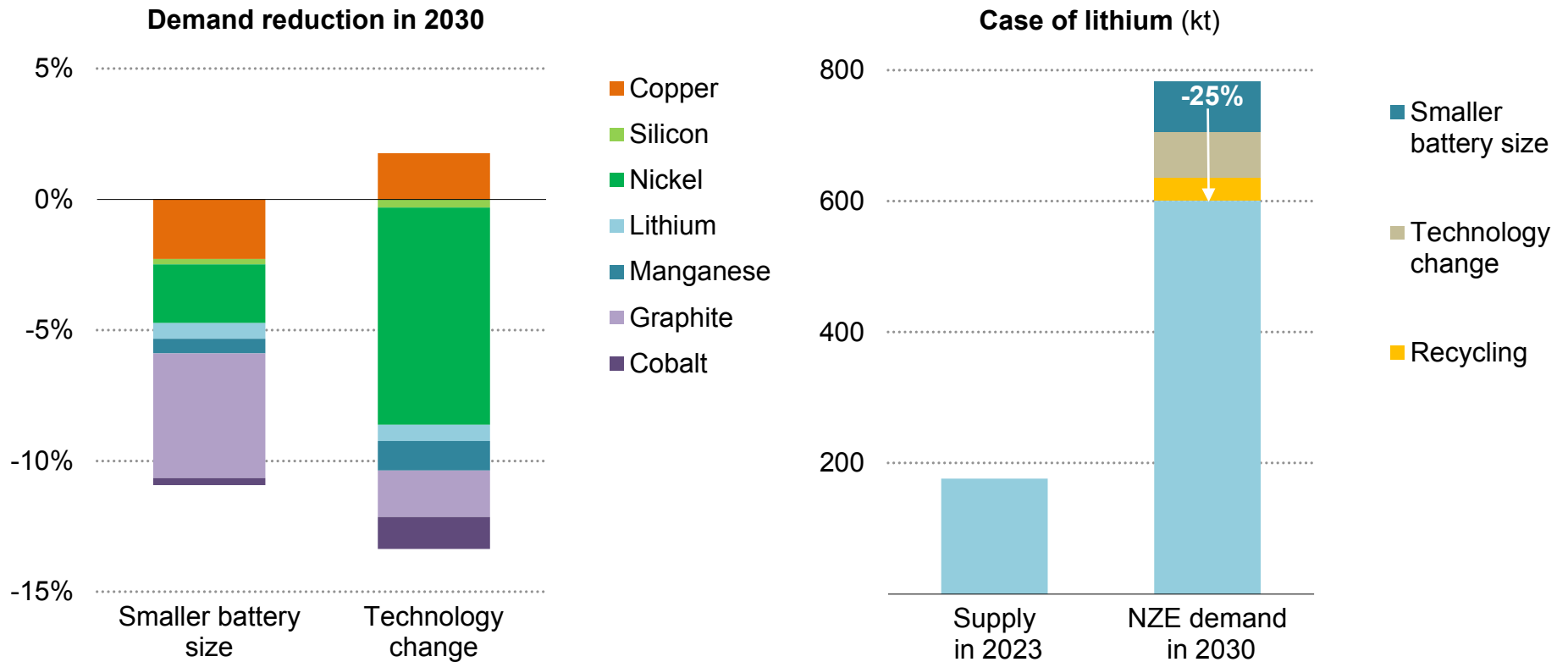


IEA. CC BY 4.0.

Note: Secondary supply of copper does not include direct use of scrap.

## Technology innovation and demand-side measures can play significant roles in reducing mineral demand

Mineral demand reduction potential for electric vehicle batteries and battery storage, 2030



IEA. CC BY 4.0.

Note: Technology change assumes a higher share of lithium-ion phosphate chemistries and sodium-ion batteries.

## Scaling up recycling, continued investment in technology innovation, and promoting consumer behavioural changes play a crucial role in ensuring the security of mineral supplies

Every country's strategy on critical minerals will inevitably reflect its specific circumstances, but it would be a mistake for such strategies to focus only on increased exploration, mining and refining investment. A comprehensive approach to security and sustainability of supply needs to also address the demand side of the equation, which plays a crucial role in narrowing supply-demand gaps while simultaneously mitigating the potential environmental and social harms associated with resource extraction and use. This encompasses elements such as innovation, recycling, behavioural measures and rigorous sustainability standards. The importance of unlocking the power of technology and recycling has long been a theme of IEA analysis and this was one of the key takeaways from the first-ever [IEA Critical Minerals and Clean Energy Summit in September 2023](#)<sup>1</sup>.

### Recycling

Recycling creates a secondary supply of minerals that relieves the pressure on primary supply from mining and refining. A strong focus on recycling can deliver triple benefits: complementing primary

mineral supplies, improving security of supply for regions with limited resource endowments and enhancing environmental performance and waste management.

For base metals such as aluminium, recycling practices are well established, but this is not yet the case for many energy transition minerals such as lithium, nickel (from electric vehicle [EV] and storage batteries) and rare earth elements (from wind turbines and EV motors). For battery metals, today's feedstock for recycling is dominated by electronic waste and scrap from manufacturing processes, but this is set to change by the end of the decade as the first generation of electric vehicles reach the end of their life. Globally, around 30 GWh of spent electric car batteries is expected to be available for recycling by the end of the decade.

While recycling would not eliminate the need for continued investment in new supplies, we estimate that by 2040, recycled quantities of copper, lithium, nickel and cobalt from clean energy applications could reduce primary supply requirements for key minerals by 10-30%. The security benefits of recycling can be far

<sup>1</sup> The IEA will delve deeper into the topic of recycling – covering various topics such as battery recycling, industrial scrap and mine waste – in a forthcoming report for the Italian G7 presidency.

greater for regions with wider deployment of clean energy technologies due to greater economies of scale. A strong example of the environmental benefits comes from the aluminium industry, where recycling of post-consumer scrap has been [shown to reduce emissions by 90% compared with primary aluminium](#). Furthermore, recent studies show that total GHG emissions for manufacturing a nickel-rich lithium-ion battery cell can be around [28% lower if made from recycled materials rather than virgin minerals](#).

Recovering minerals from mine waste, also known as tailings reprocessing, is a growing area of interest. As ore grades decline, larger amounts of wastes are generated during mining, increasing the economic and environmental cost of tailings management. [Advancements in processing technologies mean that some tailings have grades comparable to currently economical ore deposits](#). Thus, reprocessing can have various benefits: revenue opportunities, water recovery and environmental impact mitigation.

## Technology and innovation

Technology advances also have a major role in alleviating potential supply strains. For example, significant reductions in the use of silver and silicon in solar cells over the past decade have contributed to a spectacular rise in deployment of solar PV. For grids, our projections indicate that deploying high-voltage direct current transmission lines more widely in electricity networks has the potential to shrink their material demand by 3% in 2030 and 10% in 2050. Similarly, a

sensitivity case covering an accelerated global adoption of lithium-iron phosphate chemistries and sodium-ion batteries could reduce mineral demand for EV batteries by around 13% in 2030 and 18% in 2050 compared to the NZE Scenario's base case.

## Behavioural changes

Energy demand depends on the behavioural choices of millions of consumers worldwide. [Behavioural changes are actions that energy consumers take to reduce wasteful or unnecessary energy consumption](#). Many of these changes take place as part of daily life, and involve using energy differently or using less of it. These changes depend in part on individual choices and evolving socio-cultural norms. However, it is systemic transformations brought about by targeted and well-designed policy interventions that count most in changing consumer behaviour, and these often depend on the availability of infrastructure of one kind or another.

Behavioural changes in the NZE Scenario help to bring about a more equitable and just energy transition. But in terms of critical minerals, behavioural changes can also imply a more tempered demand that can help narrow the demand-supply gap, especially changes in behaviour related to transport needs.

In 2022, electric SUVs accounted for over half of global electric car sales for the [first time ever and took up 16% of total SUV sales](#). Such a consumer preference is contributing to a further increase in mineral demand as SUVs require larger batteries to power them. Behavioural

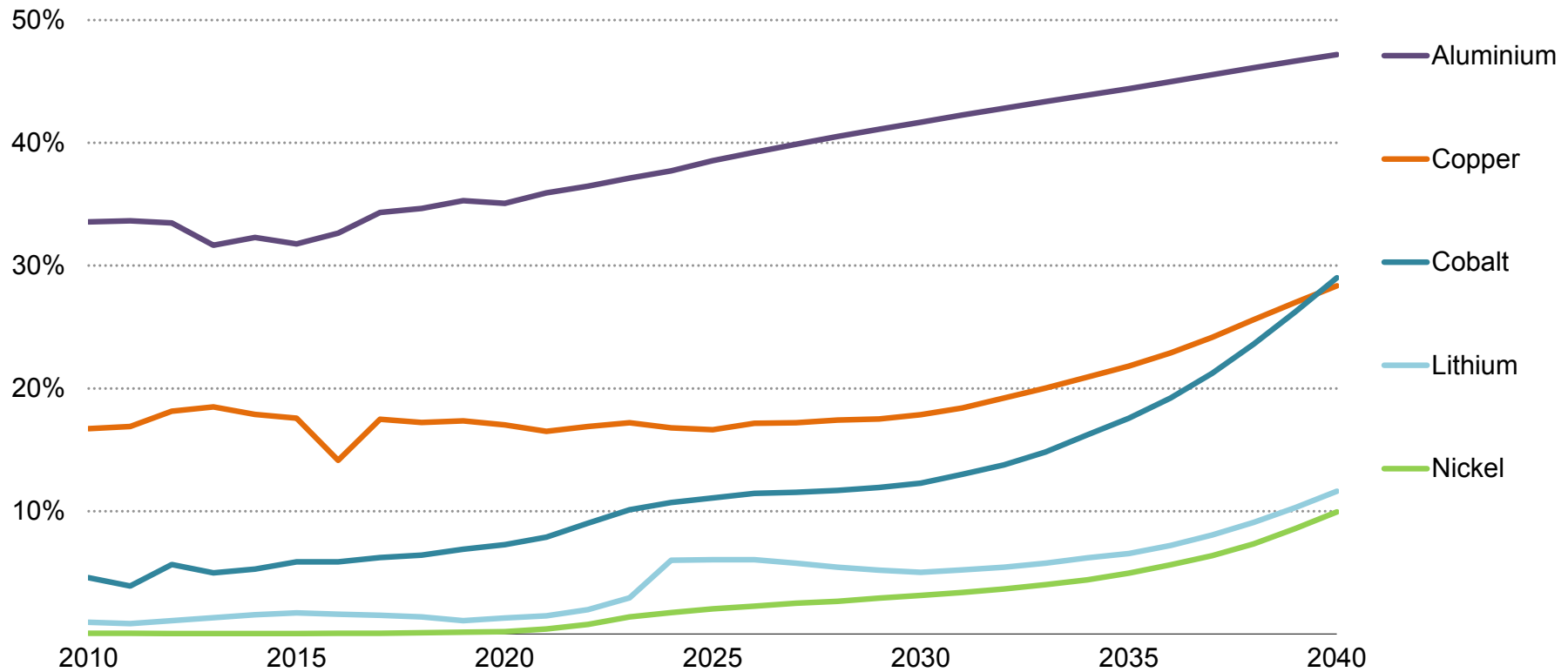
changes and targeted measures to tame the appetite for SUVs and other large vehicles could result in considerable demand reduction for battery metals. IEA projections based on these specific sensitivity cases show that measures to promote smaller electric cars lead to a more than 10% reduction in battery mineral demand by 2030 projected in the NZE Scenario, compared with a counterfactual case where SUV demand continues to grow. In February 2024, the city of Paris took measures to moderate the average size of cars on the roads by [voting for elevated parking tariffs for larger private vehicles](#). Other behavioural measures that can reduce car traffic and thereby, not just gasoline demand from internal combustion engine vehicles but also demand for battery metals for EVs, include increased share

of carpooling, active modes of transportation and public transit in total road passenger transport.

[The IEA recently showed](#) that, in the case of lithium, the combination of smaller EV battery sizes, alternative chemistries and recycling could reduce demand for lithium by 25% in 2030 in the NZE Scenario, saving an amount similar to today's production volumes. With these reductions, new supplies would need to grow by 20% per year between today and 2030. The lithium industry managed to deliver this scale of growth in recent years. For example, lithium raw material supply grew by roughly 20% per year over the past five years.

## Recycling rates for many materials have exhibited limited growth in the past, but growing policy attention and the rise of battery recycling are set to change the picture

Share of secondary supply in total demand for selected materials in the NZE Scenario



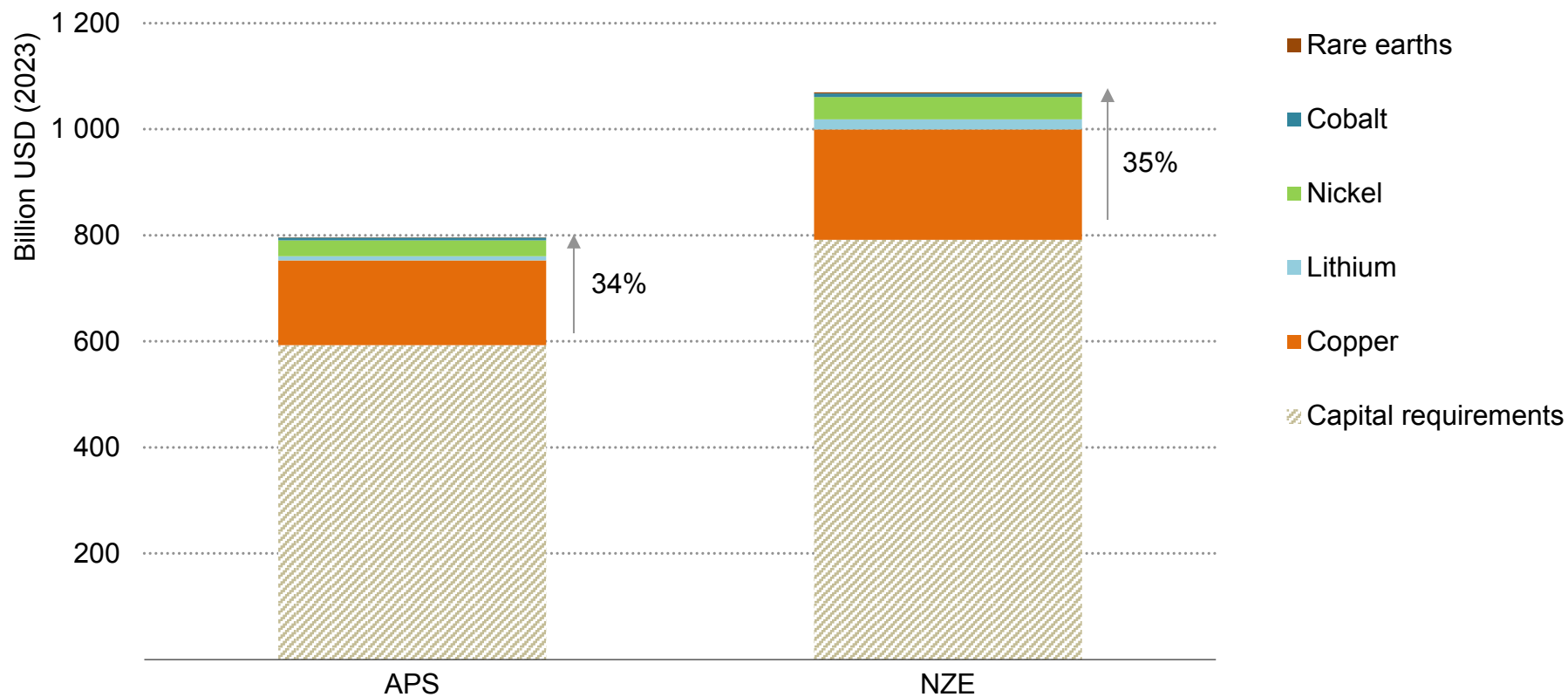
IEA. CC BY 4.0.

Note: Secondary supply of copper excludes direct use of scrap.



## Without the uptake of recycling and reuse, mining capital requirements to meet demand would have been a third higher

Reduced mining capital requirements due to higher recycling and reuse in the APS and NZE Scenario



IEA. CC BY 4.0.

## Much stronger efforts are needed to scale up recycling and ease the strains on mineral supply in a net zero pathway

Global battery recycling capacity surpassed [300 GWh in 2023, of which more than 80% was located in China](#), far ahead of Europe and the United States with under 2% each. Many technology developers and industry actors are seeking to position themselves in the future market for end-of-life EV management and have announced considerable capacity expansions. If all announced projects are developed in full and on time, global battery recycling capacity could exceed 1 500 GWh in 2030, of which 70% is in China, and about 10% each in Europe and the United States. The main sources of supply for battery recycling plants in 2030 will be [EV battery production scrap](#), accounting for half of supply, and retired EV batteries, accounting for about 20%. From 2030, end-of-life batteries surpass manufacturing scrap as the primary source of recycling.

Policy measures, including standardisation and alignment of battery waste and transportation codes (e.g. for black mass handling and cross-border transport to high-quality recyclers), the implementation of extended producer responsibility principles for EV batteries, the development of comprehensive collection infrastructure, and the initiation of information and communication campaigns, all play pivotal roles in encouraging the uptake of battery recycling.

Despite the undeniably significant role of batteries in total mineral demand, as the clean energy transition ramps up in almost every

major region, recycling efforts will need to extend to technologies beyond batteries as well. In addition to scaling up recycling infrastructure, efforts also need to be directed towards the maintenance and repair of products that will enable longer use.

The share of secondary supply in mineral demand has remained fairly stable for the last decade, but this changes rapidly in the NZE Scenario. The share of secondary supply for nickel needs to grow from around 1% today to 3% in 2030, and that of lithium from 3% to 5% in the same period. By 2040, secondary supply share of most major critical minerals would need to reach at least 15% under the NZE Scenario.

If the share of secondary supply were to stay at today's levels, capital requirements for mining to meet demand in climate-driven scenarios would have been a third higher, highlighting the significance of recycling in alleviating pressure on primary supply.

## Policies and actions to mitigate increases in demand for critical minerals

| Policy area                                      | Description   | Examples  |
|--|---|---|
| <b>Repair, refurbishment and remanufacturing</b> | Extending product lifetimes, reducing the need for new production                                   | <ul style="list-style-type: none"> <li>Siemens Gamesa's lifetime extension programme for wind turbines</li> </ul>   |
| <b>Recycling</b>                                 | Collecting, processing, and reusing materials that would otherwise be discarded as waste            | <ul style="list-style-type: none"> <li>Minimum recycled content requirements, extended producer responsibility regulations</li> </ul>                                       |
| <b>Substitution</b>                              | Replacing materials with renewable or more sustainable alternatives                                 | <ul style="list-style-type: none"> <li>Chemistry change for EV batteries</li> <li>Adoption of alternative battery technologies</li> </ul>                                   |
| <b>Material efficiency</b>                       | Designing products and processes to minimise material use, waste, and environmental impact          | <ul style="list-style-type: none"> <li>Iridium loading reduction in proton exchange membrane electrolyser manufacturing</li> <li>Reduced silicon use in solar PV</li> </ul> |
| <b>Product-as-a-Service</b>                      | Business models that provide services instead of selling products                                   | <ul style="list-style-type: none"> <li>Vehicle-sharing schemes to increase utilisation of assets</li> </ul>   |
| <b>Behavioural changes</b>                       | Encouraging individuals to adopt more sustainable habits and practices such as reducing consumption | <ul style="list-style-type: none"> <li>Opting for optimal size vehicles than larger cars</li> <li>Reducing private car journeys via public transport</li> </ul>             |

## Market transparency

## Market transparency brings important benefits to all aspects of the supply chain

Despite strong expected increases in demand, market transparency of commodities such as cobalt, lithium, and rare earth elements remains limited, challenging price-hedging and discouraging investment and risk assessments. Market transparency covers both the question of **pricing** – including efficient market price discovery mechanisms and financial tools to hedge price risks – and **information** – the importance of publicly available data on consumption, supply, inventories, trade and ESG performance.

Transparency of pricing and market information brings important benefits to all aspects of the supply chain: producers and consumers are able to hedge their price risk, plan their stocks and production, and negotiate fair contracts. Merchants and intermediaries are able to correct global supply and demand imbalances as efficiently as possible. Governments benefit by being able to plan ahead and ensure supply continuity. Information transparency enables the anticipation of potential risk areas, allowing policymakers to target support where it is most needed.

### Price transparency: Tailoring actions to each critical mineral's market maturity level

The primary element of a well-functioning market for minerals and metals is transparency of pricing. Efficient price discovery processes provide two main benefits to the market: first, they offer clearer

market signals, aiding informed investment decisions; second, they facilitate the development of financial tools to mitigate risks, allowing for hedging by midstream operators (refining, recycling) and downstream consumers.

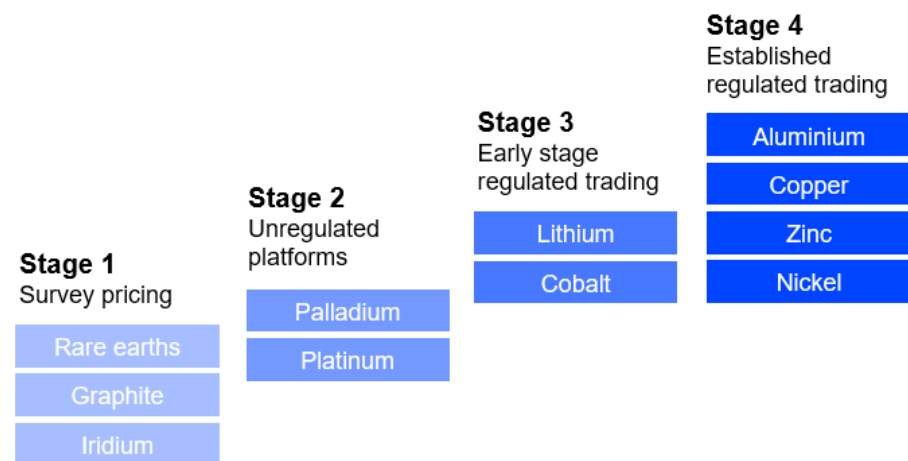
In a developed, sophisticated market, this means that there is a clear “spot” price (i.e. for immediate delivery), as well as a futures price curve – i.e. information about prices for delivery months or years into the future. While some commodities such as copper and aluminium already benefit from established and regulated exchanges with ample liquidity, not all critical minerals benefit from such levels of market maturity. Many of their markets contend with market concentration, insufficient liquidity, and reliance on bilateral contracts.

There are broadly four stages of development in price transparency. Some commodities, such as copper and nickel, are already traded on regulated exchanges, where both spot and future contracts can be publicly traded – but derivatives can also often be traded outside of these exchanges, as over-the-counter (OTC) forward contracts, where prices are less easily tracked (see figure below – “Stage 4. Established and regulated trading”). For others, such as lithium and cobalt, there are signs of growing trade activities at major exchanges, while remaining significantly less liquid (“Stage 3. Early-stage regulated trading”). Although traded derivatives markets are important in assessing market participants’ expectations, OTC

financial contracts are of particular utility in risk management, as they allow more effective price hedging.

For the less liquid markets, market players rely on unregulated spot auction platforms (“Stage 2”) or surveys from price reporting agencies (PRAs) (“Stage 1”) or other key market actors, who may – or may not – meet the principles set out by the International Organization of Securities Commissions (IOSCO). The different stages of market maturity discussed here are indicative, and each element may face different circumstances.

#### Market maturity levels for selected minerals



IEA. CC BY 4.0.

Price data are often much more limited for midstream processing than refined material. While for some commodities, such as copper, “treatment and refining charges” (the amount mines need to pay to smelt concentrate into cathodes) are tracked by agencies, data are less available for other commodities. The absence of data on refining costs and prices, as well as existing capacities and stockpiles, restricts further investments in midstream capacities, and thus their diversification.

Some of the smaller commodities may have structurally insufficient liquidity pools for market-based price discovery mechanisms. In these cases, policymakers could consider various ways to incentivise or encourage contributions by market participants to PRAs’ platforms who adhere to the IOSCO principles or their equivalents, or to enhance data collection from businesses. Regulated markets also require deep liquidity pools for effective price discovery. In this context, governments could avoid actions that would further fragment liquidity pools. For cobalt and lithium in particular, there is a question as to whether physically-deliverable contracts could be possible. This would have the advantage of providing stocks data to the market, which gives some proxy data to the market as to supply and demand.

Finally, there is a growing interest in pricing schemes that incorporate ESG performance. While many PRAs are introducing new price indices, it is uncertain whether these indices would achieve sufficient liquidity without policy and regulatory support to encourage consumers to consider sustainability aspects in their procurement decisions.

## Classification of commodity markets by maturity level

|                                  | Stage 1                         | Stage 2   | Stage 3                              | Stage 4                                  |
|----------------------------------|---------------------------------|---|--------------------------------------|--|
|                                  | <b>Survey pricing</b>           | <b>Unregulated platforms</b>                      | <b>Early stage regulated trading</b> | <b>Established and regulated trading</b> |
| <b>Price discovery mechanism</b> | PRAs and market participants    | PRAs and trading platform                         | Exchange                             | Exchange                                 |
| <b>Reporting frequency</b>       | Monthly                         | Weekly-daily                                      | Instant                              | Instant                                  |
| <b>Risk management tools</b>     | Limited to bilateral agreements | Futures and options with financial intermediaries | Traded futures and options           | Active derivative markets                |
| <b>Examples</b>                  | Rare earth elements, graphite   | Platinum, palladium                               | Lithium, cobalt                      | Aluminium, copper, zinc, nickel          |

## Market information transparency

Understanding critical mineral production and refining also relies both on public data and on mining and supply chain actors, with multiple benefits: allowing more informed investment decisions, facilitating supply risk identification along the supply chain, enabling systematic tracking of ESG performance, informing due diligence efforts, facilitating audit and verification of claims and ensuring better accountability.

However, information transparency faces significant challenges – insufficient publicly available data, particularly on the midstream, underlaid by a lack of consensus on what data could or should be shared through the supply chain, and further disclosed to the public and consumers.

Some nations already disclose significant data on mining volumes, given the economic and social importance of this activity in their jurisdictions. Stock exchanges and their regulators, particularly in Canada ([NI National Instrument 43-101 Standards of Disclosure for Mineral Projects](#)) and Australia ([Joint Ore Reserves Committee \[JORC\] reporting code](#)), have also played a crucial role in making more data on production and reserves of publicly traded mining companies accessible.

Public data initiatives have the potential to offer valuable insights to stakeholders in the market. While some disclosures have been made under the Extractive Industries Transparency Initiative (EITI),

countries do not necessarily systematically disclose the information even if it is required under EITI. In addition to private disclosures from publicly traded companies, efforts are underway to classify and make data on resources more readily available, often held by geological surveys, with the United Nations [Framework Classification for Resources](#) (UNFC).

For refining and trade, public statistics face challenges in portraying what is now becoming an essential section of many economies – even though they play a critical role in understanding complex supply chains. In particular, the Harmonised System (HS) codes can facilitate access to trade data for materials of growing importance. However, key commodities such as lithium ore, concentrate and chemicals or cobalt and manganese sulphates, essential to the EV battery, do not yet have harmonised codes, hindering efficient tracking of trade flows.

Likewise, information about regional consumption is relatively lacking compared with production volumes, which hampers the granular understanding of market balances. All of these underscore the necessity of launching efforts to systematically collect reliable data consistently, beginning with identifying areas where publicly available data are most lacking.

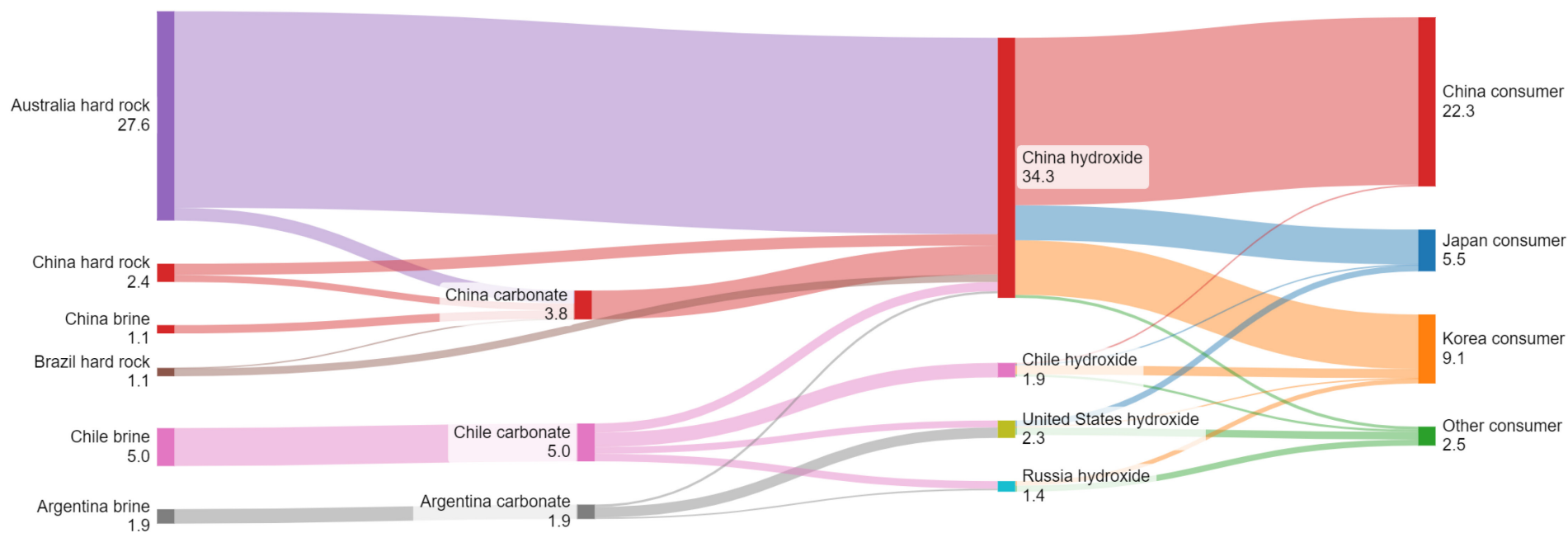
Traceability tools can also be a technical enabler, though not an end goal in themselves. There is a growing interest in decentralised databases, but the underlying challenge often lies in defining i) which data should be shared to achieve transparency objectives, in what

frequency; ii) with whom this data should be shared; iii) how accountable data producers are; and iv) whether public enforcement is necessary to provide adequate incentives and ensure adherence to best practices.



## Trade analysis is key to identifying bottlenecks in complex supply chains

Lithium hydroxide supply chain, 2021



IEA. CC BY 4.0.

Notes: Values in kt of elemental Li. Lithium hydroxide supply chain includes trade of lithium-containing commodities (carbonates, ore concentrates) used as inputs for hydroxide production.

Sources: IEA analysis, based on UN Comtrade and Wood Mackenzie.

## There is scope to improve codes for trade reporting to better track trade flows of raw and refined materials

### World Customs Organization HS codes for critical mineral trades

|                                    | Copper   | Lithium   | Nickel  | Cobalt   | Graphite   | Rare earth elements  | Manganese  |
|------------------------------------|--|---|---|--|--|--|--|
| <b>Mined</b>                       | 2603.00 ("Copper ores and concentrates")   | Included in 2530.90 ("Mineral substances not elsewhere specified or included")  | 2604.00 ("Nickel ores and concentrates")  | 2605.00 ("Cobalt ores and concentrates")   | 2504.10 and 2504.90 ("Natural graphite")   | Included in 2530.90 ("Mineral substances not elsewhere specified or included")               | 2602.00 ("Manganese ores and concentrates")  |
| <b>Processed</b>                   | 2825.50, 2827.41, 2833.25 (copper chemicals) and the complete 74 chapter ("Copper and articles thereof") | 2825.20 (Li oxide and hydroxide)<br>2836.91 (Li carbonates), also included in 2805.19 ("Alkali metals, including lithium metal"), 2833.29 ("Sulphates") and 2827.39 ("other chlorides") | 2825.40, 2827.35, 2833.24 (Nickel chemicals), 7202.60 (Ferronickel) and the complete 75 chapter ("Nickel and articles thereof") | 2822.00 (Co oxides and hydroxides), 8105.20 (Co mattes) and also included in 2833.29 ("Sulphates") | 3801.1 (synthetic graphite) and 3801.2 (natural graphite)                            | 2805.30, 2846.10, 2846.90  | 2820.10, 2820.90 (manganese oxide and dioxide), 7202.11, 7202.19 (ferro-manganese), 8111.00 (manganese metal) and also included in 2833.29 (sulphates) |
| <b>Secondary (waste, scrap...)</b> | 7404.00 ("Cu waste and scrap")   |   | 7503.00 ("Ni waste and scrap")  | 8105.30 ("Co waste and scrap")   |  |  | Manganese waste and scrap is also included in 8111.00  |
| <b>Notes</b>                       |  | EU imports lithium ores under domestic code 25309040, China uses a ten-digit code for various lithium ores (2530909902 for spodumene...)  |   |  | No distinction between raw and refined battery-grade graphite in the HS code system. | EU imports rare earth ores under domestic code 25309050, China under domestic code 25309020. |  |

## Sustainable and responsible supplies

## Critical minerals cannot be truly secure, reliable and resilient unless they are also sustainably and responsibly produced

The foremost reason to address the ESG risks within the mineral supply chain is to protect people, communities and the environment. Robust efforts to ensure that supply chains are responsible and sustainable will be necessary to ensure that energy transitions are people-centred and that the benefits associated with mineral production, such as revenue and jobs, are captured in producer countries and communities. In parallel, improving the ESG performance of mineral supply chains can yield important security-of-supply benefits.

In fact, without serious efforts to mitigate the ESG risks associated with mineral supply chains, there may not be sufficient supplies to support the rapid scale-up of clean energy technologies that is needed to reach climate goals and to avert the worst effects of climate change. Governments and companies alike have a role in developing sustainable and responsible supply chains. While companies may champion sustainable and responsible practices and transparently monitor progress, governments play a crucial role in incentivising corporate action and creating a regulatory environment conducive to high ESG standards.

While there are many ESG risks that can lead to supply disruptions, we have identified six priority areas that have particularly important implications for security of supply: water, GHG emissions,

biodiversity, human rights, communities and corruption. Each of these risks impacts security of supply in a different way, but broadly, failures in these areas can limit market access, create legal barriers, discourage investment, damage reputation, increase the likelihood of opposition from local communities, and in some cases physically prevent projects from operating.

Critical minerals are often situated in regions characterised by elevated water stress. Developing infrastructure that ensures secure water access for local communities can help companies prevent conflicts where water access is limited. Policy responses that encourage water stewardship include conditioning public investment to or establishing specific targets for water quality, use and effluents that improve over time.

Companies that do not reduce and report GHG emissions face risks to market access and their reputation. Corporate reporting can build onto existing standards and external verification to provide transparent and credible data. Investment in on-site renewables and energy efficiency can help drive decarbonisation efforts. Governments can improve or expand GHG reporting requirements and ensure that data on emissions are publicly available.

Operations that fail to address biodiversity impacts may face regulatory barriers and reputational and investment risks – especially for mineral deposits located in key biodiversity areas. Companies can minimise land use and related impacts by working on project design and implementing technologies tailored to each site. Governments can strengthen biodiversity protections in mining regulations and permits and improve monitoring and disclosure of biodiversity data.

Enhancing human rights standards in mining operations can mitigate operational disruptions and reduce divestment resulting from human rights violations, including child labour and forced labour. Corporations and governments can enable supply chain transparency by embedding human rights risks in due diligence systems or regulatory frameworks, while supporting the continued implementation and enforcement of protections.

Meaningful engagement with local communities and Indigenous Peoples can help projects obtain and maintain a social licence to operate. This rests on credible local community and Indigenous Peoples-led consultation schemes. Free, prior and informed consent of Indigenous Peoples and potentially impacted communities is a best practice, where not already required by law.

Reducing corruption and governance risks can facilitate investment and strengthen public confidence in mining operations. This can be supported by targeted policies and the disclosure of permits,

licences, and contracts; company beneficial ownership; and payments to governments.

Considering the available levers for action, we have developed [five key recommendations for policy makers](#) to ensure that critical mineral value chains are sustainable and responsible:

- **Better regulations.** Ensure legal and regulatory protections for the environment, workers, Indigenous Peoples and communities, backed by sufficient means of implementation and enforcement.
- **Targeted public spending.** Channel public spending to encourage the development of better practices and to incentivise good performance.
- **Improved data.** Strengthen the collection and reporting of granular and standardised data to enable benchmarking and progress tracking throughout the supply chain.
- **Increased transparency.** Improve transparency throughout the supply chain, including by enhancing traceability, undertaking due diligence and reporting publicly on risks and mitigation actions.
- **Support sustainability standards.** Support the development of initiatives that help companies demonstrate that their operations are sustainable and responsible while ensuring cross-compatibility and interoperability.

Governments can play an important role in promoting improvements by incorporating the recommendations into their policy and investment decisions. These five recommendations are cross-cutting and can apply to all ESG risks

---

# Annex

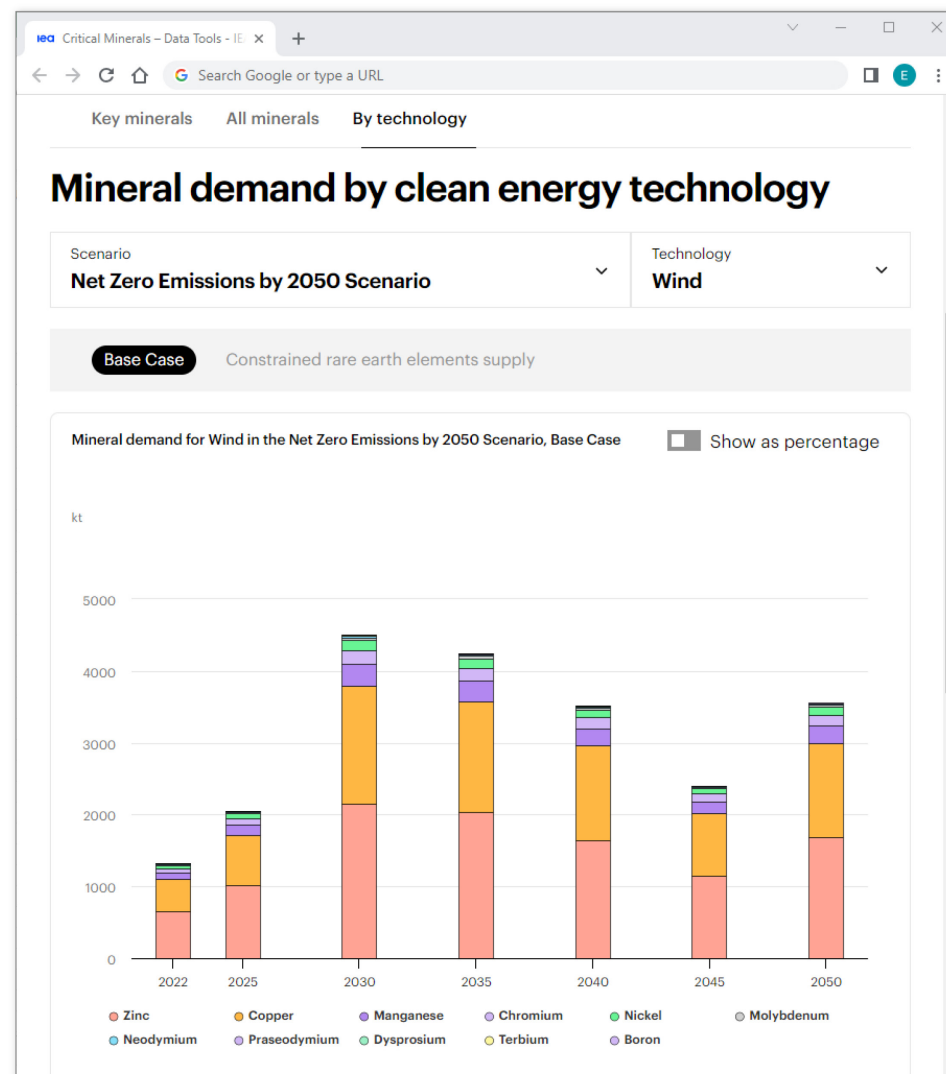
---

## IEA Critical Minerals Data Explorer

The IEA has integrated critical minerals into its long-term energy modelling framework. Last year, alongside the [Critical Minerals Market Review 2023](#), the [IEA Critical Minerals Data Explorer](#) was launched. The explorer is an interactive online tool that allows users to easily access the IEA's projection data. This year the data explorer has been updated to now include long-term supply projection data as well as demand projection data for the key energy transition minerals (copper, lithium, nickel, cobalt, graphite and rare earth elements).

The tool provides users with access to the IEA's demand projection results under various energy scenarios and technology evolution trends (through various alternative technology cases). Users can look up total demand for key energy transition minerals and projected mineral demand in the clean energy sector by technology and commodity, scenario and technology case. Long-term supply projections for the key energy transition minerals are now accessible in the tool. Supply projections are based on the project pipeline for each mineral in a base case and high production case based on the project's probability of coming online.

The numbers are regularly updated to align with the latest energy projections.



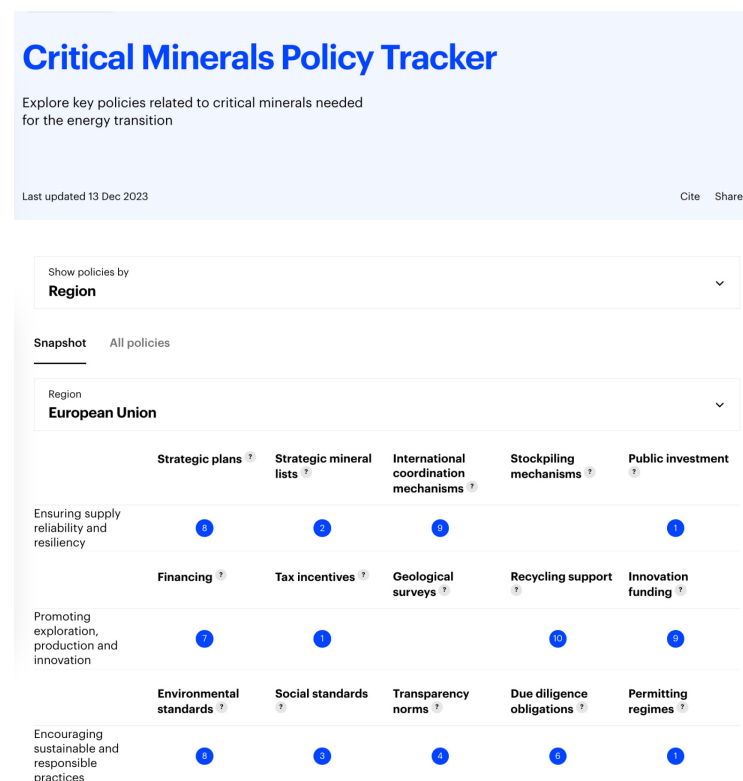
## IEA Critical Minerals Policy Tracker

The IEA launched the [Critical Minerals Policy Tracker](#) in November 2022, which monitors and analyses the development of policies concerning critical minerals. This tool tracks policies across over 35 countries, starting from an initial dataset of 200 policies and expanded to 450 policies by 2023. Updated annually to ensure the inclusion of new policies and any amendments, the latest update was completed in December 2023. While not exhaustive, this data tool provides an overview of the evolving landscape in mineral supply chain governance in the context of clean energy transitions.

The data for the Tracker is primarily sourced from the [IEA Policies Database](#), which encompasses an array of government-issued policies, laws, and regulations relevant to the energy sector. The methodology for data collection for the [Critical Minerals Policy Tracker](#) includes desk research and stakeholder submissions to capture policies in place within each of the focus countries and regions. For the 2023 update, a questionnaire was circulated among all IEA member countries via the IEA’s Working Party on Critical Minerals. Feedback from country delegates and external researchers further refines and validates the database entries.

Policies tracked by this tool are categorised into three key areas: ensuring supply reliability and resiliency, promoting exploration, production, and innovation, and encouraging sustainable and

responsible practices. Within each category, policies are further divided into five subcategories. This categorisation aids in the IEA’s systematic analysis of policy trends and differences across various countries and regions, providing stakeholders with insights into the global policy approaches to managing critical mineral resources.





## Methodology

### Scope

The critical minerals model, added as a permanent module in the [Global Energy and Climate \(GEC\) Model](#) during the 2022 modelling cycle, assesses the mineral requirements for the following clean energy technologies:

- low-emissions power generation
  - solar PV (utility-scale and distributed)
  - wind (onshore and offshore)
  - concentrating solar power (parabolic troughs and central tower)
  - hydropower
  - geothermal
  - bioenergy for power
  - nuclear power
- electricity networks (transmission, distribution, and transformer)
- electric vehicles (battery electric and plug-in hybrid electric vehicles)

- battery storage (utility-scale and residential)
- hydrogen (electrolysers and fuel cells)

All of these energy technologies require metals and alloys, which are produced by processing mineral-containing ores. Ores – the raw, economically viable rocks that are mined – are beneficiated to liberate and concentrate the minerals of interest. Those minerals are further processed to extract the metals or alloys of interest. Processed metals and alloys are then used in end-use applications. While this analysis covers the entire mineral and metal value chain from mining to processing operations, we use “minerals” as a representative term for the sake of simplicity.

We focus specifically on the use of minerals in clean energy technologies, given that they generally require considerably more minerals than their fossil fuel counterparts. Our model also focuses on the requirements for building a plant (or making equipment) and not on operational requirements (e.g. uranium consumption in nuclear plants).

Our model considers a wide range of minerals used in clean energy technologies. They include copper, major battery metals (lithium, nickel, cobalt, manganese and graphite), rare earth elements, arsenic, boron, cadmium, chromium, gallium, germanium, hafnium, indium,

iridium, lead, magnesium, molybdenum, niobium, platinum group metals, selenium, silicon, silver, tantalum, tellurium, tin, titanium, tungsten, vanadium and zinc.

Steel and aluminium are widely used across many clean energy technologies, but we have excluded them from the scope of this analysis. Steel does not have substantial security implications and the energy sector is not a major driver of growth in steel demand. Aluminium demand is assessed for electricity networks only as the outlook for copper is inherently linked with aluminium use in grid lines, but is not included in the aggregate demand projections.

For the six key energy transition minerals – copper, lithium, nickel, cobalt, graphite and rare earth elements – we model total demand including uses in clean energy applications and other segments. Consumption outside the clean energy sector has been estimated using historical consumption by end-use applications, relevant activity drivers (e.g. GDP, industry value added, steel production, etc.) and material intensities.

## Demand

For each of the clean energy technologies, we estimate overall mineral demand using five main variables:

- clean energy deployment trends under different scenarios
- sub-technology shares within each technology area

- mineral intensity of each sub-technology
- mineral intensity improvements
- material efficiency measures (recycling, reuse and behavioural change)

Clean energy deployment trends under the Stated Policies Scenario (STEPS), the Announced Pledges Scenario (APS), and the Net Zero Emissions by 2050 (NZE) Scenario are taken from the projections from the [World Energy Outlook 2023](#), adjusted by latest information from the [Global EV Outlook 2024](#) and other sources.

Mineral intensity assumptions were developed through extensive [literature review](#) and expert and industry consultations, including with IEA Technology Collaboration Programmes. The pace of mineral intensity improvements varies by scenario, with the STEPS generally seeing minimal improvement over time as compared with modest improvement (around 10% in the longer term) assumed in the APS and NZE Scenario. In areas that may particularly benefit from economies of scale or technology improvement (e.g. silicon and silver use in solar PV, platinum loading in fuel cells, rare earth elements use in wind turbines, copper in buildings), specific improvement rates have been applied based on the review of underlying drivers.

## Supply

For the six key energy transition minerals, primary supply requirements have been assessed by deducing projected secondary supply from projected total demand.

Secondary production is estimated with two parameters: the average recycling rate and the lifetime of each end-use sector. The recycling rate is the combination of the end-of-life collection rate (the amount of a certain product being collected for recycling) and the yield rate (the amount of material a recycling process can actually recover). For emerging technologies such as lithium-ion batteries, we assume collection rates increase at a faster pace. For batteries, the collection rates gradually increase from around 45% in the early-2020s to 80% by 2040 in the NZE Scenario. The yield rate is assumed to vary according to the technical limitations for the extraction of each mineral using the currently available recycling methods. The reuse rates are much lower than the collection rate for recycling as the use

of second-life batteries (in grid applications) faces many technical and regulatory obstacles. Losses from manufacturing processes are also taken into account. For primary supply requirements for mined materials, a certain level of loss ratio during refining processes is assumed.

Supply projections for the key energy transition minerals are built using the data for the pipeline of operating and announced mining and refining projects by country. These projections are divided into a base case and a high production case, whose categorisation is assessed through their probability of coming online based on various factors such as the status of financing, permitting and feasibility studies.

We acknowledge the use of data on mining and refining projects from various professional information sources such as [S&P Global Market Intelligence](#), [Wood Mackenzie](#), [Benchmark Mineral Intelligence](#), and [Project Blue](#).

## Mineral-specific clean energy transition risk assessment – detailed evaluation criteria

| Supply risks  | Assessment methodology   | Weight | High   | Medium   | Low   |
|---|--|--------|--|--|---|
|   |  |        |  |  |   |
| Expected pace of demand growth                        | Annual average demand growth rates in climate-driven scenarios vis-à-vis historical growth rates | 10%    | Expected pace of growth between 2023 and 2030 in the APS is over 2 times higher than historical growth rates | Expected pace of growth between 2023 and 2030 in the APS is more than 20% higher than historical growth rates    | Expected pace of growth between 2023 and 2030 in the APS is similar or lower than historical growth rates |
| Short-term market balances                            | Balances between expected supply (base case) and primary supply requirements in 2026             | 20%    | Expected supply (base case) falls short of STEPS primary supply requirements in 2026                         | Expected supply (base case) able to meet STEPS primary supply requirements in 2026, but falls short of APS needs | Expected supply (base case) is higher than APS primary supply requirements in 2026                        |
| Long-term market balances in climate-driven scenarios | Balances between expected supply and primary supply requirements in 2040                         | 30%    | Expected supply (base case) meets less than 60% of APS primary supply requirements in 2040                   | Expected supply (base case) meets 60-80% of the APS primary supply requirements in 2040.                         | Expected supply (base case) meets over 80% of the APS primary supply requirements in 2040.                |
| Observed price volatility                             | Historical monthly price volatility between 2011 and 2023  | 20%    | Standard deviation of indexed historical monthly prices above 35   | Standard deviation of historical monthly prices between 25 and 35 (range of oil and gas)                         | Standard deviation of historical monthly prices below 25  |
| Impact on clean energy cost                           | Share of a material in total cost of end-use technologies  | 20%    | Price spikes could hamper the deployment of final technologies   | Modest impact on final clean energy cost   | Limited impact on final clean energy cost   |

|  |   |        | High   | Medium   | Low   |
|--|---|--------|--|--|---|
| Geopolitical risks                                     | Assessment methodology  | Weight |  |  |   |
| Geographical concentration of mined supply             | Expected share of top 3 producing mining countries in 2030  | 20%    | Projected top 3 country share remains above 80% in 2030 or top 1 country controls more than two thirds of global   | Projected top 3 country share between 65% and 80% in 2030 or top 1 country controls more than 50% of global supply | Projected top 3 country share remains below 65% and top 1 country controls less than 50% of global supply |
| Geographical concentration of refined supply           | Expected share of top 3 producing refining countries in 2030  | 30%    | Projected top 3 country share remains above 80% in 2030 or top 1 country controls more than two thirds of global   | Projected top 3 country share between 65% and 80% in 2030 or top 1 country controls more than 50% of global supply | Projected top 3 country share remains below 65% and top 1 country controls less than 50% of global supply |
| N-1 supply and demand balances                         | Share of N-1 supply in N-1 material requirements in 2030 (refined product basis)                            | 15%    | N-1 supply serves less than 35% of N-1 requirements in 2030 in the APS   | N-1 supply serves between 35% and 60% of N-1 requirements in 2030 in the APS                                       | N-1 supply serves over 60% of N-1 requirements in 2030 in the APS   |
| Export risks of major suppliers                        | Weighted average export restriction risk score of today's production portfolio both for mining and refining | 15%    | Weighted average country risk score above 4  | Weighted average country risk score between 2.5 and 4  | Weighted average country risk score below 2.5   |
| Hurdles to develop new projects in diversified regions | Difficulties in building supply chains in geographically diverse regions (qualitative)                      | 20%    | New capacities involve considerably higher capital and operating costs (than incumbent players) and long lead time | Building new capacities needs to overcome modest capital, lead time and technological barriers                     | Manageable capital, lead time and technological barriers.   |

| Barriers to respond to disruption          | Assessment methodology   | Weight |  |   |   |
|--|--|--------|--|---|---|
| Visible stock levels                       | Visible stock levels in major exchanges  | 25%    | Limited visibility in stock levels   | Possible to monitor visible stock levels in major exchanges, but volumes are low compared to historical average.          | Ample visible stock in major exchanges                          |
| Transparency of pricing schemes            | Qualitative assessment of market liquidity and transparency of pricing schemes   | 25%    | Price reporting driven through survey pricing and unregulated platforms with limited liquidity | Early stage regulated market trading but with limited liquidity   | Established regulated market trading with ample liquidity       |
| Availability of options to moderate demand | Availability of demand-side and technology switching options to moderate demand growth in case of supply tightness (qualitative) | 25%    | Limited opportunities to reduce demand without sacrificing performance                         | Scope for technology switching and behavioural change to reduce demand, but requires substantial time and cost commitment | Viable opportunities to reduce demand in a short period of time |
| Status of secondary supply                 | Share of secondary supply in total supply and potential for growth   | 25%    | Share of secondary supply remains low and is not improving significantly                       | Share of secondary supply remains low but is improving or share remains high but with limited improvement                 | Share of secondary supply remains high and is improving         |

| Exposure to ESG and climate risks                            |   |        | High  | Medium   | Low   |
|--|---|--------|---|--|---|
| Exposure to ESG and climate risks                            | Assessment methodology  | Weight |   |  |   |
| Environmental performance: mining                            | Weighted average environmental performance score of today's mined production                              | 30%    | Weighted average environmental performance score below 40                                       | Weighted average environmental performance score between 40 and 65                                     | Weighted average environmental performance score above 65   |
| Environmental performance: refining                          | Weighted average grid carbon intensity of today's refined production                                      | 30%    | Weighted average grid carbon intensity above 460 gCO <sub>2</sub> /kWh (world average)          | Weighted average grid carbon intensity between 460 gCO <sub>2</sub> /kWh and 380 gCO <sub>2</sub> /kWh | Weighted average grid carbon intensity below 380 gCO <sub>2</sub> /kWh (advanced economy average) |
| Social and governance performance                            | Weighted average corruption, human rights and conflict score of today's mined production (based on V-Dem) | 20%    | Weighted average social and governance score below 0.33   | Weighted average social and governance score between 0.33 and 0.66                                     | Weighted average social and governance score above 0.66   |
| Exposure to natural hazards and climate risks - water stress | Share of mines exposed to water stress risks  | 10%    | Share of mine production located in high, extreme high and arid areas equal or above 50%        | Share of mine production located in high, extreme high and arid areas between 25% and 50%              | Share of mine production located in high, extreme high and arid areas below 25%                   |
| Exposure to natural hazards and climate risks - earthquake   | Share of mines exposed to earthquake risks  | 10%    | Share of mine production located in high and very high earthquake risk areas equal or above 50% | Share of mine production located in high and very high earthquake risk areas between 25% and 50%       | Share of mine production located in high and very high earthquake risk areas below 25%            |

## Key projection results

## Copper demand

| Unit: kt Cu                  | Historical |        | Stated Policies |        |        | Announced Pledges |        |        | Net Zero by 2050 |        |        |
|------------------------------|------------|--------|-----------------|--------|--------|-------------------|--------|--------|------------------|--------|--------|
|                              | 2021       | 2023   | 2030            | 2040   | 2050   | 2030              | 2040   | 2050   | 2030             | 2040   | 2050   |
| <b>Clean energy</b>          | 5 380      | 6 311  | 10 314          | 12 188 | 12 972 | 12 001            | 16 343 | 17 466 | 14 842           | 19 636 | 19 416 |
| <b>Electricity networks</b>  | 4 030      | 4 171  | 5 922           | 6 305  | 6 124  | 6 632             | 8 327  | 8 158  | 7 816            | 10 632 | 9 471  |
| <b>Electric vehicles</b>     | 166        | 396    | 1 645           | 3 131  | 3 470  | 1 870             | 4 297  | 4 804  | 2 612            | 4 642  | 5 124  |
| <b>Solar PV</b>              | 694        | 1 208  | 1 691           | 1 684  | 1 959  | 2 117             | 2 049  | 2 401  | 2 564            | 2 245  | 2 390  |
| <b>Other</b>                 | 490        | 536    | 1 055           | 1 068  | 1 419  | 1 382             | 1 670  | 2 103  | 1 850            | 2 116  | 2 430  |
| <b>Other uses</b>            | 19 548     | 19 543 | 20 341          | 21 997 | 24 671 | 19 127            | 20 036 | 22 046 | 18 399           | 19 434 | 21 473 |
| <b>Total demand</b>          | 24 928     | 25 855 | 30 655          | 34 185 | 37 643 | 31 128            | 36 379 | 39 512 | 33 241           | 39 069 | 40 889 |
| <b>Share of clean energy</b> | 22%        | 24%    | 34%             | 36%    | 34%    | 39%               | 45%    | 44%    | 45%              | 50%    | 47%    |

Notes: Demand is based on refined copper and excludes direct use of scrap. Electric vehicles demand includes both EV batteries and EV motors demand.



## Copper supply

| Unit: kt Cu          | Mining     |        |           |        | Refining             |        |           |        |        |
|----------------------|------------|--------|-----------|--------|----------------------|--------|-----------|--------|--------|
|                      | Historical |        | Base case |        | Historical           |        | Base case |        |        |
|                      | 2021       | 2023   | 2030      | 2040   | 2021                 | 2023   | 2030      | 2040   |        |
| <b>Chile</b>         | 5 660      | 5 311  | 5 211     | 4 053  | <b>China</b>         | 10 383 | 11 547    | 14 788 | 14 788 |
| <b>DRC</b>           | 2 014      | 2 678  | 3 183     | 2 145  | <b>DRC</b>           | 1 562  | 1 978     | 2 235  | 1 381  |
| <b>Peru</b>          | 2 282      | 2 644  | 2 377     | 1 067  | <b>Chile</b>         | 2 270  | 2 058     | 1 719  | 1 321  |
| <b>China</b>         | 1 828      | 1 865  | 2 128     | 1 856  | <b>Japan</b>         | 1 514  | 1 499     | 1 614  | 1 614  |
| <b>Russia</b>        | 862        | 960    | 1 215     | 1 019  | <b>India</b>         | 497    | 549       | 1 060  | 1 060  |
| <b>Indonesia</b>     | 753        | 863    | 948       | 861    | -                    |        |           |        |        |
| <b>Rest of world</b> | 8 026      | 8 187  | 7 350     | 3 888  | <b>Rest of world</b> | 8 747  | 8 706     | 10 506 | 9 781  |
| <b>World</b>         | 21 426     | 22 508 | 22 412    | 14 889 | <b>World</b>         | 24 973 | 26 336    | 31 922 | 29 944 |
| <b>Top 3 share</b>   | 46%        | 47%    | 48%       | 54%    | <b>Top 3 share</b>   | 57%    | 59%       | 59%    | 59%    |

Note: DRC = Democratic Republic of the Congo.

## Lithium demand

| Unit: kt Li                  | Historical |      | Stated Policies |      |      | Announced Pledges |       |       | Net Zero by 2050 |       |       |
|------------------------------|------------|------|-----------------|------|------|-------------------|-------|-------|------------------|-------|-------|
|                              | 2021       | 2023 | 2030            | 2040 | 2050 | 2030              | 2040  | 2050  | 2030             | 2040  | 2050  |
| <b>Clean energy</b>          | 38         | 92   | 381             | 868  | 1041 | 442               | 1 203 | 1 452 | 616              | 1 308 | 1 573 |
| <b>Electric vehicles</b>     | 35         | 83   | 347             | 808  | 964  | 398               | 1 124 | 1 353 | 560              | 1 206 | 1 447 |
| <b>Battery storage</b>       | 2          | 9    | 35              | 59   | 77   | 44                | 79    | 99    | 56               | 102   | 126   |
| <b>Other uses</b>            | 63         | 73   | 90              | 123  | 155  | 90                | 123   | 155   | 90               | 123   | 155   |
| <b>Total demand</b>          | 101        | 165  | 471             | 991  | 1196 | 531               | 1 326 | 1 607 | 705              | 1 431 | 1 728 |
| <b>Share of clean energy</b> | 37%        | 56%  | 81%             | 88%  | 87%  | 83%               | 91%   | 90%   | 87%              | 91%   | 91%   |

## Lithium supply

| Unit: kt Li          | Raw materials |      |           |      | Chemicals            |      |           |      |     |
|----------------------|---------------|------|-----------|------|----------------------|------|-----------|------|-----|
|                      | Historical    |      | Base case |      | Historical           |      | Base case |      |     |
|                      | 2021          | 2023 | 2030      | 2040 | 2021                 | 2023 | 2030      | 2040 |     |
| <b>Australia</b>     | 50            | 84   | 146       | 128  | <b>China</b>         | 70   | 114       | 213  | 215 |
| <b>China</b>         | 17            | 34   | 103       | 103  | <b>Chile</b>         | 25   | 46        | 56   | 56  |
| <b>Chile</b>         | 28            | 46   | 56        | 56   | <b>Argentina</b>     | 7    | 9         | 47   | 40  |
| <b>Argentina</b>     | 6             | 9    | 47        | 40   | <b>Australia</b>     | 0    | 6         | 30   | 30  |
| <b>Zimbabwe</b>      | 2             | 9    | 34        | 34   | <b>US</b>            | 0    | 1         | 17   | 18  |
| <b>Canada</b>        | 0             | 3    | 20        | 20   | <b>Korea</b>         | 0    | 0         | 4    | 5   |
| <b>Rest of world</b> | 4             | 8    | 44        | 28   | <b>Rest of world</b> | 0    | 0         | 6    | 6   |
| <b>World</b>         | 107           | 194  | 450       | 408  | <b>World</b>         | 102  | 176       | 373  | 370 |
| <b>Top 3 share</b>   | 89%           | 85%  | 68%       | 70%  | <b>Top 3 share</b>   | 100% | 96%       | 85%  | 84% |

Note: Raw materials cover extraction of lithium from hard rock ore, as well as from clays and brines. Lithium chemicals cover the first production of lithium carbonate, hydroxide, sulphates and chlorides, and excludes reprocessing.

## Nickel demand

| Unit: kt Ni                  | Historical |       | Stated Policies |       |       | Announced Pledges |       |       | Net Zero by 2050 |       |       |
|------------------------------|------------|-------|-----------------|-------|-------|-------------------|-------|-------|------------------|-------|-------|
|                              | 2021       | 2023  | 2030            | 2040  | 2050  | 2030              | 2040  | 2050  | 2030             | 2040  | 2050  |
| <b>Clean energy</b>          | 240        | 478   | 1 585           | 2 411 | 2 074 | 1 953             | 3 381 | 3 132 | 2 794            | 3 584 | 3 094 |
| <b>Electric vehicles</b>     | 148        | 299   | 1 184           | 2 081 | 1 799 | 1 338             | 2 862 | 2 508 | 1 825            | 2 921 | 2 634 |
| <b>Battery storage</b>       | 7          | 12    | 18              | 0     | 0     | 22                | 0     | 0     | 28               | 0     | 0     |
| <b>Other</b>                 | 85         | 166   | 383             | 329   | 274   | 593               | 518   | 624   | 940              | 662   | 460   |
| <b>Other uses</b>            | 2 519      | 2 627 | 2 866           | 3 120 | 3 354 | 2 802             | 2 857 | 3 014 | 2 776            | 2 802 | 2 935 |
| <b>Total demand</b>          | 2 759      | 3 104 | 4 451           | 5 531 | 5 428 | 4 754             | 6 238 | 6 146 | 5 570            | 6 386 | 6 030 |
| <b>Share of clean energy</b> | 9%         | 15%   | 36%             | 44%   | 38%   | 41%               | 54%   | 51%   | 50%              | 56%   | 51%   |

## Nickel supply

| Unit: kt Ni          | Mining     |       |           |       | Refining             |       |           |       |       |
|----------------------|------------|-------|-----------|-------|----------------------|-------|-----------|-------|-------|
|                      | Historical |       | Base case |       | Historical           |       | Base case |       |       |
|                      | 2021       | 2023  | 2030      | 2040  | 2021                 | 2023  | 2030      | 2040  |       |
| <b>Indonesia</b>     | 1 005      | 1 787 | 2 671     | 3 278 | <b>Indonesia</b>     | 869   | 1 414     | 2 028 | 2 365 |
| <b>Philippines</b>   | 390        | 391   | 345       | 157   | <b>China</b>         | 882   | 1 065     | 965   | 964   |
| <b>New Caledonia</b> | 168        | 210   | 247       | 201   | <b>Japan</b>         | 192   | 204       | 264   | 230   |
| <b>Russia</b>        | 205        | 194   | 215       | 191   | <b>Russia</b>        | 120   | 158       | 165   | 165   |
| <b>Canada</b>        | 175        | 194   | 156       | 97    | <b>Finland</b>       | 65    | 138       | 207   | 207   |
| <b>China</b>         | 109        | 114   | 143       | 126   | <b>Canada</b>        | 107   | 136       | 157   | 147   |
| <b>Australia</b>     | 158        | 111   | 87        | 67    | <b>Australia</b>     | 105   | 132       | 213   | 213   |
| <b>Rest of world</b> | 438        | 450   | 441       | 322   | <b>Rest of world</b> | 589   | 550       | 591   | 577   |
| <b>World</b>         | 2 649      | 3 451 | 4 304     | 4 439 | <b>World</b>         | 2 929 | 3 796     | 4 590 | 4 867 |
| <b>Top 3 share</b>   | 60%        | 69%   | 76%       | 83%   | <b>Top 3 share</b>   | 66%   | 71%       | 71%   | 73%   |

Note: Nickel refining includes nickel that is processed into either a metal, oxide, nickel pig iron, ferronickel, or sulphate and excludes outputs from intermediate production steps.

## Cobalt demand

| Unit: kt Co                  | Historical |      | Stated Policies |      |      | Announced Pledges |      |      | Net Zero by 2050 |      |      |
|------------------------------|------------|------|-----------------|------|------|-------------------|------|------|------------------|------|------|
|                              | 2021       | 2023 | 2030            | 2040 | 2050 | 2030              | 2040 | 2050 | 2030             | 2040 | 2050 |
| <b>Clean energy</b>          | 36         | 64   | 155             | 187  | 216  | 177               | 260  | 303  | 243              | 279  | 323  |
| <b>Electric vehicles</b>     | 34         | 62   | 151             | 187  | 216  | 171               | 260  | 303  | 236              | 279  | 323  |
| <b>Battery storage</b>       | 2          | 3    | 4               | 0    | 0    | 5                 | 0    | 0    | 7                | 0    | 0    |
| <b>Other uses</b>            | 145        | 150  | 169             | 198  | 222  | 167               | 194  | 218  | 167              | 193  | 217  |
| <b>Total demand</b>          | 181        | 215  | 324             | 385  | 438  | 344               | 454  | 521  | 410              | 472  | 539  |
| <b>Share of clean energy</b> | 20%        | 30%  | 48%             | 49%  | 49%  | 51%               | 57%  | 58%  | 59%              | 59%  | 60%  |

## Cobalt supply

| Unit: kt Co          | Mining     |      |           |      | Refining             |      |           |      |     |
|----------------------|------------|------|-----------|------|----------------------|------|-----------|------|-----|
|                      | Historical |      | Base case |      | Historical           |      | Base case |      |     |
|                      | 2021       | 2023 | 2030      | 2040 | 2021                 | 2023 | 2030      | 2040 |     |
| <b>DRC</b>           | 121        | 157  | 215       | 135  | <b>China</b>         | 130  | 172       | 231  | 228 |
| <b>Indonesia</b>     | 3          | 20   | 50        | 47   | <b>Finland</b>       | 14   | 19        | 20   | 20  |
| <b>Russia</b>        | 6          | 8    | 8         | 8    | <b>Japan</b>         | 5    | 6         | 13   | 12  |
| <b>China</b>         | 7          | 7    | 8         | 7    | <b>Indonesia</b>     | 0    | 0         | 9    | 9   |
| <b>Australia</b>     | 8          | 8    | 6         | 5    | <b>Canada</b>        | 7    | 7         | 8    | 3   |
| <b>Philippines</b>   | 5          | 6    | 3         | 3    | <b>Korea</b>         | 2    | 3         | 5    | 5   |
| <b>Rest of world</b> | 30         | 36   | 36        | 20   | <b>Rest of world</b> | 18   | 18        | 28   | 28  |
| <b>World</b>         | 179        | 240  | 326       | 225  | <b>World</b>         | 176  | 224       | 313  | 305 |
| <b>Top 3 share</b>   | 75%        | 77%  | 84%       | 84%  | <b>Top 3 share</b>   | 86%  | 88%       | 84%  | 85% |

## Graphite demand

| Unit: kt                     | Historical |       | Stated Policies |        |        | Announced Pledges |        |        | Net Zero by 2050 |        |        |
|------------------------------|------------|-------|-----------------|--------|--------|-------------------|--------|--------|------------------|--------|--------|
|                              | 2021       | 2023  | 2030            | 2040   | 2050   | 2030              | 2040   | 2050   | 2030             | 2040   | 2050   |
| <b>Clean energy</b>          | 532        | 1 292 | 5 179           | 7 053  | 4 839  | 6 013             | 9 839  | 6 777  | 8 407            | 11 222 | 7 879  |
| <b>Electric vehicles</b>     | 495        | 1 147 | 4 671           | 6 148  | 3 707  | 5 375             | 8 629  | 5 318  | 7 592            | 9 668  | 6 012  |
| <b>Battery storage</b>       | 37         | 145   | 508             | 904    | 1 133  | 638               | 1 210  | 1 459  | 815              | 1 555  | 1 867  |
| <b>Other uses</b>            | 3 388      | 3 340 | 4 430           | 6 047  | 7 648  | 4 406             | 6 185  | 7 955  | 4 616            | 6 650  | 8 473  |
| <b>Total demand</b>          | 3 920      | 4 632 | 9 609           | 13 100 | 12 487 | 10 419            | 16 023 | 14 733 | 13 023           | 17 873 | 16 352 |
| <b>Share of clean energy</b> | 14%        | 28%   | 54%             | 54%    | 39%    | 58%               | 61%    | 46%    | 65%              | 63%    | 48%    |

Note: Demand is for raw natural flake graphite and synthetic graphite.



## Graphite supply

| Unit: kt             | Mining (natural graphite) |       |           |       | Refined battery-grade supply |      |           |       |       |
|----------------------|---------------------------|-------|-----------|-------|------------------------------|------|-----------|-------|-------|
|                      | Historical                |       | Base case |       | Historical                   |      | Base case |       |       |
|                      | 2021                      | 2023  | 2030      | 2040  | 2021                         | 2023 | 2030      | 2040  |       |
| <b>China</b>         | 1 140                     | 1 320 | 1 905     | 2 160 | <b>China</b>                 | 701  | 1 852     | 5 125 | 6 892 |
| <b>Mozambique</b>    | 77                        | 97    | 239       | 339   | <b>Japan</b>                 | 121  | 124       | 97    | 123   |
| <b>Madagascar</b>    | 82                        | 66    | 269       | 223   | <b>United States</b>         | 12   | 16        | 69    | 123   |
| <b>Russia</b>        | 28                        | 29    | 34        | 51    | <b>Canada</b>                | 0    | 0         | 31    | 80    |
| <b>Tanzania</b>      | 0                         | 0     | 33        | 39    | <b>Sweden</b>                | 0    | 0         | 35    | 56    |
| <b>Canada</b>        | 11                        | 5     | 25        | 25    | <b>Finland</b>               | 0    | 0         | 26    | 54    |
| <b>Rest of world</b> | 116                       | 100   | 237       | 215   | <b>Rest of world</b>         | 41   | 45        | 99    | 153   |
| <b>World</b>         | 1 455                     | 1 617 | 2 742     | 3 052 | <b>World</b>                 | 875  | 2 037     | 5 481 | 7 481 |
| <b>Top 3 share</b>   | 89%                       | 92%   | 88%       | 89%   | <b>Top 3 share</b>           | 97%  | 98%       | 97%   | 95%   |

Note: Refined battery-grade supply includes spherical graphite made from natural flake graphite and synthetic anode production.

## Rare earth elements demand

| Unit: kt REE                 | Historical |      | Stated Policies |      |      | Announced Pledges |      |      | Net Zero by 2050 |      |      |
|------------------------------|------------|------|-----------------|------|------|-------------------|------|------|------------------|------|------|
|                              | 2021       | 2023 | 2030            | 2040 | 2050 | 2030              | 2040 | 2050 | 2030             | 2040 | 2050 |
| <b>Clean energy</b>          | 11         | 16   | 40              | 48   | 57   | 46                | 64   | 78   | 62               | 72   | 80   |
| <b>Electric vehicles</b>     | 3          | 7    | 23              | 36   | 40   | 25                | 46   | 51   | 33               | 48   | 52   |
| <b>Wind</b>                  | 8          | 10   | 17              | 12   | 17   | 22                | 19   | 27   | 29               | 24   | 28   |
| <b>Other uses</b>            | 67         | 76   | 87              | 105  | 123  | 87                | 105  | 123  | 86               | 104  | 123  |
| <b>Total demand</b>          | 78         | 93   | 127             | 153  | 180  | 134               | 169  | 200  | 148              | 176  | 202  |
| <b>Share of clean energy</b> | 14%        | 18%  | 31%             | 32%  | 32%  | 35%               | 38%  | 39%  | 42%              | 41%  | 39%  |

Note: Rare earth elements refer only to four magnet rare earths, neodymium, praseodymium, dysprosium and terbium.

## Rare earth elements supply

| Unit: kt REE         | Mining     |      |           |      | Refining             |      |           |      |     |
|----------------------|------------|------|-----------|------|----------------------|------|-----------|------|-----|
|                      | Historical |      | Base case |      | Historical           |      | Base case |      |     |
|                      | 2021       | 2023 | 2030      | 2040 | 2021                 | 2023 | 2030      | 2040 |     |
| <b>China</b>         | 32         | 47   | 58        | 62   | <b>China</b>         | 53   | 70        | 81   | 86  |
| <b>Australia</b>     | 4          | 5    | 19        | 20   | <b>Malaysia</b>      | 4    | 4         | 13   | 13  |
| <b>Myanmar</b>       | 6          | 11   | 10        | 10   | <b>United States</b> | 0    | 0         | 4    | 4   |
| <b>United States</b> | 6          | 6    | 7         | 7    | <b>Australia</b>     | 0    | 0         | 4    | 4   |
| <b>Rest of world</b> | 6          | 6    | 13        | 14   | <b>Rest of world</b> | 2    | 2         | 5    | 5   |
| <b>World</b>         | 55         | 75   | 107       | 114  | <b>World</b>         | 59   | 76        | 106  | 110 |
| <b>Top 3 share</b>   | 81%        | 85%  | 81%       | 81%  | <b>Top 3 share</b>   | 98%  | 98%       | 92%  | 93% |

Note: Rare earth elements refer only to four magnet rare earths, neodymium, praseodymium, dysprosium and terbium.

## Acknowledgements

This report was prepared by the Office of the Chief Energy Economist of the Directorate of Sustainability, Technology and Outlooks, in co-operation with other directorates of the International Energy Agency (IEA). Tae-Yoon Kim co-ordinated the work and was the lead author, and he designed and directed the report together with Tim Gould, Chief Energy Economist.

The principal authors from across the agency were: Simon Bennett (venture capital investment), Eric Buisson (lithium, graphite, market transparency), Eléonore Carré (Chinese investment), Amrita Dasgupta (clean energy technology, rare earth elements, recycling), Shobhan Dhir (EV and batteries, copper, investment), Alexandre Gouy (modelling), Alexandra Hegarty (nickel, environmental and social issues, investment), Gyubin Hwang (investment, geospatial analysis), Yun Young Kim (cobalt, stock and trade), K.C. Michaels (environmental and social issues, uranium), Mari Nishiumi (Chinese investment), Tomás de Oliveira Bredariol (environmental and social issues), Ryszard Pospiech (data), Joyce Raboca (environmental and social issues, policy tracking), Jun Takashiro (investment, cost analysis) and Wonjik Yang (infographic). Eleni Tsoukala provided essential support.

The report benefited greatly from contributions from other experts within the IEA: Laura Cozzi, Pascal Laffont, Joel Couse, Milosz

Karpinski, Teo Lombardo, Christophe McGlade, Deniz Ugur and Michael Waldron.

Thanks also to Jethro Mullen, Poeli Bojorquez, Curtis Brainard, Astrid Dumond, Merve Erdil, Julia Horowitz, Clara Vallois, Lucile Wall, and Therese Walsh of the Communications and Digital Office. Erin Crum edited the manuscript and Lorenzo Squillace designed the cover. Jon Custer and Ivo Letra provided support for the web-based data tool.

This analysis has been supported by the Clean Energy Transitions Programme, the IEA's flagship initiative to transform the world's energy system to achieve a secure and sustainable future for all, particularly through the financial assistance of the Ministry of Foreign Affairs of Japan. Thanks also go to the IEA Working Party on Critical Minerals and the IEA Critical Minerals Expert Advisory Group who provided valuable input to the design of the report. Emissions intensity data was provided by courtesy of Skarn Associates.

Many experts from outside of the IEA provided essential input and/or reviewed preliminary drafts of the report. Their comments and suggestions were of great value. They include:

Siyamend Al Barazi      BGR Germany

Kwasi Ampofo              BloombergNEF

|                    |  |                     |  |
|--------------------|--|---------------------|--|
| Florian Anderhuber | Euromines  | Sylvain Eckert      | InfraVia   |
| David Anonychuk    | SGS  | Rod Eggert          | Colorado School of Mines                                   |
| Tsutomu Aoki       | Battery Association for Supply Chain of Japan                            | Simon Gardner-Bond  | TechMet  |
| Susan Bates        | Glencore   | Colin Hamilton      | BMO Capital Markets  |
| Stephane Bourg     | OFREMI   | Takeshi Harada      | Japan Organisation for Metals and Energy Security (JOGMEC) |
| Grant Bromhal      | US Department of Energy  | Sara Hastings-Simon | University of Calgary                                      |
| Peter Buchholz     | BGR Germany  | Corina Hebestreit   | European Carbon and Graphite Association                   |
| Ignacio de Calonie | International Finance Corporation  | Chris Heron         | Eurométaux   |
| Cyril Cassisa      | BHP  | Daniel Hill         | Natural Resources Canada                                   |
| David Clift        | South32  | Eleonore Lebre      | Sustainable Minerals Institute                             |
| Vincenzo Conforti  | Glencore   | Lilly Lee           | Columbia University, Center on Global Energy Policy        |
| Clint Cox          | The Anchor House   | John Lindberg       | International Council on Mining and Metals                 |
| Axel Darjana       | Direction de l'Industrie des Mines et de l'Energie de Nouvelle-Calédonie | Sophie Lu           | HSBC   |
| Stefan Debruyne    | SQM  | Sarlah McAlphine    | Geoscience Australia                                       |
| Aaron Delroy       | Pilbara Minerals   | Michele McRae       | US International Trade Administration                      |

|                    |  |                   |  |
|--------------------|--|-------------------|--|
| Dennis O. Mesina   | US Department of Energy                                      | Matthieu Salomon  | Natural Resources Governance Institute                       |
| Tom Moerenhout     | Columbia University, Center on Global Energy Policy          | Kotaro Shimizu    | Mitsubishi UFJ Research and Consulting Co.                   |
| Shinsuke Murakami  | The University of Tokyo                                      | Tristan Stanley   | BHP  |
| Mark Murray        | US Department of State                                       | Martin Stuermer   | International Monetary Fund                                  |
| Jane Nakano        | Center for Strategic and International Studies               | Simon Thibault    | General Motors   |
| Junhyeok Park      | Korean Institute of Geoscience and Mineral Resources (KIGAM) | Lyle Trytten      | Trytten Consulting   |
| Elsa Pernot        | Gunvor   | Vasileios Tsianos | Neo Performance Materials                                    |
| Raymond Philippe   | Skarn Associates   | Henry Van         | Trafigura  |
| Julia Poliscanova  | Transport and Environment                                    | Constanze Veeh    | European Commission  |
| Davide Puglielli   | Enel Group   | Ke Wang           | World Resources Institute                                    |
| Alina Racu         | Transport and Environment                                    | Joel Watson       | Foreign, Commonwealth and Development Office, United Kingdom |
| Sven Ulrich Renner | World Bank   |                   |  |
| Mark Richards      | Rio Tinto  |                   |  |
| Shunsuke Saka      | Mitsui   |                   |  |

Colleagues from US Departments of Commerce and Defense and US Department of Energy Advanced Manufacturing Office also provided valuable comments. The work reflects the views of the IEA Secretariat, but does not necessarily reflect those of reviewers. Any funder, supporter or collaborator that contributed to this work shall not be responsible for any use of, or reliance on, the work.

## Abbreviations and acronyms

|                          |   |                  |   |
|--------------------------|---|------------------|---|
| <b>ACSR</b>              | aluminium conductor steel reinforced  | <b>DRC</b>       | Democratic Republic of the Congo                |
| <b>ADMC</b>              | African Minerals Development Centre   | <b>DSTP</b>      | deep-sea tailings placement                     |
| <b>APS</b>               | Announced Pledges Scenario  | <b>EAF</b>       | electric arc furnace                            |
| <b>ASM</b>               | artisanal and small-scale mining  | <b>EBIT</b>      | earnings before interest and taxes              |
| <b>ASSB</b>              | all solid-state battery   | <b>ECA</b>       | export credit/insurance agencies                |
| <b>BEV</b>               | battery electric vehicle  | <b>EGC</b>       | Enterprise Générale du Cobalt                   |
| <b>BTM</b>               | behind-the-metre  | <b>EITI</b>      | Extractive Industries Transparency Initiative   |
| <b>CAD</b>               | Canadian dollar   | <b>EMDE</b>      | emerging market and developing economies        |
| <b>CATL</b>              | Contemporary Amperex Technology Co., Limited  | <b>EREV</b>      | extended-range electric vehicle                 |
| <b>CBAM</b>              | Carbon Border Adjustment Mechanism  | <b>ESG</b>       | environmental, social and governance            |
| <b>CEEP</b>              | Clean Energy Equipment Price Index  | <b>EU</b>        | European Union                                  |
| <b>CME</b>               | Chicago Mercantile Exchange   | <b>EUR</b>       | euro  |
| <b>CMETC</b>             | Critical Mineral Exploration Tax Credit   | <b>EV</b>        | electric vehicle                                |
| <b>CMOC</b>              | CMOC Group Limited  | <b>G7</b>        | Group of Seven intergovernmental forum          |
| <b>CO<sub>2</sub></b>    | carbon dioxide  | <b>GEC Model</b> | Global Climate and Energy Model                 |
| <b>CO<sub>2</sub>-eq</b> | carbon dioxide equivalent   | <b>GHG</b>       | greenhouse gas                                  |
| <b>COP28</b>             | 28th Conference of the Parties to the United Nations Framework Convention on Climate Change | <b>GHGRP</b>     | Greenhouse Gas Reporting Program                |
| <b>CRMA</b>              | Critical Raw Materials Act  | <b>GISTM</b>     | Global Industry Standard on Tailings Management |
| <b>CSDDD</b>             | Corporate Sustainability Due Diligence Directive  | <b>GM</b>        | General Motors                                  |
| <b>CSRD</b>              | Corporate Sustainability Reporting Directive  | <b>HALEU</b>     | high-assay low-enriched uranium                 |
| <b>CTP</b>               | cell-to-pack  | <b>HDPE</b>      | high-density polyethylene                       |
| <b>DFC</b>               | International Development Finance Corporation   | <b>HMS</b>       | heavy mineral sand                              |
| <b>DFI</b>               | development finance institutions  | <b>HPAL</b>      | high-pressure acid leaching                     |
| <b>DLA</b>               | Defense Logistics Agency  | <b>HPMS</b>      | Hydrogen Processing of Magnet Scrap             |
| <b>DoD</b>               | Department of Defense   | <b>HREE</b>      | heavy rare earth elements                       |
| <b>DOE</b>               | Department of Energy  | <b>HVDC</b>      | high-voltage direct current                     |

|                |  |                |  |
|----------------|--|----------------|--|
| <b>IAC</b>     | ionic adsorption clay                                | <b>MIDA</b>    | Malaysian Investment Development Authority             |
| <b>IAD</b>     | ionic adsorption deposit                             | <b>MoU</b>     | memorandum of understanding                            |
| <b>ICE</b>     | internal combustion engine                           | <b>MSP</b>     | Minerals Security Partnership                          |
| <b>ICMM</b>    | International Council on Mining and Materials        | <b>Na-ion</b>  | Sodium-ion   |
| <b>IEA</b>     | International Energy Agency                          | <b>NCA</b>     | nickel cobalt aluminium                                |
| <b>IOSCO</b>   | International Organization of Securities Commissions | <b>NDC</b>     | Nationally Determined Contributions                    |
| <b>IPCC</b>    | Intergovernmental Panel on Climate Change            | <b>NdFeB</b>   | neodymium iron boron                                   |
| <b>IRA</b>     | Inflation Reduction Act                              | <b>NMC</b>     | nickel manganese cobalt                                |
| <b>IRMA</b>    | Initiative for Responsible Mining Assurance          | <b>NPI</b>     | nickel pig iron  |
| <b>KEXIM</b>   | Korea Export-Import Bank                             | <b>NZE</b>     | Net Zero Emissions By 2050 Scenario                    |
| <b>KFM</b>     | Kisanfu copper-cobalt mine                           | <b>OECD</b>    | Organisation For Economic Co-operation and Development |
| <b>KIO</b>     | Kachin Independence Organisation                     | <b>OEM</b>     | original equipment manufacturer                        |
| <b>Korea</b>   | Republic of Korea                                    | <b>OSBF</b>    | oxygen-rich side blowing furnace                       |
| <b>LAC</b>     | Latin America  | <b>OTC</b>     | over-the-counter                                       |
| <b>LCE</b>     | lithium carbonate equivalent                         | <b>PAL</b>     | pressure acid leaching                                 |
| <b>LDV</b>     | light-duty vehicle                                   | <b>PEM</b>     | proton exchange membrane                               |
| <b>LFP</b>     | lithium iron phosphate                               | <b>PEX</b>     | polyethylene   |
| <b>LIBS</b>    | laser-induced breakdown                              | <b>PGMs</b>    | platinum group metals                                  |
| <b>LME</b>     | London Metal Exchange                                | <b>PHEV</b>    | plug-in hybrid electric vehicles                       |
| <b>LMFP</b>    | lithium manganese iron phosphate                     | <b>PIA</b>     | Promotion of Investment Act                            |
| <b>LMR-NMC</b> | lithium-manganese-rich NMC                           | <b>PV</b>      | photovoltaic   |
| <b>LNMO</b>    | lithium nickel manganese oxide                       | <b>PRA</b>     | price reporting agency                                 |
| <b>LPO</b>     | Loan Programs Office                                 | <b>R&amp;D</b> | research and development                               |
| <b>LREE</b>    | light rare earth elements                            | <b>REE</b>     | rare earth elements                                    |
| <b>M&amp;A</b> | mergers and acquisitions                             | <b>REO</b>     | rare earth oxides                                      |
| <b>MAC</b>     | Mining Association of Canada                         | <b>RKEF</b>    | rotary kiln electric furnace                           |
| <b>METC</b>    | Mineral Exploration Tax Credit                       | <b>SGPI</b>    | General Secretariat for Investment                     |
| <b>MHP</b>     | mixed-hydroxide precipitate                          | <b>SHFE</b>    | Shanghai Futures Exchange                              |
|                |  | <b>SIF</b>     | Strategic Innovation Fund                              |



|              |  |
|--------------|--|
| <b>Si-Gr</b> | silicon-doped graphite                                 |
| <b>STEPS</b> | Stated Policies Scenario                               |
| <b>SUV</b>   | sport utility vehicle                                  |
| <b>SWF</b>   | sovereign wealth fund                                  |
| <b>SxEw</b>  | solvent extraction and electrowinning                  |
| <b>TC/RC</b> | spot treatment and refining charge                     |
| <b>TFM</b>   | Tenke Fungurume mine                                   |
| <b>U-235</b> | uranium-235  |
| <b>UK</b>    | United Kingdom   |
| <b>UNFC</b>  | United Nation's Framework Classification for Resources |
| <b>US</b>    | United States  |
| <b>USD</b>   | United States dollar                                   |
| <b>VC</b>    | venture capital  |
| <b>XRF</b>   | X-ray Fluorescence                                     |

## Units of measure

|                         |                           |
|-------------------------|---------------------------|
| <b>bps</b>              | basis points              |
| <b>g CO<sub>2</sub></b> | grammes of carbon dioxide |
| <b>GW</b>               | gigawatt                  |
| <b>GWh</b>              | gigawatt-hour             |
| <b>kg</b>               | kilogramme                |
| <b>km</b>               | kilometre                 |
| <b>km<sup>2</sup></b>   | square kilometre          |
| <b>kt</b>               | kilotonne                 |
| <b>Mt</b>               | million tonnes            |
| <b>Mtpa</b>             | million tonnes per annum  |
| <b>MW</b>               | megawatt                  |
| <b>TWh</b>              | terawatt-hours            |

International Energy Agency (IEA)

This work reflects the views of the IEA Secretariat but does not necessarily reflect those of the IEA's individual member countries or of any particular funder or collaborator. The work does not constitute professional advice on any specific issue or situation. The IEA makes no representation or warranty, express or implied, in respect of the work's contents (including its completeness or accuracy) and shall not be responsible for any use of, or reliance on, the work.



Subject to the IEA's [Notice for CC-licensed Content](#), this work is licenced under a [Creative Commons Attribution 4.0 International Licence](#).

This document and any map included herein are without prejudice to the status of or sovereignty over any territory, to the delimitation of international frontiers and boundaries and to the name of any territory, city or area.

Unless otherwise indicated, all material presented in figures and tables is derived from IEA data and analysis.

IEA Publications  
International Energy Agency  
Website: [www.iea.org](http://www.iea.org)  
Contact information: [www.iea.org/contact](http://www.iea.org/contact)

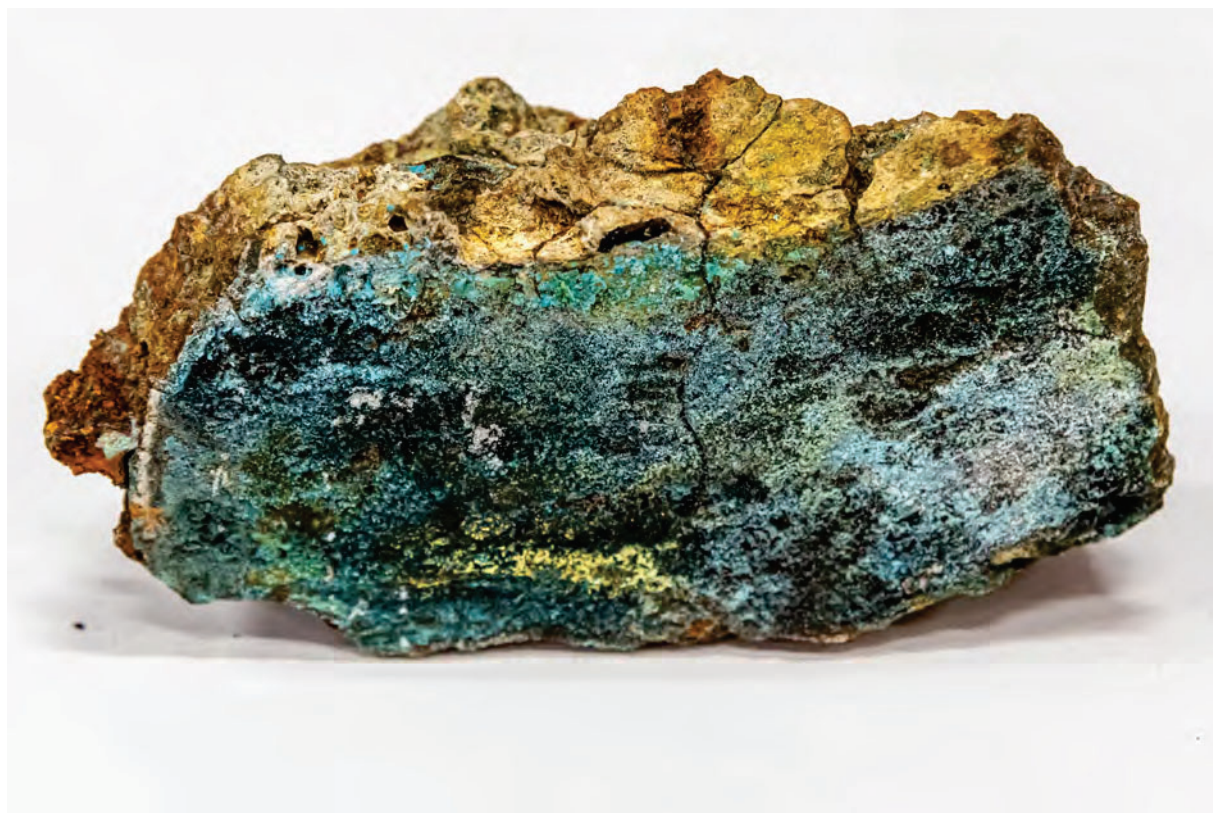
Typeset in France by IEA - May 2024  
Cover design: IEA  
Photo credits: © Shutterstock







OLJEDIREKTORATET



27. januar 2023 |

## Ressursvurdering havbunnsmineraler

Utarbeidet på oppdrag for: Olje- og energidepartementet



## Innholdsfortegnelse

|   |    |
|---|----|
| 1 Sammen drag .....   | 1  |
| 2 Innledning .....  | 5  |
| 2.1 Bakgrunn for Oljedirektoratets arbeid .....                             | 7  |
| 2.2 Forutsetninger for ressursvurderingen .....                             | 7  |
| 2.3 Metalliske mineraler .....  | 7  |
| 2.3.1 Hovedgrupper av metaller .....  | 8  |
| 2.3.2 Global metallutvinning og reserver .....                              | 8  |
| 2.4 EUs behov for kritiske metaller .....                                   | 9  |
| 3 Oljedirektoratets kartleggingsarbeid .....                                | 13 |
| 3.1 Datadekning .....   | 14 |
| 3.2 Dataoppløsning .....  | 22 |
| 4 Geologi og ressurser .....  | 23 |
| 4.1 Sulfidforekomster .....   | 28 |
| 4.1.1 Dannelsen av sulfidforekomster - aktiviteten i aksedalen .....        | 28 |
| 4.1.2 Utbredelsen av sulfidforekomster - prosessene utenfor aksedalen ..... | 30 |
| 4.1.3 Geokjemi og metallgehalt .....  | 33 |
| 4.1.4 Geologisk ressursmodell .....   | 34 |
| 4.1.5 Letemodeller for sulfidforekomster .....                              | 36 |
| 4.1.5.1 Volum .....   | 37 |
| 4.1.5.2 Tetthet .....   | 39 |
| 4.1.5.3 Antall forekomster .....  | 39 |
| 4.1.5.4 Metallgehalter .....  | 42 |
| 4.2 Sulfideksempel Mohnsskatten .....                                       | 44 |
| 4.2.1 Geologi og tektonisk ramme .....                                      | 45 |
| 4.2.2 Geokjemi og undergrunnsmodell .....                                   | 48 |
| 4.3 Skorpeforekomster .....   | 51 |
| 4.3.1 Dannelse av fjellandskapet .....                                      | 51 |
| 4.3.2 Dannelse og vekst av manganskorper .....                              | 54 |
| 4.4 Letemodeller for manganskorper .....                                    | 60 |
| 4.4.1 Volum .....   | 60 |
| 4.4.2 Tetthet .....   | 65 |
| 4.4.3 Metallgehalt .....  | 65 |
| 4.5 Manganskorpe-eksempel sjøfjell nordvest i Grønlandshavet .....          | 65 |
| 5 Metode for beregning av mineralressurser .....                            | 69 |
| 5.1 Modelleringsverktøy .....   | 69 |
| 5.1.1 GeoX .....  | 69 |
| 5.1.2 @RISK .....   | 69 |
| 5.1.3 Ranged Approach to Target and Inventory Estimates .....               | 69 |
| 5.2 Metode for beregning av areal med helning over 20 grader .....          | 70 |
| 5.3 Ressursklassifisering .....   | 71 |
| 5.3.1 Beskrivelse av ressursklassifiseringssystem .....                     | 72 |
| 6 Ressursvurdering .....  | 75 |
| 6.1 Ressursberegning .....  | 75 |
| 6.1.1 Sulfidressurser .....   | 75 |
| 6.1.1.1 Beregningsgrunnlaget .....  | 75 |
| 6.1.1.2 Resultater .....  | 76 |
| 6.1.2 Manganskorpe-ressurser .....  | 77 |
| 6.1.2.1 Beregningsgrunnlaget .....  | 77 |
| 6.1.2.2 Resultater .....  | 78 |
| 6.1.3 Forventede totale ressurser .....                                     | 79 |
| 6.2 Resurser i regneeksemplene Mohnsskatten og Sjøfjell .....               | 80 |
| 6.2.1 Mohnsskattens sulfidressurser .....                                   | 80 |

|   |     |
|---|-----|
| 6.2.2 Sjøfjell manganskorperressurser.....                                    | 81  |
| 6.3 Kunnskapsbehov.....   | 83  |
| 7 Appendiks.....  | 85  |
| 7.1 Andre sulfidforekomster kartlagt av Oljedirektoratet og akademia .....    | 85  |
| 7.1.1 Fåvne .....   | 85  |
| 7.1.1.1 Geologi og tektonisk ramme.....                                       | 85  |
| 7.1.1.2 Geokjemi og undergrunnsmodell .....                                   | 86  |
| 7.1.2 Gnitahai .....  | 87  |
| 7.1.2.1 Geologi og tektonisk ramme.....                                       | 87  |
| 7.1.2.2 Geokjemi og undergrunnsmodell .....                                   | 88  |
| 7.1.3 Lokeslottet.....  | 90  |
| 7.1.3.1 Geologi og tektonisk ramme.....                                       | 90  |
| 7.1.3.2 Geokjemi og undergrunnsmodell .....                                   | 90  |
| 7.2 Tabeller for kaledonske sulfidforekomster .....                           | 92  |
| 7.3 Tabeller for gehalter i manganskorper .....                               | 99  |
| 7.4 Ressurstabeller for letemodeller og delområder .....                      | 103 |
| 7.5 Nærmere om metaller - beskrivelse, utvinning, reserver og ressurser ..... | 105 |
| 7.5.1 Basemetaller.....   | 106 |
| 7.5.2 Edelmetaller .....  | 106 |
| 7.5.3 Spesialmetaller.....  | 107 |
| 7.5.4 Jern, titan og jernlegering.....  | 110 |
| 7.5.5 Andre metaller.....   | 111 |
| 8 Ordliste .....  | 115 |
| 9 Referanser .....  | 119 |

## Figurer

|  |    |
|--|----|
| 2.1 Påviste sulfid- og manganskorpeforekomster.....                                  | 6  |
| 2.2 EU strømmer av innsatsvarer .....  | 10 |
| 3.1 Oversikt over ODs egenopererte tokt og samarbeidstokt i perioden 1999-2021 ..... | 15 |
| 3.2 ODs egenopererte kartlegging ved Mohnsryggen i 2018 .....                        | 17 |
| 3.3 ODs egenopererte kartlegging ved Mohnsryggen i 2019 .....                        | 18 |
| 3.4 ODs borekampanje i 2020 .....  | 19 |
| 3.5 ODs kartlegging ved Knipovitsryggen i 2021 .....                                 | 20 |
| 3.6 Oversikt over dybde data OD har tilgang til .....                                | 21 |
| 4.1 Geologiske hovedtrekk i Nord-Atlanteren .....                                    | 23 |
| 4.2 Havbunns spredningen langs Mohnsryggen.....                                      | 24 |
| 4.3 Havbunns spredningen mellom Norge og Grønland .....                              | 26 |
| 4.4 Snitt av sulfidprøve .....   | 28 |
| 4.5 Geologisk ramme for sulfidforekomster .....                                      | 29 |
| 4.6 Tektonisk ramme for Mohnsryggens aksedal .....                                   | 30 |
| 4.7 Mohnsryggens flankevidder .....  | 31 |
| 4.8 Sedimentfordeling på havbunnen .....   | 32 |
| 4.9 Prospektive arealer for modellering av sulfidforekomster .....                   | 33 |
| 4.10 Geologisk modell for sulfidforekomst.....                                       | 35 |
| 4.11 TAG sulfidforekomst .....   | 35 |
| 4.12 TAG blokkmodell.....  | 36 |
| 4.13 TAG tonnasjeberegning .....   | 36 |
| 4.14 Oversikt over grunnstoff analysert for i sulfidvurderingene.....                | 42 |
| 4.15 Mohnskattens (og Lokeslottets) beliggenhet.....                                 | 45 |
| 4.16 Forkastningsskrenten ved Mohnskatten.....                                       | 46 |
| 4.17 Mohnskattens beliggenhet i skrenten.....  | 47 |
| 4.18 Mohnskatt-teigens A- og B-områder.....  | 47 |
| 4.19 Mohnskatten med soneinndeling .....   | 48 |
| 4.20 Mohnskatten Modell 1.....   | 49 |
| 4.21 Mohnskatten Modell 2.....   | 49 |
| 4.22 Mohnskattens dimensjoner .....  | 50 |
| 4.23 Regionale fjellområder i Norskehavet og Grønlandshavet .....                    | 52 |
| 4.24 Manganskorpe fra Vøringutstikkeren .....  | 55 |
| 4.25 Marine istidsvifter i Norskehavet og Grønlandshavet .....                       | 57 |
| 4.26 Havstrømmer i Norskehavet og Grønlandshavet.....                                | 58 |
| 4.27 Oversikt over grunnstoff analysert for i manganskorpe-vurderingene .....        | 59 |
| 4.28 Regionale områder for beregning av manganskorper .....                          | 61 |
| 4.29 Data brukt i arealberegningene.....   | 63 |
| 4.30 Sjøfjell beliggende nordvest i Grønlandshavet .....                             | 66 |
| 5.1 FNs rammeverk for ressursklassifisering.....                                     | 72 |
| 5.2 CRIRSCO klassifisering .....   | 72 |
| 6.1 Område for ressursberegning for sulfider .....                                   | 75 |
| 6.2 Område for ressursberegning for manganskorper .....                              | 75 |
| 6.3 Sannsynlighetsfordeling for total mengde kobber .....                            | 77 |
| 6.4 Sannsynlighetsfordeling for total mengde sink .....                              | 77 |
| 6.5 Sannsynlighetsfordeling for total mengde kobolt.....                             | 77 |
| 6.6 Sannsynlighetsfordeling for total mengde sølv .....                              | 77 |
| 6.7 Sannsynlighetsfordeling for total mengde gull .....                              | 77 |
| 6.8 Forventning tilstedeværende metallressurser.....                                 | 79 |
| 7.1 Fåvne og Gnitahai sine beliggenheter .....                                       | 85 |



|                                   |    |
|-----------------------------------|----|
| 7.2 Perspektivkart av Fåvne ..... | 86 |
| 7.3 Fåvne modellsnitt .....       | 87 |
| 7.4 Gnitahai modell 1 .....       | 89 |
| 7.5 Gnitahai modell 2 .....       | 89 |
| 7.6 Lokeslottet .....             | 90 |
| 7.7 Lokeslottet Modell 1 .....    | 91 |
| 7.8 Lokeslottet Modell 2 .....    | 91 |

## Tabeller

|   |     |
|---|-----|
| 2.1 Sjeldne jordarter (REE) .....   | 8   |
| 2.2 Global utvinning og reserver av utvalgte metalliske mineraler .....                                       | 9   |
| 2.3 EU kritiske innsatsvarer 2020 .....   | 10  |
| 3.1 Kartleggingsverktøy .....   | 13  |
| 3.2 Oversikt over datatyper der OD har vært delaktig eller har utført kartlegging selv .....                  | 13  |
| 3.3 Detaljer fra ODs egenopererte AUV- og ROV-kartleggingstokt.....   | 14  |
| 4.1 Volumtall for modellering av sulfidforekomster - aksialforekomster .....                                  | 38  |
| 4.2 Volumtall for modellering av sulfidforekomster - flankeforekomster.....                                   | 39  |
| 4.3 Tetthet for modellering av sulfidforekomster.....   | 39  |
| 4.4 Prospektive arealer, modellering av sulfidforekomster .....   | 41  |
| 4.5 Antall forekomster i hvert delareal, modellering av sulfidforekomster .....                               | 41  |
| 4.6 Sum antall forekomster, modellering av sulfidforekomster.....   | 42  |
| 4.7 Aksialmodell, metallgehalt .....  | 44  |
| 4.8 Gruntvannsmodell, metallgehalt.....   | 44  |
| 4.9 Flankemodell med Co, metallgehalt .....   | 44  |
| 4.10 Flankemodell uten Co, metallgehalt.....  | 44  |
| 4.11 Estimert areal på skråninger over 20 grader .....  | 63  |
| 4.12 Oversikt over gjennomsnittlige tykkelsesvariasjoner for manganskorper per regionale område .....         | 64  |
| 4.13 Tetthet (tørr) brukt i modellering av skorpeforekomster .....  | 65  |
| 4.14 Spredning i modellert areal for sjøfjell nordvest i Grønlandshavet.....                                  | 67  |
| 5.1 Beskrivelse av UNFC-kategoriene G1 til G4 .....   | 73  |
| 6.1 Totale mengder metaller i alle sulfid letemodeller.....   | 76  |
| 6.2 Totale mengder metaller i manganskorper .....   | 78  |
| 6.3 Totale mengder manganskorper i millioner tonn, fordelt på delområde .....                                 | 79  |
| 6.4 Gehaltstatistikk over utvalgte gehalter i Mohnsskatten .....  | 81  |
| 6.5 Dimensjoner og beregnet sulfid-tonnasje i Mohnsskatten .....  | 81  |
| 6.6 Gehalter og beregnede metall-tonnasjer i Mohnsskatten .....   | 81  |
| 6.7 Forventningsverdier for parametere for sjøfjell i Grønlandshavet .....                                    | 82  |
| 6.8 Beregnet tilstedeværende ressurser på sjøfjell i Grønlandshavet.....                                      | 82  |
| 7.1 Hydrotermale sulfidforekomster i skandinavisk del av den kaledonske fjellkjeden; mulige SMS-analoger..... | 92  |
| 7.2 Kaledonske sulfidmalmforekomster gruppert som i Tabell 7.1. Gjennomsnittstall pr gruppe .....             | 96  |
| 7.3 Tall fra Tabell 1 i Hannington et al. (2010). Kun tall fra midt-oseanrygger er tatt med.....              | 98  |
| 7.4 Gehalter for Jan Mayen-ryggen.....  | 99  |
| 7.5 Gehalter for Ægirbassenget og Jan Mayen-trauet.....   | 100 |
| 7.6 Gehalter for Vøringutstikkeren .....  | 100 |
| 7.7 Gehalter for Lofoten Basin Seamount .....   | 101 |
| 7.8 Gehalter for Greenland Basin Seamount/Greenland Sea East .....  | 102 |
| 7.9 Gehalter for Greenland Sea West.....  | 102 |
| 7.10 Metallmengder i flankemodellen .....   | 103 |
| 7.11 Metallmengder i aksialmodellen .....   | 103 |
| 7.12 Metallmengder i gruntvannsmodellen .....   | 103 |
| 7.13 Skorperessurser på Mohnsryggen .....   | 103 |
| 7.14 Skorperessurser på Knipovitsjryggen.....   | 104 |
| 7.15 Skorperessurser på Jan Mayen-ryggen.....   | 104 |
| 7.16 Skorperessurser på Vøringutstikkeren.....  | 105 |



## 1 Sammendrag

Det har lenge vært kjent at verdenshavens store dyp inneholder forekomster av metalliske mineraler. Noen steder er forekomstene av en størrelse som kan være økonomisk drivverdig.

Mineralforekomster på havbunnen deles i tre typer; mangannoduler, manganskorper og sulfider. Alle de tre typene inneholder flere metaller (er polymetalliske) og de ligger på store dyp, hovedsakelig mellom 1500 og 6000 meter. På norsk sokkel er det funnet manganskorper og sulfider. Mangannoduler på havbunnen er ikke påvist. Vi har for denne rapporten antatt at forutsetningene ikke er tilstede for dannelse av mangannoduler på grunn av høy sedimentasjonsrate. Mangannoduler er derfor ikke inkludert i ressursvurderingen.

Bergverksdrift har spilt en viktig rolle i norsk næringsliv siden begynnelsen av 1600-tallet, og er blant de eldste eksportindustriene i landet. Dypmarine sulfidforekomster (SMS - Seabed Massive Sulphides) er sagt å være moderne analoger til landbaserte vulkanogene massive sulfidforekomster (VMS). Flesteparten av kobbersulfidgruvene i Norge har startet sitt liv som skorsteiner på havbunnen.

Oljedirektoratet (OD) har siden 2011 gjennomført datainnsamling i dypvannsområder i Norskehavet og Grønlandshavet i samarbeid med Universitetet i Bergen (UiB), og fra 2020 også i samarbeid med Universitetet i Tromsø (UiT). Data fra ODs kartleggingstokt og samarbeid med vitenskapelige institusjoner er grunnlag for denne ressursvurderingen.

For sulfidforekomster kan kunnskapen om påviste forekomster ekstrapoleres. Det er mange flere inaktive enn aktive forekomster på norsk sokkel. Kunnskap om aktive forekomster er en forutsetning for utforskning av inaktive forekomster. For manganskorper vil havbunnstopografi og alder på underliggende bergarter ha stor betydning for tykkelsen på manganskorpene og dermed for ressursvurderingen.

ODs ressursvurdering spenner opp et utfallsrom for hvor store de tilstedeværende mineralressursene i utredningsområdet kan være. Tilstedeværende ressurser er ressurser som er påvist eller antatt å være tilstede. En del av de tilstedeværende ressursene vil kunne være utvinnbare. Mengden utvinnbare ressurser avhenger av teknologi og økonomi. Det er så langt for lite kunnskap om utvinningsteknologi og utbyggingsløsninger til at det er hensiktsmessig å vurdere malmer og estimere utvinningsgrad.

For sulfider er forventningsverdier for samlede tilstedeværende ressurser:

### Forventningsverdier for samlede ressurser for sulfider

| Metall | Mengde (i tonn) |
|--------|-----------------|
| Kobber | 38 100 000      |
| Sink   | 45 000 000      |
| Gull   | 2 317           |
| Sølv   | 85 200          |
| Kobolt | 1 000 000       |

Mohnsskatten er modellert som et regneeksempel, med forventede tilstedeværende ressurser gitt i tabellen nedenfor. Gjennomsnittlig forekomststørrelse for sulfider er: 40 000 tonn kobber, 47 100 tonn sink, 2,4 tonn gull og 89,3 tonn sølv. Forekomster i flankemodellen er betydelig større enn for aksial- og gruntvannsmodellen.

**Forventet ressurstall for en utvalgt sulfidforekomst, Mohnsskatten, modellert som et regneeksempel**

| Metall | Mengde (i tonn) |
|--------|-----------------|
| Kobber | 20 332          |
| Sink   | 60 326          |
| Gull   | 6               |
| Sølv   | 145             |
| Kobolt | 313             |

Prospektivt areal for manganskorpe er anslått å dekke i overkant av 8 500 km<sup>2</sup> av utredningsområdet, med en forventningsverdi for samlede tilstedeværende ressurser på:

**Forventningsverdier for samlede ressurser for manganskorper**

| Metall     | Mengde (i tonn) |
|------------|-----------------|
| Mangan     | 185 000 000     |
| Titan      | 8 400 000       |
| Magnesium  | 24 100 000      |
| Litium     | 229 300         |
| Vanadium   | 1 918 800       |
| Kobolt     | 3 058 100       |
| Niob       | 73 000          |
| Hafnium    | 14 700          |
| Wolfram    | 80 300          |
| Gallium    | 19 200          |
| Scandium   | 55 800          |
| Yttrium    | 300 900         |
| Lantan     | 368 800         |
| Cerium     | 1 681 200       |
| Praseodym  | 102 500         |
| Neodym     | 420 300         |
| Europium   | 23 200          |
| Gadolinium | 99 900          |
| Terbium    | 15 200          |
| Dysprosium | 86 400          |

Et regneeksempelet på et sjøfjell i Grønlandshavet på 133 km<sup>2</sup> forventes å ha ressurstill på:

**Forventet ressurstill for et sjøfjell i Grønlandshavet, modellert som et regneeksempel**

| Metall     | Mengde (i tonn) |
|------------|-----------------|
| Mangan     | 6 900 000       |
| Titan      | 270 000         |
| Magnesium  | 820 000         |
| Litium     | 9 346           |
| Vanadium   | 79 080          |
| Kobolt     | 131 586         |
| Niob       | 2 913           |
| Hafnium    | 611             |
| Wolfram    | 3 414           |
| Gallium    | 756             |
| Scandium   | 2 368           |
| Yttrium    | 12 399          |
| Lantan     | 14 475          |
| Cerium     | 71 655          |
| Praseodym  | 4 067           |
| Neodym     | 16 600          |
| Europium   | 926             |
| Gadolinium | 4 053           |
| Terbium    | 614             |
| Dysprosium | 3 519           |

OD vurderer at at de tilstedeværende ressursene er betydelige. For flere av metallene tilsvarer ressursene mange år med global utvinning. De modellerte mengdene er metallinnhold - ikke oksider eller sulfider.

Ressursvurderingen gir en første, samlet vurdering av havbunnsmineraler i utredningsområdet. Datagrunnlaget kan videre styrkes og metodikk for ressursmodellering videreutvikles. Teknologiutvikling, sammen med mer og bedre data, vil forbedre forståelsen av ressurspotensialet og dermed også kvantifiseringen av usikkerheten i ressursanslagene, og gi mulighet for å flytte ressurser til mer modne ressursklasser.



## 2 Innledning

Det har lenge vært kjent at verdenshavenes store dyp inneholder forekomster av metalliske mineraler. Noen steder er forekomstene av en størrelse som kan være økonomisk drivverdig. Interessen for slike forekomster var en av de viktigste drivkreftene for å forhandle fram Havrettstraktaten i årene 1973-1982, der rettighetene til disse ble regulert.

FNs havrettskonvensjon sier at en kyststat har suverene rettigheter til ressursene på og under havbunnen på landets kontinentalmargin, i hele dens utstrekning – også der kontinentalmarginen strekker seg utover 200 nautiske mil. Havrettskonvensjonen definerer dette området som kyststatens kontinentalsokkel.

Mineralforekomstene deles inn i tre typer; mangannoduler, manganskorper og sulfider. Alle sammen inneholder flere slags metaller (polymetalliske) og de ligger på store dyp, hovedsakelig mellom 1500 og 6000 meter.

- Mangannoduler ligger på bløt bunn på de store havdypene. De inneholder mye mangan og jern med mindre mengder kobber, nikkel, kobolt, titan og platina.
- Manganskorpene inneholder også mest mangan og jern og mindre mengder titan, kobolt, nikkel, cerium, zirkonium og sjeldne jordarter (REE - Rare Earth Elements). Disse vokser som laminerte belegg på fast fjell der det stikker opp på havbunnen, typisk på dyp mellom 1500 og 3000 meter.
- Sulfidene inneholder hovedsakelig bly, sink, kobber, kobolt, gull og sølv. De er knyttet til varme kilder på verdenshavenes vulkanske spredningsrygger der det dannes «svarte skorsteiner» («Black Smokers»). Slike svarte skorsteiner er aktive i noen tusen år før de dør ut og etterlater seg «sulfidhauger» (mounds). Hovedmengden av sulfidmalmressursene ligger i disse haugene.

På norsk sokkel er det funnet manganskorper og sulfider, se [Fig. 2.1](#). Mangannoduler på havbunnen er ikke påvist. Vi har for denne rapporten antatt at forutsetningene ikke er tilstede for dannelse av mangannoduler på grunn av for høy sedimentasjonsrate. Mangannoduler er derfor ikke inkludert i ressursvurderingen.



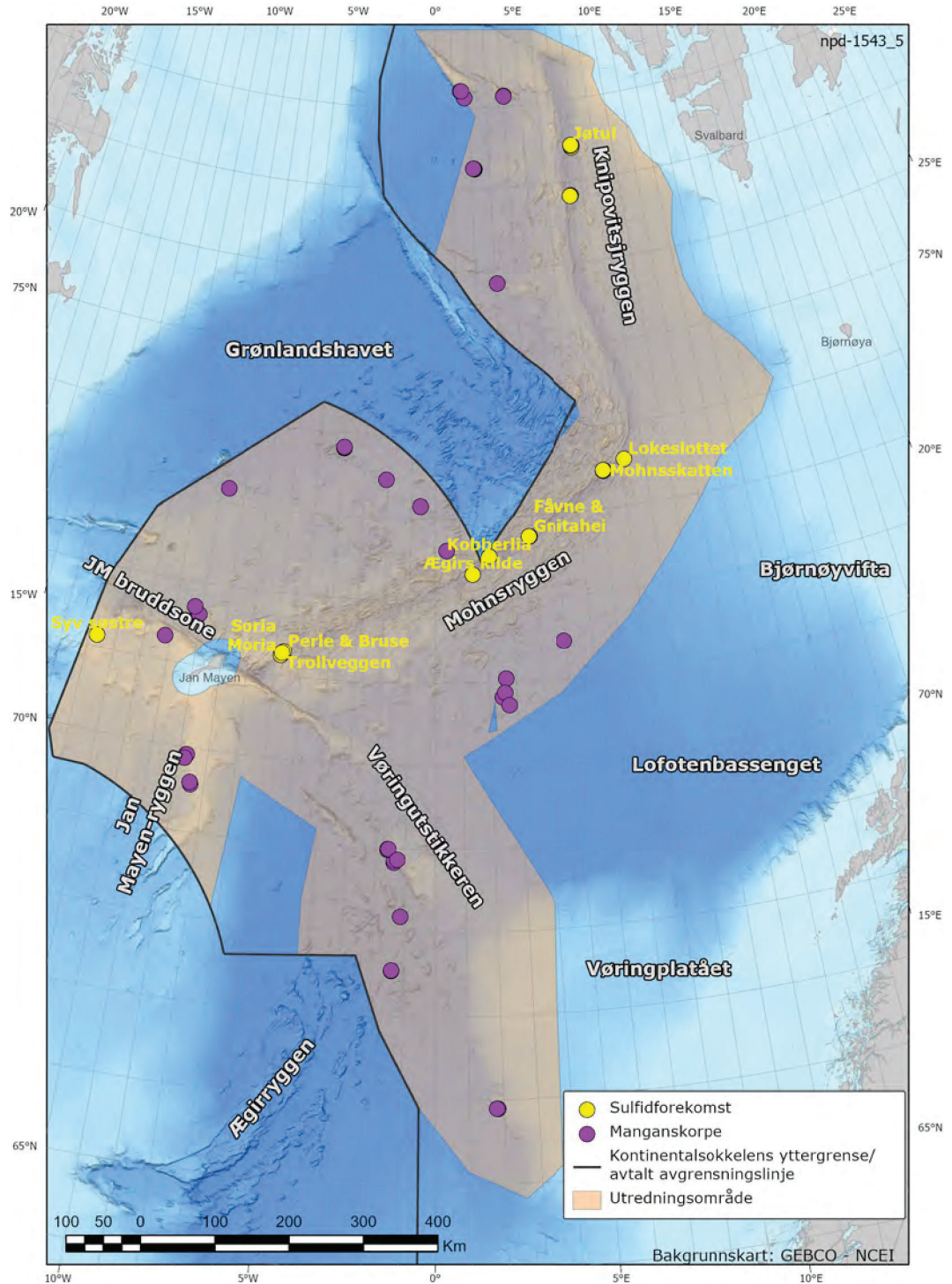


**Fig. 2.1 Påviste sulfid- og manganskorpeforekomster**

Kart over Norskehavet og Grønlandshavet med påviste hydrotermale sulfidforekomster. Kartet viser også påviste manganskorpe-lokaliteter fra samarbeidstokt mellom Universitetet i Bergen og Oljedirektoratet.

Ifølge Hein et al. (2013) har den økonomiske interessen for de ulike forekomstene ofte dreid seg om nikkel-kobber-mangan (Ni-Cu-Mn) for mangannoduler, kobolt-nikkel-mangan (Co-Ni-Mn) for manganskorpe og kobber-sink-gull-sølv (Cu-Zn-Au-Ag) for sulfidforekomster. Sjeldne jordartene (REE) i skorpeforekomster kan også være mulige produkter fra disse.

## 2.1 Bakgrunn for Oljedirektoratets arbeid

Olje- og energidepartementet igangsatte, i medhold av havbunnsmineralloven, våren 2020 en åpningsprosess for mineralvirksomhet på norsk kontinentalsokkel. Oljedirektoratet (OD) er gitt i oppdrag å kartlegge de kommersielt mest interessante mineralforekomstene på norsk kontinentalsokkel, og på basis av kartleggingen utarbeide en vurdering av ressurspotensialet. Ressursvurderingen vil inngå som egen del av beslutningsgrunnlaget for åpning av områder for mineralvirksomhet.

## 2.2 Forutsetninger for ressursvurderingen

Det finnes per i dag ingen spesifikk, akseptert og utbredt modell for ressursvurdering av havbunnsmineraler. ODs ressursvurdering baseres på ODs kartleggingstokt supplert med andre data og vitenskapelig arbeid.

For forekomster av sulfider og skorper hvor det er hentet opp prøver, vil man ha et mineralogisk og geologisk utgangspunkt for ressursvurdering av påviste forekomster. For sulfider kan kunnskapen om påviste forekomster ekstrapoleres langs spredningsaksen og ressurser modelleres for områder med forventet tilsvarende geologiske forutsetninger<sup>1</sup>. I tillegg kan modellerte forekomster ut fra spredningsaksen inkluderes i ressursvurderingen. Det er mange flere inaktive enn aktive forekomster på norsk sokkel. Kunnskap om aktive forekomster er en forutsetning for utforskning av inaktive forekomster. Parametere for den enkelte forekomst, frekvens/avstand mellom forekomster og tykkelse på sedimentoverdekning vil ha stor betydning for ressursvurderingen for sulfider.

For manganskorper vil havbunnstopografi og alder på underliggende bergarter ha stor betydning for tykkelsen på manganskorperne og dermed for ressursvurderingen.

ODs ressursvurdering spenner opp et utfallsrom for hvor store de tilstedeværende mineralressursene i utredningsområdet kan være. Tilstedeværende ressurser er ressurser som er påvist eller antatt å være tilstede. En del av de tilstedeværende ressursene vil kunne være utvinnbare. Mengden utvinnbare ressurser avhenger av teknologi og økonomi. Det er så langt for lite kunnskap om utvinningsteknologi og utbyggingsløsninger til at det er hensiktsmessig å vurdere malmer og estimere utvinningsgrad.

## 2.3 Metalliske mineraler

Norges geologiske undersøkelse (NGU, 2023) beskriver at bergverksdrift har spilt en viktig rolle i norsk næringsliv siden begynnelsen av 1600-tallet, og er blant de eldste eksportindustriene i landet. Norge har tradisjoner i gruvedrift på en del metaller, som kobber, sink, jern, titan, gull, sølv, bly, niob, vanadium, kobolt og nikkel. Kun titan og jern utvinnes i dag<sup>2</sup>.

Mineralutvinning på land i Norge i dag deles etter Direktoratet for mineralforvaltning sin kategorisering (DMF, 2022) i fem mineralgrupper – byggeråstoff, industrimineral, metallisk malm, naturstein og energimineral. Det ble solgt mineraler for 12 867 millioner kroner i 2021. Byggeråstoff var størst med drøyt 54 pst. av den totale salgsværdien, mens industrimineral, metallisk malm, naturstein og energimineral utgjorde hhv. 16 pst., 21

pst., 8 pst. og <1 pst. av total salgsverdi. Eksportverdien på 6 245 millioner kroner utgjorde nesten halvparten av den totale salgsverdien. Mineralnæringen sysselsatte 4 436 årsverk i 2021.

For mineralressurser på land er Direktoratet for mineralforvaltning med Bergmesteren for Svalbard forvalter av råstoffene og for leting og utvinning, mens Norges geologiske undersøkelse er forvalter av geologiske databaser og kunnskap om ressurser i bakken.

Metallisk malm er en betegnelse på bergarter som inneholder metaller med en egenvekt på over 5 gram/cm<sup>3</sup> (Gvein, Rui og Dahl, 2022). For at en forekomst skal kunne defineres som en malm må det være en naturlig forekommende, økonomisk brytbar konsentrasjon av et mineral som kan brukes til metallfremstilling (NGU, 2023).

### 2.3.1 Hovedgrupper av metaller

Metalliske mineraler inneholder metaller. Metaller defineres kjemisk som elementer/ grunnstoff som lett avgir elektroner (danner positive ioner), og danner metallbindinger (NGU, 2023). En enklere definisjon er at metaller er skinnende, duktile (myke og bøyelige), smibare og gode elektriske ledere. Metalliske malmer opptrer vanligvis i form av oksider (bundet til oksygen) eller sulfider (bundet til svovel og oksygen), og deles av NGU inn i følgende hovedgrupper:

- Basemetaller (kobber, sink, bly, arsen, antimon, vismut og tinn)
- Edelmetaller (gull, sølv og platinagruppens elementer)
- Spesialmetaller (niob, tantal, hafnium, beryllium, litium, yttrium, scandium og sjeldne jordartselementer)
- Jern, titan og jernlegeringsmetaller (jern, mangan, titan, krom, nikkel, kobolt, vanadium, molybden og wolfram)
- Energimetaller (uran og thorium)
- Andre metaller (Cs, Ga, Ge, In, Cd, Hg, Re, Rb, Se, Si, Sr, S, Te, Tl, Zr, Al, Mg og metalliske elementer med andre bruksområder enn til metallformål: Ba, K, Ca, Na, Rb).

**Tab. 2.1 Sjeldne jordarter (REE)**

Sjeldne jordarter er en samlebetegnelse for grunnstoffene scandium og yttrium i gruppe 3 i periodesystemet, i tillegg til de 15 lantanoidene. Alle de sjeldne jordartene er metaller. De sjeldne jordartene er (i stigende rekkefølge etter atomnummer): scandium, yttrium, lantan, cerium, praseodym, neodym, promethium, samarium, europium, gadolinium, terbium, dysprosium, holmium, erbium, thulium, ytterbium og lutetium. Betegnelsen kommer av at man lenge mente at disse grunnstoffene kun finnes i små og vanskelig tilgjengelige mengder i naturen. For de fleste gjelder dette fremdeles, men noen av dem, for eksempel yttrium, cerium, lantan og neodym, forekommer i større mengde i jordskorpen enn for eksempel bly. Sjeldne jordarter brukes som legering- eller dopingstoffer i teknologiske materialer og elektronikk for å lage materialer med spesifikke ønskede elektriske og magnetiske egenskaper<sup>3</sup>. Gielen, D. and M. Lyons (2022) deler de sjeldne jordartene opp i lette elementer (LREE) og tunge elementer (HREE) basert på atomnummer. Lantan, cerium, praseodym, neodym, promethium, samarium, europium og gadolinium kategoriseres som LREE. Terbium, dysprosium, holmium, erbium, thulium, ytterbium og lutetium kategoriseres som HREE.

### 2.3.2 Global metallutvinning og reserver

U.S. Geological Survey utarbeider årlig publikasjonen Mineral commodity summaries (U. S. Geological Survey, 2022), med oversikt over bl.a. global utvinning og globale reserver for ulike metaller. Tall for utvinning (primærproduksjon) og reserver i 2020 i Tab. 2.2 er i

all hovedsak hentet herfra. Tall for utvinning av sjeldne jordarter er hentet fra Minor Metals Trade Association (MMTA, 2022). Se [7.5 Nærmere om metaller - beskrivelse, utvinning, reserver og ressurser](#) for detaljer og kilder.

**Tab. 2.2 Global utvinning og reserver av utvalgte metalliske mineraler**

| Grunnstoff                       | Global utvinning (tonn) | Globale reserver (tonn)                   |
|----------------------------------|-------------------------|---|
| Kobber (Cu)                      | 20 600 000              | 880 000 000                               |
| Sink (Zn)                        | 12 000 000              | 250 000 000                               |
| Bly (Pb)                         | 4 400 000               | 90 000 000                                |
| Gull (Au)                        | 3 030                   | 54 000                                    |
| Sølv (Ag)                        | 23 500                  | 530 000                                   |
| REE*                             | 240 000                 | 120 000 000                               |
| Yttrium (Y)                      | 8 000-12 000            | >500 000 (Y <sub>2</sub> O <sub>3</sub> ) |
| Scandium (Sc)                    | 2                       |   |
| Litium (Li)                      | 82 500                  | 22 000 000                                |
| Titan (Ti)** (TiO <sub>2</sub> ) | 8 600 000               | 750 000 000                               |
| Kobolt (Co)                      | 142 000                 | 7 600 000                                 |
| Mangan (Mn)                      | 18 900 000              | 1 500 000 000                             |
| Vanadium (V)                     | 105 000                 | 24 000 000                                |
| Magnesium (Mg)                   | 1 000 000               | Tilnærmet uendelig og vidt spredt         |
| Niob (Nb)                        | 67 700                  | 17 000 000                                |
| Hafnium (Hf)                     |                         |   |
| Wolfram (W)                      | 78 400                  | 3 700 000                                 |
| Gallium (Ga)                     | 327                     |   |
| Lantan (La)                      | 12 500                  | 6 000 000                                 |
| Cerium (Ce)                      | 24 000                  |   |
| Praseodym (Pr)                   | 2 500                   | 2 000 000                                 |
| Neodym (Nd)                      | 35 000                  | 8 000 000                                 |
| Europium (Eu)                    | 270                     |   |
| Gadolinium (Gd)                  | 7 500                   | 1 000 000                                 |
| Terbium (Tb)                     | 10                      |   |
| Dysprosium (Dy)                  | 2 500                   |   |

\* Tonn REO - Rare Earth Oxide, \*\* Titandioksid fra ilmenitt og rutil

## 2.4 EUs behov for kritiske metaller

Europakommisjonen (Kommisjonen) presenterte sist i 2020 sin oversikt over kritiske innsatsvarer, herunder kritiske metaller (European Commission, 2020a). Oversikten oppdateres hvert tredje år, og følges også av en fremskrivning av behovet for kritiske innsatsvarer i 2030 og 2050.

Økonomisk betydning og forsyningsrisiko er hovedkriterier for å fastsette kritikalitet for EU. Økonomisk betydning ser i detalj på hvor viktig enkelte innsatsvarer er for industriell fremstilling av sluttprodukter. Forsyningsrisiko ser på geografisk konsentrasjon i utvinning



og forsyning til EU, styresett i leverandørland inkl. miljøspørsmål, muligheter for resirkulering og gjenbruk som alternativ, substitusjon, EUs importavhengighet og handelsrestriksjoner i tredjeland.

Kommisjonens liste for 2020 inneholder 30 innsatsvarer, sammenlignet med 14 i 2011, 20 i 2014 og 27 i 2017. Bauksitt, litium, titan og strontium er nye på 2020-listen. Helium tas ut, mens nikkel overvåkes utenfor listen pga. økt etterspørsel som innsatsvare for batterier.

**Tab. 2.3 EU kritiske innsatsvarer 2020**

|           |                   |                          |                          |                         |
|-----------|-------------------|--------------------------|--------------------------|-------------------------|
| antimon   | <b>bauksitt</b>   | barytt                   | beryllium                | bor                     |
| flusspat  | fosfatstein       | fosfor                   | gallium                  | germanium               |
| grafitt   | hafnium           | indium                   | kobolt                   | <b>litium</b>           |
| magnesium | metallurgisk kull | naturgummi               | niob                     | platinumgruppe metaller |
| scandium  | silisium          | sjeldne jordarter, lette | sjeldne jordarter, tunge | <b>strontium</b>        |
| tantalum  | <b>titan</b>      | vanadium                 | vismut                   | wolfram                 |

Kommisjonens fremskrivning av behovet for kritiske innsatsvarer i 2030 og 2050 beskriver behovet i et 2050 klimanøytralt scenario (European Commission, 2020b). Kommisjonen vektlegger at EUs behov må sees i en global sammenheng, der befolkningsvekst, industrialisering, dekarbonisering av transport, energisystemer og andre industrielle sektorer, økende etterspørsel fra fremvoksende økonomier og nye teknologiske anvendelser, alle medfører økt etterspørsel etter kritiske innsatsvarer. For metaller viser Kommisjonen til OECDs anslag om en etterspørselsvekst på 150 pst. frem til 2060. EU er 75-100 pst. importavhengig for de fleste metaller.

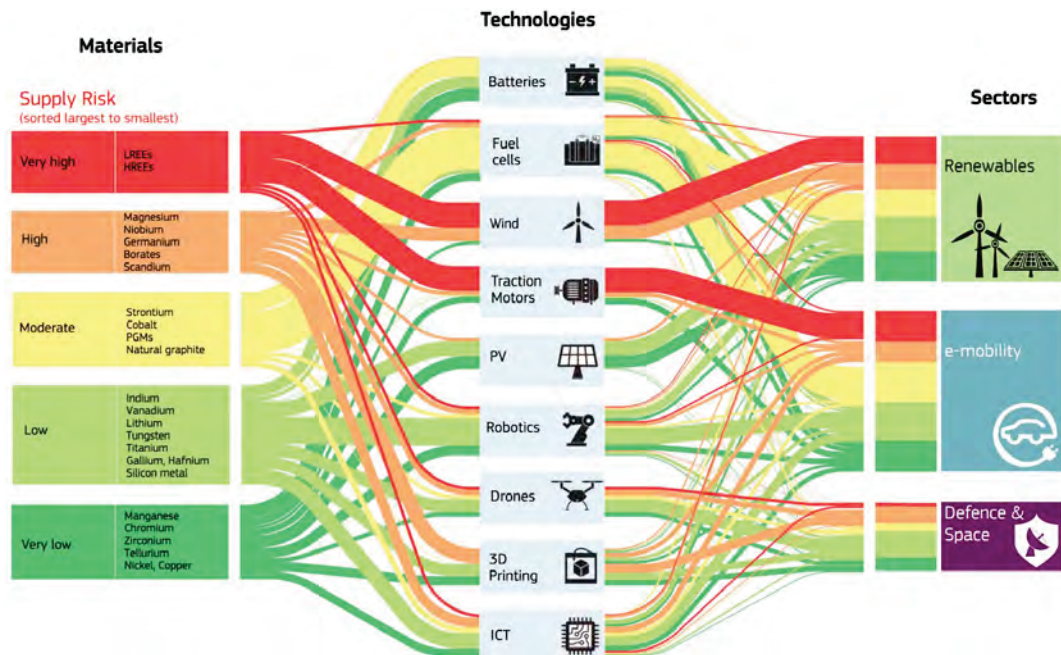


**Fig. 2.2 EU strømmen av innsatsvarer**

Semi-kvantitativ fremstilling av strømmen av innsatsvarer og deres nåværende forsyningsrisiko for ni utvalgte teknologier og tre sektorer. Kilde: Europakommisjonen

- 1 Forekomster på land gir også viktig kunnskap. Dypmarine sulfidforekomstene er sagt å være moderne analoger til landbaserte vulkanogene massive sulfid- (VMS) forekomster. I Norge har mineralutvinning av basemetaller på land historisk vært drevet på VMS-forekomster. Flesteparten av kobbersulfidgruvene i Norge har startet sitt liv som skorsteiner på havbunnen. Det gjelder blant annet gruvene på Løkken og Røros i Trøndelag, og Visnes på Karmøy i Rogaland.
- 2 Per 2015 var det i Norge hovedsakelig drift på jerntitanoksidet ilmenitt (Sokndal, Rogaland) og jernoksidet hematitt (Rana, Nordland). Disse bearbeides til høyt spesialiserte produkter og brukes til andre formål enn metallproduksjon. De siste årene har også vært noe drift på molybden (Knaben, Vest-Agder).
- 3 sjeldne jordarter (2022) i Store norske leksikon på snl.no. Tilgjengelig fra: [https://snl.no/sjeldne\\_jordarter](https://snl.no/sjeldne_jordarter) (Hentet 12. desember 2022).



### 3 Oljedirektoratets kartleggingsarbeid

Oljedirektoratet (OD) sitt kartleggingsarbeid tilknyttet havbunnsmineraler omfatter bruk av en rekke datatyper av både nyere og eldre dato. For eksempel er batymetriske data innsamlet for arbeidet relatert til avgrensing av Norges yttergrenser i 1999/2000 brukt som grunnlagsdata for ODs dedikerte kartleggingsoperasjoner i 2018 og 2019.

En generell fremgangsmåte for ODs kartleggingsarbeid har vært bruk av skipsbasert batymetrisk data-innsamling for å få et overordnet bilde av havbunnen. Deretter har AUV-innsamling blitt utført for å gi et mer detaljert bilde, etterfulgt av ROV-operasjoner for å dokumentere og hente opp prøvemateriale av havbunn. OD har også gjennomført boreoperasjoner på sulfidforekomster ved bruk av kveilerørsteknologi.

**Tab. 3.1 Kartleggingsverktøy**

| Verktøy                             | Forklaring  |
|-------------------------------------|---|
| MBES (Multi Beam Echo Sounder)      | Multistråle ekkolodd som gir topografiske kart over havbunn, også kalt batymetriske data eller dybde-data. Innsamlet fra båt gir dette oppløsning på kart i størrelsesorden 30-100 m. |
| AUV (Autonomous Underwater Vehicle) | Autonome undervannsfarkoster som utfører en rekke målinger både på havbunn og i vannsøylen. Kan også samle inn MBES og da med oppløsning på cm til 1 m.                               |
| ROV (Remotely Operated Vehicle)     | Undervannsrobot som opererer på havbunn og som er styrt fra båten. Kan både utføre målinger og samle inn havbunnsmateriale.   |

Kartleggingstokt som OD har gjennomført har vært basert på anbudsprosesser, hvor internasjonale og nasjonale aktører har utført oppdrag. Samarbeidstoktene med Universitetet i Bergen (UiB) og Universitetet i Tromsø (UiT) har blitt utført gjennom samarbeidsavtaler, hvor Norges forskningsskip har blitt benyttet.

Tab. 3.2 gir informasjon om de ulike datatypene som er benyttet for datainnsamling i forbindelse med ressursvurderingen. De geofysiske dataene som er samlet inn er tilgjengeliggjort og kan bestilles hos OD.

Det arbeides med å systematisere havbunns- og kjernemateriale med mål om at det tilgjengeliggjøres på tilsvarende måte som kjerner fra letebrønner for petroleum.

**Tab. 3.2 Oversikt over datatyper der OD har vært delaktig eller har utført kartlegging selv**

| År/ansvarlig      | Data               | Område             | Tilgjengeliggjort | Oppløsning (MBES) |
|-------------------|--------------------|--------------------|-------------------|-------------------|
| 1999/00 - OD      | MBES (skipsbasert) | Norskehavet        | X                 | Nær 100 m         |
| 2008 - UiB        | MBES (skipsbasert) | Mohnsryggen        | X                 | Nær 100 m         |
| 2010 - OD         | MBES (skipsbasert) | Jan<br>Mayenryggen | X                 | Nær 100 m         |
| 2011 - OD/<br>UiB | ROV                | Jan<br>Mayenryggen |                   |                   |
| 2012 - OD/<br>UiB | ROV                | Jan<br>Mayenryggen |                   |                   |
| 2013 - OD/<br>UiB | MBES (skipsbasert) | Vøringutstikkeren  | X                 | Nær 50 m          |



|                    |  |                 |   |                   |
|--------------------|--|-----------------|---|-------------------|
| 2016 - UiB/<br>OD  | AUV  | Mohnsryggen     | X | 1-2 m             |
| 2017 - UiB/<br>OD  | AUV  | Mohnsryggen     | X | 1 -2m             |
| 2018 – UiB/<br>OD  | MBES (skipsbasert) og ROV-MBES inkl. prøvetaking | Mohnsryggen     | X | Nær 50 m og 1 m   |
| 2018 - OD          | AUV og ROV                                       | Mohnsryggen     | X | 3 cm              |
| 2019 – UiB/<br>UiB | AUV og MBES                                      | Mohnsryggen     | X | 1 m               |
| 2019 - OD          | AUV og ROV                                       | Mohnsryggen     | X | 1 m               |
| 2020 - OD          | Kjerneboring                                     | Mohnsryggen     |   |                   |
| 2020 – UiB/<br>OD  | MBES (skipsbasert)                               | Mohnsryggen     | X | Nær 50 m          |
| 2020 – UiT/<br>OD  | MBES (skipsbasert)                               | Knipovitsryggen | X | Nær 50 m          |
| 2021 - OD          | AUV og ROV                                       | Knipovitsryggen | X | 0,5 m             |
| 2021 – UiT/<br>OD  | MBES (skipsbasert)                               | Knipovitsryggen | X | Nær 50 m          |
| 2021 – UiB/<br>OD  | MBES (skipsbasert) og ROV-MBES inkl. prøvetaking | Mohnsryggen     | X | Nær 50 m og 1-2 m |
| 2022 – UiB/<br>OD  | MBES (skipsbasert) og ROV-MBES inkl. prøvetaking | Mohnsryggen     |   | Nær 50 m og 1-2 m |
| 2022 – UiB/<br>OD  | MBES (skipsbasert) og ROV-MBES inkl. prøvetaking | Knipovitsryggen |   | Nær 50 m og 1-2 m |
| 2022 –<br>Atlab3   | Seismikk og Elektromagnetiske målinger           | Mohnsryggen     |   |                   |

**Tab. 3.3 Detaljer fra ODs egenopererte AUV- og ROV-kartleggingstokt**

| År   | AUV -<br>operativt | Sensor for AUV   | ROV-<br>dykk | Operative<br>døgn | Datamengde<br>innsamlet | Km/<br>dag | Km/<br>dag/<br>AUV |
|------|--------------------|--|--------------|-------------------|-------------------------|------------|--------------------|
| 2018 | 1 Hugin<br>3000    | HiSAS, SSS, SP, Magnetometer (SCM), SBP, MBES, Geokjemi (CH <sub>4</sub> , turbiditet, pH, ORP), Video | 10           | 16 døgn           | 750 km                  | 47         | 47                 |
| 2019 | 3 Hugin<br>6000    | SSS, SP, Magnetometer (SCM), SBP, MBES, Geokjemi (CH <sub>4</sub> , turbiditet, pH, ORP), Video        | 5            | 17 døgn           | 3868 km                 | 227        | 76                 |
| 2021 | 2 Hugin<br>6000    | SSS, SP, Magnetometer (SCM), SBP, MBES, Geokjemi (turbiditet, pH, ORP), Video                          | 4            | 13 døgn           | 2200 km                 | 169        | 85                 |

### 3.1 Datadekning

ODs kartapplikasjon «Deep Sea Surveys» er vist i [Fig. 3.1](#) og gir en geografisk oversikt over kartleggingstoktene som OD har vært involvert i. Dette omfatter multistråle ekkolodds-data (MBES) helt tilbake fra 1999 og fremover i sentrale deler av Norskehavet, deler av Jan Mayen mikrokontinent, Vøringsutstikkeren, Mohnsryggen, deler av Grønlandshavet og Knipovitsryggen.

OD har i senere år prioritert kartlegging over områder som ut ifra dagens kunnskap har størst potensial for interessante mineralforekomster.

Innenfor utredningsområdet er det 280 000 km<sup>2</sup> havbunn som ikke er dekket med skipsbasert MBES-data. Dette tilsvarer 47 pst. av utredningsområdet. I disse områdene er kartgrunnet satellittdata og oppløsningen på kart som viser havbunn i størrelsesorden 200-500 meter.

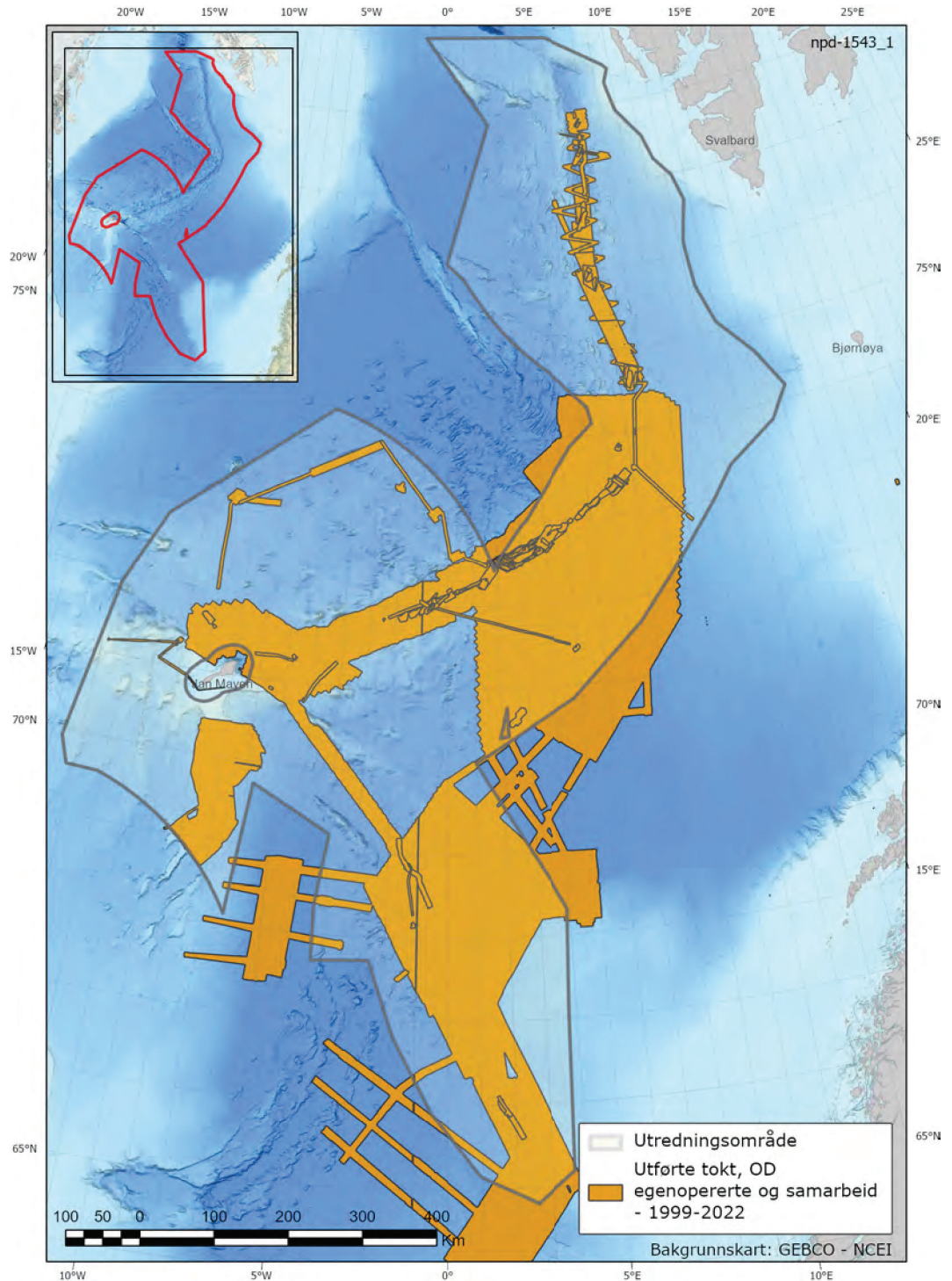


Fig. 3.1 Oversikt over ODs egenopererte tokt og samarbeidstokt i perioden 1999-2021

### Samarbeidstokt med UiB

OD har siden 2011 gjennomført datainnsamling i dypvannsområder i Norskehavet i samarbeid med UiB. Kunnskapsinnhenting både innenfor geologi og biologi har hatt

fokus, i all hovedsak med bruk av forskningsfartøyet G.O. Sars. Materiale fra havbunnen har blitt hentet opp med bruk av Kystdesign Aegir 6000 ROV, og kartlegging av havbunnen har blitt utført med bruk av Kongsberg Maritime Simrad EM 302/710 MBES. Data fra samarbeidstokt med UiB har vært sentrale som grunnlagsdata for gjennomføring av ODs egenopererte tokt ved Mohnsryggen og Knipovitsryggen i 2018-2021.

### **Samarbeidstokt med UiT**

Bedre oppløsning på kartgrunnet for havbunnen ved Knipovitsryggen var nødvendig før OD skulle gjennomføre et større kartleggingstokt med bruk av AUV i 2021. Multistråle-ekkoloddsdata ble hentet inn med forskningsfartøyene Kronprins Haakon og Helmer Hanssen i 2020 og 2021, i samarbeid med UiT. FF Kronprins Haakon er utstyrt med Kongsberg Maritime Simrad EM302/710 MBES og Helmer Hanssen EM302.

Samarbeidstoktene med academia har gitt en bedre forståelse for utbredelsen av mangankorpe og økt kunnskap om sulfidavsetninger på norsk kontinentalsokkel.

### **Samarbeidstokt med Atlab 3**

Kartlegging av lagrekker like under havbunnen var ODs mål med deltakelse i det vitenskapelige prosjektet Atlab 3 i 2022, et prosjekt ledet av Norges teknisk-naturvitenskapelige universitet (NTNU). Geofysiske metoder kjent fra kartlegging av de grunnere deler av kontinentalsokkelen ble tilpasset og testet ut i de dypere deler av sokkelen. En tidlig versjon av Atlab3-data bekrefter de storskala geologiske trekk som ODs geologiske modeller bygger på.

### **ODs egenopererte tokt i 2018**

ODs egenopererte tokt i 2018 var direktoratets første tokt for å kartlegge potensialet for havbunnsmineraler. Kartleggingen ble gjennomført uten samarbeidspartnere, men erfaringer fra tidligere samarbeid med UiB var nyttig for planleggingen. Området som ble valgt ut var en mindre del av Mohnsryggen, og for kartlegging av havbunn ble det benyttet én AUV og én ROV. Oppdragstaker var selskapet Swire Seabed, hvor AUV'en som ble benyttet var Kongsberg Maritime Hugin 3000 og ROV'en var av typen Schilling HD23.

Totalt 750 linjekilometer med AUV-data ble samlet inn, 10 ROV-dykk ble gjennomført og en ny aktiv sulfidforekomst ble funnet, «Fåvne».



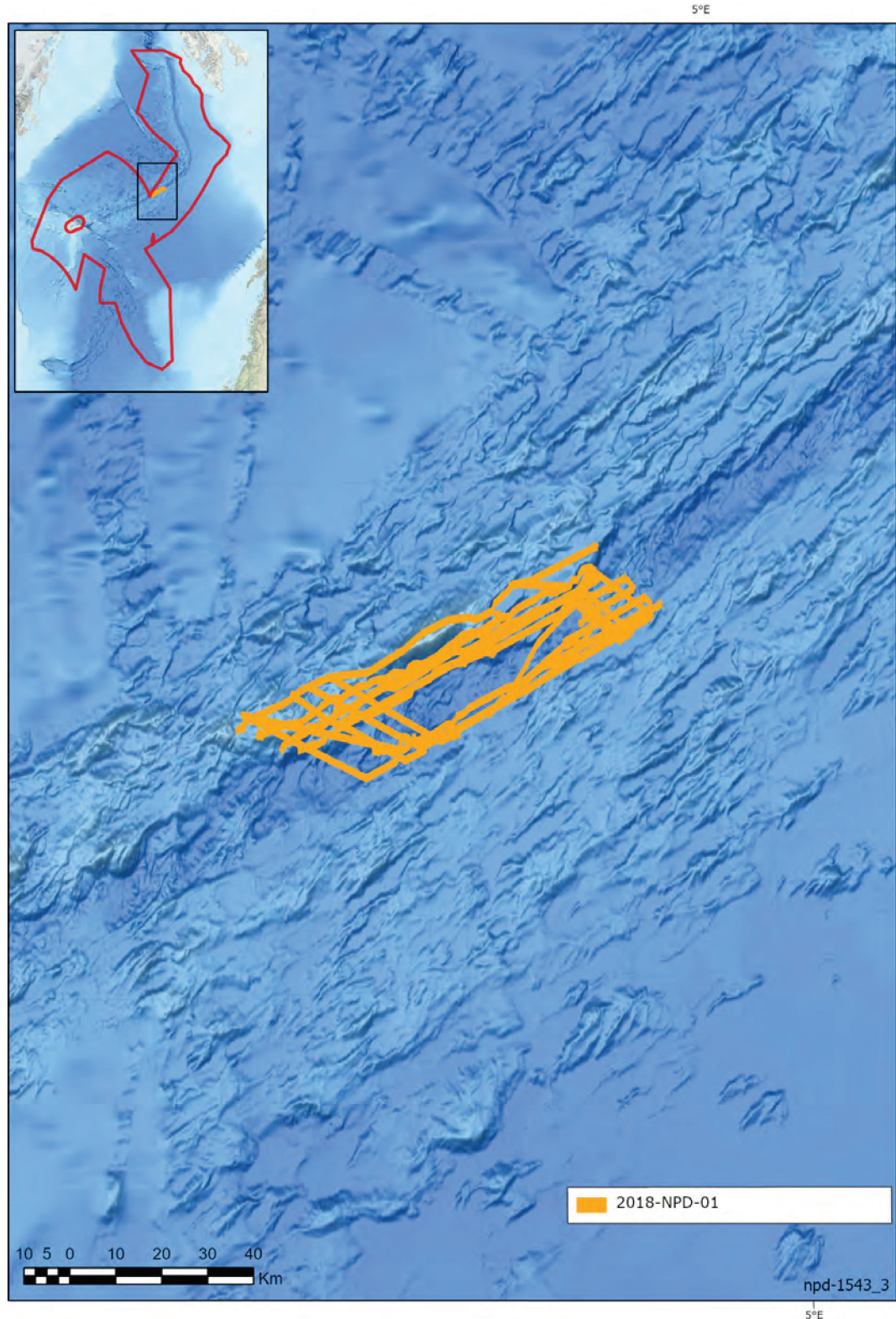


Fig. 3.2 ODs egenopererte kartlegging ved Mohsryggen i 2018

### ODs egenopererte tokt i 2019

Erfaring fra kartleggingstokt i 2018 var sentralt for planleggingen av 2019-toktet. Blant annet ble det nå valgt å benytte tre AUV'er som opererte samtidig. Området ved

Mohnsryggen som ble kartlagt var en forlengelse fra 2018-kartleggingen. Selskapet Ocean Infinity utførte oppdraget for OD, og AUV av typen Kongsberg Hugin 6000 og ROV Kystdesign KD31 ble benyttet til datainnhenting.

Totalt 3800 linjekilometer med AUV-data ble hentet inn, og det ble gjennomført 5 ROV-dykk. En ny inaktiv sulfidforekomst, «Gnitahei», ble funnet, og sulfidforekomsten «Mohnsskatten» ble verifisert.

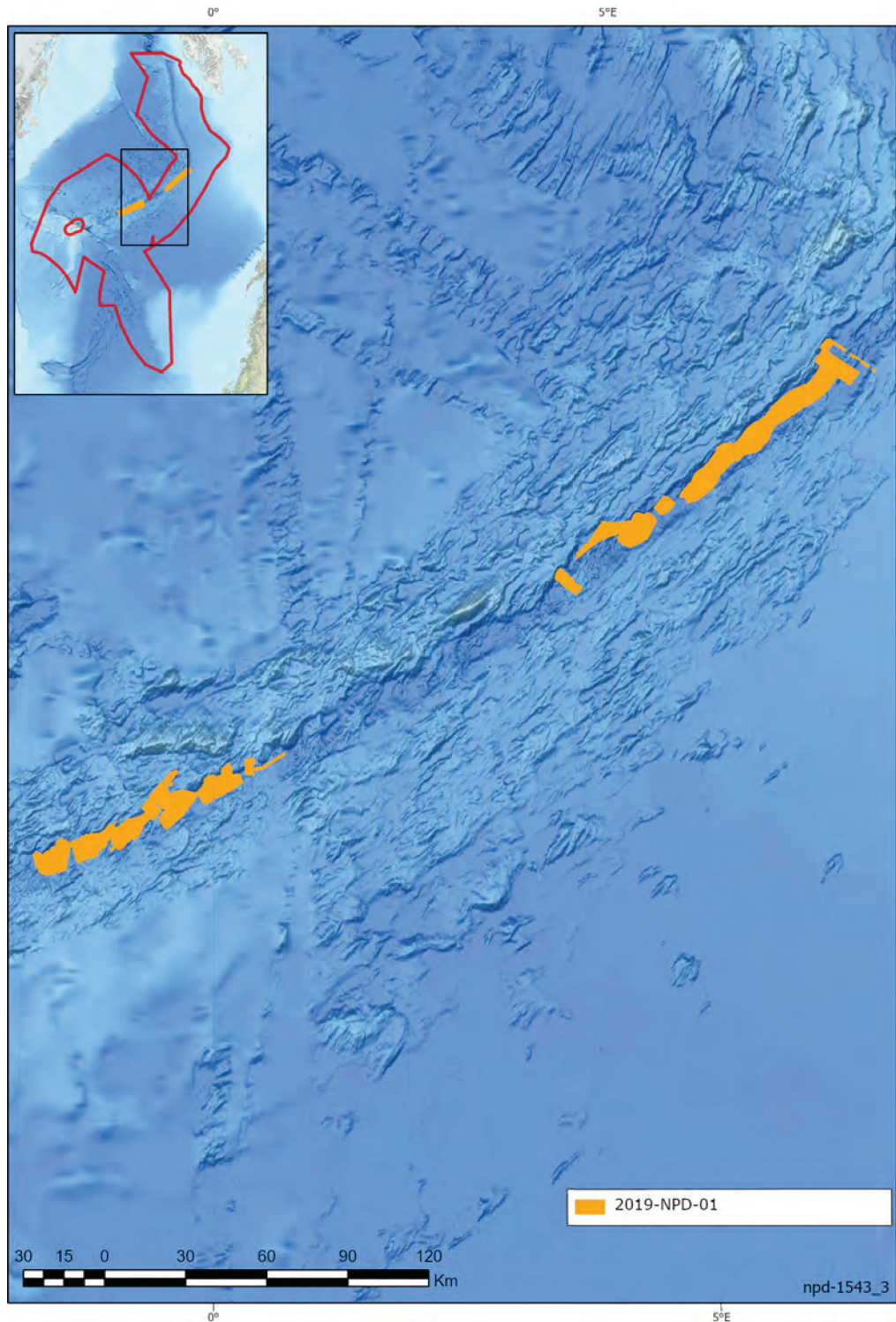


Fig. 3.3 ODs egenopererte kartlegging ved Mohnsryggen i 2019



### ODs egenopererte tokt i 2020

ODs kartlegging i 2018 og 2019 gav informasjon om sulfidavsetninger på havbunnen, men det var til nå ingen kunnskap om sulfidmektigheter i undergrunnen på norsk sokkel. Økt forståelse for utstrekning av sulfidavsetninger under havbunn var dermed mål for ODs kjerneboreoppdrag i 2020. Oppdraget skulle gjennomføres ved kartlagte sulfidforekomster ved Mohnsryggen. Selskapet TIOS vant anbuds konkurransen og utførte oppdraget sammen med Halliburton, Island Offshore og Oceaneering. Kjernemateriale ble hentet opp både ved Fåvne og Gnitahoi (sørlig gul sirkel på Fig. 3.4) og «Mohnskatten» (nordlig gul sirkel på Fig. 3.4) ved bruk av kveilerørsteknologi.

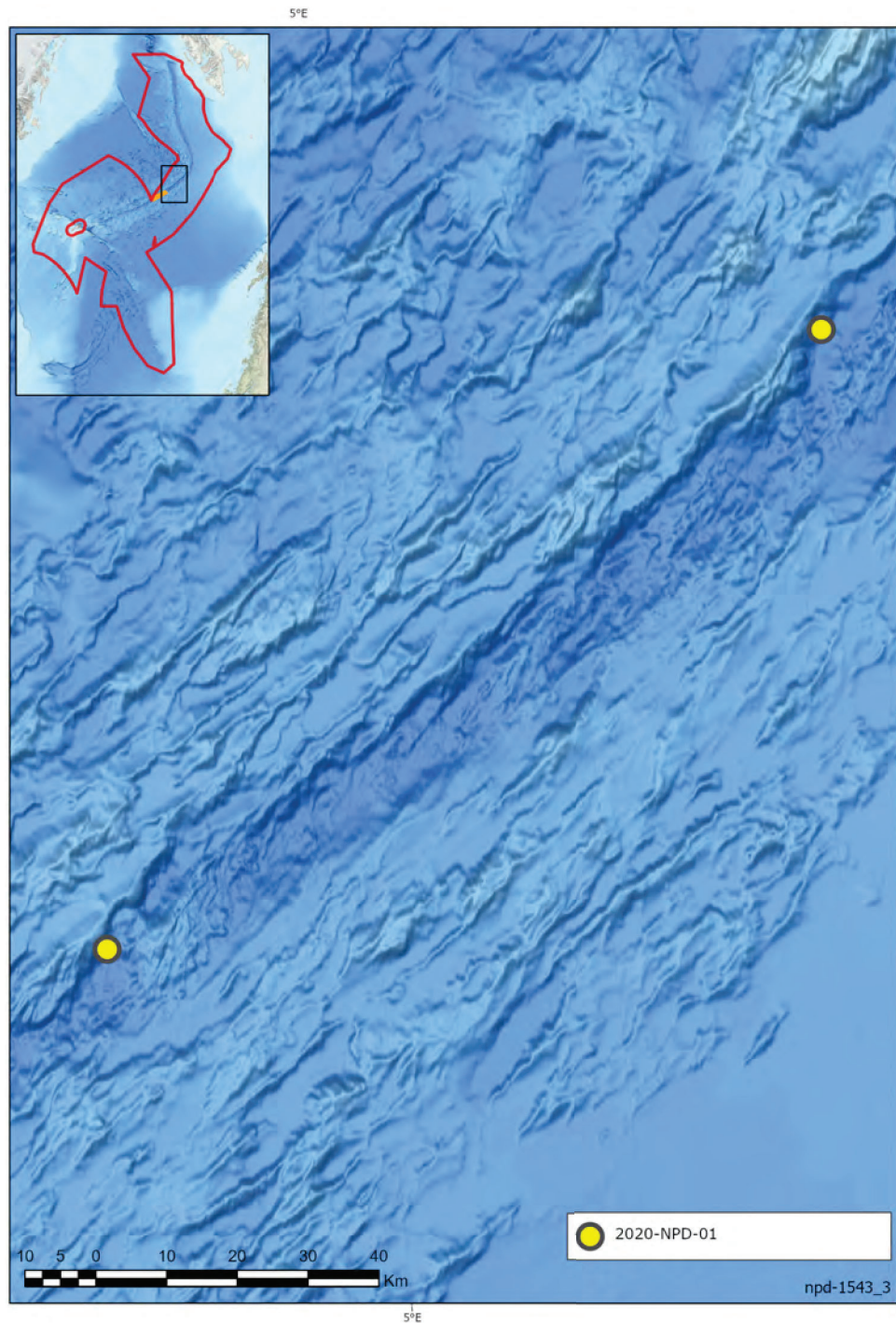


Fig. 3.4 ODs borekampanje i 2020

### ODs egenopererte tokt i 2021

OD prioriterte i 2020 å øke forståelsen for Knipovitsjryggen ved å samle inn MBES-data sammen med UiT. Disse dataene var grunnlagsdata for ODs AUV- og ROV-kartlegging i 2021 i denne delen av utredningsområdet. Ocean Infinity utførte oppdraget for OD, og fartøyet som ble benyttet var mobilisert med tre AUV'en av typen Kongsberg Maritime Hugin 6000, og én Schilling WROV 150 utførte tre ROV-dykk. Kartleggingen resulterte i anomalier på innsamlet datasett – men disse ble på grunn av dårlig vær ikke nærmere undersøkt.

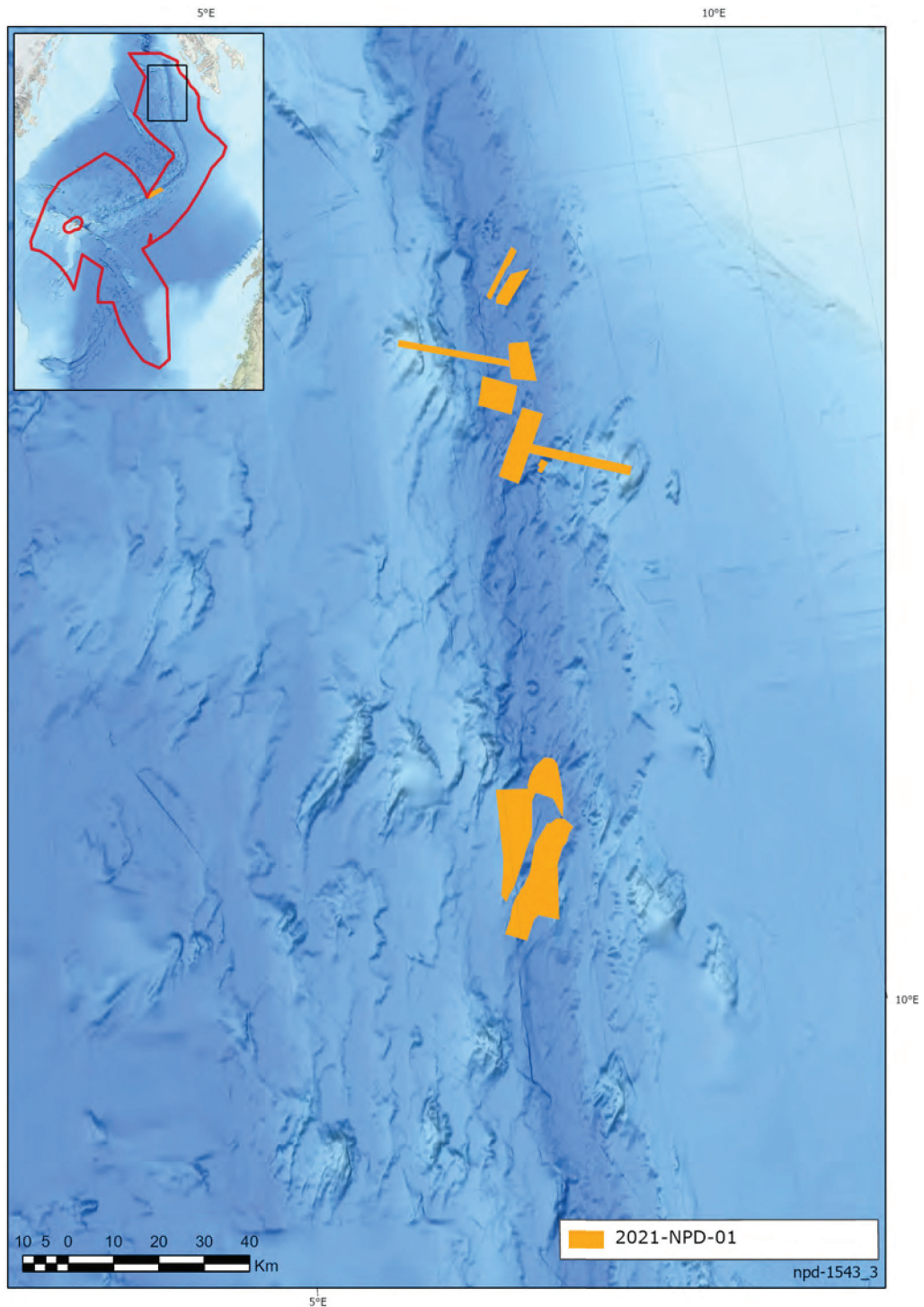


Fig. 3.5 ODs kartlegging ved Knipovitsjryggen i 2021



### Data fra andre

MBES-datasett fra de akademiske institusjonene GIN RAS og Marum har blitt benyttet til å komplettere kartgrunnlaget for Knipovitsj-området, mens datasett fra kartleggingsprogrammet Mareano og transittlinjer fra Marum-tokt på tilsvarende måte har blitt benyttet for Grønlandshavet og Lofotbassenget. Disse vitenskapelig innsamlede datasettene har generelt sett en oppløsning på nær 50 m.

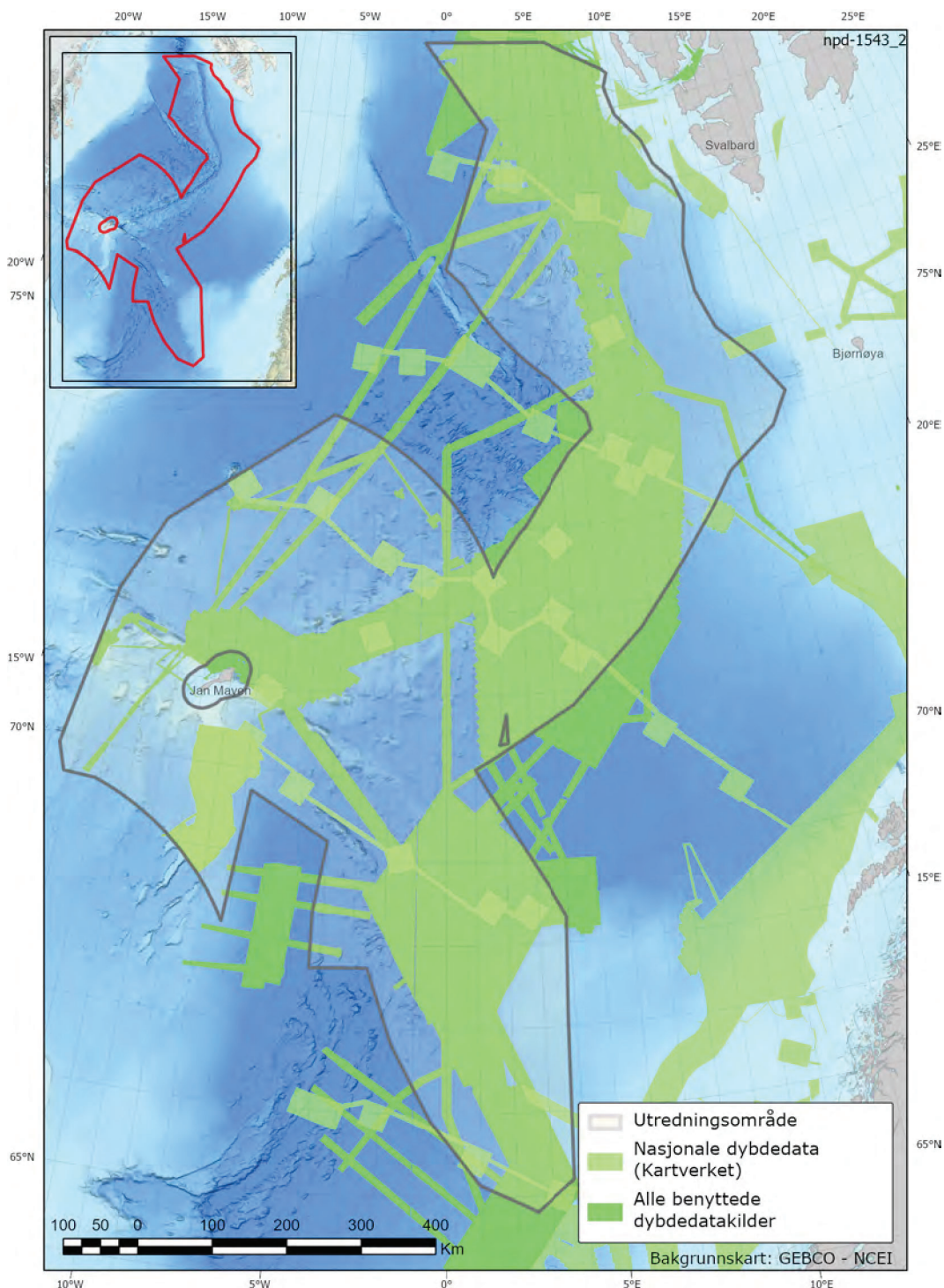


Fig. 3.6 Oversikt over dybdedata OD har tilgang til



## 3.2 Dataoppløsning

Batymetriske data innsamlet med bruk av AUV gir en oppløsning på dybde data i størrelsesorden 1 cm til 1-2 m. Oppløsning er avhengig av flere faktorer, blant annet flyhøyde over havbunn og type påmontert sensor for innsamling.

Batymetriske data innsamlet fra skip gir en kartoppløsning fra 30 m til 100 m. Havdyp, topografi, hastighet for datainnsamling og fokus for ekkoloddsstråle er med å styre oppløsning på innsamlede havdypsdata.

Batymetriske data innsamlet med ROV gir en oppløsning på dybde data på cm-nivå.

Skipsbasert MBES-data som eksisterer innenfor utredningsområdet er generelt sett målt i henhold til versjon av S-44 standard, utgitt av "International Hydrographic Organization". For inngående prosesseringsdetaljer henvises til datainnsamler.

Havbunnstopografiske data (MBES) som er brukt i denne rapporten vurderes å ha god kvalitet, og tilstrekkelig for kartleggingsarbeidet som OD har utført.

## 4 Geologi og ressurser

Jordklodens ytre skall, litosfæren, er delt opp i plater (litosfæreplater) som «flyter» rundt på mantelen i jordens indre og derved beveger seg i forhold til hverandre. Det er dette som er jordens platetektonikk. Havområdene mellom Norge og Grønland er en del av Atlanterhavet, som er et resultat av denne platetektonikken.

For omtrent 300 millioner år siden var verdens kontinenter samlet i ett superkontinent, Pangea. Superkontinentet begynte deretter å sprekke opp og det ble dannet nye litosfæreplater; og nye verdenshav, deriblant Atlanterhavet. Kontinent-oppsprekningen og åpningen av Atlanterhavet startet sørfra mellom Afrika og Sør-Amerika i juratiden, og migrerte deretter nordover. For 55 millioner år siden nådde oppsprekningen våre breddegrader, og havområdet mellom Norge og Grønland begynte å åpne seg – med den amerikanske litosfæreplaten i vest og den eurasiske litosfæreplaten i øst.

Dette havområdet utgjør den nordligste delen av den midt-atlantiske havbunnsbredningen og består av de tre spredningssegmentene Kolbeinseyryggen, Mohnsryggen og Knipovitsryggen. En regional, oseansk bruddsone, Jan Mayen-bruddsonen, deler dette havområdet på tvers av spredningsryggene, med Kolbeinseyryggen på sørsiden og Mohnsryggen og Knipovitsryggen på nordsiden (Fig. 4.1).

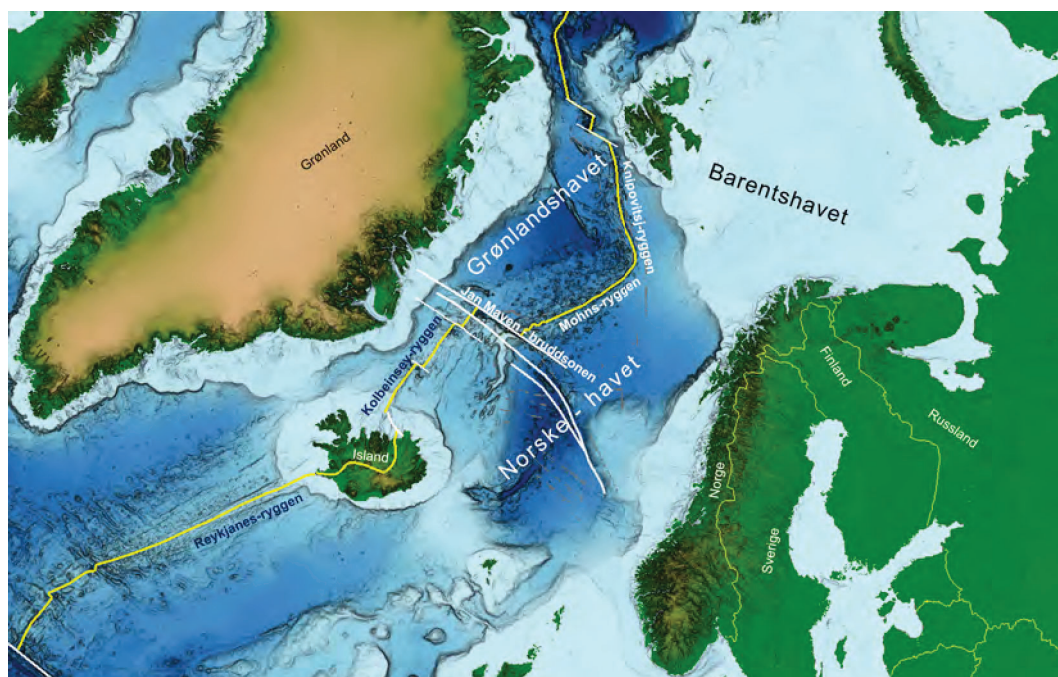


**Fig. 4.1 Geologiske hovedtrekk i Nord-Atlanteren**

Kartfiguren viser de geografiske og geologiske hovedtrekkene i den nordlige delen av Atlanterhavet. Dybdeforholdene er vist med sjatteringer i blått og er basert på det globale havdypsgridet SRTM 30 v8. Aksene for midthavsryggene der den aktive havbunnsbredningen foregår er vist med gul linje, og de viktigste segmentene er navngitt i hvit og blå skrift. De viktigste oseanske bruddsonene er markert med hvite linjer.

Langs Mohnsryggen, i området mellom Jan Mayen-bruddsonen og Barentshavsranden, har havbunnsbredningen etterlatt seg en havbunn med et regelmessig landskap av fjellrygger parallelt med aksedalen i spredningsryggen. Denne symmetrien gjenspeiler seg også i mønsteret av de magnetiske spredningsanomaliene i området (Fig. 4.2).

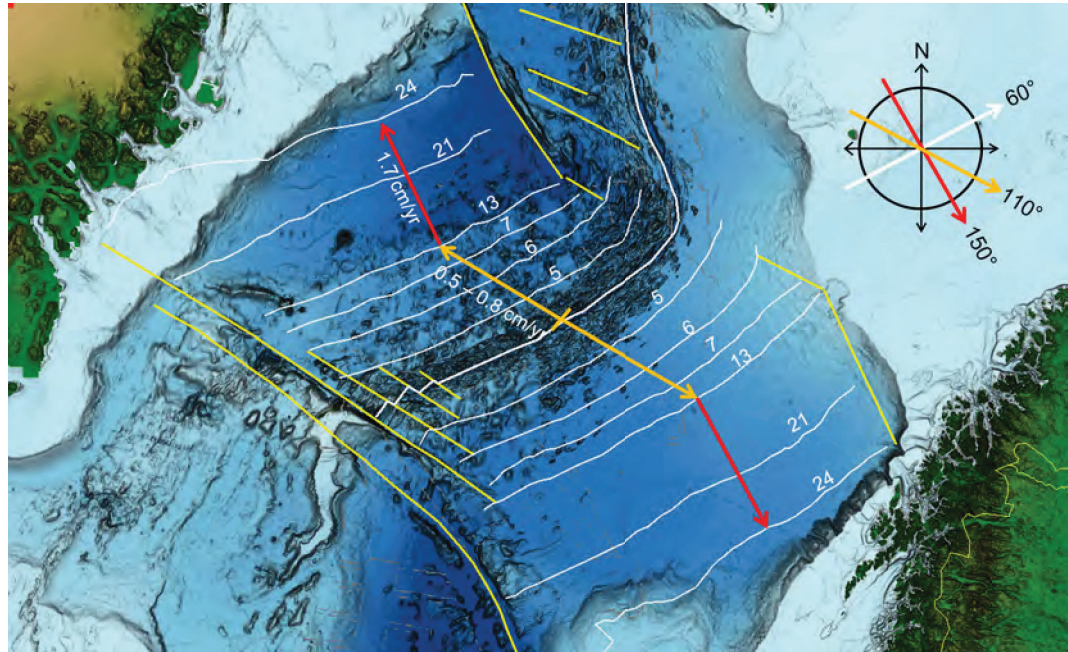


**Fig. 4.2 Havbunnsbredningen langs Mohnsryggen**

Batymetriske kart som viser sammenhengen mellom spredningsanomalier, og hastighet og retning for havbunnsbredningen langs Mohnsryggen i Norskehavet og Grønlandshavet. De viktigste, magnetiske spredningsanomalier er vist med hvite linjer og er nummerert i henhold til den internasjonale standard. De viktigste, oseanske bruddsoner er vist med gule linjer. Anomali 24 ble dannet ved kontinentoppsprekningen for 55 millioner år siden, mens anomali 13 ble dannet på den tiden den relative platebevegelsen mellom den amerikanske og den eurasiske endret seg (33 millioner år siden). Anomali 6 markerer begynnelsen på havbunnsbredningen langs Knipovitsryggen (ca 20 millioner år siden). De røde pilene viser retningen på havbunnsbredningen mellom anomali 24 og 13. Denne var på 150 grader som vist med rød pil i kompassrosen, og var vinkelrett på aksedalen. I denne perioden var spredningshastigheten på ca 1,7 cm/år. Ved anomali 13 skiftet spredningsretningen til ca 110 grader (oransje pil) og hastigheten sank til 0,5 - 0,8 cm/år. Dette var, og er, skrått på aksedalens retning som er på ca 60 grader (hvit pil). Dagens aksedal (0 millioner år) er markert som den sentrale, hvite linjen.

Magnetiske spredningsanomalier kommer av at jordens magnetfelt endrer seg ved at de magnetiske polene bytter plass (reversering av polariteten). Dette skjer hyppig med ujevne mellomrom gjennom geologisk tid (i snitt ca. hvert 0,5-1,0 millioner år). Selve skiftet skjer raskt, omtrent 5000 år. Sist det skjedde var for ca. 770 000 år siden (Haneda et al., 2020).

Basaltiske bergarter inneholder mye magnetiske mineraler. I en basaltisk smelte (lavastrømmer og gangintrusjoner) vil disse mineralene stille seg inn etter den gjeldende polretning og låses i den retningen når bergarten er kjølt ned til under 600-300 °C. På denne måten vil de vulkanske bergartene i en aksedal registrere og bevare jordens magnetiske polaritet fra den tiden aksedalen var aktiv. Over tid viser dette seg som et mønster med striper (anomalier) parallelt med aksedalen med vekselvis normal og reversert magnetisk polaritet ut til hver side av dalen. I likhet med årringene i et tre kan man da bestemme alder på havbunnen lokalt ved å gjenkjenne og telle disse anomalistripene utover fra aksedalen. De anomalierne som er kraftigst og lettest å gjenkjenne, vil være de viktigste for å få en oversikt over den geologiske utviklingen av et havområde.

Havbunnsbredningen langs Mohnsryggen har foregått i to perioder siden anomali 24. Denne anomalien markerer kontinentoppsprekningen for 55 millioner år siden. Havbunnsbredningen foregikk deretter vinkelrett på anomaliretningen (150 grader)

med 1,7 cm per år til hver side fram til anomali 13 (33 millioner år siden) (Fig. 4.2). Fra anomali 13 endret spredningsretningen seg til 110 grader og spredningshastigheten sank til 0,5-0,8 cm per år (Dauteuil og Brun, 1996; Mosar et al., 2002). Dette har holdt seg frem til i dag. Retningen på aksedalen (og dermed retningen på spredningsanomaliene) har derimot holdt seg på 60 grader helt siden oppsprekningen for 55 millioner år siden og synes å representere en stabil tektonisk trend i mantelen nedarvet fra kontinenttoppsprekningen. Dermed står dagens spredningsretning skrått på aksedalen med ca. 30-40 grader fra vinkelrett (Fig. 4.2). Spredningsprosessen innebærer kontinuerlig dannelse av bruddsoner i jordskorpen i aksedalen. Disse bruddene opptrer som ekstensjonsforkastninger som utvikler seg normalt på spredningsretningen, og stryker dermed 30-40 grader på skrått over aksedalen. Denne ekstensjonsprosessen utløser også vulkanske sprekke-utbrudd som bygger opp aksiale vulkanrygger langs disse forkastningene. De aksiale vulkanryggene utgjør derved korte spredningssegmenter som er bundet sammen av overføringssoner i et sikk-sakk-mønster som fordeler spredningen (ekstensjonen) langs aksedalen (Pedersen et al., 2010a).

Taktskiftet i havbunnsbredningen som skjedde ved anomali 13 (33 millioner år siden) førte til en endring i oppbygningen av havbunnskorpen. Skorpen som ble dannet langs Mohnsryggen etter anomali 13 ligger 300 – 400 meter grunnere enn den som ble dannet før. Dette kan sees som et markant trinn i havdypet opp til anomali 13 (Fig. 4.8).

Den sørligste delen av Mohnsryggen er delt opp av mindre bruddsoner i tre små segmenter der aksedalen er orientert mer eller mindre normalt på spredningsretningen (Fig. 4.2). I dette området ser man spor av denne aksedalsretningen helt ut til anomali 6 til hver side. Dette området ligger betydelig grunnere enn resten av spredningsryggen nordover (2000-600 meters dyp) på grunn av økt magmatisk oppbygning av skorpen. Disse forholdene skyldes at dette området ligger i ytterkanten av den store varmpunktadiapiren i mantelen under Island, og påvirkes sterkt av denne (Pedersen et al., 2010a).

Inntil anomali 13 ble åpningsbevegelsen i dette havområdet overført sidelengs inn i Polhavet via en kontinental bruddsone langs Barentshavsranden, kalt de Geer-sonen. Denne sonen utgjorde del av plategrensen mellom den amerikanske og den eurasiske platen. Endringen av spredningsretning og hastighet ved anomali 13 skjedde på grunn av en justering i den relative bevegelsen mellom disse to platene. Dette førte antagelig til at sidelengs-bevegelsen langs plategrensen også fikk en ekstensjons-komponent som førte til strekking og tynning av den kontinentale jordskorpen langs de Geer-sonen. Nyere data indikerer at for ca 20 millioner år siden (ved ca anomali 6) førte dette til endelig oppsprekking av jordskorpen og separasjon av kontinentene. Knipovitsryggen begynte da å åpne seg ved spredning mellom de to platene langs de Geer-sonen (med en ekstremt skeiv spredningsretning) (Dumais et al. 2021). Denne prosessen førte også til at sterkt strukket kontinentalskorpe utgjør underlaget i et område langs østsiden av Grønlandsryggen (Gernigon et al., 2020; se også Zayonchek & Brekke et al., 2011; Gusev, 2015).

I området sør for Jan Mayen-bruddsonen og nord for en ryggstruktur fra Grønland over Island til Færøyene (GIFR) (Hjartason et al., 2017) har havbunnsbredningen foregått svært komplisert og usymmetrisk (Fig. 4.3). Spredningsprosessen og åpningen av havområdet har foregått i to faser. I den første fasen foregikk spredningen langs Ægirryggen vest for Island og Jan Mayen fra åpningen for 55 millioner år siden (ved anomali 24) til ca. 20-25 millioner år siden (mellom anomali 6 og 7). Fram til anomali 13 foregikk spredningen kontinuerlig, men deretter sank spredningshastigheten betydelig.



Samtidig begynte Kolbeinseyryggen å overta en del av spredningen og utviklet seg som en kile inn langs Grønland fra sør. Kontinentalskorpen der begynte å sprekke opp og en mindre del av den ble skilt fra resten av Kolbeinseyryggen, som omtrent ved anomali 6 overtok all havbunns-spredning mellom Grønland og Norge sør for Jan Mayen-bruddsonen. På grunn av denne spredningsprosessen har det fraskilte skorpefragmentet beveget seg vekk fra Grønland og utgjør i dag et område med kontinentalskorpe midt mellom Norge og Grønland. Dette regnes nå som et eget mikrokontinent, Jan Mayen-kontinentet. Hvordan Kolbeinseyryggen ble etablert er omdiskutert. Tidlige modeller antar at det til å begynne med fantes en midlertidig, kortere spredningsrygg som styrte fraskillingen av mikrokontinentet fra Grønland, og at den aller sørligste delen av mikrokontinentet muligens kunne strekke seg til under nordøstligste del av dagens Island (Talwani og Eldholm, 1977; Brekke, 2000). Nyere modeller antar en jevn utvikling av Kolbeinseyryggen fra starten av (Gernigon et al., 2015; Blischke et al., 2022). I begge modellene inngår det at kontinentalskorpen, på den sørlige delen av mikrokontinentet, er tynn og strukket ut over et bredt område, med et havdyp på ca 2000 meter. Mot nord er ikke skorpen strukket på langt nær i samme grad, slik at kontinentfragmentet der blir betydelig smalere og tykkere og har form som en smal, langstrakt, grunn rygg (JMR i Fig. 4.3). I forlengelsen av denne ryggen mot nord ligger øya Jan Mayen med vulkanen Beerenberg.

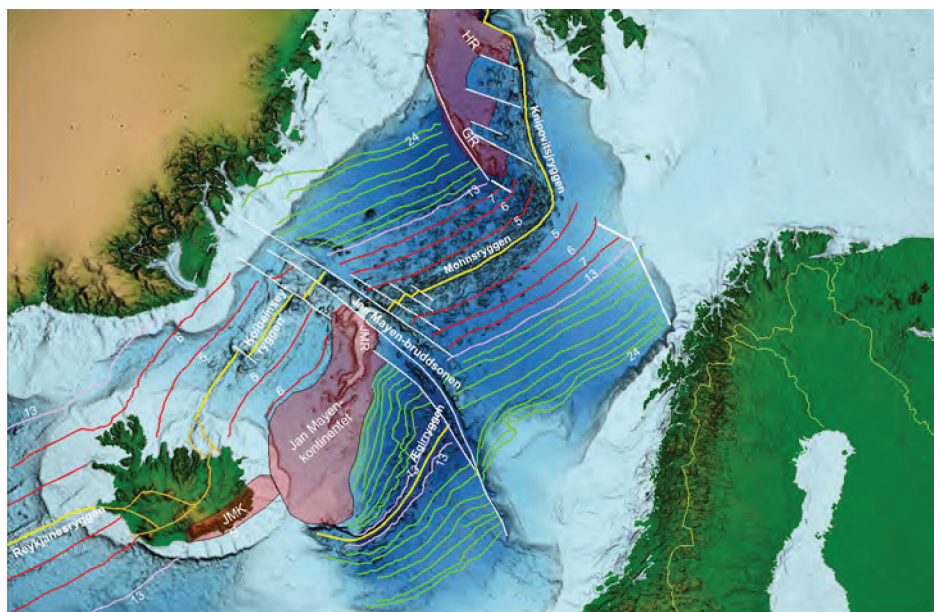


**Fig. 4.3 Havbunns-spredningen mellom Norge og Grønland**

Kartfiguren viser en oversikt over de geologiske hovedelementene i havbunns-spredningen mellom Norge og Grønland nord for Island. Aksene i de aktive og inaktive spredningsryggene er vist med gule linjer. Havbunns-spredningen gjennom Island går langs definerte vulkanske og seismiske soner - disse er vist med oransje linjer. Spredningsanomali 13 (tiden for skiftet i relative platebevegelser) er vist med rosa linjer. Spredningsanomalier eldre enn anomali 13 er vist med grønne linjer, og spredningsanomalier som er yngre enn anomali 13 er vist med røde linjer. De viktigste anomaliene er nummerert. Spredningsanomaliene er tatt fra Wessel and Müller (2018). Områdene med kontinentalskorpe i Jan Mayen-kontinentet og langs Grønlandsryggen er vist som gjennomskitige polygoner med rød farge. Avgrensingen av kontinentalskorpeområdene er gjort på grunnlag av NGUs publiserte datasett over magnetiske anomalier (se Olesen et al., 2010; Gernigon et al., 2015), med støtte i Gernigon et al. (2020) og Dumais et al. (2020). Anomalimønsteret viser tydelig den vifteformede spredningen langs Ægirryggen fram til da spredningshastigheten sank betraktelig etter anomali 13. Etter adskillelsen av Jan Mayen-kontinentet fra Grønland var Kolbeinseyryggen fullt etablert ved anomali 6. Langs Mohnsryggen viser anomaliene en stort sett symmetrisk spredning, selv om hastighet og retning endret seg noe ved anomali 13, da Ægirryggen begynte å dø ut. Spredningsmønsteret langs Knipovitsryggen er komplisert og foreløpig ikke inkludert (se Dumais et al., 2020).

Den betydelige strekkingen og utvidelsen av kontinenten i den sørlige delen av Jan Mayen-kontinentet foregikk samtidig med havbunnsbredning langs Ægirryggen. Mangelen på strekning og utvidelse i den nordlige delen av kontinentet ble kompensert ved at bredningen langs Ægirryggen fikk en vifteform med mest bredning nordover (Fig. 4.3). En grundig analyse basert på nyere bredningsanomalidata og geokjemiske data (Torsvik et al., 2015) viser at sterkt strukket kontinental skorpe ligger i en forlengelse av Jan Mayen-kontinentet under den østligste delen av Island (JMKS i Fig. 4.3).

Gjennomgangen over viser at jordskorpen opprinnelse, sammensetning, tykkelse og topografi varierer i stor grad i disse havområdene. Jordskorpen beskaffenhet har direkte innvirkning på dannelse og utvikling av de ulike havbunnsmineralene og har derfor stor betydning for vurderinger og beregninger av ressurspotensialet. Hvordan disse variasjonene påvirker ressursvurderingen er beskrevet i mer detalj videre i kapittelet.

## 4.1 Sulfidforekomster

Sulfidforekomster er sulfidforbindelser mellom svovel og metallgrunnstoffer avsatt som sulfidmineraler. Siden de inneholder flere typer metallgrunnstoffer, kalles de polymetalliske. Slike sulfidforekomster er av de viktigste kildene til metaller som kobber, sink, bly, kobolt, sølv og gull.

### 4.1.1 Dannelsen av sulfidforekomster - aktiviteten i aksedalen

De polymetalliske sulfidforekomstene (Fig. 4.4) dannes av hydrotermale prosesser drevet av magmatisk aktivitet i aksedalen i en spredningsrygg. På norsk kontinentalsokkel gjelder det Knipovitsjryggen, Mohnsryggen og nordlig del av Kolbeinseyryggen. Sulfidforekomstene her kan deles i to typer, alt etter hvilken tektonisk posisjon de har i aksedalen i spredningsryggene: flankeforekomster og aksialforekomster. Dette er også grunnlaget for inndelingen av forekomstene i to hoved-letemodeller (se 4.1.5 [Letemodeller for sulfidforekomster](#)).



**Fig. 4.4 Snitt av sulfidprøve**

Sulfidprøve fra Mohnskatten hentet opp fra 2800 meters vandndyp med ROV i 2020.

Flankeforekomstene dannes langssetter de store hovedforkastningene som utgjør flankene av aksedalen. Aksialforekomstene dannes i vulkanske rygger som utvikles i de sentrale deler av aksedalen. Ryggene dannes ved sprekke-erupsjoner som er knyttet til bruddannelse i jordskorpen, og disse bruddene dannes ortogonalt til spredningsretningen. De vulkanske ryggene utgjør derved korte spredningssegmenter som er definert av vulkanrygger omgitt av dypere, langstrakte bassenger. På grunn av det skrå spredningsmønsteret forflyttes disse ortogonale spredningssegmentene sidelengs. Dette skjer langs overføringssoner. Disse går på tvers av aksedalen. Sett i detalj følger aksedalen dermed et sikk-sakk mønster, der ortogonale spredningssegmenter knyttes sammen av overføringssonene (se Pedersen et al., 2010a).

Både hovedforkastningene langs flankene og de aksiale forkastningene går gjennom den øvre, sprø delen av havbunnskorpen ned til dypene der skorpen er duktil og tildels gjennomsett av magmakamre med smeltet masse. Bevegelser på disse forkastningene gir sprekkesystemer som stedvis i perioder åpner for sirkulasjon av hydrotermale væsker, og dermed avsetning av polymetalliske sulfider (Fig. 4.5).

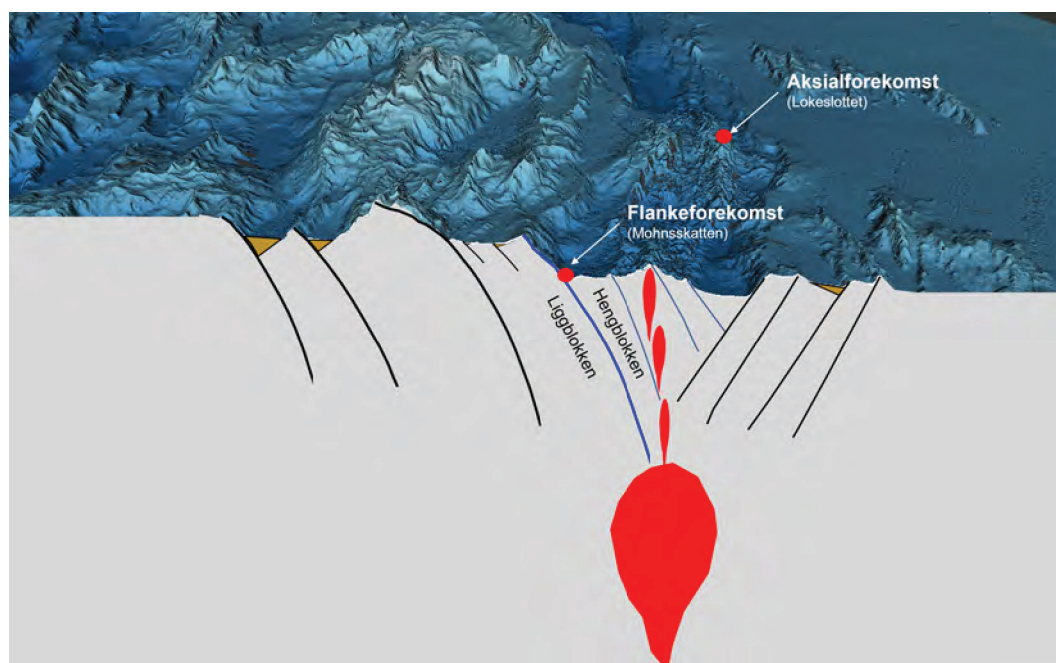


**Fig. 4.5 Geologisk ramme for sulfidforekomster**

Perspektivkart over nordligste del av Mohnsryggen. Figuren er en kombinasjon av havbunnsstopografien og et snitt av jordskorpen, som viser sammenhengen mellom skorpeprosessene i aksedalen og avsetningen av de to typene sulfidforekomster; aksialforekomstene langs aksiale vulkanrygger og flankeforekomstene langs de store flankeforkastningene. Et gruntliggende magmakammer som tilfører aksedalen lava er vist i rødt. Sedimentavsetninger i halvgrabenene utover fra flankene av aksedalen er vist som brune kiler. Figuren viser også prinsippet for liggblokken og hengblokken til en forkastning. Liggblokken er den blokken som ligger fast under forkastningsplanet, mens hengblokken er den blokken som sklir nedover oppå forkastningsplanet. I figuren er dette illustrert langs det blå forkastningsplanet. I et system av parallelle forkastninger vil liggblokken til én forkastning utgjøre hengblokken til den neste, underliggende forkastning.

Flankeforekomstene finnes både langs foten av forkastningene (eks. Fåvne, se 7.1.1 Fåvne) og oppe i forkastningsskrenten (eks. Gnitahei og Mohnsskatten, se 7.1.2 Gnitahei og 4.2 Sulfideksempel Mohnsskatten). Forekomstene ved foten av forkastningene kan ligge helt nede i, og på tvers av, overgangen mellom liggblokken og hengblokken (overgangen mellom skrenten og dalbunnen, se Fig. 4.5). Alle flankeforekomster følger med liggblokken og vil med tiden løftes sammen med skrenten opp og ut av aksedalen. De flankeforkastninger som så langt er undersøkt i Mohnsryggens aksedal har kun eksponert basalt. Ultramafiske bergarter kan til dels opptre i dypere deler av jordskorpen og inngå i reaksjonssonen i den hydrotermale prosessen uten at de er eksponert på overflaten. Noen flankeforkastninger som er aktive over spesielt lang tid vil kunne utvikle såkalte kjernekomplekser, der også mantelen med de ultramafiske bergartene blir eksponert. Slike forkastninger synes ikke å være, eller å ha vært, dominerende i våre deler av det atlantiske spredningssystemet — men flere kandidater er beskrevet (Pedersen et al., 2007; Reimers, 2020). Aksedalen i Mohnsryggen er asymmetrisk der forkastningene langs nordvestflanken er størst. Flankeforekomstene oppdaget i Mohnsryggen til nå, ligger alle i den nordvestlige flanken. Det er ikke dokumentert at dette har sammenheng med denne asymmetrien, men skyldes heller at det er den nordvestlige flanken som et blitt mest undersøkt. UiB har påvist sulfidrike lag i en kjerne



tatt nær den sørøstre flanken. Kilden til dette laget er trolig en forekomst som har rast ut ved denne flanken. Ved anslag av antall forekomster langs aksedalen må man derfor ta hensyn til at den sør-østre flanken er underrepresentert.

Den samme asymmetrien ser ikke til å være utviklet i Knipovitsryggen.

Aksialforekomstene forekommer både sentralt og på flankene av de aksiale vulkanryggene (eks. Lokeslottet og Ægirs kilde). Retningen på aksedalen går skjevt på spredningsretningen. De aksiale vulkanryggene og de tilhørende, tverrgående forkastningene går derfor på skrå over aksedalen (Fig. 4.6) (se også 4 Geologi og ressurser).

Mohnsskatten er nærmere beskrevet i eger avsnott (4.2 Sulfideksempel Mohnsskatten). De øvrige kjente sulfidforekomstene på norsk kontinentalsokkel er beskrevet i mer detalj i appendiks (Appendiks 7.1 Andre sulfidforekomster kartlagt av Oljedirektoratet og akademia).

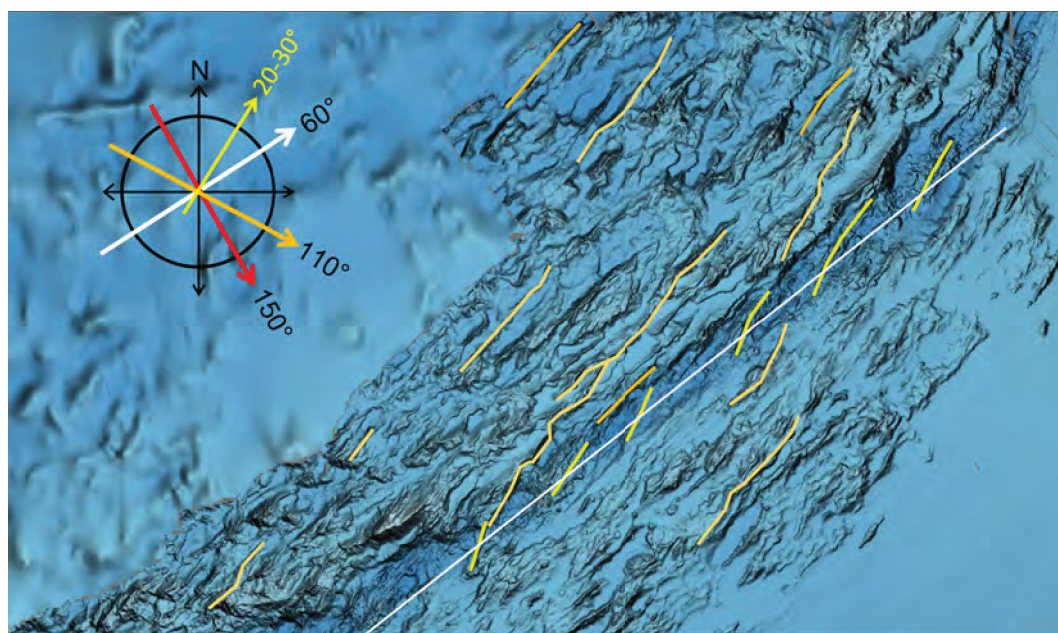


**Fig. 4.6 Tektonisk ramme for Mohnsryggens aksedal**

Batymetrisk kart som viser sammenhengen mellom havbunnsbredningen og ekstensjonsforkastningene. Den hvite linjen går langs aksens retning på 60° som vist med den hvite pila. Spredningsretningen er på 110° og vist med den oransje kompasspila. Dette fører til ekstensjonsforkastninger vinkelrett på denne spredningsretningen som antydtes med de gule og oransje linjene; de gule viser aktive forkastninger i den aksedalen, mens de oransje viser noen av de gamle, passive ekstensjonsforkastningene utover på flankene. Ekstensjonsforkastningene avviker med 30 – 40° fra retningen på aksedalen (som ville vært forkastningsretningen hvis spredningen hadde foregått vinkelrett på aksedalen som vist med rød kompasspila).

#### 4.1.2 Utbredelsen av sulfidforekomster - prosessene utenfor aksedalen

Forkastningene langs flankene av aksedalen vil over tid bli inaktive og nye flankeforkastninger blir utviklet langs noen av de store forkastningene assosiert med de aksiale vulkankompleksene. Dette ser ut til å skje når den gamle flankeforkastningen forlater området med aktive magmakamre i jordskorpen, og denne konsolideres og hever seg isostatisk. Relieffet på forkastningsskrentene er da i størrelsesorden 1200-2000 meter (Fig. 4.7). De gamle forkastningsblokkene med sine forkastningsskrenter og deler

av paleo-aksedalene blir da en del i rekken av halvgrabener som danner den inaktive havbunnskorpen og med tiden beveger seg vekk fra den aktive aksedalen (Fig. 4.7). De fossile sulfidforekomstene følger med i disse skrentene og paleo-kompleksene, og kan utgjøre store mineralressurser. Men flere faktorer begrenser tilgjengeligheten av disse fossile forekomstene.

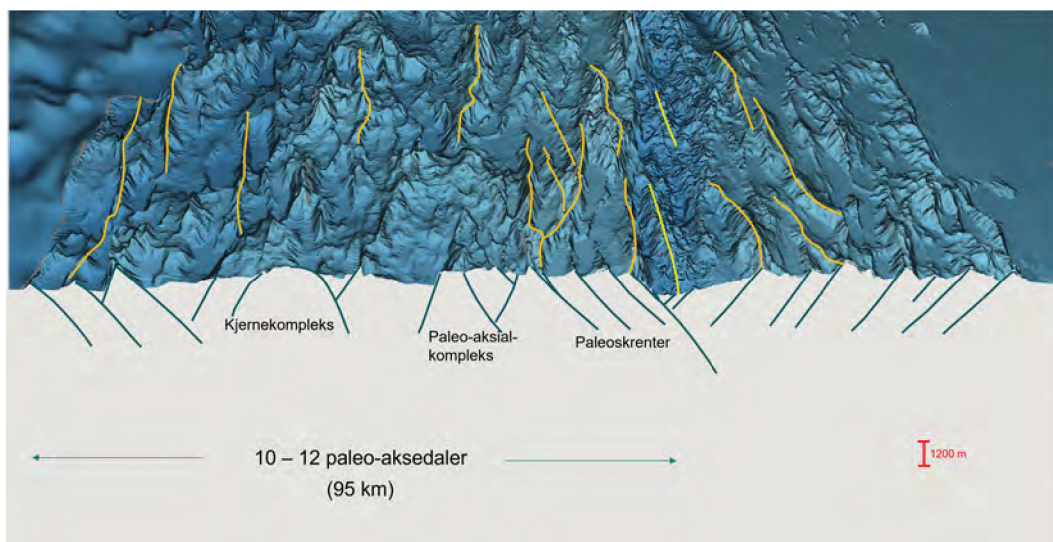


**Fig. 4.7 Mohnsryggens flankevidder**

Perspektivkart over Mohnsryggen sett fra sør. Kartet er en kombinasjon av havbunnsstopografien og et snitt av jordskorpen på tvers av aksedalen. Kartet viser at havbunnens berggrunn med sine fjelltopper, rygger, daler og gamle forkastningsskrenter i sin tid ble dannet av de tektoniske og vulkanske prosessene i aksedalen og deretter transportert utover i flankene av spredningsprosessen.

Dalbunnen i aksedalen er vulkansk aktiv og blir kontinuerlig tilført lava fra vulkanske utbrudd spredt rundt om i dalen. Selv om de enkelte utbrudd er spredt, vil de over tid ha dekket hele dalbunnen. Kartlegging og datering utført av UiB viser hvor dynamisk utviklingen av dagens dalbunn er. Undersøkelsene viser at 70 pst. av overflaten ved aksiale vulkanrygger er blitt vulkansk fornyet i løpet av de siste 25 000 årene. For de dype områdene som omgir de aksiale vulkanryggene, og overføringssonene som binder dem sammen i et spredningssystem, er omkring 40 pst. av havbunnen blitt vulkansk fornyet i løpet av de siste 25 000 årene. For aksedalen som helhet er bildet at: 1) omkring 75 pst. av arealet er blitt vulkansk fornyet i løpet av de siste 50 000 årene, 2) mindre enn 10 pst. er eldre enn 100 000 år, 3) det er ikke påvist områder der de øverste lavastrømmene er eldre enn 180 000 år (Stubseid et al., 2023). Dette betyr at store deler av overflaten av dalbunnen blir fornyet med lava i løpet av 25 000-50 000 år, og dermed må man ta i betraktning at en del av fossile aksialforekomster vil være dekket av lava før de eventuelt inkorporeres i et paleo-kompleks og blir transportert ut av aksedalen. På land klarer man å utvinne forekomstene selv med slik lagdeling. For havbunnsmineraler er det stor sannsynlighet for at fossile sulfidforekomster som er dekket av lava vil være utilgjengelige med dagens teknologi. Aksialforekomster uten lavadekke derimot, må regnes å ha et stort bevaringspotensial og vil være lett tilgjengelig dersom de er lokalisert nær kanten av forkastningsblokkene.

Flankeforekomstene utvikler seg stort sett i selve forkastningsskrentene eller i overgangen mellom skrent og dalbunn og dermed helt i ytterkantene av aksedalen. De har dermed mye mindre sannsynlighet enn aksialforekomstene for å bli dekket av ny lava. Disse forekomstene kan da utvikle seg over langt lengre perioder og bli betydelig større før vertsforkastningen blir inaktiv. Imidlertid er det en rekke forhold som kan føre

til at en god del av disse forekomstene vil kunne bli begravet så mye at de blir utilgjengelige med dagens teknologi. En forekomst som utvikles på hengblokken, nær en forkastning, kan ha minst fire utviklingsforløp: 1) den kan bli begravd av neste lavastrøm, 2) den kan bli begravd av ras, 3) den kan bli inkorporert i liggblokken som del av en rytterblokk, eller 4) den kan forbli på liggblokken og bli løftet ut av riftdalen når den neste hovedforkastningen dannes. Bevaringspotensialet for en forekomst som utvikles på liggblokken vil avhenge av hvor høyt i forkastningsskrenten den ligger. Topografien til havbunnen utenfor aksedalen består stort sett av en serie med halvgrabener adskilt av gamle forkastningsskrenter (Fig. 4.7). Sedimentene akkumuleres nede i halvgranbenene med skrentene stikkende opp i bakkant (Fig. 4.5). Dette betyr at jo høyere opp i forkastningsskrenten en fossil forekomst befinner seg, jo større sannsynlighet er det for at den vil være tilgjengelig for utnyttelse.

Store mengder sedimenter har kommet inn i Mohnsryggområdet fra den grunne Barentshavssokkelen i nord, særlig under istidene i kvartær. Ved endringen i spredningshastighet ved anomali 13 begynte Knipovitsryggen (inklusive Grønlandsryggen) å utvikle seg og dannet en barriere mot sedimenttilførselen fra nord og inn i områdene vest for Mohnsryggen (Fig. 4.8). Men selv med denne barrieren er dagens sedimentasjonsrate på ca. 3 cm per 1000 år. Med denne raten vil sedimentdekket på vestsiden av Mohnsryggens aksedal være 0 meter på dagens flanke av dalen og øke gradvis vestover til ca. 900 meter ute ved trinnet i oseanskorpene (anomaliene 13 - 18), som ligger ca. 250 km vest for aksedalen (Fig. 4.8). Dette betyr at andelen tilgjengelige flankeforekomster avtar med avstanden vekk fra aksedalen. Foreløpig kartlegging viser at sedimenttykkelsene i halvgrabenene ved anomali 13 er 800-900 meter. Det betyr generelt sett at mindre enn den øverste halvparten av paleoskrentene stikker opp over sedimentdekket i dette området (gitt at skrentene opprinnelig er 1200-2000 meter høye). Overordnet sett anslås det derfor at 40 - 50 pst. av de potensielle forekomstene i arealet ut til anomali 13 vil være tilgjengelig med dagens teknologi. På østsiden av Mohnsryggen er det ingen barriere mot sedimenttilførselen fra nord, og 50-100 km mot øst er den vulkanske havbunstopografien fullstendig begravet. De prospektive områdene i øst er dermed begrenset til dette 50-100 km brede beltet.

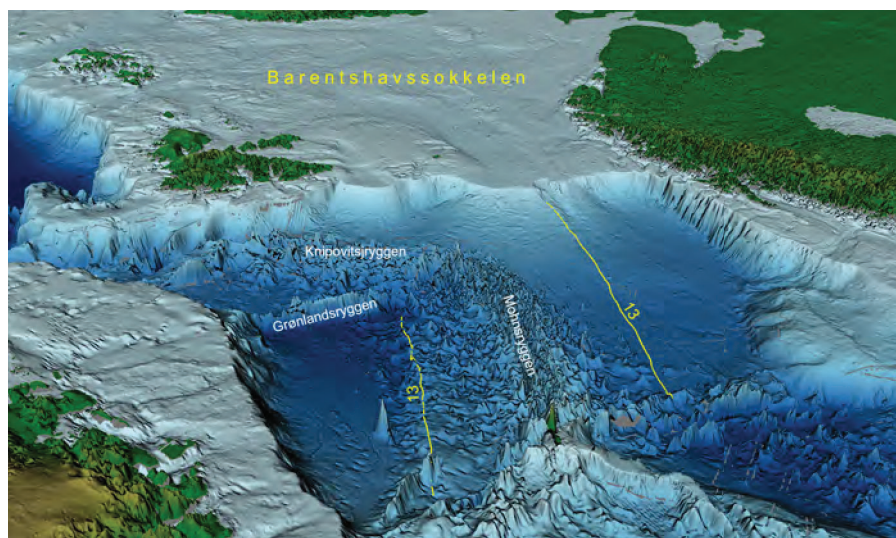


**Fig. 4.8 Sedimentfordeling på havbunnen**

Perspektivkart over havbunnen nord for Jan Mayen sett fra sør. Det viser hvordan endringen i spredningshastighet ved anomali 13 (vist i gult) førte til økt havbunntopografi, og hvordan utviklingen av Knipovitsryggen og Grønlandsryggen, sammen med Mohnsryggen, effektivt har skjermet områdene vest for Mohnsryggen fra den massive sedimenttilførselen fra nord.



Områdene sørvest for Knipovitsryggen ut til grensen for kontinentalskorpe (ca 80 km fra ryggen) vil også inneholde fossile sulfidforekomster (Fig. 4.9). Men her er sedimenttilførselen betydelig høyere enn i områdene vest for Mohnsryggen. Områdene langs nordøstsiden av Knipovitsryggens aksedal er fullstendig begravet av sedimenter fra Barentshavssokkelen. Aksedalen skjærer delvis områdene på sørvestsiden, slik at man her finner en vulkansk topografi som langs Mohnsryggen. Men batymetri- og SBP-data viser at dette landskapet er dekket av vesentlig mer sediment enn langs Mohnsryggens vestsida.

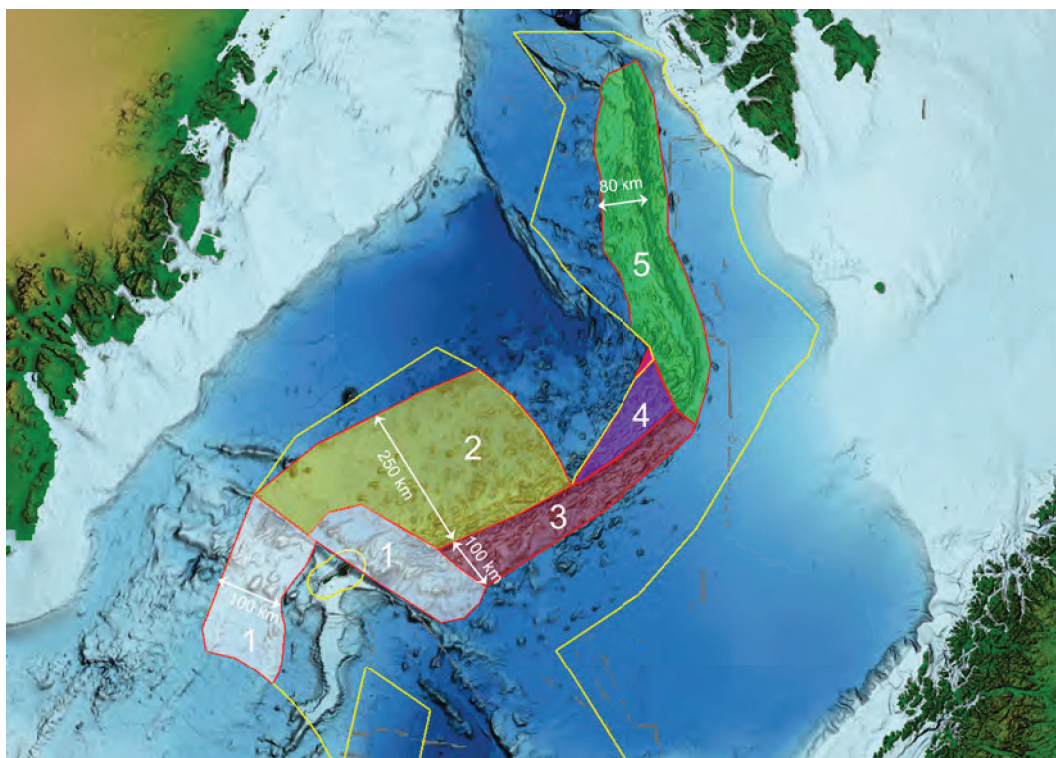


**Fig. 4.9 Prospektive arealer for modellering av sulfidforekomster**

Batymetriske kart som viser havbunnsområdene på norsk sokkel der sulfidforekomster kan være tilgjengelig for leting og utnyttelse med dagens teknologi. Disse områdene er delt opp i delareal nummerert fra 1 til 5 til bruk for estimering av sulfidressursene (se 4.1.5.3 *Antall forekomster*). Den gule linjen viser grensen for utredningsområdet. Det røde polygonet viser en mulig overlapp med Grønlands kontinentalsokkel.

#### 4.1.3 Geokjemi og metallgehalt

Den geokjemiske sammensetningen av sulfidforekomstene avhenger av mineralogien i vertsbergartene og temperaturen på den gjennomstrømmende hydrotermale væsken.

Undergrunnen inne i aksedalen består stort sett av basalter. Langs flankene kan vertsbergartene variere mer ved at de store flankeforkastningene kan bringe de dypere, ultramafiske bergartene opp i det hydrotermale systemet. Det generelle bildet fra litteraturen er at basalter gir høyere innhold av jern (Fe) og lavere innhold av kobber (Cu) og sink (Zn) enn ultramafiske bergarter, særlig der serpentin er involvert (Hannington et al., 2010; Cherkashov et al., 2010; Firstove et al., 2016). Forholdet mellom disse tre elementene avhenger også av temperaturen på væsken. Zn og Fe felles ut ved lavere temperaturer enn Cu. Det ser ut til at anrikning av kobolt (Co) er avhengig av at det finnes ultramafiske vertsbergarter. I publisert litteratur viser noen til at gull (Au) har sammenheng med ultramafiske bergarter, mens andre mener at Au-anrikning også har med temperaturen å gjøre (lav fallende temperatur gir mer Au).

Innblanding av sedimenter i prosessene vil også kunne påvirke geokjemi og metallgehalt. Hydrotermale reaksjoner som involverer sedimenter, resulterer i væsker med høyere pH og mindre evne til metalltransport. Dette fører til relativt metallfattige mineralavsetninger. Dette ser ut til å gjøre seg gjeldende i de nordlige deler av Mohnsryggens aksedal som er i kontakt med Bjørnøyvifta (se Fig. 4.25). Lokeslottet og Ægirforekomsten er således sterkt påvirket av sedimenter (Pedersen et al., 2010b; Baumberger et al., 2016), mens flankeavsetninger som Fåvne og Mohnsskatten er i liten grad preget av dette.

Vanddypet ser ut til å være en annen lokal faktor som kan påvirke geokjemien. Dette kan skyldes at det omgivende trykket kontrollerer kokepunkt og dermed temperaturen på den hydrotermale væsken der den når havbunnen. Grunne områder (grunnere enn 1500 meter) vil typisk være rike på Zn og fattige på Cu (Monecke et al., 2014).

Det ser ut til at man kan konkludere med at flankeforekomster gjennomgående har høyere innhold av Cu og Zn enn aksialforekomster. I tillegg må man ta hensyn til lokale forhold som sedimenttilførsel og generelt vanddyp. En del flankeforekomster inneholder interessante mengder Co. Det er derfor opprettet en egen Co-underklasse for flankeforekomstene. Innholdet av sølv (Ag) ser ikke ut til være systematisk forskjellig mellom de to typene forekomster. Innholdet av Au er varierende, og man bør legge inn muligheten for noe høyere Au-innhold i Co-underklassen.

Valg av gehalter er mer detaljert diskutert under avsnittet om letemodellparametere.

#### 4.1.4 Geologisk ressursmodell

Den aktive sulfidforekomsten TAG på Den midt-atlantiske rygg sør for Azorene er valgt som grunnmodell for den tredimensjonale formen av en typisk hydrotermal sulfidforekomst, inkludert den interne fordelingen av mineralressursene. Valget er gjort fordi dette er en av de best studerte hydrotermale sulfidforekomster i verden. TAG ligger i hengblokken i dalbunnen helt inn mot flankeforkastningen langs østsiden av aksedalen, på den Midt-atlantiske spredningsryggen mellom Azorene og ekvator. I dette området former liggblokken en utstikker under hengblokken der TAG befinner seg, noe som kan påvirke porøsitet og temperatur i liggblokken (Canales et al., 2007). De vesentligste aspekter for vår bruk når det gjelder forekomstens geometri, mineralogi og mineralfordeling, er publisert av Hannington et al. (1998) basert på deres resultater fra ODP-tokt 158<sup>1</sup>, og av Humphris et al. (2015).

En meget nyttig og mye brukt figur framstiller et snitt av undergrunnen i den grunnleggende TAG-modellen (Fig. 4.10). Den viser at forekomsten har form som et kremmerhus med en indre stratigrafi av forskjellige nivåer og soner av mineralinnhold, tekstur og hydrotermal omvandling av avsetninger og sidebergarter. Dette er basert på resultatene fra ODP-boringene på TAG-forekomsten (Fig. 4.11). Øverst i «kremmerhuset» ligger det et lokk av massive sulfidmineraler (mest pyritt) over en sone med massiv sulfidbreksje og anhydritt. Under dette er det utviklet en stockwerksone med breksjer av sulfidmineraler, anhydritt og amorf silika, som lenger ned går over i silifiserte og kloritiserte sidebergartsbreksjer. Stockwerksonen smalner nedover i dypet.

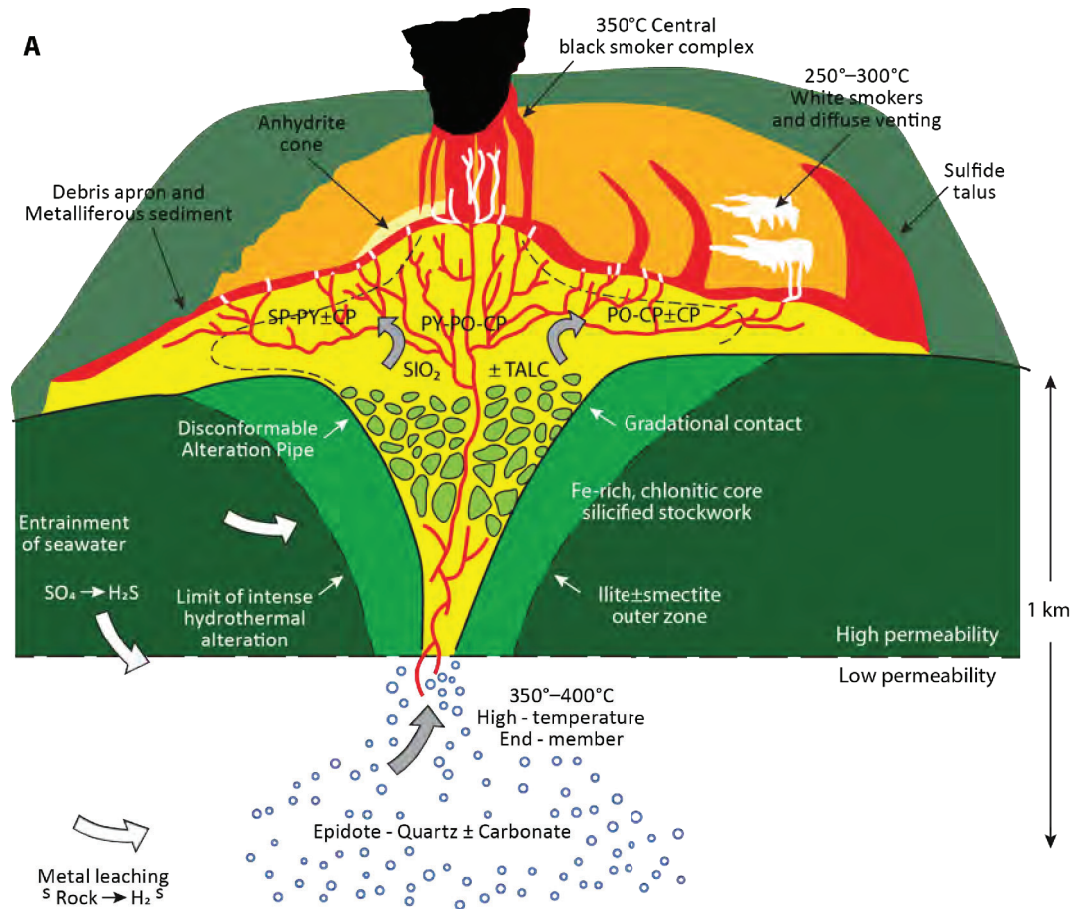


**Fig. 4.10 Geologisk modell for sulfidforekomst**

Generell geologisk modell for hydrotermale sulfidforekomster basert på TAG-forekomsten. Fra Piranjo (2009), etter Hannington et al. (1995).

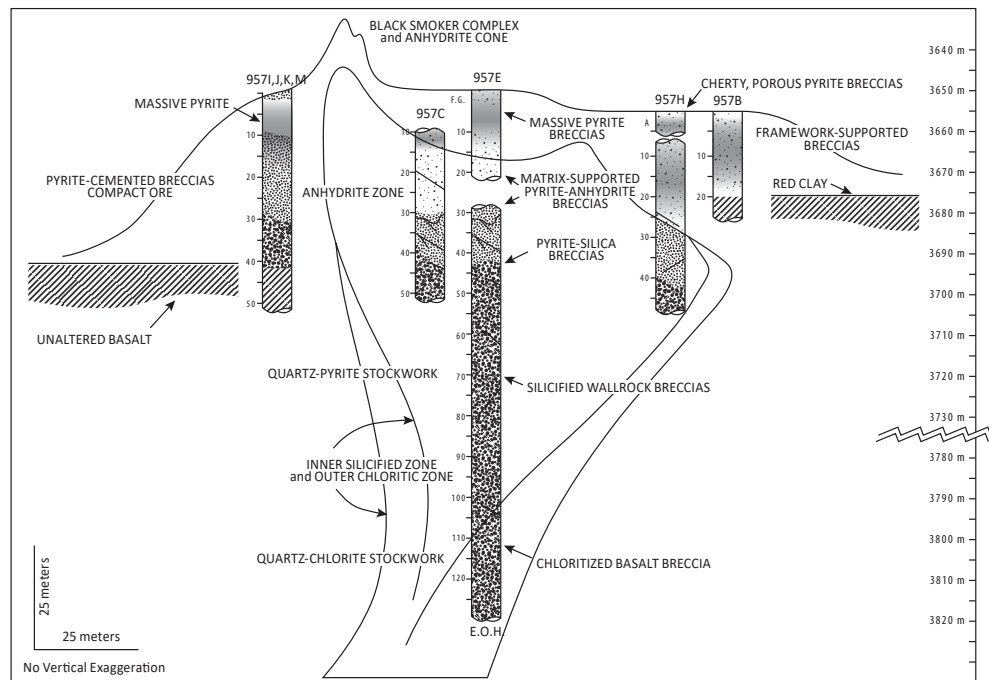


**Fig. 4.11 TAG sulfidforekomst**

Den geologiske strukturen for TAG-forekomsten tolket ut fra borekjernene fra Leg 158 av ODP-programmet (Hannington et al., 1998).

For estimering av mineralressursene er TAG-strukturen videre delt inn i ti soner alt etter mineralogi, metallgehalt, og hvor rene og massive litologiene er (eks. massiv sulfid, breksjert sulfid, breksjer med sidebergart). Ut fra boreresultatene har man anslått de forskjellige sonenes tre-dimensjonale form og størrelse (volum), beregnet massen av sulfid og metall i hver sone, og summert de totale ressursene (se Fig. 4.12 og Fig. 4.13). Denne modellbyggingen og ressursberegningen ville ikke vært mulig uten boreprøvene som viser utviklingen og avgrensingen av forekomsten i dypet.

| Block # | Dimensions | Rock type           | Density | Pyrite (vol%) | Volume (m <sup>3</sup> ) | Σ Tonnes (t) | Pyrite (t) |
|---------|------------|---------------------|---------|---------------|--------------------------|--------------|------------|
| 1       | 40 X 35    | Massive pyrite      | 4       | 80            | 87,970                   | 351,860      | 281,500    |
| 2       | 60 X 15    | Semi-massive pyrite | 4       | 60            | 226,200                  | 904,780      | 542,870    |
| 3       | 70 X 10    | Massive pyrite      | 4       | 80            | 38,480                   | 153,940      | 123,150    |
| 4       | 45 X 25    | Massive pyrite      | 4       | 80            | 238,570                  | 954,260      | 763,410    |
| 5       | 20 X 30    | Anhydrite zone      | 3       | <50           | 9,420                    | 28,270       | 14,140     |
| 6       | 80 X 20    | Anhydrite zone      | 3       | <50           | 100,530                  | 301,590      | 150,800    |
| 7       | 90 X 15    | Pyrite-silica       | 3.75    | 50            | 95,430                   | 357,850      | 178,930    |
| 8       | 85 X 15    | Silicified wallrock | 3.75    | 40            | 85,120                   | 319,190      | 127,680    |
| 9       | 80 X 20    | Silicified wallrock | 3.5     | 30            | 100,530                  | 351,860      | 105,560    |
| 10      | 50 X 25    | Quartz-chlorrite    | 3.5     | 20            | 49,090                   | 161,990      | 32,400     |
|         |            |                     |         |               | 1,031,340                | 3,885,590    | 2,320,440  |

**Fig. 4.12 TAG blokkmodell**

Blokk-modell for TAG-forekomsten (Hannington et al., 1998)

| Dimension                            | Blocks                      | Volume (m <sup>3</sup> ) | Calculated tonnage (t) |
|--------------------------------------|-----------------------------|--------------------------|------------------------|
| Total size of deposit                | Blocks 1–10                 | 1,031,300                | 3,885,600              |
| Exposed mound of massive sulfides*   | Blocks 1–6                  | 701,163                  | 2,695,000              |
| Subseafloor stockwork mineralization | Blocks 7–10                 | 330,160                  | 1,190,900              |
| Total pyrite content                 | Blocks 1–10                 | —                        | 2,320,440              |
| Total Cu                             | 1–2% Cu in blocks 1–10      | —                        | 30,000–60,000          |
| Anhydrite zone                       | 50% anhydrite in blocks 5,6 | 109,950                  | 329,860                |

Note: \* = to a depth of 20–25 m

**Fig. 4.13 TAG tonnasjeberegning**

Størrelsen på TAG-avsetningen inkludert den øvre, massive SMS-sonen og den underliggende stockwerk-sonen.

Foreløpig har vi ikke nok data i den tredje dimensjonen (dypet) i de forekomstene vi har påvist på norsk sokkel, men vi har informasjon om form og areal i kartplanet (overflaten). Ved å kombinere størrelsesforholdene i 3D-modellen for TAG-strukturen med våre form- og arealkart, kan vi beregne hva som kan være realistiske volumer av malm i våre forekomster. I den grad vi har gode tall for metallgehalten i de enkelte forekomstene, får vi da realistiske, mulige ressurstall for disse. Dette brukes til å kalibrere våre letemodeller.

#### 4.1.5 Letemodeller for sulfidforekomster

OD har definert to hovedletemodeller for hydrotermale sulfidforekomster ut fra forekomstenes tektoniske posisjon i spredningsryggens aksedal: Aksialmodellen og flankemodellen. Flankemodellen er delt i to underpopulasjoner: forekomster med mer enn 0,1 pst. Co og forekomster med lavere koboltinnhold. En tredje letemodell er opprettet for to områder med vesentlig grunnere vann: Langs Kolbeinseyryggen i sørvest og i et område med magmatisk oppbygninger rett nord for Jan Mayen ligger havbunnen på vesentlig grunnere dyp (2000 - 300 m) enn i de øvrige områdene. Dette kommer av at



disse områdene er sterkt påvirket av den store varmpunktsdiapiren i jordens mantel under Island. Metallinnholdet i disse områdene skiller seg distinkt fra de øvrige, dypere områdene når det gjelder sink (Zn) og kobber (Cu) (data fra UiB). Dette kan skyldes et lavere vanntrykk, og dermed lavere temperatur på den hydrotermale væsken som strømmer ut (Monecke et al., 2014). Disse områdene er derfor skilt ut i en egen letemodell kalt Gruntvannsmodellen (se også [4.1.5.4 Metallgehalter](#) og [4.1.5.3 Antall forekomster](#)).

For hver letemodell er det definert et sett med de nødvendige parametre som inngår i de statistiske beregningene, og deres tallverdier. Tallverdiene for disse parametrene oppgis med spredning; minimum, forventning og maksimum. I det følgende oppsummeres hvordan, og med hvilken begrunnelse, man har valgt parametre og fastsatt tallverdiene for våre beregninger.

Beregningen av mengden sulfid i hver letemodell er gitt ved:

(Antatt tonn sulfid pr forekomst) x (Antatt antall forekomster) = Tonn sulfid i letemodell

Alternativt kan man beregne antatt tonn malm pr forekomst ved å bruke volum og tetthet:

(Volum<sup>1</sup> sulfid pr forekomst) x (Tetthet sulfid pr forekomst) x (Antall forekomster) = Tonn sulfid i letemodell

<sup>1</sup>Volumer beregnes ved hjelp av areal og tykkelse (dyp) av forekomstene.

For forekomster på land finnes det mye informasjon om variasjonen og fordelingen av mengde per forekomst. For estimering av ressurser på land kan man benytte antatt mengde per forekomst direkte uten å gå veien om volum og tetthet. Denne landstatistikken vil være viktig å bruke som kalibrering for forekomster til havs, men foreløpig ikke som direkte analog.

For forekomster på havbunnen er den tilgjengelige informasjonen om overflatearealer av de enkelte forekomstene langt sikrere enn eventuelle tall for mengde. OD ha derfor valgt å beregne antatt mengde per forekomst ved hjelp av volum (beregnet ved areal og tykkelse (dyp)) og tetthet.

#### 4.1.5.1

#### Volum

For å beregne volumer trenger man overflatearealet av forekomsten, utstrekningen av forekomsten i dypet («tykkelsen»/dypet) og en modell for hvordan areal og dyp henger sammen. Oljedirektoratet har valgt den publiserte TAG-modellen (se [4.1.4 Geologisk ressursmodell](#)) som grunnlag for sin beregningsmodell for sulfidforekomster (Hannington et al., 1998). I beregningsmodellen deles forekomsten i to: øverst en sone kalt den massive sulfidkappen (inneholder lag av massive sulfidutfellinger, sementerte sulfidbreksjer og anhydritt), og under denne en stockwerksone (sulfidmineraliserte breksjer av sidebergart). Den massive sulfidkappen er dannet i overflaten og gir overflatearealet av forekomsten. I henhold til TAG-modellen er arealet i toppen av stockwerksonen ca. en fjerdedel av overflatearealet (sulfidkappen). Volumet av den massive sulfidkappen beregnes som et flak med en gjennomsnittstykkelse. Stockwerksonen har form som et kremmerhus som strekker seg nedover i dypet. I TAG er stockwerksonen ca. 80-100 meter dyp og utgjør ca en tredjedel av den totale



tonnasjen beregnet for TAG (se Hannington et al., 1998). Det vil si at forholdet mellom tonnasjen i stockwerksonen og tonnasjen i den massive sulfidkappen er ca. 0,45. I ressursmodellen brukes dette forholdstallet til å beregne ressursene i stockwerksonen som et tillegg til ressursene i den massive sulfidkappen.

Tall for overflatearealer av marine sulfidforekomster er tilgjengelig fra publikasjoner og ODs egen kartlegging. Hannington et al. (2010) presenterer en global oversikt over størrelser og gehalter fra kjente forekomster i dagens spredningsrygger i oseanene og øybuebassenger. Tallene som er oppgitt for forekomster fra spredningsryggene er benyttet i "kalibreringen" av våre valgte parameterverdier (se Tab. 7.3). Det aritmetriske gjennomsnitt av forekomster med areal større enn 1000 m<sup>2</sup> (30 stk.) fra midt-oseanryggene er ca. 35 000 m<sup>2</sup>. Dette er valgt som middelveidien for forekomststørrelsen i ODs beregninger. Til sammenligning er dette større enn grunnarealene av Lokeslottet (26 000 m<sup>2</sup>) og Fåvne (10 000 m<sup>2</sup>), mens Mohnsskatten er ca. dobbelt så stor.

Den massive sulfidkappen i en forekomst består i overflaten av områder med skorsteiner og kjegleoppbygninger opp til 20-30 meters høyde. Men den gjennomsnittlige høyden av sulfidkappen må settes slik at den representerer den gjennomsnittlige tykkelsen av sulfidkappen utjevnet over hele arealet. Solwara-1-feltet, som består av et svært variert landskap av 10-20 meter høye skorsteinskjegler, ble i 2008 beregnet til å inneholde ca. 2,1 millioner tonn sulfider på et areal på ca 90 000 m<sup>2</sup> (Hannington et al., 2010). Dette tilsvarer en gjennomsnittstykkelse på 6 meter, gitt en tetthet på 3,5. En detaljert reserveberegning gjort seinere (Lipton et al., 2012) gir ca. samme resultat. En slik utjevning av terrenget kan sammenlignes med at man samler volumet fra en 18 meter høy kjegle i en 6 meter høy sylinder på samme areal. Ved en slik betraktning vil Lokeslottet, som består av to kjegler på drøyt 20 meter, få en gjennomsnittstykkelse på 6-7 meter. Mange av de publiserte forekomstene oppgis å ha en gjennomsnittstykkelse på den massive sulfidkappen på 4-10 meter (Cherkashov et al., 2010), og OD ha valgt å legge seg på dette nivået i sine beregninger. TAG-forekomsten er spesiell ved at den har en gjennomsnittstykkelse på 23 meter på et areal på 31 000 m<sup>2</sup>. TAG er en ung forekomst på ca 20 000 år (Cherkashov et al., 2017). Den må derfor ha hatt en høy og jevn aktivitet for å kunne ha jevnet seg så godt ut under oppbygging.

På grunn av den magmatiske aktiviteten i aksedalen, vil en god del av aksialforekomstene generelt sett ikke bli eldre enn 25 000 - 50 000 år. Denne begrensingen gjelder ikke for flankeforekomstene, som dermed i enkelte tilfeller kan være aktive over flere titalls- til hundretusener år og dermed vokse til betydelig større maksimumsstørrelser. Dette må det tas høyde for i spredningen i størrelser.

Derfor benyttes følgende parametre (Tabell 4.1 og 4.2) for beregning av volumet i forekomstene basert på den massive sulfidkappen:

**Tab. 4.1 Volumtall for modellering av sulfidforekomster - aksialforekomster**

|   |                     |
|---|---------------------|
| Overflateareal, massiv sulfidkappe (km <sup>2</sup> ) | 0,001 – 0,035 – 0,3 |
| Tykkelse, massiv sulfidkappe (m)                      | 1,5 – 6 – 15        |
| Stockwerksonen beregnes som tillegg med forholdstall  | 0,4 - 0,45 - 0,5    |

**Tab. 4.2** Volumtall for modellering av sulfidforekomster - flankeforekomster

|   |                           |
|---|---------------------------|
| <b>Overflateareal, massiv sulfidkappe (km<sup>2</sup>)</b>  | <b>0,001 – 0,04 – 0,5</b> |
| <b>Tykkelse, massiv sulfidkappe (m)</b>                     | <b>1,5 – 6 – 15</b>       |
| <b>Stockwerksonen beregnes som tillegg med forholdstall</b> | <b>0,4 - 0,45 - 0,5</b>   |

OD har benyttet denne beregningsmodellen på tre forekomster med data fra egen kartlegging og universitetene - Mohnsskatten, Fåvne og Lokeslottet. Resultatene stemmer godt med størrelser publisert for marine forekomster andre steder, som referert til ovenfor.

#### 4.1.5.2 Tetthet

Tettheten av sulfidavsetningene varierer med innholdet av anhydritt og breksjert materiale. Tettheten av massiv sulfid er 4. Ved innblanding av anhydritt eller breksjer blir den lavere. I TAG er tettheten i anhydrittsonene satt til 3 og i stockwerksonen til 3,5 – 3,75. Imidlertid blir anhydritten oppløst og mobilisert etter at den hydrotermale aktiviteten opphører. Tettheten i denne sonen vil da øke og bli nær tettheten av massiv sulfid.

For modellene benyttes følgende tetthet:

**Tab. 4.3** Tetthet for modellering av sulfidforekomster

|                       |                        |
|-----------------------|------------------------|
| <b>Kappesonen</b>     | <b>3,75 – 3,9 – 4</b>  |
| <b>Stockwerksonen</b> | <b>3,5 – 3,7 – 3,8</b> |

#### 4.1.5.3 Antall forekomster

Beregnet antall forekomster i letemodellene blir fastsatt ut fra en antatt frekvens av forekomster langs aksedalen i spredningsryggen og en ekstrapolering av denne til de fossile aksedalerestene som ligger i flankeviddene, begrenset av graden av overdekning av sedimenter (se [4.1.2 Utbredelsen av sulfidforekomster - prosessene utenfor aksedalen](#)).

Ifølge vitenskapelig litteratur er det omtrent 100 km mellom hver aktiv hydrotermalforekomst langs ultrasakte spredningsrygger (Hannington et al., 2010). Men det påpekes også at tallet med stor sannsynlighet ikke er representativt for den reelle frekvensen av alle sulfidforekomster, som antas å være til dels mye høyere. Særlig må en forvente at det finnes langt flere inaktive forekomster enn til nå oppdaget (Cherkashov et al., 2010).

Til nå er det påvist seks aktive forekomster langs den 600 km lange Mohnsryggen (fra Jan Mayen til Lokeslottet), altså én forekomst pr 100 km. Disse er fra sentralt i aksedalen og den nordvestre flanken. I tillegg er det funnet to inaktive forekomster (Gnitahei og Mohnsskatten), samt spor av en til (Kobberåsen). Dette gir ni oppdagede forekomster totalt langs Mohnsryggens aksedal, ca 1,5 pr 100 km. Til sammenligning har man i det russiske kontraktsområdet på den midt-atlantiske rygg nå rapportert til sammen 24 forekomster, hvorav ni aktive, over en avstand på 880 km, dvs. 2,7 forekomster per 100 km (Cherkashov et al., 2010; Sudarikov et al., 2021). Fra litteraturen ser det ut til at frekvensen av flankeforekomster kan være betydelig høyere enn for aksialforekomster

(Cherkashov et al. 2010; 2017). Den sørøstre flanken av Mohnsryggen er lite undersøkt og det forventes at det vil finnes et tilsvarende antall forekomster langs denne som langs nordvestflanken, altså opp mot en dobling av dagens registrerte (dvs. antallet aktive kan økes til 12). Dette støttes ved at det er registrert to anomalier i vannsøylen i de sørlige delene av aksedalen (Stensland et al., 2019).

I det russiske kontraktområdet har man datert en rekke av forekomstene (Cherkashov et al., 2017). Det viser at de fleste forekomstene har vært aktive i flere perioder. Forekomstene der deles inn i tre aldersklasser etter sin eldste registrerte, aktive periode (maksimumsalder): unge, 0-25 000 år, middelaldrende, 25 000-90 000 år, og gamle, over 100 000 år. Forekomsten Petersburgskoye har den høyeste maksimumsalder med ca. 225 000 år. Levetiden for nye forekomster kan da antas å ligge omtrent midt mellom de unge og middelaldrende forekomstene her. På Mohnsryggen kan dette representeres av Lokeslottet med sine på 20 000 år. Å anta 12 slike forekomster til enhver tid langs Mohnsryggens aksedal, vil teoretisk sett innebære dannelsen av 600 forekomster i løpet av 1 million år.

Aksedalen er generelt 15-20 km bred innenfor kantene av flankeforkastningene. Flankeforkastningene er 1-2 km brede i kartplanet, og utgjør dermed 10-20 pst. av hele aksedalens bredde. Vi antar da at av de forekomstene som utvikles i løpet av 1 mill år, vil ca. 90 utvikles i flankesonene mens resten (510) utvikles i dalbunnen. I følge Stubseid et al. (2023) blir grovt sett halvparten av arealet av dalbunnen vulkansk fornyet i løpet av 25 000 år, og mer enn 90 pst. blir fornyet i løpet av 100 000 år. Det betyr at så godt som alle de ca 450 forekomster som ble dannet i dalbunnen før 100 000 år siden ikke lenger finnes i overflaten, men er begravet av lava. Av de som er yngre kan man anta at i størrelsesorden halvparten (25-30), fremdeles finnes i overflaten. I flankesonene, som er langt mindre magmatisk aktive enn dalbunnen, vil en langt større andel av forekomstene forbli i overflaten. Innen det russiske kontraktområdet er anslagsvis 80 pst. av de aktive forekomstene oppdaget utenfor dalbunnsområdene (Cherkashov et al. 2010; 2017).

Dette innebærer at det kan finnes ca. 115 forekomster innenfor aksedalen. Det totale arealet av aksedalen, med flanker, regnes som ca. 1 200 km<sup>2</sup> (20 km x 600 km). Basert på dette, får vi en antatt forventet tetthet (**F**) på 9,5 forekomster per 1 000 km<sup>2</sup> i områdene av dagens og fortidens aksedaler. Tallet er usikkert; dette er det tatt høyde for ved at det er satt en minimums- og maksimumstetthet til hhv. 4 og 12 forekomster per 1 000 km<sup>2</sup>.

Man kan anta samme tetthet (med spredning) av forekomster i gjennomsnitt i de tidligere aksedalene som i dagens. Dette snittet er gjort gjeldene for de områder som er prospektive til hver side av av dagens aksedal for alle de tre spredningsryggene, Kolbeinseyryggen, Mohnsryggen og Knipovitsryggen. I sør gjelder det områdene i Gruntvannsmodellen, dvs langs Kolbeinseyryggen og i de magmatisk oppbygningene nord for Jan Mayen (se [4.1.1 Dannelsen av sulfidforekomster - aktiviteten i aksedalen](#) og [4.1.5.4 Metallgehalter](#)). Langs Mohnsryggens nordvestside vil det gjelde fjellandskapet i Grønlandshavet nord for Jan Mayen-bruddsonen ut til trinnet i havbunnskorpen ved anomali 13 - 18. Vestenfor ligger havbunnen 300-400 meter dypere og er blitt overdekket av sedimenter. I Grønlandshavet omfatter norsk kontinentalsokkel områdene innenfor 200-milssonen rundt Jan Mayen og et mindre, smalere område langs nordre del av Mohnsryggen. I sørøst er fjellandskapet blottet kun i en relativt smal sone langs aksedalen, resten er dekket av Bjørnøyviftas sedimenter i Lofotbassenget. Langs Knipovitsryggen brukes samme forekomst-tetthet som langs Mohnsryggen i en relativt

smal sone (80 km) langs ryggens vestsida. Østsida er dekket av sedimenter fra de submarine viftene langs kanten av Barentshavet (se også [4.1.2 Utbredelsen av sulfidforekomster - prosessene utenfor aksedalen](#)).

Områdene beskrevet ovenfor er delt inn i fem med hvert sitt areal for beregning av det totale antallet forekomster innenfor arealet som er angitt som prospektivt for sulfider (Fig. 4.9 ,Tab. 4.4 )

**Tab. 4.4 Prospektive arealer, modellering av sulfidforekomster**

|    |   |                        |
|----|---|------------------------|
| 1. | Områder nord og vest for Jan Mayen-ryggen         | 53 200 km <sup>2</sup> |
| 2. | Grønlandshavet innenfor Jan Mayens fiskerisone    | 80 850 km <sup>2</sup> |
| 3. | Sone langs Mohnsryggens aksedal i Lofotbassenget  | 24 850 km <sup>2</sup> |
| 4. | Grønlandshavet vest for nordre del av Mohnsryggen | 10 600 km <sup>2</sup> |
| 5. | Områdene langs Knipovitsjryggen                   | 53 000 km <sup>2</sup> |

På grunn av sedimentasjonen gjennom tid vil en del av forekomstene i tre av disse områdene (1, 2, 3 og 5) være overdekket av sedimenter og ikke tilgjengelige (se [4.1.2 Utbredelsen av sulfidforekomster - prosessene utenfor aksedalen](#)). Antallet forekomster blir derfor nedkortet tilsvarende. Det gjøres også nedkorting i gruntvannsområdet nord og vest for Jan Mayen-ryggen (område 1) fordi området/havbunnsstopografien ikke gjenspeiler systematisk de magnetiske anomaliene med klare paleo-flankeskrenter slik de gjør langs Mohnsryggen. Beregning av antall forekomster med spredning innenfor hvert delareal blir da som i [Tab. 4.5](#).

**Tab. 4.5 Antall forekomster i hvert delareal, modellering av sulfidforekomster**

|    |                                      |                    |                          |
|----|--------------------------------------|--------------------|--------------------------|
| 1. | Antall = 53 200 x F (= 4 - 9,5 - 12) | nedkortet med 40 % | 128 - 303 - 383          |
| 2. | Antall = 80 850 x F (= 4 - 9,5 - 12) | nedkortet med 60 % | 129 - 307 - 388          |
| 3. | Antall = 24 850 x F (= 4 - 9,5 - 12) | nedkortet med 60 % | 40 - 94 - 119            |
| 4. | Antall = 10 600 x F (= 4 - 9,5 - 12) | nedkortes ikke     | 42 - 101 - 127           |
| 5. | Antall = 53 000 x F (= 4 - 9,5 - 12) | nedkortet med 60 % | 85 - 201 - 254           |
|    |                                      |                    |                          |
|    | <b>Totalt antall forekomster</b>     |                    | <b>424 - 1007 - 1272</b> |

Tallene gjelder for alle letemodeller samlet. Antallet forekomster i Gruntvannsmodellen er gitt direkte fra beregningen av delområde 1. Det resterende antallet fordeles med 75 pst. på Flankemodellen og 25 pst. på Aksialmodellen. Dette fordi litteraturen sier at frekvensen av flankeforekomster er vesentlig høyere enn for aksialforekomstene. I tillegg er oppbevaringspotensialet for aksialforekomstene lavere enn for flankeforekomstene (se [4.1.2 Utbredelsen av sulfidforekomster - prosessene utenfor aksedalen](#)). Videre fordeles antallet forekomster i Flankemodellen med 65 pst. på Cu-Zn-typen og 35 pst. på Co-typen. Det samlede antall forekomster fordeles derfor som i [Tab. 4.6](#).

Tab. 4.6 Sum antall forekomster, modellering av sulfidforekomster

|  |                        |
|--|------------------------|
| <b>Gruntvannsmodellen, antatt antall forekomster</b>         | <b>128 - 303 - 383</b> |
| <b>Aksialmodellen, antatt antall forekomster</b>             | <b>74 - 176 - 222</b>  |
| <b>Flankemodellen, Co-type, antatt antall forekomster</b>    | <b>78 - 185 - 233</b>  |
| <b>Flankemodellen, Cu-Zn-type, antatt antall forekomster</b> | <b>144 - 343 - 433</b> |

4.1.5.4

Metallgehalter

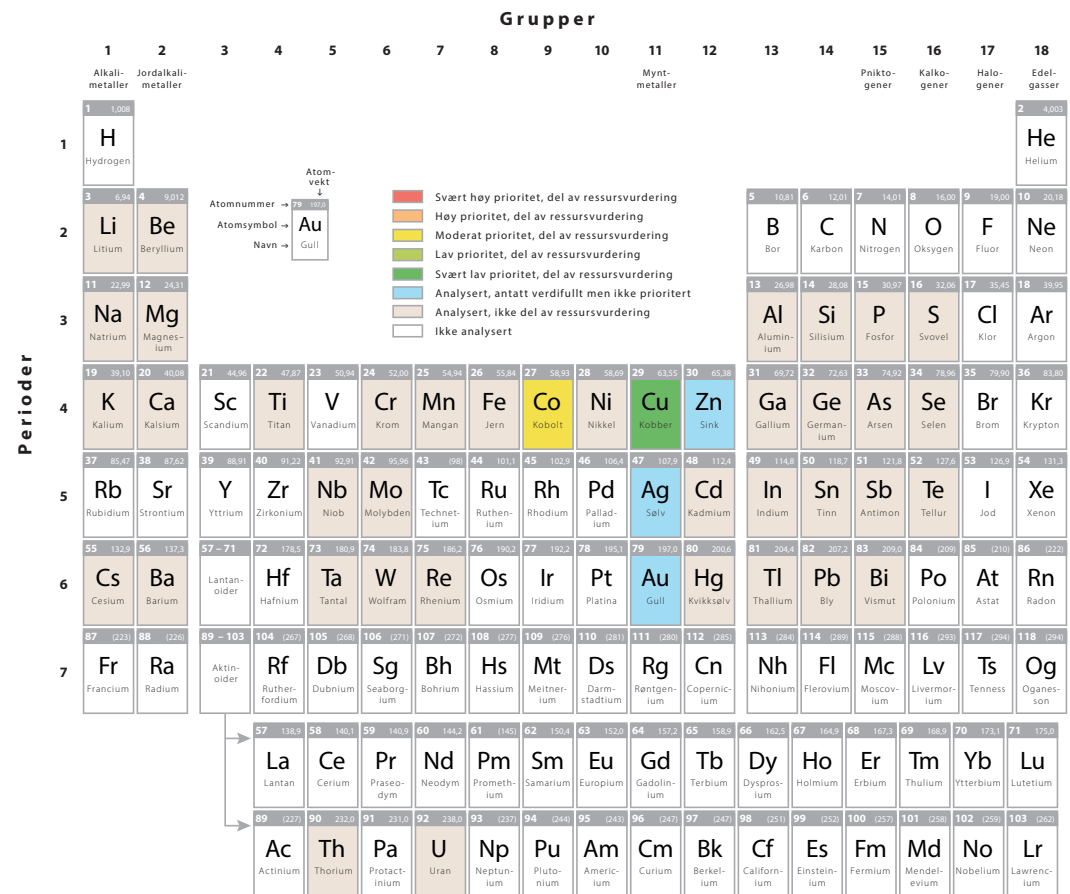


Fig. 4.14 Oversikt over grunnstoff analysert for i sulfidvurderingene

I tabellene Tab. 4.7, Tab. 4.8, Tab. 4.9 og Tab. 4.10 oppgis antatt metallgehalt for Cu, Zn, Co, Au og Ag. Det antas at aksialforekomstene vil generelt ha noe lavere innhold av Cu og Zn enn flankeforekomstene. Representative gehalter er vurdert ved å benytte tall publisert fra andre steder på Den midt-atlantiske rygg (se Hannington et al., 2010). Som gjennomsnitt for midt-oseanske rygger oppgir Hannington 5,9 pst. Cu og 6,1 pst. Zn. Samtidig påpeker forfatterne at dette er gjennomsnittet av analyser av prøver som er plukket fra overflaten av havbunnen. Slike prøver er plukket selektivt for andre formål enn å få et statistisk representativt utvalg, og kan slik sett gi en skjev fordeling. Mest sannsynlig har dette gitt en overestimering av gjennomsnittsgehaltene. Dette understøttes av at analyser fra borekjerne tatt under havbunnen stort sett gir vesentlig lavere gehalter, ofte en halvering (Hannington et al., 2010). I sine egne beregninger av

ressursene i TAG, har de samme forfatterne brukt 2,0 pst. Cu i SMS-sonen og 1,0 pst. Cu i stockwerksonen (Hannington et al., 1998; Hannington et al., 2010). Dette er basert på boreresultat foretatt på TAG under ODP 158.

Gjennomsnittsgeneholdene for Cu og Zn i dagens spredningsrygger ligger stort sett høyere enn i de analoge VMS-avsetningene på land (vulkanogene massive sulfidforekomster). De landforekomstene som er de beste analogene til dyphavsforekomstene er de som har mafiske vertsbeararter og ligger i fjellkjedene. Franklin et al. (2005) oppgir et gjennomsnitt på 1,82 pst. Cu og 0,84 pst. Zn for slike avsetninger. Barrie og Hannington (1999) oppgir hhv 2,04 pst. Cu og 1,82 pst. Zn for mafiske forekomster. Årsaken til forskjellen i nivået på gjennomsnittet for Zn i publikasjonene er ukjent, men det kan komme av utvalget og antallet forekomstanalyser. Tallene fra Barrie og Hannington (1999) er videre underbygget av Galley et al. (2007). Gjennomgang av databasen over Fennoskandiske malmavsetninger i Kaledonidene (se Tab. 7.1, Tab. 7.2), viser gjennomsnitt på 1,68 pst. Cu og 2,77 pst. Zn for alle forekomstene (gjennomsnitt fra hhv. 112 og 95 forekomster). Men disse gjennomsnittene inkluderer også forekomster med sedimenter og alle typer vulkanitter som vertsbeararter, som hver for seg gir noe forskjellige gjennomsnitt. For utvalget av de med mafisk vertsbearart (grønnstein og amfibolitt), får man et gjennomsnitt på 1,80 pst. Cu og 2,39 pst. Zn (gjennomsnitt fra hhv. 32 og 24 forekomster) fra samme database. Dette er i samsvar med tallene til Barrie og Hannington (1999).

Forskjellen i de oppgitte gjennomsnittsgeneholdene for forekomstene langs de oseanske spredningsryggene og landforekomstene, ser ut til å være reell selv om man tar hensyn til den mulige skjevheten i utvalget fra havbunnen. Dette gjelder særlig for havbunnsforekomster med ultramafiske vertsbeararter. For disse ligger de gjennomsnittlige geneholdene for Cu og Zn ofte på 10-15 pst. (Cherkashov et al., 2010; Hannington et al., 2010). Dette er bl.a. rapportert fra den midt-atlantiske rygg sør for Azorene (Cherkashov et al., 2010), men til nå har man ikke påvist slike forekomster langs Mohnsryggen eller Knipovitsjryggen. Gjennomsnittsgeneholdene for Cu og Zn for forekomster med mafiske vertsbeararter (basalt) fra Midt-Atlanteren viser en variasjon på 1,7-3,7 pst. for Cu og 0,4-2,4 pst. for Zn (Cherkashov et al., 2010). Til sammenligning er gjennomsnittet for analysene av Cu og Zn fra Mohnsskatten på hhv. 0,9 og 2,7 pst. (tall fra Oljedirektoratet), og fra Fåvne på hhv. 3,6 og 7,2 pst. (tall fra Oljedirektoratet, UiB, og Sahlström et al., 2022).

I de sedimentpåvirkede områdene aksialforekomstene er metallinnholdet generelt lavere. Lokeslottet inneholder et snitt på 0,96 pst. Cu, 1,52 pst. Zn, 0,4 ppm (parts per million) Au og 20 ppm Ag (tall fra UiB, Snook et al., 2018, Sahlström et al., 2022). I gruntvannsområdene er metallinnholdet på nivå med flankeforekomstene, men forskjøvet mot Zn. Snittet for forekomstene Soria Moria, Perle & Bruse og Trollveggen er 0,36 pst. Cu, 8,25 pst. Zn, 0,92 ppm Au og 40,75 pst. Ag (alle data fra UiB). Dette er det tatt hensyn til i spredningen i tallene for Aksialmodellen og Gruntvannsmodellen.

Med unntak av de sedimentpåvirkede forekomstene, varierer Au og Ag moderat mellom forekomster med mafiske vertsbeararter på spredningsryggene, rundt 2 ppm Au og 70 ppm Ag. Dette ligger konsekvent markant høyere enn i analogene på land. En del dyphavsforekomster med ultramafiske vertsbeararter har vesentlig høyere gjennomsnitt for Au, opp til 40-50 ppm (se Cherkashov et al., 2010). Dette er det forsøkt tatt vare på ved å øke maksverdiene for geneholdene i den koboltførende letemodellen.

I vurderingen av gehaltverdier for våre beregninger er det lagt mest vekt på analyser av materiale kjernetatt under overflaten av havbunnen. Samtidig tar vi høyde for at gehaltene i dyphavet faktisk ligger høyere enn i de fossile analogene på land (se diskusjonen ovenfor). Tall for beregningene er gitt i tabellene [Tab. 4.7](#), [Tab. 4.9](#) og [Tab. 4.10](#).

**Tab. 4.7 Aksialmodell, metallgehalt**

| Cu (% wt) | 0,5 | 1,2 | 4   |
|-----------|-----|-----|-----|
| Zn (% wt) | 0,5 | 1,5 | 5   |
| Au (ppm)  | 0,1 | 0,3 | 3   |
| Ag (ppm)  | 1   | 17  | 100 |

**Tab. 4.8 Gruntvannsmodell, metallgehalt**

| Cu (% wt) | 0,2 | 0,5 | 5   |
|-----------|-----|-----|-----|
| Zn (% wt) | 0,5 | 5   | 9   |
| Au (ppm)  | 0,5 | 1   | 3   |
| Ag (ppm)  | 0,5 | 40  | 150 |

**Tab. 4.9 Flankemodell med Co, metallgehalt**

| Cu (% wt) | 0,8  | 3    | 7   |
|-----------|------|------|-----|
| Zn (% wt) | 0,5  | 3    | 7   |
| Co (% wt) | 0,03 | 0,33 | 0,6 |
| Au (ppm)  | 1    | 2    | 5   |
| Ag (ppm)  | 1    | 70   | 170 |

**Tab. 4.10 Flankemodell uten Co, metallgehalt**

| Cu (% wt) | 0,8 | 4  | 7   |
|-----------|-----|----|-----|
| Zn (% wt) | 0,5 | 3  | 5   |
| Au (ppm)  | 1   | 2  | 3   |
| Ag (ppm)  | 1   | 70 | 170 |

## 4.2 Sulfideksempel Mohnsskatten

For konkretisering av sulfidforekomster, er det gjort en mer detaljert modellering i form av et regneeksempel på Mohnsskatten. Mohnsskatten er sulfidforekomsten hvor OD har best datadekning. Mohnsskatten er lokalisert i skrenten på en av de store hovedforkastningene som utgjør nordvestflanken av aksedalen i nordlig del av Mohnsryggen (se [Fig. 4.15](#)).



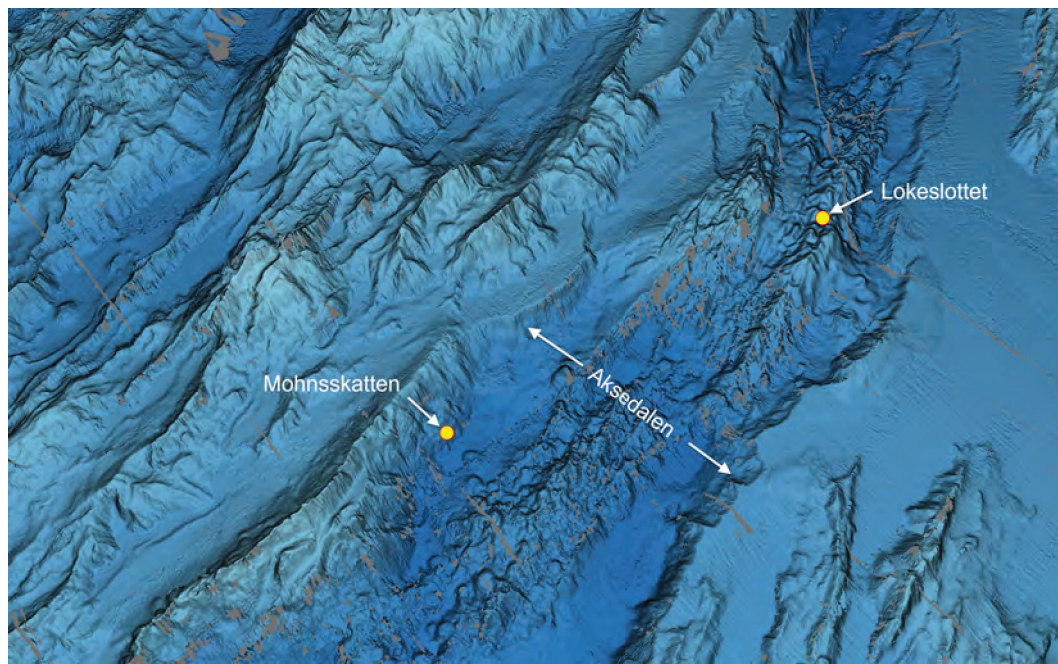


**Fig. 4.15 Mohnsskattens (og Lokeslottets) beliggenhet**

Perspektiv kart over nordlig del av Mohnsryggen sett fra sørøst. Det viser Lokeslottets tektoniske plassering på en vulkanrygg sentralt i aksedalen i nord, og Mohnsskatten på flanken lenger sør.

#### 4.2.1 Geologi og tektonisk ramme

Spranget på hovedforkastningen ved Mohnsskatten er på ca 1200 meter, slik at dagens forkastningsskrent går fra eggen på ca 2000 meters dyp til foten langs dalbunnen på 3200 meter. Denne skrenten representerer overflaten av ligg-blokken av forkastningen og vil vokse videre så lenge forkastningen er aktiv og ligg-blokken hever seg. Forkastningen er fremdeles aktiv, og dagens spranghøyde har utviklet seg ved gjentatte episoder med større og mindre sprang gjennom forkastningens levetid. Disse forkastningsepisodene har påvirket og modifisert den store forkastningsskrenten.

Batymetrikartene viser at i området ved Mohnsskatten er hoved-forkastningsskrenten internt forkastet og glidd ut langs et 7-8 km langt og skålformet (listrisk) forkastningsplan (Fig. 4.16). Området innenfor denne forkastningsblokken ble da brutt opp i et system av mindre forkastninger. En sentral, sidelengs forkastning går i fallretningen og deler blokken i to deler med hvert sitt system av normalforkastninger i strøkretningen. I tillegg er området karakterisert av mer eller mindre skålformede skredgroper og tilhørende skredvifter. Skredviftene ligger langs dalbunnen ved foten av hovedforkastningsskrenten og langs foten av en større normalforkastning lenger opp i skrenten (Fig. 4.16).



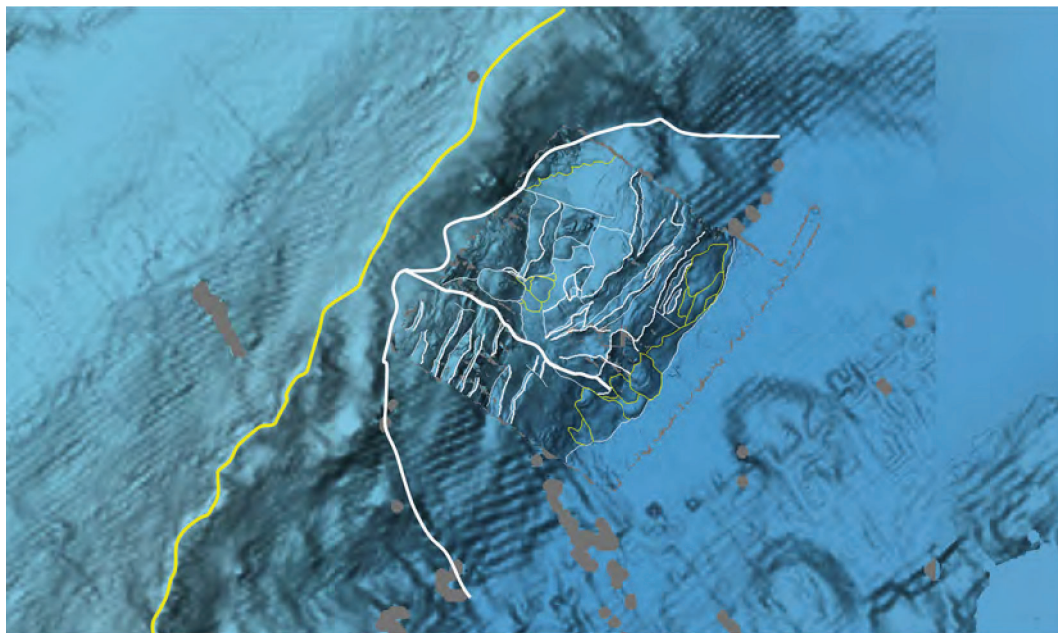


**Fig. 4.16 Forkastningsskrenten ved Mohnsskatten**

Kart over hovedforkastningsskrenten i området omkring Mohnsskatt-teigen. Eggen på skrenten er vist med tykk, gul linje. Bakkanten av den listriske forkastningsblokken og den sentrale sidelengsforkastningen som deler blokken i to er vist med tykk, hvit linje. De mindre, interne forkastningene i den listriske blokken er vist med tynn, hvit linje. Omrisset av de lokale skredviftene er vist med tynn, gul linje.

Mohnsskatten ligger på 2800-3000 meters vanddyb innenfor den nordlige forkastningsblokken i den nedre del av hovedskrenten, ca. 200 meter over den flate dalbunnen. Mohnsskatten er en sulfidteig bestående av inaktive skorsteiner, kjegler og hauger. En lokal, skålformet skredgrop er dannet i dette området, og sulfidteigen er utviklet på oversiden av og nedover skråningen i denne gropen (Fig. 4.17). Langs kanten på toppen av skråningen består sulfidteigen av en rekke med 18-20 meter høye, sammengrodde hauger og kjegler. Disse sammengrodde strukturene strekker seg videre nedover skråningen i skredgropen. Haugene langs kanten ser ut til å ha blitt kuttet av den opprinnelige skredflaten, men nye kjegler og hauger har vokst oppå og dekker nå denne flaten (Fig. 4.18). Dette betyr at skredgropen er dannet etter at den hydrotermale aktiviteten begynte, men en god tid før den sluttet. Det er mulig at den hydrotermale aktiviteten har svekket og destabilisert undergrunnen og dermed utløst skredet.

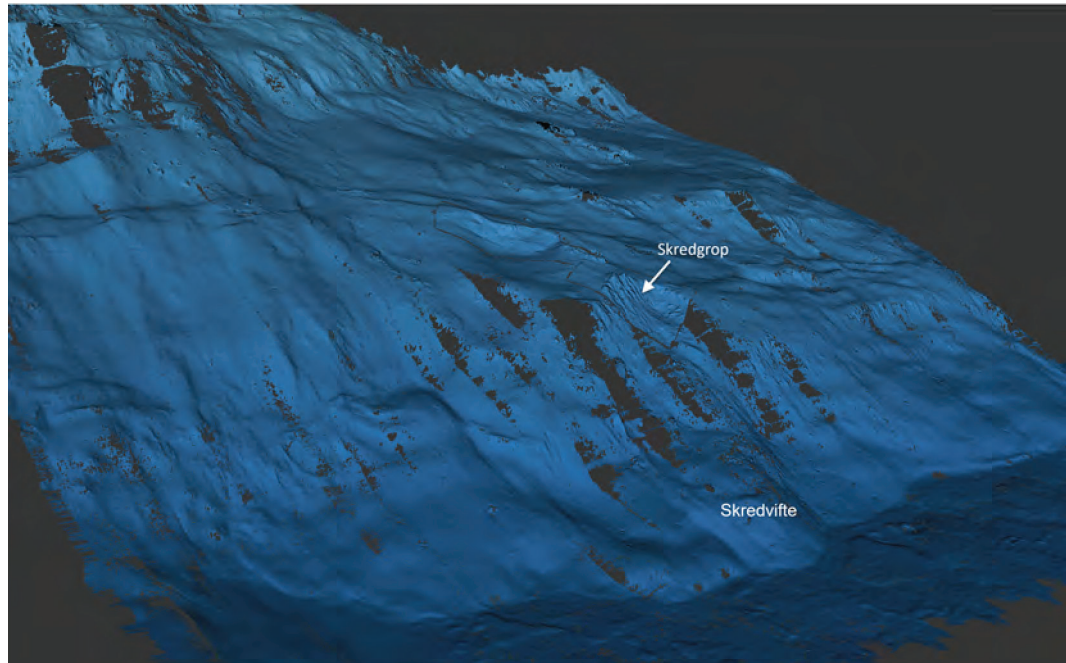


**Fig. 4.17 Mohnsskattens beliggenhet i skrenten**

Perspektivkart som viser beliggenheten av Mohnsskatten i flankeforkastningsskrenten. Her vises skredgropen sentralt i forekomsten og skredviften nedenfor.

Ovenfor haugene og kjeglene på skråningskanten fortsetter sulfidteigen som en 70 m bred og 150 m lang sulfidrygg av hauger og kjegler. Denne delen av teigen er skilt fra sulfidavsetningene på kanten av skredgropa av en 30 m bred sone uten synlige sulfidavsetninger (Fig. 4.18). Mohnsskatt-teigen består altså av to deler i overflaten (A og B). Selv om avstanden mellom er liten, har man vurdert to modeller for hvordan disse fortsetter ned i undergrunnen (se 4.2.2 Geokjemi og undergrunnsmodell).

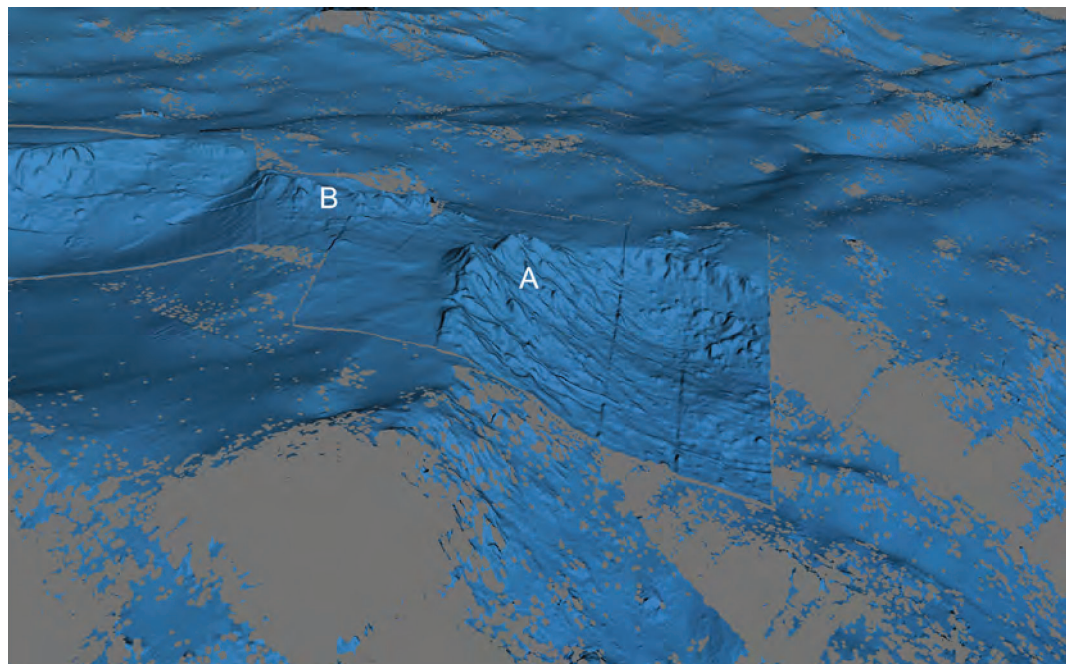


**Fig. 4.18 Mohnsskatt-teigens A- og B-områder**

Perspektivkart som viser skredgropen med sulfidhauger langs øvre kant. Litt vest for kanten på skredgropen ligger en mindre sulfidrygg omtalt i teksten.



Nedenfor den lokale skredgropen, ved foten av flankeforkastningen, ligger det en skredvifte som antagelig inneholder massene fra det lokale skredet (se Fig. 4.17). Da det antas at skredet gikk mens sulfidene ble avsatt, regner en med at denne viften også kan inneholde betydelige mengder med sulfid.

#### 4.2.2 Geokjemi og undergrunnsmodell

OD har analysert 61 sulfidprøver tatt på Mohnsskatten i 2020. Analysene ble utført på AtLab i Canada (se excelark tilgjengelig på ODs hjemmeside). Ved å skille ut prøver med mer enn 1 pst. Cu og 1 pst. Zn, fikk man en klar indikasjon på at Mohnsskatten kan inndeles i Cu-rike og Zn-rike soner (Fig. 4.19). Det ble også tatt 75 prøver av sidebergartene. 38 av disse prøvene ser ut til å være hydrotermalt påvirket (mineralogi og struktur) og gir grunnlag for å indikere en hydrotermal sone som omslutter sulfidavsetningene (Fig. 4.19).

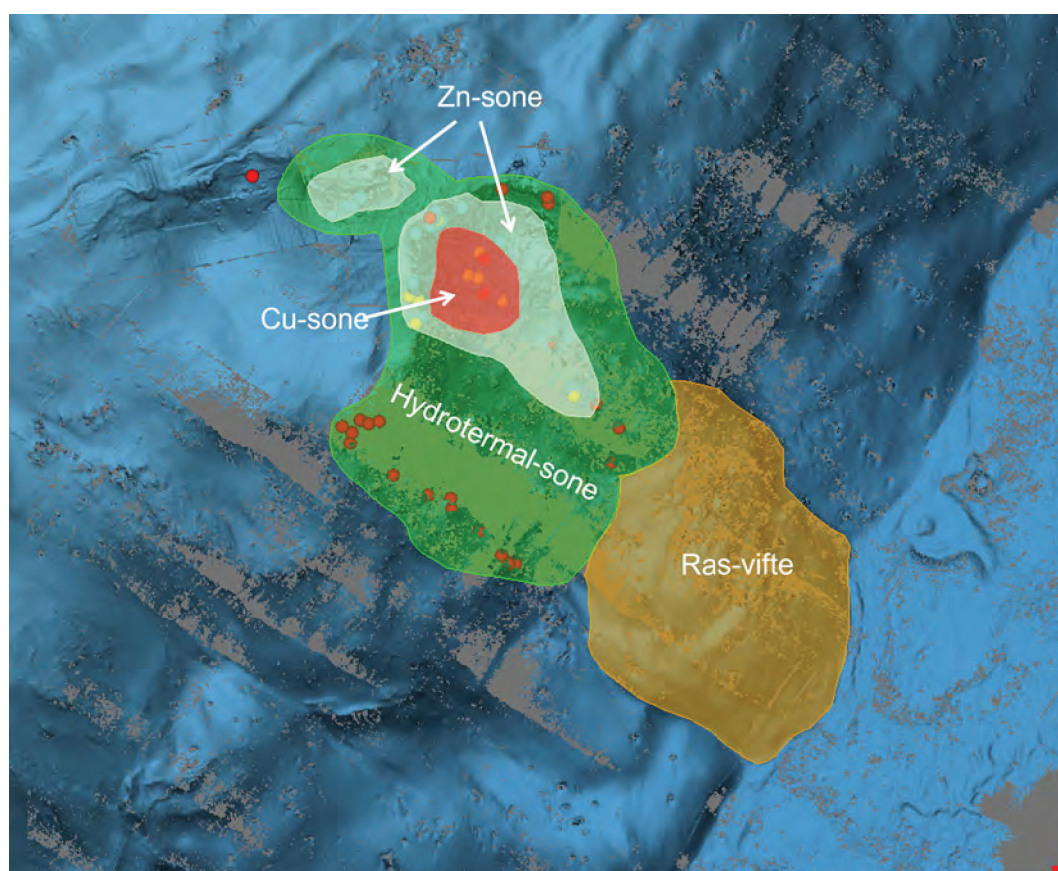


**Fig. 4.19 Mohnsskatten med soneinndeling**

Kart over Mohnsskatten sulfidvang. Den kopperrike sonen er vist med rødt, de sinkrike sonene vist med hvitt, den hydrotermalt påvirkede sonen i sidebergartene er vist med grønt, og skredviften som antas å inneholde sulfidressurser nedenfor er vist med oransje.

Denne soneinndelingen i kartplan er kombinert med den tredimensjonale TAG-modellen for å predikere to mulige, realistiske, tredimensjonale modeller for Mohnsskatten (se Fig. 4.20 og Fig. 4.21). I den ene, Modell 1, løper sulfidavsetningene i de to delene av Mohnsskatten sammen i undergrunnen, adskilt av 30 meter med hydrotermalt påvirkede sidebergart øverst mot overflaten (Fig. 4.20) I Modell 2 sitter de to delene over hvert sitt tilførselsrør (med stockwerksone) langs adskilte sprekkesoner ned i dypet til raksjonssonen (Fig. 4.21). Dimensjonene i modellene er tatt fra TAG-modellen kombinert med kartbildet i overflaten (Fig. 4.22).

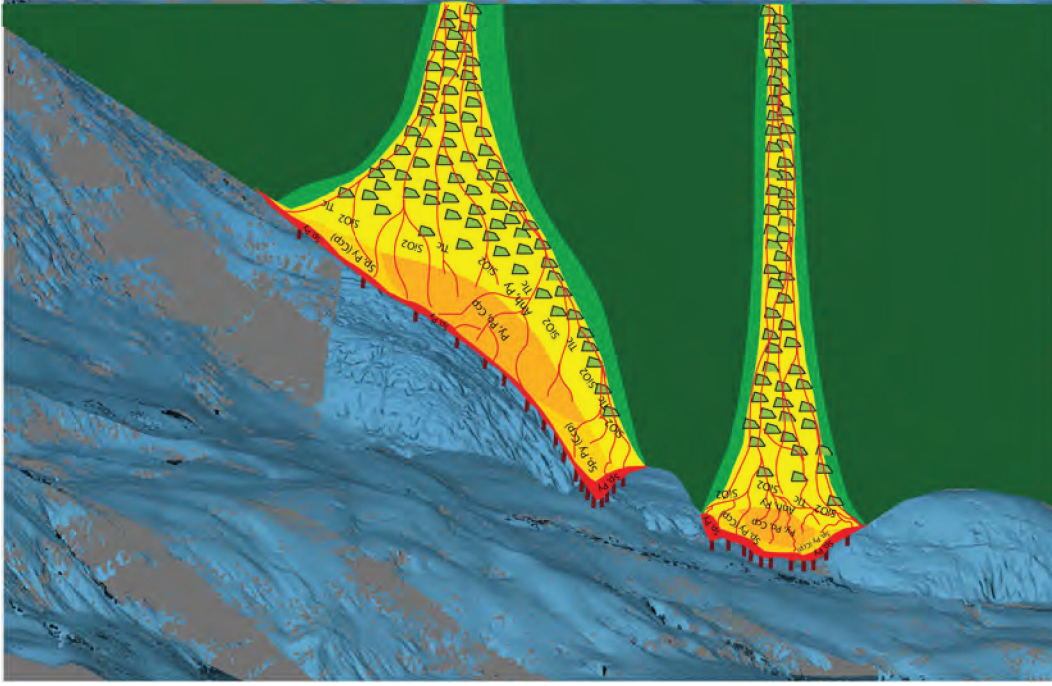


Fig. 4.21 Mohnskatten Modell 2

Modell 2 for Mohnskatten. Her har de to delene i overflaten adskilte tilførselsrør og stockverksjoner. Snittet og fargekodene er de samme som i Fig. 4.20.

Fig. 4.20 Mohnskatten Modell 1: Et snitt av jordskorpen på tvers av Mohnskattens sulfidteig kombinert med havbunnsstopografien sett i perspektiv fra sørøst. Et «toppløkk» av massiv sulfid er antydnet i rødt, de Cu-rike sonene er antydnet i mørk oransje, de Zn-rike sonene er antydnet i lys oransje, sonen med hydrotermalt påvirket sidebergart er antydnet i lyst grønn, og sidebergarten er antydnet i mørkt grønn. Stockverksjonen med mineralisering og bergartsbrekksjer er antydnet i gult med grønne fragmenter.

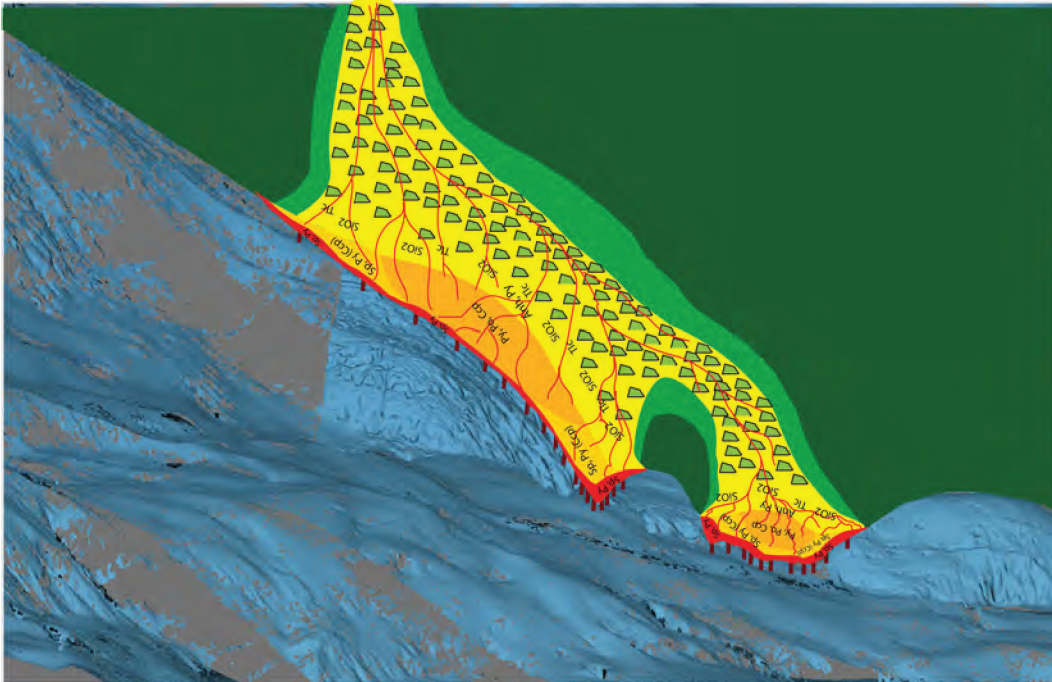
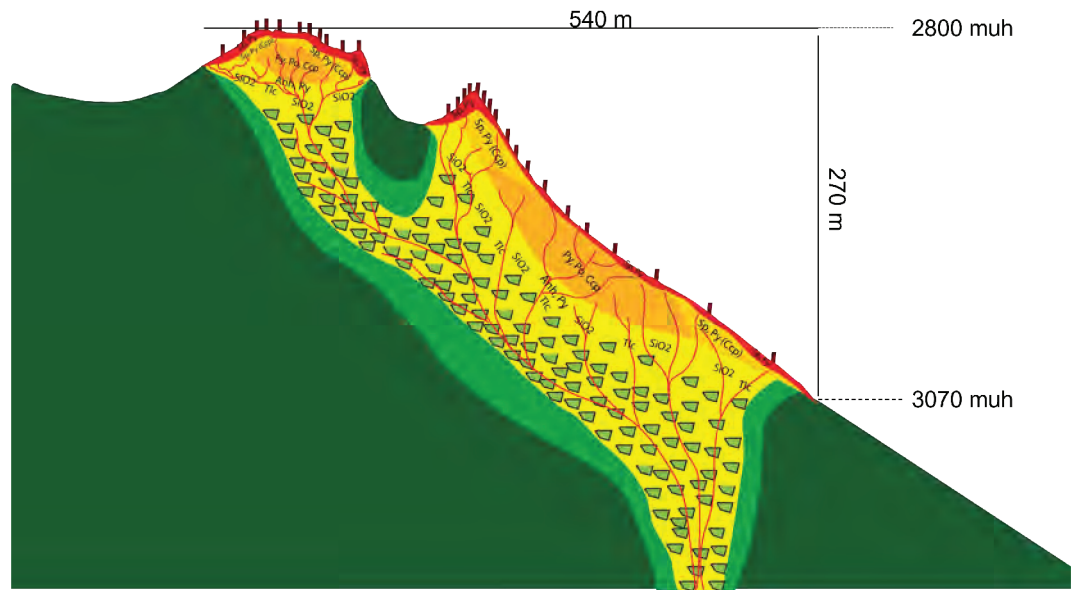


Fig. 4.20 Mohnskatten Modell 1



**Fig. 4.22 Mohnsøkketens dimensjoner**

Snitt gjennom Modell 1 for Mohnsøkket som i Fig. 4.20 med målte dimensjoner i meter. Meter under havoverflaten er forkortet muh. De samme mål i overflaten gjelder også Modell 2 i Fig. 4.21.

## 4.3 Skorpeforekomster

### 4.3.1 Dannelse av fjellandskapet

Fjellandskap utvikles i varierende grad i flankeviddene langs midthavsryggene. Spredningshastighet og magmatisk aktivitet påvirker de mekaniske egenskapene til litosfæren som igjen kontrollerer den tektoniske utviklingen og landskapsdannelsen (Pedersen et al., 2021). Havområdene ved spredningsryggene på norsk sokkel ble formet ved hyppig rifting som til slutt førte til separasjon av Norge og Grønland for over 55 millioner år siden (Mosar et al., 2002). Siden den gang har nye fjellandskap blitt dannet langs spredningsryggene på norsk sokkel. Dette skjer ved at det magmatiske landskapet i aksedalen blir forkastet og løftet opp fra dalbunnen langs dalens flankeforkastninger, og ender opp som fjellrygger langs flankene av dalen når den aktive generasjonen av flankeforkastninger til slutt blir inaktiv og erstattes av den neste.

Med unntak av Jan Mayen-ryggen og områdene langs nordsiden av Grønlandsryggen, er havbunnsområdene av oseansk karakter. Bunntopografien i resten av Norske-/Grønlandshavet styres av tre hovedelementer:

1. Et system av spredningsrygger (midthavsrygger) som strekker seg gjennom hele havområdet fra Island til Framstredet,
2. Bruddsoner som danner dallandskap og som går på tvers av spredningsryggene,
3. Dyphavsletter og sedimentære vifter med utspring ved kanten av kontinentalsokkelen (Pedersen et al., 2021).

De viktigste fjellandskapene i utredningsområdet er (se [Fig. 4.23](#)) :

- Østlige Jan Mayen bruddsone (55-25 millioner år gammel)
- Jan Mayen-ryggen (ca. 25 millioner år)
- Fjellområdene ved Mohnsryggen (ca. 40-0 millioner år)
- Fjellområdene ved Knipovitsryggen (33(?)-0 millioner år)

Nærmere beskrivelse av hvordan havbunnen med disse fjellområdene er dannet er gitt i innledningen ([4 Geologi og ressurser](#)).



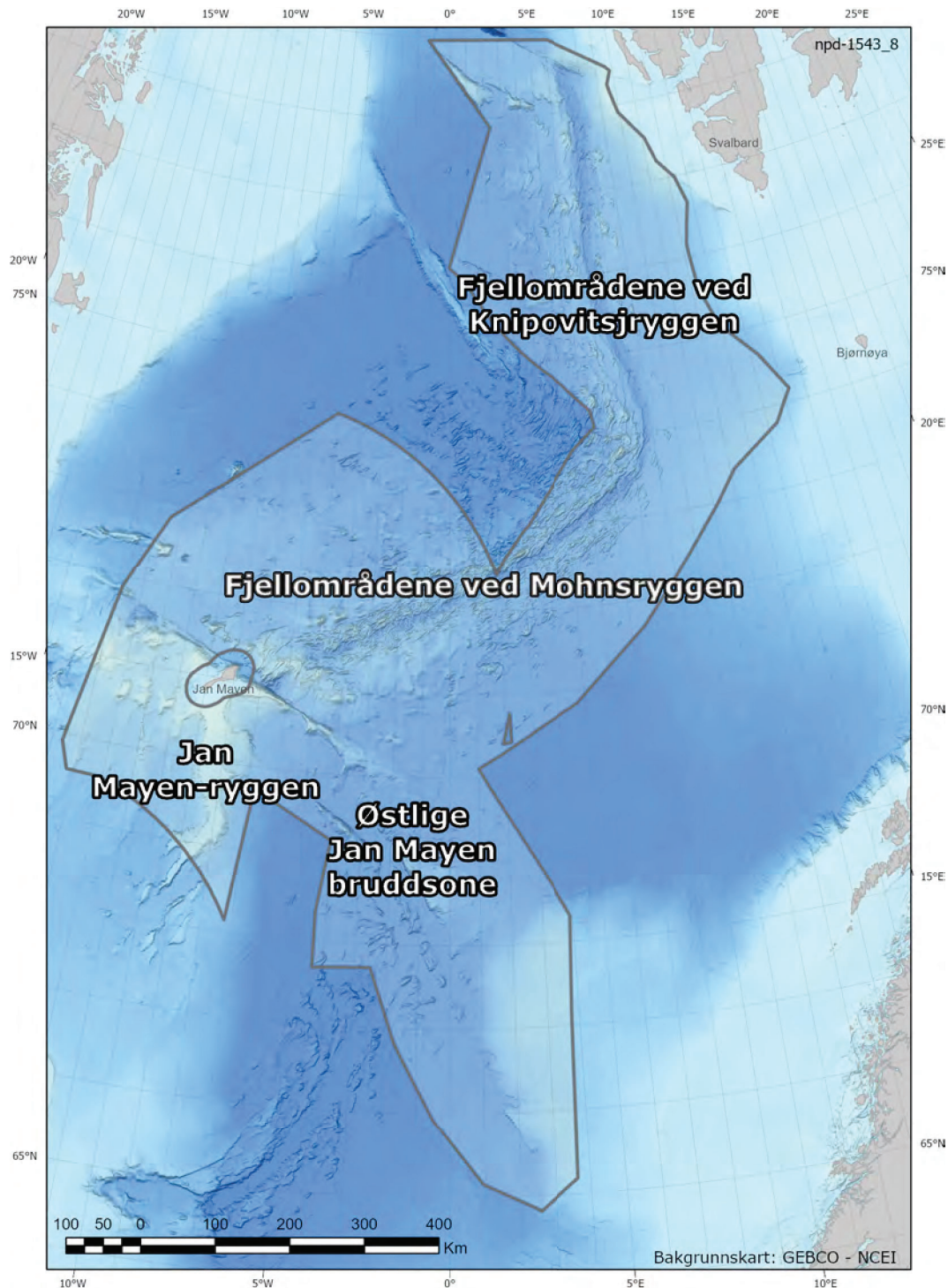


Fig. 4.23 Regionale fjellområder i Norskehavet og Grønlandshavet

**Østlige Jan Mayen bruddsone (55-25 millioner år)**

Spredningsryggene deles opp av bruddsoner som danner markerte landskapstrekk på tvers av ryggene. Bruddsonene består av den seismisk aktive delen av plategrensen der litosfæreplatene beveger seg sidelengs i forhold til hverandre og definerer en transformforkastning, og de seismisk inaktive, fossile delene av plategrensen i fortsettelsen av hver ende av transformforkastningen. Østlige Jan Mayen-bruddsone er en inaktiv, eldre del av bruddsone-systemet som strekker seg på tvers av Norske-/

Grønlandshavet. Bruddsonen er her definert av to parallelle daler som strekker seg 700 km fra Jan Mayen-ryggen til Møremarginen. Dalbunnen danner et slettelandskap med dybde på 3500-3700 m (Pedersen et al., 2021).

De to dalene, som representerer fossile transformforkastninger, er adskilt av en kjede av sjøfjell med fjelltopper som står 800-1400 m over slettelandskapet. Mot nordøst er slettelandskapet avgrenset av Vøringplatået, og videre vestover av Vøringutstikkeren og av fjellområder som skiller den østlige Jan Mayen-bruddsonen fra den aktive Jan Mayen-bruddsonen i vest. Avgrensningen mot Vøringplatået (kalt Vøring transform-margin) består av en 260 km lang fjellskråning, der det dype slettelandskapet går brått over i bratte skrenter og klipper som leder opp til Vøringplatået (Pedersen et al., 2021). Fjellutspringene består her av utgående sedimentære lag av kritt og paleocene alder (Polteau et al., 2020), og spektakulære magmatiske sill-intrusjoner (Styve, 2015; Bjerga et al., 2022). Ved Vøringutstikkeren avgrenses det dype slettelandskapet mot nordøst av en 120 km lang sammenhengende fjellside, der toppene rager 1000-1500 m over dalbunnen. Her er det også utgående lag av sedimenter og vulkanske bergarter (Pedersen et al., 2021).

### ***Jan Mayen-ryggen (ca. 25 millioner år)***

Jan Mayen-ryggen (JMR) var før spredningen mellom Grønland og den eurasiske platen en del av den grønlandske platen. Dannelsen av den nye spredningsryggen Reykjanesryggen, førte til at Jan Mayen-mikrokontinent med JMR begynte å løsne fra grønlandsplaten. For mellom 21 og 25 millioner år siden (anomali 6) ble Ægirryggen inaktiv og spredningen flyttet seg til Kolbenseyryggen vest for JMR, og JMR ble en del av den eurasiske platen (Gernigon et al., 2019).

### ***Fjellområdene ved Mohnsryggen (ca. 40-0 millioner år)***

Fjellområdene langs Mohnsryggen deles inn i Grønlandsbassenget nordvest og Lofotbassenget sørøst for Mohnsryggen. De høyeste fjelltoppene rager her 3000 meter over sletteområdene som omgir ryggen. Den gjennomsnittlige dybden av fjellandskapet er omkring 2000 meter i områdene nær aksedalen. Mot nordvest øker den gjennomsnittlige dybden og når 3400 meter der fjellandskapet går over i et slettelandskap, vest for magnetisk anomali 13 (Fig. 4.8).

Landskapstrekkene i fjellområdene er i stor grad definert av fossile forkastninger som var aktive da områdene ble dannet langs aksedalen. Pedersen et al. (2021) beskriver hvordan landskapet er bygget opp av fire hovedelementer:

1. Langstrakte forkastningsrygger,
2. Forkastningsbassenger som utvikles i halvgrabener mellom ryggene,
3. Kjernekomplekser som er blitt utviklet ved langvarig forkastingsaktivitet og som danner større fjellpartier,
4. Fjellmassiv som er blitt dannet ved et mer komplekst samspill av tektoniske og magmatiske prosesser.

Forkastningsryggene, som er det dominerende landskapstrekket, består av tre elementer: a) forkastningsskråninger som representerer forkastingsplan der dypere deler av skorpen og mantelen er/kan være eksponert; b) forkastingskanter, som definerer bruddkanten til forkastingene; c) skråstilt havbunn som består av vulkanitter som ble dannet i aksedalen og som siden er blitt løftet opp og skråstilt som følge av



forkastningsaktivitet. Områder med skråstilt havbunn har gradienter som vanligvis er mindre enn  $10^\circ$ . Forkastningsskråningene har derimot mange steder gradienter over  $20^\circ$  (Pedersen et al., 2021).

### ***Fjellområdene ved Knipovitsryggen (33(?)-0 millioner år)***

Fjellandskapet langs Knipovitsryggen er mindre markert enn langs Mohnsryggen. Langs hele ryggsegmentet har flankeviddene dybder mellom 2000 og 2500 meter. I to områder ( $76,4^\circ\text{N}$  og  $77,3^\circ\text{N}$ ) er det utviklet fjellområder i flankeviddene på begge sider av aksedalen. På vestsiden står disse 500-1500 meter over landskapet rundt. Disse sjøfjellene danner lineamenter som står skrått på aksedalen, men som er parallelle med spredningsretningen. I begge disse områdene er det i dag relativt høy vulkansk og tektonisk aktivitet i aksedalen. Her opptrer unge vulkanske ryggstrukturer som er flankert av normalforkastinger og lokale fjellformasjoner. Fjell-lineamentene indikerer at dagens vulkanske og tektoniske mønster har vedvart over mange millioner år (Hellevang og Pedersen, 2005). I Knipovitsryggen er aksedalen svært skråstilt i forhold til spredningsretningen. Dette har i stor grad påvirket den magmatiske og tektoniske aktiviteten. Bortfall av et markert fjellandskap er trolig forårsaket av dette skråstilte spredningsmønsteret og av en svært lav effektiv spredningshastighet (Pedersen et al., 2021).

Det har også tidligere vært debattert om Hovgaardryggen og Grønlandsryggen består av oseansk havbunn eller er fragmenter av kontinentalskorpe. Flymagnetisk datainnsamling utført av Norges geologiske undersøkelse sommeren 2016 og 2018 viser lav til medium intensitet på de magmatiske anomaliene (Dumais et al., 2021). Dette er indikasjon på at det ikke er havbunnskorpe dannet ved havbunnsbredning (se [4 Geologi og ressurser](#) og [Fig. 4.3](#)). Foreløpige tolkninger av prøver tatt av Hovgaardryggen og Grønlandsryggen på tokt i november 2022 (UiB/OD) tyder på at dette er sedimentære bergarter. Dette støtter teorien om at Hovgaardryggen ikke er et resultat av spredningsvulkanisme.

### **4.3.2 Dannelselse og vekst av manganskorper**

Manganskorper ([Fig. 4.24](#)) dannes ved utfelling av grunnstoffer fra havvannet. Utfelling av grunnstoff vil skje overalt i havet, men manganskorper dannes i hovedsak på bart fjell der det ikke er i konkurranse med sedimentasjon. Slikt bart fjell finner vi på undersjøiske rygger og fjellformasjoner i mesteparten av dyphavsområdene på norsk sokkel.



**Fig. 4.24 Manganskorpe fra Vøringutstikkeren**

Prøven ble hentet opp fra 2200 meters havdyp ved bruk av ROV i 2016.

Det er flere faktorer som kontrollerer og påvirker dannelse, vekst og bevaring av manganskorper. De viktigste er:

1. Alder på fjellandskapet
2. Stabiliteten og helning av fjellskråningene
3. Sedimenttilførsel og avstand til kontinenter,
4. Type og konsentrasjon av grunnstoff i havvannet,
5. Havstrømmer og lokale strømforhold.

#### ***Alder på fjellandskapet***

Manganskorper vokser med noen få millimeter per millioner år. Skorpene i Norskehavet ser ut til å vokse med omkring en millimeter per hundre tusen år. Observasjoner gjort av UiB viser at tykkelsen på skorpene blir 20 cm eller mer i områder med 25-30 millioner år gammel havbunn, og tilsvarende at skorpene er 3-4 mm langs aksedalene der havbunnen er 0,5 millioner år gammel. Kunnskap om alderen på fjellandskapet har derfor stor betydning for å kunne forutsi tykkelsen av manganskorper i de forskjellige områdene (Pedersen et al., 2021).

#### ***Stabilitet og helning av fjellskråningene***

For å få en viss tykkelse på manganskorpene må skråningene de ligger i vært stabile over lengre perioder. I tillegg må skråningene være steilere enn 20 grader slik at sedimenter sklir av og ikke blir akkumulert på bergflaten. Observasjoner fra 12 år med samarbeidstokt med UiB viser klare variasjoner i skråningsstabilitet innenfor utredningsområdet og at geologiske egenskaper kontrollerer om et sjøfjell/-rygg er prospektivt.

Sjøfjellene på hver side av Mohnsryggen og Knipovitsryggen består i hovedsak av magmatiske bergarter som i sin tid ble dannet i aksedalen ([4.3.1 Dannelse av](#)

**fjellandskapet** ). Videotransekter (undersøkelser med ROV med innsamling av video, samt prøvetaging) opp langs skråninger med ulik og varierende helningsgrad indikerer at disse sjøfjellene har relativt stabile skråninger. Dette betyr at man i stor grad kan bruke alderen på sjøfjellet og helningen på skråningen til å beskrive forventet tykkelse av manganskorper. (Se kapittel 4.5 **Manganskorpe-eksempel sjøfjell nordvest i Grønlandshavet** for eksempel).

Foreløpige vurderinger av prøver tatt på Hovgaardryggen vest for Knipovitsryggen, viser derimot at bergartene under manganskorpene er konsoliderte sedimenter. Dette tyder på at grunnfjellet her kan være kontinentalt. Det ble også her utført videotransekter (undersøkelser med ROV) opp skråninger med varierende helningsgrad. Disse transektene viste mer ustabile skråninger med liten eller ingen vekst av manganskorper. Tykke manganskorper ble kun funnet i et par områder mot toppen av skråningene. Dette kan tyde på at svak skråningstabilitet og erosjon forhindrer vekst av manganskorper.

Undersøkelsene utført på Jan Mayen-ryggen, Vøringutstikkeren og Vøringplatået viser i likhet med Hovgaardryggen en stor variasjon i tilstedeværelsen av manganskorpe i fjellskråninger på over 20 grader. Dette indikerer at geologiske egenskaper har betydning for vekst av manganskorper.

### ***Sedimenttilførsel og avstand til kontinenter***

Tilførsel av sedimenter til dyphavet har stor innvirkning på dannelsen av manganskorper. Etter at spredningen mellom Norge og Grønland startet for over 50 millioner år siden har sedimenttilførsel fra kontinentalmarginen variert over tid. Også i dag ser vi stor forskjell i sedimenttilførsel innenfor utredningsområdet. Sedimentasjonshastigheten i områdene rundt Mohnsryggen er på 3-4 cm per tusen år (Flesland et al., in prep; Stubseid et al., 2023). I selve aksedalen er sedimentasjonshastigheten 6 cm per tusen år (Stubseid et al., 2023). Det vulkanske landskapet begravnes derfor relativt hurtig av sedimenter.

Til sammenligning er sedimentasjonshastigheten ved den ekvatoriale delen av Den midtatlantiske ryggen 30 ganger lavere (0,1-10 mm; Agius et al., 2018).

På en aksial vulkanrygg i den sentrale delen av Knipovitsryggen er sedimentasjonshastigheten målt til 7 cm per tusen år (Stubseid et al., 2023). Dette er over dobbelt så mye som ved tilsvarende vulkaner langs Mohnsryggen (Stubseid et al., 2023). Den raske sedimentasjonen skyldes at aksedalen i Knipovitsryggen ligger nær inntil kontinentalskråningen og nær viftene som tilfører sedimenter ut fra Spitsbergen og Barentshavet ().

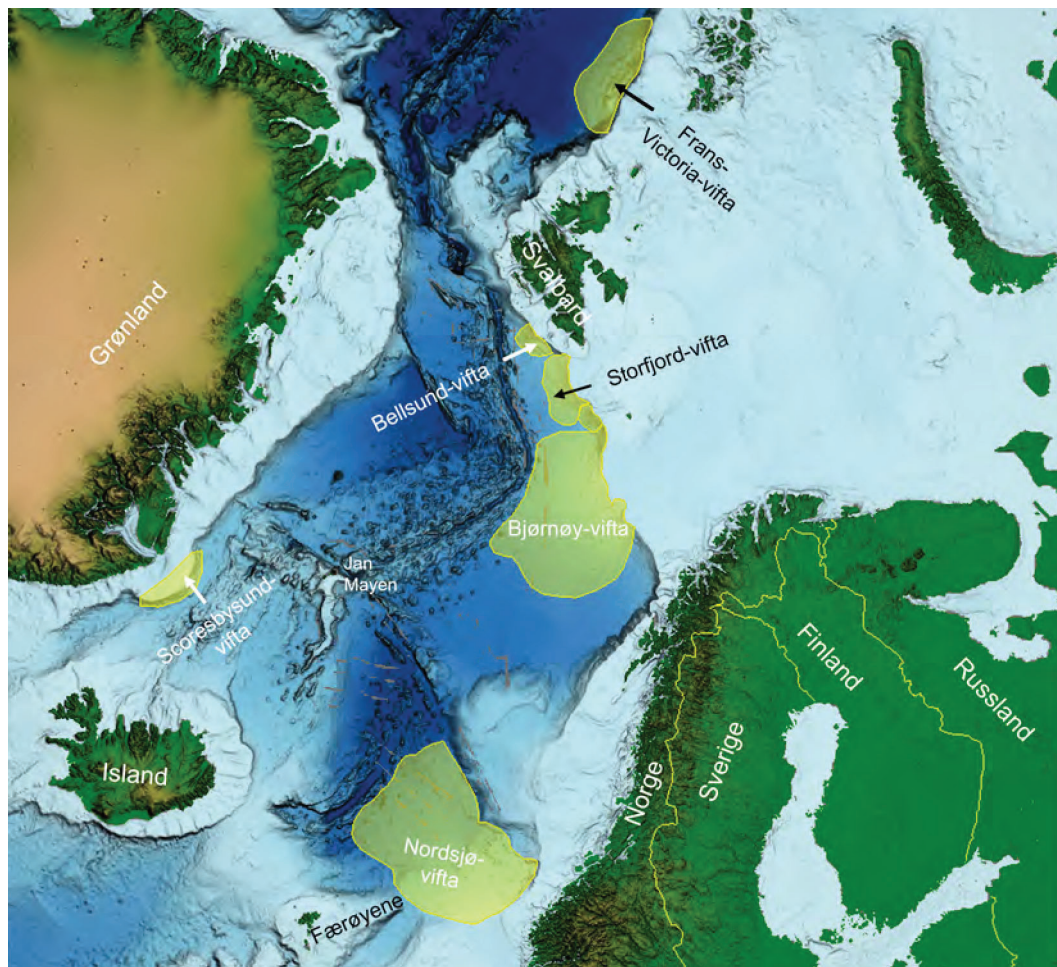


Fig. 4.25 Marine istidsvifter i Norskehavet og Grønlandshavet

Sedimenter fra Øst-Grønland vil i liten grad bli transportert ut til sjøfjellene nordvest for Mohnsryggen. Dette skyldes i hovedsak at sedimentene blir fraktet med den sterke øst-grønlandske havstrømmen sørover langs grønlandskysten. Ved Jan Mayen deler strømmen seg og får en gren som går østover. Dette bidrar antagelig til høyere sedimenttilførsel i den sørvestlige delen av utredningsområdet. Dette støttes av satellittdata som viser at det synes å være færre sjøfjell i den sørvestlige del av området enn lenger nordøst. Videre er det et abyssalt basseng vest for et topografisk trinn opp til sjøfjellene ved anomali 13 (C13) (Fig. 4.8). Dette bassenget kan fungere som en sedimentfelle og dermed begrense sedimentasjonen i områdene øst for anomali 13 der det ikke er beskrevet vesentlige havstrømmer.



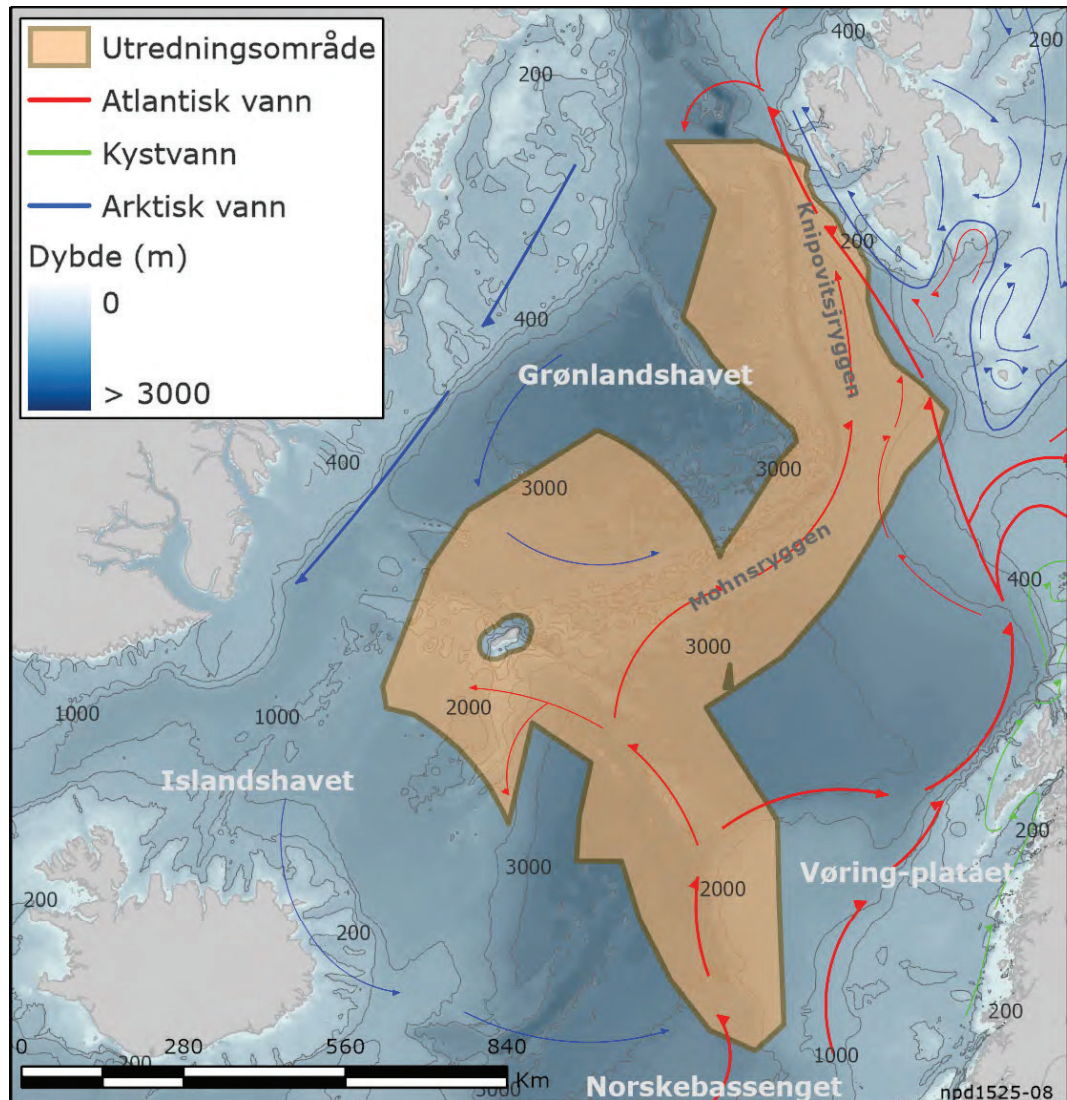


Fig. 4.26 Havstrømmer i Norskehavet og Grønlandshavet

Kart over Norskehavet med bunntopografi og viktigste havstrømmer (atlantehavsvann - rødt, arktisk vann - blått, kystvann - grønt).

### **Type og konsentrasjon av grunnstoff i havvannet**

Manganskorpene felles ut direkte fra havvannet og fester seg i tynne lag på sjøfjellene. Dersom overflaten ikke begravnes av sedimenter eller raser ut, men forblir i direkte kontakt med sjøvann gjennom millioner år, kan utfellingene vokse til skorper som er flere titalls centimeter tykke. Manganskorper av denne typen dannes direkte fra sjøvann ved utfelling av jern-oksidhydroksid og mangan-hydroksid. Materialets høye spesifikke overflateareal og dipolare ladning gjør at det også tar opp en rekke sporstoffer fra sjøvannet (Hein et al., 2000).

Mengden av jern (Fe), mangan (Mn) og sporstoff i havvannet er i hovedsak bestemt av nærheten til kontinentalmarginen, oksygeninnholdet i vannkolonnen, nærheten til hydrotermal aktivitet og havstrømmene. I den periodiske tabellen (Fig. 4.27) er alle analyserte grunnstoff markert. Grunnstoff som er tatt med i ressursvurderingen for manganskorper er uthevet.

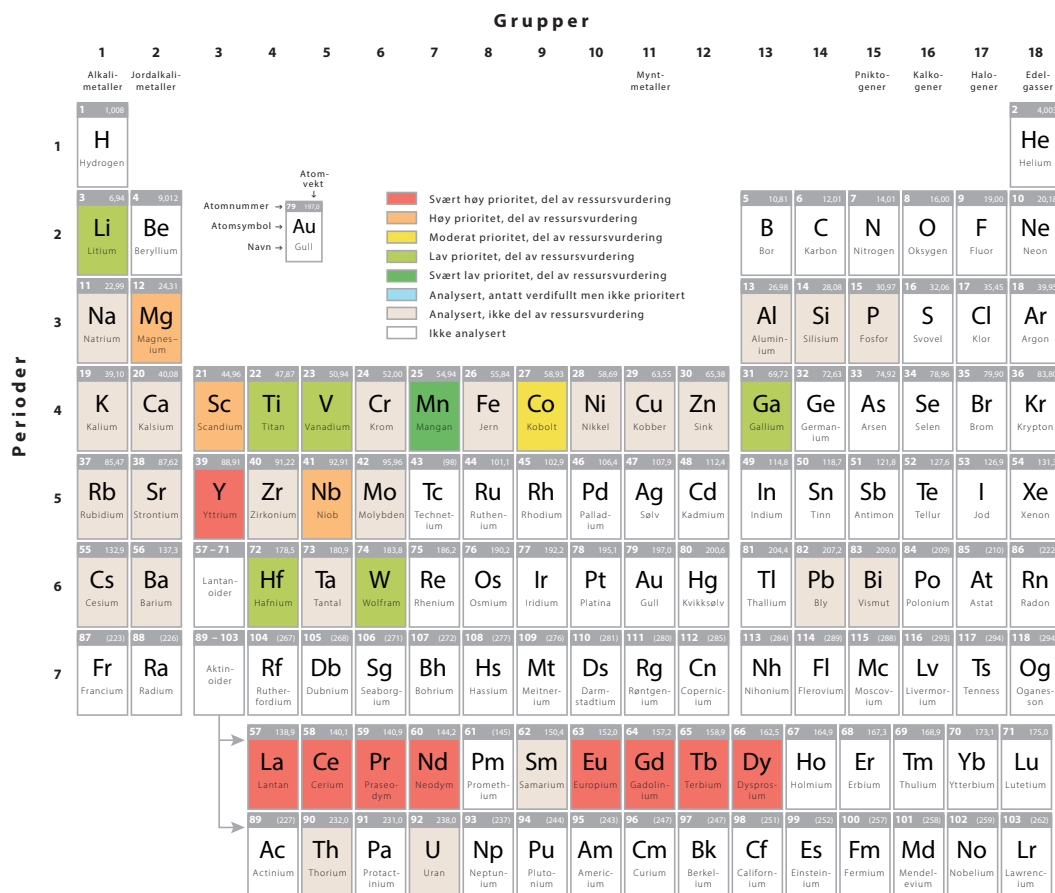


Fig. 4.27 Oversikt over grunnstoff analysert for i manganskorpe-vurderingene

**Havstrømmer og lokale strømforhold**

Siden manganskorper felles ut fra havvannet, vil sirkulasjon av havvann ha betydning for tilgang på jern, mangan og andre grunnstoff. Havstrømmene inneholder grunnstoff fra bl.a. sedimenter fra land og hydrotermal aktivitet. Dette fraktes rundt i havområdene.

Fig. 4.26 viser de viktigste havstrømmene i Norskehavet og Grønlandshavet.

Bunntopografien styrer i stor grad havstrømmene og utveksling av vannmasser. Strømmene i Norskehavet og Grønlandshavet er i hovedsak dominert av en grunnere og varmere havstrøm som går nordover på østsidene og en dypere og kaldere havstrøm som går sørover på vestsiden. Den varme, norske atlantehavsstrømmen som kommer opp fra sør deler seg ved Vøringutstikkeren, hvor en del går utover mot Jan Mayen og Mohnsryggen, og en del går nordover langs kysten av Norge. Lenger nord deler denne seg i en strøm inn i Barentshavet og en strøm nordover langs Spitsbergen. Deler av strømmen i dyphavet ved Mohnsryggen går nordover langs ryggen til Knipovitsryggen og videre til Framstredet. Her sirkulerer den og blander seg med polare strømmer og danner den kalde øst-grønlandske strømmen sørover langs grønlandskysten.

Vi har lite kunnskap om strømforhold nær havbunnen.

## 4.4 Letemodeller for manganskorper

For ressursvurdering av manganskorper er utredningsområdet delt inn i fire regionale områder. Inndelingen er basert på sammenlignbare geologiske og topografiske hovedtrekk. De regionale områdene er delt inn i subområder for å speile variasjoner i tykkelse på skorpene.

Beregningen av mengden ressurser i hvert område er gitt ved:

$$(\text{Volum}^1 \text{ ressurser}) \times (\text{Tetthet tørr bergart}) = \text{Tonn tørre ressurser i området}$$

<sup>1</sup>Volumer beregnes ved hjelp av areal og tykkelse.

### 4.4.1 Volum

Skorpevolum kan beregnes når man kjenner arealet av områder som oppfyller kriteriene for vekst av manganskorpe, variasjoner i skorpetykkelse og har en modell for hvordan areal og tykkelse henger sammen.

For å illustrere beregningen av skorperessurser har OD brukt fire regionale områder:

- Området ved Vøringutstikkeren og Vøringplatået
- Jan Mayen Ryggen og sjøfjellene rundt
- NV og SØ for Mohnsryggen
- V og Ø for Knipovitsryggen

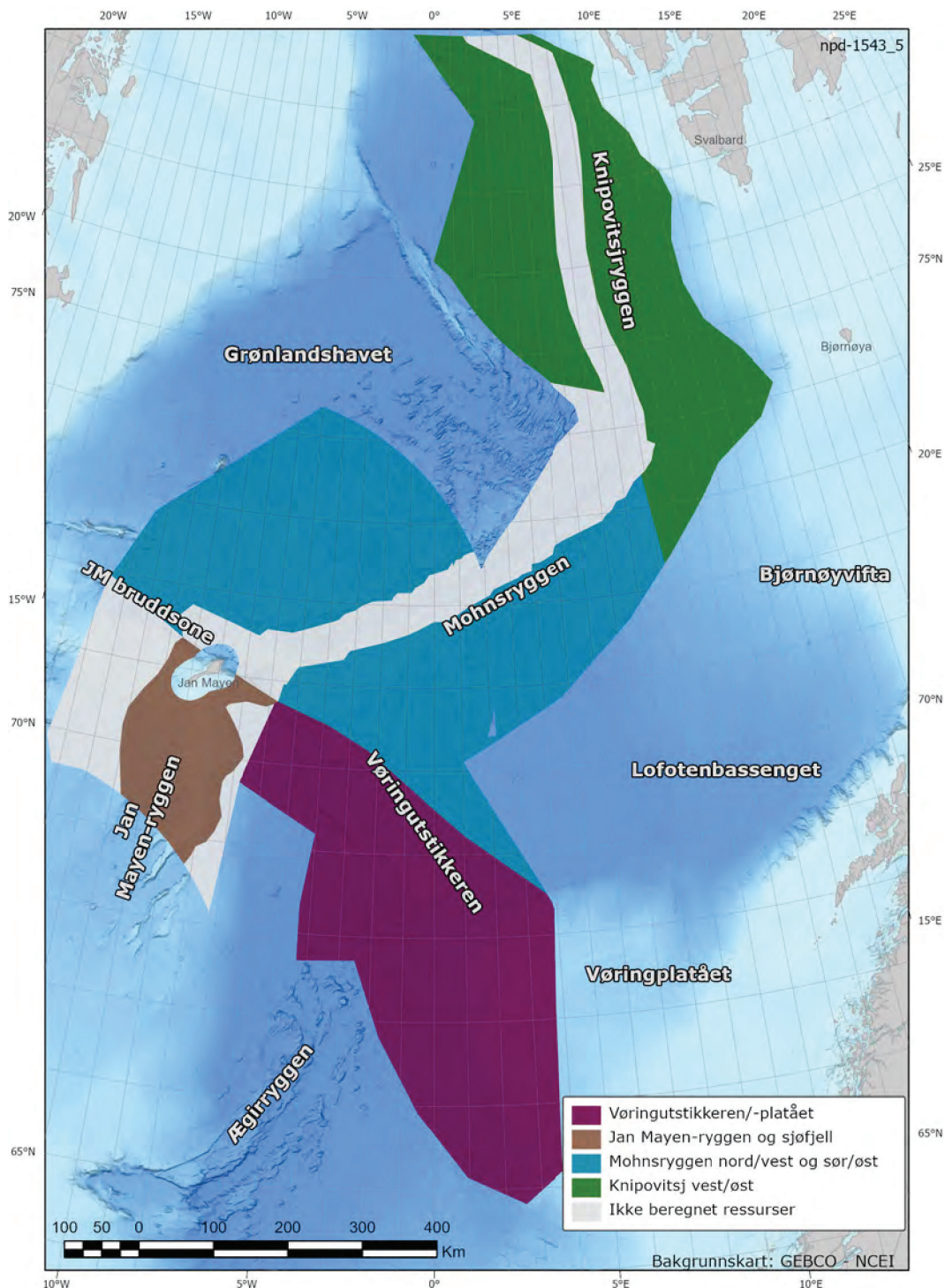


**Fig. 4.28 Regionale områder for beregning av manganskorper**  
 Hvert delområde har sammenlignbare geologiske og topografiske hovedtrekk.

Disse regionale områdene er delt inn i subområder. For hvert subområde er det beregnet størrelse på areal med helning over 20 grader, og det er valgt en tykkelsesspredning for subområdet. Fordi sjøfjellene er av varierende alder og har ulike geologiske egenskaper, må spredningen i mulig skorpetykkelse reflektere minimum, forventet og maksimum gjennomsnittstykkelse for hele subområdet. Dette vil være ulikt en minimum, forventet og maksimumsverdi for et gitt sjøfjell/-rygg innenfor subområdet.



### Areal

Det er benyttet ca. 20 graders helning på terrenget for å skille mellom områder dominert av bløtbunn og skråninger/fjellsider med hardbunn. Denne grenseverdien bygger på kartlegging av sedimenttykkelser med bunnpenetrerende ekkolodd over store områder i aksedalen (Stubseid et al., 2023; Pedersen et al., 2021), samt en serie videotransekter med ROV opp skråninger med ulik og varierende helningsgrad. Kartleggingen viser at de hemipelagiske sedimentlagene tynner ut i områder med helning mellom 17 og 20 grader, og at hemipelagiske sedimenter ikke akkumuleres i vesentlig grad i brattere terreng. Økende helning av terrenget fører til ras og massetransport ned skåningene. Dokumenterte undersøkelser viser at skråninger på under 15-20 grader vil få sedimentdekning, mens i brattere skråninger vil sediment gli av og/eller rase ut. Det ser ut som manganskorper kan vokse også med noe sedimenttilførsel, hvor sedimentet fletter seg sammen med manganskorpen. Dette gjør at metallgehalten vil bli lavere enn i rene manganskorper uten sedimenttilførsel. I skråninger med helning på 20-30 grader ser man en blanding av mangankonsoliderte sedimenter, utraste sedimenter og relativt uforstyrret manganskorpevekst. Er skråningene på over 30 grader har manganforbindelsene fått feste seg på bart fjell relativt uforstyrret (Pedersen et al., 2021).

For å avgrense områder med skråninger på over 20 graders helning, er det brukt kartdata med 10-200 meters oppløsning (Fig. 4.29). I områdene som ikke er kartlagt med MBES er det blitt estimert areal med helning over 20 grader basert på nærliggende MBES-data med sammenlignbare geologiske og topografiske hovedtrekk. Beskrivelse av metode for utregning av areal finnes i kapittel 5.2 [Metode for beregning av areal med helning over 20 grader](#).

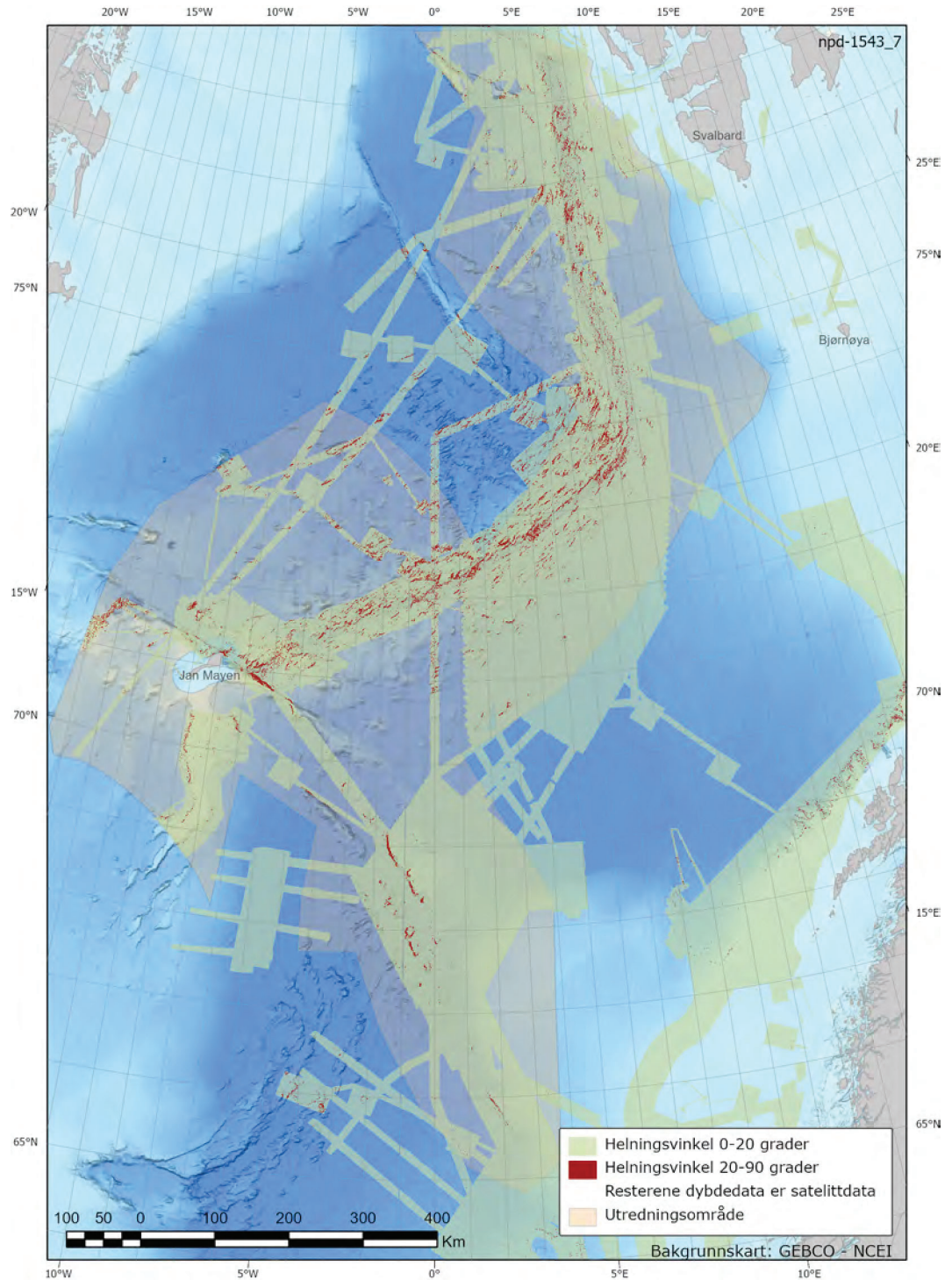


**Fig. 4.29 Data brukt i arealberegningene**  
Kartet viser områder med helningsvinkel på over 20 grader.

Tabellen under oppsummerer arealet med helning på over 20 grader innenfor hver av de regionale områdene vist i Fig. 4.28

**Tab. 4.11 Estimert areal på skråninger over 20 grader**

| Regionale områder                              | Forventningsverdi (km <sup>2</sup> ) |
|--|--------------------------------------|
| Området ved Vøringutstikkeren og Vøringplatået | 888                                  |
| Jan Mayen-ryggen og sjøfjellene rundt          | 528                                  |

|                             |      |
|-----------------------------|------|
| NV og SØ for Mohnsryggen    | 5383 |
| V og Ø for Knipovitsjryggen | 1735 |
| Total:                      | 8534 |

### Variasjoner i skorpetykkelse

En sammenstilling av spredning av gjennomsnittlige tykkelse brukt i ressursvurderingen innenfor de regionale områdene er summert i [Tab. 4.12](#). Parameterne i tabellen tar høyde for at det er observert større variasjon i skorpevekst i stabile skråninger med 20 og 30 graders helning, enn på skråninger med over 30 graders helning.

**Tab. 4.12 Oversikt over gjennomsnittlige tykkelsesvariasjoner for manganskorper per regionale område**

| Regionale områder                              | min (cm) | maks (cm) |
|--|----------|-----------|
| Området ved Vøringutstikkeren og Vøringplatået | 2,5      | 32        |
| Jan Mayen-ryggen og sjøfjellene rundt          | 1,5      | 10        |
| NV og SØ for Mohnsryggen                       | 2,5      | 32        |
| V og Ø for Knipovitsjryggen                    | 5        | 20        |

#### **Jan Mayen-ryggen og sjøfjellene rundt**

For å gi en indikasjon på variasjoner i skorpetykkelse i området på og rundt Jan Mayen er det inkludert skorpetykkelser fra Gilje et al. (in prep). Observasjoner og prøvetakning med ROV viser skorpeprøver med opp mot 20 cm tykkelse, mens gjennomsnittet var rundt 3 cm. Videobildene viser varierende geologiske egenskaper på underliggende fjellskråning. Vi forventer derfor at det kan finnes skråninger med over 20 graders helning der det kan være lite eller ingen manganskorpe.

#### **Området ved Vøringutstikkeren og Vøringplatået**

I området på og rundt Vøringutstikkeren og Vøringplatået er skorpetykkelser fra Gilje et al. (in prep) benyttet for å gi en indikasjon på tykkelsesvariasjonene. Her er den tykkeste skorpen over 20 cm og gjennomsnitts-tykkelsen målt på prøvene er rundt 5 cm. I likhet med Jan Mayen-ryggen viser videobilder fra kartleggingstokt varierende geologiske egenskaper til underliggende fjellskråning. Tilsvarende som for Jan Mayen-ryggen kan det finnes skråninger med over 20 graders helning der det kan være lite eller ingen manganskorpe.

#### **NV og SØ for Mohnsryggen**

I områdene nordvest og sørøst for Mohnsryggen er alder og de reologiske egenskapene til havbunnen relativt godt forstått ([5.4.1 Dannelse av fjellandskapet](#) og [5.4.2 Dannelse og vekst av manganskorper](#)). Alderen på sjøfjellene varierer fra rundt 5 millioner år nærmest aksedalen og ut til over 40 millioner år ved grensen av utredningsområdet.

#### **V og Ø for Knipovitsjryggen**

Langs Knipovitsjryggen er alder av havbunnen mer usikker ([5.4.1 Dannelse av fjellandskapet](#)) og færre sjøfjell er kartlagt og prøvetatt med ROV. De geologiske egenskapene til sjøfjellene dannet i aksedalen antas å være relativt lik det man finner ved Mohnsryggen. Unntaket er Hovgaardryggen, der observasjoner indikerer mer ustabile fjellskråninger og lite manganskorpevekst.

#### 4.4.2 Tetthet

Det er brukt tørr tetthet i utregningene. Det betyr at volumtallene som blir oppgitt i ressursvurderingen er tørre ressurser. Input-parametrene er basert på gjennomsnittlig tørr tetthet beskrevet av Hein et al. (2000).

For alle områdene er følgende benyttet:

**Tab. 4.13 Tetthet (tørr) brukt i modellering av skorpeforekomster**

|                           | min  | forventet | maks |
|---------------------------|------|-----------|------|
| Tørr tetthet manganskorpe | 1,25 | 1,3       | 1,35 |

#### 4.4.3 Metallgehalt

I overkant av 100 prøver er analysert for 48 forskjellige grunnstoff. Det er utført en ressursvurdering på 20 av disse grunnstoffene. Analysene er gjort av UiB på prøver som samlet inn på samarbeidstokt med UiB gjennom de siste 12 årene.

Spredningen i gehalter er delt inn i fire områder: Vøringutstikkeren, Jan Mayen-ryggen, Mohnsryggen og Knipovitsjryggen. Prøver innsamlet på tokt til Knipovitsjryggen i november 2022 er ikke ferdig analysert. Derfor har vi benyttet fordeling i gehalter fra Mohnsryggen i dette området. Når det foreligger analyser fra bergartsprøver samlet inn på tokt til Knipovitsjryggen, vil de gi grunnlag for en ny vurdering. Tabell med alle gehalter som er brukt i ressursvurderingen er oppsummert i [7.3 Tabeller for gehalter i manganskorper](#).

### 4.5 Manganskorpe-eksempel sjøfjell nordvest i Grønlandshavet

For konkretisering er det gjort mer detaljert modellering i form av et regneeksempel på et sjøfjell nordvest i Grønlandshavet (i utredningsområdet), i et område som er kartlagt, og hvor det er påvist manganskorper.

#### **Prospektivt areal og skorpetykkelser**

Som eksempel er det valgt et sjøfjell nordvest for Mohnsryggen. Det befinner seg nordvest i Grønlandshavet, 350 km nord for Jan Mayen. Sjøfjellet er kartlagt med skipsbatymetri (30 meters oppløsning) og det er brukt ROV for å samle inn bergartsprøver, film og stillbilder. Data ble samlet inn med forskningsfartøyet G.O.Sars sommeren 2022 under et samarbeidstokt mellom Senter for dyphavsforskning ved UiB og OD. Havydpet er mellom 2500 meter på toppen av sjøfjellet ned til 3800 meter ved foten av fjellet. Prøvene av manganskorpe er samlet inn i fjellskråninger med over 20 graders helning ([4.4 Letemodeller for manganskorper](#))

Metoden for å beregne areal med helning på over 20 grader er den samme som er benyttet i hele utredningsarealet. For beskrivelse se kapittel [5.2 Metode for beregning av areal med helning over 20 grader](#).

Arealet for forekomsten er vist i det røde polygonet i [Fig. 4.30](#). Her er 596 km<sup>2</sup> dekket med skipsbatymetri. Dette utgjør 66 pst. av arealet i polygonet. I denne delen av polygonet har 14,8 pst. av arealet en helning på mer enn 20 grader.



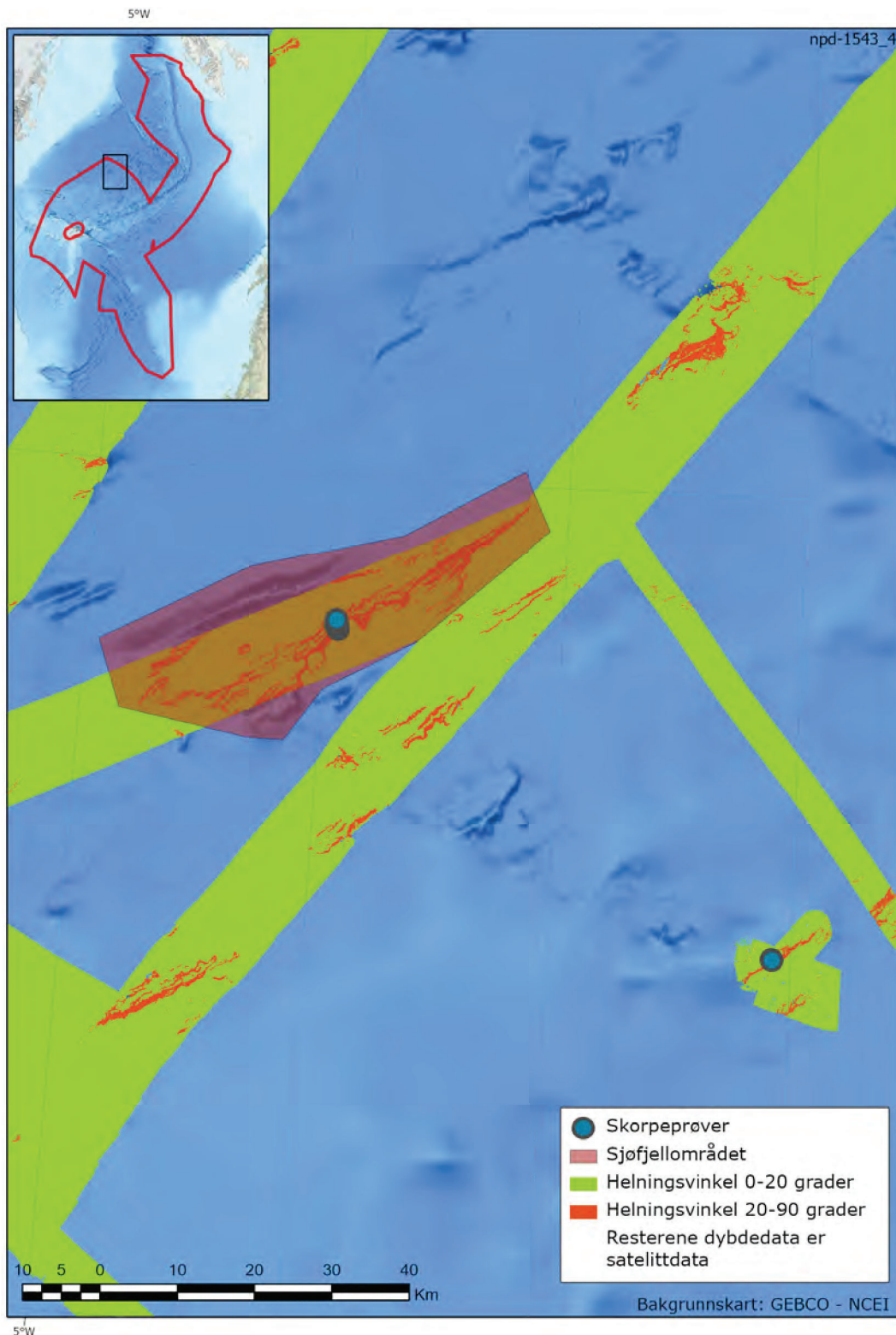


**Fig. 4.30 Sjøfjell beliggende nordvest i Grønlandshavet**

Kart som viser lokasjonen til sjøfjellet og lokalitetene til skorpeprøvene som er blitt analysert.

Basert på metoden i kapittel 5.2 Metode for beregning av areal med helning over 20 grader, kan vi da beregne at det resterende arealet i polygonet (34 pst. uten MBES-data) har samme fordeling av helning, altså at 14 pst. av dette arealet er over 20 grader. Dette betyr at det er tilsammen 133 km<sup>2</sup> som har mer enn 20 graders helning og som utgjør prospektivt areal innenfor sjøfjellområdet (Fig. 4.30).

Skipsbatymetrien har en oppløsning på 30 meter og det er usikkerhet rundt det faktiske arealet med helning på over 20 grader. Dette er ivare tatt ved å benytte en usikkerhet på +/- 20 pst. for areal over 20 grader i forekomsten:

**Tab. 4.14 Spredning i modellert areal for sjøfjell nordvest i Grønlandshavet**

| P95 (km <sup>2</sup> ) | Forventningsverdi (km <sup>2</sup> ) | P05 (km <sup>2</sup> ) |
|------------------------|--------------------------------------|------------------------|
| 106,5                  | 133                                  | 159,5                  |

Det benyttes samme usikkerhet i hele polygonet for dette sjøfjellet.

Basert på den geologiske spredningshistorikken for Mohnsryggen, samt de magnetiske anomaliene, er det estimert at området er rundt 40 millioner år gammelt. Prøver tatt med ROV viser manganskorper med tykkelser på opp mot 40 cm i de bratte fjellskråningene. Dette indikerer en vekstrate på rundt 1 cm per millioner år, noe som samsvarer med andre målinger lengre øst i Grønlandshavet.

Ettersom det er observert variasjon i skorpevekst i skråninger på mellom 20 og 30 grader, og det er usikkert om målte tykkelser er representativt for alle skråningene på forekomsten, er det lagt inn en spredning på tykkelsen som reflekterer dette.

### **Geokjemi**

For det utvalgte sjøfjellet har UiB analysert 15 manganskorpeprøver samlet inn i den nordlige delen av Grønlandshavet i 2022. Det er analysert for 48 forskjellige grunnstoff og utført ressursvurdering på 20 av disse. En oversikt over analyseresultatene finnes i kapittel 7.3 [Tabeller for gehalter i manganskorper](#).

Ressursvurderingen dette sjøfjellet er beskrevet i kapittel [6.2.2 Sjøfjell manganskorperressurser](#).

- 1 International Ocean Discovery Program, tidligere Ocean Drilling Program.



## 5 Metode for beregning av mineralressurser

### 5.1 Modelleringsverktøy

Denne ressursvurderingen er første gang det gis en helhetlig ressursvurdering for havbunnsmineraler på norsk sokkel. Ressursvurderingen er basert på Oljedirektoratets (OD) sine kartleggingstokt supplert med andre data og vitenskapelig arbeid. OD modellerer med flere stokastiske metoder for å kvalitetssikre resultatene.

#### 5.1.1 GeoX

OD benytter GeoX for å utarbeide ressursestimat for uoppdagede petroleumsressurser i prospekter og letemodeller. GeoX er et sett med verktøy for stokastiske beregninger av petroleumsressurser og -verdier i letefasen. GeoX ble utviklet av det norske selskapet GeoKnowledge AS, som senere ble kjøpt av oljeserviceselskapet Schlumberger.

GeoX er ikke tilrettelagt for å beregne mineralressurser, men beregningsmodellene kan likevel brukes for slike beregninger med noen tilpasninger og begrensninger. Vi har benyttet GeoX for beregning av sulfidforekomster i en tidlig fase i denne ressursvurderingen. Vi har også brukt GeoX til å validere våre egne modeller laget i @RISK som er beskrevet i kap.5.1.2 @RISK.

#### 5.1.2 @RISK

@RISK er en software – en Excel Add-In – for å bygge egne modeller for Monte Carlo-simulering uten programmering. Andre beslutningsstøtte-verktøy, bl.a. Precision Tree (lager beslutningstrær), kan brukes sammen med @Risk.

Med @RISK er det lett å bygge ut og teste modeller, og det er mer fleksibelt enn ferdigprogrammerte verktøy som GeoX. Excel er et kjent brukergrensesnitt. Med @RISK kan man bruke egne begreper/navn, og man har ikke de begrensninger som er i GeoX mht. antall metaller som kan estimeres.

@RISK er filbasert, så resultater som skapes ligger i den enkelte fil. Det er ingen database i bunnen som tilbyr uttrekk av data, lagringssikkert og tilgangssikkerhet. Derfor fordres god versjonskontroll på modeller.

#### 5.1.3 Ranged Approach to Target and Inventory Estimates

"Ranged Approach to Target and Inventory Estimates" kom opprinnelig fra ressursestimering i petroleum (BP) til landbasert mineralutvinning (BHP), og er etter sigende 'best practice' for stokastisk modellering av landbaserte mineraler. "Ranged Approach" er et tidligfase hjelpemiddel for ressursvurdering og etablering av et "Mineral Inventory". Et "Mineral Inventory" forutsetter ikke at mineralene kan utvinnes, ei heller at en forretningsidé skal være modnet frem til en forretningsmulighet. Det er "Mineral Inventory" som modelleres – ikke "Mining Inventory".



"Ranged Approach" følger seks steg frem til et "Mineral Inventory":

1. Utarbeide faktakart for geografisk å definere og avgrense prosjektet
2. Klassifisere dataene i prosjektet, oppdelt i
  - a. Fakta
  - b. Tolkninger
  - c. Antakelser
  - d. Ukjente faktorer
3. Utarbeide et geologisk influensdiagram/flytdiagram for ressursakkumulasjonen, samt bestemme geologiske nøkkelfaktorer i diagrammet
4. Etablere tre (eller flere) deterministiske ressursutfall, oppdelt i
  - a. Minimumsanslag (garantert minimum)
  - b. Maksimumsanslag (kan ikke bli større)
  - c. Mest sannsynlige utfall (typetall/modalverdi)
  - d. (Ev. flere case for ressursutfall på halene – som 10 pst. High – dersom max-min gjør troverdig modellering krevende)
5. Fastsette hvorledes tykkelse, horisontal kontinuitet og gehalt ('Grade') skal ivaretas i modelleringen
6. Stokastisk modellering av utfallsrommet for "Mineral Inventory"

## 5.2 Metode for beregning av areal med helning over 20 grader

Metoden for beregning av areal for manganskorper er i hovedsak gjennomgått i [4.4 Letemodeller for manganskorper](#). Detaljer om metoden er utdypet nedenfor.

Det er utarbeidet helningskart innenfor utredningsområdet med formål å tallfeste arealer med gitte helningsgrader. Med helning menes hvor bratt det er i et område.

Det er benyttet dybde data (MBES) med oppløsning ned mot 10 meter (se kap. [3 Oljedirektoratets kartleggingsarbeid](#)). Variasjon i oppløsningen ligger mellom 10 og 200m.

Data ble konvertert til celler på 25 x 25 meter. Helningsgrad for hver celle er beregnet ved å bruke dybde i hver celle og tilgrensende celler. Disse ble videre klassifisert i ulike kategorier. Antall celler i hver kategori ble så brukt for å beregne arealet pr. kategori.

Helning i områder uten MBES-data ble ekstrapolert fra tiliggende områder med MBES datadekning. For å ta hensyn til ulik topografi ble satellittdata benyttet for å definere områder for ekstrapolering. (Fig. 4.28) Disse subområdene er delt inn i delområder basert på lignende topografisk karakter for å ta hensyn til at «fjelltetthet» varierer i utredningsområdet. Det er for eksempel ulik grad av begravning av sjøfjell i de ulike områdene av utredningsarealet.

I ressursvurderingen er det benyttet usikkerhet for areal av sjøfjell. Det er større usikkerhet i områder hvor det kun finnes satellittdata. Tilsvarende er det lavere usikkerhet i områder med MBES data. I områder med MBES data er det valgt en usikkerhet på +-20%. I områder med kun satellittdata er det valgt en usikkerhet på +-50%. Disse verdiene er satt basert på ODs erfaring med tilsvarende arbeid innenfor estimering av uoppdagede ressurser i petroleum. Ved å vurdere sensitiviteter vil en slik usikkerhet bli mer velfundert. Dette vil inkluderes i fremtidig arbeid.

### 5.3 Ressursklassifikasjon

Forvaltningen av ressurser er en viktig oppgave for enhver nasjonalstat. En standardisert og funksjonell klassifisering av ressursene er en avgjørende forutsetning for:

- Utforming av internasjonal energi- og mineralpolitikk
- Myndighetenes ressursforvaltning
- Industriens aktivitetsplanlegging
- Finansanalyser og kapitalallokering

OD utviklet i 1996 et klassifikasjonssystem for petroleumsressurser. Dette systemet er basert på prosjektmodenhet, og ble sist oppdatert iht. ny ressursforskrift i 2018 (Oljedirektoratet, 2018).

#### Definisjoner

**Ressurs:** er elementer eller menneskelige egenskaper som kan utnyttes økonomisk, eller som er til nytte på annen måte<sup>1</sup>. Naturressurser er luft, vann, dyrkbare arealer, petroleum, mineraler og andre råstoffer. Man skiller gjerne mellom fornybare og ikke-fornybare ressurser<sup>2</sup>.

**Klassifikasjon:** er en sammenstilling av ting eller omgrep i grupper eller klasser etter hvor like de er. Ordet klassifikasjon blir også brukt om resultatet av ei slik sammenstilling. Klassifikasjon spiller en viktig rolle både i det daglige og i vitenskapelige sammenhenger, for å få oversikt, økt innsikt og forståelse<sup>3</sup>.

**Malm:** bergart som inneholder ett eller flere mineraler eller grunnstoffer i økonomisk drivverdige mengder<sup>4</sup>.

I denne rapporten benyttes ikke begrepet malm, heller vil begrepet ressurser (knyttet til havbunnsmineraler) bli benyttet.

#### Klassifiseringssystemer

Det eksisterer flere ulike systemer for ressursklassifisering, de mest relevante for havbunnsmineraler er:

- UNFC: United Nations Framework Classification for Resources<sup>5,6,7</sup>
- CRIRSCO: Committee for Mineral Reserves International Reporting Standards<sup>8</sup>

To andre klassifikasjonssystem som ofte er benyttet og referert er:

- Petroleum Resources Management System (PRMS)<sup>9</sup>
- EUs taksonomi<sup>10</sup>

Disse to siste vil ikke bli omtalt videre her – PRMS er relatert til petroleum og EUs taksonomi er et system som i hovedsak er laget for styring av finansielle virkemiddel mot bærekraftige investeringer.

#### Institusjoner og gjeldende rammeverk

I Norge er mineralforvaltningen på land ivaretatt av Direktoratet for mineralforvaltning med Bergmesteren for Svalbard (DMF) og Norges geologiske undersøkelse (NGU), se kapittel 2 [Innledning](#).

Forvaltningsansvaret for havbunnsmineraler på norsk sokkel er lagt til Olje- og energidepartementet, og ODer er departementets fagetat på området.

Den internasjonale havbunnsmyndigheten (International Seabed Authority - ISA) er opprettet under FNs Havrettskonvensjon for å forvalte ressursene i de internasjonale havbunnsområdene på vegne av menneskeheten. ISA har 167 medlemsland, deriblant Norge.

### 5.3.1 Beskrivelse av ressursklassifiseringssystem

UNFC sitt klassifikasjonssystem for ressurser omfatter en rekke naturressurser: mineraler, petroleum, energi – også fornybar, antropogene, hydrogen etc., og det er nært knyttet til FNs mål for bærekraftig utvikling og bærekraftmålene («2030 Agenda»)<sup>11</sup>. OD har siden 2009 presentert ressursregnskap for petroleum i samsvar med UNFC-systemet.

Rammeverket for UNFC klassifikasjonssystem består av tre akser med ulik grad av modenhet for prosjekter / ressurser: G-aksen for geologi / undergrunn, F-aksen for teknisk modenhet («Feasibility») og E-aksen for sosio-økonomiske forhold («Economy/ Environment»).

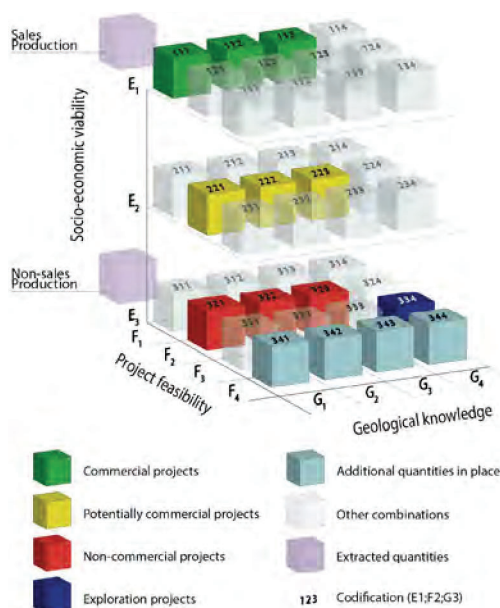


**Fig. 5.1 FNs rammeverk for ressursklassifisering**  
United Nations Framework Classification for Resources - UNFC.

Den internasjonale havbunnsmyndigheten – ISA – har tidligere (2015) publisert et forslag til klassifisering av havbunnsmineralressurser som er basert på CRIRSCO<sup>12</sup>, men ISA vurderer også å benytte UNFC for ressursklassifisering<sup>13</sup>. Det er utarbeidet et «Bridging document» mellom UNFC og CRIRSCO<sup>14</sup>, og det er tilsvarende laget «bridging document» for mineralressurser på land i Finland, Norge og Sverige, koblet mot UNFC<sup>15</sup>.

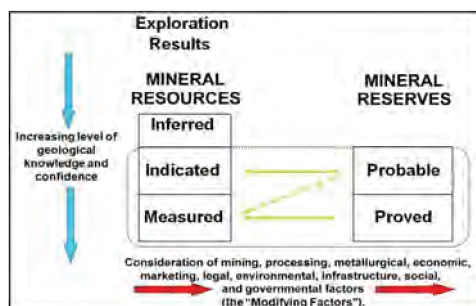


**Fig. 5.2 CRIRSCO klassifisering**  
Viser sammenheng mellom leterresultater, mineralressurser og -reserver.

Begrepene «ressurser» og «reserver» kan være begrep som er vanskelig å forholde seg til, blant annet fordi noen ressurstyper og reserver er strengt definert i finansmarkedet. Som NGU beskriver i sin mineralstatistikk/ressursrapport (Heldal et al, 2017):

I grove trekk er en "reserve" et nøye oppmålt volum av malm eller annen bergart som man vet er produserbar og økonomisk lønnsom ut fra dagens marked. I realiteten gjelder dette aktive bergverk eller nye bergverk like før oppstart. Det er meget dyrt å fremskaffe nok

informasjon til å definere reserver, derfor har mange selskap lagt seg på en kost-nyttelinje der man har reserver for 10-12 år, tilstrekkelig for å tilfredsstille investorer og aksjonærer. En "ressurs" kan derimot være både et nøye oppmålt volum eller et løst estimat, der det ikke er like stor sikkerhet for at volumet er produserbart og lønnsomt. Ressurser kan altså inkludere reserver i en mer nøytral kontekst.

I ressursklassifisering skiller det også mellom tilstedeværende og utvinnbare ressurser. Oppdelingen i ulike kategorier reflekteres også i systemer som UNFC og CRIRSCO.

En beskrivelse av UNFCs geologiske ressursdata er gitt i [Tab. 5.1](#). Det er beskrevet fire kategorier fra G1 (svært stor sikkerhet) til G4 (estimat med liten sikkerhet). Denne tilnærmingen er også i overensstemmelse med NGUs ressursklassifisering på land.

**Tab. 5.1 Beskrivelse av UNFC-kategoriene G1 til G4**

|    |  |
|----|--|
| G1 | Ressursvolum tilknyttet kjente forekomster, som kan beregnes med stor grad av sikkerhet (inkluderer påviste reserver og påviste ressurser)   |
| G2 | Ressursvolum tilknyttet kjente forekomster, som kan beregnes med moderat grad av sikkerhet (inkluderer sannsynlige reserver og indikerte ressurser)  |
| G3 | Ressursvolum tilknyttet kjente forekomster, som kan beregnes med lav grad av sikkerhet (inkluderer estimerte ressurser)  |
| G4 | Usikre ressursvolum tilknyttet mulige forekomster, basert på grove estimater, indirekte estimater eller overslag basert på statistiske sannsynligheter NB; inkluderer ikke-standardiserte historiske data som ikke er nærmere vurdert. |

Med det eksisterende grunnlaget for kartleggingen av havbunnsmineraler på norsk sokkel, har OD ikke grunnlag for å kategorisere noen ressurser som reserver, se [6.1 Ressursberegning](#).

- 1 ressurs (2023) i Store norske leksikon på snl.no. Tilgjengelig fra: <http://snl.no/ressurs> (Hentet 24. januar 2023).
- 2 naturressurs (2023) i Store norske leksikon på snl.no. Tilgjengelig fra: <https://snl.no/naturressurs> (Hentet 24. januar 2023).
- 3 Ådland, Marit Kristine (2023) klassifikasjon i Store norske leksikon på snl.no. Tilgjengelig fra: <http://snl.no/klassifikasjon> (Hentet 24. januar 2023).
- 4 Rui, Ingolf Jarle (2023) malm i Store norske leksikon på snl.no. Tilgjengelig fra: <http://snl.no/malm> (Hentet 24. januar 2023).
- 5 UNFC (og UNECE) (2023): <https://unece.org/sites/default/files/2020-12/UNFC2020.pdf> (Hentet 24. januar 2023).
- 6 UNFC og mineraler (2023): <https://unece.org/sustainable-energy/unfc-and-sustainable-resource-management/unfc-and-minerals> (Hentet 24. januar 2023).
- 7 UNFC og CRIRSCO (2023): [https://unece.org/DAM/energy/se/pdfs/UNFC/UNFC\\_specs/Revised\\_CRIRSCO\\_Template\\_UNFC\\_Bridging\\_Document.pdf](https://unece.org/DAM/energy/se/pdfs/UNFC/UNFC_specs/Revised_CRIRSCO_Template_UNFC_Bridging_Document.pdf) (Hentet 24. januar 2023).
- 8 CRIRSCO: Committee for Mineral Reserves International Reporting Standards (2023). Etablert i 1994, medlemmer er JORC (Australasia), CBRR (Brazil), CIM (Canada), Comision Minera (Chile), CCRR (Colombia), PERC (Europe (mainly UK)), NACRI (India), KCMi (Indonesia), KAZRC (Kazakhstan), MPIGM (Mongolia), OERN (Russia), SAMCODES (South Africa), UMREK (Turkey), SME (United States of America)). <https://www.criirSCO.com> (Hentet 24. januar 2023).
- 9 PRMS: Petroleum Resources Management System (2023): et etablert system for klassifisering av petroleumsressurser – utarbeidet over flere år og forankret i SPE/WPC/AAPG/SPEE/SEG. <https://www.spe.org/en/industry/reserves/> (Hentet 24. januar 2023).
- 10 EUs taksonomi: et klassifikasjonssystem for bærekraftig aktivitet forankret i «European green deal» og har hovedvekt på finansiell aktivitet (styring). [https://finance.ec.europa.eu/sustainable-finance/tools-and-standards/eu-taxonomy-sustainable-activities\\_en](https://finance.ec.europa.eu/sustainable-finance/tools-and-standards/eu-taxonomy-sustainable-activities_en) (Hentet 24. januar 2023).
- 11 FNs mål for bærekraftig utvikling er De forente nasjoners (FN) felles arbeidsplan for å utrydde fattigdom, bekjempe ulikhet og stoppe klimaendringene innen 2030. De består av 17 hovedmål og 169 delmål. Bærekraftsmålene skal fungere som en felles global retning for land, næringsliv og sivilsamfunn. <https://unsdg.un.org/2030-agenda> (Hentet 24. januar 2023).
- 12 ISA 2015: Recommendations for the guidance of contractors on the content, format and structure of annual reports – Annex V: Reporting standard of the International Seabed Authority for mineral exploration results assessments, mineral resources and mineral reserves: [https://isa.org.jm/files/files/documents/isba-21lrc-15\\_1.pdf](https://isa.org.jm/files/files/documents/isba-21lrc-15_1.pdf) (Hentet 24. januar 2023).
- 13 Bruk av UNFC av ISA: <https://unece.org/sustainable-energy/news/unfc-under-consideration-international-seabed-authority-classification> (Hentet 24. januar 2023).
- 14 Bridging mellom UNFC og CRIRSCO: [https://unece.org/DAM/energy/se/pdfs/UNFC/UNFC\\_specs/Revised\\_CRIRSCO\\_Template\\_UNFC\\_Bridging\\_Document.pdf](https://unece.org/DAM/energy/se/pdfs/UNFC/UNFC_specs/Revised_CRIRSCO_Template_UNFC_Bridging_Document.pdf) (Hentet 24. januar 2023).
- 15 Bridging mellom UNFC og mineraler på land i Finland, Norge og Sverige: [https://unece.org/DAM/energy/se/pdfs/UNFC/2018/UNFC\\_Nordic\\_guidelines/180212\\_A\\_guidance\\_for\\_the\\_application\\_of\\_the\\_UNFC.pdf](https://unece.org/DAM/energy/se/pdfs/UNFC/2018/UNFC_Nordic_guidelines/180212_A_guidance_for_the_application_of_the_UNFC.pdf) (Hentet 24. januar 2023).



## 6 Ressursvurdering

### 6.1 Ressursberegning

De to typene av havbunnsmineraler som er påvist på norsk kontinentalsokkel, sulfider og manganskorper, er geologisk sett svært forskjellige. Ressursgrunnlaget i hver av dem er et resultat av hvordan de er blitt dannet og hvordan de forekommer. De ressursberegnes derfor hver for seg som beskrevet i de påfølgende avsnittene. Metoden som er benyttet for beregning av tilstedeværende ressurser for havbunnsmineraler er «Mineral Inventory», som beskrives i kapittel 5.1.3 [Ranged Approach to Target and Inventory Estimates](#). De totale ressursene for manganskorpe og sulfider er beregnet for et stort område (se Fig. 6.1 og Fig. 6.2) og har ikke blitt klassifisert i UNFC-kategorier. De individuelle sjøfjellene og sulfidforekomstene kan ev. klassifiseres i kategori G4 og G3.

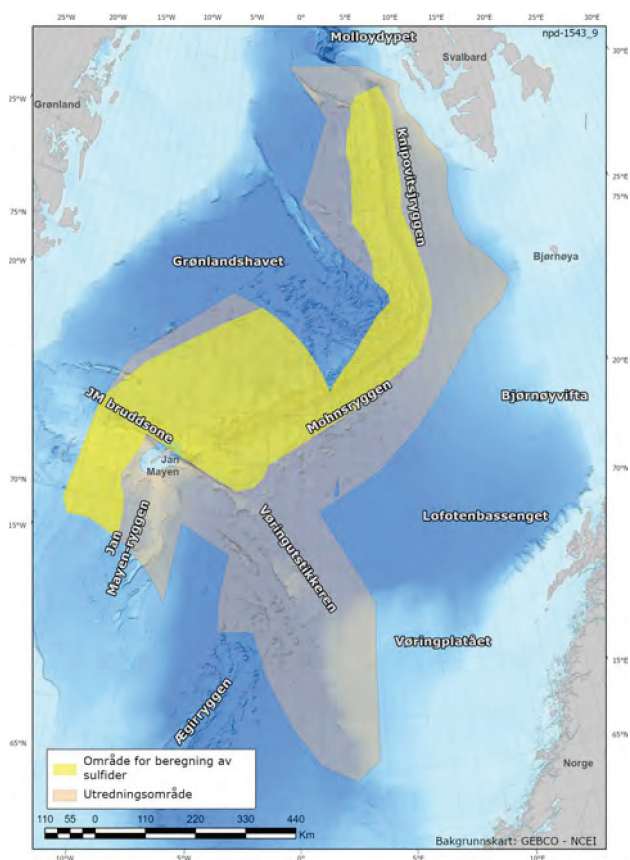


Fig. 6.1 Område for ressursberegning for sulfider

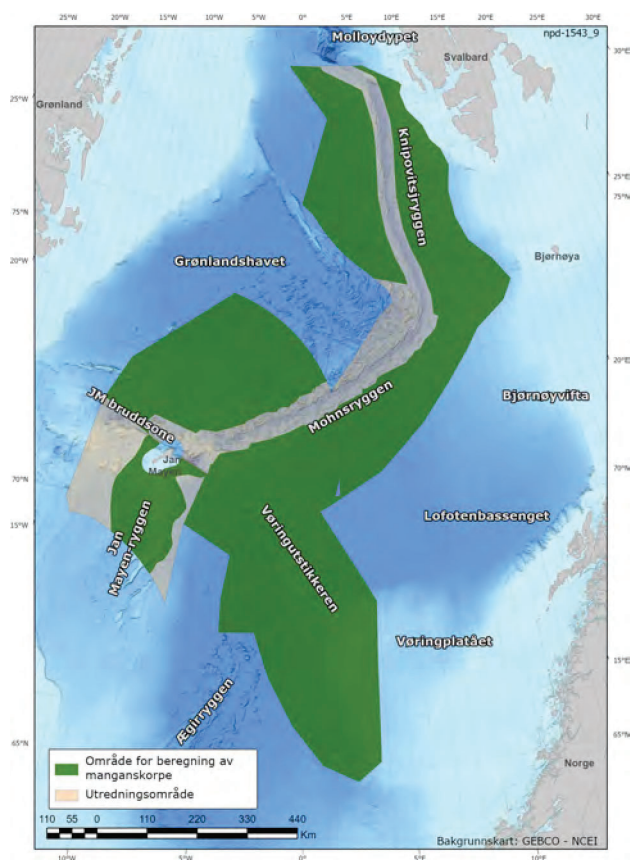


Fig. 6.2 Område for ressursberegning for manganskorper

#### 6.1.1 Sulfidressurser

##### 6.1.1.1 Beregningsgrunnlaget

Ifølge 4.1.1 [Dannelsen av sulfidforekomster - aktiviteten i aksedalen](#) er sulfidforekomstene delt i to hovedtyper alt etter hvor de er dannet i forkastningssystemene i aksedalen i spredningsryggene. Flankeforekomstene dannes langssetter de store hovedforkastningene som utgjør flankene av aksedalen. Aksialforekomstene dannes i vulkanske rygger som utvikler seg over forkastninger i sentrale deler av aksedalen. Som forklart i 4.1.1 [Dannelsen av sulfidforekomster - aktiviteten i aksedalen](#) gir disse forholdene grunnlaget for å definere de to hoved-

letemodellene som brukes i ressursvurderingen: hhv flankemodellen og aksialmodellen. Flankemodellen er delt i to underpopulasjoner: forekomster med mer enn 0,1% Co i gjennomsnitt og forekomster med mindre. I tillegg er det opprettet en tredje letemodell for to områder med vesentlig grunnere vann enn resten av området: langs Kolbeinseyryggen i sørvest og i et område med magmatisk oppbygninger rett nord for Jan Mayen (se [4.1.5 Letemodeller for sulfidforekomster](#)).

For hver letemodell er det definert et sett av nødvendige parametere som inngår i beregningene. Disse er som følger:

Areal (m<sup>2</sup>), Tykkelse (m), Tetthet (tonn/m<sup>3</sup>), Gehalt (%), ppm), og Antall forekomster

Beregningen av mengden sulfid i hver letemodell er gitt ved den generelle formelen:

$$\text{Tonn sulfid} = \text{Areal (m}^2\text{)} \times \text{Tykkelse (m)} \times \text{Tetthet (tonn/m}^3\text{)} \times \text{Antall}$$

Beregningen av mengden metall i hver letemodell følger da ved den generelle formelen:

$$\text{Tonn metall} = \text{Tonn sulfid} \times \text{Gehalt}$$

Beregningen av ressursene i hver letemodell er gjort ved Monte Carlo-simulering med programmet @Risk. Denne simuleringen krever at tallverdiene for parameterne oppgis med spredning; minimum, gjennomsnitt og maksimum. I [4.1.5 Letemodeller for sulfidforekomster](#) er det redegjort for hvordan, og med hvilken begrunnelse, man har valgt parameterne og fastsatt tallverdiene deres for beregningene av sulfidressursene.

### 6.1.1.2

#### Resultater

Resultatene av beregningene er gitt i de følgende tabeller og grafer. I [Tab. 6.1](#) vises estimerte mengder av metallene kobber, sink, kobolt, sølv og gull totalt for alle letemodeller. For hvert metall er det oppgitt en forventningsverdi samt et lavt (P95) og høyt (P05) estimat. Tilsvarende er vist i [7.4 Ressurstabeller for letemodeller og delområder](#) for de enkelte letemodellene.

**Tab. 6.1 Totale mengder metaller i alle sulfid letemodeller**

| Metall         | P95    | Forventning | P05     |
|----------------|--------|-------------|---------|
| Cu (mill tonn) | 28,4   | 38,1        | 47,6    |
| Zn (mill tonn) | 35,6   | 45,0        | 54,2    |
| Co (mill tonn) | 0,6    | 1,0         | 1,3     |
| Ag (tonn)      | 64 870 | 85 200      | 105 530 |
| Au (tonn)      | 1 755  | 2 317       | 2 856   |

I [Fig. 6.3](#) er vist den resulterende sannsynlighetsfordelingen for total mengde kobber i de tre letemodellene. På fordelingen er også angitt P95- og P05-verdiene. Tilsvarende fordelinger er gitt for de øvrige metallene i figurene [Fig. 6.4](#), [Fig. 6.5](#), [Fig. 6.6](#) og [Fig. 6.7](#)

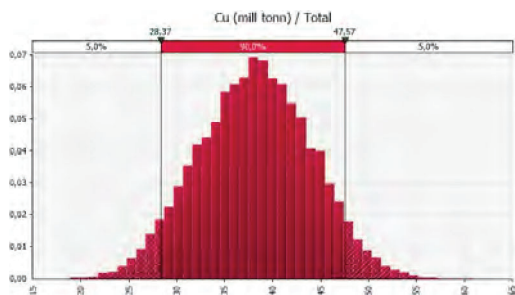


Fig. 6.3 Sannsynlighetsfordeling for total mengde kobber

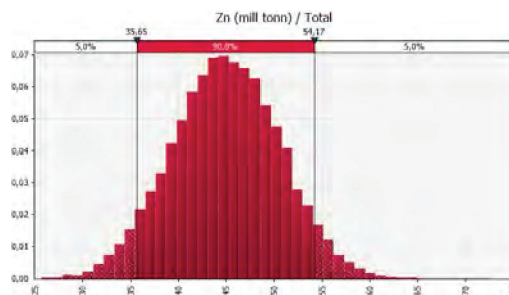


Fig. 6.4 Sannsynlighetsfordeling for total mengde sink

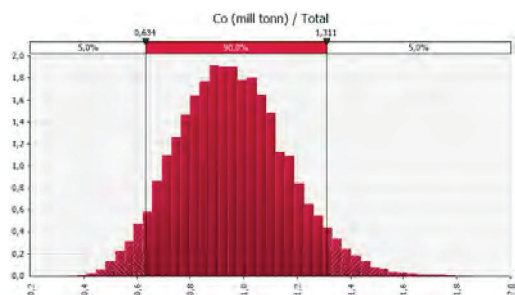


Fig. 6.5 Sannsynlighetsfordeling for total mengde kobolt

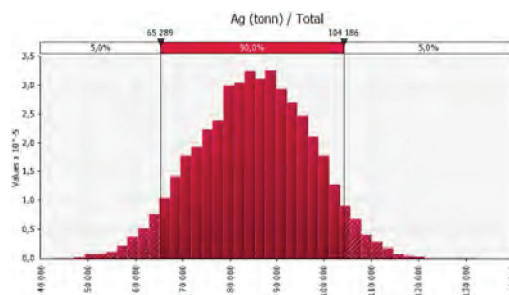


Fig. 6.6 Sannsynlighetsfordeling for total mengde sølv

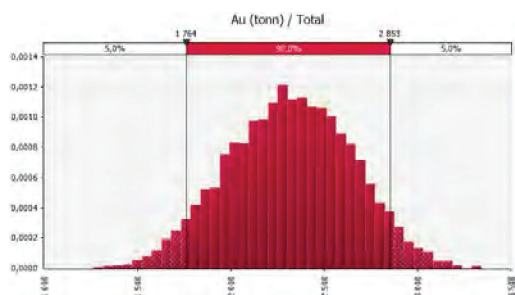


Fig. 6.7 Sannsynlighetsfordeling for total mengde gull

## 6.1.2 Manganskorpe-ressurser

### 6.1.2.1 Beregningsgrunnlaget

Dannelsen av manganskorpe vil være avhengig av minst fem viktige faktorer:

1. Alder på fjellandskapet
2. Stabilitet og helning av fjellskråninger
3. Sedimenttilførsel og avstand til kontinenter,
4. Type og konsentrasjon av grunnstoff i havvannet,
5. Havstrømmer og lokale strømforhold.

Disse faktorene er nærmere beskrevet i kapittel 4.3.2 [Dannelse og vekst av manganskorper](#).

Basert på forskjeller i geologisk utvikling av fjellandskapet ([4.4 Letemodeller for manganskorper](#)) er utredningsområdet delt inn i fire regionale områder. For hvert av disse regionale områdene er det definert subområder med prospektivt areal, manganskorpe-tykkelser og metallgehalter.



For hvert subområde er det definert parametere som inngår i beregningene:

Areal over 20 grader (m<sup>2</sup>), Tykkelse (m), Tørr Tetthet (tonn/m<sup>3</sup>), Gehalt (% , ppm)

Beregningen av mengden mangan i hvert subområde er gitt ved den generelle formelen:

Tonn Manganskorpe = Areal (m<sup>2</sup>) x Tykkelse (m) x Tørr Tetthet (tonn/m<sup>3</sup>)

Beregningen av mengden metall følger da ved den generelle formelen:

Tonn metall = Tonn Manganskorpe x Gehalt

Disse er så summert opp for å få et representativt tall for hele utredningsområdet.

Beregningen av ressursene i utredningsområdet er gjort ved Monte Carlo-simulering med programmet @Risk. Denne simuleringen krever at tallverdiene for parameterne oppgis med spredning; minimum, forventningsverdi og maksimum. I kapittel 4.4 [Letemodeller for manganskorper](#) er parametervalg redegjort for og begrunnet. Videre er det beskrevet hvordan tallverdier er fastsatt for beregninger av ressurser i manganscorpene.

#### 6.1.2.2

#### Resultater

Resultatene av beregningene av metaller i skorper er vist i de følgende tabeller.

I [Tab. 6.2](#) er vist alle metaller som det er gjort ressursberegninger for. Tabellen viser forventede mengder (mean) samt P95- og P05-verdier. Fordelingen av skorperessurser på de fire regionale områdene ([Fig. 4.28](#)) er vist i [Tab. 6.3](#). Totale mengder metaller per område er vist i kapittel 7.4 [Ressurstabeller for letemodeller og delområder](#).

**Tab. 6.2 Totale mengder metaller i manganskorper**

| Metall              | P95       | Forventning | P05       |
|---------------------|-----------|-------------|-----------|
| Mn (millioner tonn) | 126       | 185         | 257       |
| Ti (millioner tonn) | 5,8       | 8,4         | 11,4      |
| Mg (millioner tonn) | 16,7      | 24,1        | 33,0      |
| Li (tonn)           | 137 700   | 229 300     | 360 600   |
| Sc (tonn)           | 36 400    | 55 800      | 79 500    |
| V (tonn)            | 1 256 700 | 1 918 800   | 2 713 500 |
| Co (tonn)           | 1 937 900 | 3 058 100   | 4 416 700 |
| Nb (tonn)           | 48 000    | 73 000      | 103 200   |
| Hf (tonn)           | 9 600     | 14 700      | 21 000    |
| W (tonn)            | 46 100    | 80 300      | 131 200   |
| Ga (tonn)           | 12 400    | 19 200      | 27 900    |
| Y (tonn)            | 196 200   | 300 900     | 427 600   |
| La (tonn)           | 241 500   | 368 800     | 521 700   |
| Ce (tonn)           | 1 078 800 | 1 681 200   | 2 414 100 |
| Pr (tonn)           | 67 100    | 102 500     | 145 900   |
| Nd (tonn)           | 274 000   | 420 300     | 596 000   |
| Eu (tonn)           | 15 100    | 23 200      | 32 900    |
| Gd (tonn)           | 65 100    | 99 900      | 141 800   |

|           |        |        |         |
|-----------|--------|--------|---------|
| Tb (tonn) | 9 900  | 15 200 | 21 600  |
| Dy (tonn) | 56 400 | 86 400 | 122 500 |

**Tab. 6.3 Totale mengder manganskorper i millioner tonn, fordelt på delområde**

| Område                                | P95 | Forventning | P05   |
|---------------------------------------|-----|-------------|-------|
| V og Ø for Knipovitsryggen            | 157 | 278         | 427   |
| NV og SØ for Mohnsryggen              | 642 | 1 022       | 1 459 |
| Jan Mayen-ryggen og sjøfjellene rundt | 14  | 31          | 55    |
| Vøringutstikkeren og Vøringplatået    | 44  | 120         | 235   |
| Totalt                                | 968 | 1 451       | 2 023 |

Se Fig. 4.28 for kart med markering av områdene.

### 6.1.3 Forventede totale ressurser

Forventningsverdier for samlede, tilstedeværende metaller i både sulfider og manganskorper i utredningsområdet, er vist i Fig. 6.8. Spredningen i utfallsrommet (P95 og P05) vises ikke i figuren.

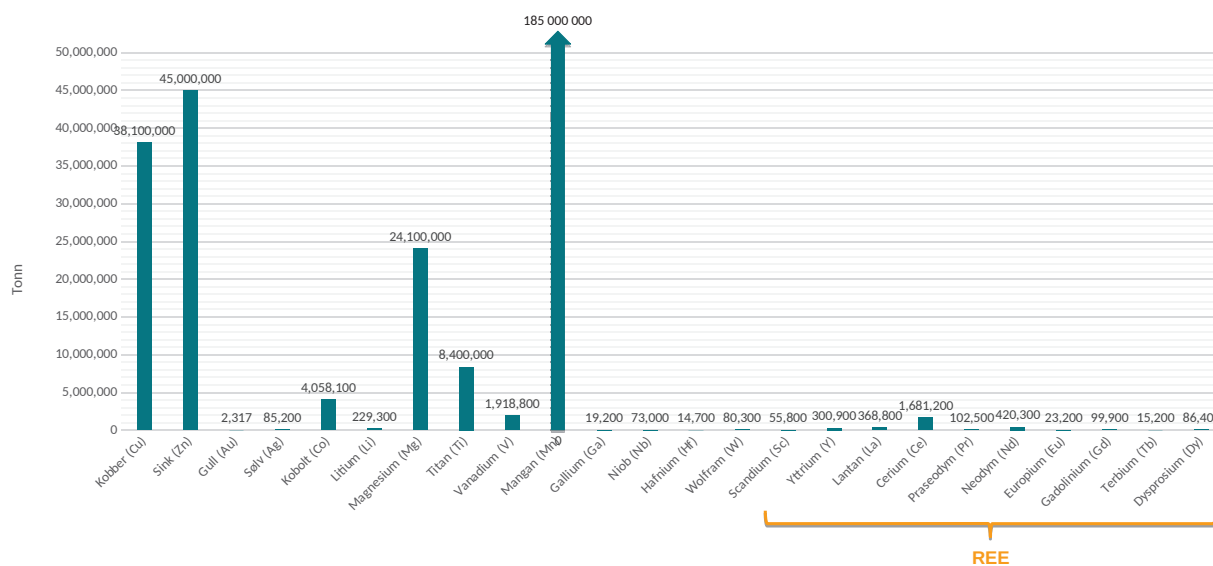


**Fig. 6.8 Forventning tilstedeværende metallressurser**

## 6.2 Ressurser i regneeksemplene Mohnsskatten og Sjøfjell

### 6.2.1 Mohnsskattens sulfidressurser

I dette avsnittet brukes Mohnsskatten, hvor vi har best datadekning, som eksempel på beregning av ressurser i en enkelt sulfidteig. Mohnsskatten består av to forekomster, A og B, og ligger på nordvestflanken av aksedalen i nordre del av Mohnsryggen. Det er beskrevet to geologiske modeller for Mohnsskatten. De geologiske modellene og tilhørende geologisk informasjon og nødvendige parametere er presentert i [4.2 Sulfideksempel Mohnsskatten](#) med underkapitler. TAG-forekomsten som ligger på den midt-atlantiske ryggen sør for Azorene, brukes som modell for ressursberegningen slik den er beskrevet i seksjon [4.1.4 Geologisk ressursmodell](#). Beregningene regner først ut volumet av den massive sulfidkappen som ligger på havbunnen øverst i strukturen. Deretter legger man til volumet av den underliggende stockwerksonen beregnet med forholdstallet mellom sulfidkappen og stockverket i TAG (=0,45). Siden disse beregningene dermed gjøres på grunnlag av overflatearealet i de to delene (A og B), vil det bli samme resultat for begge geologiske modeller.

Tonnasje malm i Mohnsskatten beregnes ut fra den generelle formelen:

$$(\text{Volum}^1 \text{ malm}) \times (\text{Tetthet malm}) = \text{Tonn malm i letemodell}$$

<sup>1</sup>Volumer beregnes ved hjelp av areal og tykkelse (dyp) av forekomstene.

Tonnasje av de enkelte metaller beregnes så ut fra gehaltene:

$$(\text{Tonn malm}) \times (\text{Gehalt av metall i \% eller ppm}) = \text{Tonn metall}$$

I det følgende oppgis de enkelte parametere for beregningen

Volum:

$$\text{Overflatearealet} = 68\,705 \text{ m}^2$$

$$\text{Gjennomsnittstykkelse av massiv sulfid-kappe} = 6 \text{ meter}$$

$$\text{Volum av stockwerk-sonen} = (\text{Volum av sulfid-kappen}) \times 0,45$$

Overflatearealet av sulfidkappen er digitalisert fra kartet over Mohnsskatten ([Fig. 4.19](#)). Tykkelsen er fastsatt i følge prinsipp beskrevet i avsnitt [4.1.5.1 Volum](#).

Tettheten:

$$\text{Gjennomsnitt tetthet i den massive sulfidkappen} = 3,8$$

$$\text{Gjennomsnitt tetthet i stockwerk-sonen} = 3,6$$

## Metallgehalter:

Tab. 6.4 Gehaltstatistikk over utvalgte gehalter i Mohnsskatten

| Metall | Mohnsskatten 2020 |        |       |       |    |
|--------|-------------------|--------|-------|-------|----|
|        | Gjennomsnitt      | MEDIAN | STDV  | Max   | N  |
| Cu %   | 0,91              | 0,48   | 1,92  | 14,30 | 65 |
| Zn %   | 2,70              | 0,13   | 5,19  | 24,40 | 65 |
| Co %   | 0,014             | 0,005  | 0,031 | 0,140 | 65 |
| Au ppm | 2,58              | 1,16   | 3,62  | 19,2  | 65 |
| Ag ppm | 64,5              | 8,25   | 123,5 | 548   | 65 |

Gehaltene som er brukt representerer gjennomsnittene av analyser av 65 prøver. Det benyttes samme gehalter for stockwerksonen som for sulfidkappen. De fem valgte metallene er de som ansees som mest økonomisk interessante.

Oppsummeringstabeller over parametere og beregninger:

Tab. 6.5 Dimensjoner og beregnet sulfid-tonnasje i Mohnsskatten

| Mohnsskatten, soner      | Areal m <sup>2</sup> | Volum m <sup>3</sup> | Tykkelse/ forholdstall | Tetthet | Ressurser, Mt |
|--------------------------|----------------------|----------------------|------------------------|---------|---------------|
| Sulfidkappe A            | 58720                | 352320               | 6                      | 3,8     | 1,339         |
| Sulfidkappe B            | 9985                 | 59910                | 6                      | 3,8     | 0,228         |
| <b>Sulfidkappe A + B</b> | <b>68705</b>         | <b>412230</b>        |                        |         | <b>1,566</b>  |
| Stockwerksone A          |                      | 158544               | 0,45                   | 3,6     | 0,571         |
| Stockwerksone B          |                      | 26960                | 0,45                   | 3,6     | 0,097         |
| <b>Stockwerk A + B</b>   |                      | <b>185504</b>        |                        |         | <b>0,668</b>  |
| <b>Totalt</b>            | <b>68705</b>         |                      |                        |         | <b>2,234</b>  |

Tab. 6.6 Gehalter og beregnede metall-tonnasjer i Mohnsskatten

| Gehalt, gjennomsnitt     | Cu %         | Zn %         | Co %       | Au ppm   | Ag ppm     |
|--------------------------|--------------|--------------|------------|----------|------------|
| Mohnsskatten A + B       | 0,91         | 2,7          | 0,014      | 2,6      | 65         |
| Tonnasje, metaller       | Cu tonn      | Zn tonn      | Co tonn    | Au tonn  | Ag tonn    |
| Sulfidkappe A            | 12183        | 36148        | 187        | 3        | 87         |
| Sulfidkappe B            | 2072         | 6147         | 32         | 1        | 15         |
| <b>Sulfidkappe A + B</b> | <b>14255</b> | <b>42295</b> | <b>219</b> | <b>4</b> | <b>102</b> |
| Stockwerk sone A         | 5194         | 15410        | 80         | 1        | 37         |
| Stockwerk sone B         | 883          | 2620         | 14         | 0        | 6          |
| <b>Stockwerk A + B</b>   | <b>6077</b>  | <b>18031</b> | <b>93</b>  | <b>2</b> | <b>43</b>  |
| <b>Totalt</b>            | <b>20332</b> | <b>60326</b> | <b>313</b> | <b>6</b> | <b>145</b> |

### 6.2.2 Sjøfjell manganskorperressurser

I dette avsnittet brukes sjøfjellet nordvest i Grønlandshavet og området rundt som regneeksempel på ressurser i et område med manganskorpe. Den geologiske modellen for forekomsten, og tilhørende geologisk informasjon og nødvendige parametere, er

presentert i [4.5 Manganskorpe-eksempel sjøfjell nordvest i Grønlandshavet](#). Regneeksempelet sjøfjell dekker et areal på 133 km<sup>2</sup> hvor det er relativt god datadekning, gunstig topografi og tykke manganskorper.

Tonnasje manganskorpe i området beregnes ut fra den generelle formelen:

$$(\text{Volum}^1) \times (\text{Tetthet tørre ressurser}) = \text{Tonn tørre ressurser}$$

<sup>1</sup>Volumer beregnes ved hjelp av areal og tykkelse.

Tonnasje av de enkelte metaller beregnes så ut fra gehaltene:

$$(\text{Tonn tørr manganskorpe}) \times (\text{Gehalt av metall i \% eller ppm}) = \text{Tonn metall}$$

Nøkkelparametre fra ODs beregning er vist i [Tab. 6.7](#), der beregnet gjennomsnittsareal over 20 grader er 133 km<sup>2</sup> og forventet gjennomsnittstykkelse av manganskorpen er 28 cm.

Nærmere beskrivelse av arealberegning og tykkelsespredning er gitt i kapittel [4.4.1 Volum](#)

Metallgehalter brukt er oppsummert i [7.3 Tabeller for gehalter i manganskorper](#)

**Tab. 6.7 Forventningsverdier for parametere for sjøfjell i Grønlandshavet**

|                                     | Areal km <sup>2</sup> | Volum millioner m <sup>3</sup> | Tykkelse/ forholdstall (cm) | Tetthet | Ressurser millioner tonn |
|-------------------------------------|-----------------------|--------------------------------|-----------------------------|---------|--------------------------|
| <b>Sjøfjell NV i Grønlandshavet</b> | 133                   | 43                             | 28                          | 1,3     | 56                       |

**Tab. 6.8 Beregnet tilstedeværende ressurser på sjøfjell i Grønlandshavet**

| Metall              | P95    | Forventning | P05     |
|---------------------|--------|-------------|---------|
| Mn (millioner tonn) | 3,4    | 6,9         | 11,2    |
| Ti (millioner tonn) | 0,14   | 0,27        | 0,41    |
| Mg (millioner tonn) | 0,51   | 0,82        | 1,18    |
| Li (tonn)           | 3 614  | 9 346       | 18 970  |
| Sc (tonn)           | 1 224  | 2 368       | 3 708   |
| V (tonn)            | 49 242 | 79 080      | 115 187 |
| Co (tonn)           | 57 329 | 131 586     | 219 283 |
| Nb (tonn)           | 1 518  | 2 913       | 4 591   |
| Hf (tonn)           | 342    | 611         | 936     |
| W (tonn)            | 1 228  | 3 414       | 7 198   |
| Ga (tonn)           | 418    | 756         | 1 153   |
| Y (tonn)            | 8 149  | 12 399      | 17 338  |
| La (tonn)           | 7 829  | 14 475      | 22 300  |
| Ce (tonn)           | 43 837 | 71 655      | 105 249 |
| Pr (tonn)           | 2 337  | 4 067       | 6 086   |
| Nd (tonn)           | 9 703  | 16 600      | 24 732  |
| Eu (tonn)           | 579    | 926         | 1 339   |
| Gd (tonn)           | 2 566  | 4 053       | 5 807   |

|           |       |       |       |
|-----------|-------|-------|-------|
| Tb (tonn) | 392   | 614   | 881   |
| Dy (tonn) | 2 316 | 3 519 | 4 971 |

### 6.3 Kunnskapsbehov

Ressursvurderingen gir en første, samlet vurdering av havbunnsmineraler i utredningsområdet. Datagrunnlaget kan videre styrkes og metodikk for ressursmodellering videreutvikles. Teknologitviking, sammen med mer og bedre data, vil forbedre forståelsen av ressurspotensialet og dermed også kvantifisering av usikkerheten i ressursanslagene, og gi mulighet for å flytte ressurser til mer modne ressursklasser. Viktige bidrag for å øke treffsikkerhet i ressursanslagene er:

#### **Innsamling av mer batymetri for bedre havbunnskart**

53 pst. av utredningsområdet er per 01.12.2022 dekket av skipsbatymetri. Dette gir grunnlag for å utarbeide topografiske havbunnskart med god oppløsning (25 meter eller bedre). Det er behov for å dekke hele utredningsområdet i samme oppløsning. Dette er viktig for å kunne beregne areal av fjellområder som møter kriteriene for dannelse av manganskorper, og som grunnlag for AUV-tokt på leting etter eldre sulfidforekomster øst og vest for dagens spredningsrygger.

#### **Leteboring på sulfidforekomster**

For å redusere usikkerhet knyttet til tykkelse og utbredelse av sulfidforekomster i dypet, vil det være behov for grunne leteboringer. Seismiske metoder forventes også å kunne bidra til bedre forståelse av sulfidforekomstene i utredningsområdet og ressurser i dypet av disse, spesielt der disse kan kalibreres til grunne leteboringer.

#### **Høyfrekvent seismikk for å avbilde sedimentpakker og paleo-sulfidforekomster**

Store paleosulfid-ressurser vil være helt eller delvis begravd under sedimenter. Høyfrekvent seismikk og videreutviklede geofysiske metoder kan skille sedimenter og underliggende bergarter, samt sulfidforekomster fra basalter/vulkansk havbunn.

#### **Tykkelsesmålinger for manganskorper på AUV**

Det er behov for å utvikle teknologi som kan måle tykkelse på manganskorper raskt og effektivt. Det arbeides med å utvikle geofysiske verktøy som kan monteres på AUV'er og kontinuerlig samle inn denne type data.

#### **Prøvetaking av manganskorper med ROV**

I dag benyttes ROV med kutteverktøy (motorsag, vinkelsliper o.l.) for å ta prøver. Dette er en tidkrevende teknikk, og mer effektive metoder må utvikles.





## 7 Appendiks

### 7.1 Andre sulfidforekomster kartlagt av Oljedirektoratet og academia

I dette appendikset beskrives modeller for noen av de andre sulfidforekomster i utredningsområdet. Modellene bidrar til kunnskap og kalibrering av ressursvurderingen, men det er ikke gjort detaljerte ressursvurderinger for disse forekomstene.

#### 7.1.1 Fåvne

Fåvne er en sulfid-teig som ligger nesten 140 km sør for Mohnskatten på ca 72° 45' N i skrenten på en av de store hovedforkastningene som utgjør nordvestflanken av aksedalen i nordlig del av Mohnsryggen. Gnitahei ligger i samme skrenten omtrent 700 meter sør for Fåvne (Fig. 7.1).

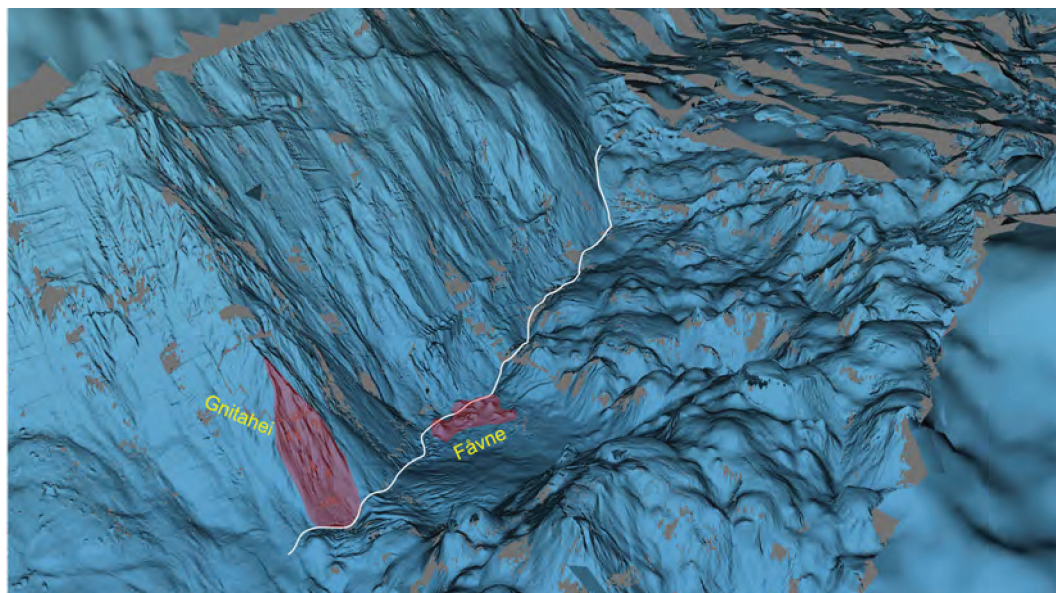


**Fig. 7.1 Fåvne og Gnitahei sine beliggenheter**

Perspektivkart som viser plasseringen av sulfidteigene Fåvne og Gnitahei sett fra sørøst. Sulfidteigenes utstrekning er antydnet med gjennomsiktige polygoner. Den hvite linjen antyder foten av skråningen på hovedforkastningen på vestflanken av aksedalen.

##### 7.1.1.1 Geologi og tektonisk ramme

Spranget på hovedforkastningen ved Fåvne er på ca 1000 meter, slik at dagens forkastningsskrent går fra eggen på ca 2 000 meters dyp til foten langs dalbunnen på 3 000 meter. Denne skrenten representerer overflaten av liggblokken av forkastningen. Forkastningen er fremdeles aktiv, og dagens spranghøyde vil fortsette å øke ved gjentatte episoder med større og mindre sprang gjennom forkastningens levetid.

Fåvne-teigen ligger ved foten av hovedforkastningen, delvis på tvers av overgangen mellom liggblokken og hengblokken (overgangen mellom skrenten og dalbunnen) (Fig. 7.2). Teigen består av syv store og flere små, separate sulfidkjegler innenfor et område på ca 250 x 130 meter, et område på 90 x 50 meter av dette ligger i liggblokken, mens resten ligger i hengblokken. To av de store kjeglene er bekreftet aktive, mens de øvrige må antas nylig å ha vært det eller være i en periode med redusert aktivitet. Dette fordi

skorsteinene er bygget av meget porøst og lite konsolidert materiale og er fortsatt helt intakte uten spor av erosjon. Dette viser at denne sulfidteigen er meget ung der sulfidavsetningene ennå ikke er begynt å bli massive og konsoliderte.

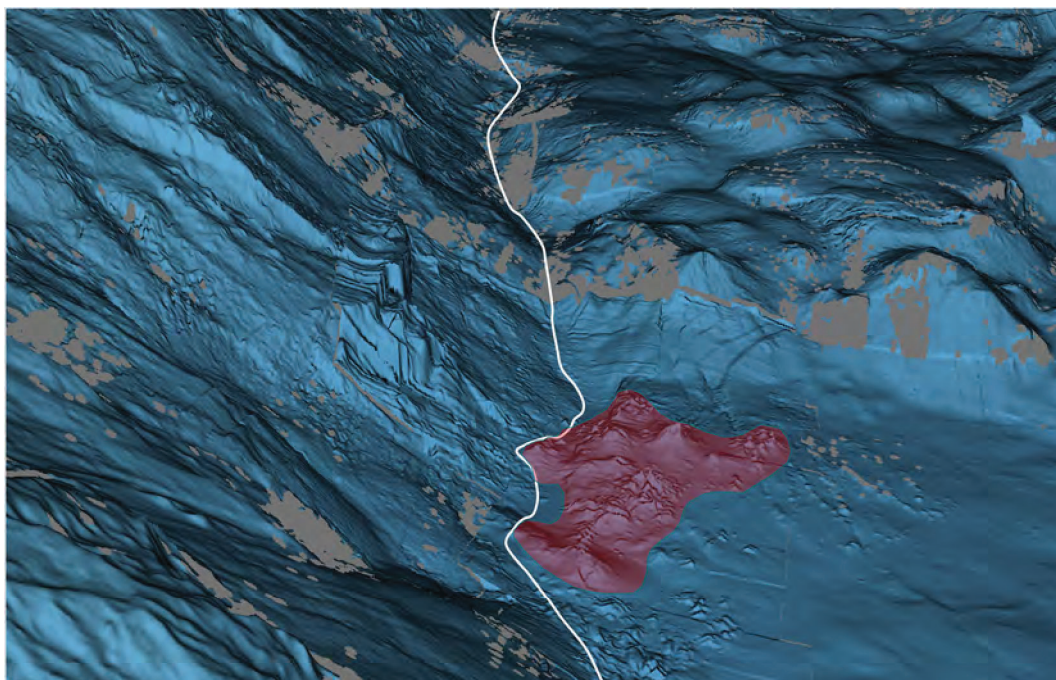


**Fig. 7.2 Perspektivkart av Fåvne**

Utstrekningen av sulfidteigen er antydnet med et polygon i gjennomsiktig burgunder. Topografien internt i polygonet gjenspeiler sulfidteigens skorsteiner, kjepler og hauger.

Sulfidavsetningen i kjeplene er så løs at det ikke var mulig å bore ut kjerner. I stedet produserte boringen kun en løs masse av borekaks og støv som ble fanget opp i store plastsylindere. På en lokalitet lykkes man med å få ut en 2,2 m kerne av den underliggende, sterkt breksjerte basalten. Breksjen i borekjernen har ennå ikke utviklet årer av utfelte mineraler slik at klastene ikke er kittet sammen, men ligger løst inntil hverandre. Men klastene har alle en mørk sone ytterst som viser at de var breksjert før den hydrotermale aktiviteten startet.

#### 7.1.1.2

#### Geokjemi og undergrunnsmodell

Vulkankjeplene i Fåvne-teigen ligger adskilt med innbyrdes avstander på 20 til 50 meter. Som beskrevet ovenfor, er denne sulfidteigen ung, med kjepler og skorsteiner bygget av løst sulfidmateriale oppå en berggrunn av ikke-mineralisert basaltbreksje. Det betyr at i dagens sulfidteig stiger de hydrotermale væskene opp gjennom soner bestående stort sett kun av breksjerte sidebergarter. Dersom aktiviteten fortsetter, vil disse breksjene kunne utvikle seg til å bli en mineralisert stockwerksone. Man må da også vurdere om de enkelte kjeplene utvikles over separate tilførselsrør eller om de utvikler seg til å løpe sammen en felles stockwerksone.

Resultatene fra 15 analyser fra Oljedirektoratet, 12 fra Sahlström et al. (2020) og 8 fra UiB gir til sammen et gjennomsnitt på 3,55 pst. Cu, 7,20 pst. Zn og 0,32 pst. Co for Fåvne. De gjennomgående høye verdiene for Co (0,1 til 0,98 pst.) tyder på at de hydrotermale væskene har vært i kontakt med ultramafiske bergarter i undergrunnen. Det er ikke påvist slike bergarter internt eller i nærheten av Fåvne-teigen, hverken i hengblokken eller liggblokken. Men det må regnes som sannsynlig at ultramafiske bergarter er brakt

så høyt i skorpen langs forkastningsplanet i liggblokken at de er blitt en del av det hydrotermale systemet. Som for Mohnsskatten er den tredimensjonal TAG-modellen benyttet for å predikere en mulig, realistisk, tredimensjonal modell for Fåvne (se snitt i Fig. 7.3). Dimensjonene i modellen er tatt fra TAG-modellen kombinert med kartbildet i overflaten. Denne modellen gir grunnlag for beregning av ressurser i Fåvne. Dette vil også gi grunnlag for å predikere hvor store ressursene i Fåvne vil bli i fremtiden dersom den utvikler seg med en sonering (vertikalt og horisontalt) som i TAG og Mohnsskatten.

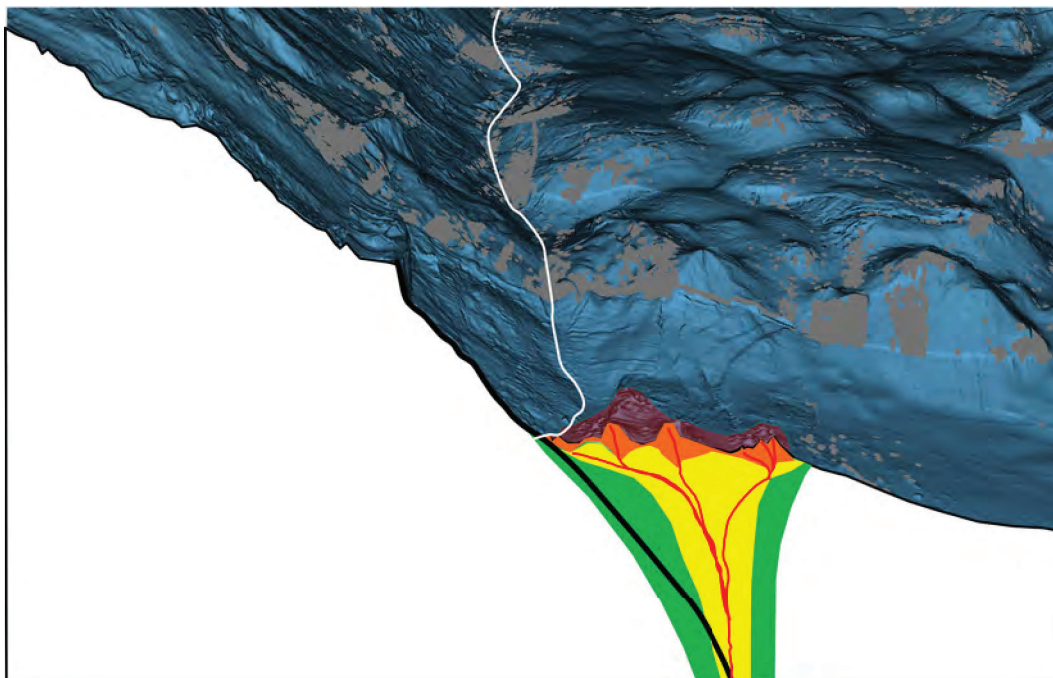


**Fig. 7.3 Fåvne modellsnitt**

Et snitt av jordskorpen på tvers av Fåvneteigen kombinert med havbunnstopografien sett i perspektiv fra sørøst. Utstrekningen av sulfidteigen bak snittet er antydnet som burgunder polygon. De massive sulfidene og sulfidbreksjene er antydnet i mørk orange, stockwerksonen med mineralisering og bergartsbreksjer er antydnet i gult med mineraliserte årer skjematisk antydnet i rødt, og sonen med hydrotermalt påvirket sidebergart er antydnet i lyst grønn. Hovedforkastningsplanet er vist som svart linje.

## 7.1.2 Gnitahei

Gnitahei er en sulfid-teig som ligger nesten 140 km sør for Mohnsskatten på ca 72° 45' N i skrenten på en av de store hovedforkastningene som utgjør nordvestflanken av aksedalen i nordlig del av Mohnsryggen. Fåvne ligger i samme skrenten omtrent 700 meter nord for Gnitahei (Fig. 7.1).

### 7.1.2.1

#### Geologi og tektonisk ramme

Spranget på hovedforkastningen her er på ca 1 000 meter, slik at dagens forkastningsskrent går fra eggen på ca 2 000 meters dyp til foten langs dalbunnen på 3 000 meter. Denne skrenten representerer overflaten av liggblokken av forkastningen. Forkastningen er fremdeles aktiv, og dagens spranghøyde vil fortsette å øke ved gjentatte episoder med større og mindre sprang gjennom forkastningens levetid.

Gnitahei ligger i en lokal skredgrop oppe i forkastningsskrenten på liggblokken. Denne skredgropen strekker seg fra 2 775 meters dyp og ender mot dalbunnen ved foten av forkastningsskrenten. Den har en trekantet form, med en bredde på ca 200 meter ved foten og smalner til en spiss mot toppen. Sulfidteigen strekker seg fra den øvre kanten



på skredgropa på 2 775 meters dyp helt ned til foten (Fig. 7.1). Utover på dalbunnen nedenfor skredgropen ligger en stor vifte som sannsynligvis inneholder massene fra skredet.

I skredgropen i dag er det bare stockwerksonen av den opprinnelige Gnitaheiforekomsten som er blottet i forkastningsskrenten. De øvre delene med de massive sulfidavsetningene og deres skorsteiner, kjegler og hauger er fjernet ved utrasningen(e) som dannet skredgropen. Det er ikke funnet noen skorsteiner, kjegler eller hauger, hverken nede i skredgropen eller langs kantene, unntatt noen få skorsteinsfragmenter litt ovenfor raskanten (Wold, 2022). Det betyr at utrasningen(e) skjedde etter at den hydrotermale aktiviteten døde ut. At det nesten ikke er spor etter de typiske sulfidstrukturene utenfor skredgropen heller, tyder på at denne sulfidteigen er gammel og fullstendig nederodert.

#### 7.1.2.2 Geokjemi og undergrunnsmodell

ROV-videoene og prøvetaking viser at mye av skredgropen består av breksjert sidebergart og utrast materiale av samme. Opp av disse massene stikker det en del langstrakte, smale rygger med sammenkittede breksjer. Disse representerer antagelig rester av store, mineraliserte årer som har vært transportveier for hydrotermale væsker. I disse og spredt langs skredkantene er det funnet prøver av massivt sulfid og basaltbreksjer med mineralisert matriks. Oljedirektoratet har gjort analyser av 16 sulfidprøver fra Gnitahei. De inneholder vesentlig Fe og viser svært lave verdier av både Cu og Zn, henholdsvis 0,15 og 0,2 pst. En ekstra analyse tatt med håndholdt XRF viser 2,5 pst. Zn, som er den høyeste verdi som er registret til nå. UiB rapporterer også lave verdier; et snitt på 0,5 pst. Cu i de massive sulfidene (Wold, 2022). Oljedirektoratets prøver inneholder markert mindre Co i Gnitahei (ca 0,04 pst) enn i Fåvne, men representerer likevel en anrikning i Co. Studier av Wold (2022) viser til det samme nivået for Co og at dette, sammen med et forhøyet Ni-nivå tyder på at det hydrotermale systemet knyttet til Gnitahei kan ha vært i noekontakt med ultramafiske vertsbergarter slik tilfellet synes å være også med Fåvne-teigen.

Avgrensingen av Gnitahei-teigen er ikke helt avklart – til det trengs det mer prøvetaking. Imidlertid ser det ikke ut til at den strekker seg mye utover den lokale skredgropen. Det er også sannsynlig at en stor del, kanskje mesteparten av sulfidressursene ligger i skredviften i dalbunnen nedenfor.

Det er to mulige modeller for strukturen av Gnitahei-teigen i undergrunnen. I den ene (Modell 1) antas det at sulfidteigen har utviklet seg ved foten av skåningen i samme tektoniske posisjon som Fåvne-teigen i dag, og at de hydrotermale væskene har fulgt hovedforkastningssonen. Etter at sulfidteigen er blitt inaktiv, er den delen som ble utviklet i hengblokken blitt hevet til dagens plassering i skrånningen, der dagens skredgrop er dannet ved seinere utrasninger (Fig. 7.4). I den andre modellen (Modell 2) antas det at hele Gnitahei-teigen ble utviklet i selve hengblokken med en hydrotermal breksjesone vertikalt under forekomsten. Etter at den ble inaktiv har så store deler rast ut og etterlatt seg skredgropen (Fig. 7.5).

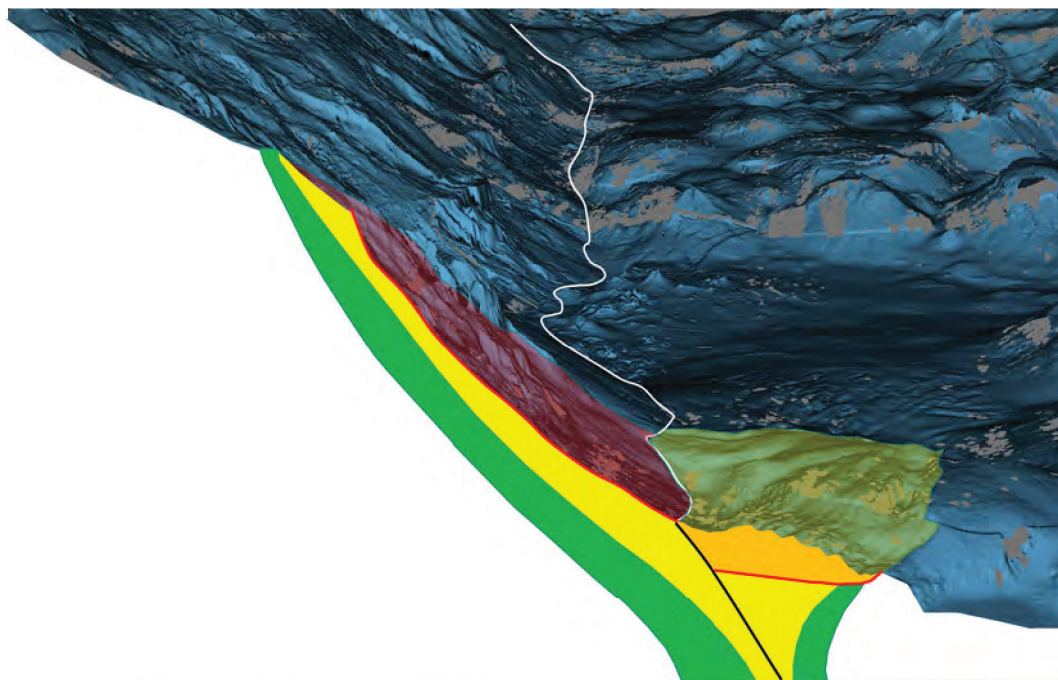


**Fig. 7.4 Gnitahai modell 1**

Et snitt av jordskorpen på tvers av Gnitahai-teigen kombinert med havbunnsstopografien sett i perspektiv fra sørøst. Utstrekningen av sulfidteigen og skredgropa bak snittet er antydnet som burgunder polygon. Stockwerksonen med mineralisering og bergartsbreksjer er antydnet i gult, og sonen med hydrotermalt påvirket sidebergart er antydnet i lyst grønn. Skredviften nedenfor skredgropen er vist med gjennomsiktig, gul overflate og oransje snitt. Skredets glideplan er vist i rødt. Hovedforkastningsplanet er vist som svart linje.

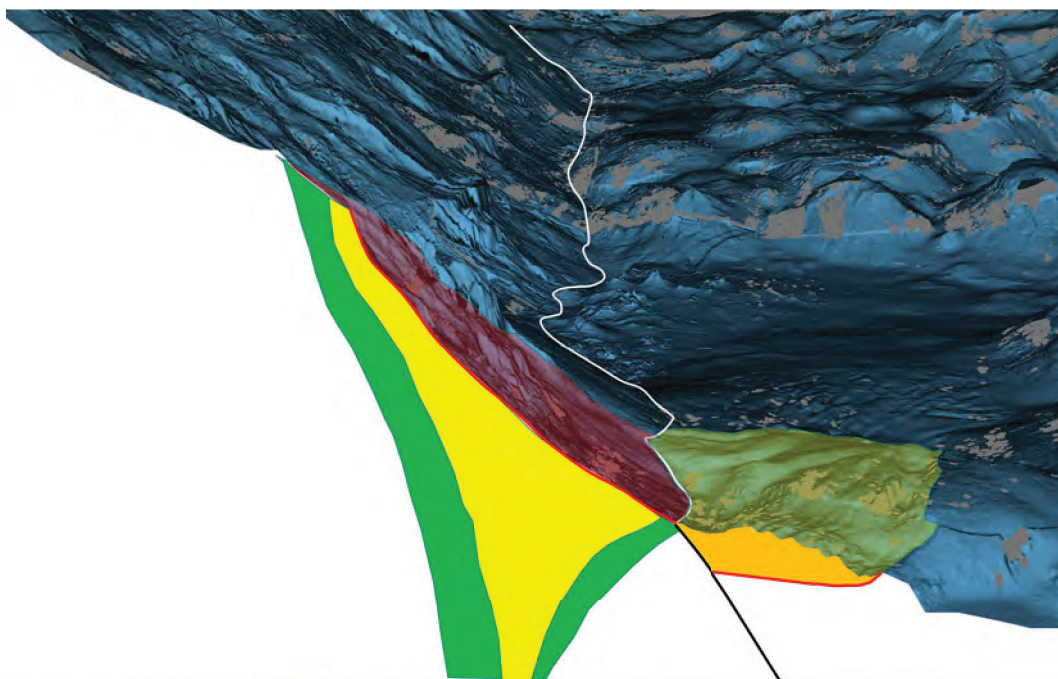


**Fig. 7.5 Gnitahai modell 2**

Et snitt av jordskorpen på tvers av Gnitahai-teigen kombinert med havbunnsstopografien sett i perspektiv fra sørøst. Utstrekningen av sulfidteigen og skredgropa bak snittet er antydnet som burgunder polygon. De massive sulfidene og sulfidbreksjene er antydnet i mørk oransje, stockwerksonen med mineralisering og bergartsbreksjer er antydnet i gult, og sonen med hydrotermalt påvirket sidebergart er antydnet i lyst grønn. Skredviften nedenfor skredgropen er vist med gjennomsiktig, gul overflate og oransje snitt. Skredets glideplan er vist i rødt. Hovedforkastningsplanet er vist som svart linje.

### 7.1.3 Lokeslottet

Lokeslottet er en sulfid-teig som ligger 32 km nord for Mohnskatten på ca 73° 33' N på en aksial vulkanrygg der aksedalen i Mohnsryggen begynner å svinge inn i aksedalen i Knipovitsryggen (Fig. 2.1).

#### 7.1.3.1 Geologi og tektonisk ramme

Lokeslottet er en sulfidteig som består av to store, sammengrodde, kjegleformede sulfidhauger med aktive skorsteiner på toppen. De to haugene er ca 30 meter høye og ligger innenfor et område på ca 250 x 150 meter. Den aksiale vulkanryggen de ligger på, består av basaltisk lava (Fig. 7.6).

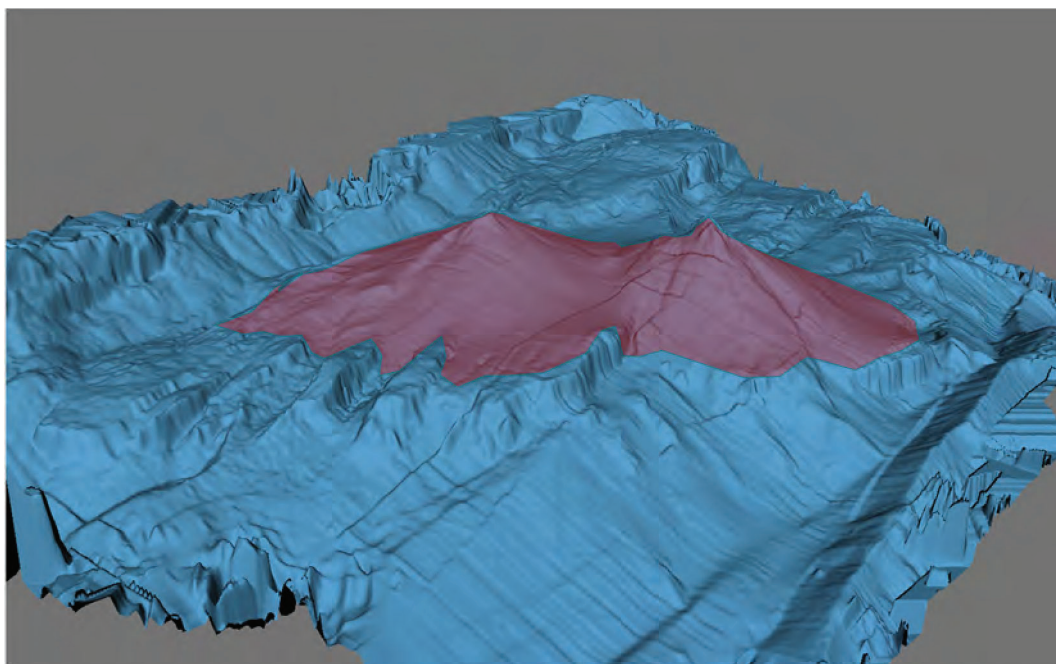


**Fig. 7.6 Lokeslottet**

Perspektivkart av sulfidforekomsten Lokeslottet med sine to sulfidhauger og sentrale skorsteiner, sett fra sørøst. Utstrekningen av forekomsten er antydnet med et polygon i gjennomsiktig burgunder.

#### 7.1.3.2 Geokjemi og undergrunnsmodell

De aktive skorsteinene viser at vulkanryggen har sprekkesoner som når ned i den hydrotermale reaksjonssonen i undergrunnen. På batymetrien ser det ut til at disse sprekkesonene ligger i et sett med forkastninger som stryker langsetter den vulkanske ryggen, både sentralt på ryggen og langs flankene. Den regulære kjegleformen og høyden på de to haugene viser at det er to tilførselssoner til overflaten og at disse har vært stabile over tid. Det foreligger da to mulige undergrunnsmodeller for de to sulfidhaugene. De kan være tilknyttet reaksjonssonen i dypet ved en felles sprekkesone som fordeles på to tilførselsrør langs hvert sitt forkastningsplan opp mot overflaten (Modell 1) (Fig. 7.7), eller de to haugene kan ha separate tilførselsrør helt ned til reaksjonssonen i dypet (Modell 2) (Fig. 7.8).



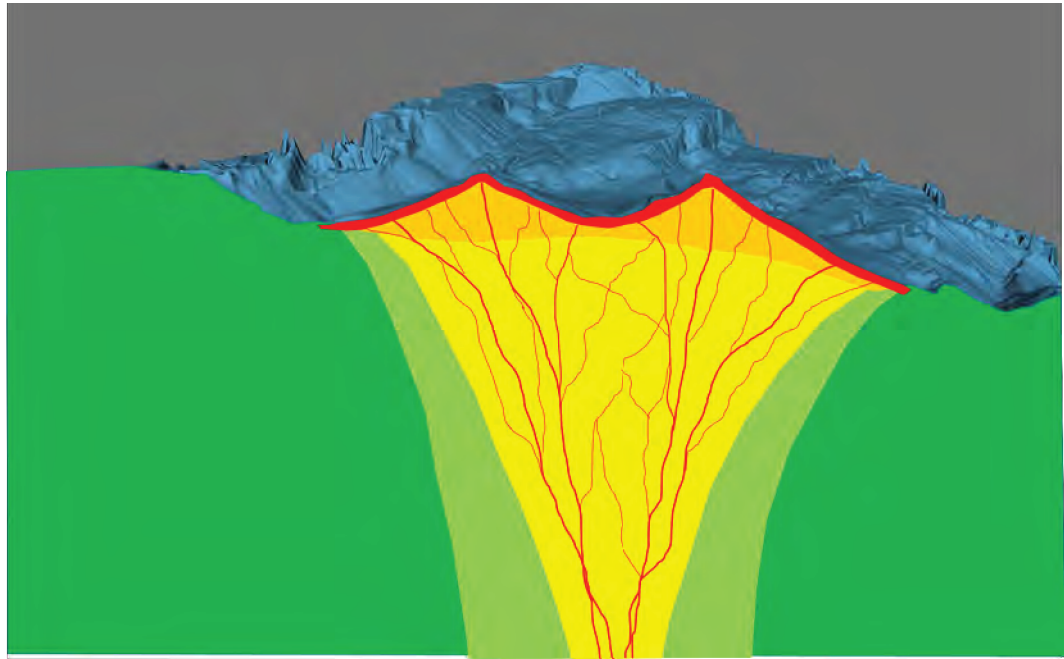


**Fig. 7.7 Lokeslottet Modell 1**

Et snitt av jordskorpen på tvers av Lokeslottet kombinert med havbunnsstopografien sett i perspektiv fra sørøst. Et «topplukk» av massiv sulfid er antydnet i rødt, de massive sulfidene og sulfidbreksjene er antydnet i mørk oransje, stockwerksonen med mineralisering og bergartsbreksjer er antydnet i gult med mineraliserte årer skjematisk antydnet i rødt, sonen med hydrotermalt påvirket sidebergart er antydnet i lyst grønn, og sidebergarten er antydnet i mørkt grønn.

**Fig. 7.8**

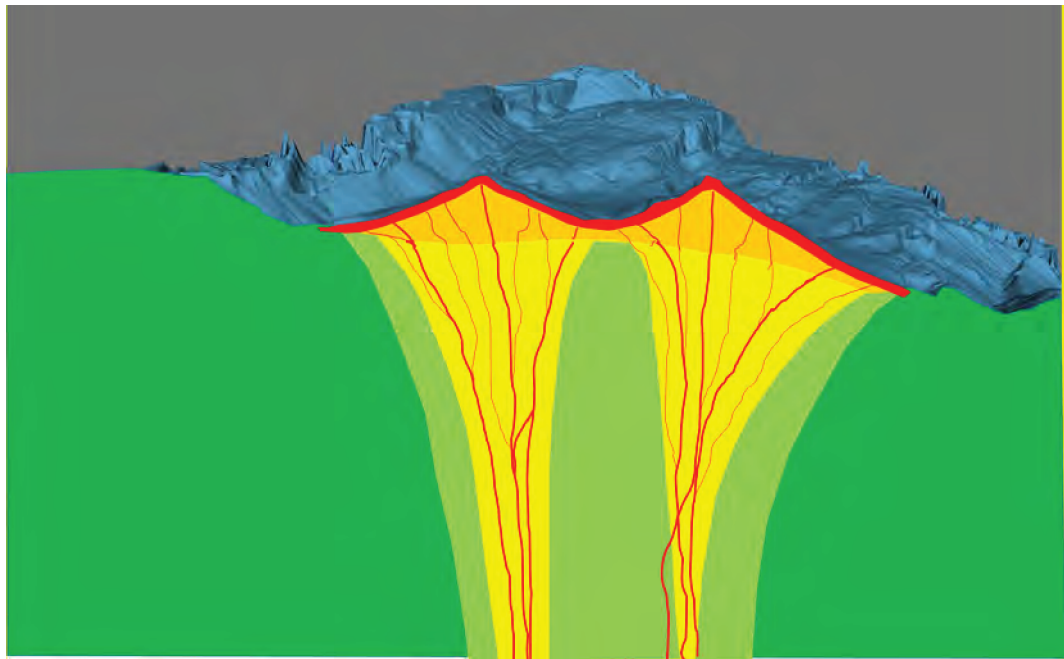


**Fig. 7.8 Lokeslottet Modell 2**

Modell 2 for Lokeslottet. Her har de to sulfidhaugene i overflaten adskilte tilførselsrør og stockwerksoner. Snittet og fargekodene er de samme som i Fig. 7.7

Resultatene fra 46 analyser fra UiB, 7 fra Snook et al. (2018) og 7 fra Sahlström et al. (2020) gir til sammen et gjennomsnitt på 0,96 pst. Cu, 1,52 pst. Zn for Lokeslottet. Dette er noe lavere konsentrasjoner enn for Mohnsskatten, og betydelig lavere enn for Fåvne.

Lokeslottet har svært lav konsentrasjon av Co. De generelt lave metallkonsentrasjonene i Lokeslottet skyldes antagelig innblanding av sedimenter i systemet som beskrevet tidligere (4.1.3 Geokjemi og metallgehalt).

## 7.2 Tabeller for kaledonske sulfidforekomster

Tab. 7.1 Hydrotermale sulfidforekomster i skandinavisk del av den kaledonske fjellkjeden; mulige SMS-analoger

| Navn, forekomst   | Sone           | Produsert Mt | Opprinnelig Mt | Cu%  | Zn%  | Au ppm | Ag ppm | Co%  | Pb%  | Hovedmalm      | Vertsbjergart    | Type   | Gruppe |
|-------------------|----------------|--------------|----------------|------|------|--------|--------|------|------|----------------|------------------|--------|--------|
| Gravdal           | Hardanger      | 0,141        | 0,141          | 1,35 | 0,7  |        |        |      |      | Cu             | Rhyd             | VMS    | A      |
| Grev Moltke Gruve | Folldal-Meråk. | 0,3          | 0,3            | 2    | 5    | 0,35   | 48     |      | 0,45 | Cu, Zn, Ag     | Dac, tuff        | VMS    | A      |
| Søndre Geitryggen | Folldal-Meråk. | 0,5          | 0,5            | 0,7  | 2,7  | 0,35   | 27     |      | 0,15 | Cu, Zn, Au, Ag | Dac, tuff        | VMS    | A      |
| Stekenj. enjokk   | Grong-Stekenj. | 6,97         | 11,93          | 1,29 | 3,81 | 0,4    | 53,1   |      | 0,59 | Cu, Zn, Au     | Tuff, Qzp        | ExVo   | A      |
| Levimalmen        | Grong-Stekenj. | 0            | 5,14           | 1,25 | 1,84 |        | 24,21  |      | 0,14 | Cu, Zn, Ag     | Qzp              | ExVo   | A      |
| Tjokkola          | Grong-Stekenj. | 0            | 0,17           | 0,89 | 2,2  | 0,1    | 22     |      | 0,1  | Cu, Zn, Ag     | Tuff, Qzk        | ExVo   | A      |
| Beitsetjenjunje   | Grong-Stekenj. | 0            | 0,2            | 0,85 | 1,06 | 0,19   | 13     |      | 0,16 | Cu, Zn         | Qzk              | ExVo   | A      |
| Raudvatnet        |                | 0            | 0,365          | 0,49 | 2,5  | 0,4    | 39     |      |      | Zn, Cu, Ag, Au | Fels             | VMS    | A      |
| Hamarfjell Østre  |                |              |                |      | 4,3  | 0,12   |        |      | 1,5  | Zn, Pb, Cu     | Andprf           | VMS    | A      |
| Skorovas          | Grong-Stekenj. | 5,6          | 6,9            | 1,14 | 2,71 |        |        |      |      | Cu, Zn         | Grstn, And, Fels | VMS    | MA     |
| Visletten         | Grong-Stekenj. | 0            | 0,78           | 0,92 | 3,86 | 0,5    |        |      |      | Zn, Cu         | Grstn, Fels      | VMS    | MA     |
| Gjersvik          | Grong-Stekenj. | 0,45         | 1,6            | 2,15 | 0,6  |        |        |      |      | Cu, Zn         | Grstn, And, Fels | VMS    | MA     |
| Bjørkvatnet       | Grong-Stekenj. | 0            | 0,08           | 0,85 | 0,35 | 0,13   | 3,9    |      | 0,04 | Cu, Zn         | Grsk, tuff       | ExVo   | MA     |
| Anna              | Sulitjelma     | 0,29         | 0,29           | 3,86 |      |        |        |      |      | Cu, Zn         | Amf              | VMS    | MV     |
| Nygruva           | Hardanger      | 0,006        | 0,049          | 0,7  | 3,4  | 0,8    |        |      | 0,05 | Zn, Cu, Au     | Grstn            | VMS    | MV     |
| Valaheien         | Hardanger      | 0,17         | 0,484          | 0,27 | 0,1  |        |        |      |      | Cu, Zn         | Grstn            | VMS    | MV     |
| Nedre rustgruva   | Sel            | Lite         | Liten          |      |      |        |        |      |      | Cu             | Grstn            | VMS    | MV     |
| Åsåren            | Sel            |              | 0,73           | 1,43 | 1,32 |        |        | 0,07 |      | Cu, Co, Zn     | Grstn            | VMS    | MV     |
| Grimeli           | Sunnfjord      | 0,05         | 1,5            | 2    | 1    |        |        |      |      | Cu             | Grstn            | VMS    | MV     |
| Svanøy            | Sunnfjord      | 0,039        | 0,102          | 1,75 |      |        |        |      |      | Cu, Zn         | Grstn            | VMS    | MV     |
| Gammelgruva       | Folldal-Meråk. | 1,15         | 3              | 1,9  | 1,1  |        |        |      |      | Cu, Zn         | Amf, Trd         | VMS    | MV     |
| Fredrik IV        | Folldal-Meråk. | 0,003        | 0,003          | 6    |      | 1,7    |        | 0,1  |      | Cu             | Gabbro           | ÅreCu* | MV     |



|                   |                |        |        |      |      |      |     |      |      |  |                |                 |          |    |
|-------------------|----------------|--------|--------|------|------|------|-----|------|------|--|----------------|-----------------|----------|----|
| Hersjøgruva       | Folldal-Meråk. | 0,004  | 2,99   | 1,7  | 1,4  | 0,1  | 4   |      |      |  | Cu, Zn         | Grstn           | VMS      | MV |
| RødhamMeråk.      | Folldal-Meråk. | 0      | 0,9    | 0,5  |      |      |     |      |      |  | Cu, Zn         | Dol, Amf        | VMS      | MV |
| Gressli           | Folldal-Meråk. | 0,005  | 0,085  | 0,9  | 5,5  |      |     |      |      |  | Cu, Zn         | Grstn, Dac      | VMS      | MV |
| Heimtjønnhø       | Støren-Løkken  | 0      | 1,6    | 0,01 | 0,04 |      |     |      |      |  | Cu, Zn         | Maf             | VMS      | MV |
| Tverrfjellet      | Støren-Løkken  | 15     | 19     | 1    | 1,2  | 0,08 | 10  |      | 0,2  |  | Cu, Zn         | Maf             | VMS      | MV |
| Oscar II          | Røros-Tydal    | 0,0096 | 0,0096 | 3,5  |      |      |     |      |      |  | Cu             | Maf             | VMS      | MV |
| Løkken            | Støren-Løkken  | 24     | 30     | 2,3  | 1,8  | 0,2  | 16  | 0,07 | 0,02 |  | Cu, Zn, Fe, Co | Grstn, jaspis   | VMS      | MV |
| Høydal            | Støren-Løkken  | 0,1    | 1,159  | 1,15 | 0,45 | 0,27 | 36  |      | 0,08 |  | Cu, Ag         | Grstn           | VMS      | MV |
| Åmot              | Støren-Løkken  | 0,012  | 0,012  | 3    |      |      |     |      |      |  | Cu             | Grstn           | VMS*     | MV |
| Dragset           | Støren-Løkken  | 0,065  | 0,1    | 3,5  |      |      |     |      |      |  |                | Grstn           | VMS      | MV |
| Ytterøya          | Støren-Løkken  | 0,46   | 0,46   | 1,9  | 2,4  |      |     |      | 0,3  |  | Cu, Zn         | Grstn           | VMS      | MV |
| Ulriksdal         | Støren-Løkken  | 0,0042 | 0,0042 | 0,8  | 1,5  |      |     |      |      |  | Cu, Zn         | Grstn           | VMS      | MV |
| Åkervoll          | Støren-Løkken  | 0,025  | 0,025  | 1,5  | 20   | 0,1  | 100 |      | 1,75 |  | Cu, Zn, Ag     | Grstn, Dac      | VMS      | MV |
| Malså             | Støren-Løkken  | 0,001  | 0,5    | 4,9  | 0,2  |      |     |      |      |  | Cu             | Grstn, Dac      | VMS      | MV |
| Killingdal        | Røros-Tydal    | 2,959  | 3,242  | 1,7  | 5,5  |      |     |      | 0,4  |  | Zn, Cu         | Grstn, Plava    | VMS      | MV |
| Joma              | Grong-Stekenj. | 11,453 | 18,653 | 1    | 1,66 |      |     |      |      |  | Cu, Zn         | Grstn           | VMS      | MV |
| Remdalen          | Grong-Stekenj. | 0      | 0,38   | 1,66 | 2,66 |      |     |      |      |  | Cu, Zn         | Grstn           | ExVo     | MV |
| Jakobsbakken      | Sulitjelma     | 4,47   | 4,5    | 1,55 | 2,42 |      |     |      |      |  | Cu, Zn         | Amf             | SedExhal | MV |
| Fjelds            | Sulitjelma     | 0      | 0,25   | 1,5  |      |      |     |      |      |  | Cu, Zn         | Amf             | VMS      | MV |
| Mons Petter       | Sulitjelma     | 2,5    | 2,5    | 1,75 | 0,48 |      |     |      |      |  | Cu, Zn         | Amf             | VMS      | MV |
| Rieppe            | Vaddas-Birtav. | 0      | 3      | 0,5  | 2    |      |     |      |      |  | Zn, Cu         | Grstn           | VMS      | MV |
| Øvre Nomilolgi    | Vaddas-Birtav. | 0      | 0,15   | 0,88 | 1    |      |     |      | 0,06 |  | Cu, Co, Zn     | Grstn           | VMS      | MV |
| Loftani           | Vaddas-Birtav. | 0      | 0,22   | 1,2  | 0,1  |      |     |      | 0,05 |  | Cu, Co         | Grstn           | VMS      | MV |
| Vaddas            | Vaddas-Birtav. | 0,7    | 1,415  | 1,37 | 0,01 |      |     |      | 0,05 |  | Cu, Co         | Grstn           | VMS      | MV |
| Grimsdalen        | Folldal-Meråk. | Lite   | 14,3   | 0,5  | 2,3  |      |     |      |      |  | Cu, Zn         | Fyl, Trd        | VMS      | SA |
| Nordre Geitryggen | Folldal-Meråk. | 2,5    | 2,5    | 1,3  | 3,2  | 0,2  | 31  |      | 0,2  |  | Cu, Zn         | Fyl, Prf        | VMS      | SA |
| Mannfjell         | Folldal-Meråk. | 0,1    | 0,1    | 1,8  | 5,3  | 1    |     |      |      |  | Cu, Zn, Au     | Ssk, Prf, Grstn | VMS      | SA |

|                |                |         |        |      |      |      |      |  |      |            |               |        |    |
|----------------|----------------|---------|--------|------|------|------|------|--|------|------------|---------------|--------|----|
| Heramb         | Rana-Hemnes    |         |        | 3    | 3    |      | 45   |  | 0,2  | Cu, Zn     | Glgn, Rhyd    | VMS    | SA |
| Mos gruve      | Rana-Hemnes    | 0,052   | 0,122  | 0,5  | 1,1  |      |      |  |      | Zn, Cu     | Glgn, Rhyd    | VMS    | SA |
| Sølvberget     | Rana-Hemnes    | 0,005   | 5      | 0,4  | 1,6  |      | 2,5  |  | 0,05 | Zn, Cu     | Glgn, Rhyd    | VMS    | SA |
| Mos gruve      | Rana-Hemnes    | 0,052   | 0,122  | 0,5  | 1,10 |      |      |  |      | Zn, Cu     | Glgn, Rhyd    | VMS    | SA |
| Hesjelia       | Rana-Hemnes    |         |        | 0,6  | 3,7  |      | 11   |  | 0,3  | Zn, Cu     | Glgn, Rhyd    | VMS    | SA |
| Malmberg       | Rana-Hemnes    | 0,006   | 0,5    |      | 0,35 |      |      |  |      | Zn         | Rhyl, Glsk    | VMS    | SA |
| St. Knut       | Tron           | 0,0008  | 0,0008 | 8    |      |      |      |  |      | Cu         | Grv           | ÅreCu* | SD |
| Sivilvangen    | Folldal-Meråk. | 0       | 0,4    | 0,7  | 4,3  |      |      |  |      | Cu, Zn     | Fyl, Gffyl    | VMS    | SD |
| Vinglen        | Folldal-Meråk. | 0,03    | 0,23   | 1,3  | 3,8  |      |      |  |      | Cu, Zn     | Fyl           | VMS    | SD |
| Fosgruva       | Folldal-Meråk. | 0,017   | 0,064  | 1,3  | 1,1  |      |      |  |      | Cu         | Glsk          | VMS    | SD |
| Storvollen     | Folldal-Meråk. | 0,0085  | 0,0085 | 2    |      |      |      |  |      | Cu         | Glsk          | VMS    | SD |
| Storwartz      | Røros-Tydal    | 1,62    | 1,7    | 1,8  | 12,1 | 0,33 | 25,3 |  | 0,9  | Zn, Cu     | Klkfyl        | VMS    | SD |
| Quintus        | Røros-Tydal    | 0,75    | 0,75   | 0,9  | ???  |      |      |  |      | Cu, Zn     | Klkfyl        | VMS    | SD |
| Olavsgruva     | Røros-Tydal    | 1,131   | 1,3    | 1,39 | 1,44 |      |      |  |      | Cu, Zn     | Klkfyl        | VMS    | SD |
| Nyberget       | Røros-Tydal    | 0,12    | 0,12   | 4    |      |      |      |  |      | Cu         | Klkfyl        | VMS    | SD |
| Gamle Solskinn | Røros-Tydal    | 0,09    | 0,09   | 3    |      |      |      |  |      | Cu         | Klkfyl        | VMS    | SD |
| Svenskemenna   | Røros-Tydal    | 0,0012  | 0,0012 | 1,37 | 1,8  |      |      |  |      | Cu, Zn     | Qzglsk        | VMS    | SD |
| Kjøli I        | Røros-Tydal    | 0,25    | 0,25   | 2,1  | 0,1  |      |      |  |      | Cu         | Leistein, Grv | VMS    | SD |
| Grøbskard      | Røros-Tydal    |         |        | 2,5  |      |      |      |  |      | Cu         | Qzglsk        | VMS    | SD |
| Allergot       | Røros-Tydal    |         |        | 3    | 2,4  |      |      |  |      | Cu, Zn     | Qzglsk        | VMS    | SD |
| Lillefjell     | Røros-Tydal    | 0,107   | 0,107  | 5    | 4,5  |      |      |  |      | Cu, Zn     | Grv           | VMS    | SD |
| Kviknegruvene  | Kvikne-Singsås | 0,25    | 0,25   | 2,36 | 1,81 |      | 11   |  |      | Cu, Zn     | Qzglsk        | VMS    | SD |
| Fløttum        | Kvikne-Singsås |         | 0,35   | 0,96 | 4,76 |      | 29   |  |      | Zn, Cu     | Qzt, Fyl      | VMS    | SD |
| Undal          | Kvikne-Singsås | 0,279   | 1      | 1,15 | 1,86 |      |      |  |      | Cu, Fe, Zn | Melange       | VMS    | SD |
| Jormlien       | Grong-Stekenj. | 0,00002 | 0,612  | 0,4  | 4,75 |      |      |  |      | Mn, Fe, Zn | Grv           | ExVo   | SD |
| Ankaravattnet  | Grong-Stekenj. | 0       | 0,75   | 0,45 | 5,48 | 0,2  | 17   |  | 0,37 | Zn Cu      | Grv           | ExVo   | SD |

|                      |                |       |       |      |      |      |      |      |      |                |                 |          |    |
|----------------------|----------------|-------|-------|------|------|------|------|------|------|----------------|-----------------|----------|----|
| Unna Gaisartjåkk     | Grong-Stekenj. | 0     | 1     | 0,8  | 0,5  | 0,5  | 20   |      |      | Cu, Au, Zn, Ag | Grv             | ExVo     | SD |
| Daningen             | Grong-Stekenj. | 0     | 0,05  | 9,85 | 0,6  | 0,6  | 12   |      | 0    | Cu             | Grv             | ExVo     | SD |
| Abelvattnet          | Grong-Stekenj. | 0     | 0,069 | 0,9  | 0,07 |      |      |      |      | Cu             | Grv             | ExVo     | SD |
| Storäcksdalen Västra | Grong-Stekenj. | 0     | 0,015 | 1,2  | 6,3  | 0,5  | 49   |      | 2,4  | Zn, Cu, Pb, Ag | Fyl, Srsk       | ExVo     | SD |
| Rikarsbäcken         | Grong-Stekenj. | 0     | 0,15  | 0,8  | 4,3  | 0,2  | 43   |      | 1,1  | Zn, Cu, Ag, Pb | Fyl, Srsk       | ExVo     | SD |
| Tjåter               | Grong-Stekenj. | 0     | 0,15  | 1    | 4,8  | 0,5  | 49   |      | 1,9  | Zn, Cu, Pb, Ag | Srsk, Svsk      | ExVo     | SD |
| Bleikvassli          | Rana-Hemnes    | 5,84  | 8,84  | 0,15 | 4    |      | 25   |      | 2    | Zn, Pb         | Grtglsk         | VMS      | SD |
| Gräskevardo          | Rana-Hemnes    | 0     | 0,1   | 0,35 | 3,49 |      | 34   |      | 1,23 | Zn, Pb, Cu, Ag | Glsk            | ExVo     | SD |
| Hellerfjellet        | Rana-Hemnes    |       |       | 0,5  | 10   |      | 110  |      | 3    | Zn, Pb, Ag     | Gfglsk          | VMS      | SD |
| Båsmo                | Rana-Hemnes    | 1,85  | 1,85  | 0,13 | 0,14 |      |      |      |      | Cu, Zn         | Grtklsk         | SedExhal | SD |
| Ingeborgvatn         | Sulitjelma     | 0     | 0,5   | 1,5  | 1    |      | 15   |      |      | Cu, Zn         | Klsed           | VMS      | SD |
| Ny-Sulitjelma        | Sulitjelma     | 2,59  | 2,59  | 1,99 | 0,55 | 0,3  |      | 0,01 |      | Cu             | Glsk            | VMS      | SD |
| Hankabakken          | Sulitjelma     | 1,99  | 2,49  | 1,4  | 0,4  |      |      |      |      | Cu, Zn         | Glsk            | VMS      | SD |
| Bursi                | Sulitjelma     | 1,83  | 1,845 | 1,5  | 0,31 |      |      |      |      | Cu             | Glsk            | VMS      | SD |
| Sabetok              | Vaddas-Birtav. | 0,014 | 0,35  | 1,2  |      |      |      |      |      | Cu             | Grv             | VMS      | SD |
| Moskodal             | Vaddas-Birtav. | 0,04  | 0,225 | 2,67 |      |      |      |      |      | Cu, Zn         | Grv             | VMS      | SD |
| Litlabø              | Hardanger      | 9     | 9     |      | 0,28 |      |      |      |      | Zn, S          | Fyl, Grstn      | VMS      | SD |
| Christianus Sextus   | Røros-Tydal    | 0,25  | 0,25  | 2,38 | 7,36 | 0,14 | 14,4 |      | 0,44 | Zn, Cu         | Grv, tuff       | VMS      | SV |
| Lergruvbakken        | Røros-Tydal    | 0,45  | 0,97  | 1    | 9,4  |      | 20   |      | 0,4  | Zn, Cu         | Grv, tuff       | VMS      | SV |
| Kongens Gruve        | Røros-Tydal    | 1,5   | 3     | 2,2  | 6,9  | 0,17 | 31,3 |      | 0,5  | Zn, Cu         | Grv, tuff       | VMS      | SV |
| Fjellsjø             | Røros-Tydal    |       | 1,75  |      |      |      |      |      |      | Zn, Cu         | Grv, tuff       | VMS      | SV |
| Kvernenglia          | Røros-Tydal    |       | 0,142 | 0,3  | 1,98 |      |      |      |      | Zn, Cu         | Grv, tuff       | VMS      | SV |
| Muggruva             | Røros-Tydal    | 0,65  | 0,65  | 2    | 0,3  | 0,34 | 12,7 |      |      | Cu             | Grv, tuff       | VMS      | SV |
| Skrattåsen           |                | 0,005 | 0,085 | 1    | 7    |      | 70   |      | 2    | Zn, Cu, Pb, Ag | Tuff, Glsk      | VMS      | SV |
| Godejord             | Grong-Stekenj. | 0     | 0,25  | 0,6  | 4,2  | 0,4  | 15   |      | 0,2  | Zn, Cu         | Tuff, Kalk, Kst | VMS      | SV |
| Skiftesmyr           | Grong-Stekenj. | 0     | 4,07  | 1    | 1,5  | 0,1  | 2,5  |      |      | Cu, Zn         | Tuff, Kst       | VMS      | SV |
| Finnbu               | Grong-Stekenj. | 0     | 0,25  | 0,3  | 3    |      |      |      |      | Zn, Cu         | Tuff, Kst       | VMS      | SV |

|                     |                |               |               |             |             |             |              |             |             |            |                |          |    |
|---------------------|----------------|---------------|---------------|-------------|-------------|-------------|--------------|-------------|-------------|------------|----------------|----------|----|
| Mofjellet           | Rana-Hemnes    | 4,35          | 5,35          | 0,31        | 3,61        | 0,3         | 10           |             | 0,71        | Zn, Cu     | Grv, Vlk       | SedExhal | SV |
| Rødalen             | Kvikne-Singsås | 0,04          | 0,04          | 1,13        | 0,2         | 0,3         |              |             |             | Cu         | Qzt, Amf, Glsk | VMS      | MS |
| Røstvangen          | Kvikne-Singsås | 0,388         | 0,488         | 3,09        | 0,73        | 0,28        | 12           | 0,05        |             | Cu, Co     | Msst, Amf      | VMS      | MS |
| Børsjøhø            | Kvikne-Singsås | 0,0008        | 2,0008        | 1,21        | 0,92        |             |              |             |             | Cu, Zn     | Msd, Amf       | VMS      | MS |
| Småvatnan           | Rana-Hemnes    |               |               | 0,6         | 10          |             | 140          |             | 1,9         | Zn, Pb, Ag | Glgn, Amf      | VMS      | MS |
| Gudrun              | Sulitjelma     | 0,71          | 0,71          | 1,49        | 0,55        |             |              |             |             | Cu, Zn     | Amf, Glsk      | VMS      | MS |
| Giken               | Sulitjelma     | 5,8           | 10,5          | 2,25        | 0,7         |             |              |             |             | Cu, Zn     | Glsk, Amf      | VMS      | MS |
| Charlotte           | Sulitjelma     | 3             | 3,1           | 2           | 0,58        | 0,24        |              | 0,02        |             | Cu, Co, Zn | Glsk, Amf      | VMS      | MS |
| Furuhaugen          | Sulitjelma     | 0,37          | 0,52          | 1,65        |             |             |              |             |             | Cu, Zn     | Amf, Glsk      | VMS      | MS |
| Rupsi               | Sulitjelma     | 0             | 4,2           | 1,1         |             |             |              |             |             | Cu, Zn     | Msst, Amf      | VMS      | MS |
| Bjørkåsen           | Troms Fe       | 6             | 6             | 0,45        | 1           |             |              |             |             | Cu, Zn     | Grtglsk, Amf   | VMS      | MS |
| Moskogaissa         | Vaddas-Birtav. | 0,065         | 0,065         | 4,5         |             |             |              |             |             | Cu         | Grstn, Grv     | VMS      | MS |
| Birtav. avarre      | Vaddas-Birtav. | 0,2           | 0,2           | 4,4         |             |             |              |             |             |            | Glsk, Grstn    | VMS      | MS |
| Vigsnes             | Karmøy         | 1,44          | 1,44          | 1,66        | 1,4         |             |              |             |             | Cu, Zn     | Fyl, Grstn     | VMS      | MS |
| Rødkleiv            | Karmøy         | 2,64          | 2,64          | 0,78        | 1,17        |             |              |             |             | Cu, Zn     | Fyl, Grstn     | VMS      | MS |
| <b>Sum</b>          |                | <b>135,82</b> | <b>233,94</b> |             |             |             |              |             |             |            |                |          |    |
| <b>Restmalm</b>     |                | <b>98,12</b>  |               |             |             |             |              |             |             |            |                |          |    |
| <b>Gjennomsnitt</b> |                | <b>1,306</b>  | <b>2,146</b>  | <b>1,67</b> | <b>2,74</b> | <b>0,35</b> | <b>31,32</b> | <b>0,05</b> | <b>0,74</b> |            |                |          |    |
| <b>STDV</b>         |                | <b>3,31</b>   | <b>4,38</b>   | <b>1,49</b> | <b>3,05</b> | <b>0,31</b> | <b>29,56</b> | <b>0,03</b> | <b>0,81</b> |            |                |          |    |
| <b>Antall, n</b>    |                | <b>104</b>    | <b>109</b>    | <b>112</b>  | <b>95</b>   | <b>35</b>   | <b>40</b>    | <b>9</b>    | <b>35</b>   |            |                |          |    |

Informasjon og data er tatt fra «Fennoscandian Ore Deposit Database (FOOD)», Fennoscandian Mineral Deposits (gtk.fi) .

\*Forekomst representert kun ved stockwerk/stringer-sonen

Klassifikasjonen i «Type» er tatt fra databaasen: VMS – Volcanic Massive Sulfide, SedExhal – Sedimentary Exhalative, ExVo – Volcanic Exhalative, ÅreCu – Årekopper

Sortering i «Gruppe» er gjort i henhold til beskrivelsene av vertsbjergart (se forklaring av forkortelser i Tabell 8.3)

**Tab. 7.2 Kaledonske sulfidmalmforekomster gruppert som i Tabell 7.1. Gjennomsnittstall pr gruppe**

| Gruppe            | Produsert Mt | Opprinnelig Mt | Cu%  | Zn%  | Au ppm | Ag ppm | Co%  | Pb%  |
|-------------------|--------------|----------------|------|------|--------|--------|------|------|
| Gjennomsnitt alle | 1,29         | 2,15           | 1,68 | 2,77 | 0,35   | 31,32  | 0,05 | 0,74 |

|                 |      |      |      |      |      |       |      |      |
|-----------------|------|------|------|------|------|-------|------|------|
| Antall, n       | 104  | 109  | 112  | 95   | 35   | 40    | 9    | 35   |
| Gjennomsnitt MV | 2,05 | 3,04 | 1,80 | 2,39 | 0,46 | 33,20 | 0,07 | 0,40 |
| Antall, n       | 31   | 32   | 32   | 24   | 7    | 5     | 6    | 7    |
| Gjennomsnitt SD | 0,84 | 1,09 | 1,93 | 3,00 | 0,39 | 33,79 | 0,01 | 1,43 |
| Antall, n       | 33   | 34   | 36   | 29   | 8    | 13    | 1    | 9    |
| Gjennomsnitt MS | 1,59 | 2,45 | 1,88 | 1,73 | 0,27 | 76,00 | 0,04 | 1,90 |
| Antall, n       | 13   | 13   | 14   | 10   | 3    | 2     | 2    | 1    |
| Gjennomsnitt MA | 1,51 | 2,34 | 1,27 | 1,88 | 0,32 | 3,90  |      | 0,04 |
| Antall, n       | 4    | 4    | 4    | 4    | 2    | 1     | 0    | 1    |
| Gjennomsnitt A  | 0,99 | 2,34 | 1,10 | 2,68 | 0,27 | 32,33 |      | 0,44 |
| Antall, n       | 8    | 8    | 8    | 9    | 7    | 7     | 0    | 7    |
| Gjennomsnitt SA | 0,45 | 3,23 | 1,08 | 2,41 | 0,60 | 22,38 |      | 0,19 |
| Antall, n       | 6    | 7    | 8    | 9    | 2    | 4     | 0    | 4    |
| Gjennomsnitt SV | 0,80 | 1,52 | 1,11 | 4,53 | 0,24 | 21,99 |      | 0,71 |
| Antall, n       | 9    | 11   | 10   | 10   | 6    | 8     | 0    | 6    |

Sortering i «Gruppe» er gjort i henhold til beskrivelsene av vertsbergart (se forklaring av forkortelser i Tabell 8.3)

#### Forkortelser brukt i Tabell 7.1 og Tabell 7.2

| Forkortelse | Bergart                        | Gruppe | Vertsbergart-assosiasjoner                     |
|-------------|--------------------------------|--------|--|
| Grstn       | Grønnstein                     | A      | Sure vulkanitter og intrusjoner                |
| And         | Andesitt                       | MA     | Mafiske og sure vulkanitter og intrusjoner     |
| Rhyd        | Rhyodacitt                     | MV     | Mafiske vulkanitter og intrusjoner             |
| Dac         | Dacitt                         | MS     | Mafiske vulkanitter og sedimenter              |
| Qzk         | Kvartskeratofyr                | SA     | Sedimenter, og sure vulkanitter og intrusjoner |
| Qzp         | Kvartsporfy                    | SD     | Metasedimenter                                 |
| Fels        | Felsisk vulkanitt              | SV     | Metasedimenter og vulkanitter                  |
| Grsk        | Grønnskifer                    |        |  |
| Dol         | Doleritt                       |        |  |
| Amf         | Amibolitt                      |        |  |
| Maf         | Mafiske vulkanitter/intrusiver |        |  |
| Fyl         | Fyllitt                        |        |  |
| Glg         | Glimmergneis                   |        |  |
| Rhyl        | Rhyolitt                       |        |  |
| Glsk        | Glimmerskifer                  |        |  |
| Klkfyl      | Kalkholdig fyllitt             |        |  |
| Trd         | Trondjemitt                    |        |  |
| Qzglsk      | Kvartsglimmerskifer            |        |  |
| Svsk        | Svartskifer                    |        |  |
| Sersk       | Serisittskifer                 |        |  |
| Grtglsk     | Granat-glimmerskifer           |        |  |
| Gfglsk      | Grafitt-glimmerskifer          |        |  |
| Gf          | Grafitt                        |        |  |
| Msst        | Metasandstein                  |        |  |

|         |                      |  |  |
|---------|----------------------|--|--|
| Prf     | Porfyr               |  |  |
| Gffyl   | Grafitt-fyllitt      |  |  |
| Andprf  | Andesittporfyr       |  |  |
| Grv     | Gråvakke             |  |  |
| Qzt     | Kvartsitt            |  |  |
| Grtklsk | Granat-klorittskifer |  |  |
| Klsed   | Klorittisk sediment  |  |  |
| Vlk     | Vulkanitter          |  |  |
| Msd     | Metasediment         |  |  |
| Kst     | Kiselstein           |  |  |
| Plava   | Putelava             |  |  |

**Tab. 7.3 Tall fra Tabell 1 i Hannington et al. (2010). Kun tall fra midt-oseanrygger er tatt med**

| Spredningsrygg, Forekomst | Areal m <sup>2</sup> | Antall, n | Cu % | Zn % | Au ppm | Ag ppm |
|---------------------------|----------------------|-----------|------|------|--------|--------|
| Juan de Fuca, Explorer    |                      |           |      |      |        |        |
| S. Explorer               | 5000                 | 51        | 3,2  | 5,4  | 0,72   | 125    |
| Endeavour, High           | 3000                 | 49        | 1,9  | 9,6  | 0,28   | 63     |
| Endeavour, Main field     | 5000                 | 97        | 2,6  | 6,7  | 0,14   | 260    |
| Endeavour, Clam bed       |                      | 5         | 0,3  | 2,8  | 0,12   | 145    |
| Endeavour, Mothra         | 5000                 | 20        | 3,3  | 14,9 | 0,05   | 105    |
| Co-axial                  |                      | 6         |      | 23,2 | 0,98   | 59     |
| Northern cleft            |                      | 26        | 1,7  | 26,6 | 0,25   | 225    |
| Southern cleft            |                      | 16        | 1,1  | 30,9 | 0,11   | 230    |
| East Pacific Rise         |                      |           |      |      |        |        |
| 21°N EPR                  |                      | 46        | 5,4  | 12,2 | 0,12   | 83     |
| 21°N Green Seamount       |                      | 6         | 2,6  | 0,2  | 0,16   | 1      |
| 14°N EPR                  |                      | 5         | 2,8  | 4,7  | 0,51   | 48     |
| 13°N EPR                  | 5000                 | 71        | 6,4  | 11,1 | 0,45   | 61     |
| 13°N Seamount             | 30000                | 13        | 2,4  | 4,3  | 0,8    | 32     |
| 11°30'N EPR               |                      | 23        | 3,2  | 1,8  | 0,25   | 23     |
| 11°32'N EPR               |                      | 32        | 3,4  | 0,1  | 0,13   | 4      |
| 11°N EPR                  |                      | 18        | 1,6  | 26,6 | 0,15   | 37     |
| 09°50'N EPR               |                      | 29        | 7,9  | 6,3  | -      |        |
| 07°24'S EPR               |                      | 14        | 11,1 | 2,1  | 0,05   | 23     |
| 16°43'S EPR               |                      | 19        | 10,2 | 8,5  | 0,32   | 55     |
| 17°26'S EPR               |                      | -         | 1,3  | 5,6  | 0,1    | 31     |
| 18°25'S EPR               |                      | 35        | 4,7  | 18,6 | 0,58   | 170    |
| 21°30'S EPR               |                      | 28        | 9,8  | 4,3  | 0,41   | 62     |
| 21°50'S EPR               |                      | -         | 2,4  | 21,7 | 0,36   | 120    |
| 37°40'S ERPR              |                      | 24        | 3,8  | 3,1  | 0,82   | 40     |
| Galapagos rift 86°W       | 30000                | 128       | 4,5  | 3,5  | 0,29   | 35     |
| Indian Ocean              |                      |           |      |      |        |        |
| Sonne field, CIR          | 50000                | 35        | 13,1 | 3    | 1,02   | 46     |
| Kairei field, CIR         | 3000                 | 8         | 20,4 | 10,3 | 7,99   | 101    |

|                      |        |      |       |       |       |        |
|----------------------|--------|------|-------|-------|-------|--------|
| Edmond field, CIR    | 3000   | 17   | 6,5   | 10,7  | 4,01  | 188    |
| Mt. Jourdanne, SWIR  |        | 9    | 1,9   | 16,7  | 4,29  | 630    |
| Mid-Atlantic Ridge   |        |      |       |       |       |        |
| Broken spur          | 5000   | 76   | 4,9   | 3,7   | 1,64  | 30     |
| 24°30'N, MAR         | -      | 16,2 | 4,1   | 5,3   |       |        |
| TAG, surface & core  | 30000  | 310  | 4,9   | 6,5   | 1,80  | 92     |
| Mir                  | 50000  | 137  | 5     | 8,7   | 4,2   | 115    |
| Alvin                | 100000 | 7    | 2     | 0,3   | 0,85  | 17     |
| Snakepit             | 15000  | 93   | 6,5   | 4,6   | 0,1   | 70     |
| Krasnov              | 150000 | 144  | 1,74  | 0,69  | 0,76  | 26     |
| Semyenov             | 300000 | 21   | 2,48  | 2,39  | 3,60  | 53     |
| Turtle pits, 5°S     | 5000   | 43   | 7     | 2,3   | 0,26  | 17     |
| Nibelungen, 8°S      |        | 9    | 17,3  | 16,2  | 8,95  | 37     |
| Lucky                | 3000   | 36   | 4,5   | 2     | 0,08  | 35     |
| Axial volcano, CASM  |        | 31   | 0,3   | 16,3  | 4,12  | 250    |
| Axial volcano, ASHES |        | 90   | 2,3   | 17,3  | 1,56  | 295    |
| Rainbow              | 30000  | 62   | 11    | 18    | 2,53  | 189    |
| Ashadze-1            | 50000  | 104  | 10,5  | 17,64 | 3,5   | 88     |
| Ashadze-2            | 50000  | 23   | 17,7  | 0,83  | 11,1  | 8      |
| Logatchev-1          | 5000   | 78   | 33,19 | 4,3   | 14    | 56     |
| Logatchev-2          | 1000   | 5    | 15,93 | 28,06 | 21,5  | 79     |
| Middle Valley        | 50000  | 100  | 1,1   | 2,8   | 0,16  | 7      |
| Escanaba trough      | 1000   | 51   | 1,8   | 5,6   | 1,29  | 163    |
| Guaymas basin        | 15000  | 22   | 0,4   | 2,2   | 0,15  | 82     |
| Gjennomsnitt         | 37000  | 48   | 6,00  | 9,22  | 2,24  | 98,14  |
| STDAV                | 62727  | 54   | 6,28  | 8,32  | 4,13  | 108,05 |
| Høyeste verdi        | 300000 | 310  | 33,19 | 30,90 | 21,50 | 630,00 |
| Laveste verdi        | 1000   | 5,00 | 0,30  | 0,10  | 0,05  | 1,00   |

### 7.3 Tabeller for gehalter i manganskorper

Tabellene her oppsummerer målte verdier for metallinnhold i skorper fra seks områder.

Verdiene fra tabell [Tab. 7.4](#) er brukt som basis for ressursberegningen for Jan Mayen-ryggen.

**Tab. 7.4** Gehalter for Jan Mayen-ryggen

| Metall | Enhet | Antall | Gjennomsnitt | Standardavvik | Høyeste verdi | Laveste verdi |
|--------|-------|--------|--------------|---------------|---------------|---------------|
| Mn     | % wgt | 11     | 12,55        | 5,27          | 20,00         | 4,67          |
| Ti     | % wgt | 11     | 1,27         | 0,27          | 1,60          | 0,80          |
| Mg     | % wgt | 11     | 2,40         | 0,43          | 3,21          | 1,86          |
| Li     | ppm   | 11     | 131,82       | 50,76         | 212,57        | 54,65         |
| Sc     | ppm   | 11     | 36,77        | 7,33          | 51,39         | 27,44         |
| V      | ppm   | 11     | 1149,58      | 256,72        | 1651,04       | 839,24        |
| Co     | ppm   | 11     | 1155,72      | 580,79        | 2390,36       | 551,10        |
| Nb     | ppm   | 11     | 88,86        | 46,37         | 160,23        | 47,27         |



|    |     |    |        |        |         |        |
|----|-----|----|--------|--------|---------|--------|
| Hf | ppm | 11 | 9,62   | 3,00   | 14,68   | 5,32   |
| W  | ppm | 11 | 35,00  | 13,35  | 61,62   | 16,05  |
| Ga | ppm | 11 | 15,88  | 3,59   | 21,22   | 7,97   |
| Y  | ppm | 11 | 153,51 | 71,42  | 332,20  | 88,76  |
| La | ppm | 11 | 174,49 | 101,27 | 421,24  | 93,38  |
| Ce | ppm | 11 | 574,25 | 423,15 | 1494,64 | 192,64 |
| Pr | ppm | 11 | 44,77  | 24,37  | 102,62  | 22,71  |
| Nd | ppm | 11 | 186,34 | 99,10  | 426,57  | 103,70 |
| Eu | ppm | 11 | 10,46  | 5,27   | 22,77   | 5,93   |
| Gd | ppm | 11 | 44,04  | 22,78  | 99,73   | 24,92  |
| Tb | ppm | 11 | 6,79   | 3,45   | 15,08   | 3,89   |
| Dy | ppm | 11 | 40,53  | 20,13  | 88,09   | 21,77  |

Verdiene fra tabell Tab. 7.5 er brukt som basis for ressursberegningen i den vestlige delen av Vøringutstikkeren.

**Tab. 7.5 Gehalter for Ægirbassenget og Jan Mayen-trauet**

| Metall | Enhet | Antall | Gjennomsnitt | Standardavvik | Høyeste verdi | Laveste verdi |
|--------|-------|--------|--------------|---------------|---------------|---------------|
| Mn     | % wgt | 39     | 19,49        | 6,70          | 30,26         | 1,96          |
| Ti     | % wgt | 39     | 1,33         | 0,50          | 2,80          | 0,54          |
| Mg     | % wgt | 39     | 2,29         | 0,46          | 3,41          | 1,70          |
| Li     | ppm   | 39     | 121,96       | 98,98         | 328,60        | 27,64         |
| Sc     | ppm   | 38     | 46,19        | 9,75          | 73,79         | 25,49         |
| V      | ppm   | 39     | 1569,20      | 386,73        | 2083,19       | 602,58        |
| Co     | ppm   | 39     | 2407,30      | 1306,51       | 6073,00       | 465,40        |
| Nb     | ppm   | 39     | 76,98        | 34,56         | 175,70        | 27,16         |
| Hf     | ppm   | 39     | 12,34        | 3,01          | 17,09         | 5,35          |
| W      | ppm   | 38     | 97,62        | 60,82         | 195,04        | 11,03         |
| Ga     | ppm   | 38     | 9,88         | 6,13          | 28,06         | 3,40          |
| Y      | ppm   | 39     | 270,75       | 93,53         | 398,97        | 82,53         |
| La     | ppm   | 39     | 371,85       | 173,78        | 612,14        | 76,39         |
| Ce     | ppm   | 39     | 1268,51      | 621,18        | 2129,29       | 122,01        |
| Pr     | ppm   | 39     | 97,86        | 45,92         | 161,04        | 20,65         |
| Nd     | ppm   | 39     | 404,59       | 187,02        | 660,48        | 87,01         |
| Eu     | ppm   | 39     | 21,92        | 9,68          | 35,61         | 5,38          |
| Gd     | ppm   | 39     | 90,37        | 38,70         | 141,25        | 23,02         |
| Tb     | ppm   | 39     | 13,77        | 5,78          | 21,74         | 3,58          |
| Dy     | ppm   | 39     | 79,00        | 31,24         | 122,46        | 23,07         |

Verdiene fra tabell Tab. 7.6 er brukt som basis for ressursberegningen i den østlige delen av Vøringutstikkeren.

**Tab. 7.6 Gehalter for Vøringutstikkeren**

| Metall | Enhet | Antall | Gjennomsnitt | Standardavvik | Høyeste verdi | Laveste verdi |
|--------|-------|--------|--------------|---------------|---------------|---------------|
| Mn     | % wgt | 10     | 15,18        | 8,68          | 28,45         | 1,22          |
| Ti     | % wgt | 10     | 1,39         | 0,65          | 2,34          | 0,53          |

|    |       |    |         |         |         |        |
|----|-------|----|---------|---------|---------|--------|
| Mg | % wgt | 10 | 2,06    | 0,70    | 3,55    | 0,84   |
| Li | ppm   | 10 | 308,51  | 275,07  | 918,52  | 48,22  |
| Sc | ppm   | 10 | 36,36   | 12,97   | 60,07   | 13,29  |
| V  | ppm   | 10 | 937,04  | 518,71  | 1825,95 | 243,70 |
| Co | ppm   | 10 | 1782,35 | 1399,58 | 4221,52 | 184,30 |
| Nb | ppm   | 10 | 62,47   | 27,14   | 109,27  | 32,10  |
| Hf | ppm   | 10 | 10,53   | 4,21    | 17,59   | 4,04   |
| W  | ppm   | 10 | 49,15   | 34,17   | 92,74   | 2,72   |
| Ga | ppm   | 10 | 14,18   | 6,06    | 23,50   | 6,91   |
| Y  | ppm   | 10 | 180,33  | 111,67  | 352,27  | 37,49  |
| La | ppm   | 10 | 193,05  | 124,24  | 402,66  | 46,70  |
| Ce | ppm   | 10 | 870,45  | 609,26  | 1753,25 | 134,20 |
| Pr | ppm   | 10 | 51,50   | 32,62   | 106,01  | 12,44  |
| Nd | ppm   | 10 | 214,01  | 133,57  | 439,57  | 52,07  |
| Eu | ppm   | 10 | 12,63   | 7,80    | 25,03   | 2,50   |
| Gd | ppm   | 10 | 54,58   | 33,97   | 107,78  | 10,67  |
| Tb | ppm   | 10 | 8,68    | 5,43    | 17,06   | 1,66   |
| Dy | ppm   | 10 | 51,88   | 32,41   | 98,91   | 9,38   |

Verdier fra Tab. 7.7 er brukt som basis for ressursberegningen for den østlige delen av Mohnsryggen og den østlige delen av Knipovitsryggen.

**Tab. 7.7** Gehalter for Lofoten Basin Seamount

| Metall | Enhet | Antall | Gjennomsnitt | Standardavvik | Høyeste verdi | Laveste verdi |
|--------|-------|--------|--------------|---------------|---------------|---------------|
| Mn     | % wgt | 20     | 13,61        | 4,27          | 20,20         | 1,60          |
| Ti     | % wgt | 20     | 0,52         | 0,26          | 1,06          | 0,19          |
| Mg     | % wgt | 20     | 1,70         | 0,37          | 2,49          | 1,30          |
| Li     | ppm   | 20     | 151,73       | 115,49        | 491,70        | 32,21         |
| Sc     | ppm   | 20     | 25,42        | 6,30          | 37,63         | 17,91         |
| V      | ppm   | 20     | 1063,97      | 354,33        | 1638,79       | 662,07        |
| Co     | ppm   | 20     | 1150,79      | 756,83        | 2457,00       | 362,00        |
| Nb     | ppm   | 20     | 29,88        | 16,73         | 62,25         | 9,96          |
| Hf     | ppm   | 20     | 6,73         | 3,25          | 13,87         | 2,59          |
| W      | ppm   |        |              |               |               |               |
| Ga     | ppm   |        |              |               |               |               |
| Y      | ppm   | 20     | 141,88       | 72,00         | 259,86        | 60,25         |
| La     | ppm   | 20     | 187,87       | 133,43        | 419,30        | 71,53         |
| Ce     | ppm   | 20     | 714,28       | 559,80        | 1949,00       | 184,10        |
| Pr     | ppm   | 20     | 52,96        | 37,14         | 118,10        | 19,89         |
| Nd     | ppm   | 20     | 219,89       | 152,80        | 489,50        | 83,26         |
| Eu     | ppm   | 20     | 11,76        | 7,74          | 25,28         | 4,46          |
| Gd     | ppm   | 20     | 48,72        | 31,39         | 103,20        | 18,38         |
| Tb     | ppm   | 20     | 7,50         | 4,71          | 15,46         | 2,78          |
| Dy     | ppm   | 20     | 41,54        | 25,32         | 83,82         | 15,74         |

Verdier fra Tab. 7.8 er brukt som basis for ressursberegningen for den indre, vestlige delen av Mohnsryggen.

**Tab. 7.8 Gehalter for Greenland Basin Seamount/Greenland Sea East**

| Metall | Enhet | Antall | Gjennomsnitt | Standardavvik | Høyeste verdi | Laveste verdi |
|--------|-------|--------|--------------|---------------|---------------|---------------|
| Mn     | % wgt | 42     | 11,70        | 3,71          | 17,65         | 0,05          |
| Ti     | % wgt | 42     | 0,54         | 0,17          | 1,00          | 0,28          |
| Mg     | % wgt | 41     | 1,59         | 0,22          | 2,18          | 1,28          |
| Li     | ppm   | 25     | 109,83       | 66,26         | 292,30        | 38,39         |
| Sc     | ppm   | 42     | 35,44        | 7,03          | 55,57         | 16,83         |
| V      | ppm   | 42     | 1306,64      | 257,77        | 1674,00       | 186,24        |
| Co     | ppm   | 42     | 2323,75      | 1008,41       | 4047,00       | 16,12         |
| Nb     | ppm   | 42     | 48,41        | 20,23         | 107,90        | 12,95         |
| Hf     | ppm   | 42     | 10,06        | 2,05          | 14,24         | 3,07          |
| W      | ppm   |        |              |               |               |               |
| Ga     | ppm   |        |              |               |               |               |
| Y      | ppm   | 42     | 217,18       | 55,86         | 316,10        | 24,73         |
| La     | ppm   | 42     | 304,80       | 95,86         | 473,20        | 35,19         |
| Ce     | ppm   | 42     | 1292,40      | 410,75        | 2041,00       | 74,30         |
| Pr     | ppm   | 42     | 83,38        | 25,77         | 134,90        | 9,07          |
| Nd     | ppm   | 42     | 342,75       | 103,81        | 537,20        | 35,52         |
| Eu     | ppm   | 42     | 18,44        | 5,25          | 27,61         | 1,60          |
| Gd     | ppm   | 42     | 78,07        | 21,79         | 109,90        | 5,97          |
| Tb     | ppm   | 42     | 11,96        | 3,20          | 16,44         | 0,90          |
| Dy     | ppm   | 42     | 65,90        | 17,48         | 89,57         | 4,91          |

Verdier fra Tab. 7.9 er brukt som basis for ressursberegningen for den ytre, vestlige delen av Mohnsryggen og den vestlige delen av Knipovitsryggen.

**Tab. 7.9 Gehalter for Greenland Sea West**

| Metall | Enhet | ANTALL | Average | STDV   | Høyeste verdi | Laveste verdi |
|--------|-------|--------|---------|--------|---------------|---------------|
| Mn     | % wgt | 15     | 12,11   | 3,49   | 18,07         | 7,29          |
| Ti     | % wgt | 15     | 0,47    | 0,12   | 0,67          | 0,30          |
| Mg     | % wgt | 15     | 1,45    | 0,25   | 2,04          | 1,15          |
| Li     | ppm   |        |         |        |               |               |
| Sc     | ppm   | 15     | 41,79   | 10,79  | 72,58         | 32,85         |
| V      | ppm   | 15     | 1395,33 | 242,62 | 1974,00       | 989,00        |
| Co     | ppm   | 15     | 2323,83 | 777,37 | 3635,00       | 810,40        |
| Nb     | ppm   | 15     | 51,60   | 13,60  | 88,59         | 32,52         |
| Hf     | ppm   | 15     | 10,84   | 2,57   | 19,31         | 8,63          |
| W      | ppm   |        |         |        |               |               |
| Ga     | ppm   |        |         |        |               |               |
| Y      | ppm   | 14     | 219,53  | 30,22  | 252,90        | 167,60        |
| La     | ppm   | 15     | 256,63  | 60,64  | 354,60        | 149,50        |
| Ce     | ppm   | 15     | 1265,36 | 229,09 | 1774,00       | 951,10        |
| Pr     | ppm   | 15     | 72,05   | 15,65  | 96,64         | 44,83         |

|    |     |    |        |       |        |        |
|----|-----|----|--------|-------|--------|--------|
| Nd | ppm | 15 | 294,26 | 61,65 | 395,60 | 192,10 |
| Eu | ppm | 15 | 16,37  | 2,88  | 21,11  | 12,14  |
| Gd | ppm | 15 | 71,81  | 12,02 | 92,82  | 54,97  |
| Tb | ppm | 15 | 10,88  | 1,70  | 13,96  | 8,44   |
| Dy | ppm | 15 | 62,15  | 8,96  | 78,02  | 48,44  |

## 7.4 Ressurstabeller for letemodeller og delområder

### Sulfider

Tab. 7.10 Metallmengder i flankemodellen

| Metall         | P95    | Forventning | P05    |
|----------------|--------|-------------|--------|
| Cu (mill tonn) | 21,9   | 31,4        | 40,7   |
| Zn (mill tonn) | 17,8   | 25,5        | 32,9   |
| Co (mill tonn) | 0,6    | 1,0         | 1,3    |
| Ag (tonn)      | 43 760 | 63 230      | 82 540 |
| Au (tonn)      | 1 240  | 1 780       | 2 300  |

Tab. 7.11 Metallmengder i aksialmodellen

| Metall         | P95   | Forventning | P05   |
|----------------|-------|-------------|-------|
| Cu (mill tonn) | 1,9   | 2,9         | 3,9   |
| Zn (mill tonn) | 2,4   | 3,6         | 4,9   |
| Co (mill tonn) | 0,0   | 0,0         | 0,0   |
| Ag (tonn)      | 3 490 | 5 260       | 7 190 |
| Au (tonn)      | 87    | 134         | 185   |

Tab. 7.12 Metallmengder i gruntnvansmodellen

| Metall         | P95    | Forventning | P05    |
|----------------|--------|-------------|--------|
| Cu (mill tonn) | 2,6    | 3,9         | 5,2    |
| Zn (mill tonn) | 10,8   | 15,9        | 21,2   |
| Co (mill tonn) | 0,0    | 0,0         | 0,0    |
| Ag (tonn)      | 11 360 | 16 720      | 22 320 |
| Au (tonn)      | 275    | 402         | 535    |

### Manganskorper

Tab. 7.13 Skorperressurser på Mohnsryggen

| Metall              | P95       | Forventning | P05       |
|---------------------|-----------|-------------|-----------|
| Mn (millioner tonn) | 75,9      | 125,3       | 184,1     |
| Ti (millioner tonn) | 3,0       | 5,0         | 7,4       |
| Mg (millioner tonn) | 9,4       | 15,4        | 22,6      |
| Li (tonn)           | 79 000    | 156 700     | 274 900   |
| Sc (tonn)           | 23 200    | 39 700      | 59 700    |
| V (tonn)            | 812 800   | 1 374 500   | 2 052 200 |
| Co (tonn)           | 1 291 300 | 2 242 400   | 3 383 700 |
| Nb (tonn)           | 28 700    | 49 700      | 74 600    |

|           |         |           |           |
|-----------|---------|-----------|-----------|
| Hf (tonn) | 6 100   | 10 500    | 15 700    |
| W (tonn)  | 24 600  | 53 000    | 97 400    |
| Ga (tonn) | 7 800   | 13 700    | 21 000    |
| Y (tonn)  | 125 700 | 215 500   | 321 400   |
| La (tonn) | 155 400 | 264 100   | 394 200   |
| Ce (tonn) | 718 400 | 1 236 500 | 1 854 700 |
| Pr (tonn) | 43 400  | 73 800    | 110 400   |
| Nd (tonn) | 178 000 | 302 100   | 449 800   |
| Eu (tonn) | 9 800   | 16 600    | 24 700    |
| Gd (tonn) | 42 100  | 72 100    | 107 800   |
| Tb (tonn) | 6 400   | 11 000    | 16 400    |
| Dy (tonn) | 36 100  | 62 000    | 92 500    |

**Tab. 7.14** Skorperessurser på Knipovitsryggen

| Metall              | P95     | Forventning | P05     |
|---------------------|---------|-------------|---------|
| Mn (millioner tonn) | 19,6    | 35,3        | 55,2    |
| Ti (millioner tonn) | 0,8     | 1,4         | 2,1     |
| Mg (millioner tonn) | 2,4     | 4,3         | 6,7     |
| Li (tonn)           | 20 300  | 45 000      | 84 900  |
| Sc (tonn)           | 5 600   | 10 000      | 15 700  |
| V (tonn)            | 198 000 | 356 400     | 557 900 |
| Co (tonn)           | 288 700 | 532 800     | 844 000 |
| Nb (tonn)           | 6 800   | 12 200      | 19 300  |
| Hf (tonn)           | 1 400   | 2 600       | 4 100   |
| W (tonn)            | 6 700   | 16 900      | 33 800  |
| Ga (tonn)           | 1 900   | 3 700       | 6 100   |
| Y (tonn)            | 29 700  | 53 500      | 84 000  |
| La (tonn)           | 35 700  | 64 700      | 102 100 |
| Ce (tonn)           | 164 500 | 298 400     | 471 800 |
| Pr (tonn)           | 10 000  | 18 200      | 28 700  |
| Nd (tonn)           | 41 000  | 74 600      | 117 700 |
| Eu (tonn)           | 2 300   | 4 100       | 6 500   |
| Gd (tonn)           | 9 800   | 17 800      | 28 000  |
| Tb (tonn)           | 1 500   | 2 700       | 4 200   |
| Dy (tonn)           | 8 400   | 15 300      | 24 000  |

**Tab. 7.15** Skorperessurser på Jan Mayen-ryggen

| Metall              | P95    | Forventning | P05    |
|---------------------|--------|-------------|--------|
| Mn (millioner tonn) | 1,7    | 3,9         | 7,2    |
| Ti (millioner tonn) | 0,2    | 0,4         | 0,7    |
| Mg (millioner tonn) | 0,3    | 0,7         | 1,3    |
| Li (tonn)           | 1 800  | 4 100       | 7 400  |
| Sc (tonn)           | 500    | 1 100       | 2 000  |
| V (tonn)            | 15 600 | 35 400      | 63 900 |
| Co (tonn)           | 15 000 | 35 500      | 66 300 |

|           |       |        |        |
|-----------|-------|--------|--------|
| Nb (tonn) | 1 200 | 2 700  | 5 100  |
| Hf (tonn) | 100   | 300    | 500    |
| W (tonn)  | 500   | 1 100  | 2 000  |
| Ga (tonn) | 200   | 500    | 900    |
| Y (tonn)  | 2 000 | 4 700  | 8 800  |
| La (tonn) | 2 200 | 5 400  | 10 200 |
| Ce (tonn) | 6 900 | 17 600 | 34 200 |
| Pr (tonn) | 600   | 1 400  | 2 600  |
| Nd (tonn) | 2 400 | 5 700  | 10 800 |
| Eu (tonn) | 100   | 300    | 600    |
| Gd (tonn) | 600   | 1 400  | 2 500  |
| Tb (tonn) | 100   | 200    | 400    |
| Dy (tonn) | 500   | 1 200  | 2 300  |

Tab. 7.16 Skorperessurser på Vøringutstikkeren

| Metall              | P95    | Forventning | P05     |
|---------------------|--------|-------------|---------|
| Mn (millioner tonn) | 7,6    | 21,1        | 42,2    |
| Ti (millioner tonn) | 0,6    | 1,6         | 3,2     |
| Mg (millioner tonn) | 1,3    | 3,7         | 7,3     |
| Li (tonn)           | 8 200  | 24 100      | 48 900  |
| Sc (tonn)           | 1 800  | 5 000       | 10 000  |
| V (tonn)            | 56 700 | 156 000     | 313 000 |
| Co (tonn)           | 92 300 | 256 300     | 512 600 |
| Nb (tonn)           | 3 100  | 8 500       | 16 900  |
| Hf (tonn)           | 500    | 1 400       | 2 700   |
| W (tonn)            | 3 300  | 9 200       | 18 700  |
| Ga (tonn)           | 500    | 1 400       | 2 800   |
| Y (tonn)            | 10 200 | 27 800      | 55 700  |
| La (tonn)           | 12 800 | 35 500      | 70 700  |
| Ce (tonn)           | 47 400 | 131 600     | 262 400 |
| Pr (tonn)           | 3 400  | 9 400       | 18 900  |
| Nd (tonn)           | 13 900 | 38 900      | 78 100  |
| Eu (tonn)           | 800    | 2 200       | 4 300   |
| Gd (tonn)           | 3 200  | 9 000       | 18 000  |
| Tb (tonn)           | 500    | 1 400       | 2 800   |
| Dy (tonn)           | 2 900  | 8 100       | 16 100  |

## 7.5 Nærmere om metaller - beskrivelse, utvinning, reserver og ressurser

Omtale av metaller nedenfor er i stor grad basert på NGU's beskrivelser (NGU, 2023). Tall for utvinning (primærproduksjon) og reserver i 2020 er i all hovedsak hentet fra U.S. Geological Survey (U.S. Geological Survey, 2022). Tall for utvinning av sjeldne jordarter er hentet fra Minor Metals Trade Association (MMTA, 2022).

### 7.5.1 Basemetaller

Basemetaller er metaller som oksideres når de varmes opp i kontakt med luft, og som verken er jern- og jernlegeringsmetaller eller edelmetaller. Basemetallene omfatter bl.a. kobber (Cu), sink (Zn) og kobolt (Co). Kobolt brukes i jernlegeringer og er beskrevet under denne kategorien.

#### Kobber (Cu)

Kobber fremstilles hovedsakelig fra konsentrater av kobbersulfider som kan utvinnes fra ulike forekomsttyper. Kobber brukes først og fremst som kobbertråd til elektriske ledere og i elektronikk, for eksempel trykte kretskort. Kobber legeres med gull og sølv til smykker, med tinn til bronse og med sink til messing.

I 2020 ble det i verden produsert 20,6 millioner tonn kobber. De største produsentene var Chile (5,7 mill. tonn), Peru (2,2 mill. tonn) og Kina (1,7 mill. tonn). Globale kobberreserver er 880 mill. tonn. Globale påviste kobberressurser ble i 2015 anslått til 2,1 mrd. tonn.

#### Sink (Zn)

Sink utvinnes hovedsakelig fra sinkblende som opptrer i en rekke forskjellige typer av komplekse sulfidmalmer. Sink brukes i stor grad til galvanisering, som anodemateriale i batterier, pigment i maling (sinkoksid) og i legering med kobber til messing.

I 2020 ble det produsert 12 millioner tonn sink. De tre største produsentene var Kina (4,1 mill. tonn), Peru (1,3 mill. tonn) og Australia (1,3 mill. tonn). Globale sinkreserver er 250 mill. tonn. Globale påviste sinkressurser er anslått til 1,9 mrd. tonn.

### 7.5.2 Edelmetaller

Edelmetaller er metaller som kjemisk sett er lite reaktive med tanke på korrosjon og oksidasjon. Metallene er relativt sjeldne og av høy økonomisk verdi. De mest kjente edelmetallene er gull og sølv (men også platinagruppens metaller og rhenium inkluderes blant edelmetallene).

#### Gull (Au)

Gull er et mykt, skinnende og lett formbart metall. Gull brukes fremfor alt som verdielement og i smykker. Gull har meget gode lederegenskaper for både elektrisitet og varme og er et viktig element i elektronikkindustrien. Metallet brukes også i tannindustrien, spesielt i kroner og broer.

Malmer hvor gull er hovedprodukt dannes gjerne ved hydrotermale prosesser (varme løsninger). Ellers er gull et viktig biprodukt ved prosessering av magmatiske nikkel-, kobber- og platinamalmer, samt vulkanogene kismalmer (VMS) med kobber og sink og porfyr-kobbermalmer.

I 2020 ble det på verdensbasis produsert 3 030 tonn gull, hvorav Kina (365 tonn), Australia (328 tonn), og Russland (305 tonn) var de største produsentene. Globale gullreserver er 54 000 tonn.

#### Sølv (Ag)

Sølv har høyere ledningsevne for varme og elektrisitet enn noe annet metall, og er et meget smibart materiale. Det har også en meget høy glans. I likhet med gull brukes også



sølv som verdielement og i smykker. De viktigste anvendelsene er til fotografiske formål, elektronikk, i mynter, forsølving, smykker, som katalysator, til vannrensing og i medisin.

Sølv forekommer rent (gedigent), i form av sulfider eller bundet til arsen og/eller antimon. Det utvinnes i stor grad som biprodukt ved prosessering av kobber-, sink- eller blyforekomster av forskjellig opprinnelse. Rene sølvmalmer finnes som gangforekomster.

Verdensproduksjonen i 2020 var 23 500 tonn, hvor Mexico (5 540 tonn), Kina (3 380 tonn) og Peru (2 770 tonn) var de største produsentene. Globale sølvreserver er 530 000 tonn.

### 7.5.3 Spesialmetaller

Det finnes en rekke metalliske grunnstoffer som verken kan klassifiseres som jern- og jernlegeringsmetaller, basemetaller, energimetaller eller edelmetaller. NGU kategoriserer gruppen som "spesialmetaller", hvor bl.a. niob (Nb), hafnium (Hf), scandium (Sc), yttrium (Y) og de 15 lantanoidene – samlet betegnet som sjeldne jordartselementer (REE; Rare Earth Elements) – inkluderes.

#### Niob (Nb)

Niob fremstår i ren form som et lysegrått metall. Det er mykt og formbart og kan lett vales og smis. Den viktigste bruken av niob er som legeringsgrunnstoff i lavlegerte og rustfrie stål samt høytemperaturlegeringer<sup>1</sup>. Niob brukes i stål- og superlegeringer til fly- og rakettmotorer.

Niob (Nb) og tantal (Ta) finnes ofte i de samme forekomstene, da de kan erstatte hverandre i ulike mineraler. De viktigste Nb-førende mineralene er columbitt, euxenitt, fergusonitt og pyroklor (NGU, 2023).

Verdensproduksjonen av niob i 2020 var på 67 700 tonn, med Brasil som største produsent (59 800 tonn), etterfulgt av Canada (6 500 tonn). Globale niobreserver overstiger 17 mill. tonn. Verdens ressurser av niob anslås å være tilstrekkelig for fremtidige behov.

#### Hafnium (Hf)

Hafnium er et sølvhvitt, mykt og smibart metall med et svært høyt smeltepunkt på 2503 °C. Det oksideres lett, men beskyttes av et tynt, tett oksidlag, i likhet med aluminium. Hafnium brukes som absorpsjonsmateriale i kjernereaktorer. Metallet brukes også som legeringsgrunnstoff i høytemperaturlegeringer og som getter i høyvakuumteknikk.

I naturen forekommer hafnium i zirkoniummineraler. Kommersielt fremstilles hafnium fra konsentrater av zirkon,  $ZrSiO_4$ , som inneholder 0,5-2 pst. hafnium<sup>2</sup>.

Tall på verdensproduksjon og -reserver av hafnium er ikke tilgjengelige. I 2020 var global produksjon av zirkoniummalm og -konsentrat på 1,2 mill. tonn bruttovekt. Australia (400 000 tonn), Sør-Afrika (280 000 tonn) og Kina (140 000 tonn) var største produsenter. Globale reserver av zirkonium ( $ZrO_2$ ) er 70 mill. tonn.

### Litium (Li)

Litiumkarbonat og -silikat anvendes i produksjon av glass og keramikk for å senke smeltepunktet. Litiumkjemikalier inngår i et stort spekter av produkter, inkludert forskjellige typer av litiumbatterier. Metallisk litium anvendes i fremstilling av aluminium-litium og magnesium-litium-legeringer som er meget lette og egnet til bruk i flyindustrien. Litiumkonsumet for batterifremstilling har vokst betydelig i de senere år.

Den største delen av Li-utvinning kommer fra saltsjøer i form av litiumkarbonat. I 2020 ble det produsert 82 500 tonn litium. De største produsentene var Australia (39 700 tonn), Chile (21 500 tonn) og Kina (13 300 tonn). Globale litiumreserver er 22 mill. tonn. Globale påviste litiumressurser er anslått til 89 mill. tonn.

### Sjeldne jordartsmetaller (REE): yttrium (Y), scandium (Sc) og lantanider

Metallene av de sjeldne jordartselementene (REE) brukes i bilkatalysatorer, metallurgisk industri, TV- og dataskjermer, (permanente) magneter, ulike lys og til oljeraffinering. Eksempelvis brukes terbium (Tb) i fosforlegeringer i lamper og skjermer, og blant annet sammen med dysprosium (Dy) for å lage sterke og lette magneter som også beholder sine egenskaper under høye temperaturer. Disse magnetene brukes i både i hybridbilmotorer, vindturbiner og nedkjøling av kjernekraftreaktorer. Neodym (Nd) brukes blant annet i harddisker og hodetelefoner. Yttrium (Y) og europium (Eu) brukes blant annet for å generere rød farge i tv-skjermer/pc-skjermer. Scandium (Sc) benyttes i legeringer med aluminium for å gi stor styrke, særlig til fly- og luftfart, samt til spesielle lyskilder.

I 2020 ble det på verdensbasis produsert 240 000 tonn sjeldne jordarts-oksider (REO), med Kina (140 000 tonn), USA (39 000 tonn) og Myanmar (31 000 tonn) som største produsenter. Globale REO-reserver er 120 mill. tonn. Produksjonen av scandiumoksid på verdensbasis er beskjeden, omkring 2000 kg/år. Scandium er produsert som biprodukt og det finnes ikke gruvedrift som er basert bare på Sc-utvinning. Verdensproduksjonen av yttrium i REE-konsentrater er 8 000 – 12 000 t/år. Globale reserver av yttriumoksid-ekvivalenter ( $Y_2O_3$ ) er anslått til >500 000 tonn (U.S. Geological Survey, 2022).

### Lantan (La)

Lantan er et sølvhvitt metall. Det er så mykt at det kan skjæres med kniv, og er derfor svært lett å forme og valse. Lantan brukes som tilsetning til høytemperaturlegeringer for å forbedre oksidasjonsbestandigheten. Det brukes som tilsetning til jern og stål for å fjerne forurensninger av oksygen og svovel.

Lantan fremstilles fra anriket monazitt eller bastnäsitt<sup>3</sup>. Verdensproduksjonen av lantan er anslått til 12 500 tonn per år. USA, Brasil India, Sri Lanka og Australia er største produsenter. Globale reserver anslås til 6 mill. tonn. Lantan anslås å være den minst sjeldne av de sjeldne jordartene<sup>4</sup>.

### Cerium (Ce)

Cerium er et mykt metall med farge og glans som jern. Cerium-metall anvendes i legering med andre lantanoider til en rekke formål. Tilsats av små mengder cerium (cirka 0,1 pst.) til høytemperaturlegeringer gir økt bestandighet mot korrosjon ved høye temperaturer.

I naturen finnes cerium i form av en rekke mineraler. Cerium utgjør 68 ppm av jordskorpen, og er det mest utbredte av lantanoidene<sup>5</sup>.

Cerium utvinnes fra mineralganger av monazitt eller bastnäsitt. Verdensproduksjonen av cerium er anslått til 24 000 tonn per år. De viktigste utvinningsområdene er som for andre sjeldne jordarter: USA, Brasil, India, Sri Lanka, Australia og Kina<sup>6</sup>.

### **Praseodym (Pr)**

Praseodym er et sølvglinsende metall som er lett å forme og uedelt (oksideres lett i luft og vann). Sammen med andre lantanoider brukes praseodym blant annet som katalysator, i fosforer og lasermaterialer, og som tilsetning i legeringer.

Praseodym utgjør 7,6 ppm av jordskorpen og er vanligere enn metaller som tinn, wolfram og sølv. Metallet forekommer sammen med andre lantanoider i mineraler som monazitt og cerritt<sup>7</sup>. Årlig produksjon er omtrent 2 500 tonn<sup>8</sup>, med 2 mill. tonn i globale reserver<sup>9</sup>.

### **Neodym (Nd)**

Neodym er et sølvhvitt, duktilt (formbart) metall. Den viktigste anvendelsen for neodym er som (permanent) magnet, for bruk i bl.a. harddisker, vindturbiner og batterier<sup>10</sup>.

Nest etter cerium og lantan er neodym det vanligste av lantanoidene. I jordskorpen forekommer det gjennomsnittlig i større mengder enn metaller som bly, tinn, sølv og gull<sup>11</sup>. Monazitt og enkelte forekomster av bastnäsitt er viktigste kilder. Global produksjon av neodym i 2020 var 35 000 tonn (KU Leuven, 2022). Kina, USA, Brasil, India, Sri Lanka og Australia er viktigste produsenter, hvor Kina dominerer produksjonen. Globale reserver av neodym anslås til 8 mill. tonn<sup>12</sup>.

### **Europium (Eu)**

Europium er et metall som er sølvglinsende, pyrofort (selvantennelig) og like mykt som bly. Europium har viktige industrielle anvendelser, bl.a. i kontrollstaver i kjernereaktorer og for å generere den røde fargen i billedrør.

Europium fremstilles fra mineralene monazitt, bastnäsitt og xenotim-(Y). Det er det mest sjeldne av lantanoidene, men finnes allikevel i større mengder i jordskorpen enn metaller som sølv, gull og platina<sup>13</sup>. Kina er største produsent. Årlig verdensproduksjon av europium er omtrent 270 tonn<sup>14</sup>.

### **Gadolinium (Gd)**

Gadolinium er et sølvhvitt, duktilt og svært uedelt metall (korroderer raskt). Grunnstoffet brukes i kontrollstaver i kjernereaktorer og som nøytronabsorpsjonsmateriale. Gadoliniumholdig kontrastmiddel brukes ved MR-undersøkelser.

Gadolinium finnes i mineralene monazitt og bastnäsitt<sup>15</sup>. Verdensproduksjonen av gadolinium er anslått til 7 500 tonn per år, med Kina som største produsent. Globale reserver av gadolinium sies å være over 1 mill. tonn<sup>16</sup>.

### **Terbium (Tb)**

Terbium er metall som er sølvhvitt, duktilt og så bløtt at det kan skjæres med kniv. Det er uedelt, svært reaktivt og behandles i vakuum eller inaktive atmosfærer. Terbium brukes som aktivator i fosforer for røntgen- og elektronstråler<sup>17</sup>, og med zirkonium i brenselceller.

Terbium er en av de sjeldneste sjeldne jordartene. Global produksjon er anslått til 10 tonn per år<sup>18</sup>.

### **Dysprosium (Dy)**

Dysprosium er et sølvglinsende metall og så mykt at det enkelt kan skjæres med kniv. Bruk av dysprosium har ofte få substitutter. Dysprosium brukes i magneter for å unngå tap av magnetisme ved høye temperaturer, i motorer, hjemmeelektronikk og i vindturbiner. Det høye smeltepunktet og evnen til å absorbere nøytroner gjør at det har vært brukt som legeringsmetall i deler til kjernekraftverk.

Dysprosium er sjeldent i naturen. Det finnes i mineraler som monazitt og bastnäsitt<sup>19</sup>. Global produksjon av dysprosium i 2020 var 2 500 tonn (KU Leuven, 2022). Kina er største produsent<sup>20</sup>.

## **7.5.4 Jern, titan og jernlegering**

Jern er det nest vanligste metallet på jorda og forbrukes i store mengder. Titan brukes i stållegeringer og rustfritt stål, mens jernlegeringsmetallene gir forskjellige egenskaper til stål og støpejern.

### **Titan (Ti)**

Titan brukes i stållegeringer (ferro-titan), i rustfritt stål (for å minske karboninnholdet), og legeres blant annet med aluminium, vanadium, kobber, jern, mangan, molbybden og andre metaller. Valsede produkter som plater, barrer, wirer etc., kan brukes til en rekke formål innen industri, romfart, luftfart, medisin (som implantater og til instrumenter), sportsutstyr med mer.

I 2020 var global produksjon av titandioksid ( $\text{TiO}_2$ ) fra ilmenitt og rutil på 8,6 mill. tonn, med Kina (2,8 mill. tonn), Sør-Afrika (1 mill. tonn) og Mosambik (0,96 mill. tonn) som største produsenter fra ilmenittkonsentrat, og Australia (190 000 tonn), Sierra Leone (114 000 tonn) og Ukraina (95 000 tonn) som største produsenter fra rutilkonsentrat. Globale reserver av titandioksid fra ilmenitt og rutil er 750 mill. tonn. Globale ressurser av anatas, ilmenitt og rutil er anslått til >2 mrd. tonn.

### **Jernlegeringsmetaller**

Gruppen inkluderer bl.a. kobolt (Co), mangan (Mn), vanadium (V) og wolfram (W).

### **Kobolt (Co)**

Kobolt produseres vanligvis som biprodukt ved kobber- og nikkelproduksjon. Kobolt kan danne kjemiske forbindelser med nesten alle grunnstoffer. Det gjør at kobolt har en rekke bruksområder og er et viktig metall i miljøvennlig teknologi, bl.a. som legering i elektrodene til oppladbare batterier. Ellers brukes kobolt også i superlegeringer og hardmetall-legeringer, korrosjons- og værbestandige legeringer, og mye mer. Kobolt har også blitt brukt som blått fargestoff i glass og keramikk i flere tusen år.

I 2020 ble det på verdensbasis produsert 142 000 tonn kobolt, hvorav Kongo (98 000 tonn), Russland (9 000 tonn), og Australia (5 630 tonn) var de største produsentene. Globale koboltreserver er 7,6 mill. tonn. Påviste globale koboltressurser på land er rundt 25 mill. tonn.

### **Mangan (Mn)**

Mangan er et hardt paramagnetisk metall som lett oksideres. Det er viktig i jern- og stålproduksjon, og 85-90 pst. av verdensproduksjonen brukes her. Mangan er nødvendig i de fleste typer stål og krom og gjør stålet rustfritt. Mangan er en nøkkelbestanddel i

billig rustfritt stål og er mye brukt i aluminiumlegeringer. Det har også en rekke anvendelser innen kjemisk industri, som tilsetning i blyfri bensin for å øke oktantallet og redusere motorbanking.

I 2020 var verdens manganutvinning på 18,9 mill. tonn. De største produsentene var Sør-Afrika (6,5 mill. tonn), Australia (3,3 mill. tonn) og Gabon (3,3 mill. tonn). Globale manganmalm-reserver er 1,5 mrd. tonn. Landbaserte manganressurser er store, men ujevnt fordelt.

### **Vanadium (V)**

Vanadium finnes i en rekke mineraler. Det utvinnes vanligvis som biprodukt fra raffinering av petroleum. Vanadium er et mykt metall med god motstandsdyktighet mot korrosjon av alkalier, svovelsyre og saltsyre. 80 pst. av alt vanadium som produseres, brukes i ferrovanadium eller som tilsetning i blant annet rustfritt stål til bruk i kirurgiske instrumenter og verktøy, og blandet med aluminium i titanlegeringer til bruk i jetmotorer. Det er en viktig karbidstabilisator i stålproduksjon og brukes i brenselceller og batterier.

I 2020 ble det på verdensbasis produsert 105 000 tonn vanadium, hvor Kina (70 000 tonn), Russland (19 500 tonn), og Sør-Afrika (8 580 tonn) var de største produsentene. Globale vanadiumreserver er 24 mill. tonn. Globale ressurser av vanadium er anslått å overstige 63 mill. tonn.

### **Wolfram (W)**

Wolfram (eng. tungsten) er et lysegrått metall. Det har det høyeste smeltepunktet av alle metaller, 3422 °C. Wolfram brukes som glødetråd i lyspærer. En annen viktig anvendelse er som legeringsgrunnstoff i stål, superlegeringer og annet. Wolframkarbid har høy hardhet og inngår i hardmetaller for bruk i borekroner, fjellbor o.a.

Wolfram utgjør 1 ppm av jordskorpen. I naturlig tilstand finnes wolfram blant annet i mineralene wolframitt og scheelitt<sup>21</sup>.

I 2020 var verdens produksjon av wolfram på 78 400 tonn, hvor de største produsentene var Kina (66 000 tonn), Vietnam (4 500 tonn) og Russland (2 400 tonn). Globale reserver av wolfram er 3,7 mill. tonn. Verdens wolframressurser er geografisk spredt, men Kina er størst på ressurser og reserver.

## **7.5.5 Andre metaller**

### **Gallium (Ga)**

Gallium er et mykt, sølvglinsende metall som smelter allerede ved 30 °C. Med sitt lave smeltepunkt og høye kokepunkt er gallium flytende over et større temperaturområde enn noe annet grunnstoff. Gallium har lignende kjemiske egenskaper som aluminium. Det brukes blant annet i halvledere og som små partikler i skismøring.

Gallium forekommer i jordskorpen i omtrent samme mengder som bly. Det finnes imidlertid ikke i konsentrerte forekomster, bare spredt. Gallium fremstilles som et biprodukt ved fremstilling av aluminium og sink<sup>22</sup>.

I 2020 var global produksjon av gallium 327 tonn. Kina var største produsent (317 tonn), etterfulgt av Russland (5 tonn) og Japan (3 tonn). Reserveestimer er ikke tilgjengelige. Produksjonen deles i lav- og høy-renhetsproduksjon, samt resirkulering. Global

produksjonskapasitet i 2021 er anslått til hhv. 774 tonn, 325 tonn og 273 tonn. Gjennomsnittlig galliumgehalt i bauxitt er 50 ppm. Galliumressurser i bauxitt overstiger 1 mill. tonn, pluss en betydelig mengde i sink. Under 10 pst. av disse galliumressursene forventes å være utvinnbare.

### Magnesium (Mg)

Magnesium er et sølvhvitt, glinsende og mykt metall. Magnesium har liten tetthet, bare 25 prosent av stål, og er det letteste metallet som blir brukt i dag. Det er godt egnet til bruksgjenstander i form av legeringer som har større mekanisk styrke enn rent metall. Magnesium er et sterkt reduksjonsmiddel. I konstruksjoner er magnesium det mest brukte metallet etter stål og aluminium.

Magnesium utgjør 2,4 vektprosent av jordskorpen. I rekkefølgen av grunnstoffene i jordskorpen, er magnesium nummer seks. Magnesium er det tredje mest vanlige grunnstoffet i sjøvann<sup>23</sup>.

I 2020 ble det på verdensbasis produsert over 27 mill. tonn magnesiumoksid, med Kina (19 mill. tonn), Brasil (1,8 mill. tonn) og Tyrkia (1,47 mill. tonn) som største kjente produsenter. Globale reserver av magnesiumoksid er 7,2 mrd. tonn. Magnesium blir framstilt kommersielt ved to metoder: elektrolyse av smeltet vannfritt magnesiumklorid og ved silikotermisk reduksjon av magnesiumoksid.

Den første metoden er den langt viktigste. Global produksjon av magnesium var i 2020 på 1 mill. tonn, med Kina (886 000 tonn), Russland (19 000 tonn) og Israel (19 000 tonn) som største kjente produsenter. Tilgangen på ressurser for utvinning av magnesium vurderes som tilnærmet ubegrenset.

- 1 Kofstad, Per K.; Pedersen, Bjørn (2022): niob i Store norske leksikon på [snl.no](https://snl.no). Tilgjengelig fra: <https://snl.no/niob> (Hentet 16. desember 2022).
- 2 Kofstad, Per K.; Pedersen, Bjørn (2022): hafnium i Store norske leksikon på [snl.no](https://snl.no). Tilgjengelig fra <https://snl.no/hafnium> (Hentet 16. desember 2022).
- 3 Kofstad, Per K. (2022): lantan i Store norske leksikon på [snl.no](https://snl.no). Tilgjengelig fra <https://snl.no/lantan> (Hentet 16. desember 2022).
- 4 <https://mmta.co.uk/metals/la/> (Hentet 16. desember 2022).
- 5 Kofstad, Per K.; Pedersen, Bjørn (2022): cerium i Store norske leksikon på [snl.no](https://snl.no). Tilgjengelig fra <https://snl.no/cerium> (Hentet 18. desember 2022).
- 6 <https://mmta.co.uk/metals/Ce/> (Hentet 16. desember 2022).
- 7 Kofstad, Per K. (2022): praseodym i Store norske leksikon på [snl.no](https://snl.no). Tilgjengelig fra <https://snl.no/praseodym> (Hentet 18. desember 2022).
- 8 Årlig produksjon på 11 000 tonn oppgis av KU Leuven, April 2022, Metals for Clean Energy: Pathways to solving Europe's raw materials challenge, 117 s.
- 9 <https://mmta.co.uk/metals/Pr/> (Hentet 16. desember 2022).
- 10 <https://mmta.co.uk/metals/Nd/> (Hentet 16. desember 2022).
- 11 Kofstad, Per K. (2022): neodym i Store norske leksikon på [snl.no](https://snl.no). Tilgjengelig fra <https://snl.no/neodym> (Hentet 18. desember 2022).
- 12 <https://mmta.co.uk/metals/Nd/> (Hentet 16. desember 2022).
- 13 Kofstad, Per K.; Pedersen, Bjørn (2022): europium i Store norske leksikon på [snl.no](https://snl.no). Tilgjengelig fra <https://snl.no/europium> (Hentet 18. desember 2022).
- 14 <https://mmta.co.uk/metals/Eu/> (Hentet 16. desember 2022).
- 15 Kofstad, Per K.; Pedersen, Bjørn (2022): gadolinium i Store norske leksikon på [snl.no](https://snl.no). Tilgjengelig fra <https://snl.no/gadolinium> (Hentet 18. desember 2022).
- 16 <https://mmta.co.uk/metals/Gd/> (Hentet 16. desember 2022).

- 17 Kofstad, Per K. (2022): terbium i Store norske leksikon på [snl.no](https://snl.no). Tilgjengelig fra <https://snl.no/terbium> (Hentet 18. desember 2022).
- 18 <https://mmta.co.uk/metals/Tb/> (Hentet 16. desember 2022).
- 19 Kofstad, Per K. (2022): dysprosium i Store norske leksikon på [snl.no](https://snl.no). Tilgjengelig fra <https://snl.no/dysprosium> (Hentet 18. desember 2022).
- 20 <https://mmta.co.uk/metals/Dy/> (Hentet 16. desember 2022).
- 21 Kofstad, Per K.; Pedersen, Bjørn (2022): wolfram i Store norske leksikon på [snl.no](https://snl.no). Tilgjengelig fra <https://snl.no/wolfram> (Hentet 16. desember 2022).
- 22 Kofstad, Per K.; Pedersen, Bjørn (2022): gallium i Store norske leksikon på [snl.no](https://snl.no). Tilgjengelig fra <https://snl.no/gallium> (Hentet 16. desember 2022).
- 23 Kofstad, Per K.; Pedersen, Bjørn; Kaland, Trine; Allkunne (2022): magnesium i Store norske leksikon på [snl.no](https://snl.no). Tilgjengelig fra <https://snl.no/magnesium> (Hentet 18. desember 2022).





## 8 Ordliste

**Aksedal:** Kontinuerlig dalføre langs midten av en oseansk spredningsrygg. Aksedalen oppstår som en innsynkning (et søkk) langs grensen mellom spredningsryggens to litosfæreplater der det kontinuerlig dannes ny jordskorpe etterhvert som litosfæreplatene glir fra hverandre.

**Aksialforekomst:** Sulfidforekomster som er dannet i vulkanske rygger utviklet i de sentrale deler av aksedalen.

**Aktiv sulfidforekomst** (se også definisjon av sulfidforekomst): Sulfidmineralisering er tilstede, væske med høy temperatur strømmer ut.

**AUV (Autonomous Underwater Vehicle):** Selvstyrt undervannsfarkost som utfører en rekke målinger på havbunn og i vannsøylen.

**Avsetning:** Mineralakkumulasjon på havbunnen; opptrer i forskjellige former og strukturer som lag, skorsteiner, kjegler og hauger.

**Basalt:** Den mest utbredte magmatisk bergarten på jorden. Hovedtyngden av klodens basalter dannes ved vulkanske utbrudd tilknyttet de oseanske spredningsryggene.

**Bruddsone:** Består av seismisk aktive deler der litosfæreplatene beveger seg sidelengs i forhold til hverandre og definerer transformforkastninger, og seismisk inaktive deler der platene på begge sider av bruddsonen beveger seg i samme retning.

**Flankeforekomst:** sulfidforekomst som er dannet i og langsetter de store hovedforkastningene som utgjør flankene av aksedalen.

**Forekomst:** Alle typer avsetninger av mineraler.

**Forkastning:** Struktur som dannes i jordskorpen ved at en del av jordskorpen beveger seg i forhold til en annen langs en bruddsone eller forkastningssone. Bevegelsen inntreffer etter en periode med spenningsoppbygning og kan generere jordskjelv når spenningene utløses og forkastningen beveger seg.

**Geokjemi:** For denne rapportens formål: kjemiske og fysiske vannparametre (metan, turbiditet, pH, og oks-red. potensialet) som måles under leting etter sulfidforekomster. Disse måles med sensorer påmontert AUV.

**HiSAS:** AUV-sensor med syntetisk apertur sonar, som gir en svært detaljert oppløsning av havbunnens topografi.

**Hydrotermale (sulfid-)byggverk:** Flere hydrotermale hauger og kjegler som henger sammen i en mer kompleks struktur.

**Hydrotermal (sulfid-)haug:** En hauglignende struktur bygget opp av hydrotermale kjegler og kollapsede skorsteiner.

**Hydrotermal kilde:** Et sted der varm, mineralrik væske strømmer ut av havbunnen, ofte i forbindelse med vulkanske områder i randsonen mellom kontinentalplater.

**Hydrotermal (sulfid-)kjegle:** En kjegleformet struktur som bygges av mineralavsetninger rundt en hydrotermal skorstein

**Hydrotermal (sulfid-)skorstein:** En skorsteinslignende struktur som danner utløpet av den varme væsken i en hydrotermal kilde. Den bygges ved kontinuerlig utfelling av mineraler fra væsken som strømmer ut. Over tid kollapser de og bygger hauglignende avsetninger.

**Hydrotermal væske:** Vann fra varme kilder tilknyttet varmesentre under havbunnen.

**Inaktiv sulfidforekomst (se også definisjon av sulfidforekomst):** Sulfidmineralisering er tilstede, men ingen utstrømming av væske med høy temperatur.

**Klassifikasjon:** Sammenstilling av grupper eller klasser etter hvor like de er. Ordet klassifikasjon blir også brukt om resultatet av slik sammenstilling.

**Litosfæreplate:** Jordklodens ytre skall, litosfæren, er delt opp i plater (litosfæreplater) som «flyter» rundt på mantelen i jordens indre og derved beveger seg i forhold til hverandre.

**Magnetometer (SCM):** AUV-sensor som måler magnetisk felt.

**Manganskorpe:** Dannes ved at mineraler som er oppløst i sjøvann felles ut på fjellsider som oksid- og oksidhydroksidmineraler. Hovedkomponenter er jern og mangan.

**MBES (Multi Beam Echo Sounder):** Multistråle-ekkolodd for innsamling av dybde data som gir topografien av havbunnen.

**Ressurs:** Elementer eller menneskelige egenskaper som kan utnyttes økonomisk, eller som er til nytte på annen måte. Naturressurser er luft, vann, dyrkbare arealer, petroleum, mineraler og andre råstoffer. Man skiller gjerne mellom fornybare og ikke-fornybare ressurser<sup>2</sup>.

**ROV (Remotely Operated Vehicle):** Undervannsrobot som opererer på havbunn, og som er styrt fra overflaten.

**SBP:** AUV-sensor for bunnpenetrerende ekkoloddsdata. Måler tetthetskontraster (akustisk impedans) ned til noen ti-talls meter under havbunn og gir et bilde av sedimentenes lagdeling.

**Sjøfjell:** Undersjøisk fjell.

**Slettelandskap:** Omfatter sammenhengende arealer med mindre høydeforskjeller.

**SP:** AUV-sensor for måling av selvpotensial (elektriske egenskaper).

**Spredningsakse:** Området langs midten av aksedalen; altså ideelt sett aksene for spredningen av litosfæreplatene.

**Spredningsgrøft:** Et annet ord for aksedal.

**Spredningsrygg:** Også kalt midthavsrygg. Styr av magmatiske prosesser glir jordens litosfæreplater fra hverandre langs oseanske spredningsrygger, og ny jordskorpe dannes. For norsk kontinentalsokkel og utredningsområdet gjelder dette Kolbeinseyryggen, Mohnsryggen og Knipovitsjryggen.

**SSS:** AUV-sensor for sidesøkende sonar. Gir et «skygge-relieff» av havbunn.

**Sulfid:** Sulfider er kjemiske forbindelser mellom svovel og en eller flere grunnstoffer. Denne rapporten handler om sulfidforbindelser mellom svovel og metalliske grunnstoffer.

**Sulfidforekomst:** I denne rapporten brukes begrepet sulfidforekomster om avsetninger med svovel og metaller avsatt som sulfidmineraler på og i havbunnen av hydrotermal aktivitet. Den enkelte sulfidforekomst er avsatt gjennom en egen hydrotermal sprekkekanal separat fra andre sulfidforekomster. Sulfidforekomstene på norsk kontinentalsokkel dannes naturlig tilknyttet de aktive spredningsryggene mellom Norge og Grønland.

**Sulfid-teig:** Naturlig avgrenset område med sulfidforekomster avsatt i hydrotermale strukturer som skorsteiner, byggverk eller hauger; geografisk separert fra andre sulfidteiger.

- 1 Fossen, Haakon: forkastning i Store norske leksikon på [snl.no](https://snl.no). Hentet 6. januar 2023 fra <https://snl.no/forkastning>
- 2 naturressurs i Store norske leksikon på [snl.no](https://snl.no). Hentet 6. januar 2023 fra <https://snl.no/naturressurs>



## 9 Referanser

- Agius, M. R., Harmon, N., Rychert, C. A., Tharimena, S. and Kendall, J. M., 2018. Sediment characterization at the equatorial Mid-Atlantic Ridge from P-to-S teleseismic phase conversions recorded on the PI-LAB experiment. *Geophysical Research Letters*, 45(22)
- Barrie, C.T. and Hannington, M.D. 1999. Classification of Volcanic-Associated Massive Sulfide Deposits Based on Host-Rock Composition. *Reviews in Economic Geology*, v. 8, p 1 – 11. DOI: 10.5382/Rev.08.01
- Baumberger, T., Früh-Green, G.L., Thorseth, I.H., Lilley, M.D., Hamelin, C., Bernasconi, S. M., Okland, I.E. and Pedersen, R.B. 2016. Fluid composition of the sediment-influenced Loki's Castle vent field at the ultra-slow spreading Arctic Mid-Ocean Ridge. *Geochimica and Cosmochimica Acta*, v. 187, p 156 - 178. <https://doi.org/10.1016/j.gca.2016.05.017>
- Bjerga, A., Stubseid, H. H., Pedersen, L-E. R., & Pedersen, R. B. 2022. Radiation damage allows identification of truly inherited zircon. *Communications Earth & Environment*, 3(1), 1-7.
- Blischke, A., Brandsdóttir, B., Stoker, M.S., Gaina, C., Erlendsson, Ö., Tegner, C., Haldórsson, S.A., Helgadóttir, H.M., Gautason, B., Planke, S., Koppers, A.A.p. and Hopper, J.R. 2022. Seismic Volcanstratigraphy: The Key to Resolving the Jan Mayen Microcontinent and Iceland Plateau Rift Evolution. *Geochemistry, Geophysics, Geosystems*, 23, e2021GC009948. <https://doi.org/10.1029/2021GC009948>
- Brekke, H. 2000. The tectonic evolution of the Norwegian Sea Continental Margin with emphasis on the Vøring and Møre Basins. In: Nøttvedt, A., Larsen, B.T., Gabrielsen, R.H., Olaussen, S., Brekke, H., Tørudbakken, B., Birkeland, Ø. and Skogseid, J. (eds): *Dynamics of the Norwegian Margin*. *GSL Special Publication*, 167, p 327 - 378.
- Canales, J.P., Sohn, R.A. and deMartin, B.J. 2007. Crustal structure of the Trans-Atlantic Geotraverse (TAG) segment (Mid-Atlantic Ridge, 26\_100N): Implications for the nature of hydrothermal circulation and detachment faulting at slow spreading ridges. *Geochem. Geophys. Geosyst.*, 8, Q08004, doi:10.1029/2007GC001629.
- Cherkashov, G., Poroshina, I., Tepanova, T., Ivanov, V., Bel'tenev, B., Lazareva, L., Rozhdestvenskaya, I., Samovarov, M., Shilov, V., Glasby, G.P., Fouquet, Y., and Kuznetsov, V. 2010. Seafloor Massive Sulfides from the Northern Equatorial Mid-Atlantic Ridge: New Discoveries and Perspectives. *Marine Georesources & Geotechnology*, v. 28, Issue 3, pp 222 – 239.
- Cherkashov, G., Kuznetsov, V., Kuksa, K., Tabuns, E., Maksimov, F., and Bel'tenev, V. 2017. Sulfide geochronology along the Northern Equatorial Mid-Atlantic Ridge. *Ore Geology Reviews*, p 147 - 154. <http://dx.doi.org/10.1016/j.orgeorev.2016.10.015>
- DMF - Direktoratet for mineralforvaltning med Bergmesteren for Svalbard 2022. Mineralstatistikk 2021, Harde fakta om mineralnæringen 2021. Tilgjengelig fra: <https://dirmin.no/harde-fakta-om-mineralnaeringen-mineralstatistikk-2021> (Hentet: 24. januar 2023).

Dauteuil, O. and Brun, J.-P. 1996. Deformation partitioning in a slow spreading ridge undergoing oblique extension: Mohns Ridge, Norwegian Sea. *Tectonics*, vol. 15, no. 4, p 870 - 884.

Dumais, M.A., Gernigon, L., Olesen, O., Johansen, S. E., and Brønner, M., 2021. New interpretation of the spreading evolution of the Knipovich Ridge derived from aeromagnetic data, *Geophysical Journal International*, Volume 224, Issue 2, February 2021, Pages 1422–1428.

European Commission 2020a. Communication from the Commission to the European Parliament, the Council, the European Economic and Social Committee and the Committee of the Regions. Critical Raw Materials Resilience: Charting a Path towards greater Security and Sustainability, Brussels, 3.9.2020 COM(2020) 474 final. Tilgjengelig fra: <https://ec.europa.eu/docsroom/documents/42849>.

European Commission 2020b. Critical materials for strategic technologies and sectors in the EU - a foresight study, 2020. Tilgjengelig fra: <https://ec.europa.eu/docsroom/documents/42881>.

Faleide, J.I., Tsikalas, F., Breivik, A., Mjelde, R., Ritzmann, O., Engen, Ø., Wilson, J., and Eldholm, O., 2008. Structure and evolution of the continental margin off Norway and Barents Sea, *Episodes*, 31, 82–91.

Firstova, A., Stepanova, T., Cherkashov, G., Goncharov, A. and Babaeva, S. 2016. Composition and Formation of Gabbro-Peridotite Hosted Seafloor Massive Sulfide Deposits from the Ashadze-1 Hydrothermal Field, Mid-Atlantic Ridge. *Minerals* 2016, 6, 19; doi:10.3390/min6010019 . [www.mdpi.com/journal/minerals](http://www.mdpi.com/journal/minerals)

Flesland, K., Hafliðason, H., Thorseth, I.H. and Pedersen, R.B. Manganese-enriched sediment layers at the Mohns Ridge, Norwegian-Greenland Sea (in prep)

Franklin, J.M., Gibson, H.L., Jonasson, I.R. and Galley, A.G. 2005. Volcanogenic Massive Sulfide Deposits. Society of Economic Geologists, Inc. *Economic Geology* 100th Anniversary Volume pp. 523–560.

Gernigon, L., Franke, D., Geoffroy, L., Schiffer, C., Foulger, G.R. and Stoker, M., 2020. Crustal fragmentation, magmatism, and the diachronous opening of the Norwegian-Greenland Sea. *Earth Sci. Rev.*

Gernigon, L., Blischke, A., Nasuti, A. and Sand, M. 2015. Conjugate volcanic rifted margins, seafloor spreading, and microcontinent: Insights from high-resolution aeromagnetic surveys in the Norway Basin. *Tectonics*, 34, pp 27. <https://doi.org/10.1002/2014TC003717>

Gielen, D. and M. Lyons 2022. Critical materials for the energy transition: Rare earth elements, International Renewable Energy Agency, Abu Dhabi.

Gilje, S., Thorseth I.H., Pedersen R.B. Composition and characteristics of the ferromanganese crusts from the Norwegian-Greenland Sea, (in prep).

Gusev, E.A. 2015. Some features of the geological structure of the Greenland-Spitsbergen Plateau. *Advances in current natural sciences*, no. 1, 2015 (in Russian). *VNIIOkeangeologia*, St. Petersburg, p 29 - 32.



- Gvein, Ø., Rui, I.J., Dahl, R.M. 2022. Bergverksdrift i Norge i Store norske leksikon på snl.no. Tilgjengelig fra: [https://snl.no/Bergverksdrift\\_i\\_Norge](https://snl.no/Bergverksdrift_i_Norge) (Hentet 12. desember 2022).
- Haneda, Y., Okada, M., Suganuma, Y. and Kitamura, T. 2020. A full sequence of the Matuyama-Bruhnes geomagnetic reversal in the Chiba composite section, Central Japan. *Progress in Earth Planetary Science*, 7:44, pp 22. <https://doi.org/10.1186/s40645-020-00354-y>
- Hannington, M.D., Jamieson, J., Monecke, T. and Petersen, S. 2010. Modern Sea-Floor Massive Sulfides and Base Metal Resources: Toward an Estimate of Global Sea-Floor Massive Sulfide Potential. *Society of Economic Geologists, Inc. Special Publication 15*, pp. 317–338
- Hannington, M.D., Galley, A.G, Herzig, P.M. and Petersen, S. 1998. Comparison of the TAG Mound and Stockwork Complex with Cyprus-Type Massive Sulfide Deposits. In: Herzig, P. M., Humphris, S.E., Miller, D.J., and Zierenberg, R.A. (Eds.), *Proceedings of the Ocean Drilling Program, Scientific Results, Vol. 158*, pp 389-415.
- Hein, J.R., Koschinsky, A., Bau, M., Manheim, F.T., Kang, J.-K. and Roberts, L., 2000. Cobalt-rich ferromanganese crusts in the Pacific. In: Cronan, D.S. (Ed.), *Handbook of Marine Minerals Deposit*. CRC Press, Boca Raton, Florida, pp. 239–279
- Heldal, T., Erichsen, E., Aasly, K. A., Schiellerup, H. og Raaness, A. 2017. Mineralske ressurser i bakken - oversikt og analyser 2016. Trondheim: Norges geologiske undersøkelse. Tilgjengelig fra: <https://www.ngu.no/publikasjon/mineralske-ressurser-i-bakken-oversikt-og-analyser-2016> (Hentet 24. januar 2023).
- Hellevang, B., and Pedersen, R. B., 2005. Magmatic segmentation of the northern Knipovich Ridge: Evidence for high-pressure fractionation at an ultraslow spreading ridge. *Geochemistry, Geophysics, Geosystems*, 6(9).
- Hjartarson, A., Erlendsson, Ö. and Blischke, A. 2017. The Greenland-Iceland-Faroe Ridge Complex. In: Péron-Pinvidic, G., Hopper, J.R., Stoker, M.S., Gaina, C., Doornenbal, J.C., Funck, T. and Árting, U.E. 2017. *GSL, Special Publication*, 447, p 127 - 148.
- Kandilarov, A., Mjelde, R., Pedersen, R. B., Hellevang, B., Papenberg, C., Petersen, C. J., Planert, L., and Flueh, E., 2012. The northern boundary of the Jan Mayen microcontinent, North Atlantic determined from ocean bottom seismic, multichannel seismic, and gravity data. *Marine Geophysical Research*, 33(1), 55-76.
- KU Leuven 2022. Metals for Clean Energy: Pathways to solving Europe's raw materials challenge, 117 s. Tilgjengelig fra: <https://eurometaux.eu/media/jmxf2qm0/metals-for-clean-energy.pdf> (Hentet 21. juni 2022).
- Lipton, I.T., Jankowski, P.E., Munro, P. and Lowe, J.J. 2012. Mineral Resource Estimate, Solwara Project, Bismarck Sea, PNG. *Golder Associates Report No SL01-NSG-RPT-7020-001 Rev 1.*, Nautilus Minerals Nuigini Limited Report 10631040-003-R-Rev 1., 217 p.
- MMTA - Minor Metals Trade Association 2023. Minor Metals. Tilgjengelig fra: <https://mmta.co.uk/metals/> (Hentet 17. januar 2023).

- Monecke, T., Petersen, S. and Hannington, M.D. 2014. Constraints on water depth of massive sulfide formation: Evidence from modern seafloor hydrothermal systems in arc-related settings. *Economic Geology*, vol. 109, No. 8, p 2079 - 2101.
- Mosar, J., Eide, E.A., Osmundsen, P.T., Sommaruga, A. and Torsvik, T.H., 2002. Greenland - Norway separation: a geodynamic model for the North Atlantic. *Nor. J. Geol.* 82 (4), 281–298.
- Nemčok, M., Sinha, S.T., Doré, A.G., Lundin, E.R., Mascle, J., and Rybár, S., 2016. Mechanisms of microcontinent release associated with wrenching-involved continental break-up; a review, *Geol. Soc., London, Spec. Publ.*, 431, 323.
- NGU - Norges geologiske undersøkelse 2023. Mineralressurser - Metaller. Tilgjengelig fra: <https://www.ngu.no/emne/metaller> (Hentet: 24. januar 2023).
- Olesen, O., Brønner, M., Ebbing, J. and Koziel, J. 2010. New aeromagnetic and gravity compilations from Norway and adjacent areas: Methods and applications. *Petroleum Geology Conferences series 2010; v.7*, p 559 - 586. doi:10.1144/0070559
- Oljedirektoratet 2018. Klassifisering av petroleumsressursene på norsk kontinentalsokkel - Oljedirektoratets ressursklassifikasjonssystem 2016. Tilgjengelig fra: <https://www.npd.no/regelverk/veiledninger/> (Hentet: 23. januar 2023).
- Pedersen, R. B., Thorseth, I. H., Olson, E. J., Hellevang, H., Okland, I., Baumberger, T., Lilley, M. D., Bruvoll, V., Mjelde, R., & Hafliðason, H. (2007). Hydrothermal activity and core complex formation at the Arctic Mid-Ocean Ridge: An overview of preliminary results of the H2DEEP expedition to the southern Knipovich Ridge at 73N. *American Geophysical Union, Fall Meeting 2007, Abstract #OS41C-05*, 5–7.
- Pedersen, R.B., Thorseth, I.H., Nygård, T.E., Liley, M.D and Kelley, D.S. 2010 a. Hydrothermal Activity at the Arctic Mid-Ocean Ridges. In: *Diversity of Hydrothermal Systems on Slow Spreading Ocean Ridges. Geophysical Monograph Series 188. American Geophysical Union*, p 67 - 89. DOI: 10.1029/2008GM000783.
- Pedersen, R.B., Rapp, H.T., Thorseth, I.H., Lilley, M.D., Barriga, F.J.A.S., Baumberger, T., Flesland, K., Fonseca, R., Früh-Green, G. and Jørgensen, S.L. 2010 b. Discovery of a black smoker vent field and vent fauna at the Arctic Mid-Ocean Ridge. *Nature Communications*, 1:106, p 1 - 6. DOI: 10.1038/ncomms1124
- Pedersen, R.B, B.R. Olsen, T. Barreyre, A. Bjerga, A. Denny, M. Heggernes Eilertsen, I. Fer, H. Hafliðason, J. Thomassen Hestetun, S Jørgensen, P.A. Ribeiro, I.H. Steen, H. Stubseid, A.H. S. Tandberg and I. Thorseth, 2021. Fagutredning mineralressurser i Norskehavet. Landskapstrekk, naturtyper og bentiske økosystemer. Rapport fra senter for dyphavsforskning, Universitetet i Bergen.
- Polteau, S., Planke, S., Zastrozhnov, D., Abdelmalak, M. M., Lebedeva-Ivanova, N., Planke, E. E., Svendsen, H. H., Mazzini, A., Gernigon, L., Myklebust, R., Kjølhamar, B. E., Pedersen, R. B., Sandstå, N. R. and Bünz, S., 2020. Upper cretaceous-paleogene stratigraphy and development of the Mimir High, Vøring transform margin, Norwegian Sea. *Marine and Petroleum Geology*, 122.

- Reimers, H. 2020. Identifying oceanic core complexes and associated detachment faulting on the ultraslow-spreading Mohs Ridge and links to SMS-deposits. *Mineralproduksjon, No 9, Norsk bergforening, ISSN 1893-1170 (online edition) ISSN 1893-1057 (printed edition)*, p. A25 - A53.
- Sahlström, F., Palinkaš, S. S., Dundas, S. H., Sendula, E., Cheng, Y., Wold, M., & Pedersen, R. B. (2022). Mineralogical distribution and genetic aspects of cobalt at the active Fåvne and Loki's Castle seafloor massive sulfide deposits, Arctic Mid-Ocean Ridges. *Ore Geology Reviews*, 105261
- Snook, B., Drivenes, K., Rollinson, G.K. and Aasly, K. 2018. Characterisation of mineralized Material from the Loki's Castle hydrothermal vent on the Mohn's Ridge. *Minerals*, 8, 576; doi:10.3390/min8120576
- Stensland, A., Baumberger, T., Mork, K.A., Lilley, M.D., Thorseth, I.H. and Pedersen, R.B. 2019. <sup>3</sup>He along the ultraslow spreading AMOR in the Norwegian-Greenland Seas. *Deep Sea Research Part I: Oceanographic Research Papers*, 147, 1-11.
- Stubseid, H., Bjerga, A., Halfidason, H., Pedersen, R.B., 2023. Volcanic evolution of an ultraslow-spreading ridge (in review). Preprint: <https://www.researchsquare.com/article/rs-2393567/v1>
- Styve, E., 2015. Petrogenesis of igneous samples from the Gjallar Ridge and the Vøring Spur. Master thesis, Department of Earth Science, University of Bergen
- Sudarikov, S., Narevsky, E. and Petrov, V. 2021. Identification of Two New Hydrothermal Fields and Sulfide Deposits on the Mid-Atlantic Ridge as a Result of the Combined Use of Exploration Methods: Methane Detection, Water Column Chemistry, Ore Sample Analysis, and Camera Surveys. *Minerals* 2021, 11, 726. <https://doi.org/10.3390/min11070726>
- Talwani, M., Eldholm, O., 1977. Evolution of the Norwegian–Greenland Sea, *Bull. geol. Soc. Am.*, 88, 969–999.
- Torsvik, T., Amundsen H.E.F., Trønnes, R.G., Doubrovine, P.V., Gaina, C., Kuznir, N.J., Steinberger, B., Corfu, F., Lewis, D.A., Griffin, W.L., Wemer, S.C. and Jamtveit, B. 2015. Continental crust beneath southeast Iceland. *PNAS*, pp 10. [www.pnas.org/cgi/doi/10.1073/pnas.1423099112](http://www.pnas.org/cgi/doi/10.1073/pnas.1423099112)
- U.S. Geological Survey 2022. Mineral commodity summaries 2022: U.S. Geological Survey, 202 p., <https://doi.org/10.3133/mcs2022>.
- Vorren, T. O., Laberg, J. S., Blaume, F., Dowdeswell, J. A., Kenyon, N. H., Mienert, J., Rumohr, J., and Werner, F., 1998. The Norwegian–Greenland Sea continental margins: morphology and late Quaternary sedimentary processes and environment. *Quaternary Science Reviews*, 17(1-3), 273- 302.
- Wessel, P., Müller, R.D. 2018. Published Magnetic Picks for Tectonic Reconstruction. Site: [www.soest.hawaii.edu/PT/GSFML/index.html](http://www.soest.hawaii.edu/PT/GSFML/index.html)
- Wold, M., 2022. Geochemical characterization of the Gnitahai seafloor massive sulfide deposit, Arctic Mid-Ocean Ridge, Master thesis, Department of Earth Science, University of Bergen

Zayonchek, A., Brekke, H., Leonov, J., Sokolov, S., Khytorskoj, M., Lundschien, B.A., Høy, T. and Stenløkk, J. 2011. Norwegian-Russian joint investigations around Svalbard and Franz Josef Land – evidence of a plate boundary in the making? **Abstract, Sixth International Conference on Arctic Margins (ICAM VI).**



DET KONGELIGE  
OLJE- OG ENERGIDEPARTEMENT

Ifølge liste

|           |            |                    |
|-----------|------------|--------------------|
| Deres ref | Vår ref    | Dato               |
|           | 19/2012-21 | 13. september 2021 |

### Fastsetting av konsekvensutredningsprogram for mineralvirksomhet på deler av norsk kontinentalsokkel

Det vises til Deres høringsinnspill til forslag til konsekvensutredningsprogram for mineralvirksomhet på deler av norsk kontinentalsokkel som hadde frist for kommentarer 12. april d.å.

Olje- og energidepartementet mottok til sammen 53 høringsinnspill i høringen. Departementet har behandlet innspillene og har på basis av Oljedirektoratets faglige gjennomgang av høringsinnspillene, fastsatt konsekvensutredningsprogrammet.

Utredningsprogrammet består av forslaget til utredningsprogram som ble sendt på høring og departementets behandling av innkomne høringsinnspill. Dokumentene er publisert på regjeringens nettsider: <https://www.regjeringen.no/no/aktuelt/program-for-konsekvensutredningen-for-mineralvirksomhet-pa-havbunnen-fastsatt/id2871090/>

Med hilsen

Dag Erlend Henriksen (e.f.)  
avdelingsdirektør

Cecilie Myklatun  
fagsjef

*Dokumentet er elektronisk signert og har derfor ikke håndskrevne signaturer*

Postadresse  
Postboks 8148 Dep  
0033 Oslo  
postmottak@oed.dep.no

Kontoradresse  
Akersgata 59  
oed.dep.no

Telefon\*  
22 24 90 90  
Org.nr.  
977 161 630

Avdeling  
Olje- og  
gassavdelingen

Saksbehandler  
Cecilie Myklatun  
22 24 61 72

## Mottakerliste

|   |                                   |      |                |
|---|-----------------------------------|------|----------------|
| Adepth Minerals AS                              | Solheimsgaten 7c                  | 5058 | BERGEN         |
| Allsite Geo AS                                  | Professor Olav Hanssens<br>vei 7A | 4021 | STAVANGER      |
| Artsdatabanken                                  | 1285 Torgarden                    | 7462 | TRONDHEIM      |
| Arunima Sen (Nord<br>Universitet)               |                                   |      |                |
| Direktoratet for<br>mineralforvaltning          | Postboks 3021 Lade                | 7441 | TRONDHEIM      |
| Direktoratet for strålevern og<br>atomsikkerhet |                                   |      |                |
| Equinor ASA                                     |                                   | 4035 | STAVANGER      |
| Fiskebåt  | Røysegata 15                      | 6003 | ÅLESUND        |
| Fiskeridirektoratet                             | Postboks 185 Sentrum              | 5804 | BERGEN         |
| Framtiden i våre hender                         | Fredensborgveien 24 G             | 0177 | OSLO           |
| GCE Node  | Tordenskjoldsgt. 9                | 4612 | KRISTIANSAND S |
| GCE Ocean Technology                            |                                   |      |                |
| Greenpeace Norge                                | Postboks 33 Torshov               | 0412 | OSLO           |
| Havforskningsinstituttet                        | Postboks 1870 Nordnes             | 5817 | BERGEN         |
| Helse- og<br>omsorgsdepartementet               | Postboks 8011 Dep                 | 0030 | OSLO           |
| Industri Energi                                 | Youngsgate 11                     | 0181 | OSLO           |
| Justis- og<br>beredskapsdepartementet           | Postboks 8005 Dep                 | 0030 | OSLO           |
| Kartverket                                      | Postboks 600 Sentrum              | 3507 | HØNEFOSS       |
| Klima- og miljødepartementet                    | Postboks 8013 Dep                 | 0030 | OSLO           |
| Kristiansund kommune                            | Postboks 178                      | 6501 | KRISTIANSUND N |
| Kunnskapsdepartementet                          | Postboks 8119 Dep                 | 0032 | OSLO           |
| Kystverket                                      | Postboks 1502                     | 6025 | Ålesund        |
| Landbruks- og<br>matdepartementet               | Postboks 8007 Dep                 | 0030 | OSLO           |
| Landsorganisasjonen i Norge                     | Youngsgate 11                     | 0181 | OSLO           |
| Meteorologisk institutt<br>MHWirth              | Postboks 43 Blindern              | 0313 | OSLO           |
| Miljødirektoratet                               | Postboks 5672 Sluppen             | 7485 | TRONDHEIM      |
| Møre og Romsdal<br>fylkeskommune                | Fylkeshuset                       | 6404 | MOLDE          |
| Natur og Ungdom                                 | Postboks 4783 Sofienberg          | 0506 | OSLO           |
| Naturvernforbundet                              | Mariboegate 8                     | 0183 | OSLO           |
| NORCE Norwegian Research<br>Centre AS           | Nygårdsgaten 112                  | 5008 | BERGEN         |
| Nordic Ocean Resources                          |                                   |      |                |
| Nordland fylkeskommune                          | Fylkeshuset                       | 8048 | BODØ           |

|   |                               |      |              |
|---|-------------------------------|------|--------------|
| Norges Fiskarlag  | Postboks 1233 Sluppen         | 7462 | TRONDHEIM    |
| Norges geologiske undersøkelse  | Postboks 6315 Sluppen         | 7491 | TRONDHEIM    |
| Norges rederiforbund  | Postboks 1452 Vika            | 0116 | OSLO         |
| Norges Teknisk-Naturvitenskapelige Universitet NTNU                           | Høgskoleringen 1              | 7491 | TRONDHEIM    |
| Norges vassdrags- og energidirektorat   | Postboks 5091 Majorstuen      | 0301 | OSLO         |
| Norsk Bergindustri  |                               | 0362 | OSLO         |
| Norsk forum for marine mineraler  | S.P. Andersens veg 15a        | 7031 | TRONDHEIM    |
| Norsk Industri  |                               |      |              |
| Norsk institutt for vannforskning - NIVA                                      | Gaustadalleen 21              | 0349 | OSLO         |
| Norsk olje og gass  | Postboks 8065                 | 4068 | STAVANGER    |
| Norsk Polarinstitutt  | Postboks 6606 Langnes         | 9296 | TROMSØ       |
| Norwegian Energy Partners (NORWEP)  | Postboks 631 Skøyen           | 0214 | OSLO         |
| Pelagisk forening   | Slottsgaten 3                 | 5003 | BERGEN       |
| Petro Arctic  | Postboks 301                  | 9615 | HAMMERFEST   |
| Petroleumstilsynet  | Postboks 599                  | 4003 | STAVANGER    |
| Riksantikvaren  | Postboks 1483 Vika            | 0116 | OSLO         |
| SABIMA - Samarbeidsrådet for biologisk mangfold                               | Postboks 6784 St. Olavs plass | 0130 | OSLO         |
| Samferdselsdepartementet  | Postboks 8010 Dep             | 0030 | OSLO         |
| Universitet i Bergen Senter for Dyphavforskning og Institutt for biovitenskap | Postboks 7803                 | 5020 | BERGEN       |
| Sjøfartsdirektoratet  | Postboks 2222                 | 5509 | HAUGESUND    |
| Statistisk Sentralbyrå  | Postboks 8131 Dep             | 0033 | OSLO         |
| Sysselmannen på Svalbard  | Postboks 633                  | 9171 | LONGYEARBYEN |
| Universitetet i Stavanger   |                               | 4036 | Stavanger    |
| Utenriksdepartementet   | Postboks 8114 Dep             | 0032 | OSLO         |
| WWF-Norge   | Postboks 6784 St. Olavs plass | 0130 | OSLO         |



## Åpningsprosess for utforskning og utvinning av havbunnsmineraler på norsk kontinentalsokkel

### Grunnlagsstudie: Pelagisk økosystem

#### Bakgrunn

Lov om mineralvirksomhet på kontinentalsokkelen (havbunnsmineralloven) trådte i kraft 1. juli 2019. Loven gir bestemmelser om hvordan områder kan åpnes for undersøkelser og utvinning, herunder krav til gjennomføring av en konsekvensutredning. Regjeringen har igangsatt en slik åpningsprosess for relevante områder.

Olje- og energidepartementet har forvaltningsansvaret for havbunnsmineraler og vil lede arbeidet med åpningsprosessen. Oljedirektoratet er departementets fagdirektorat og vil bistå departementet i gjennomføringen av konsekvensutredningen. Oljedirektoratet vil koordinere det faglige utredningsarbeidet og vil samhandle med andre relevante fagdirektorater herunder Miljødirektoratet som vil være miljømyndighet for mineralutvinning til havs.

Et forslag til program for konsekvensutredning er under utarbeidelse og vil være gjenstand for en høringsprosess. Programforslaget foreslår tematiske fagstudier for utredning av virkninger på henholdsvis naturforhold og miljø, og antatte næringsrelaterte, økonomiske og sosiale virkninger.

Vurdering av virkninger på naturressurser og miljø krever kunnskap om miljøtilstand og naturforhold innenfor område med mulig virksomhet og tilhørende influensområde. I tillegg er det viktig å ha oversikt over mangler og usikkerhet i kunnskapsgrunnlaget og videre kunnskapsbehov.

Det er vurdert at den beste kunnskapsoversikten for natur- og miljøforhold i norske farvann finnes hos statlige forskningsinstitutter samt academia. Det er derfor naturlig at de statlige instituttene utarbeider grunnlagsrapporter til konsekvensutredningen for sine respektive fagområder.

For tema «pelagisk økosystem<sup>1</sup>» er det vurdert at Havforskningsinstituttet har den beste kunnskapen om utredningsområdet. Dersom ytterligere kunnskap besittes av andre institusjoner eller academia, oppfordres det til dialog med disse for å sikre et best mulig kunnskapsgrunnlag. Bunndyrsamfunn tilknyttet dyphavsområdene blir beskrevet i en parallell studie ledet av Universitet i Bergen<sup>2</sup>, og inngår derfor ikke i arbeidsomfanget, men dialog og samarbeid er forutsatt som en del av dette oppdraget.

#### Utredningsområde

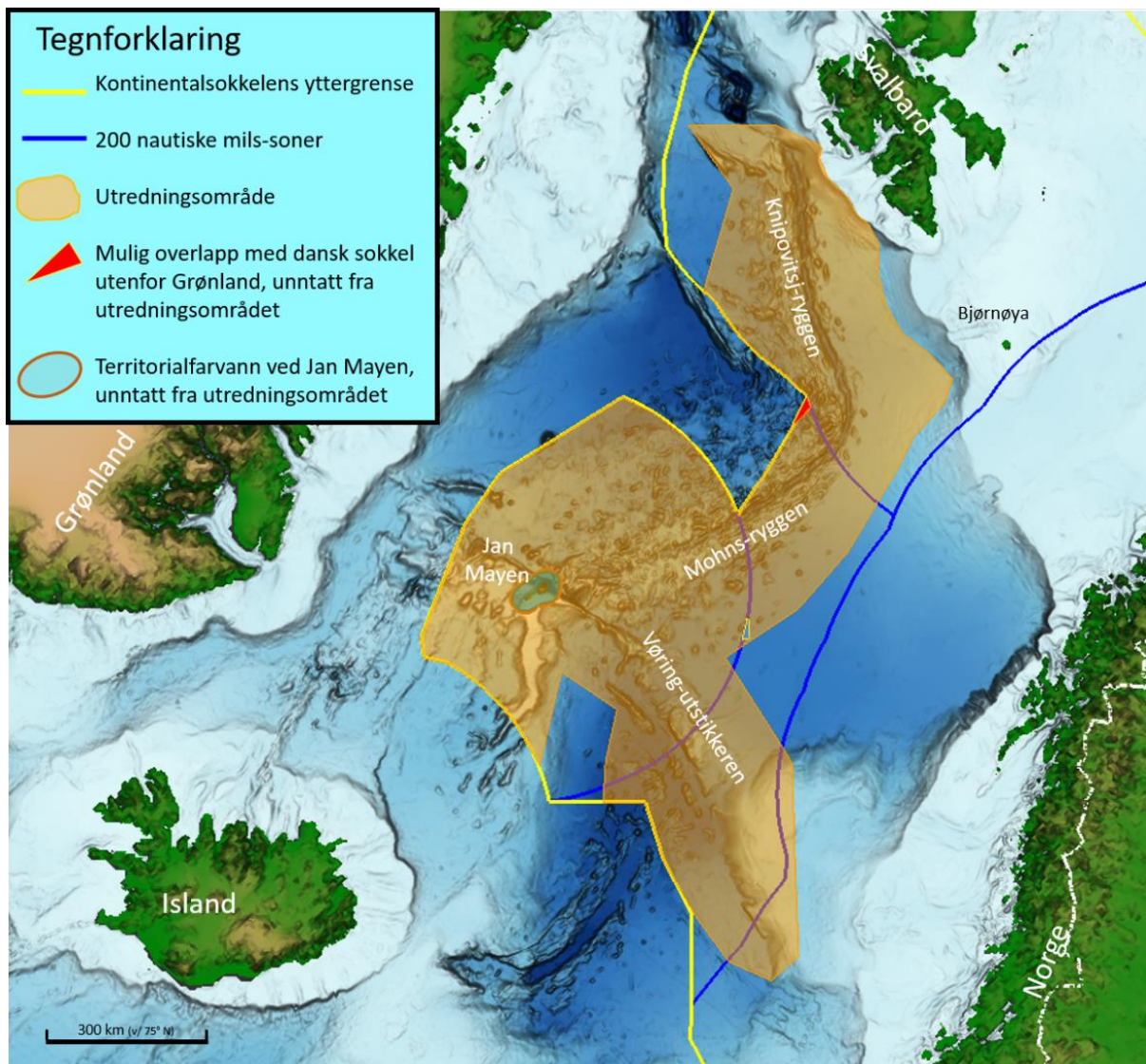
Det foreslåtte utredningsområdet omfatter områder med 100 - 4000 meters havdyp – generelt dypere enn 1500 meter, men med enkelte grunnere områder rundt Jan Mayen<sup>3</sup>. Utredningsområdet er vist i brunt i figur 1 og områder hvor havbunnsmineraler er identifisert ligger i hovedsak langs spredningsryggene (figur 2). De aktuelle områdene for mineralvirksomhet forventes å ligge langt fra kysten.

---

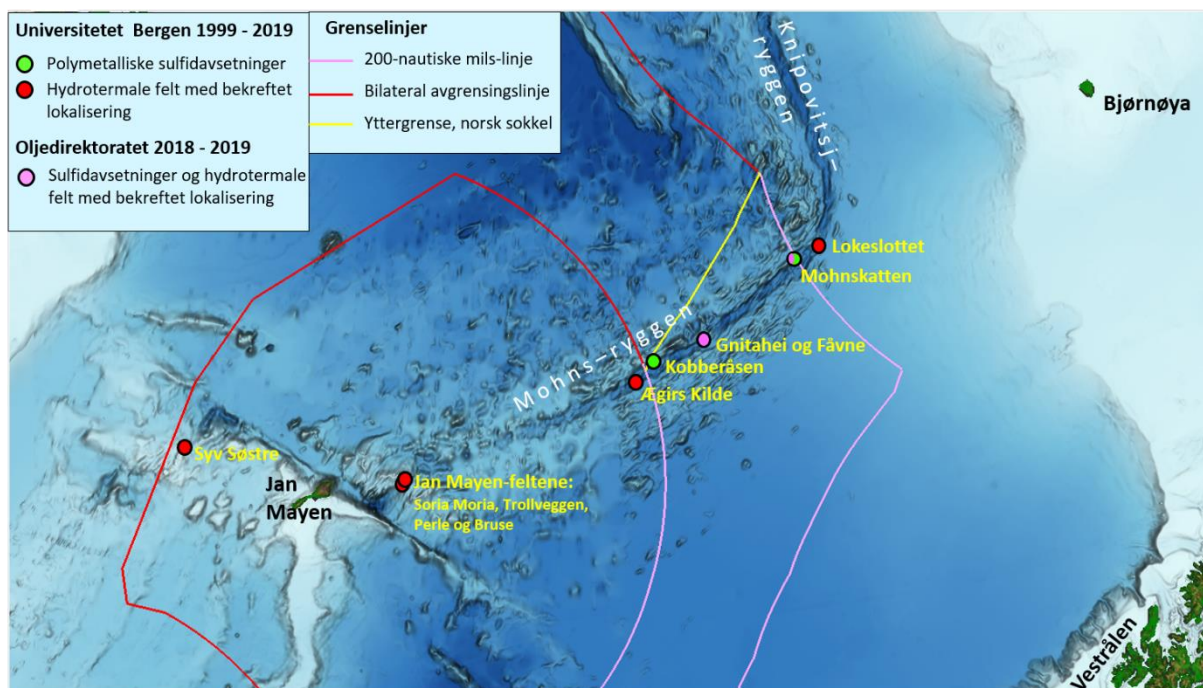
<sup>1</sup> Økosystemkomponenter og prosesser som er av særlig interesse for konsekvensutredningen med hensyn til det pelagiske økosystem

<sup>2</sup> Oljedirektoratet vil iinledningvis i arbeidet introdusere de to fagmiljøene for hverandre.

<sup>3</sup> Øya Jan Mayen, og en sone på 12 nm rundt denne, er vernet som naturreservat og inngår ikke i utredningsområdet.



Figur 1. Kart som viser området der de geologiske betingelsene er tilstede for å påvise økonomisk interessante forekomster av polymetalliske sulfider og manganskorper. Det markerte området (i brunt) foreslås som utredningsområde for konsekvensutredningen.



Figur 2. Kart som viser områder med kjente sulfidfunn langs spredningsryggene.

## Arbeidsbeskrivelse

Utvinning av havbunnsmineraler fra dyphavsområder kan medføre påvirkning i øvre vannlag og vannsøylen, eksempelvis relatert til utslipp av vannstrømmer og partikulært materiale. Mulige virkninger på miljø- og naturforhold fra slik virksomhet skal utredes gjennom spesifikke fagutredninger, anslagsvis i 2021/2022. Som bakgrunn for disse utredningene er det behov for en grunnlagsrapport som beskriver fysiske, kjemiske og biologiske prosesser i vannsøylen innen utredningsområdet. Siden det i disse områdene er tildels store vanddyb, og siden utredningsområdet også dekker et betydelig geografisk område, vil både fysiske, kjemiske og biologiske forhold ha stor variasjon, og sannsynligvis også svært ulike kunnskapsgrunnlag. En del av utredningsområdet overlapper eksempelvis med den Arktiske Front, normalt omtalt som av stor økologisk viktighet.

Følgende forhold skal beskrives:

- Oseanografi:
  - Kunnskap om havstrømmer i overflatelag og ulike vanddyb, herunder strømmønster, hastighet og retninger, vannmassefordeling.
  - Temperaturforhold varierende geografisk og med havdyp, samt sesongmessige variasjoner.
  - Næringsalter, klorofyll, oksygeninnhold og og havforsuring
  - Den Arktiske Front
  - Isutbredelse som relevant
- Planktonsamfunn:
  - Sammensetning og fordeling «i tid og rom», inkl. relevante mikrobiologiske samfunn /marinkjemi/biogeokjemi
- Fisk:
  - Relevante arter av bunnfisk og pelagisk fisk

- Evt. gyte- og oppvekstområder, beiteområder
- Sjøpattedyr:
  - Arter av sel og hval, eventuelle viktige områder med (sesongmessig) aggregering av dyr
- Bentisk-Pelagisk kobling (jf. arbeid i regi av UiB)
- Fremtidsutsikter; naturlig variabilitet og klimaendringer

Det er viktig at det tydelig kommer fram hva vi har kunnskap om og hva vi ikke har kunnskap om innenfor utredningsområdet, og i hvilke geografiske områder vi har kunnskap og hvor vi evt. mangler kunnskap. Rapporten skal derfor angi en vurdering av kvaliteten på tilgjengelig kunnskap (både hos HI og basert på gjennomgang av litteratur) og, som relevant, beskrive ytterligere kunnskap som vurderes som nyttig knyttet til eventuelle fremtidige prosjekter for utvinning av havbunnsmineraler i området.

### **Leveranse og tidsplan**

Resultatene fra arbeidet skal presenteres i en rapport (eksempelvis tilsvarende HI rapport 16-2012 til Olje- og energidepartementet i 2012 i struktur og detaljering) utgitt av aktuelt institutt og som skal være offentlig tilgjengelig.

Et rapportutkast skal leveres for kommentarer forut for ferdigstillelse. Rapportutkastet forventes for kommentarer innen 15. mai 2021.

Endelig rapport forventes levert i løpet av juni 2021.

Eventuelle leveranser av data på GIS-format vil bli avklart i løpet av oppdraget.

### **Budsjettramme**

Prosjektet har en ramme på inntil NOK 750 000,- eks. eventuell merverdiavgift.



## Havbunnsmineraler - Konsekvensutredningsprogram

### Naturforhold

Forslag til utredning i regi av Universitetet i Bergen.

Universitetet i Bergen (UiB) har siden slutten av 1990-årene hatt et omfattende marint forskningsprogram i dyphavet. Forskningene har vært rettet mot midthavsryggene og Norske-Grønlandshavet har vært det primære undersøkelsesområdet. Siden 2007 har forskningen vært drevet frem av et senter for fremragende forskning i geobiologi, og de siste fire årene gjennom et K.G. Jebsen Senter for dyphavsforskning.

Forskningsinnsatsen har i stor grad vært rettet mot grunnleggende problemstillinger. Den har primært omhandlet geologiske og geobiologiske prosesser og liv i ekstreme miljø. Forskningen har ført til viktige gjennombrudd og ny grunnleggende forståelse - og til oppdagelsen av marine mineralressurser og særegne økosystemer i norske havområder. Den har også resultert i bred ny kunnskap om ulike naturtyper og økosystemer i norske dyphavsområder. Senter for dyphavsforskning ved UiB vil kunne sammenfatte denne omfattende kunnskapsbasen for å etablere et best mulig faktagrunnlag omkring naturforhold.

Den tilgjengelig kunnskap er fordelt mellom publiserte forskningsartikler, PhD-avhandlinger og masteroppgaver, toktrapporter, observasjoner, datasett som foreløpig er upublisert, og individuell kunnskapsbase og innsikt. Store variasjoner i topografi og vandyp, geologi, oseanografi, vannkjemi og geokjemi resulterer i et mangfold av naturtyper og stor variasjon i biologiske samfunn. Relevant kunnskap er fordelt over en rekke fagområder og fagpersoner. For at faktagrunnlaget skal bli dekkende vil vi engasjere en rekke forskere som i dag arbeider ved senteret, og forskere som tidligere har vært tilknyttet forskningsmiljøet. Alle har viktig førstehånds kunnskap som er fremskaffet gjennom egen forskning.

### Tema som vil bli dekket i faktagrunnlaget

Faktagrunnlaget vil inneholde en generell del som inkluderer faglig bakgrunn og kontekst, samt en oversikt over forskningsaktiviteten i disse områdene. Den vil så ha en systematisk gjennomgang av de ulike økosystemene (naturtypene og deres biologiske samfunn) og deres sårbarhet. Kunnskapshull og usikkerheter knyttet til økosystemene sårbarhet vil også bli behandlet.

#### *Dyphavsmiljø og naturtyper*

- Vulkansk havbunn og naturtyper
- Sjøfjell, klipper og tilhørende naturtyper - deriblant områder med manganskorper
- Sedimentære avsetninger og naturtyper
- Aktive hydrotermale kilder og deres naturtyper
- Fossile (inaktive) hydrotermale avsetninger og deres naturtyper
- Dyphavsvannmasser og hydrotermale plumer

#### *Biologiske samfunn knyttet til ulike naturtyper*

For de aktuelle naturtypene vil følgende bli beskrevet og omtalt:

- Organismer rett over bunnen (*hyperbenthos*)
- Organismer tilknyttet bunnen (*benthos*)
- Organismer under havbunnen (*infauna*)
- Organismer i vannmassene (*pelagiske organismer*)
- Mikrobielle samfunn knyttet til aktive og fossile hydrotermale felt og annen havbunn
- Den geografiske utbredelsen av artene, grad av genutveksling mellom populasjoner og økosystemer (konnektivitet)

#### *Andre naturressurser*

- Genetiske og molekylære ressurser
- Fiskeriressurser
- Geotermiske ressurser

### *Usikkerhet og metodikk*

Beskrivelse av usikkerhet og kunnskapshull vil utgjøre en viktig del av faktagrunnlaget. Dette vil bli fremhevet under hvert tema, og det vil også bli behandlet overordnet som et eget tema. En gjennomgang av metodikken vil også være en viktig del av faktagrunnlaget.

### **Bidragstere**

**Naturtyper:** *Prof. Rolf B. Pedersen*, Senter for dyphavsforskning, UiB (vulkansk havbunn, tektoniske landskapsformer, aktive og inaktive hydrotermale felt), *Prof. Haflidi Haflidason*, Senter for dyphavsforskning, UiB, (sedimentær havbunn), *Prof. Ingunn Thorseth* (hydrotermale felt, geobiologiske samspill), *Dr. Thibaut Barreyre*, Senter for dyphavsforskning, UiB, (hydrotermale felt, hydrotermale plumer, geotermiske ressurser).

**Biologiske samfunn:** *Dr. Bernt Rydland Olsen*, Rådgivende Biologer AS / Høgskulen på Vestlandet, (plankton). *Dr. Mari H. Eilertsen*, Senter for dyphavsforskning, UiB (benthos). *Dr. Jon T. Hestetun*, NORCE Miljø (benthos). *Dr. Anne Helene Tandberg*, Universitetsmuseet i Bergen, UiB (hyperbenthos). *Dr. Pedro Ribeiro*, Senter for dyphavsforskning, UiB (benthos), *Dr. Steffen Jørgensen*, Senter for dyphavsforskning, UiB (dyp biosfære). *Prof. Ida Steen*, Senter for dyphavsforskning, UiB (hydrotermale mikrobielle samfunn, genetiske ressurser).

Det skal opprettes dialog med andre universiteter og forskningsmiljø i Norge for å sikre at all relevant tilgjengelig kunnskap blir vurdert og omtalt.

### **Omfang og kostnader**

Gruppen v bidragstere består av forskere som alle har arbeidet ved Senter for Geobiologi og/eller K. G. Jebsen Senter for dyphavsforskning. Syv av bidragstere er enten tilsatt i midlertidige stillinger ved UiB, eller i selskaper som krever timebasert inntjening. Det er beregnet av hver av disse trenger ett månedsverk for å sammenstille eksisterende kunnskap, til koordinering, rapportskrivning etc. Fire av bidragstere er i faste vitenskapelige stillinger. Hver av disse vil trenge to uker med teknisk assistanse for å gjennomføre oppdraget. Totalt vil dette utgjøre en kostnad på kr 1.350.000 ekskl. mva.

## Åpningsprosess for utforskning og utvinning av havbunnsmineraler på norsk kontinentalsokkel

### Grunnlagsstudie: Sjøfugl

#### Bakgrunn

Lov om mineralvirksomhet på kontinentalsokkelen (havbunnsmineralloven) trådte i kraft 1. juli 2019. Loven gir bestemmelser om hvordan områder kan åpnes for undersøkelser og utvinning, herunder krav til gjennomføring av en konsekvensutredning. Regjeringen har igangsatt en slik åpningsprosess for relevante områder.

Olje- og energidepartementet har forvaltningsansvaret for havbunnsmineraler og vil lede arbeidet med åpningsprosessen. Oljedirektoratet er departementets fagdirektorat og vil bistå departementet i gjennomføringen av konsekvensutredningen. Oljedirektoratet vil koordinere det faglige utredningsarbeidet og vil samhandle med andre relevante fagdirektorater herunder Miljødirektoratet som vil være miljømyndighet for mineralutvinning til havs.

Et forslag til program for konsekvensutredning er under utarbeidelse og vil være gjenstand for en høringsprosess. Programforslaget foreslår tematiske fagstudier for utredning av virkninger på henholdsvis naturforhold og miljø, og antatte næringsrelaterte, økonomiske og sosiale virkninger.

Vurdering av virkninger på naturressurser og miljø krever kunnskap om miljøtilstand og naturforhold innenfor område med mulig virksomhet og tilhørende influensområde. I tillegg er det viktig å ha oversikt over mangler og usikkerhet i kunnskapsgrunnlaget og fremtidig kunnskapsbehov.

Det er vurdert at den beste kunnskapsoversikten for natur- og miljøforhold i norske farvann finnes hos statlige forskningsinstitutter samt academia. Det er derfor naturlig at de statlige instituttene utarbeider grunnlagsrapporter til konsekvensutredningen for sine respektive fagområder.

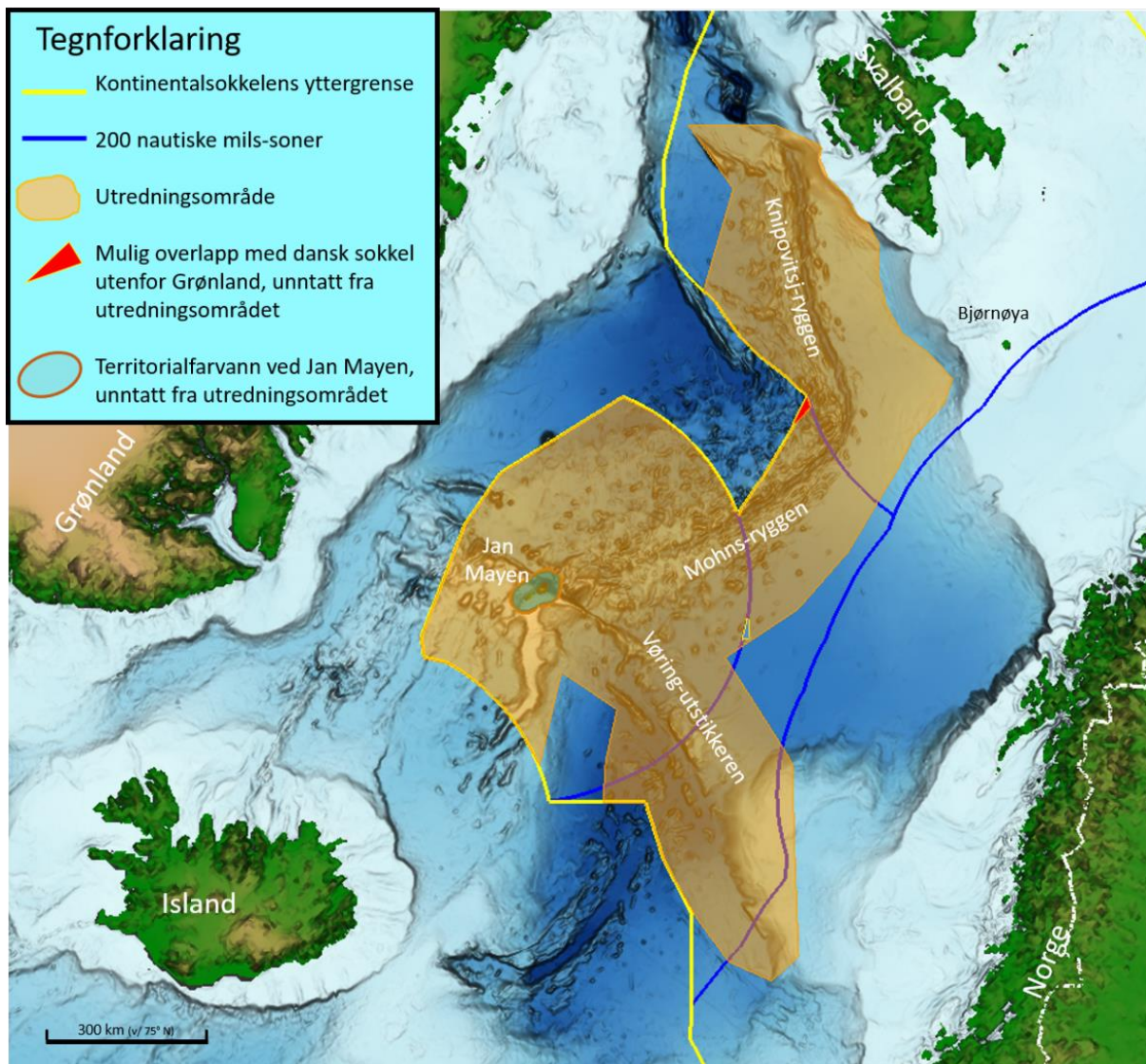
For tema sjøfugl er det vurdert at Norsk polarinstitutt (NP) og Norsk institutt for naturforskning (NINA) sammen har den beste kunnskapen om sjøfugl i utredningsområdet, hvor NP har hovedfokus overlappende med aktuelt geografisk område. Dersom viktig ytterligere kunnskap besittes av andre institusjoner eller academia, oppfordres det til dialog med disse for å sikre et best mulig kunnskapsgrunnlag.

#### Utredningsområde

Det foreslåtte utredningsområdet omfatter områder med 100 - 4000 meters havdyp – generelt dypere enn 1500 meter, men med enkelte grunnere områder rundt Jan Mayen<sup>1</sup>. Utredningsområdet er vist i brunt i figur 1 og områder hvor havbunnsmineraler er identifisert ligger i hovedsak langs spredningsryggene (figur 2). De aktuelle områdene for mineralvirksomhet forventes å ligge langt fra kysten.

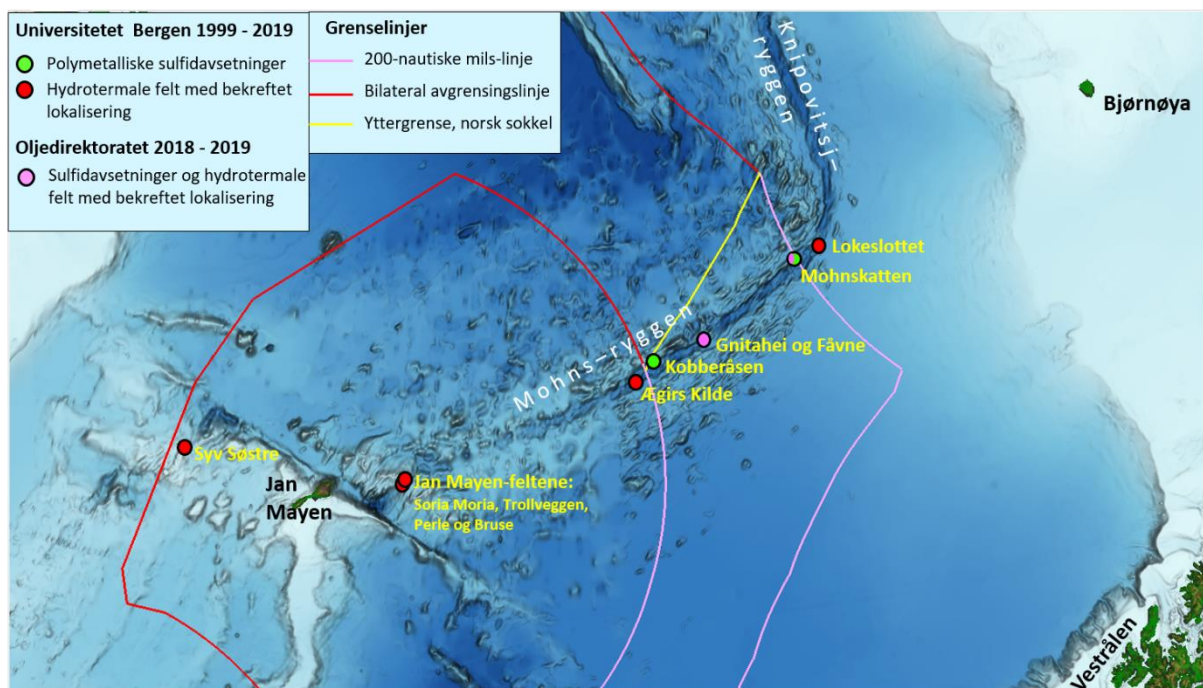
---

<sup>1</sup> Øya Jan Mayen, og en sone på 12 nm rundt denne, er vernet som naturreservat og inngår ikke i utredningsområdet.



Figur 1. Kart som viser området der de geologiske betingelsene er tilstede for å påvise økonomisk interessante forekomster av polymetalliske sulfider og manganskorper. Det markerte området (i brunt) foreslås som utredningsområde for konsekvensutredningen.





Figur 2. Kart som viser områder med kjente sulfidfunn langs spredningsryggene.

## Arbeidsbeskrivelse

Havbunnsmineralvirksomhet vurderes i utgangspunktet å ikke medføre høy risiko for direkte skade på sjøfugl, selv om mindre utslipp av drivstoff, hydraulikkvæske eller kjemikalier ikke kan utelukkes. Det kan imidlertid være problemstillinger som indirekte kan ha virkninger på sjøfugl, av ulik grad og karakter, herunder mulige partikkelutslipp som påvirker næringstilgang, lys på innretninger, osv. For å kunne vurdere virkninger på sjøfugl av denne type påvirkning er en grunnlagsrapport nødvendig.

Grunnlagsrapporten skal adressere følgende tema basert på tilgjengelig kunnskap:

- Arter som forekommer i området, omfang og bestandstilhørighet
- Status for hekkebestander (Jan Mayen evt. andre bestander som benytter området til næringssøk i hekkeperioden)
- Fordeling av sjøfugl i området i ulike sesonger, eksempelvis basert på SEATRACK
- En vurdering av viktigheten av ulike delområder for sjøfugl (innenfor utredningsområdet)

Rapporten skal videre angi en vurdering av kvaliteten på tilgjengelig kunnskap, kunnskapsmangler og, beskrive ytterligere kunnskapsbehov som vurderes som nødvendig for å avdekke eventuelle virkninger av mineralutvinning til havs på sjøfugl.

## Leveranse og tidsplan

Resultatene fra arbeidet skal presenteres i en rapport utgitt av aktuelt institutt og som skal være offentlig tilgjengelig.

Et rapportutkast skal leveres for kommentarer forut for ferdigstilling. Rapportutkastet forventes for kommentarer innen 15. mai 2021.

Endelig rapport forventes levert i løpet av juni 2021.

Eventuelle leveranser av data på GIS-format vil bli avklart i løpet av oppdraget.

**Budsjettramme**

Prosjektet har en ramme på inntil NOK 500 000,- eks. eventuell merverdiavgift.



Rapportvedlegg til grunnlagsrapport - Fiskeriaktiviteten i utredningsområdet for mineralvirksomhet

## Utenlandsk fiskeriaktivitet i deler av utredningsområdet hvor Norge ikke har fiskerijurisdiksjon

Kristian L. Skaar mars 2023

# Rapportvedlegg

Utenlandsk fiskeriaktivitet i deler av utredningsområdet hvor Norge ikke har fiskerijurisdiksjon

|  |   |   |
|--|---|---|
| <b>Årstall</b><br>2023                           | <b>Ansvarlig avdeling:</b><br>Avdeling for areal, miljø og statistikk | <b>Emneord:</b><br>Havbunnsmineraler, fiskeriaktivitet, kontinentalsokkel |
| <b>Arkivsaksnummer:</b><br>[Arkivsaksnummer]     | <b>Dato utgitt:</b><br>[Dato utgitt]                                  | <b>Totalt antall sider:</b><br>8  |
| <b>Saksansvarlig:</b><br>Kristian Landmark Skaar |   |   |

Utenlandsk fiskeriaktivitet i deler av utredningsområdet hvor Norge ikke har fiskerijurisdiksjon

Sammendrag

I forbindelse med åpningsprosessen for undersøkelse og utvinning av havbunnsmineraler på norsk kontinentalsokkel utarbeidet Fiskeridirektoratet en grunnlagsrapport om fiskeriaktiviteten i havområdene som skal utredes for åpning av mineralvirksomhet. Rapporten beskrev norsk og utenlandsk fiskeriaktivitet i de deler av utredningsområdet som er underlagt norsk fiskerijurisdiksjon, men ikke utenlandsk aktivitet i de delene av utredningsområdet som er internasjonalt farvann og som forvaltes av kyststatene via NEAFC. Utenlandske data fra internasjonalt farvann, for perioden 2013-2019, ble senere tilgjengeliggjort via ICES og publiseres nå som et vedlegg til grunnlagsrapporten.

Rapporten beskriver fiskeriaktiviteten fra utenlandske fartøy i området basert på fisketimer og totalkvantum innenfor ruter på 15 km<sup>2</sup>.



# Rapportvedlegg

Utenlandsk fiskeriaktivitet i deler av utredningsområdet

## Innholdsfortegnelse

|   |   |
|---|---|
| 1. Bakgrunn for rapporten .....                       | 2 |
| 2. Aktivetsbeskrivelse .....                          | 2 |
| 2.1. Datagrunnlag og metode.....                      | 2 |
| 2.2. Fiskeriaktivitet .....                           | 2 |
| 2.2.1. Generell vurdering av fiskeriaktiviteten ..... | 5 |
| 3. Begrensinger i analysen.....                       | 6 |
| 3.1. Manglende data.....                              | 6 |
| 3.2. Redskapsopplysninger .....                       | 6 |
| 4. Kildeliste .....                                   | 7 |

## 1. Bakgrunn for rapporten

I forbindelse med åpningsprosessen for undersøkelse og utvinning av havbunnsmineraler på norsk kontinentalsokkel utarbeidet Fiskeridirektoratet en grunnlagsrapport om fiskeriaktiviteten i havområdene som skal utredes for åpning av mineralvirksomhet. Rapporten beskrev norsk og utenlandsk fiskeriaktivitet i de deler av utredningsområdet som er underlagt norsk fiskerijurisdiksjon, men ikke utenlandsk aktivitet i de delene av utredningsområdet som er internasjonalt farvann og som forvaltes av kyststatene via NEAFC. Det ble derfor sendt en forespørsel via ICES om utlevering av sammenholdte sporingsdata og fangststatistikk for utenlandske fartøy i delene av utredningsområdet som er internasjonalt farvann. Data for perioden 2013-2019 ble oversendt Fiskeridirektoratet i slutten av 2022 og publiseres nå som et vedlegg til grunnlagsrapporten.

## 2. Aktivitetsbeskrivelse

### 2.1. Datagrunnlag og metode

For å beskrive fiskeriaktiviteten for utenlandske fartøy i det gitte området ble det oversendt årsvise data for fisketimer og totalfangst basert på satellittsporingsdata (VMS) og loggbok data. For analyser av romlige fiskeridata benytter ICES seg av en standard metode (ICES, 2017) hvor fisketimer og totalfangst summeres innenfor såkalte «c-squares» (0,05° x 0,05°, omtrent 15 km<sup>2</sup> ved 60°N breddegrad). For mer om metode, metadata og begrensninger i data se kildeliste.

VMS- og fangstdata for perioden 2013-2019 ble samlet inn på forespørsel til ICES medlemsland. I påfølgende tabell listes landene som leverte data av tilfredsstillende kvaliteten og hvilke land som ikke gjorde det.

Tabell 1: Oversikt over hvilke medlemsland som har sendt inn av data og er med i analysen. Land i uthevet skrift er utelatt fra analysen.

| Land            | Innsendt data | Land            | Innsendt data                  |
|-----------------|---------------|-----------------|--------------------------------|
| Belgia          | Ja            | Litauen         | Ja                             |
| Danmark         | Ja            | Nederland       | Ja                             |
| <i>Færøyene</i> | <i>Nei</i>    | <i>Norge</i>    | <i>Ja, men tatt ut</i>         |
| Frankrike       | Ja            | Polen           | Ja                             |
| Tyskland        | Ja            | <i>Portugal</i> | <i>Ja, men dårlig kvalitet</i> |
| <i>Grønland</i> | <i>Nei</i>    | <i>Russland</i> | <i>Nei</i>                     |
| Irland          | Ja            | Spania          | Ja                             |
| Island          | Ja            | Sverige         | Ja                             |
| Latvia          | Ja            | Storbritannia   | Ja                             |
| Estland         | Ja            |                 |                                |

### 2.2. Fiskeriaktivitet

Følgende kapittel viser fiskeriaktiviteten som fisketimer og totalfangst fra omtrent 15 km<sup>2</sup> store ruter. Mørkere farge representerer høyere kvantum fisket.



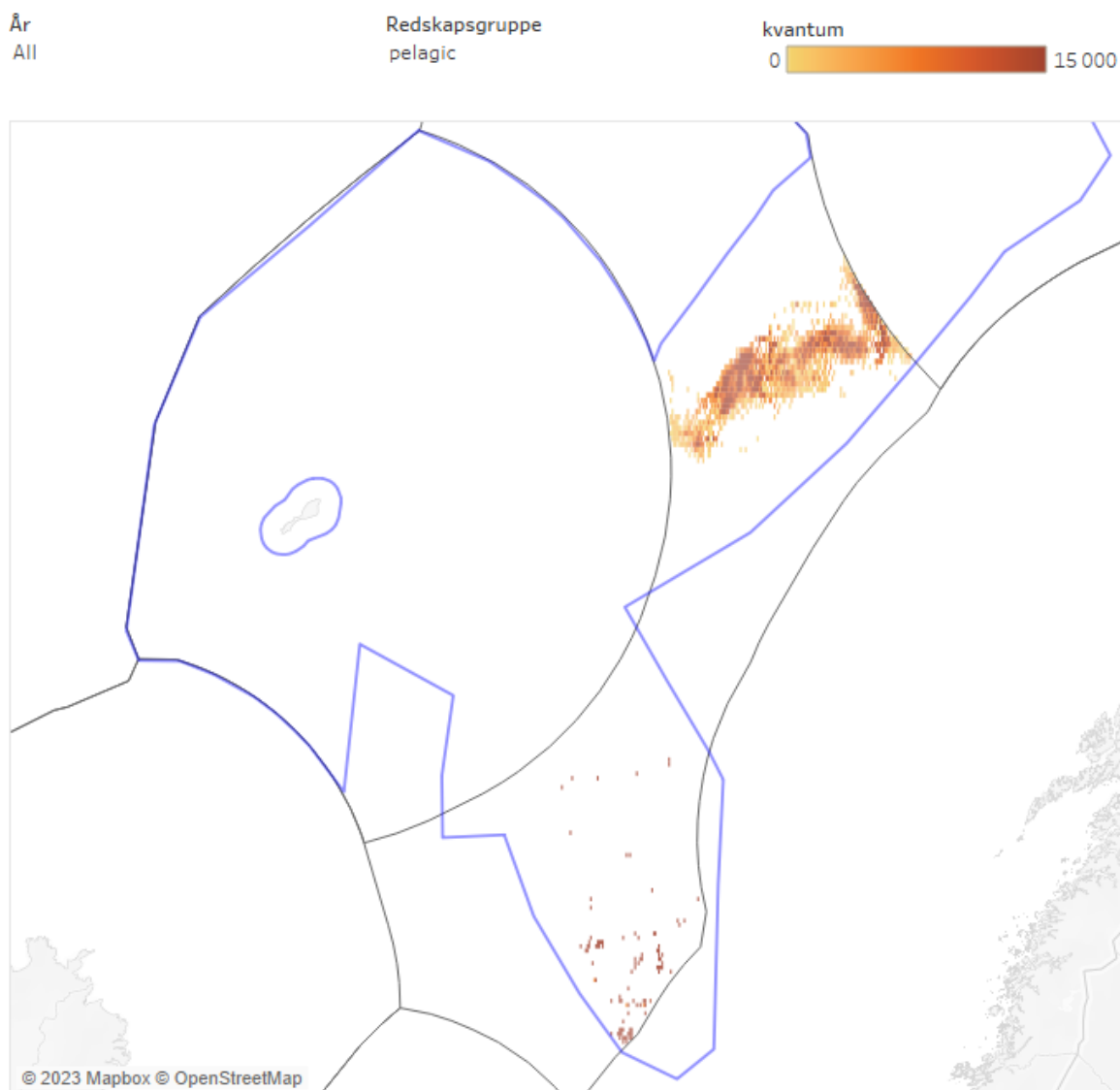


Figur 2.1 Oversikt over fiskeriaktiviteten fra utenlandske fartøy i de delene av internasjonalt farvann som er med utredningsområdet for mineralvirksomhet. Figuren viser årlig totalkvantum fisket fra den pelagiske flåten i perioden 2013-2016. Tabellen under viser totalfangst (kg) for hele området og timer som fisketimer basert på fart (1,5 kn – 4,5 kn).





Figur 2.2 Oversikt over fiskeriaktiviteten fra utenlandske fartøy i de delene av internasjonalt farvann som er med utredningsområdet for mineralvirksomhet. Figuren viser årlig totalkvantum fisket fra den pelagiske flåten i perioden 2017-2019. Tabellen under viser totalfangst (kg) for hele området og timer som fisketimer basert på fart (1,5 kn – 4,5 kn).

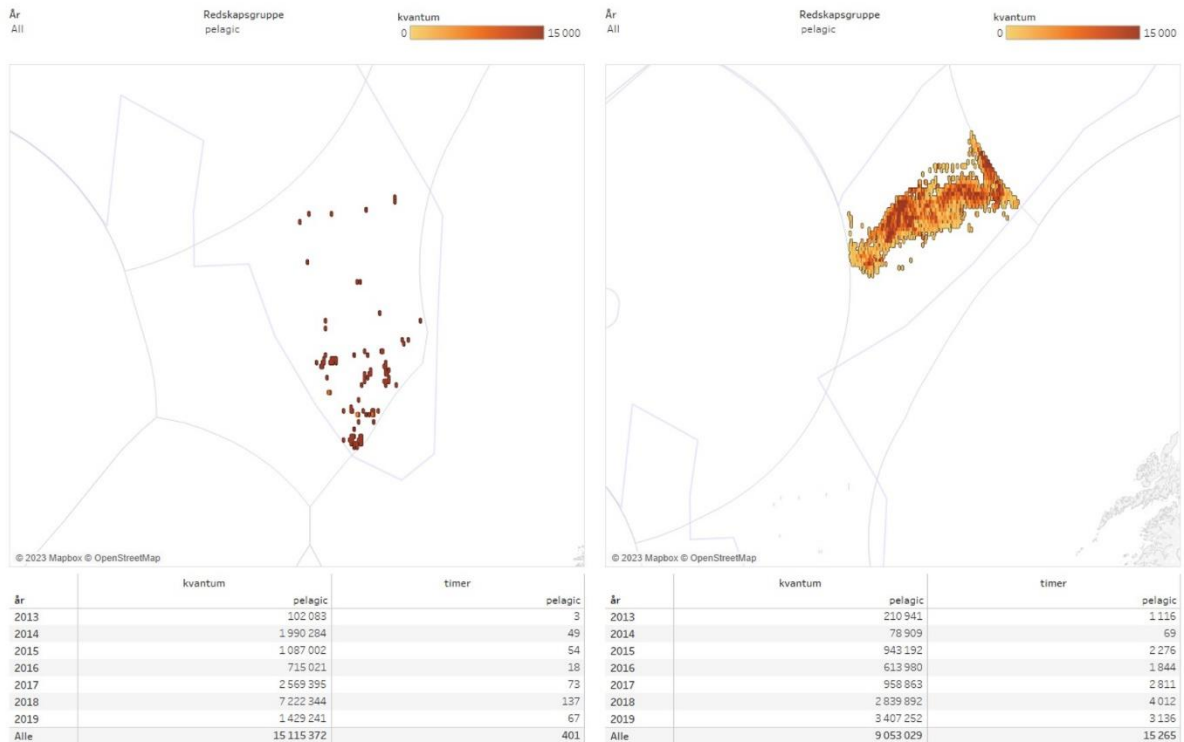


| år   | kvantum |            | timer |         |
|------|---------|------------|-------|---------|
|      |         | pelagic    |       | pelagic |
| 2013 |         | 313 024    |       | 1 119   |
| 2014 |         | 2 069 193  |       | 118     |
| 2015 |         | 2 030 194  |       | 2 331   |
| 2016 |         | 1 329 001  |       | 1 862   |
| 2017 |         | 3 528 258  |       | 2 885   |
| 2018 |         | 10 062 236 |       | 4 149   |
| 2019 |         | 4 836 494  |       | 3 203   |
| Alle |         | 24 168 401 |       | 15 666  |

Figur 2.3 Totaloversikt over fiskeriaktiviteten fra utenlandske fartøy for perioden 2013-2019. Figuren viser årlig totalkvantum fisket fra den pelagiske flåten i perioden 2017-2019. Tabellen under viser totalfangst (kg) for hele området og timer som fisketimer basert på fart (1,5 kn – 4,5 kn).

### 2.2.1. Generell vurdering av fiskeriaktiviteten

Figurene viser hvor det har vært aktivitet av utenlandske fartøy og gir et anslag over hvilke områder som kan være mer viktige enn andre. De viser også at det er kan være relativt store variasjoner fra år til år. Jevnt over fiskes det større kvantum i områdene sør for 69°N, samtidig som antall fisketimer i dette området er færre enn i området nord for 69°N. Sett fra et verdiskapings perspektiv vil området i sør dermed kunne betraktes viktigere enn i nord.



Figur 2.4 T.v. totalkvantum fisket og antall fisketimer for området sør for 69°N i perioden 2013-2019. T.h. totalkvantum fisket og antall fisketimer for området nord for 69°N i perioden 2013-2019.

I dataene fra ICES er det kun oppgitt totalfangst per rute og det er derfor ingen opplysninger om art. Det fiskes både sild og makrell i området av den norske flåten og det derfor sannsynlig at dette gjelder også for den utenlandske flåten. Dette kan videre forklare noe av svingningene i kvantum fra år til år.

### 3. Begrensinger i analysen

#### 3.1. Manglende data

I grunnlagsdataene mangler det opplysninger fra fiskerinasjoner som blant annet Russland, Færøylene og Grønland. Dette fører til at den faktiske fiskeriaktiviteten sannsynligvis er høyere enn analysen viser. Det er likevel sannsynlig at områdene det fiskes i er de samme som vist på figurene, men at kvantum og intensitet er høyere.

#### 3.2. Redskapsopplysninger

I grunnlagsdataene er not og flytetrål definert som pelagiske redskap, mens bunnredskaper som bunntrål, bomtrål, snurrevad og skrape er definert som bentiske redskaper. Havdypet i området som er med i analysen varierer fra 1800 m – 4000 m, og det er ikke kjent at det foregår et kommersielt fiskeri med bentiske redskaper i disse områdene. Likevel er det noen år oppgitt fangst med bentiske redskaper. Dette kan skyldes feil opplysninger i dagboken, men vi har likevel valgt å utelate fangst og fisketimer som er oppgitt å være tatt med bentiske redskaper. Fangst tatt med det som opplyses å være bentiske redskaper utgjør mindre enn 0,5 prosent av totalkvantum og mindre enn 4 prosent av totalt antall fisketimer, og anses derfor ikke å kunne påvirke totalbildet av fiskeriaktiviteten.

#### 4. Kildeliste

ICES 2017. OSPAR request on the production of spatial data layers of fishing intensity/pressure. In Report of the ICES Advisory Committee, 2017. ICES Advice 2017, ICES Technical Service, sr.2017.17. 8 pp

ICES. 2022. Norwegian special request on the production of spatial data layers of fishing in areas relevant to future extraction of deep sea minerals. In Report of the ICES Advisory Committee, 2022. ICES Advice 2022, sr.2022.16.

<https://doi.org/10.17895/ices.advice.10.17895>

[https://github.com/ices-taf/2022\\_sr.2022.16\\_TechnicalService](https://github.com/ices-taf/2022_sr.2022.16_TechnicalService)

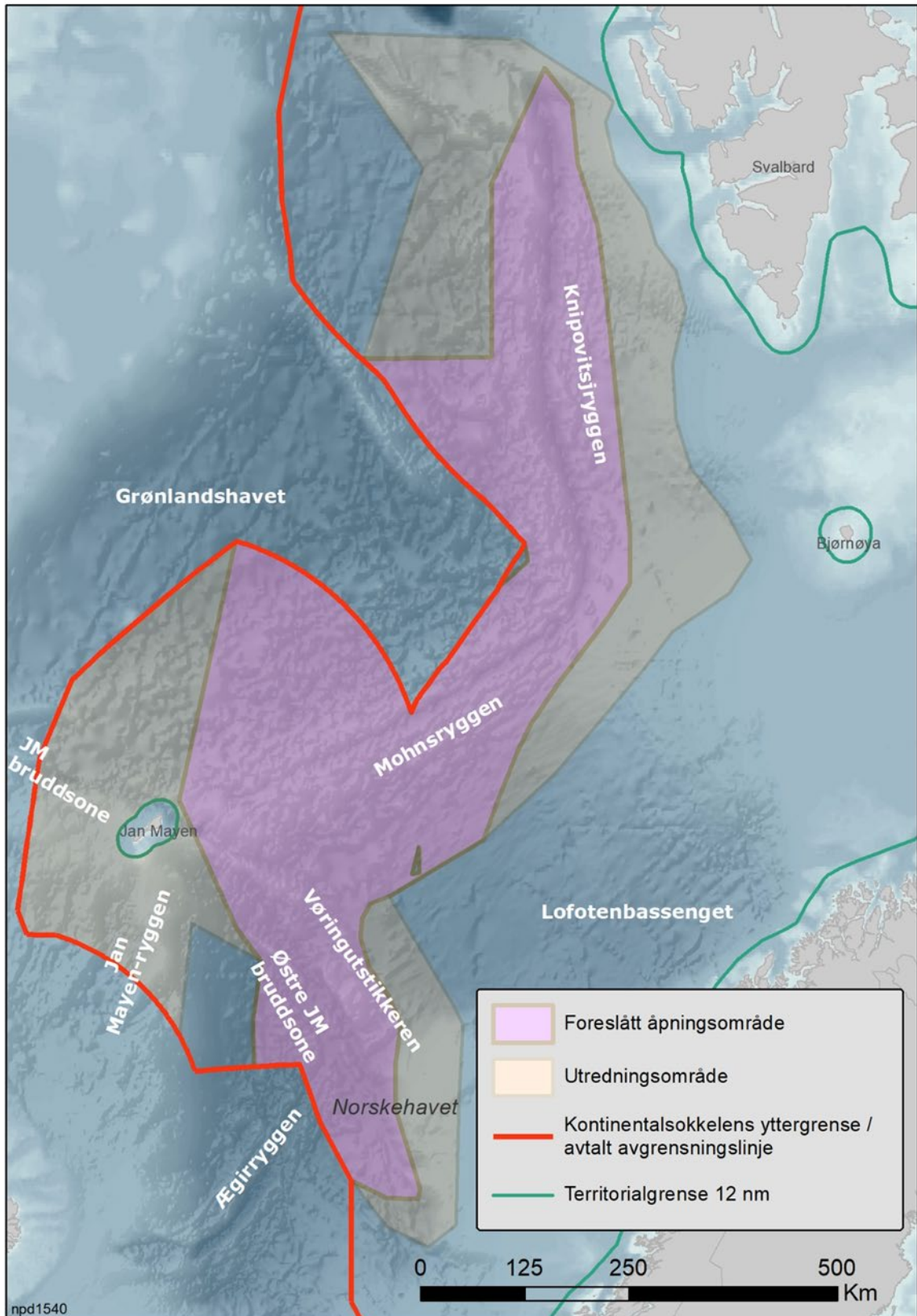




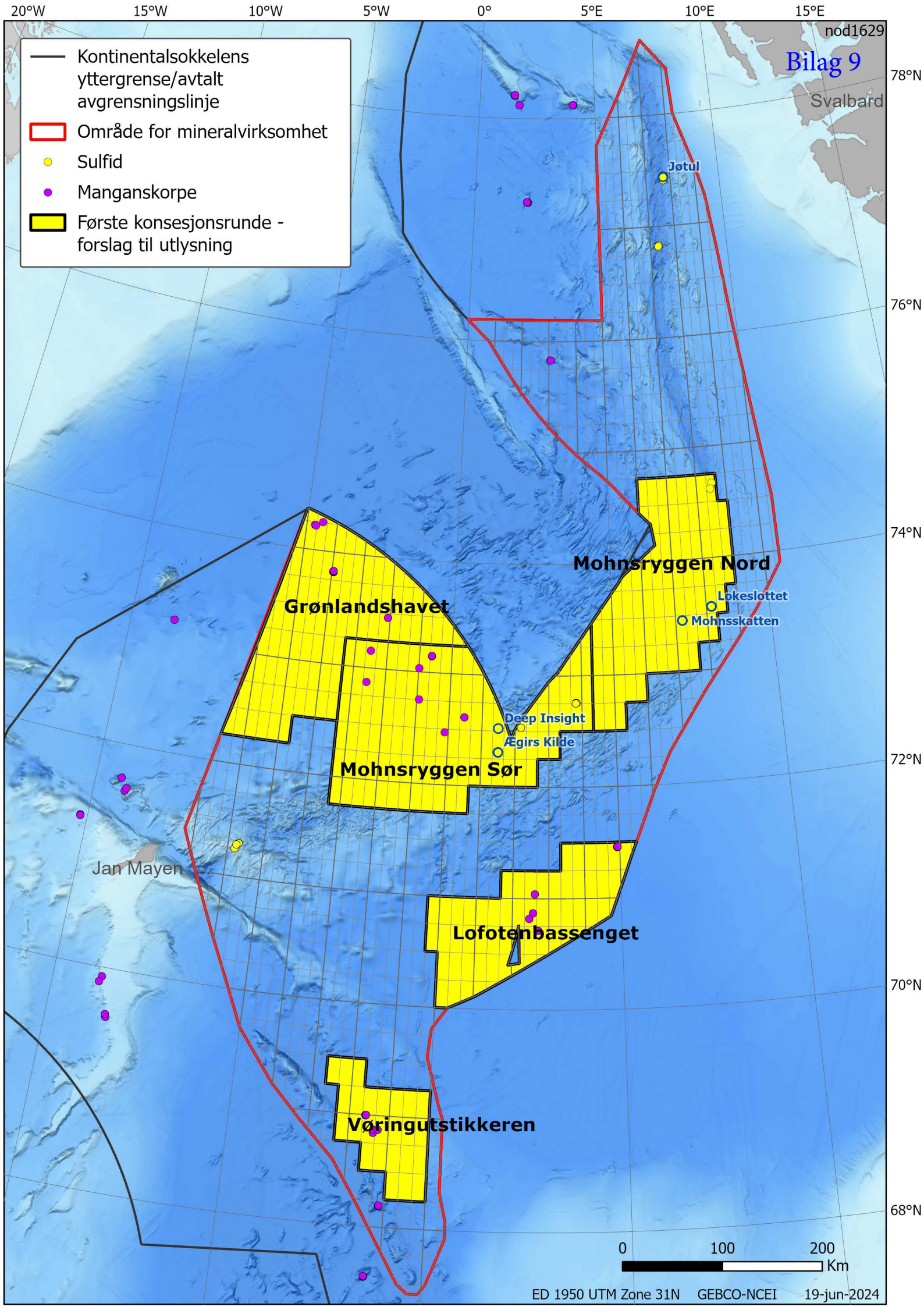
## FISKERIDIREKTORATET

Telefon: 55 23 80 00  
E-post: [postmottak@fiskedir.no](mailto:postmottak@fiskedir.no)  
Internett: [www.fiskeridir.no](http://www.fiskeridir.no)

Livet i havet - vårt felles ansvar







- Kontinentalsokkelens yttergrense/avtalt avgrensningslinje
- ▭ Område for mineralvirksomhet
- Sulfid
- Manganskorpe
- ▭ Første konsesjonsrunde - forslag til utlysning







# Høring av arealforslag – Utlysning av områder for mineralvirksomhet på havbunnen

Høring | Dato: 26.06.2024 | Energidepartementet (<http://www.regjeringen.no/no/dep/ed/id750/>)

**Status:** På høring

**Høringsfrist:** 26.09.2024

## Høringsbrev

Vår ref.: 24/1690

Regjeringen presenterte sitt forslag til åpning av område og sin strategi for forvaltning av havbunnsmineralressursene på norsk kontinentalsokkel i Meld. St. 25 (2022-2023) «*Mineralverksemd på norsk kontinentalsokkel – opning av areal og strategi for forvaltning av ressursane*». Stortinget sluttet seg til hovedlinjene i strategien, herunder forslaget om å åpne et gitt område for slik virksomhet, i januar 2024 ved sin behandling av Innst. 162 S (2023-2024). Kongen i statsråd fattet i april i år det formelle vedtaket om åpning av et nærmere avgrenset område for havbunnsmineralvirksomhet.

Denne høringen av arealforslag i den første konsesjonsrunden er det neste, viktige skrittet i den etablerte ressursforvaltningsstrategien. De vilkår som framgår av Meld. St. 25 (2022-2023) og Innst. 162 S (2023-2024), herunder for å ivareta hensynet til miljø, kunnskapsinnhenting, sameksistens og nasjonal sikkerhet, vil ligge til grunn for departementets gjennomføring av konsesjonsrunden.

Den etablerte forvaltningsstrategien fastslår at Norge skal være verdensledende når det gjelder en fakta- og kunnskapsbasert forvaltning av havbunnsmineralressursene som er helhetlig, bærekraftig og forsvarlig. Hensynet til miljø vil bli ivaretatt i alle faser av virksomheten. Rammene for virksomheten skal være basert på føre-var-prinsippet og en økosystembasert tilnærming.

Stabile og forutsigbare rammebetingelser forankret i fakta og kunnskap er viktig for å legge til rette for verdiskaping knyttet også til havbunnsmineraler. Departementet vil vektlegge det å etablere og opprettholde klare og forutsigbare rammevilkår for aktørene innenfor havbunnsmineralvirksomheten. Det vil videre legges opp til konkurranse om oppdrag til næringen slik at konkurransedyktige norskbaserte aktører kan delta i konkurransen om oppdrag knyttet til havbunnsmineralvirksomheten på kontinentalsokkelen.

I tråd med den etablerte strategien for forvaltning av havbunnsmineralressursene, følges åpningsbeslutningen nå opp med å sette i gang prosessen med å utlyse områder og tildele tillatelser under havbunnsmineralloven. Den første konsesjonsrunden som nå sendes på høring markerer starten på arealtildelinger for havbunnsmineraler. Departementet vil føre en arealpolitikk som legger til rette for en skrittvis, kunnskapsbasert og rasjonell utforskning av det arealet som er åpnet for slik virksomhet.

Gjennom konsesjonsrunden legges det til rette for konkurranse om arealer fra ulike kommersielle aktører. Departementet vil som del av dette legge til rette for at kommersielle aktører gradvis kan bygge opp en portefølje av tillatelser, slik at virksomhet kan vare over tid. Hensynet til nasjonal sikkerhet vil bli ivaretatt ved tildelinger av tillatelser under havbunnsmineralloven.

Enhver tillatelse som tildeles vil bli gitt med et tilpasset arbeidsprogram for hvilken kartlegging som rettighetshaveren må gjennomføre. Disse arbeidsprogrammene vil bidra til kunnskapsoppbygging. Relevante data som hentes inn av rettighetshaverne, herunder data om geologiske forhold, biologisk materiale, informasjon om temperatur, strømforhold mv., må deles med staten. Kartleggingen under tildelte tillatelser vil skje i tillegg til den kartleggingen staten vil holde frem med framover. Den statlige kartleggingen av natur- og miljøforhold, herunder gjennom Mareano-programmet, vil legge til rette for en effektiv og skrittvis utforskning fra næringen samtidig som den styrker kunnskapsgrunnlaget til staten.

Aktiviteten i arbeidsprogrammene består av undersøkelsesaktivitet og avsluttes med en ev. søknad om godkjenning av en utvinningsplan. Utvinning vil kun bli godkjent av departementet dersom rettighetshaverens utvinningsplan godtgjør at den planlagte utvinningen kan skje på bærekraftig og forsvarlig vis, slik at hensynet til miljø, sikkerhet og ev. annen virksomhet til havs i det aktuelle området er godt ivaretatt, og slik at sameksistensen med andre virksomheter, og både eksisterende og potensielt nye havnæringer, ivaretas. Utvinning av aktive hydrotermale strukturer vil ikke tillates. Videre vil slike strukturer beskyttes slik at de ikke blir skadet av virksomhet i tilstøtende områder. En utvinningsplan vil kun bli godkjent dersom det kan godtgjøres at utvinningen kan gjennomføres slik at det ikke medfører vesentlige negative virkninger for naturmangfoldet knyttet til de aktive strukturene. De første planene for utvinning av havbunnsmineraler som departementet legger opp til å godkjenne vil bli framlagt for Stortinget før departementet gjør dette.

Forslaget til utlysning av områder for mineralvirksomhet på havbunnen som nå sendes på høring er innenfor de rammene Stortinget har lagt og er faglig forankret for å legge til rette for en skrittvis, kunnskapsbasert og rasjonell utforskning av det arealet som er åpnet for slik virksomhet.

I arbeidet med forslaget til utlysning har departementet bedt Sokkeldirektoratet om å foreslå områder som direktoratet mener bør prioriteres for utlysning i den første konsesjonsrunden, innenfor det området som er åpnet. Dette innspillet, sammen med egne vurderinger, er grunnlaget for forslaget til utlysning som nå sendes på høring. Arealet som foreslås utlyst omfatter til sammen hele eller deler av 386 blokker.

Høringsforslaget er basert på den oppdaterte kunnskapen som framkom gjennom åpningsprosessen og som åpningsbeslutningen ble tatt på bakgrunn av. Konsekvensutredningen som var en del av åpningsprosessen viser blant annet at aktivitet knyttet til leting etter havbunnsmineraler er generelt funnet å gi små miljømessige virkninger. Som det fremgår av forvaltningsstrategien for næringen vil departementet i forbindelse med utlysning av områder basere seg på ny, oppdatert kunnskap innhentet av både statlige og kommersielle aktører. Det bes på bakgrunn av dette om innspill til områder som kan være aktuelle å unnta av hensyn til miljø og sameksistens i høringen.

Energidepartementet sender med dette forslag til utlysningsområder for en første konsesjonsrunde for mineralvirksomhet på norsk kontinentalsokkel, på offentlig høring. **Kommentarer må være Energidepartementet i hende innen 26. september 2024.**

Med hilsen

Dag Erlend Henriksen (e.f)

avdelingsdirektør

Jannicke Sahl

seniorrådgiver

## Høringsnotat

[Kart - Forslag til utlysningsareal mineralvirksomhet.pdf](#)

(<http://www.regjeringen.no/contentassets/05ec18fa77324f85b808227a9697d69a/forslag-til-utlysningsareal-mineralvirksomhet.pdf>)

## Energidepartementet

### RELATERT

- [Høring av første konsesjonsrunde for havbunnsmineraler](http://www.regjeringen.no/no/aktuelt/horing-av-forste-konsesjonsrunde-for-havbunnsmineraler/id3047008/)  
(<http://www.regjeringen.no/no/aktuelt/horing-av-forste-konsesjonsrunde-for-havbunnsmineraler/id3047008/>)  
Pressemelding | 26.06.2024



Regjeringen.no

Ansvarlig for [Energidepartementets sider](#):

Ansvarlig redaktør: [Arvid Samland](#)

Nettredaktør: [Eivind Windingstad Stensrud](#)

Tlf: 22 24 90 90

E-post: [postmottak@ed.dep.no](mailto:postmottak@ed.dep.no)

Ansatte i ED: [Depkatalog](#)

[Personvernerklæring for Energidepartementet](#)

Organisasjonsnummer: 977 161 630



# Høring av første konsesjonsrunde for havbunnsmineraler

Pressemelding | Dato: 26.06.2024 | Energidepartementet

(<http://www.regjeringen.no/no/dep/ed/id750/>)

[Read in English \(http://www.regjeringen.no/en/aktuelt/public-consultation-of-the-first-licensing-round-for-seabed-minerals/id3047008/\)](http://www.regjeringen.no/en/aktuelt/public-consultation-of-the-first-licensing-round-for-seabed-minerals/id3047008/)

Energidepartementet har sendt forslag til utlysning av første konsesjonsrunde for havbunnsmineraler på offentlig høring. Dette er områder der selskapene vil kunne søke om utvinningstillatelser, slik at arbeidet med å undersøke og innhente kunnskap om hvorvidt det er grunnlag for bærekraftig mineralutvinning på norsk sokkel kan starte.

– Verden trenger mineraler til det grønne skiftet, og regjeringen vil undersøke om det kan være mulig å utvinne havbunnsmineraler på en bærekraftig måte fra norsk sokkel. Et bredt flertall i Stortinget støtter regjeringens skrittvisе tilnærming til forvaltningen av havbunnsmineraler. Denne utlysningen er et viktig neste skritt i forvaltningen av våre havbunnsmineralressurser. Hensyn til miljø vil ivaretas i alle faser av virksomheten. I dag sender vi på høring det området vi foreslår å lyse ut i første konsesjonsrunde. Planen er at tildeling av tillatelser kan skje i første halvår 2025, sier energiminister Terje Aasland.

Regjeringen la frem forslag til åpning av areal og forvaltningsstrategien for havbunnsmineraler i Meld. St. 25. (2022-2023). Et bredt flertall på Stortinget ga i januar i år sin tilslutning til regjeringens forslag om å åpne et område på norsk kontinentalsokkel for havbunnsmineralvirksomhet og hovedlinjene i forvaltningsstrategien. På bakgrunn av dette vedtok Kongen i statsråd 12. april i år formelt å åpne et område i Norskehavet og Grønlandshavet for mineralvirksomhet.

- Tilgang på mineraler er avgjørende for at verden skal lykkes med overgangen til lavutslippssamfunnet. Mineraler fra den norske havbunnen kan bli en kilde til å dekke deler av dette behovet. Den lange og gode erfaringen vi har i Norge med forsvarlig og bærekraftig forvaltning av ressurser til havs gjør oss godt posisjonert til å gå foran og forvalte disse ressursene på en forsvarlig og bærekraftig måte, sier Aasland.

Sokkeldirektoratet har fått i oppgave å utarbeide et forslag til hvilken del av det åpnete området som bør gjøres tilgjengelig for søknader i første konsesjonsrunde. Som ledd i dette har direktoratet hatt kontakt med næringen for å avklare hvilke områder det er størst interesse for å kartlegge. Forslaget som nå sendes på høring er basert på forslaget fra Sokkeldirektoratet. Arealet i forslaget utgjør til sammen 386 blokker, og utgjør rundt 38 prosent av det området som ble åpnet i april.



Fristen for høringsinnspill er 26. september 2024.

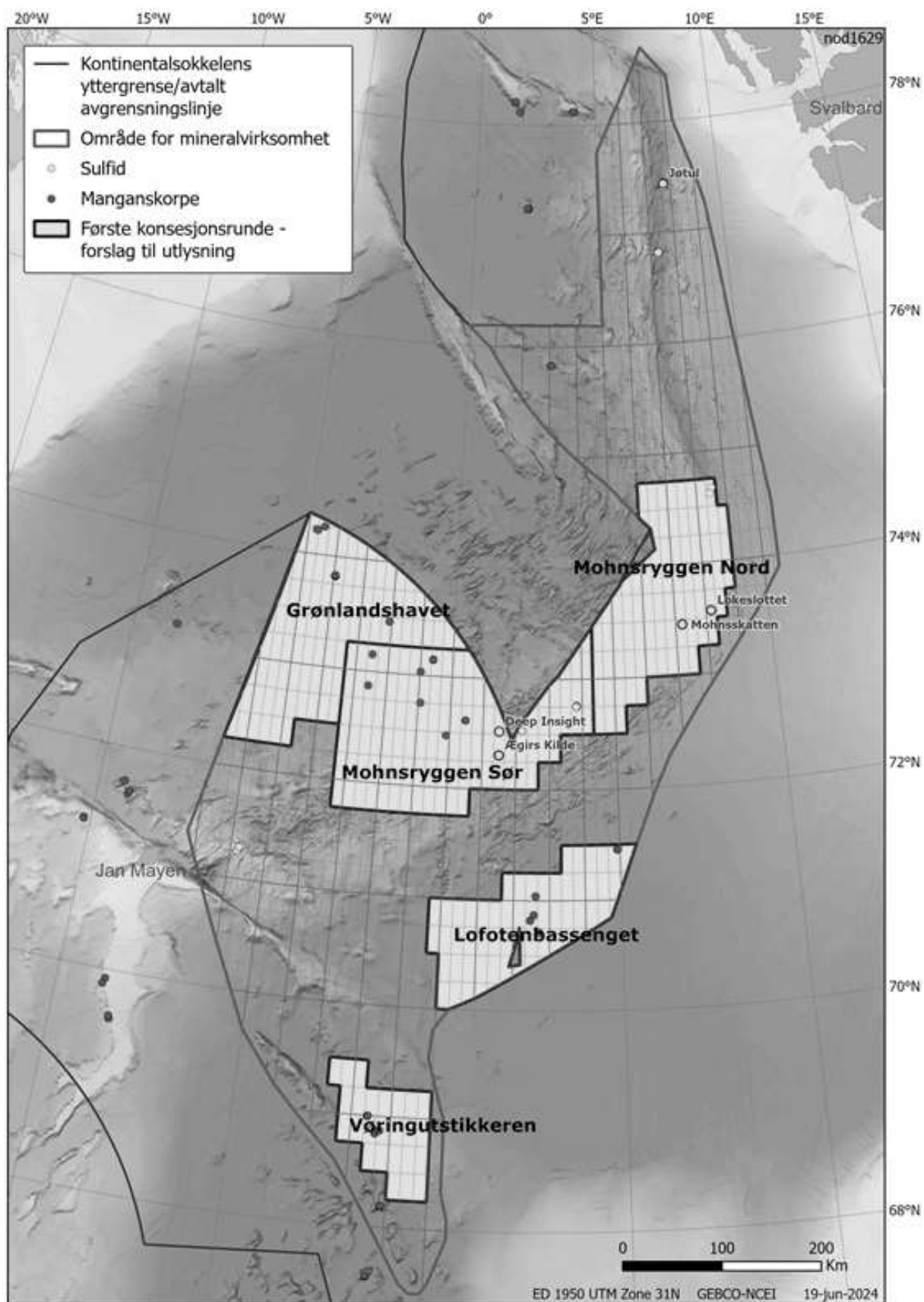


Foto: Sokkeldirektoratet.

## Bakgrunn

Høringsrunden er en del av første konsesjonsrunde for mineralvirksomhet på norsk kontinentalsokkel. Etter høringen vil departementet gjennomgå høringsinnspillene. Deretter vil konsesjonsrunden bli utlyst. Utlysningen vil blant annet inneholde en søknadsfrist for selskapene, og opplysninger om krav og vilkår som vil pålegges søkere knyttet til blant annet miljø. Som en del av søknadene, vil selskapene også bli bedt om å inkludere et forslag til arbeidsprogram for arealet de søker på.

Mottatte søknader vil behandles i henhold til publiserte og kjente tildelingskriterier. Departementet tar sikte på å tildele tillatelser i løpet av første halvår 2025. Rettighetshavere i en utvinningstillatelse må utarbeide et detaljert arbeidsprogram tilpasset det arealet som omfattes av tillatelsen, og de ressurser som man antar finnes der. Slik aktivitet antas kun å ha små miljøvirkninger, men vil bidra til viktig kunnskaps- og kompetansebygging. Arbeidsprogrammet vil normalt ha innlevering av utvinningsplan eller tilbakelevering av areal som siste milepæl.

Rettighetshaverne vil også ha som krav å dele data med myndighetene, som er viktig for kunnskapsbygging om ressurser, miljø og naturverdier. Norge vil ha en skrittvis og forsvarlig utvikling av havbunnsmineralvirksomhet på norsk kontinentalsokkel. Hensynet til miljø og sikkerhet skal ivaretas i alle faser av virksomheten.

Det er en nødvendig forutsetning for eventuell fremtidig utvinning av havbunnsmineraler å tildele utvinningstillatelser. Tildeling betyr imidlertid ikke at utvinning kan settes i gang. Før en eventuell utvinning kan starte, kreves det at rettighetshaverne har påvist ressurser, har identifisert en teknisk løsning som gjør utvinning lønnsom og har tatt investeringsbeslutning for prosjektet. Rettighetshaverne må deretter utarbeide en utvinningsplan, som inkluderer gjennomføring av en konsekvensutredningsprosess, som må godkjennes av departementet. For at departementet skal kunne godkjenne konkrete utvinningsplaner, må planen vise at prosjektet kan gjennomføres på en bærekraftig og forsvarlig måte. De første planene skal også forelegges Stortinget.

Høringsforslaget er basert på den oppdaterte kunnskapen som framkom gjennom åpningsprosessen og som åpningsbeslutningen ble tatt på bakgrunn av. Konsekvensutredningen som var en del av åpningsprosessen viser blant annet at leteaktivitet kun vil ha små miljøvirkninger. Konsekvensutredningen viste også at med omfang av fiskeri og mulige arealkonflikter/virkninger av havbunnsmineralvirksomhet er det vanskelig å se for seg betydelige konsekvenser for fiskeriene innenfor det åpnede området. Som det fremgår av forvaltningsstrategien for næringen vil departementet i forbindelse med utlysning av områder basere seg på ny, oppdatert kunnskap innhentet av både statlige og kommersielle aktører. Det bes på bakgrunn av dette i høringen om innspill til områder som kan være aktuelle å unnta av hensyn til miljø og sameksistens.

## Energidepartementet

### TEMA

Havbunnsmineraler

### RELATERT

- Høring av arealforslag – Utlysning av områder for mineralvirksomhet på havbunnen (<http://www.regjeringen.no/no/dokumenter/horing-av-arealforslag-utlysning-av-omrader-for-mineralvirksomhet-pa-havbunnen/id3046676/>)
- Åpning av område på norsk kontinentalsokkel for mineralvirksomhet (<http://www.regjeringen.no/no/aktuelt/apning-av-omrade-pa-norsk-kontinentalsokkel-for-mineralvirksomhet/id3033970/>)  
Nyhet | 12.04.2024
- Se mer informasjon på Sokkeldirektoratet sine nettsider (<https://www.sodir.no/aktuelt/nyheter/generelle-nyheter/2024/anbefalte-blokker-til-utlysning-pa-offentlig-horing/>)

## KONTAKT

Kommunikasjonsenheten i ED (<http://www.regjeringen.no/no/dep/ed/org/avdelinger/komm/id86785/>).

E-post: [info@ed.dep.no](mailto:info@ed.dep.no) (<mailto:info@ed.dep.no>).

Telefon: 41 57 35 00 (ikke sms)

Adresse: Postboks 8148 Dep, 0033 Oslo

Besøksadresse: Akersgata 59, Oslo



Regjeringen.no

Ansvarlig for Energidepartementets sider:

Ansvarlig redaktør: Arvid Samland

Nettredaktør: Eivind Windingstad Stensrud

Tlf: 22 24 90 90

E-post: [postmottak@ed.dep.no](mailto:postmottak@ed.dep.no)

Ansatte i ED: Depkatalog

Personvernerklæring for Energidepartementet

Organisasjonsnummer: 977 161 630

## The biological carbon pump

**Uta Passow<sup>a</sup> and Thomas Weber<sup>b</sup>**, <sup>a</sup>Ocean Sciences Centre, Memorial University, Newfoundland, NL, Canada; <sup>b</sup>Department of Earth and Environmental Science, University of Rochester, Rochester, NY, United States

© 2023 Elsevier Inc. All rights reserved.

This is an update of C.L. De La Rocha, U. Passow, 8.4 - The Biological Pump, Editor(s): Heinrich D. Holland, Karl K. Turekian, Treatise on Geochemistry (Second Edition), Elsevier, 2014, Pages 93–122, <https://doi.org/10.1016/B978-0-08-095975-7.00604-5>.

|  |           |
|--|-----------|
| <b>Introduction</b>  | <b>2</b>  |
| <b>Description of the biological carbon pump</b>   | <b>4</b>  |
| Carbon fixation: Photosynthesis and biomineralization                                    | 4         |
| Levels of primary production   | 4         |
| Patterns in space and time   | 4         |
| New, export and regenerated production   | 6         |
| Organic matter size continuum  | 6         |
| <b>Pathways of the pump</b>  | <b>7</b>  |
| Gravitational sinking  | 7         |
| Marine snow  | 8         |
| Feeding structures   | 8         |
| Fecal pellets  | 8         |
| Active vertical migration  | 9         |
| Physical export  | 9         |
| <b>Flux attenuation</b>  | <b>9</b>  |
| Controls on particle sinking velocities  | 9         |
| Controls on loss rates   | 10        |
| Flux attenuation with depth  | 11        |
| <b>Sedimentation and burial</b>  | <b>11</b> |
| <b>Quantifying organic matter fluxes</b>   | <b>11</b> |
| Measurement of sinking particle flux   | 11        |
| Sediment traps   | 12        |
| Particle reactive radionuclides  | 13        |
| Marine snow catchers and UVP   | 13        |
| BioARGO  | 13        |
| Comparison of measurement methods  | 14        |
| <b>Remineralization tracers</b>  | <b>14</b> |
| Oxygen utilization rates   | 14        |
| Remineralized nutrients  | 14        |
| <b>Upscaling gravitational POC export</b>  | <b>15</b> |
| Upscaling methods  | 15        |
| Global patterns and rates  | 16        |
| Estimating physical export and active transport  | 17        |
| Total export and double counting   | 17        |
| <b>Carbon Sequestration by the biological pump</b>                                       | <b>17</b> |
| Metrics of carbon sequestration  | 18        |
| Geographic variability of POC flux attenuation   | 18        |
| Sequestration timescales   | 20        |
| Carbon sequestration by the pump pathways  | 21        |
| Climate sensitivity of carbon storage  | 21        |
| <b>The future of the biological pump</b>   | <b>22</b> |
| Effects on processes driving the BCP   | 22        |
| The surface ocean: Phytoplankton community composition, primary production & respiration | 22        |
| Changes to flux attenuation  | 23        |
| Earth system model predictions   | 24        |
| Missing processes and feedbacks in ESMs  | 26        |
| Geoengineering the BCP   | 27        |
| <b>Conclusion</b>  | <b>28</b> |
| <b>References</b>  | <b>29</b> |

### Abstract

This chapter summarizes the Biological Carbon Pump (BCP) – a series of biologically mediated processes that together sequester carbon in deep ocean waters and regulate the ocean-atmosphere partition of carbon dioxide. First, the component processes of the system are reviewed, including primary production, pathways of organic matter transfer to depth, and flux attenuation. Next, the approaches used to quantify BCP carbon fluxes are compared, ranging from direct measurements to indirect geochemical constraints, and technological advances are highlighted. The chapter then explores how carbon sequestration by the BCP is quantified, and understood in terms of carbon remineralization depth and sequestration timescales. The final section examines expected responses of BCP processes to anthropogenic climate change, spanning from organism-level acclimation, to ecosystem restructuring, to global scale trends predicted by Earth System Models. The chapter closes by exploring geoengineering strategies that aim to mitigate climate change by deliberately altering the BCP.

### Keywords

Biological carbon pump; Carbon flux; Carbon sequestration; Climate change; Earth system models; Export production; Flux attenuation; Flux pathways; Geoengineering; Marine snow; Organic matter; Primary production; Remineralization; Sedimentation; Sinking velocity

### Key points

- Describe the processes driving the Biological Carbon Pump (BCP), the different pathways of carbon flux, and their spatial-temporal variability
- Review and compare approaches to quantify the BCP, ranging from small scale direct measurements to Earth System Models (ESMs)
- Discuss the sequestration of carbon in the deep ocean by the BCP
- Explore expected responses of the BCP to climate change, and assess carbon dioxide removal (CDR) options involving the BCP.

### Introduction

The Biological Carbon Pump (BCP) comprises a series of biologically mediated processes that together sequester carbon in deep ocean waters (Passow and Carlson, 2012; Boyd et al., 2019). Photosynthesis, only possible in the well-lit surface ocean, generates organic carbon from dissolved inorganic carbon (DIC) species. The bulk of this organic matter is recycled in the upper ocean via grazing and microbial hydrolysis, but a small fraction is transported, by sinking and other processes, into the deep sea, a process known as export. Much of the exported material decomposes as it settles through the water column, whereas a much smaller fraction survives to reach the seafloor sediments and is buried. Just as photosynthesis by autotrophs removes dissolved inorganic materials (DIC and nutrients) from surface waters, the decomposition of sinking biogenic particles and excretion from heterotrophs returns inorganic materials to the seawater, which is referred to as remineralization. Organic matter production in the surface and remineralization in deeper waters has the net effect of transferring DIC to depth, against a concentration gradient (Fig. 1A), which is why it is referred to as a pump. DIC sequestered at depth cannot exchange with the atmosphere, so the BCP acts to lower atmospheric CO<sub>2</sub>.

Observed profiles of the ocean's three main carbon pools reflect the cycling of carbon through the water column (Fig. 1). Particulate and dissolved organic carbon (POC and DOC respectively) concentrations are relatively high near the surface where organic matter is produced, and decrease rapidly with depth (Fig. 1B and C), whereas DIC increases with depth due to the accumulation of remineralized carbon (DIC<sub>rem</sub>) in the ocean interior (Passow and Carlson, 2012). Globally averaged, the BCP maintains a vertical DIC gradient of ~150 μmol between the surface and deep ocean (Fig. 1A). The remaining ~100 μmol increase is explained by the "solubility pump," which describes the physical transport of surface water to depth in cold high latitude regions where, "preformed" DIC (DIC<sub>pre</sub>, the sum of saturation and disequilibrium) is elevated (Fig. 1A) due to the temperature-dependence of CO<sub>2</sub> solubility (Ito and Follows, 2003). Concentrations of DIC are typically 2–3 orders of magnitude higher than those of organic carbon, and the fact that a ~ 150 μmol vertical DIC gradient is maintained by much smaller gradients in POC and DOC implies fast turnover of organic carbon, relative to the timescale of ocean circulation. In addition to vertical gradients, the interaction of the BCP with large-scale circulation drives lateral gradients in dissolved carbon species. Recently-formed ("young") deep water, e.g. in the North Atlantic, contains less remineralized DIC and more DOC than older deep waters, e.g. in the North Pacific (Fig. 1C).

Transport of organic carbon to depth by the BCP may happen by three different pathways: physical transport, gravitational settling and transport via vertically migrating organisms (Fig. 2). These transfer pathways provide sustenance to subsurface

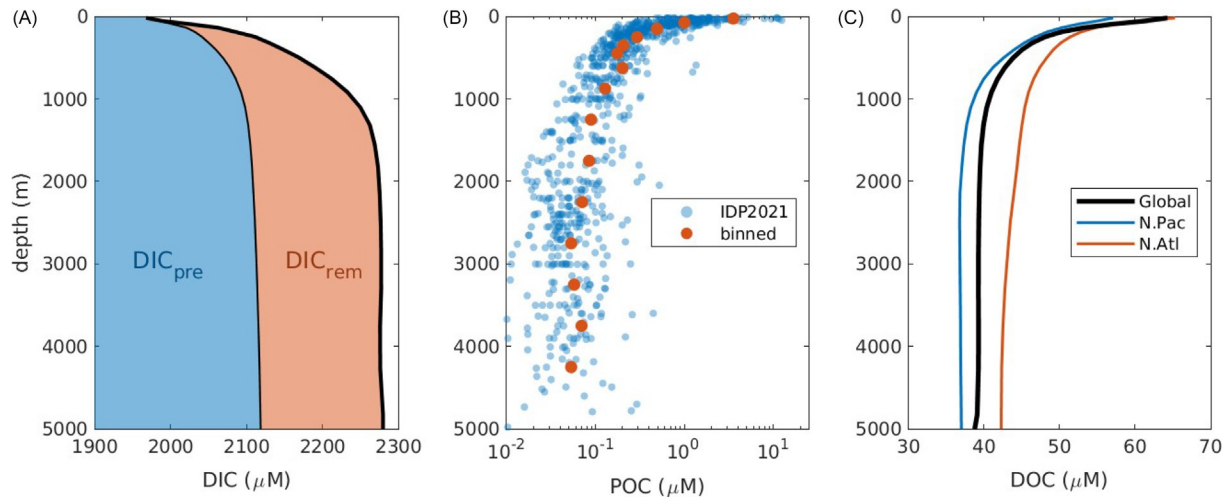


**Fig. 1** Geochemical constituents of the biological carbon pump. (A) Global-mean depth profile of dissolved inorganic carbon (DIC) concentration from the GLODAPv2 preindustrial climatology (thick black line). DIC is divided into a “preformed” component ( $\text{DIC}_{\text{pre}}$ ) transported from the surface and a remineralized component ( $\text{DIC}_{\text{rem}}$ ) that accumulates from organic matter decomposition.  $\text{DIC}_{\text{pre}}$  is calculated in the OCIM circulation model following Carter et al. (2021) and  $\text{DIC}_{\text{rem}}$  is calculated by difference. (B) Particulate organic carbon (POC) concentrations from the GEOTRACES IDP2021 archive (translucent blue dots), which combines data from the Atlantic, Pacific, Southern and Arctic Oceans. Red dots are averaged within depth bins that increase in thickness from 100 m to 500 m over depth. (C) Dissolved organic carbon (DOC) concentrations from the climatology of Roshan and Devries (2017), averaged globally and in the North Atlantic and Pacific Oceans ( $>40^\circ\text{N}$ ), representing the beginning and end of the thermohaline overturning circulation respectively.

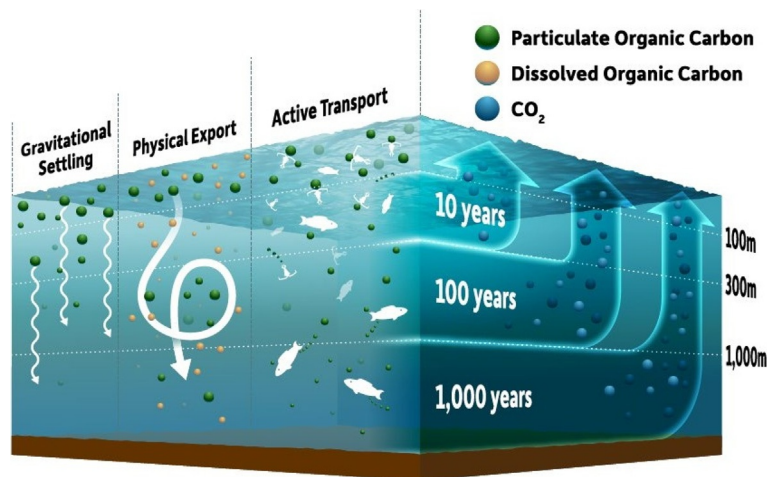


**Fig. 2** Pathways of the biological carbon pump. Left face shows the three main export pathways for organic carbon from the surface euphotic zone to the ocean interior: gravitational settling of POC, physical export of POC and DOC, and active transport of carbon by vertically migrating organisms (zooplankton and fish). Right face shows the return of respired  $\text{CO}_2$  to the surface via the large-scale ocean circulation, annotated with characteristic recirculation timescales for different depth intervals, which reflect the time that respired carbon is sequestered out of contact with the atmosphere. Illustration by M. Osadciw, University of Rochester.

heterotrophic communities and thus enable life in the dark ocean. The depth to which organic matter is transported before remineralizing, determines the timespan that carbon is isolated from contact with the atmosphere, and thus the effectiveness of carbon sequestration by the BCP (Fig. 2). Carbon remineralized above the wintertime mixed layer depth will be returned to the surface within a year, whereas remineralization beneath  $\sim 300$  m can result in carbon storage for 100 years or more (often considered a critical timescale for sequestration) and remineralization below 1000 m can lead to extremely efficient sequestration for 1000 years or more (Fig. 2), (Passow and Carlson, 2012).

Two additional suites of biological processes also exert leverage on the ocean-atmosphere carbon balance. The *Microbial Carbon Pump* (MCP) describes the process in which carbon is sequestered in a reservoir of very recalcitrant dissolved organic compounds. These recalcitrant compounds may be produced in the surface ocean or released at depth during POC remineralization, and on average remineralize on timescales of hundreds to thousands of years (Jiao and Azam, 2011). Because this turnover time is similar to or longer than the timescale of ocean circulation, recalcitrant DOC accumulates throughout the ocean, explaining why considerable DOC concentrations are observed even in the ocean’s oldest waters (Fig. 1C). Because carbon stored in the recalcitrant DOC pool does not participate in ocean-atmosphere exchange, the MCP has the net effect of reducing atmospheric  $\text{pCO}_2$  (Legendre et al., 2015).



The *Carbonate or Hard Tissue Pump* (Rost and Riebesell, 2004) refers to the activity of organisms like coccolithophores, pteropods, and foraminifera that use DIC to produce inorganic carbon shells or tests. Calcium carbonate production modifies inorganic carbon speciation, lowering alkalinity and leading to outgassing of CO<sub>2</sub> (Wolf-Gladrow and Zeebe, 2001). The Carbonate Pump is also referred to as the Counter Pump, given that it works counter to the other carbon pumps, at least on short timescales (see chapter by Hain).

The relative magnitude of these different carbon pumps is a key question of current research, but on immediate human timescales the BCP is thought to be of central importance. Here, in this chapter, we will focus on the BCP, and on timescales relevant for humans. We will describe the BCP, its functions, pathways and effects, as well as its quantification and efficiency. We will end the chapter by looking at the future of the pump and possible opportunities to engineer our environment consciously with the goal of removing CO<sub>2</sub> from the atmosphere.

## Description of the biological carbon pump

Primary production, defined as the amount of organic carbon generated by photosynthesis in the surface ocean, is the theoretical maximum amount of carbon that may be exported by the BCP. Most of the organic carbon will be recycled within a few hundred meters of the surface (Martin et al., 1987), but some portion will be exported to deeper waters or even to the sediments before decomposition, or may even escape decay entirely and be deposited in the sedimentary reservoir. We will therefore first look at primary production in the ocean (Section “Levels of primary production”), at drivers and spatial patterns (Section “Patterns in space and time”), and introduce the concepts of new, export and regenerated production (Section “New, export and regenerated production”) and the organic matter size continuum (Section “Organic matter size continuum”). Second, we will examine the different pathways (“Pathways of the pump”) by which organic matter is exported from the surface to the deep ocean: Gravitational sinking of particles (Sections “Gravitational sinking,” “Marine snow,” “Feeding structures,” and “Fecal pellets”), the activity of vertically migrating organisms (Section “Active vertical migration”), and physical transport processes (Section “Physical export”), that move both dissolved and particulate organic matter to depth. Each carbon molecule may experience a mix of these pathways on its journey downward through the water column. Third, we will explore organic carbon flux attenuation (Section “Flux attenuation”) and the processes that drive organic matter loss over depth (Fig. 1B and C), before finally examining the burial of a tiny fraction of the organic matter produced in the surface ocean in seafloor sediments (Section “Sedimentation and burial”).

## Carbon fixation: Photosynthesis and biomineralization

### Levels of primary production

In the initial step of the BCP, phytoplankton convert CO<sub>2</sub> into organic matter via photosynthesis, with the rate a function of the average light climate that the phytoplankton cells experience. Photosynthesis is thus restricted to the sunlit surface waters. When light is sufficient, the upper limit of primary production is set by the supply of macro- and micronutrients to the euphotic zone. Nitrogen frequently limits primary productivity over annual timescales, whereas phosphorus is thought to limit global primary production on timescales approaching its oceanic residence time of 9000–80,000 years (Tyrrell, 1999; Benitez-Nelson et al., 2000). Besides C, H, and O, the two main components of phytoplankton organic matter are N and P, in the variable (Geider and La Roche, 2002; Weber and Deutsch, 2010) but roughly average molar proportion of 106C: 16 N: 1 P (Redfield et al., 1963), which is known as the Redfield ratio. Diatoms which are often limited by low concentrations of silicic acid, have an average C: Si ratio of 8 (Brzezinski, 1985), although this ratio may vary from 3 to 40 depending on the species and the environmental conditions (Harrison et al., 1990; Hoffmann et al., 2007). Diazotrophic (N<sub>2</sub>-fixing) phytoplankton are not susceptible to N limitation, but may be more susceptible to P and Fe limitation than other taxa. In some parts of the ocean, N and P are both replete, and Fe limits phytoplankton growth (de Baar et al., 2005; Martin and Fitzwater, 1988; Boyd et al., 2007). Trace elements such as Fe, Zn, Cd, Mg, I, Se, and Mo are required for the synthesis of carbohydrates, lipids, proteins, biominerals, amino acids, enzymes, DNA, and other essential compounds (Falkowski and Raven, 2007). Coccolithophorids produce external scales, called coccoliths, made of calcium carbonate (CaCO<sub>3</sub>) (Paasche, 1999). Elements such as Na, Mg, P, Cl, K, and Ca are important for osmoregulation, buoyancy control, and the maintenance of charge balance (Fagerbakke et al., 1999). Primary production depends on the availability of all elements a specific phytoplankton species requires.

Global marine net primary production (NPP = gross primary production minus phytoplankton respiration and photorespiration) has been estimated from satellite retrievals as 50–60 Pg C (4–5 Pmol C) each year (Westberry et al., 2008; Silsbe et al., 2016; Field et al., 1998; Martin et al., 1987; Carr et al., 2006). This represents roughly half of the total (marine plus terrestrial) annual 105 Pg C fixed each year (Field et al., 1998), despite the fact that marine phytoplankton comprise less than 1% of the total photosynthetic biomass on Earth.

### Patterns in space and time

Because NPP depends on light, nutrients and trace elements, its magnitude varies spatially and seasonally (Fig. 3). Rates of NPP in coastal regions average 2000 g C m<sup>-2</sup> year<sup>-1</sup>, significantly outpacing the oligotrophic open ocean, where NPP averages 440 g C m<sup>-2</sup> year<sup>-1</sup> (Chavez et al., 2011). However, because the open ocean constitutes 90% of the area of the ocean, the bulk (~ 80%) of the ocean’s annual carbon fixation occurs there rather than in productive coastal regions. Oligotrophic open ocean areas include

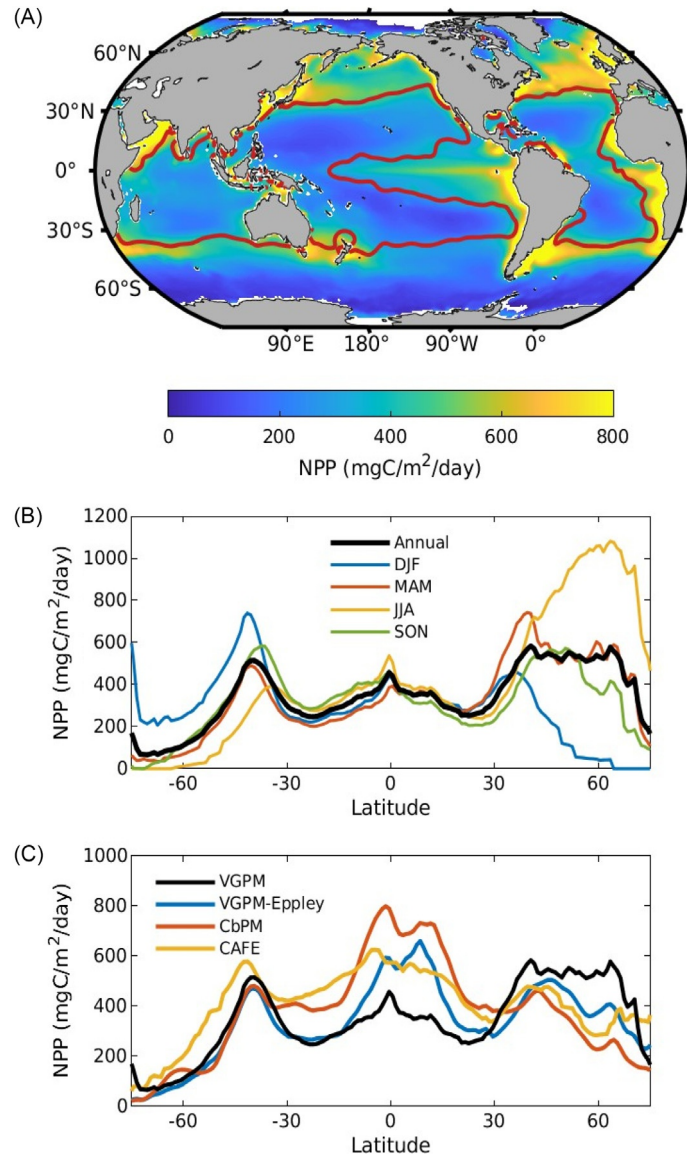


**Fig. 3** Spatial and temporal variability of organic matter production. (A) Annual-mean net primary production (NPP) estimated by the VGPM satellite algorithm. Red line is the  $1 \mu\text{M}$   $\text{NO}_3$  contour (lower  $\text{NO}_3$  lies inside the contour, in subtropical regions). (B) Zonal-mean seasonal NPP climatology from the VGPM algorithm (DJF=December–January–February; MAM = March–April–May; JJA = June–July–August; SON=September–October–November). (C) Zonal-mean annual NPP compared between four different satellite algorithms (see text for details).

the subtropical ocean basins, where nitrate concentrations are low and limiting (red line in Fig. 3A), as well as the Southern Ocean, where N is abundant but Fe scarcity and a short growth season limit NPP (Fig. 3A) (Behrenfeld and Kolber, 1999). Upwelling of nutrient-rich subsurface water near the equator, allows for elevated NPP compared to surrounding subtropical waters. Elevated, but seasonal phytoplankton growth is obvious poleward of  $\sim 40^\circ$  north and south (Lutz et al., 2007). In the Northern Hemisphere, NPP peaks in the boreal spring months (March–April–May, Fig. 3B) at  $\sim 40^\circ\text{N}$ , and in the boreal summer (June–July–August) further poleward. Peak production in the southern hemisphere occurs in austral summer (December–January–February) and the growth of the bloom is lower in magnitude than in the northern hemisphere and spatially confined to the Subantarctic band ( $\sim 40\text{--}50^\circ\text{S}$ ) and the Antarctic coastline (Fig. 3B).

NPP in Fig. 3 uses the Vertically-Generalized Production Model (VGPM, (Behrenfeld and Falkowski, 1997), the first satellite-based global NPP algorithm, which takes reflected-light estimates of chlorophyll abundance as its primary input variable and temperature and photosynthetically active radiation as additional inputs. Other algorithms have been developed since, including a modified version of VGPM (Carr et al., 2006) the Carbon-based Production Model (CbPM, Westberry et al., 2008) that uses backscatter-estimated POC rather than chlorophyll as its primary input, and the Carbon, Absorption, and Fluorescence Euphotic model (CAFE, Silsbe et al., 2016) that is primarily based on energy absorption. These more recent algorithms predict broadly similar spatial patterns and seasonal cycles, but tend to yield systematically higher NPP in the tropics and lower NPP at high latitudes than VGPM (Fig. 3C).

Different phytoplankton dominate NPP in the different marine regions. This spatial heterogeneity in phytoplankton composition and abundance reflects differences in ecosystem structure and function and ultimately impacts the efficiency of the BCP. Diatoms, often dominate in upwelling and coastal regions of the ocean (Nelson et al., 1995), whereas in the open ocean prokaryotic and eukaryotic picoplankton tend to dominate NPP (Chisholm et al., 1988; Liu et al., 1999; Steinberg et al., 2001). Coccolithophores prefer stratified conditions (Le Quéré et al., 2005) and often form a bloom after the spring diatom bloom in the North Atlantic, but are generally common around 60° N and 60° S (Iglesias-Rodríguez et al., 2002). *Phaeocystis*, may form large blooms in nutrient-enriched areas such as the Ross Sea or the Arabian Gulf (Schoemann et al., 2005), whereas *Trichodesmium*, a nitrogen-fixing taxa, thrives in oligotrophic regions (Westberry and Siegel, 2006; Capone et al., 2005). Dinoflagellates, which are motile and frequently mixotrophic, are typically abundant in systems dominated by recycling. This spatial heterogeneity is overlaid by temporal and/or seasonal succession of taxa as local conditions change.

Differences in environmental conditions and ecosystem structure can lead to seasonal successions in the plankton community that vary between regions: Outside of the tropics, levels of marine primary productivity vary systematically throughout the year (Heinrich, 1962; Smetacek et al., 1984) (Fig. 3B and C). Phytoplankton standing stocks and NPP peak in the spring following the onset of water column stratification and the increase in available light (Smetacek and Passow, 1990), or in response to alterations in the balance between rates of phytoplankton growth and zooplankton grazing (Behrenfeld, 2010). Depletion of nutrients in the stratified water column by the summer inhibits phytoplankton growth and grazing by zooplankton reduces standing stocks. Some areas may experience a small bloom of phytoplankton in the autumn when light levels are still adequate and the onset of winter convection and overturning injects nutrients into the euphotic zone. Within the tropics, fluctuations in standing stocks of phytoplankton are smaller and more frequent, often dominated by physical (e.g., mixing and upwelling) events. When iron limits NPP, blooms may be associated with iron input events (Martin et al., 1991; Nishioka and Takeda, 1997), such as upwelling (Coale et al., 1996), dust storms, icebergs (Lin et al., 2011) or coastal or river runoff (Johnson et al., 1999).

### **New, export and regenerated production**

Whereas NPP sets the theoretical upper limit of carbon available for export via the BCP, the actual export flux is much smaller, because the majority of NPP is converted back into CO<sub>2</sub> and dissolved nutrients within the euphotic zone. These recycled nutrients may then be used to fuel further carbon fixation. At steady state, carbon export may be approximated by operationally separating NPP fueled by nutrients supplied from outside the euphotic zone (*new production*) from that fueled by recycled nutrients (*regenerated production*). Such a separation can be achieved by considering the form nitrogen used for NPP, as winter mixing provides nitrate from deeper layers, whereas recycled N is mostly in the form of ammonia (NH<sub>3</sub>) (Dugdale and Goering, 1967). In addition to upwelling and mixing, new production can also be supported by external nutrient sources such as river inputs, nitrogen fixation, and atmospheric deposition. The ratio of new to total primary production in the ocean, known as the *f*-ratio (Eppley and Peterson, 1979), is generally higher in upwelling environments than it is in oligotrophic regions of the ocean (Harrison et al., 1990; Laws et al., 2000). On average, about 25% of the total global marine primary production is thought to be new production (Yool et al., 2007), ranging from 7% to 70% from region to region (Laws et al., 2000).

When averaged over appropriate temporal and spatial scales, new production should be equivalent to export production, where export production is defined as the net vertical transport of organic matter out of the euphotic zone. This concept is theoretically useful, because estimates of new production are often easier to achieve than direct estimates of export. However, export and new production may be spatially and temporally decoupled due to time lags, horizontal advection and other processes, complicating the translation from new to export production (Plattner et al., 2005; Laws and Maiti, 2019).

### **Organic matter size continuum**

Organic matter in the ocean exists as a spectrum of different sized particulate organic matter (POM, which includes POC), as well as in the form of dissolved organic matter (DOM, which includes DOC). Acoustic and optical particle counters reveal a continuous particle size spectrum spanning from microns to centimeters, in which particle number density is often well described as a power-law function of diameter (Stemmann and Boss, 2012; Picheral et al., 2010) (Fig. 4A). The “slope” of the particle size spectrum (log-log plot) determines the relative abundance of small vs. large particles (steeper slope means small particles are more dominant) and usually lies in the range -5 to -2. Particles larger than 0.5 mm, referred to as “marine snow” (Section “Marine snow”), are thought to make the largest contribution to POC export despite their relative scarcity due to the strong relationships between particle size and mass, and size and sinking velocity. Smaller particles may make an important indirect contribution to export by aggregating into larger, faster-sinking particles.

DOC is released by actively growing phytoplankton (Sondergaard et al., 2000; Teira et al., 2001; Mykkestad, 1995), during grazing by zooplankton (Strom et al., 1997; Saba et al., 2011), during solubilization of POM by exoenzymes released by bacteria (Smith et al., 1995; Ogawa et al., 2001), and by viruses (Suttle, 2007). DOC is operationally separated into different fractions (Amon and Benner, 1996): The labile fraction is rapidly remineralized (in minutes to weeks) by microbes, meaning that it makes up a small fraction of the total pool of DOC at any given time, the semi-labile fraction persists for months to a few years (Davis and Benner, 2007; Repeta and Aluwihare, 2006), and the refractory fraction has an average age of ~5000 years (Jiao et al., 2018). It has been suggested that this refractory portion of DOC survives, because concentrations of each compound are too low to compensate for metabolic costs of its utilization (Arrieta et al., 2015).

A fraction of DOM, specifically some exopolymers exuded by phytoplankton and bacteria, may spontaneously form gel-like particles, such as transparent exopolymer particles (TEP) (Passow, 2000; Kepkay, 1994; Nagata et al., 2021) and protein-rich

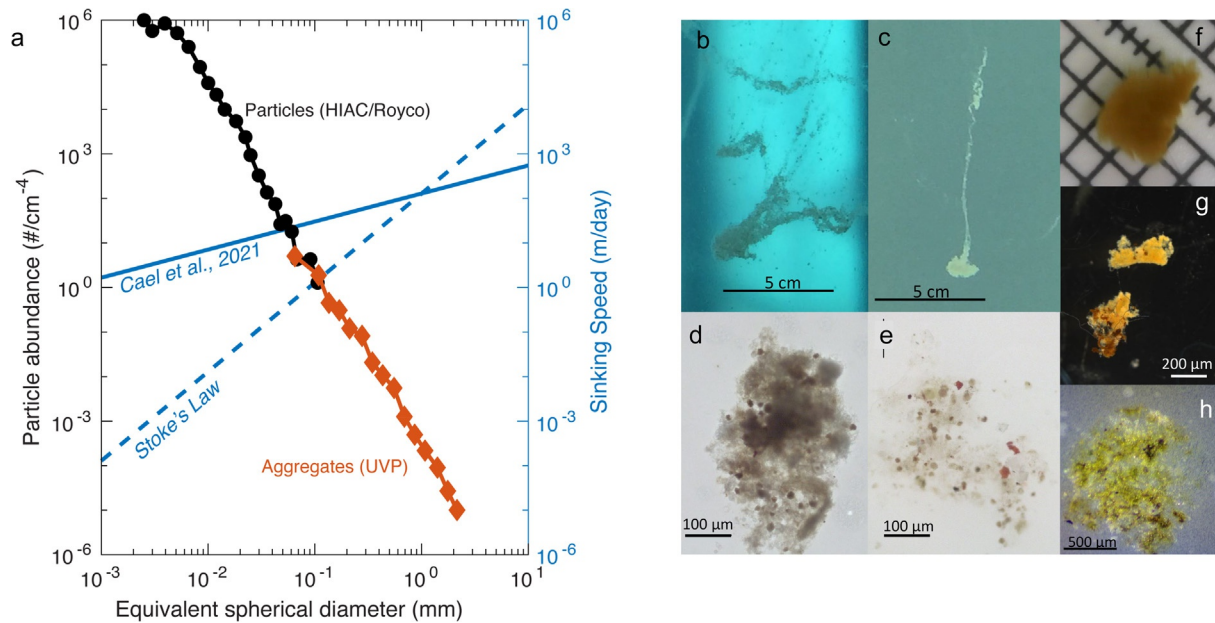


**Fig. 4** Characteristics of the POC assemblage. (A) Abundance vs. size spectrum of POC (left y-axis) measured by a combination of acoustic (black dots) and visual (red diamonds) particle counters, spanning 4 orders of magnitude in particle diameter. Blue lines (right y-axis) show two sinking speed vs. size relationships (see text for details). (B–H), photographs of different organic particle types: Mucus-rich aggregates in mesocosm (B, C), small natural aggregates collected with the snow catcher, degrading salp pellet (F, 2 x 4 mm), degrading euphausiid strings, large phytoplankton aggregate collected with snow catcher. (A) Adapted from Stemmann L and Boss E (2012) Plankton and particle size and packaging: From determining optical properties to driving the biological pump. *Annual Review of Marine Science* 4: 263–290 and Cael BB, Cavan EL and Britten GL (2021) Reconciling the size-dependence of marine particle sinking speed. *Geophysical Research Letters* 48: e2020GL091771. (D, E) photos: C. Cisternas Novoa. (G) photo: K. Sharpe. (H) photo: E. Romanelli.

Coomassie stainable particles (CSP) (Cisternas-Novoa et al., 2014; Long and Azam, 1996). TEP, which can be made visible by staining with Alcian blue (Passow, 2002), exist in a size continuum from colloidal fibers to gel-like particles (Verdugo, 2012) and are rich in acidic polysaccharides, especially deoxysugars (Mopper et al., 1991; Zhou et al., 1998), which grants them their surface active properties. TEP contain C and N in proportions exceeding Redfield ratios (Engel and Passow, 2001), supplying a mechanism for pumping of carbon in excess of what would be predicted from the availability of nitrogen (Schneider et al., 2004).

The role of DOC and gel-like particles within the BCP are varied, and not fully understood. DOC may be transformed into recalcitrant material (the microbial pump). Physical transport processes may move DOC to the deep ocean (Section “Physical export”). DOC utilized by bacteria, may become part of the sinking flux either when bacteria associate with fast sinking marine snow or when bacteria enter the food-web, e.g. via grazing by protists (Azam et al., 1983). Aggregates have been shown to host complete microbial loop communities (Azam and Long, 2001; Azam and Malfatti, 2007). Significant amounts of DOM also sink within aggregates (Alldredge, 2000; Antia, 2005), where pore-water concentrations of dissolved materials are frequently elevated. TEP are essential for the formation of sinking marine snow (Logan et al., 1995; Passow and Alldredge, 1995; Jackson, 1995), and impact the exchange with the atmosphere, when accumulating at the sea surface microlayer (SML) (Cunliffe et al., 2013).

### Pathways of the pump

Generally, three main export pathways that transport carbon from the surface ocean to the mesopelagic are recognized (Fig. 2): Gravitational settling, transport due to active vertical migration, and physical transport processes. Rapidly settling particles may be formed due to aggregation of smaller particles or due to biological activity, e.g. production of fecal pellets, feeding structures, carcasses and molts. The mass vertical migration of zooplankton and fish between surface waters where they feed at night and the mesopelagic zone, where they respire  $\text{CO}_2$ , excrete DOC or egest POC as feces during the day, also efficiently moves carbon to depth. Whereas the impact of zooplankton activity on these flux pathways has been investigated for decades, the potential role of fish is only slowly emerging. Mixing processes, or subduction of water masses may move non- or slow sinking particles or DOC to depth. The relative importance of the three pathways depends on physical conditions such as mixing and ecological factors including the food-web structure (Laws and Maiti, 2019; Steinberg and Landry, 2017).

### Gravitational sinking

Marine snow, defined as composite particles (“aggregates”)  $>0.5$  mm (Alldredge and Silver, 1988; Silver, 2015), are viewed as the major vehicle for gravitational settling of organic matter in the ocean, because they can traverse the distance between surface and mesopelagic in a space of days to weeks (Beaulieu, 2002; Billet et al., 1983). Rapid transit time to depth and is a prerequisite for



organic matter to reach 1000 m, beneath which carbon sequestration is particularly efficient (Fig. 2). Slowly sinking particles, such as solitary phytoplankton cells, that sink at  $\approx 1 \text{ m day}^{-1}$  (Smayda, 1971) would require more than a year to reach the benthos of even a relatively shallow continental shelf. Given the rapid rate of microbial decomposition of organic material in the ocean and the abundance of zooplankton grazers, it is virtually impossible for a slowly sinking particle to reach the mesopelagic or seabed. However, more recently, the paradigm that size is paramount in determining sinking velocity is being challenged (Section “Controls on particle sinking velocities”).

### Marine snow

Marine snow is formed either by biological activity of zooplankton or fish, which can produce mucus feeding structures, fecal pellets, molts and carcasses, or by the physical aggregation of smaller particles, such as algae cells or detritus as well as inorganic material such as biogenic silica frustules, calcium carbonate tests, or lithogenic minerals (Alldredge et al., 1993; McCave, 1984). Physical aggregation requires collision followed by attachment of particles. Particles collide due to processes such as Brownian motion, shear, and differential settling (Kepkay, 1994; Jackson, 1990), and collision rates depend on size and abundance of particles (Burd and Jackson, 2009). The probability of particles attaching following a collision is controlled by the physical and chemical properties of the particles' surfaces, that is, their “stickiness” (Alldredge and Jackson, 1995; Burd and Jackson, 2009), which makes TEP essential for aggregate formation and sedimentation (Logan et al., 1995; Passow and Alldredge, 1995; Passow et al., 2001).

Characteristics (size, porosity, fragility) of marine snow vary widely depending on formation conditions (Fig. 4). In coastal areas and in regions hosting large phytoplankton blooms, organic material reaching the deep often does so as aggregated phytoplankton (Fig. 4F) (Turner, 2002). However, spatial and temporal variability is high, and fecal pellets may dominate flux as well (Fig. 4D and E) (Turner, 2015; Ebersbach and Trull, 2007). Salp fecal pellets (Fig. 4D), appendicularian houses, or detrital aggregates may dominate flux (Fig. 4G and H) (Phillips et al., 2009; Silver et al., 1998; Passow et al., 2001; Alldredge and Silver, 1988). Although recognized as important for vertical carbon flux, sinking of dead organisms are exceedingly difficult to quantify (Steinberg and Landry, 2017).

Diatom aggregates are a common type of marine snow and form after the large spring diatom blooms observed in many areas (Alldredge and Silver, 1988). Phaeocystis, especially when co-occurring with diatoms or in the presence of lithogenic mineral particles, may also contribute significantly to sinking marine snow, depending on conditions (Passow and Wassman, 1994; Hamm et al., 2001; Dybwad et al., 2021). Even picoplankton are regularly observed in deep sediment traps, sinking as part of marine snow formed via aggregation (Cruz and Neuer, 2019; Deng et al., 2016), or from feeding structures or feces (Richardson and Jackson, 2007). Dynamics in the surface ocean, especially food-web structure and particle composition determine the timing and type of marine snow that dominates.

Sinking marine snow consists of structured microenvironments, offering surfaces, hiding places, enclosed spaces, and hot spots of biological activity (Simon et al., 2002) that provide food and substrate to organisms in the meso-, bathy-, and abyssopelagic zones and benthos, thereby coupling the surface layer with the dark ocean. Even though marine snow represents sites of elevated rates of decomposition and nutrient regeneration, it contributes significantly to the transport of C, N, P, Si, and other materials to the deep. Besides providing food for deep food-webs, sinking of marine snow contributes to the sequestration of carbon by the ocean.

### Feeding structures

Appendicularia (larvacea) generate intricate mucus houses, and pteropods and certain planktonic foraminifera produce relatively large webs, also made of mucopolysaccharides, all of which are used to collect food particles (Alldredge, 2005; Kiørboe, 2011). When these structures become clogged with material, they are discarded by the organism, which then builds another. In the case of appendicularia, these feeding structures may be produced and discarded 6–26 times a day per individual (Sato et al., 2001; Fenaux, 1985). The abandoned structures, become marine snow (Alldredge, 2005; Lombard and Kiørboe, 2010), causing distinct sedimentation events (Passow et al., 2001). In systems where appendicularia and dolioids dominate, fecal pellets and feeding structures have been observed to provide fast sinking marine snow, whereas high copepod abundance resulted in comparably reduced aggregate formation (Taucher et al., 2018). Recent surveys using cameras to monitor their abundance and sinking have suggested that discarded appendicularian houses may be responsible for roughly a third of the particulate organic carbon (POC) flux to depth in the ocean (Robinson et al., 2010).

### Fecal pellets

Zooplankton also package material into potentially fast-sinking marine snow through their production of fecal pellets (Steinberg and Landry, 2017; Ebersbach and Trull, 2007). Depending on the type of zooplankton, fecal pellets range in shape from oval, spherical, conical, rectangular, or cylindrical, to coiled, (Yoon and Rosson, 1991) with their size also quite variable (Frangoulis et al., 2004; Steinberg and Landry, 2017). The contribution of zooplankton fecal pellet carbon to total POC flux varies widely among seasons, regions and with depth (Turner, 2015; Steinberg and Landry, 2017). The theoretical upper limit for fecal pellet flux is their production rate, estimated as  $6.2 \text{ Gt C Y}^{-1}$  globally (Dilling and Alldredge, 2000; Anderson et al., 2013). The contribution of recognizable fecal pellets to POC flux is usually <40% of POC flux (Turner, 2015). High fecal export may occur episodically, during salp blooms (Stone and Steinberg, 2016; Steinberg et al., 2023). Copepod size, rather than abundance seems to determine most

significantly which fraction of fecal carbon reaches great depth (Stamieszkin et al., 2015). First estimates on the relative importance of fish pellet flux suggest regional contributions vary between 5% and 35% of the measured flux and are in the same range as flux due to zooplankton pellets (Saba et al., 2021).

### Active vertical migration

The active transport of carbon to depth by swimming organisms varies with migrator biomass and composition (Longhurst et al., 1990). Migrating zooplankton and fish feed near the surface at night, then migrate to depth during the day where they respire organic carbon to CO<sub>2</sub> and excrete dissolved and particulate (fecal) material, transferring carbon from surface waters to depths of 200–800 m (Hidaka et al., 2001; Longhurst et al., 1990; Bianchi et al., 2013b). Migrant-mediated carbon flux is comparable to 8–80% of the sinking POC flux (Steinberg and Landry, 2017). Transport of respiratory carbon tends to be high when migrator biomass is high, but environmental conditions like temperature and oxygen minimum zones impact this relationship (Steinberg and Landry, 2017). Flux due to DOC excretion, fecal production and mortality at depth is challenging to quantify. The active flux of carbon by vertically migrating zooplankton may partially explain the observed discrepancy between heterotrophic respiratory demands for carbon in the mesopelagic realm and the observed sinking flux of POC (Burd et al., 2010; Steinberg et al., 2008). Frequently ignored in BCP budgets is flux due to the ontogenetic (seasonal) migration of zooplankton, which is best understood for the large copepods common in the North Atlantic and North Pacific (Steinberg and Landry, 2017). The annual transport and metabolism of lipid-rich material (lipid pump) by large herbivorous *Calanus* is on the order of sinking POC flux (Jónasdóttir et al., 2015). Respiratory and other active flux by migrating fish is roughly in the same order as that of zooplankton (Saba et al., 2021).

### Physical export

Physical transport and mixing provide important conduits for organic matter to depth, owing to the strong vertical gradients of particulate and dissolved organic carbon (Fig. 1B and C). For larger particles, physical transport is often negligible compared to gravitational settling, but for small suspended particles and DOC physical export dominates the total export flux (Boyd et al., 2019). Three discrete pathways have been recognized for physical export of organic carbon from the upper ocean, which operate at different spatial and temporal scales. At the largest scale, suspended POC and DOC are advected to depth by the vertical component of the ocean general circulation, which includes Ekman pumping (downwelling) in subtropical gyres, and subduction along sloping isopycnals in regions of thermocline ventilation and water mass formation (Levy et al., 2013). In mid and high latitude regions, strong seasonal variability in mixed layer depth drives carbon export by the “mixed layer pump.” Organic matter accumulates in the surface mixed layer during spring and summer and is then diluted over depth during deep wintertime mixing. When the mixed layer shoals in the following spring, much of the organic matter is left behind in the ocean interior at depths up to ~400 m (Dall’olmo and Mork, 2014; Bishop et al., 1986), therefore bypassing the upper few hundred meters of the water column where remineralization is fastest and potentially driving efficient carbon sequestration (Boyd et al., 2019). The “eddy subduction pump” drives physical export at the shortest temporal and spatial scales, including the mesoscale (10–100 km) and submesoscale (1–10 km). Carbon export occurs when the strong vertical circulation associated with downwelling eddies and frontal systems carries POC and DOC from the surface to depths of 100–350 m, although it should be noted that upwelling systems can have the opposite effect, returning exported organic matter to the surface.

### Flux attenuation

Physical export and active transport by migrating organisms can provide direct pathways to “shunt” or “inject” organic matter directly to depths of hundreds of meters (Boyd et al., 2019), often bypassing flux measurement approaches (Steinberg and Landry, 2017). For gravitationally settling particles, the POC flux is generally observed to decrease (or “attenuate”) rapidly over depth in the few hundred meters beneath the euphotic zone, and then more gradually in deeper waters (Martin et al., 1987). The rate of flux attenuation is essentially driven by the balance between sinking velocity and POC loss rates due to microbial remineralization or grazing (Banse, 1990). Either faster remineralization or slower sinking will result in faster flux attenuation, and therefore shallower remineralization of organic matter.

The nature of sinking particles continuously changes during their downward journey due to microbial, zooplankton and fish activity, making carbon export and flux attenuation difficult to monitor or predict.

### Controls on particle sinking velocities

Following Stokes Law, which describes solid spheres in laminar flow, sinking velocity would be expected to increase with the size squared of the sinking particle and its excess density compared to seawater. Excess density of an aggregate is determined by the excess density of individual components and the porosity of the aggregate. Assuming that Stokes Law is principally applicable, only marine snow sized particles would sink at speeds high enough to reach the mesopelagic and beyond. Sinking velocities of marine snow are mostly greater than 50–100 m day<sup>-1</sup> and may exceed 500 m day<sup>-1</sup> (Alldredge and Gotschalk, 1989; Armstrong et al., 2009; Ploug et al., 2008b). Fecal pellets sink even more rapidly, from 10’s to 100’s m per day for copepods and euphausiid pellets to more than 1000 m day<sup>-1</sup> for salp pellets (Steinberg and Landry, 2017; Ploug et al., 2008a). Abandoned feeding structures collapse and accumulate more particles, they reach sinking velocities of 50–800 m day<sup>-1</sup> (Alldredge, 2005; Lombard and Kiørboe, 2010).

Recently, variance in the POC flux through 400 m in several ocean basins was tied to the phytoplankton community, with the largest fluxes associated with larger phytoplankton that tend to form aggregates (Guidi et al., 2009), supporting the role of particle size as a dominant driver of efficient POC transfer to depth.

Sinking velocities of smaller particles, were traditionally considered too slow to carry significant amounts of carbon to the mesopelagic or beyond (Alldredge and Gotschalk, 1989; Billet et al., 1983). However, more recent observations suggest, that small particles can contribute significantly to sinking particle mass at depth (Giering et al., 2016; Richardson and Jackson, 2007; Durkin et al., 2015; Dall'olmo and Mork, 2014; Guidi et al., 2009). Small particles may reach the mesopelagic due to fragmentation of marine snow, or due to physical transport events, such as the mixed layer pump (Richardson, 2019). BGC-Argo data also suggest that small particles are not efficient contributors to carbon sequestration, but their contribution to flux remains significant in the mesopelagic due to fragmentation of large sinking particles, (Wang and Fennel, 2022). However, in-situ measurements using neutrally buoyant devices, suggest that size is far less important in determining sinking velocities of particles than previously believed (Iversen and Lampitt, 2020). A Bayesian hierarchical model framework was used to analyze a large data set of measured sinking velocities, finding that sinking velocity of marine particles scales more closely with the square root of the particle diameter than with diameter squared (Cael et al., 2021). This implies that excess density and aggregate porosity play a larger role in determining sinking velocity than previously assumed.

The importance of aggregate density for POM flux was widely discussed as the so-called Ballast Hypothesis, which interpreted the strong correlation between fluxes of mineral particles such as calcium carbonate, biogenic and lithogenic silica (e.g., from dust) with POC fluxes (Deuser et al., 1983) to suggest that mineral incorporation enhances POC flux (Armstrong et al., 2002; Klaas and Archer, 2002; Francois et al., 2002). However, this regression approach cannot differentiate between cause and effect (Passow, 2004; Passow and De La Rocha, 2006). Moreover, the accumulation of minerals on organic aggregates causes aggregates to condense and fragment into smaller particles (Passow and De La Rocha, 2006; De La Rocha and Passow, 2007). The competing processes of density addition and size reduction mean that the relationship between sinking velocity and mineral content is not straightforward (Hamm, 2002; Lee et al., 2009; Ploug et al., 2008a). Nevertheless, an impact of ballasting minerals on sinking velocity has been observed in laboratory experiments (De La Rocha and Passow, 2007; Iversen and Ploug, 2010) and in field observations (Sanders et al., 2010; Fischer and Karakaş, 2009; Lee et al., 2009).

In contrast, positively buoyant Transparent Exopolymer Particles, TEP, may reduce sinking velocity when abundant in aggregates (Engel and Schartau, 1999; Azetsu-Scott and Passow, 2004). Whereas originally it was thought that high TEP concentrations would lead to high sedimentation rates (Riebesell et al., 2007), it is now clear that an overabundance of TEP compared to non-TEP POC will lead to reduced sinking velocities and delayed POC sedimentation events (Mari et al., 2017).

### **Controls on loss rates**

Flux attenuation and its spatial and temporal variability is influenced not only by sinking velocity, but also by the physical, physiological, and ecological factors that drive loss rates of POM due to zooplankton and bacterial and viral activities.

Consumption of POM through feeding decreases the total amount of carbon potentially available for sinking, and, in addition, the feeding activities of zooplankton change the size, number, composition, and sinking velocity of the remaining carbon (Dilling and Alldredge, 2000; Goldthwait et al., 2005; Noji, 1991; Koski et al., 2007; Lombard and Kiørboe, 2010) by repackaging the portion of the organic matter that is not assimilated into fecal pellets (Turner, 2002; Steinberg and Landry, 2017). Like other types of marine snow, fecal pellets (especially crustacean fecal pellets) frequently fall victim to ingestion (coprophagy) and fragmentation (coprorhexy) by copepods and protozoa-plankton while sinking (Noji, 1991; Poulsen and Iversen, 2008). Mesozooplankton also reduce the particle flux by breaking up aggregates into smaller particles while swimming, which affects not only sinking velocity but also remineralization rate (Goldthwait et al., 2005). Fragmentation of sinking particles via swimming zooplankton has been estimated to account for up to half of all flux attenuation (Briggs et al., 2020). In addition, this fragmentation can release DOM from the aggregate that would have otherwise been transported to depth within the pore water of the sinking particle (Alldredge, 2000).

Marine snow, including fecal pellets and aggregates are hotspots of activity with high remineralization and solubilization rates resulting in turnover times within hours to days (Azam, 1998; Azam and Long, 2001; Kiørboe et al., 2004; Smith et al., 1992). Bacterial hydrolysis (Arnosti et al., 2012) plays a major role in the decomposition and carbon specific remineralization rates of marine snow, which were determined experimentally to range from 0.08 day<sup>-1</sup> to 0.20 day<sup>-1</sup>, and are temperature dependent with a 3.5 fold decrease at 4°C compared to 15°C (Iversen and Ploug, 2010; Iversen and Robert, 2015). Hydrolytic enzymes, such as proteases, polysaccharidases, and glucosidases released by bacteria, are especially effective within the confined spaces of marine snow (Grossart et al., 2007; Simon et al., 2002; Zierovogel et al., 2010). These enzymes act to digest dissolved and particulate organic matter, turning it into lower molecular weight DOM that is directly available for uptake and consumption. Although some of the solubilized material is taken up by aggregate-associated bacteria, sinking aggregates leave behind them a plume enriched in nutrients and DOM that serve as a food source for free-living bacteria and as a chemical cue for colonizing and/or feeding organisms to locate the organic-rich aggregate (Kiørboe and Jackson, 2001; Ploug and Grossart, 2000; Cho and Azam, 1988). These complex interactions between attached and free microbial communities, POC, and DOC (Azam, 1998; Azam and Malfatti, 2007) affect colonization and turnover rates of particles, (Ploug et al., 2008b; Ploug and Grossart, 2000) resulting in high spatial and temporal variability in loss rates of marine snow. Bacteria not only participate in the degradation of sinking aggregates, but may also have a key role in the aggregation process through their stimulation of phytoplankton to produce sticky, surface-active exudates, like TEP (Gaerdes et al., 2011; Koch et al., 2014). The role of viruses, while acknowledged, has rarely been quantified (Suttle, 2007).



### Flux attenuation with depth

When applied to an individual marine snow particle the ratio between sinking velocity (in m/day) and the loss rate due to remineralization, fragmentation or solubilization (in day<sup>-1</sup>) determine the particle's remineralization length scale (in m), defined as the distance over which the carbon flux declines by about 63% (1/e) (Kwon et al., 2009). If the concept is applied to all organic carbon sinking out of the surface ocean, then the average remineralization rate and sinking velocities of all organic carbon, which include non-sinking organic matter, determine overall flux attenuation. A number of empirical models have been fit to in-situ measurements of POC flux, of which the "Martin Curve" has become the most widely used (Martin et al., 1987; Buesseler et al., 2020). The Martin Curve relates the flux ( $F$ ) at any depth ( $z$ ) beneath the euphotic zone depth ( $z_{eu}$ ) to the flux at the base of the euphotic zone ( $F_{eu}$ ) via a power-law relationship:

$$F_{eu} = F \left( \frac{z}{z_{eu}} \right)^{-b} \quad (1)$$

Here  $b$  is the Martin exponent, which determines the rate of flux attenuation over depth - larger  $b$  means faster attenuation and shallower POC remineralization. Qualitatively, the Martin Curve is similar to an exponential decline over the top few hundred meters, but attenuates more slowly at depth. Quantitatively, the relationship can be derived by assuming a linear increase in the remineralization length scale over depth, which could reflect either increasing velocity or decreasing remineralization rate with depth (Kriest and Oschlies, 2008). An exponent of  $-0.858$  was derived by fitting Eq. (1) to flux trap data from the North Pacific Ocean (Martin et al., 1987), and this has been adopted as a canonical value in modeling and flux estimation. However, subsequent observations have revealed significant variability in  $b$  ( $-0.4$  to  $-1.6$ ), indicating that the canonical version of the Martin Curve cannot be applied universally. Recent work has focused on identifying systematic regional patterns in  $b$ , and understanding its mechanistic controls (Section "Carbon sequestration by the biological pump").

### Sedimentation and burial

Of the net 50–60 Pg C (4–5 Pmol C) fixed into organic matter in the surface ocean each year, approximately 0.5 Pg C reaches the seafloor (at depths greater than 1000 m) but only about 0.002–0.16 Pg C (0.01–0.3% of NPP) are preserved in ocean sediments (Hedges and Keil, 1995; Seiter et al., 2005). The accumulation of sedimentary organic carbon varies greatly from place to place, with continental margin sediments accounting for the majority (Hedges and Keil, 1995; Deb and Mandal, 2021; de Haas et al., 2002). Only a small fraction of the total sedimentary organic carbon accumulates in the open ocean, although it accounts for 80% of the NNP, suggesting a low preservation efficiency of 0.02% compared to 1.4% on continental shelves and slopes. In low productivity regimes the underlying seabed experiences low sedimentation rates, low rates of organic matter degradation, and deep oxygen penetration that reduces preservation (Jørgensen et al., 2022). Additional variability in preservation efficiency can be driven by the nature of settling organic matter, and the biological, geochemical, and physical attributes of its environment (LaRowe et al., 2020; Jørgensen et al., 2022). It has been noted that estimates of organic carbon oxidation and burial in the global seafloor often exceed measured organic carbon fluxes in the water column, emphasizing uncertainties in BCP budgets (Jørgensen et al., 2022).

### Quantifying organic matter fluxes

Building a quantitative and mechanistic understanding of the BCP at the global scale requires the accurate measurement and upscaling of the organic matter fluxes that redistribute carbon from the surface to the deep ocean. A wide range of methodologies have been developed to achieve this, from direct measurement of sinking particles (Section "Measurement of sinking particle flux") to indirect geochemical constraints (Section "Remineralization tracers"). In general, sinking particle fluxes have received the most attention and are routinely measured across a range of spatial and temporal scales, facilitating global upscaling using remote sensing and empirical models (Section "Upscaling gravitational POC export"). Organic matter fluxes mediated by migrating organisms and physical processes have proven more challenging to quantify (Section "Estimating physical export and active transport"), and global rates of these processes remain relatively unconstrained (Section "Total export and double counting").

### Measurement of sinking particle flux

Various approaches have been developed to quantify the sinking flux of POC, each with unique strengths and weaknesses. Moored or free-floating sediment or particle interceptor traps directly collect sinking particles (Section "Sediment traps"). Particle-reactive nuclides can be used to estimate particle fluxes based on disequilibrium conditions (Section "Particle reactive radionuclides"). Visual estimates of particle concentration can be converted to flux estimates by applying empirical estimates of sinking velocity (Section "Marine snow catchers and UVP"). Most recently, BGC-Argo floats have been used to estimate seasonal export based on beam attenuation (Section "BioARGO"). Direct comparisons between these different approaches are often difficult because each integrates over different temporal and spatial scales (Section "Comparison of measurement methods").

### Sediment traps

The collection of particles in sediment traps is perhaps the most direct method for estimating sinking POC fluxes in the ocean (Estapa et al., 2020; Buesseler et al., 2007a). Although there are many different sediment trap designs in operation, sediment traps generally comprise a funnel or cylinder that channels sinking material into a cup for collection (Fig. 5), where it is poisoned with formalin or mercuric chloride to prevent microbial decomposition. Traps can be tethered to the seafloor (usually deployed at a fixed location at >1000 m depth), or they may drift at a fixed depth in the water column supported either by tether to a surface float or by regulating their buoyancy in the case of modern Neutrally Buoyant Sediment Traps (NBSTs, Buesseler et al., 2007a). NBSTs follow the local currents at their deployment depth, whereas surface-tethered trap trajectories are governed by a combination of surface currents and winds (Estapa et al., 2020). Trap deployments may span days to a year. Fluxes are then calculated by dividing the accumulated organic matter mass by the collection time and trapping area, yielding average rates over days to months.

Overall, sediment traps have provided an incredible wealth of information concerning the flux of POM as well as of  $\text{CaCO}_3$ , biogenic and lithogenic silica to depth (e.g. Armstrong et al., 2002; Francois et al., 2002; Honjo et al., 2008). In addition to flux, they allow changes in particle composition over depth to be quantified, revealing for example the preferential remineralization of nitrogen and phosphorus relative to carbon (Schneider et al., 2003), and preservation of ballast minerals relative to organic matter (Armstrong et al., 2002). Further recent advances in sediment trap design have allowed particles to be trapped in gel layers for microscope analysis, imaging, and classification (Durkin et al., 2015) or incubated in-situ to quantify POC respiration rates via oxygen consumption (McDonnell et al., 2015).

Like all observational methods, sediment traps are not without their limitations (Buesseler et al., 2007a; Honjo et al., 2008). Migrating zooplankton ('swimmers') may swim into the traps and be retained and measured, although they are not actually part of the sinking flux. Traps may also over- or under-collect particles due to hydrodynamic effects, especially near the surface where rapid flow of water over collectors can result in the advection of material into or around the traps (Estapa et al., 2020). In particular, surface-tethered traps are thought to over collect swimmers and POM in general (Buesseler et al., 2000) and traps with conical/funnel shaped collectors are thought to preferentially collect larger particles (Baker et al., 2020). NBSTs with cylindrical collectors appear to largely mitigate most biases and are increasingly seen as the "gold standard" for accurate collection (Baker et al., 2020; Estapa et al., 2020). Following collection, both POM and undersaturated biominerals such as celestite and biogenic silica, may be solubilized in sediment traps, especially during long deployments (Antia, 2005), thereby underpredicting the total flux of all these constituents.

Further problems are encountered when attempting to interpret flux profiles from arrays of sediment traps as a record of a 1-dimensional "rain" of sinking particles originating in the surface. Depending on their deployment depth, traps may collect particles that were transported to depth in part by vertical migration or physical mixing. Additionally, due to the advection of sediment traps and sinking particles by depth-varying ocean currents, traps integrate the flux across a "statistical funnel" that collect

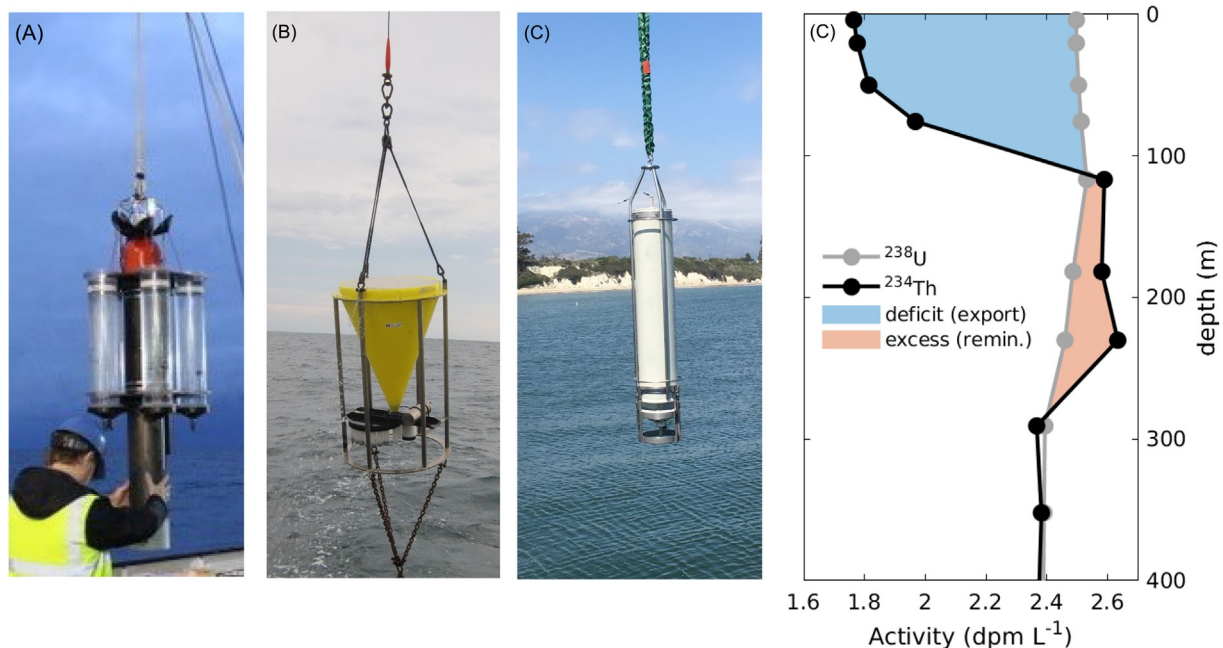


**Fig. 5** Common approaches for measuring gravitational POC flux. (A) Neutrally-buoyant sediment trap with cylindrical collectors. (B) Surface-tethered sediment trap with conical collector. (C) Marine snow catcher. (D) Depth profiles of the  $^{238}\text{U}$ - $^{234}\text{Th}$  parent-daughter radionuclide pair. POC export from the top 100 m can be estimated by integrating the deficit of  $^{234}\text{Th}$  (blue shading) relative to secular equilibrium, in which parent and daughter activities are equivalent. Excess  $^{234}\text{Th}$  below 100 m (red shading) reflects release during POC remineralization (data: E. Black). (A) Photo from M. Estapa.

from a surface source region of 10s to 100s of square km (Siegel et al., 2008; Liu et al., 2018). Together, these effects can lead to particles “appearing” at depth without being recorded by shallower traps (Boyd et al., 2019).

### Particle reactive radionuclides

Radionuclides in the uranium decay series serve as useful tracers of POC flux, owing to the propensity of decay products to scavenge (adsorb) onto sinking organic particles (Bacon and Anderson, 1982). Tracer pairs consist of a soluble parent nuclide and a particle-reactive daughter, and include  $^{238}\text{U}$ - $^{234}\text{Th}$ ,  $^{234}\text{U}$ - $^{230}\text{Th}$ , and  $^{235}\text{U}$ - $^{231}\text{Pa}$ . In each case, the half-life of the parent exceeds the mixing time of the ocean and its distribution throughout the ocean is uniform or correlated to salinity (Buesseler et al., 1992). In the upper ocean the observed activities of  $^{234}\text{Th}$ ,  $^{230}\text{Th}$ , and  $^{231}\text{Pa}$  are lower than expected from secular equilibrium (parent activity = daughter activity). The disequilibrium provides a measure of the uptake of the daughter onto sinking particles, which can then be vertically integrated to estimate the flux of the particle-adsorbed nuclide (Coale and Bruland, 1985; Buesseler et al., 1992). By measuring the ratio of nuclide to POC in particles collected at that depth horizon, the flux of nuclide can be converted into an estimate of the POC particle flux (Buesseler et al., 1992).

In the  $^{238}\text{U}$ - $^{234}\text{Th}$  pair, the daughter nuclide decays rapidly with a half-life of 24.1 days and the  $^{234}\text{Th}$  deficit is largely confined to the upper  $\sim 100$  m where particles are abundant and scavenging is fast enough to maintain disequilibrium (Fig. 5). Vertical profiles of  $^{234}\text{Th}$  are therefore commonly used to gauge POC export from the surface euphotic zone (e.g., Buesseler et al., 1998) and the method was recently applied over large basin scales during the GEOTRACES program (e.g. Anand et al., 2018; Black et al., 2018). Beneath the euphotic zone, a layer exceeding secular equilibrium is sometimes observed, which can be used to quantify  $^{234}\text{Th}$  from remineralizing particles (Black et al., 2018, Fig. 5). In the  $^{234}\text{U}$ - $^{230}\text{Th}$  pair, radioactive decay is a negligible sink of dissolved  $^{230}\text{Th}$  (75,400 year half-life) compared to particle scavenging, meaning the flux of particle-adsorbed  $^{230}\text{Th}$  can be approximated by simply integrating  $^{234}\text{U}$  activity down to the depth horizon of interest (Anderson et al., 2016; Pavia et al., 2019). This nuclide pair can therefore be used to reconstruct particle fluxes through the entire water column (Pavia et al., 2019), and integrates over the scavenging residence time of  $^{230}\text{Th}$ , on the order of tens of years (Pavia et al., 2020).

The main weakness of these methods lie in the estimation of reactive nuclide to carbon ratios, which vary widely with the composition of POM (Buesseler et al., 2006) and may be biased if only a subset of the scavenging particles are collected (Pavia et al., 2019).

### Marine snow catchers and UVP

Marine snow catchers (MSC) (Lampitt et al., 1993) are large volume (about 100 Liter) water sampler that partition particles by their sinking velocity (Riley et al., 2012; Giering et al., 2016). Following deployment and retrieval, the MSC is secured in an upright position, and particles allowed to gravimetrically settle for commonly exactly 2 h. Non-sinking particles are then collected from the top section of the MSC, while the water in the base section includes slow and fast sinking particles as well as macroscopically visible marine snow that can be hand collected. Particle flux is calculated from the measured particle concentration in each speed category and a range of sinking velocities estimated from settling time and height of the MSC.

Underwater Vision Profilers (UVPs, Picheral et al., 2010) provide another opportunity to convert measured particle abundance to estimated fluxes, but provides no internal estimate of sinking velocity for the conversion. Instead, size spectra observations derived from particle imaging (Fig. 4) are converted to POC mass and flux using allometric relationships that link aggregate carbon content and sinking velocity to size. The parameters are constrained by comparison to independent flux estimates from sediment traps (Guidi et al., 2008, 2015; Cram et al., 2018).

The strength of the UVP approach is that observations are relatively fast and economical compared to sediment traps, and data can be retrieved from the entire water column (usually down to 2000 m in a single cast (Kiko et al., 2022)). Therefore, if a universal scaling relationship exists between size and flux, this approach can expand the number and range of flux profiles by orders of magnitude. However, such a universal scaling is unlikely given that other particle properties such as shape (spherical aggregate vs. cylindrical pellets) and density (ballast content and porosity) vary significantly between regions and likely even between size categories (Stemmann and Boss, 2012). It is therefore desirable to calibrate the relationships at local scales and across narrower size ranges, which is currently a challenge given the small number of overlapping UVP and sediment trap observations. Another limitation is that UVP provides (quite literally) an instantaneous snapshot of the particle assemblage in  $\sim 5$  L of water per meter (Picheral et al., 2010), making this method especially prone to biases by under or oversampling episodic events (Stemmann and Boss, 2012).

### BioARGO

To overcome the gaps in spatial and temporal resolution that limit most flux measurement methods (Section “Sediment traps,” “Particle reactive radionuclides,” and “Marine snow catchers and UVP”), seasonally-integrated export estimates are increasingly conducted using data collected by autonomous platforms, especially BGC-Argo floats. These floats, which on average work continuously for 4 years once deployed, measure a range of parameters at regular intervals (e.g. every 10 days), including: beam attenuation (optical backscattering), a proxy for POC; in vivo chlorophyll fluorescence, a proxy for phytoplankton biomass; and oxygen concentration between the surface and 2000 m. When the float surfaces, data is transmitted back to researchers via satellite. The high temporal and spatial resolution of data collected via a large array of Argo floats provides statistically strong information, likely accounting for episodic events more robustly than other techniques.

The vertical POC flux across the base of the euphotic zone can be estimated from such data assuming that it equals the accumulation of POC within the mesopelagic during the transition between winter and summer (Dall'olmo and Mork, 2014; Wang and Fennel, 2022). Flux of large and small particles may be assessed individually by separating the baseline and spike signals in beam attenuation data and applying inversion models. Remineralization and fragmentation of particles as they sink can be quantified by incorporating O<sub>2</sub> data (Wang and Fennel, 2022), using a series of assumptions including constant sinking velocities, remineralization and fragmentation rates.

Underwater gliders are another class of autonomous platforms that have found success in closing spatio-temporal gaps that elude traditional measurement methods. Specifically, they have found use in mapping the POC distribution across small-scale physical features like fronts and eddies (Omand et al., 2015), allowing physical particle export by these ephemeral events to be quantified (Section “Estimating physical export and active transport”).

### Comparison of measurement methods

It is difficult to directly compare fluxes measured by different methods, as each method integrates over different temporal and spatial scales, and includes different pathways of downward transport. UVP and MSC based flux estimates cover the smallest spatio-temporal scales, whereas traps integrate over days to weeks, radionuclides integrate over weeks (<sup>234</sup>Th) to years (<sup>230</sup>Th) and regional scales, and Bio-ARGO can integrate up to seasonal and basin scales. Additionally, drifting sediment traps underestimate small particles due to hydrodynamics (Buesseler et al., 2007a), whereas MSC and UVP can undersample rare large particles that may be absent from the volume of water collected or imaged (100 L for MSC, 5 L per meter for UVP). Whereas traps, UVP, MSC, and Bio-ARGO floats collect or observe sinking particles directly, <sup>234</sup>Th export measures particle disappearance, hence the degree to which active migration is included in the measurements differs between these approaches. Nevertheless, despite their differences it is desirable to combine data from multiple approaches to build large particle flux datasets to calibrate upscaling methods (Section “Upscaling gravitational POC export”) and validate prognostic biogeochemical models. Recently, sediment trap and <sup>234</sup>Th-based export estimates have been compiled for this purpose (Bisson et al., 2018) given that both estimates integrate export over timescales (days to weeks) suitable for constraining monthly flux climatologies, yielding a dataset of >1700 measurements that records spatial and seasonal flux variations (Fig. 6A).

### Remineralization tracers

An alternative approach for quantifying particulate organic matter fluxes is to examine the geochemical signatures of their remineralization (oxygen depletion, nutrient release) in the ocean interior, rather than the particles themselves. Remineralization tracers must be combined with information about water mass ventilation to quantify remineralization rates and the flux of organic matter that supplies them (Jenkins, 1987). These approaches integrate over ocean basins and ventilation timescales (years to hundreds of years depending on depth) and therefore provide a stronger time-mean flux constraint than the methods discussed in Section “Measurement of sinking particle flux”. However, while oxidation of organic particles is often assumed to be the only source of remineralization tracers (Keeling et al., 2010; Weber et al., 2016), they can also accumulate due to the decomposition of dissolved organic matter, complicating their interpretation (Burd et al., 2010).

### Oxygen utilization rates

Oxygen is supplied from the surface into the ocean interior by the physical processes of advection and mixing, largely in mid-high latitude regions. After leaving the surface, water masses accumulate an oxygen deficit due to the oxidation of organic matter during remineralization, referred to as apparent oxygen utilization (AOU) and quantified based on undersaturation (Jenkins, 1982; Kadko, 2009). Dividing AOU at a point in the ocean interior by an estimate of ventilation age (time since water mass left the surface) yields the oxygen utilization rate (OUR), averaged across the transport pathway from the surface. Integrating OUR over depth then yields the total amount of oxygen consumed beneath the euphotic zone each year, which can be converted stoichiometrically to estimate the POC export flux (Jenkins, 1982).

In these applications, it is critical to select an appropriate tracer for the ventilation age of subsurface water from the available options (e.g., chlorofluorocarbons, radiocarbon, <sup>3</sup>H–<sup>3</sup>He, <sup>7</sup>Be). The timescales recorded by some of these tracers are not suitable for resolving the circulation of the upper mesopelagic zone (Kadko, 2009), and in all cases the measurements are not trivial and subject to uncertainty. Even with perfect ventilation age information, the OUR approach can overestimate remineralization rates by up to a factor 3 in shallow waters close to water mass formation regions, where rapid diffusive mixing can decouple AOU and age (Koeve and Kahler, 2016). In other regions, POC fluxes estimated from depth-integrated OUR have been shown to significantly exceed direct constraints from sediment traps, partially because DOC remineralization accounts for upwards of 20% of the oxygen loss (Burd et al., 2010).

### Remineralized nutrients

Like oxygen, subsurface macronutrient distributions can be broken into two components: one transported from the surface ocean (preformed nutrients) and one that accumulates along circulation pathways due to organic matter decomposition (remineralized nutrients) (Broecker et al., 1985). The remineralized nutrient distribution contains information about the rates and patterns of remineralization in the water column (Anderson and Sarmiento, 1994). Recently, an approach was developed to extract this rate information in a data-constrained ocean circulation model, by computing the remineralization source required to balance transport



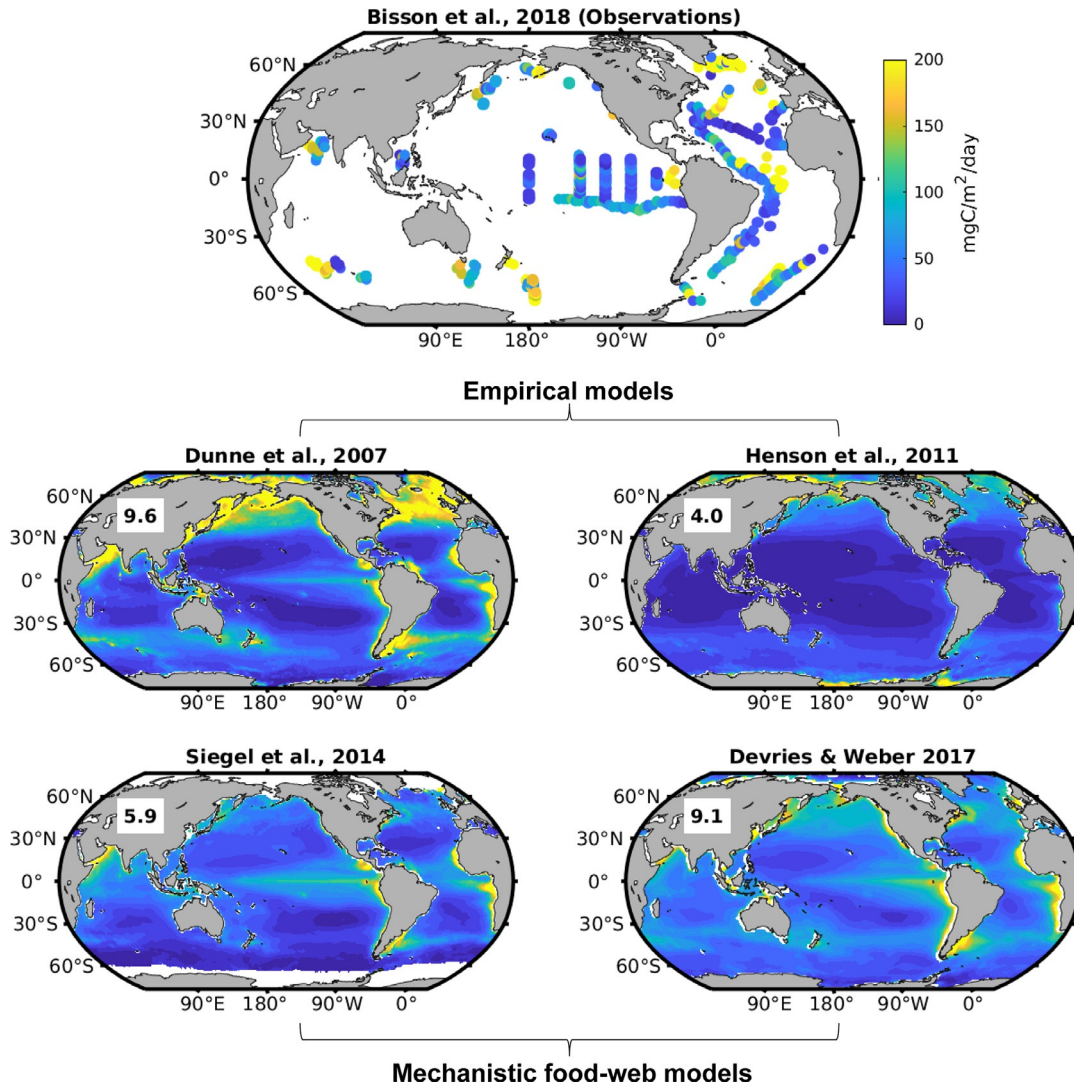


**Fig. 6** Global patterns of POC export. Top: Observed POC flux at the base of the euphotic zone measured by sediment traps and the  $^{238}\text{U}$ – $^{234}\text{Th}$  nuclide pair, compiled by Bisson et al. (2018). Bottom: Global upscaling estimates from studies that use empirical and mechanistic (food-web) models trained by subsets of the observations. Numbers in the top left give the integrated global POC export flux in Pg. C/yr. Number in the top left give the integrated global POC export in units of.

divergence of  $\text{PO}_4$  in the ocean interior (Weber et al., 2016; Weber and Bianchi, 2020). Replacing the ventilation age tracer used in OUR calculations with a circulation model that is optimized to match CFC, radiocarbon, and  $^3\text{He}$  observations circumvents the limitations of any one tracer, and better accounts for the effects of diffusive mixing near the surface (Koeve and Kahler, 2016). Furthermore, remineralization rates can be diagnosed at sufficient vertical resolution to reconstruct the POM flux profile through the entire water column (Weber et al., 2016), revealing systematic regional differences in flux attenuation (see Section “Metrics of carbon sequestration”).

Limitations of this approach include the assumption that dissolved organic phosphorous (DOP) remineralization makes a negligible contribution to  $\text{PO}_4$  remineralization at depth (Abell et al., 2000; Torres-Valdés et al., 2009) and the need to assume an organic C: P ratio to convert to POC flux. In principle, the latter limitation could be overcome by applying the same method to AOU instead of remineralized  $\text{PO}_4$ , given that the  $\text{O}_2$ : C respiratory quotient is much more stable than organic matter C: P (Tanioka and Matsumoto, 2020; Martiny et al., 2013). However AOU does not record organic carbon oxidation during denitrification and is more strongly influenced by DOM remineralization since DOC penetrates much deeper than DOP (Abell et al., 2000), so is a more ambiguous tracer of the particle flux than remineralized  $\text{PO}_4$ .

### Upscaling gravitational POC export

#### Upscaling methods

To quantify carbon export at the global scale, sparse in-situ measurements of the sinking POC flux must be extrapolated to spatially continuous global products. In general, this is achieved by leveraging the high spatiotemporal resolution of satellite NPP estimates,

and using observations to train empirical or mechanistic models that predict the so-called “particle export ratio” (*pe*-ratio), i.e. the fraction of NPP routed to sinking particles that leave the surface euphotic zone or top 100 m (Dunne et al., 2005). In the case of mechanistic food-web models, in-situ measurements are used to calibrate uncertain parameters governing aggregation, grazing, egestion of fecal pellets, and POC loss due to respiration by the surface microbial community.

Empirical analyses find that temperature is a key variable relating POC export to NPP, with lower fractional export in warmer waters (Dunne et al., 2005; Laws et al., 2011; Henson et al., 2011). Food-web models have linked this relationship to the temperature-dependence of microbial respiration of POC (Laws et al., 2000; DeVries and Weber, 2017; Nowicki et al., 2022), which require a 2–3 increase in respiration for each 10 °C warming to reproduce in-situ flux measurements. The empirical model of Henson et al. (2011) finds that temperature alone can explain ~50% of variance in <sup>234</sup>Th-based measurements of the *pe*-ratio, whereas other empirical models (Dunne et al., 2005; Laws et al., 2011) find that NPP is a secondary key predictor, with higher NPP resulting in higher fractional export. The same relationship emerges indirectly in food-web models, because, when NPP is high, large phytoplankton dominate, and aggregate into large fast-sinking particles (Siegel et al., 2014).

### Global patterns and rates

In general, the global patterns of POC export predicted by upscaling methods (Fig. 6) resemble the satellite-derived NPP estimates (Fig. 3) they are derived from. However, spatial gradients in POC export tend to be stronger than NPP, due to the compounding effects of higher *pe*-ratios in cold, productive regions. In low latitudes, most approaches agree that POC export increases strongly between oligotrophic subtropical gyres (20–50 mg/m<sup>2</sup>/day) and productive tropical upwelling regions (50–100 mg/m<sup>2</sup>/day), while high latitude regions are less well constrained. The food-web models of Siegel et al. (2014), DeVries and Weber (2017), and Nowicki et al. (2022) predict annual-mean POC export rates in the subarctic Atlantic and Pacific that are similar to (or slightly lower than) tropical regions, whereas the empirical models of Dunne et al. (2005) and Henson et al. (2011) suggest that subarctic export is ~2-fold higher than any other region (Fig. 6). These differences likely stem from two factors. First, the empirical models link POC to chlorophyll-based NPP products, whereas the more recent food-models tend to use carbon-based NPP products that estimate higher tropical productivity (Fig. 3C). Second, food-web models tend to predict a weaker overall effect of temperature on the *pe*-ratio than empirical models (Siegel et al., 2014; Henson et al., 2011), especially for larger particles that are rapidly exported from the surface. In the Antarctic region of the Southern Ocean, direct measurements of particle flux (traps and <sup>234</sup>Th) are especially scarce (Bisson et al., 2018); Fig. 6A) making it a particularly challenging region to upscale, and recent compilation of Bio-ARGO data suggests that all models significantly underpredict POC export south of 50°S (Arteaga et al., 2018).

Globally, upscaling models estimate that 4–9.6 Pg C/yr. is exported from the euphotic zone as sinking POC (Fig. 7), with the empirical models of Henson et al. (2011) and Dunne et al. (2005) representing the upper and lower limits, respectively. In both limiting cases, it is possible that the global estimate is biased by the choice of in-situ data used to fit the model. Henson et al. (2011) used a compilation of <sup>234</sup>Th-based export measurements available at that time, which may be biased low compared to a more complete compilation of <sup>234</sup>Th and trap-based measurements (Bisson et al., 2018). On the other hand, Dunne et al., 2005 combined sediment trap and <sup>234</sup>Th measurements with “net community production” data, which integrate the effect of all export pathways and would therefore overestimate the sinking POC flux (see Section “Estimating physical export and active transport”). Averaging the available upscaling estimates yields a range of  $7 \pm 1.5$  Pg C/yr., which closely overlaps with the range of  $7.1 \pm 2$  predicted by the CMIP6 suite of Earth System Models (ESMs) that resolve ocean biogeochemical cycles (Henson et al., 2022). Unlike the upscaling methods discussed here (which link satellite NPP to particle export measurements) ESMs attempt to predict

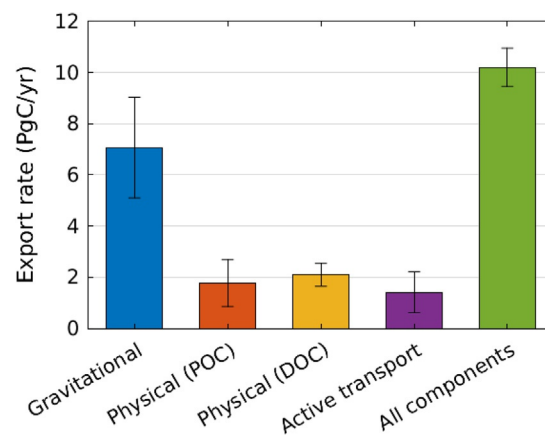


**Fig. 7** Global carbon export by each pathway of the BCP. Gravitational, Physical (POC), and Active transport estimates are from Boyd et al. (2019), which compiles prior global estimates and scales up local-scale rates; Physical (DOC) is from Roshan and DeVries (2017), which combines machine learning mapping of DOC with an ocean circulation model. All components is from Nowicki et al. (2022), which is the first study that attempts to simultaneously constrain all of the export pathways in a data-assimilation model. Error bars are uncertainty estimates from the original data sources.

the entire marine organic carbon cycle mechanistically, from phytoplankton growth to particle export and remineralization. The convergence of these distinct methods suggests that gravitational POC export is now relatively well constrained at the global scale (Boyd et al., 2019).

### Estimating physical export and active transport

Organic carbon export by physical advection and mixing, and by vertically migrating zooplankton and fish (Fig. 2) have only recently been recognized as globally-significant processes, and their large-scale rates remain poorly constrained compared to gravitational POC export (Boyd et al., 2019). Of these pathways, physical export of dissolved organic carbon is perhaps best understood (Hansell et al., 2009). By combining observed DOC profiles with measurements of mixed layer depth and AOU, down-welling and detrainment of DOC from the mixed layer have been estimated to export 10% to 75% as much carbon as gravitational POC settling at local scales (Carlson et al., 1994; Emerson, 2014). Globally, two recent modeling studies that leveraged large DOC datasets found that physical DOC export sums to  $\sim 2$  Pg. C/yr. globally (Roshan and DeVries, 2017; Nowicki et al., 2022).

Small, slow-sinking organic particles are also detrained from the mixed layer during spring, driving annual POC export that is 25–100% as large as the gravitational flux, according to calculations using satellite-derived POC and ARGO mixed layer estimates (Dall'olmo and Mork, 2014). Eddy subduction provides an additional conduit for POC supply to depth, given that eddies can mix down to  $>300$  m and POC exhibits a very strong concentration gradient across this depth range (Fig. 1B). By mapping POC, oxygen, and temperature anomalies using an array of gliders in the North Atlantic, recent work showed that subduction of POC can rival or exceed the gravitational flux at the scale of an individual eddy (Omand et al., 2015). At the global scale, a high resolution modeling study found that all physical pathways combined export  $\sim 2$  Pg. C/yr. of POC from the mixed layer (Levy et al., 2013), similar to the physical DOC export, while extrapolating local measurements leads to a large uncertainty range of 0.1–2.6 Pg. C/yr. (Boyd et al., 2019; Fig. 7).

Carbon export by vertically migrating zooplankton has traditionally been quantified by combining sediment traps with net trawls that measure the diel change in biomass (Hidaka et al., 2001), and more recently by leveraging acoustic ADCP data and metabolic models (Bianchi et al., 2013b; Davison et al., 2013). Together, these approaches find that “active transport” amounts to 10–60% of the local gravitational POC flux. A simple upscaling of these local rates to the global ocean suggests a global export flux of 0.9–3.6 Pg. C/yr. by active transport (Boyd et al., 2019, Fig. 7), whereas predictions of global biogeochemical models that resolve the process mechanistically (Aumont et al., 2018; Nowicki et al., 2022) lie at the low end of this range ( $\sim 1$  Pg. C/yr.).

### Total export and double counting

A recent global modeling study (Nowicki et al., 2022) explicitly resolved all export pathways (gravitational, physical, and active transport) and constrained them with NPP POC, DOC, and  $O_2$  datasets, finding a combined carbon export of  $10.2 \pm 0.5$  Pg. C/yr. This is close to the estimate of 11.1 Pg. C/yr. derived from an older upscaling (Laws et al., 2000) that used net community production, rather than sediment trap and  $^{234}\text{Th}$  data, to link satellite NPP to export. Net community production quantifies the total organic carbon loss from the surface ocean based on nutrient and oxygen budget analysis, and therefore this estimate should also combine all three export pathways. Interestingly, summing the central values from ranges of independent estimates for gravitational settling, physical export, and active transport (Fig. 6) yields  $\sim 12.5$  Pg. C/yr., around 20% higher than the Nowicki et al., 2022 estimate.

This suggests that some previous studies focused on single export pathways may have overestimated their global magnitude, which could occur if there is overlap in the carbon export attributed to different pathways by the methods described in Sections “Measurement of sinking particle flux,” “Remineralization tracers,” “Upscaling gravitational POC export,” and “Estimating physical export and active transport” (referred to as “double-accounting” by Boyd et al., 2019). For instance, sediment trap and  $^{234}\text{Th}$  estimates of the gravitational flux may also capture the active transport pathway to some degree, and some physical pathways like eddy subduction may export POC that would have otherwise settled out of the surface ocean, and would therefore be included in estimates of the gravitational pump (Boyd et al., 2019). Better distinguishing and quantifying the carbon export by each pathway is an important challenge for the next decade of BCP research, because each pathway will likely respond differently to global change and the overall perturbation of the BCP hinges on their relative importance.

### Carbon Sequestration by the biological pump

From the perspective of the global carbon cycle and climate, the most important metric of the BCP is not the export flux of organic carbon from the surface ocean, but the magnitude of the regenerated DIC inventory it maintains in the ocean interior (Fig. 1A) (Nowicki et al., 2022). This is often referred to as sequestered carbon, and represents the total amount of carbon isolated from exchange with the atmosphere in the deep ocean due to the net effect of organic matter export from the surface and remineralization at depth (Devries et al., 2012; Boyd et al., 2019).



### Metrics of carbon sequestration

Because oxygen is consumed while DIC accumulates during remineralization, ocean-integrated AOU provides a simple diagnostic metric for the total amount of carbon sequestered by the BCP (Ito et al., 2004; Carter et al., 2021; Wilson et al., 2022). The observed AOU inventory of  $\sim 200$  Pmol  $O_2$  (Gregoire et al., 2021) translates to  $\sim 1700$  Pg of stored carbon assuming standard C:  $O_2$  remineralization stoichiometry of  $-117:170$  (Anderson and Sarmiento, 1994). However, AOU may significantly overestimate the true oxygen utilization (TOU) in deep ocean waters that are ventilated from undersaturated high latitude surface regions (Ito et al., 2004). A model-based decomposition of the oxygen distribution that better accounts for high latitude undersaturation finds a TOU inventory of  $\sim 140$  Pmol  $O_2$ , which implies biological carbon sequestration of  $\sim 1200$  Pg C (Carter et al., 2021).

A closely related concept to the AOU-based definition of carbon storage is the so-called “efficiency” of the BCP, based on the degree of biological nutrient (usually  $PO_4$ ) utilization (Toggweiler, 2003). In this framework, subsurface  $PO_4$  is broken into: a preformed component ( $P_{pre}$ ) that represents  $PO_4$  that goes unutilized by plankton in the surface ocean and is transported physically to depth (Broecker et al., 1985), and a remineralized component ( $P_{rem}$ ) that accumulates in the ocean interior alongside respired carbon and AOU (Anderson and Sarmiento, 1994). Because the oceanic  $PO_4$  inventory is conserved on millennial timescales (Paytan and McLaughlin, 2007), the BCP can be thought to have weak and strong limits, in which the entire  $PO_4$  inventory is either preformed or remineralized, respectively (Ito and Follows, 2005). More complete nutrient utilization transforms  $P_{pre}$  into  $P_{rem}$  and drives the BCP toward its strong (or “efficient”) limit (Toggweiler, 2003). Phosphate is chosen as the defining nutrient in this framework, because even though nitrate is generally more limiting to phytoplankton growth and has a shorter oceanic residence time (Gruber and Galloway, 2008), the marine nitrogen inventory is thought to be closely coupled to  $PO_4$  by regulatory feedbacks linking denitrification and nitrogen fixation (Tyrrell, 1999; Deutsch et al., 2007). In the contemporary ocean, subsurface waters hold  $\sim 1.1$  Pmol of remineralized  $PO_4$ , which translates to  $\sim 1300$  Pg of sequestered carbon assuming a C: P remineralization ratio of 106 (Carter et al., 2021). This represents only a third of the total  $PO_4$  inventory of  $\sim 3.3$  Pmol, indicating that biological carbon storage lies closer to its weak theoretical limit than the strong limit and highlighting the potential leverage of high latitude nutrient utilization over global climate (Section “Climate sensitivity of carbon storage”).

Recently, a mechanistic metric has become popular that links carbon storage to both the organic matter supply to depth and the time required for respired DIC to recirculate back to the ocean surface, referred to as the “sequestration timescale,” and denoted  $\tau_{seq}$  (Devries et al., 2012; Weber et al., 2016; Siegel et al., 2022). For a given carbon remineralization rate, slower recirculation to the surface results in more efficient sequestration, and the total regenerated DIC that accumulates in the ocean interior is proportional to  $\tau_{seq}$  (Devries et al., 2012). The total ocean carbon storage ( $C_{seq}$ ) by the BCP is calculated as:

$$C_{seq} = \int_V r_{remin}(\mathbf{x}) \tau_{seq}(\mathbf{x}) dV \quad (2)$$

Here  $r_{remin}$  is the time-mean remineralization rate in units of carbon/ $m^3$ /time, and  $\mathbf{x}$  is the three-dimensional location vector (Siegel et al., 2022). In practice, this framework (referred to hereafter as the  $\tau_{seq}$  framework) is most applicable for quantifying carbon storage in the context of an ocean biogeochemical/circulation model, where the distribution of  $r_{remin}$  is known and  $\tau_{seq}$  can be calculated as the “first-passage” from each location ( $\mathbf{x}$ ) in the ocean interior to the surface (Primeau, 2005). Conceptually however, it provides insights that are equally applicable to the real ocean. Because deeper waters take longer to recirculate to the surface, the  $\tau_{seq}$  framework identifies the remineralization depth of organic matter as a critical determinant of carbon storage by the BCP (Weber et al., 2016; Kwon et al., 2009).

### Geographic variability of POC flux attenuation

Climate model simulations support the importance of remineralization depth in driving carbon sequestration, and therefore the ocean-atmosphere carbon balance (Kwon et al., 2009). In a model that assumes a “Martin-Curve” POC flux profile, adjusting the Martin exponent from 0.4 (slow attenuation, deep remineralization) to 1.4 (fast attenuation, shallow remineralization) results in a 100-200 ppm increase in atmospheric  $pCO_2$  (Kwon et al., 2009). In particular, the amount of organic carbon that remineralizes deeper than 1000 m is a key determinant of carbon storage by the BCP in climate models (Wilson et al., 2022), because respired DIC released beneath this horizon can be sequestered for hundreds of years before recirculating to the surface (Fig. 2). The “transfer efficiency” ( $T_{eff}$ ) of organic carbon to 1000 m (fraction of the export flux that reaches 1000 m) is therefore often used as a simple metric of remineralization depth (Lam et al., 2011).

Predicting the impact of climate change on ocean carbon sequestration, requires a mechanistic understanding of the controls on remineralization depth (Henson et al., 2022). While POC flux attenuation is broadly understood as a balance between particle sinking velocities and remineralization rates, each of these factors is influenced by numerous properties of the environment and the particles themselves, whose relative importance is poorly understood (Section “Flux attenuation”). To disentangle the first-order controls on remineralization depth, work over the last decade has focused on understanding the drivers of geographic variability in POC transfer efficiency. Efforts to identify systematic geographic patterns have applied many of the measurement approaches described in Section “Quantifying organic matter fluxes” and have reached differing conclusions.

Studies combining deep ocean ( $\sim 2000$  m) carbon fluxes measured by moored sediment traps (Honjo et al., 2008) with  $^{234}Th$  export estimates (Henson et al., 2012) and UVP-reconstructed flux profiles (Guidi et al., 2015) found evidence for slow POC flux attenuation (high transfer efficiency) in low latitude regions compared to high latitudes. A potential explanation for this pattern is

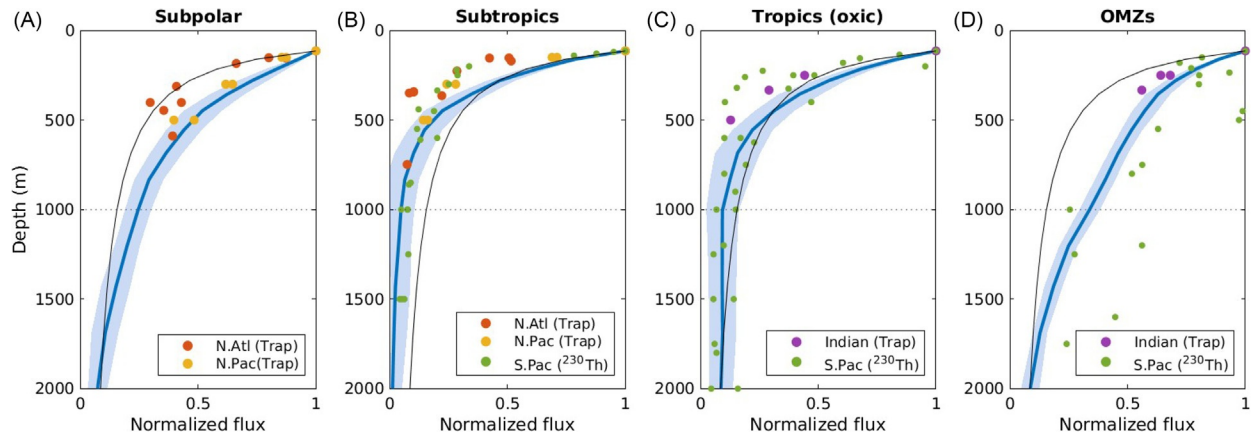


**Fig. 8** Converging lines of evidence for spatial variability in POC flux attenuation. Blue lines are regionally-averaged POC flux profiles reconstructed from remineralized nutrient distributions in an ocean circulation model by Weber et al. (2016) (A–C) and Weber and Bianchi, 2020 (D). Blue envelope gives the standard error of the regional-mean flux, quantified using a Monte Carlo procedure. Large red, yellow, and purple dots are fluxes measured using arrays of sediment traps in recent studies that focused on quantifying regional variability in flux attenuation in the North Atlantic (Marsay et al., 2015), North Pacific (Buesseler et al., 2007b), and Indian Oceans (Keil et al., 2016). Small green dots are fluxes reconstructed from particulate  $^{230}\text{Th}$  measurements along the GEOTRACES GP16 transect, crossing the Peruvian upwelling zone and South Pacific Subtropical gyre (Pavia et al., 2019). All fluxes are normalized to the flux at 100 m, the euphotic zone depth in the model of Weber et al. (2016) (fluxes shallower than 100 m are not shown). For observed flux profiles, the 100 m flux is estimated by extrapolating from the nearest measurement using the empirical fits provided in the original publications. In each panel, the thin black line is the canonical Martin Curve, for comparison, and the dashed line marks the 1000 m horizon, beneath which remineralized carbon is very efficiently sequestered.

that high latitude regions export “fresh” labile organic matter during seasonal blooms that decomposes quickly over depth, whereas low latitudes export the recalcitrant POC that escaped the rapid surface microbial loop (Henson et al., 2012; Lam et al., 2011). More recently, a consensus seems to be emerging from multiple lines of evidence for an opposite latitudinal pattern of transfer efficiency (Fig. 8). Arrays of NBSTs deployed down to  $\sim 500$  m in the subtropical and subarctic Pacific (Buesseler et al., 2007b) and Atlantic (Marsay et al., 2015) measured fast-attenuating fluxes in the top subtropics and slow-attenuating fluxes in high latitudes, compared to the canonical Martin Curve (Fig. 8A and B; Martin et al., 1987). A global time-mean flux reconstruction from remineralized  $\text{PO}_4$  (Weber et al., 2016) confirmed this latitudinal pattern and showed it extends to  $>2000$  m and into the southern hemisphere. Finally,  $^{230}\text{Th}$ -based flux profile reconstructions in the South Pacific provided additional support for very fast flux attenuation (Fig. 8B) in oligotrophic subtropical systems (Pavia et al., 2019).

While the flux profiles identified by these methods are not identical, they paint a consistent picture of systematic regional variability in POC transfer efficiency from 100 m to 1000 m, which is highest in subpolar oceans ( $\sim 25\%$ ), lowest in subtropical gyres ( $\sim 5\%$ ), and intermediate in tropical upwelling systems ( $\sim 10\%$ ) (Weber et al., 2016). Conspicuous outliers to this large-scale pattern are found in oxygen minimum zones (OMZs) of the Eastern Tropical Pacific and Arabian sea. In these regions, where the water column is functionally anoxic between  $\sim 100$  m down to 500–800 m, sediment traps (Devol and Hartnett, 2001; Keil et al., 2016),  $^{230}\text{Th}$ -based reconstructions (Pavia et al., 2019) and remineralized  $\text{PO}_4$  reconstructions (Weber and Bianchi, 2020) all find slower flux attenuation than oxygenated waters at similar latitudes, and extremely efficient POC transfer from 100 m–1000 m ( $>40\%$ ).

As with the  $pe$ -ratio (Section “Sediment traps”), a combination of empirical and mechanistic models have been used to explore the factors controlling regional variability in  $T_{\text{eff}}$  and extrapolate globally. Marsay et al. (2015) found that upper-ocean temperature could explain  $\sim 80\%$  of the variance in POC attenuation between subtropical and subarctic regions, presumably because warmer water boosts the metabolism of heterotrophic microbes and drives faster decomposition. Extrapolating globally, this relationship suggests extremely efficient carbon transfer to depth ( $T_{\text{eff}} > 40\%$ ) throughout the Antarctic sector of the Southern Ocean, although remineralization tracers (Weber et al., 2016) do not support  $T_{\text{eff}}$  values quite this high. Weber et al. (2016) found that the global pattern of transfer efficiency is well explained statistically by the size structure of the phytoplankton community, likely because smaller phytoplankton produce smaller slower-sinking particles (Section “Upscaling methods”), which remineralize shallow in the water column. Size-resolved mechanistic models of particle sinking and remineralization find an equally important role for temperature-dependent decomposition and size-dependent sinking speeds in controlling latitudinal  $T_{\text{eff}}$  variability (DeVries and Weber, 2017; Cram et al., 2018), and secondary roles for mineral ballasting and oxygen-dependent remineralization in enhancing  $T_{\text{eff}}$  at smaller scales (Cram et al., 2018).

The precise mechanisms explaining the extremely efficient POC transfer to depth observed in OMZs (Fig. 8D) remain poorly understood. Mechanistic models require a slowing of remineralization when oxygen drops below 5–30  $\mu\text{M}$  (Laufkötter et al., 2017; Cram et al., 2018) in order to reproduce observed particle flux profiles and remineralization tracers in OMZs, but oxygen availability does not appear to directly limit microbial respiration until nanomolar levels (Giovannoni et al., 2021). A number of hypotheses

have been advanced to explain the oxygen sensitivity of POC flux attenuation. First, POC remineralization may be limited by the catabolism of complex organic compounds to glucose, which is more sensitive to oxygen than the cellular respiration process itself (Giovannoni et al., 2021). Second, sinking organic aggregates can develop anoxic interiors and undergo slow anaerobic respiration even in oxygenated water columns, due to diffusion-limitation of the oxygen supply into the particle (Ploug, 2001; Bianchi et al., 2018). Finally, reduced zooplankton migration into oxygen-deficient layers of the water column (Bianchi et al., 2013a,b) could curtail particle fragmentation in the OMZ, preserving large particles that efficiently sink to depth (Cavan et al., 2017). Determining which of these processes explain the efficient POC transfer to depth in OMZs would improve our ability to predict carbon-climate feedbacks in a warming and deoxygenating ocean (Weber and Bianchi, 2020; Cram et al., 2022).

### Sequestration timescales

The sequestration time of respired  $\text{CO}_2$  increases strongly as a function of depth, reaching 100 years by  $\sim 300$  m and 1000 yrs. by  $\sim 3000$  m on average (Fig. 9A, (DeVries and Holzer, 2019, DeVries and Primeau, 2011)). For POC exported gravitationally from the euphotic zone, the majority remineralizes in waters shallower than 300 m that recirculate to the surface on decadal timescales (Fig. 2; Fig. 9A; DeVries and Holzer, 2019). This contributes very little to carbon sequestration ( $\sim 10\%$  according to Nowicki et al., 2022) compared to the smaller fraction of POC that penetrates into deeper waters where respired  $\text{CO}_2$  is sequestered for centuries (Fig. 9A). In fact, remineralization beneath 1000 m is estimated to be responsible for  $>50\%$  of total carbon sequestration even though only  $\sim 10\%$  of the sinking POC flux reaches this depth (Wilson et al., 2022; Nowicki et al., 2022; Siegel et al., 2014).

The mean sequestration time for exported carbon varies systematically between regions (Fig. 9B), controlled primarily by spatial variability in flux attenuation (Weber et al., 2016; Boyd et al., 2019). The mechanistic particle flux model of Cram et al. (2018), combined with the Ocean Circulation Inverse Model (DeVries and Holzer, 2019), predicts that carbon exported from the subtropical gyres (where  $T_{\text{eff}}$  is lowest, Fig. 8) is sequestered for only 50–150 years, compared to 150–250 years for most of the tropical and high latitude oceans. Sequestration time can exceed 400 years for regions with particularly slow flux attenuation, including tropical OMZs, the Subarctic North Pacific, and the Antarctic Southern Ocean. A secondary effect of the overturning circulation on the regional pattern is evident (Fig. 9B). Sequestration time is longer than expected from  $T_{\text{eff}}$  alone in tropical shadow zones and shorter than expected in regions of deep mixing such as the Subantarctic Southern Ocean, and tends to be slightly longer than in the Pacific than the Atlantic at similar latitudes (Fig. 9B), due to longer recirculation time for deep Pacific waters (Fig. 9A). Averaging across this pattern yields a global-mean sequestration time of  $\sim 140$  years for carbon exported via the gravitational pathway, consistent with other estimates of 120–150 years (Boyd et al., 2019; Nowicki et al., 2022; Siegel et al., 2014).

The relative importance of the gravitational export, physical export and active transport (Fig. 2) for carbon sequestration hinges not only on their export rates (Fig. 7), but also differences in sequestration time between pathways (Boyd et al., 2019). Eddy subduction and mixed-layer detrainment can deliver DOC and suspended POC rapidly to depths  $>300$  m (Levy et al., 2013; Omand et al., 2015), “bypassing” the shallow zone of rapid recirculation to the surface (Fig. 2). However, because DOC and suspended particles do not sink, they cannot deliver organic matter to the depths of most efficient sequestration ( $>1000$  m) before remineralization occurs. Physical export therefore results in shorter sequestration than gravitational export on average ( $\sim 50$  years and  $\sim 130$  years, respectively (Nowicki et al., 2022), and would sequester less carbon for a given export rate (Boyd et al., 2019).

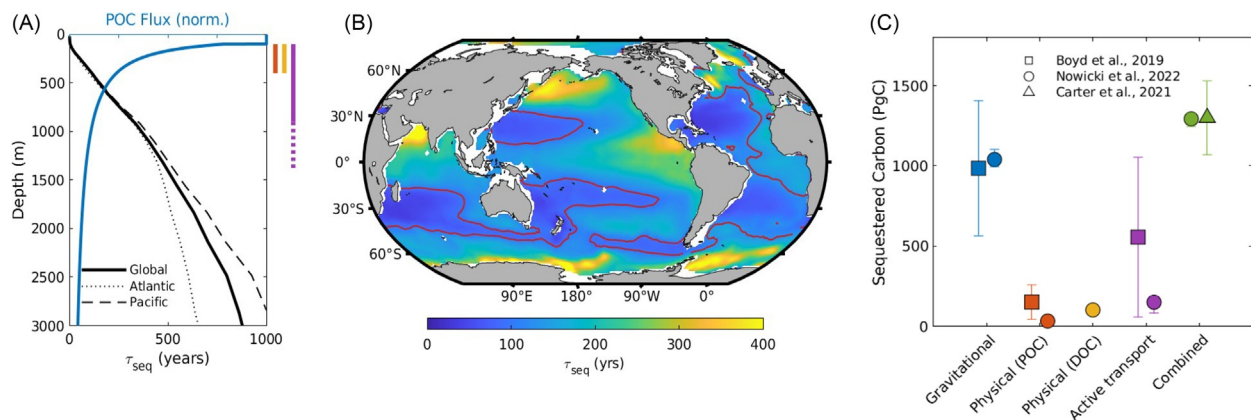


**Fig. 9** Carbon sequestration by the biological pump. (A) The sequestration time for respired carbon produced by organic matter remineralization at depth, averaged globally and in the Atlantic and Pacific Oceans (black lines, bottom axis). A characteristic POC flux profile (Martin Curve) is shown for comparison (blue line, top axis). Vertical lines to the right show the “injection depth” of other export pathways: Physical export of POC (red) and DOC (yellow), and active transport by diel migration (solid purple line) and seasonal hibernation (dashed purple line). Deep injection allows organic matter to bypass the first few hundred meters where remineralization is fast. (B), Mean sequestration time of carbon exported at each surface location. The spatial pattern reflects both regional variability in flux attenuation (from Cram et al., 2018) and recirculation pathways to the surface. Red contour is  $\tau_{\text{seq}} = 100$  yrs. (C) Estimated carbon sequestration by each BCP export pathway, and by all pathways combined. Boyd et al. (2019) compiles data from a range of sources and provides wide uncertainty ranges for each pathway. Nowicki et al. (2022) simulates all pathways simultaneously in a data-constrained model. Carter et al. (2021) use geochemical constraints on total carbon storage.

However, differences in bioavailability between suspended and sinking particles could change the carbon sequestration potential of the physical export pathway and is currently poorly constrained. Migrating zooplankton and fish can transport organic matter even deeper in the water column before it is remineralized, either due to respiration at their daytime migration depth (up to 800 m, Bianchi et al., 2013b) or production of fecal pellets that sink and remineralize deeper still (Turner and Holmes, 2015). The average sequestration time for carbon exported via this pathway is poorly constrained but is likely longer than for gravitational settling (up to 300 years according to Boyd et al., 2019). In an extreme case, wintertime hibernation and lipid catabolism by copepods at depths up to 1400 m (Jónasdóttir et al., 2015) could drive extremely efficient carbon sequestration on ~500 year timescales (Fig. 9A; Boyd et al., 2019), but the global significance of this process are unknown.

### Carbon sequestration by the pump pathways

To date, very few studies have directly attempted to quantify the total carbon sequestration contributed by the gravitational, physical, and active transport export pathways. Boyd et al. (2019) combined a range of previous export flux estimates (including global upscaling of sparse rate measurements) with model-based estimates of  $\tau_{seq}$ , finding sequestration ranges of  $\sim 1000 \pm 500$  Pg. C for gravitational export,  $\sim 200 \pm 100$  Pg. C for physical export (suspended POC only, not DOC), and  $\sim 800 \pm 600$  Pg. C for active transport (Fig. 9C). More recently, Nowicki et al. (2022) used a data-constrained global model to derive internally-consistent predictions of export, remineralization, and sequestration for each pump pathway, finding  $\sim 1040 \pm 200$  Pg. C for gravitational export,  $\sim 130 \pm 5$  Pg. C for physical export (DOC and a crude estimate of suspended POC), and  $\sim 150 \pm 50$  Pg. C for active transport (Fig. 9C). These components sum to  $\sim 1300 \pm 20$  Pg. C (Nowicki et al., 2022), in good agreement with the strong constraint of 1000–1500 Pg. C imposed by true oxygen utilization and remineralized nutrients (Carter et al., 2021; Fig. 9C). To reconcile the estimates of Boyd et al. (2022) with the same geochemical constraints, carbon sequestration by active transport must lie toward the lower bound of the range proposed, likely because the extrapolation of in-situ measurements placed an excessive upper bound on carbon export by this pathway (3.6Pg./yr.), compared to model-based estimates of  $\sim 1$  Pg. C/yr. (Aumont et al., 2018; Nowicki et al., 2022). Taken together, these studies suggest that the gravitational export pathway dominates carbon sequestration by the BCP, but physical export and active transport make important secondary contributions that are currently poorly resolved in Earth System Models used in climate forecasts (Section “Earth system model predictions”; Henson et al., 2022).

### Climate sensitivity of carbon storage

The various metrics for quantifying carbon storage outlined in Sections “Metrics of carbon sequestration,” “Geographic variability of POC flux attenuation,” “Sequestration timescales,” and “Carbon sequestration by the pump pathways” provide a framework for understanding the impact of past and future climate change on the BCP, and the potential for physically and biologically mediated climate feedbacks. The preformed nutrient framework suggests that changing biological carbon storage requires a change in the efficiency of surface nutrient utilization by phytoplankton communities, especially at high latitudes (Toggweiler, 1999). The best-known case study for changes in the BCP efficiency during Earth’s history are the Pleistocene glacial-interglacial cycles, and especially the last deglaciation that occurred between  $\sim 19$  k–11 k years ago (Clark et al., 2012). While this event was initiated by orbital forcing, the  $\sim 5$  °C increase in global-mean temperature since the Last Glacial Maximum (LGM) cannot be explained without significant degassing of CO<sub>2</sub> from the ocean to the atmosphere, largely driven by weakening of the BCP (Toggweiler, 2003; Clark et al., 2012). This is supported by multiple lines of sedimentary geochemical evidence for more complete nutrient utilization in the Southern Ocean during the LGM compared to the modern ocean (Elderfield and Rickaby, 2000; Francois et al., 1997).

Two hypotheses have been advanced to explain the efficient BCP of the LGM. The Iron Hypothesis (Martin, 1990), proposes that Southern Ocean productivity was boosted in glacial periods by Fe fertilization due a stronger supply of windblown dust to the Southern Ocean (Deangelis et al., 1987; Mahowald et al., 2006). The potential for Fe fertilization to enhance carbon export were later demonstrated in the Southern Ocean Iron Experiment (SOFeX, Buesseler et al., 2005; Moore and Doney, 2006), and dust-climate feedback loops were hypothesized to amplify orbital forcing into glacial-interglacial cycles (Jickells et al., 2005; Mahowald et al., 2006): Cooler drier climate states increase the dust supply from desert regions to the open ocean, fueling NPP and increasing carbon storage, driving further cooling (and reversed for a warming climate). Sedimentary records suggest that reduced Fe supply to the Subantarctic sector of the Southern Ocean explains  $\sim 50\%$  of the deglacial increase in atmospheric CO<sub>2</sub> (Martínez-García et al., 2014). The remainder is likely explained through a weakening of the BCP in the Antarctic sector of the Southern Ocean, driven by a poleward shift in the mid-latitude westerly winds (Toggweiler et al., 2006). This resulted in stronger upwelling around Antarctica (Anderson et al., 2009; Ai et al., 2020) during deglaciation, reducing nutrient utilization and flushing respired CO<sub>2</sub> from the deep ocean to the atmosphere (Toggweiler et al., 2006; Studer et al., 2015; Sigman et al., 2021). This mechanism is best understood through the  $\tau_{seq}$  framework. Because the majority of deep ocean waters are eventually re-exposed in the Southern Ocean (DeVries and Holzer, 2019), faster upwelling there can dramatically reduce the global-mean sequestration time for remineralized carbon, thereby reducing ocean carbon sequestration (Eq. 2).

Ocean circulation changes can drive perturbations of the BCP that often seem counter-intuitive, but are important to understand in light of ongoing ocean warming and stratification (Section “Earth system model predictions”). Simple box models have long predicted that slowing the overturning circulation would reduce the global POC export flux by stifling the nutrient supply to the surface, while simultaneously increasing carbon storage by the BCP (Toggweiler, 1999, 2003), thus breaking the intuitive link between export and storage. This is because slower overturning allows more complete surface nutrient utilization (transfer of



$P_{pre}$  to  $P_{rem}$ ) while lengthening the carbon sequestration time, thereby driving the accumulation of respired  $\text{CO}_2$  and AOU in the ocean interior. These box model predictions are qualitatively mirrored in Earth System Model predictions for the next 100 years of global warming (Henson et al., 2022; Wilson et al., 2022, Section “Earth system model predictions”).

## **The future of the biological pump**

As climate change progresses, the functioning and efficiency of the BCP may respond in a multitude of ways. The oceans are affected both directly and indirectly by rising atmospheric  $\text{pCO}_2$ , with a multitude of down-stream consequences for the biotic and abiotic processes comprising the BCP (Doney et al., 2012). Increased  $\text{pCO}_2$  leads to ocean acidification, a term used to describe the changes in the carbonate chemistry of the ocean as it takes up more inorganic carbon (Wolf-Gladrow and Zeebe, 2001). These changes include a drop in the pH, shifts in alkalinity and speciation of inorganic carbon. Rising  $\text{pCO}_2$  also drives atmospheric warming, which then warms the ocean, starting at the surface. This spatially inhomogeneous warming will increase stratification with consequences for the distribution of nutrients and oxygen, mixed layer depth, and the average light climate experienced by phytoplankton in the mixed layer (Rost et al., 2008). Temperature also directly affects many biological and chemical rate processes, such as photosynthesis and respiration. While the effects of these multiple stressors on the growth of autotrophic and heterotrophic plankton are challenging to assess, the consequences for linkages between trophic levels and ecosystems and thus for the functioning of the BCP are currently near impossible to predict reliably. This section will first give examples of expected shifts in individual processes of importance for the BCP (Section “Effects on processes driving the BCP”), then discuss holistic modeling approaches that aim to assess overall global trends in carbon export and storage by the BCP (Section “Earth system model predictions” and “Missing processes and feedbacks in ESMs”) and end by exploring knowledge about geoengineering options of the BCP (Section “Geoengineering the BCP”).

### **Effects on processes driving the BCP**

#### ***The surface ocean: Phytoplankton community composition, primary production & respiration***

Even small climate driven changes of the phytoplankton community composition and physiology may have potentially significant consequences for the functioning, and magnitude of the BCP (Rost et al., 2008; Basu and Mackey, 2018). The most important abiotic factors that impact phytoplankton composition and production, include increased temperature, PAR, UV exposure and  $\text{pCO}_2$ , as well as decreased pH and nutrient availability. Experimental and observational work have focused on assessing responses to these changes, which affect export production.

A particular species of phytoplankton is able to function in a more-or-less optimal manner over a finite range of environmental conditions, and growth responses decline rapidly outside of that range, as quantified as a response curve. When different abiotic conditions change simultaneously, interactive effects need to be considered. Multistressor experiments have proven that predictions based on individual response curves are essentially impossible, because multiple simultaneous stressors lead to highly non-linear and non-uniform cellular response patterns that may be antagonistic, additive or supra-additive, or there may be no interaction at all (Boyd et al., 2018; Passow and Laws, 2015). The outcome of species succession in a natural community exposed to multiple stressors, is thus impossible to predict reliably (Feng et al., 2009).

Responses of phytoplankton to these changing abiotic parameters are highly species specific, rather than universal, with some exceptions. Increased temperatures, if within the growth range of the species, generally increase metabolic rates, including growth rates. Increased irradiance may increase productivity if nutrients are available, but the simultaneous increase in UV exposure may have deleterious effects on phytoplankton (Basu and Mackey, 2018; Beardall et al., 2009). In terms of carbon acquisition, ocean acidification will benefit some photoautotrophic species, but not others (Mustaffa et al., 2021; Giordano et al., 2005; Basu and Mackey, 2018), depending on the existence of carbon concentrating mechanisms (CCMs). The concomitant decrease in pH appears to incur additional metabolic costs, once it falls below a certain level, leading to overall negative effects on NPP. Overall effects of increased  $\text{pCO}_2$  on rates of photosynthesis may thus range from positive (Tortell et al., 2008) to minimal (Trimbom et al., 2009) to negative, depending on the species and the magnitude of change (Nagelkerken and Connell, 2015). The changes in growth conditions will influence competition and succession, likely resulting in changes in phytoplankton community composition.

Response patterns are in some cases specific to a functional group. The ability of diazotrophic cyanobacteria to fix nitrogen appears to generally increase under ocean acidification conditions (Hutchins et al., 2013; Kranz et al., 2010); a response that is supported by increased iron use efficiency due to elevated temperatures. However, nitrogen fixation may be inhibited by pH effects that reduce the efficiency of the nitrogenase enzyme (Shi et al., 2012), or due to changes in oxygen flux, caused by elevated temperature and inhibition of enzyme activity (Van de Waal and Litchman, 2020). Such complex interactions make it difficult to predict the overall consequences of climate change with respect to nitrogen fixation. Since the saturation state of the ocean with respect to  $\text{CaCO}_3$  minerals will drop along with the pH, calcification rates of calcifiers are expected to decrease, but the consequences of weak or deformed tests and shells for competitive success are not clear (Rost et al., 2008; Hutchins, 2011; Fabry, 2008; Riebesell et al., 2000). To complicate matters, responses may vary not only between species but also strains, indicating that the physiological basis are not well understood (Hutchins, 2011; Iglesias-Rodriguez et al., 2008). Nevertheless, on global and geological scales, coccolith mass declined as  $\text{pCO}_2$  increased, in part due to shifts toward weakly calcified species (Hutchins, 2011).

Since NPP is largely nutrient limited in the oceans (e.g. nitrogen, silica, iron limited), changes in nutrient availability and composition (e.g. shifts from inorganic to organic nitrogen sources) seem especially relevant (Van de Waal and Litchman, 2020; Basu and Mackey, 2018). Reduced nutrient availability is expected to shift the size spectrum of primary producers toward smaller cells, because the large surface area to volume ratio facilitates nutrient uptake (Van de Waal and Litchman, 2020; Litchman et al., 2007), with increasing temperature reinforcing the response (Moran et al., 2010). The relationship between size of primary producers and nutrient availability is visible in today's oceans, where oligotrophic regions are dominated by small cells and eutrophic areas by large ones, and is also supported by the geological record, targeted experiments and modeling exercises (Van de Waal and Litchman, 2020). Although this trend is well established, some traits of large cells may off-set their competitive disadvantage in nutrient acquisition in the future ocean: Large cells would benefit relatively more than small cells from enhanced CO<sub>2</sub> diffusion rates, and increased light availability, and may be more resilient due to their ability to store nutrients in vacuoles, and their potential for size acclimatization and genomic plasticity (Van de Waal and Litchman, 2020).

Biogeochemical feedbacks may drive changes in ocean nutrient distributions and inventories that alter their availability and differ between nutrients. If ocean deoxygenation due to warming and stratification (Keeling et al., 2010) leads to an expansion of oxygen minimum zones then increased denitrification rates may deplete the ocean's N inventory over time (Lam and Kuypers, 2011), exacerbating N limitation (Voss et al., 2013). The degree to which N loss will be compensated by increased N<sub>2</sub>-fixation due to stabilizing N-cycle feedbacks (Deutsch et al., 2007) remains unclear, because diazotrophs may become Fe-limited (Moore et al., 2007). Another feedback may be initiated in the marine Si cycle. Mesocosm experiments revealed slower chemical silica dissolution at lower pH, and sediment trap studies confirmed the influence of pH on the Si: N ratio (Taucher et al., 2022). This implies that silica frustules will be transferred to greater depth before dissolving, trapping silicic acid in the deep ocean and reducing its availability in the surface by the year 2200 (Taucher et al., 2022). This would influence the competitiveness of diatoms.

Increased temperature, ocean acidification, and nutrient limitation, all lead to carbon overconsumption and increased DOC exudation, although this response too is species specific (Taucher et al., 2015; Seebah et al., 2014; Burkhardt et al., 1999; Conan et al., 2007; Tortell and Morel, 2002). Increased exudation, especially of TEP, could lead to increased aggregate formation (Wohlers et al., 2009; Riebesell et al., 2007), although the buoyancy of TEP, may delay and decrease sedimentation, reducing the depth of organic matter remineralization (Mari et al., 2017). A general decrease in "ballasting" material will reinforce this effect, although the timing of TEP production and input of ballasting material, rather than annual bulk amounts will determine settling flux (Mari et al., 2017). Thus the expected shift in the partitioning between DOC and POC production will likely mean reduced export flux: Currently the gravitational settling pathway makes a much larger contribution to carbon export than the physical transport pathways (Fig. 7), which will likely diminish even further under future, more stratified conditions.

The complexity of responses to climate change is further amplified when biotic interactions are considered. Lifecycles of zooplankton grazers are often tightly coupled to those of their phytoplankton prey, and as warming impacts the timing of phytoplankton blooms such linkages may be lost with unknown outcomes for the trophic structure of food-webs. Similarly, alterations in nutritional quality of phytoplankton, due to temperature driven shifts in the stoichiometry of phytoplankton cells (Basu and Mackey, 2018), may lead to reduced fecundity and growth in higher trophic levels that play an important part in the BCP, e.g. as vertical migrators or producers of marine snow. Evolutionary effects and the high phenotypic plasticity of phytoplankton add an additional layer of uncertainty over their response to environmental change (Van de Waal et al., 2019; Collins et al., 2014). Both acclimatization (after days to weeks) and adaptation (after generations) of cells may expand or shift the range where growth is possible (Collins and Bell, 2004; Brennan et al., 2017; Lohbeck et al., 2012), given that phytoplankton lifecycles are short enough for adaptive measures to be relevant on the timescales of climate change (Bach et al., 2018).

Because the amplifying effect of temperature on metabolic rates seems stronger for respiration than photosynthesis, a decline in net carbon fixation rates is expected (Wohlers et al., 2009; Regaudie-de-Gioux and Duarte, 2012). Likewise, ocean acidification conditions have been shown to lead to increased bacterial carbon demand (James et al., 2017). Such a shift toward heterotrophy implies reductions in both, net primary and secondary production, e.g. of organic matter production by heterotrophs (Nagelkerken and Connell, 2015), with consequences for POC flux attenuation and remineralization depth.

### Changes to flux attenuation

Whereas climate change effects on phytoplankton and their production have been studied experimentally, albeit with limitations (Riebesell et al., 2008; Boyd et al., 2018), less experimental evidence exists to assess climate change impacts on the transport pathways of the BCP and on flux attenuation. With reduced viscosity of warmer water, the sinking velocity of particles will increase (Taucher et al., 2014) – but this change is much smaller than the uncertainties in biologically driven factors influencing sinking velocity. Increased TEP production and decreased calcification, both point to decreased sinking velocities and shallower remineralization of marine snow sized particles, especially given the expected increased respiration rates due to warming. Moreover, the expected shift in phytoplankton community composition has potentially severe consequences for the formation of fast sinking marine snow: The large flux events are often diatom driven, as diatoms form fast sinking aggregates as part of their lifecycle (Smetacek, 1985; Alldredge et al., 1995). Dinoflagellates, in contrast, seem to rarely form aggregates (Alldredge et al., 1998), but their ability to migrate between the sunlit surface and a nutrient rich subsurface layer (Passow, 1991) may allow them to outcompete other taxa in a more nutrient-limited future ocean. Whereas coccolithophorid aggregates sink rapidly (Iversen and Ploug, 2010), their sinking velocity decreases appreciably under ocean acidification conditions, when the organic carbon to calcium carbonate ratio increases (Biermann and Engel, 2010). Picoplankton, including eukaryotic cells as well as Prochlorococcus and Synechococcus (cyanobacteria) may form small aggregates (Cruz and Neuer, 2019; Deng et al., 2016), but in the current ocean the

overall contribution of such aggregates to carbon export seems low (De Martini et al., 2018). Currently processes explaining observations of small particles sinking at significant speeds (Durkin et al., 2015; Richardson, 2019) are debated, and potentially point to the importance of unaccounted biological and physical fragmentation processes. Overall, a shift in phytoplankton composition, and especially one away from diatoms and toward picoplankton, is thought to reduce the transfer of carbon to the deep ocean where it can be efficiently sequestered.

Likewise, because zooplankton species vary widely in their feeding strategies and behavior, climate-driven shifts in their biogeography (Dam and Baumann, 2017; Brun et al., 2019) will have consequences for export (Wassmann, 1998). For example, decreased abundance of krill with a simultaneous increase in salps has impacted export production in the Southern Ocean, as the very rapid sinking velocity of salp pellets provides a fast pathway of organic carbon to depth (Phillips et al., 2009; Pfannkuche and Lochte, 1993). The quantitative effect of shallower stratification on vertical migration is currently unknown. A simplification of trophic structure and reduced diversity of food-webs is expected in the future, and is thought to lead to diminished functional redundancy (Nagelkerken and Connell, 2015), potentially making systems more vulnerable to change.

As a result of ongoing and future changes to marine food webs, migratory and fecal pellet flux may change substantially, as will flux attenuation via grazing and fragmentation of marine snow. In a mesocosm study degradation processes during a bloom were less pronounced under ocean acidification conditions, likely because of differences in micro- and mesozooplankton abundance (Stange et al., 2018). Small copepods and flux feeders are known to intensely graze on marine snow (Kjørboe, 2000; Koski et al., 2007), and a shift toward these smaller taxa could increase flux attenuation, in addition to the increased respiration rates expected due to elevated temperatures (Marsay et al., 2015).

### Earth system model predictions

Predicting the overall impact of climate warming on the ocean's biological carbon cycle – at the global scale and in a quantitative way – requires mechanistic global models that link marine microbial ecosystems to their physical and chemical environment. Most of the Earth System Models (ESMs) that are used to inform the International Panel on Climate Change (IPCC) Assessment Reports now include prognostic ocean biogeochemistry modules that are fully coupled to ocean physics and other model components (Seferian et al., 2020). Ten such models were evaluated in the 5th Coupled Model Intercomparison Project (CMIP5), associated with the IPCC Assessment Report 5 (AR5) in 2013 (Bopp et al., 2013), increasing to 19 models in the recent CMIP6 that is associated with the IPCC AR6 (Seferian et al., 2020). These models differ significantly in their treatment of biogeochemical processes and trophic levels, but some common features can be identified. Most resolve multiple phytoplankton classes (generally at least distinguishing diatoms from small phytoplankton) whose growth is limited by up to four nutrients ( $\text{NO}_3$ ,  $\text{PO}_4$ , Fe, and Si for diatoms) and who are grazed by one or more zooplankton class (Seferian et al., 2020; Wilson et al., 2022). Organic matter is routed to DOM and one or more particle classes (distinguished by size, sinking speed, or lability) that remineralize as they sink through the water column at rates that are usually dependent on temperature and sometimes on oxygen, although in some cases simple flux attenuation parameterizations are still used (Seferian et al., 2020).

In both CMIP5 and CMIP6, models were integrated forwards to the year 2100 (although sometimes to 2300) under a range of future emissions scenarios, predicting changes in a host of biogeochemical tracers, rates, and properties. Here we focus on three of central importance: NPP, which supplies energy to the upper-ocean marine food-web and supports marine biodiversity, ecosystem services, and commercial fisheries (Tagliabue et al., 2021); POC export from the upper ocean (100 m), which delivers sustenance to the midwater ecosystem and sequesters carbon out of contact with the atmosphere (Boyd et al., 2019; Henson et al., 2022); and biological carbon sequestration, which determines the overall impact of the BCP on global climate (Wilson et al., 2022). We review changes under the “business as usual scenarios,” in which no special measures are taken to curb future greenhouse gas emissions and the anthropogenic radiative climate forcing reaches  $\sim 8.5 \text{ W/m}^2$  by 2100.

Predicted changes in carbon export are relatively straightforward to interpret as a direct response to the changing physical environment (Bopp et al., 2013; Moore et al., 2018). At small scales, there is significant disagreement between models in the magnitude and even direction of export changes by 2100, even when driven by the exact same climate forcing (Henson et al., 2022). However, a coherent spatial pattern emerges in the model ensemble-mean that has remained unchanged between CMIP5 (Bopp et al., 2013) and CMIP6 ((Henson et al., 2022), Fig. 10A). POC export is expected to decline throughout most of the low latitude and mid latitude ocean, especially in the tropics and North Atlantic Ocean where the ensemble-mean export flux is  $>20\%$  lower in 2100 compared to the 1850–1900 baseline (Fig. 10A). These changes can ultimately be traced to the physical nutrient supply to the surface ocean, which places a limit on the “new” production of organic matter. Stratification of the upper ocean imposes a barrier to vertical mixing (Bopp et al., 2013), and wintertime mixed layer depths shoal by an average of  $\sim 20 \text{ m}$  in the CMIP6 models, significantly reducing nutrient entrainment especially in regions of deep mixing like the North Atlantic (Kwiatkowski et al., 2020). Counter to the global trend, some high latitude regions including the Arctic Ocean, subarctic North Pacific, and most of the Southern Ocean, are expected to see an increase in carbon export, which can also be attributed to stratification (Bopp et al., 2013). At high latitudes, where phytoplankton growth is usually limited by light rather than nutrient scarcity, shoaling mixed layers can help increase phytoplankton exposure to sunlight and lengthen the growth season (Steinacher et al., 2010). Globally, the CMIP6 model ensemble predicts a carbon export decline of  $12 \pm 10\%$  (ensemble-mean  $\pm$  s.d.) by 2100 relative to preindustrial (Fig. 10B), which is remarkably similar to the CMIP5 prediction of  $12 \pm 6\%$ .

The predicted response of NPP to climate warming is more complex, and can be decoupled from the physical nutrient supply by the recycling of organic matter within the euphotic zone. In general, the ensemble-mean NPP changes in the CMIP5 and CMIP6



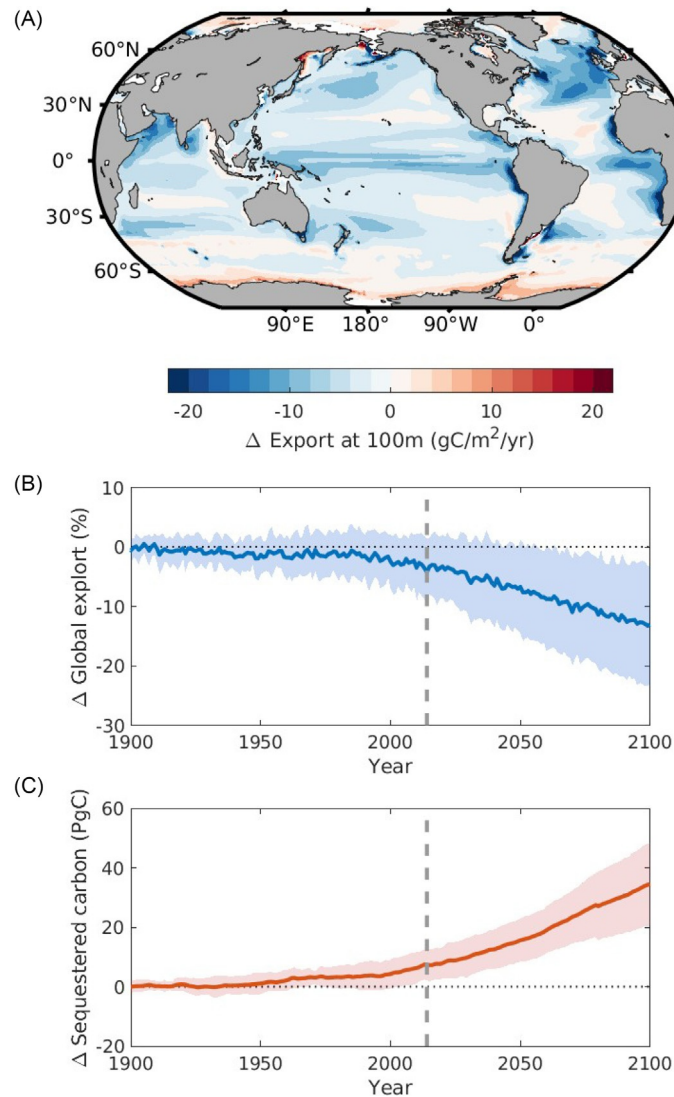


**Fig. 10** Future of the BCP predicted in the CMIP6 climate model ensemble. (A) Spatial pattern of change in gravitational POC export by the year 2100, relative to the preindustrial baseline, averaged across 9 CMIP6 models (Henson et al., 2022). (B + C), Timeseries of ensemble-mean % change in global POC export (B, Henson et al., 2022) and absolute change in carbon sequestration by the biological pump (C, Wilson et al., 2022), relative to preindustrial baseline. In both panels, shaded envelope shows standard deviation between individual CMIP6 models, and vertical grey dashed line shows when the historical hindcast portion of the simulation ends, and the forecast begins.

models exhibit the same geographical pattern as carbon export (Bopp et al., 2013) but are smaller in magnitude, with global NPP declining by  $\sim 8.5 \pm 6\%$  in the CMIP5 ensemble (Bopp et al., 2013) and  $\sim 3 \pm 9\%$  in the CMIP6 ensemble (Kwiatkowski et al., 2020). The muted NPP response can largely be explained by the temperature-dependent organic matter remineralization rates resolved in most ESMs, which accelerates nutrient recycling in the euphotic zone as the upper ocean warms, buffering NPP against the declining physical nutrient supply (Bopp et al., 2013; Moore et al., 2018). This buffering effect appears to be enhanced in the CMIP6 ensemble relative to CMIP5, likely because CMIP6 models predict more ocean warming due to their generally higher climate sensitivity, and often resolve additional pathways of nutrient recycling via zooplankton activity (Kwiatkowski et al., 2020; Tagliabue et al., 2021). Additionally, disagreement between models in the pattern and magnitude of NPP changes has grown significantly in the CMIP6 ensemble relative to CMIP5 (Tagliabue et al., 2021). This is likely because attempts to advance the biological realism in marine ecosystem models have added new processes that are handled differently between models and are not well constrained by observations (Tagliabue et al., 2021).

Changes in ocean carbon sequestration by the BCP in ESMs are less widely reported than carbon export and NPP, because it is difficult to quantify in a precise way. Because these models are not at equilibrium, the  $\tau_{seq}$  framework cannot be cleanly applied to compute integrated carbon sequestration as for simpler steady-state model solutions (Nowicki et al., 2022). Recently, ocean-integrated AOU was instead used to estimate changing carbon storage in the subset CMIP6 models that resolve dissolved  $O_2$  (Wilson et al., 2022), with the caveat that disequilibrium effects introduce uncertainty into the proxy (Ito et al., 2004).

These models predict that biological carbon storage will increase by  $\sim 34 \pm 14$  Pg. C by the year 2100, comprising a negative feedback on atmospheric  $p\text{CO}_2$  and global temperature, albeit relatively weak compared to direct oceanic uptake of anthropogenic  $\text{CO}_2$  (Wilson et al., 2022). As in simple box models (Section 4.5), the increased future carbon storage predicted by ESMs is driven by the same physical mechanism that reduces carbon export: stratification of the upper ocean and slower overturning leads to more efficient carbon sequestration (longer  $\tau_{\text{seq}}$ ) and trapping of respired  $\text{CO}_2$  in the deep ocean (Wilson et al., 2022). To some degree, physically-induced changes in both carbon export and sequestration appear to be curtailed by a negative feedback involving POC transfer efficiency to depth in this CMIP6 subset. These models predict that as the ocean warms, a larger fraction of exported POC is remineralized above 1000 m, either due to the direct effect of temperature on remineralization rates or in some cases due to ecosystem shifts toward small phytoplankton that export smaller, slower-sinking particles (Wilson et al., 2022; Henson et al., 2022). Shallower remineralization leads to faster recirculation of nutrients and respired carbon to the surface, which buffers NPP and carbon export, and limits changes in biological carbon sequestration (Wilson et al., 2022).

While the majority of CMIP5 and CMIP6 simulations end in 2100, some ESMs have been used to forecast forward to the year 2300, with the caveat that future emissions trajectories become even more uncertain on this timescale. One such simulation found that changes in NPP and carbon export become even more precipitous and spatially variable after 2300 (Moore et al., 2018). In this model, sustained climate warming causes Southern Ocean upwelling to migrate toward the Antarctic coastline, where warming and alleviation of light limitation by sea ice loss boost phytoplankton growth and carbon export, while efficiently stripping nutrients from surface waters. In turn, this prevents the nutrient transport toward low latitudes trapping nutrients in the Southern Ocean and deep water masses. By 2300, the model predicts a major redistribution of nutrients from the upper ocean to the deep ocean which drives a  $>40\%$  decline in global carbon export, and a  $\sim 25\%$  decline in global NPP that propagates up through the food-web and impacts potential fishery yields (Moore et al., 2018). This prediction provides a stark example of a non-linear biogeochemical response to climate warming, and a warning that critical tipping points in the biological carbon cycle may be crossed in the not-too-distant future.

### Missing processes and feedbacks in ESMs

Future trends in NPP, organic matter export, and carbon sequestration by the BCP predicted in Earth System Models may be limited by their simple representation of marine ecosystems and biological carbon cycle. To facilitate their incorporation into computationally expensive ESMs (which represents all major components of the global climate system), ocean biogeochemistry models must be streamlined and tend to focus on capturing processes and responses that are relatively well understood from an empirical standpoint (Seferian et al., 2020). Of all the processes that make up the BCP, NPP is generally the most realistically resolved in ESMs. The first-order controls on phytoplankton growth are usually well represented, and predicted future trends are predominantly driven by changes in the physical nutrient supply, temperature, and light (Section “Earth system model predictions”). However, complex responses of phytoplankton communities to “multi-stressor” environmental perturbations (Section “Effects on processes driving the BCP”) are rarely resolved in global models, nor are phytoplankton acclimation and adaptation to their changing environment.

Beyond NPP, parameterizations of organic carbon cycling in ESMs tend to become even simpler, often excluding even relatively well-understood first-order effects. Around half of the 19 CMIP6 models assessed by Henson et al. (2022) do not link POC remineralization to temperature or oxygen, despite mounting evidence that these factors impose a strong control on POC transfer efficiency to depth (Fig. 8). As a result, the CMIP6 ensemble as a whole likely under-predicts the magnitude of the effects of shallower remineralization due to ocean warming, and enhanced carbon sequestration in the tropics due to OMZ expansion (Wilson et al., 2022). Closing these gaps represents a low-hanging fruit for future model development, without requiring major updates to model architecture. Even models that represent POC remineralization implicitly through a flux attenuation parameterization (i.e. by assuming a Martin-Curve flux profile) can account for these effects using empirical relationships between flux profile shape and environmental factors (Marsay et al., 2015).

The impact of particle size, density and composition on sinking speed and remineralization depth is even less well represented in most global models. The majority of the CMIP6 models do not resolve mineral ballasting effects, and either resolve a single particle size class with a fixed sinking velocity or do not explicitly resolve sinking particles at all, instead parameterizing remineralization implicitly (Seferian et al., 2020; Henson et al., 2022). Even when multiple POC size classes with different sinking velocities are resolved, the relative abundance of particle sizes may be specified a priori, rather than dynamically linked to the phytoplankton community structure (Henson et al., 2022). As a whole then, the CMIP6 ensemble is poorly equipped to resolve changes in remineralization associated with the expected ecological transition toward smaller phytoplankton (Section “Earth system model predictions”). In a targeted modeling study, these transitions were predicted to decrease the mean size of exported particles, resulting in shallower remineralization and faster resupply of nutrients to the surface, which significantly weakened the declining future trend in POC (Leung et al., 2021). Taken together, the missing temperature and particle size feedbacks could lead the CMIP6 ensemble to overpredict future trends in carbon export and sequestration.

A range of other biogeochemical processes are also missing from the current generation of ESMs, whose impact on predicted BCP trends is more challenging to assess. While most CMIP6 models include at least one zooplankton class, none resolve the vertical migration of these organisms, nor their impact on particle disaggregation (Henson et al., 2022). These processes are increasingly recognized as important drivers of carbon export and flux attenuation respectively, and their representation in global models should be prioritized (Aumont et al., 2018). However, the potential response of zooplankton migration and metabolism to ocean

warming, ocean acidification and associated environmental change remains a topic of open enquiry (Section “Earth system model predictions”). The direction and magnitude of biases caused by omitting zooplankton activity from ESMs is therefore unclear at this time (Henson et al., 2022). In addition, while ESMs resolve ocean CO<sub>2</sub> uptake and acidification (Bopp et al., 2013), they do not account for plankton responses to lower pH, which may be direct (physiological) or indirect, e.g. due to pH effects on the chemical speciation of trace metals, including micronutrients like Fe and toxic elements like Cu (Millero et al., 2009).

The complexity of ocean biogeochemical models that are incorporated into ESMs is advancing quickly, and even between CMIP5 and CMIP6 many models were expanded to resolve additional nutrient cycles, microbial functional groups, and trophic levels (Seferian et al., 2020). In principle, it is assumed that increasing biological realism in these models will lead to more accurate future predictions, but in practice it has also led to wider discrepancies between models and therefore greater uncertainty in ensemble predictions (Kwiatkowski et al., 2020). The next stages of biogeochemical model development should therefore focus on validation, and aim for increased consistency between modeling frameworks in the adoption of parameterizations that allow models to best reproduce observations.

### Geoengineering the BCP

Carbon dioxide removal (CDR) technology and other climate geoengineering techniques purposefully alter environmental processes with the goal to counteract increases in atmospheric pCO<sub>2</sub> and global warming. Although many marine CDR techniques, such as marine alkalinity enhancement, will impact the functioning of the BCP (Hartmann et al., 2013; Köhler et al., 2013), they do not purposefully manipulate it. Other CDR techniques do aim to stimulate the BCP with the goal of increasing the carbon sequestration in the deep ocean. These tend to focus on increasing NPP, with the expectation that this will increase both carbon flux and sequestration. Four means of fertilization are being discussed (Lampitt et al., 2008): in-situ ocean iron fertilization (OIF) to (i) HNLC (high nutrient low chlorophyll) regions to enhance macro-nutrient uptake, or to (ii) LNLC (low nutrient low chlorophyll) regions to promote nitrogen fixation, as well as (iii) macronutrient addition to surface water or (iv) translocation of macronutrients by artificially promoting upwelling. Techniques to grow and sink macro-algae such as kelp in open ocean systems, called ocean afforestation, aim to enhance carbon flux by changing the autotrophic community.

None of these methods has been fully explored by adequate field experimentation and appropriate computational modeling to determine the likelihood that additional carbon will be sequestered (removed from the atmosphere for more than 100 years) on a global scale. Locally stimulating carbon export may not fulfill the criteria for global sequestration, if this carbon would have been exported naturally at a later time, or if the exported material is rapidly upwelled again elsewhere (Lampitt et al., 2008). Likewise, feedbacks involving other climate relevant gasses such as N<sub>2</sub>O, also need to be considered, but such downstream effects are largely unexplored (Williamson et al., 2012; Dutreuil et al., 2009). Here we focus on current knowledge about the net sequestration potential of each technology, but a full assessment will need to evaluate feasibility, costs and ecological impacts (Lampitt et al., 2008; Williamson et al., 2012), as well as societal impacts including ethical permissibility and justification (Hale and Dilling, 2011).

Thirteen artificial ocean iron fertilization (OIF) experiments were carried out between 1993 and 2004; (Yoon et al., 2018; Williamson et al., 2012; Boyd et al., 2007). These experiments largely aimed to confirm that iron limits growth in various ocean regions, and were not designed to measure export or sequestration of carbon. Supplementing these areas with iron clearly enhanced growth of phytoplankton, promoted uptake of CO<sub>2</sub> from the atmosphere, and altered elemental cycling, but responses to iron fertilization varied widely depending on macro-nutrient availability, food-web structure and physical regime (Yoon et al., 2018; Williamson et al., 2012; Boyd et al., 2007). Significant export flux was only observed in one of the experiments. Overall, the experiments and modeling exercises revealed that the potential for carbon sequestration by iron fertilization was much smaller than originally anticipated, as other limiting factors (nutrients, light), grazing, the speciation of iron and physiological responses of phytoplankton curtailed carbon export (Lampitt et al., 2008; Yoon et al., 2018). Overall, the estimated amount of carbon that might be taken out of circulation via iron fertilization is small relative to human emissions (1 GTC/yr.; Position Analysis: The Antarctic Climate & Ecosystems Cooperative Research Centre 2016, Australian Government).

The potential capacity of carbon sequestration due to ocean macronutrient fertilization (OMF), whether as nitrogen only, or as nitrogen and phosphorus has been explored using a biochemical model, which assumed that micronutrients and light are non-limiting (Harrison, 2017) and suggested that up to 1.5 Pg. C/yr. could be sequestered via OMF. However, experiments adding macronutrients to low nutrient waters revealed that although bacteria production increased, phytoplankton biomass decreased unexpectedly or was grazed, indicating that food-webs and growth limiting factors are not well understood in low nutrient systems (Williamson et al., 2012; Passos, 2018). Whereas nutrients in these experiments were released from ships, release from land has also been discussed (Lampitt et al., 2008), but the role of coastal oceans is poorly represented in Earth System Models, due to a lack of process understanding and temporal-spatial resolution of data (Cao et al., 2019), hindering predictions of even the potential.

Artificial (ocean) upwelling (AU), which uses different technologies (Pan et al., 2016) to enhance the upwelling of nutrient rich water from depth, has been proposed for a wide variety of purposes, including as a CDR technology (Pan et al., 2018; Lampitt et al., 2008; Williamson et al., 2012; Dutreuil et al., 2009). AU is, in all cases, a significant disturbance to the environment, because upwelled water will also carry elevated concentrations of DIC and change the temperature, salinity and total alkalinity of surface waters. The input of high DIC into warm and shallow waters enhances its CO<sub>2</sub> fugacity counteracting decreases in pCO<sub>2</sub> due to enhanced photosynthesis. Higher temperatures at depth will decrease transfer efficiency during sinking further limiting sequestration (Jürchott et al., 2023). Effectiveness of this approach will therefore vary between regions, seasons and ecosystem

types (Pan et al., 2018; Oschlies et al., 2010; Dutreuil et al., 2009). The most optimistic model assumption, suggest an annual carbon sequestration rate of  $\approx 0.9$  Pg. C/yr., but most of this carbon would be sequestered on land, rather than in the ocean (Oschlies et al., 2010). Both  $N_2O$  (a greenhouse gas) and DMS may simultaneously increase, at least temporarily (Dutreuil et al., 2009) impacting the net effect. Detailed field work monitoring carbon sequestration based on AU is lacking (Williamson et al., 2012).

The massive culturing of macro-algae, which are native to coastal regions, on 9% of the surface ocean, dubbed ocean macro-algae afforestation (OMA) has been heralded as the solution to a wide variety of problems, including carbon sequestration, often without critical consideration of consequences and feed-backs (N'Yeurt et al., 2012; Duarte et al., 2022). Deliberate deposition of these macro-algae to the deep ocean, which functionally replaces the BCP based on phytoplankton, is envisioned to increase carbon sequestration, although in the absence of nutrient fertilization, nutrients will be re-allocated from phytoplankton to macro-algae, diminishing the existing BCP (Boyd et al., 2022; Bach et al., 2021). Translocation of macro-algae, which have relatively high nutrient requirements, to open ocean systems, will drastically change off-shore ecosystems, including food-web structure and ocean chemistry, as well as microbial physiology and ecology (Boyd et al., 2019, 2022). Additionally, they would impact the light climate of deeper growing phytoplankton, as well as change quantity and quality of DOC release by primary producers (Ricart et al., 2022; Bach et al., 2021; Boyd et al., 2022).

A recent assessment of ocean based negative emission technologies, evaluated all the marine fertilization techniques discussed above, as being in the *concept stage*, with high potential disbenefits (Gattuso et al., 2021). Furthermore, a recent modeling exercise suggests that the carbon sequestration potential of these marine CDR strategies is low, because the export is "leaky" over a 50–100 yr. timespan, with only about 32% remaining sequestered after 50 years (Siegel et al., 2021).

## Conclusion

The BCP maintains a vertical DIC gradient of  $\sim 150$   $\mu M$  due to the rapid cycling of organic matter over depth, and lowers atmospheric  $pCO_2$  by 100–200 ppm. The system is ultimately driven by the primary production of 50–60 Pg./yr. of organic carbon in the sunlit surface ocean, which is limited by macronutrient and micronutrient availability and seasonally regulated by light levels. Decades of direct and indirect measurements, synthesized by upscaling models, have revealed that globally 4–9.6 Pg. C/yr. escapes recycling and is exported from the euphotic zone as sinking POC. Recently, physical transport and vertical migration by zooplankton and fish, have been recognized as important alternative pathways for carbon export. Accurately quantifying each of the three pathways is an important challenge for the next decade of BCP research, because each pathway will likely respond differently to global change and the overall perturbation of the BCP hinges on their relative importance.

The regenerated DIC inventory maintained in the ocean interior is referred to as sequestered carbon, and represents the total amount of carbon isolated from exchange with the atmosphere due to the net effect of organic matter export from the surface and remineralization at depth. Sequestration is not only controlled by the carbon export flux, but also the timescale before respired carbon recirculates to the surface ocean, set by the depth of organic carbon remineralization. For the gravitational pathway, POC remineralization depth hinges on the structure of the surface microbial ecosystem, which can determine the sinking velocity of exported particles, and on physical conditions of the water column that regulate microbial metabolism and POC losses over depth. In general, ecosystems dominated by large plankton, and watercolumns with low temperature and low  $[O_2]$ , appear to promote deep POC remineralization.

Globally, biological carbon sequestration is estimated as  $\sim 1200$  Pg. C, which lies closer to the weak theoretical limit than the strong limit, based on the relative magnitude of the remineralized and preformed  $PO_4$  inventories. This sequestration is largely limited by the inefficient utilization of nutrients in high latitude regions like the Southern Ocean, highlighting the potential leverage of polar microbial ecosystems over global climate. The gravitational export pathway is thought to dominate carbon sequestration by the BCP accounting for  $\sim 1000 \pm 500$  Pg. C, compared to  $\sim 200 \pm 100$  Pg. C for physical export and  $\sim 800 \pm 600$  Pg. C for active transport. Again, improving our quantitative estimates and mechanistic understanding of carbon sequestration by these pathways are critical goals for future BCP research.

As the ocean warms and acidifies, responses by organisms, populations and communities are complex and vary widely. Earth System Models (ESMs) generally predict a decline in carbon export as the ocean warms and stratifies, and some predict that a larger fraction of exported POC will remineralize above 1000 m, due to the effects of warming and deoxygenation on remineralization rates. However, most ESMs remain biologically quite simple and do not resolve complex feedbacks linking microbial physiology, ecosystem structure, and particle size and density, nor do they adequately capture the physical and active transport carbon pathways. Improving our predictive understanding of these processes remains a major challenge for both observational and modeling communities. Proposed geoengineering options, meant to increase carbon sequestration by strengthening the BCP, likely all have limited potential because the export is "leaky" over a 50–100 yr. timespan, with little carbon remaining sequestered after 50 years.



## References

- Abell J, Emerson S, and Renaud P (2000) Distributions of Top, TON and TOC in the North Pacific subtropical gyre: Implications for nutrient supply in the surface ocean and remineralization in the upper thermocline. *Journal of Marine Research* 58: 203–222.
- Ai XE, Studer AS, Sigman DM, Martinez-Garcia A, Fripiat F, Thöle LM, Michel E, Gottschalk J, Arnold L, Moretti S, Schmitt M, Oleynik S, Jaccard SL, and Haug GH (2020) Southern Ocean upwelling, Earth's obliquity, and glacial-interglacial atmospheric CO<sub>2</sub> change. *Science* 370(6522): 1348. <https://doi.org/10.1126/science.abd211>.
- Aldredge AL (2000) Interstitial dissolved organic carbon (DOC) concentrations within sinking marine aggregates and their potential contribution to carbon flux. *Limnology and Oceanography* 45: 1245–1253.
- Aldredge AL (2005) *The Contribution of Discarded Appendicularian Houses to the Flux of Particulate Organic Carbon from Oceanic Surface Waters*. GB Science Publishers-Éditions Scientifiques GB.
- Aldredge AL and Gotschalk CC (1989) Direct observations of the mass flocculation of diatom blooms: Characteristics, settling velocities and formation of diatom aggregates. *Deep-Sea Research* 36: 159–171.
- Aldredge AL and Jackson GA (1995) Aggregation in marine systems. *Deep-Sea Research* 42: 1–7.
- Aldredge AL and Silver MW (1988) Characteristics, dynamics, and significance of marine snow. *Progress in Oceanography* 20: 41–82.
- Aldredge AL, Passow U, and Logan BE (1993) The abundance and significance of a class of large, transparent organic particles in the ocean. *Deep-Sea Research Part I* 40: 1131–1140.
- Aldredge AL, Gotschalk C, Passow U, and Riebesell U (1995) Mass aggregation of diatom blooms: Insights from a mesocosm study. *Deep-Sea Research* 42: 9–28.
- Aldredge AL, Passow U, and Haddock HD (1998) The characteristics and transparent exopolymer particle (TEP) content of marine snow formed from thecate dinoflagellates. *Journal of Plankton Research* 20: 393–406.
- Amon RMW and Benner R (1996) Bacterial utilization of different size classes of dissolved organic matter. *Limnology and Oceanography* 41: 41–51.
- Anand SS, Rengarajan R, and Sarma VSS (2018) Th-234-based carbon export flux along the Indian GEOTRACES G102 section in the Arabian Sea and the Indian Ocean. *Global Biogeochemical Cycles* 32: 417–436.
- Anderson LA and Sarmiento JL (1994) Redfield ratios of remineralization determined by nutrient data analysis. *Global Biogeochemical Cycles* 8: 65–80.
- Anderson RF, Ali S, Bradtmiller LI, Nielsen SHH, Fleisher MQ, Anderson BE, and Burckle LH (2009) Wind-driven upwelling in the Southern Ocean and the deglacial rise in atmospheric CO<sub>2</sub>. *Science (New York, N.Y.)* 323: 1443–1448.
- Anderson T, Hessen D, Mitr AA, Mayor D, and Yool A (2013) Sensitivity of secondary production and export flux to choice of trophic transfer formulation in marine ecosystem models. *Journal of Marine Systems* 125: 41–53.
- Anderson RF, Cheng H, Edwards RL, Fleisher MQ, Hayes CT, Huang KF, Kadko D, Lam PJ, Landing WM, Lao Y, Lu Y, Measures CI, Moran SB, Morton PL, Ohnemus DC, Robinson LF, and Shelley RJ (2016) How well can we quantify dust deposition to the ocean? *Philosophical Transactions of the Royal Society a-Mathematical Physical and Engineering Sciences* 374.
- Antia AN (2005) Solubilization of particles in sediment traps: Revising the stoichiometry of mixed layer export. *Biogeosciences* 2: 189–204.
- Armstrong RA, Lee C, Hedges JL, Horjio S, and Wakeham SG (2002) A new, mechanistic model for organic carbon fluxes in the ocean based on the quantitative association of POC with ballast minerals. *Deep-Sea Research Part II: Topical Studies in Oceanography* 49: 219–236.
- Armstrong RA, Peterson ML, Lee C, and Wakeham SG (2009) Settling velocity spectra and the ballast ratio hypothesis. *Deep Sea Research Part II: Topical Studies in Oceanography* 56: 1470–1478.
- Arnosti C, Fuchs BM, Amann R, and Passow U (2012) Contrasting extracellular enzyme activities of particle-associated bacteria from distinct provinces of the North Atlantic Ocean. *Frontiers in Microbiology* 3.
- Arrieta JM, Mayol E, Hansman RL, Herndl GJ, Dittmar T, and Duarte CM (2015) Dilution limits dissolved organic carbon utilization in the deep ocean. *Science* 348: 331–333.
- Arteaga L, Haentjens N, Boss E, Johnson KS, and Sarmiento JL (2018) Assessment of export efficiency equations in the southern ocean applied to satellite-based net primary production. *Journal of Geophysical Research-Oceans* 123: 2945–2964.
- Aumont O, Maury O, Lefort S, and Bopp L (2018) Evaluating the potential impacts of the diurnal vertical migration by marine organisms on marine biogeochemistry. *Global Biogeochemical Cycles* 32: 1622–1643.
- Azam F (1998) Microbial control of oceanic carbon flux: The plot thickens. *Science* 280: 694–696.
- Azam F and Long RA (2001) Sea snow microcosms. *Nature* 414: 495–498.
- Azam F and Malfatti F (2007) Microbial structuring of marine exosystems. *Nature* 5: 782–791.
- Azam F, Fenchel T, Field GJ, Gray JS, Meyer-Reil LA, and Thingstad F (1983) The ecological role of water column microbes in the sea. *Marine Ecology Progress Series* 10: 257–263.
- Azetsu-Scott K and Passow U (2004) Ascending marine particles: Significance of transparent exopolymer particles (TEP) in the upper ocean. *Limnology and Oceanography* 49: 741–748.
- Bach LT, Lohbeck KT, Reusch TBH, and Riebesell U (2018) Rapid evolution of highly variable competitive abilities in a key phytoplankton species. *Nature Ecology & Evolution* 2: 611–613.
- Bach LT, Tamsitt V, Gower J, Hurd CL, Raven JA, and Boyd PW (2021) Testing the climate intervention potential of ocean afforestation using the Great Atlantic Sargassum Belt. *Nature Communications* 12: 2556.
- Bacon MP and Anderson RF (1982) Distribution of thorium isotopes between dissolved and particulate forms in the deep sea. *Journal of Geophysical Research: Oceans* 87: 2045–2056.
- Baker CA, Estapa ML, Iversen M, Lampitt R, and Buesseler K (2020) Are all sediment traps created equal? An intercomparison study of carbon export methodologies at the PAP-SO site. *Progress in Oceanography* 184.
- Banse K (1990) New views on the degradation and disposition of organic particles as collected by sediment traps in the open ocean. *Deep-Sea Research* 37: 1177–1195.
- Basu S and Mackey KRM (2018) Phytoplankton as key mediators of the biological carbon pump: Their responses to a changing climate. *Sustainability* 10: 869.
- Beardall J, Sobrino C, and Stojkovic S (2009) Interactions between the impacts of ultraviolet radiation, elevated CO<sub>2</sub>, and nutrient limitation on marine primary producers. *Photochemical & Photobiological Sciences* 8: 1257–1265.
- Beaulieu SE (2002) Accumulation and fate of phytodetritus on the seafloor. *Oceanography and Marine Biology. Annual Review* 40: 171–232.
- Behrenfeld MJ (2010) Abandoning Sverdrup's Critical Depth Hypothesis on phytoplankton blooms. *Ecology* 91: 977–989.
- Behrenfeld MJ and Falkowski PG (1997) Photosynthetic rates derived from satellite-based chlorophyll concentration. *Limnology and Oceanography* 42: 1–20.
- Behrenfeld MJ and Kolber ZS (1999) Widespread iron limitation of phytoplankton in the South Pacific Ocean. *Science* 283: 840–843.
- Benitez-Nelson CR, Buesseler KO, and Crossin G (2000) Upper ocean carbon export, horizontal transport, and vertical eddy diffusivity in the southwestern Gulf of Maine. *Continental Shelf Research* 20: 707–736.
- Bianchi D, Galbraith ED, Carozza DA, Mislán KAS, and Stock CA (2013a) Intensification of open-ocean oxygen depletion by vertically migrating animals. *Nature Geoscience* 6: 545–548.
- Bianchi D, Stock C, Galbraith ED, and Sarmiento JL (2013b) Diel vertical migration: Ecological controls and impacts on the biological pump in a one-dimensional ocean model. *Global Biogeochemical Cycles* 27: 478–491.
- Bianchi D, Weber TS, Kiko R, and Deutsch C (2018) Global niche of marine anaerobic metabolisms expanded by particle microenvironments. *Nature Geoscience* 11: 263–268.
- Biermann A and Engel A (2010) Effect of CO<sub>2</sub> on the properties and sinking velocity of aggregates of the coccolithophore *Emiliania huxleyi*. *Biogeosciences* 7: 1017–1029.

- Billet DSM, Lampitt RS, Rice AL, and Mantoura RFC (1983) Seasonal sedimentation of phytoplankton to the deep sea benthos. *Nature* 302: 520–522.
- Bishop JKB, Conte MH, Wiebe PH, Roman MR, and Langdon C (1986) Particulate matter production and consumption in deep mixed layers: Observations in a warm-core ring. *Deep-Sea Research Part I: Oceanographic Research Papers* 33: 1813–1841.
- Bisson KM, Siegel DA, Devries T, Cael BB, and Buesseler KO (2018) How data set characteristics influence ocean carbon export models. *Global Biogeochemical Cycles* 32: 1312–1328.
- Black EE, Buesseler KO, Pike SM, and Lam PJ (2018) Th-234 as a tracer of particulate export and remineralization in the southeastern tropical Pacific. *Marine Chemistry* 201: 35–50.
- Bopp L, Resplandy L, Orr JC, Doney SC, Dunne JP, Gehlen M, Halloran P, Heinze C, Ilyina T, Seferian R, Tziputra J, and Vichi M (2013) Multiple stressors of ocean ecosystems in the 21st century: Projections with CMIP5 models. *Biogeosciences* 10: 6225–6245.
- Boyd PW, Jickells T, Law CS, Blain S, Boyle EA, Buesseler KO, Coale KH, Cullen JJ, de Baar HJW, Follows M, Harvey M, Lancelot C, Levasseur M, Owens NPJ, Pollard R, Rivkin RB, Sarmiento J, Schoemann V, Smetacek V, Takeda S, Tsuda A, Turner S, and Watson AJ (2007) Mesoscale iron enrichment experiments 1993–2005: Synthesis and future directions. *Science* 315: 612–617.
- Boyd PW, Collins S, Dupont S, Fabricius K, Gattuso J-P, Havenhand J, Hutchins DA, Riebesell U, Rintoul MS, Vichi M, Biswas H, Ciotti A, Gao K, Gehlen M, Hurd CL, Kurihara H, McGraw CM, Navarro J, Nilsson GE, Passow U, and Pörtner H-O (2018) Experimental strategies to assess the biological ramifications of multiple drivers of global ocean change – A review. *Global Change Biology* 24: 2239–2261.
- Boyd PW, Claustre H, Levy M, Siegel DA, and Weber T (2019) Multi-faceted particle pumps drive carbon sequestration in the ocean. *Nature* 568: 327–335.
- Boyd PW, Bach LT, Hurd CL, Paine E, Raven JA, and Tamsitt V (2022) Potential negative effects of ocean afforestation on offshore ecosystems. *Nature Ecology & Evolution* 6: 675–683.
- Brennan GL, Colegrave N, and Collins S (2017) Evolutionary consequences of multidriver environmental change in an aquatic primary producer. *Proceedings of the National Academy of Sciences* 114: 9930–9935.
- Briggs N, Dall'olmo G, and Claustre H (2020) Major role of particle fragmentation in regulating biological sequestration of CO<sub>2</sub> by the oceans. *Science* 367: 791–793.
- Broecker WS, Takahashi T, and Takahashi T (1985) Sources and flow patterns of deep-ocean waters as deduced from potential temperature, salinity, and initial phosphate concentration. *Journal of Geophysical Research-Oceans* 90: 6925–6939.
- Brun P, Stamieszkin K, Visser AW, Licandro P, Payne MR, and Kiørboe T (2019) Climate change has altered zooplankton-fuelled carbon export in the North Atlantic. *Nature Ecology & Evolution* 3: 416–423.
- Brzezinski M (1985) The Si: C: N ratio of marine diatoms: Interspecific variability and the effect of some environmental variables. *Journal of Phycology* 21: 347–357.
- Buesseler KO, Cochran JK, Bacon MP, Livingston HD, Casso SA, Hirschberg D, Hartman MC, and Fleer AP (1992) Determination of thorium isotopes in seawater by nondestructive and radiochemical procedures. *Deep-Sea Research Part I: Oceanographic Research Papers* 39: 1103–1114.
- Buesseler K, Antia A, Chen M, Gardner WD, Gustafsson O, Harada K, Michaels AF, Rutgers Van Der Loeff MM, Sarin MM, Steinberg DK, and Trull TW (2007a) An assessment of the use of sediment traps for estimating upper ocean particle fluxes. *Journal of Marine Research* 65: 345–416.
- Buesseler K, Ball L, Andrews J, Benitez-Nelson C, Belostock R, Chai F, and Chao Y (1998) Upper ocean export of particulate organic carbon in the Arabian Sea derived from thorium-234. *Deep-Sea Research Part II: Topical Studies in Oceanography* 45: 2461–2487.
- Buesseler KO, Lamborg CH, Boyd PW, Lam PJ, Trull TW, Bishop JKB, Casciotti KL, Dehairs F, Elskens M, et al. (2007b) Revisiting carbon flux through the ocean's twilight zone. *Science* 316: 567–570. <https://doi.org/10.1126/science.1137959>.
- Buesseler KO, Steinberg DK, Michaels AF, Johnson RJ, Andrews JE, Valdes JR, and Price JF (2000) A comparison of the quantity and composition of material caught in a neutrally buoyant versus surface-tethered sediment trap. *Deep-Sea Research Part I-Oceanographic Research Papers* 47: 277–294.
- Buesseler KO, Andrews JE, Pike S, and Charette MA (2005) Particle export during the Southern Ocean Experiment (SOFEX). *Limnology and Oceanography* 50: 311–327.
- Buesseler KO, Benitez-Nelson CR, Moran SB, Burd A, Charette M, Cochran JK, Coppola L, Fisher NS, Fowler SW, Gardner W, Guo LD, Gustafsson O, Lamborg C, Masque P, Miquel JC, Passow U, Santschi PH, Savoye N, Stewart G, and Trull T (2006) An assessment of particulate organic carbon to thorium-234 ratios in the ocean and their impact on the application of Th-234 as a POC flux proxy. *Marine Chemistry* 100: 213–233.
- Buesseler KO, Boyd PW, Black EE, and Siegel DA (2020) Metrics that matter for assessing the ocean biological carbon pump. *Proceedings of the National Academy of Sciences* 117: 9679–9687.
- Burd AB and Jackson GA (2009) Particle aggregation. *Annual Review of Marine Science* 1: 65–90.
- Burd AB, Hansell DA, Steinberg DK, Anderson TR, Aristegui J, Baltar F, Beaufort SR, Buesseler KO, Dehairs F, Jackson GA, Kadko DC, Koppelman R, Lampitt RS, Nagata T, Reinthaler T, Robinson C, Robinson BH, Tamburini C, and Tanaka T (2010) Assessing the apparent imbalance between geochemical and biochemical indicators of meso- and bathypelagic biological activity: What the @#! is wrong with present calculations of carbon budgets? *Deep-Sea Research Part II: Topical Studies in Oceanography* 57: 1557–1571.
- Burkhardt S, Zondervan I, and Riebesell U (1999) Effect of CO<sub>2</sub> concentration on C: N: P ratio in marine phytoplankton: A species comparison. *Limnology and Oceanography* 44: 683–690.
- Cael BB, Cavan EL, and Britten GL (2021) Reconciling the size-dependence of marine particle sinking speed. *Geophysical Research Letters* 48. e2020GL091771.
- Cao Z, Yang W, Zhao Y, Guo X, Yin Z, Du C, Zhao H, and Dai M (2019) Diagnosis of CO<sub>2</sub> dynamics and fluxes in global coastal oceans. *National Science Review* 7: 786–797.
- Capone DG, Burns JA, Montoya JP, Subramaniam A, Mahaffey C, Gunderson T, Michaels AF, and Carpenter EJ (2005) Nitrogen fixation by *Trichodesmium* spp.: An important source of new nitrogen to the tropical and subtropical North Atlantic Ocean. *Global Biogeochemical Cycles* 19.
- Carlson CA, Ducklow HW, and Michaels AF (1994) Annual flux of dissolved organic-carbon from the euphotic zone in the northwestern Sargasso Sea. *Nature* 371: 405–408.
- Carr M-E, Friedrichs MAM, Schmeltz M, Noguchi Aita M, Antoine D, Arrigo KR, Asanuma I, Aumont O, Barber R, Behrenfeld M, Bidigare R, Buitenhuis ET, Campbell J, Ciotti A, Dierssen H, Dowell M, Dunne J, Esaias W, Gentili B, Gregg W, Groom S, Hoepffner N, Ishizaka J, Kameda T, Le Quérec C, Lohrenz S, Marra J, Mélin F, Moore K, Morel A, Reddy TE, Ryan J, Scardi M, Smyth T, Turpie K, Tilstone G, Waters K, and Yamanaka Y (2006) A comparison of global estimates of marine primary production from ocean color. *Deep Sea Research Part II: Topical Studies in Oceanography* 53: 741–770.
- Carter BR, Feely RA, Lauvset SK, Olsen A, Devries T, and Sonnerup R (2021) Preformed properties for marine organic matter and carbonate mineral cycling quantification. *Global Biogeochemical Cycles* 35.
- Cavan EL, Trimmer M, Shelley F, and Sanders R (2017) Remineralization of particulate organic carbon in an ocean oxygen minimum zone. *Nature Communications* 8: 14847.
- Chavez F, Messie M, and Pennington JT (2011) Marine primary production in relation to climate variability and change. *Annual Review of Marine Science* 3: 227–260.
- Chisholm SW, Olson RJ, Zettler ER, Goericke R, Waterbury JB, and Welschmeyer NA (1988) A novel free-living prochlorophyte abundant in the oceanic euphotic zone. *Nature* 334: 340–343.
- Cho BC and Azam F (1988) Major role of bacteria in biogeochemical fluxes in the ocean's interior. *Nature* 332: 441–442.
- Cisternas-Novoa C, Lee C, and Engel A (2014) A semi-quantitative spectrophotometric, dye-binding assay for determination of Coomassie Blue stainable particles. *Limnology and Oceanography: Methods* 12: 604–616.
- Clark PU, Shakun JD, Baker PA, Bartlein PJ, Brewer S, Brook E, Carlson AE, Cheng H, Kaufman DS, Liu ZY, Marchitto TM, Mix AC, Morrill C, Otto-Blieneser BL, Pahnke K, Russell JM, Whitlock C, Adkins JF, Blois JL, Clark J, Colman SM, Curry WB, Flower BP, He F, Johnson TC, Lynch-Stieglitz J, Markgraf V, McManus J, Mitrovica JX, Moreno PI, and Williams JW (2012) Global climate evolution during the last deglaciation. *Proceedings of the National Academy of Sciences of the United States of America* 109: E1134–E1142.
- Coale KH and Bruland KW (1985) Th-234: U-238 disequilibria within the California Current. *Limnology and Oceanography* 30: 22–33.
- Coale KH, et al. (1996) A massive phytoplankton bloom induced by an ecosystem-scale iron fertilization experiment in the equatorial Pacific Ocean. *Nature* 383: 495–501.
- Collins S and Bell G (2004) Phenotypic consequences of 1,000 generations of selection at elevated CO<sub>2</sub> in a green alga. *Nature* 431: 566–569.
- Collins S, Rost B, and Rynearson TA (2014) Evolutionary potential of marine phytoplankton under ocean acidification. *Evolutionary Applications* 7: 140–155.

- Conan P, Sondegaard M, Kragh T, Thingstad F, Pujo-Pay M, Williams PJLB, Markager S, Cauwet G, Borch NH, Evans D, and Riemann B (2007) Partitioning of organic production in marine plankton communities: The effects of inorganic nutrient ratios and community composition on new dissolved organic matter. *Limnology and Oceanography* 52: 753–765.
- Cram JA, Weber T, Leung SW, McDonnell AMP, Liang J-H, and Deutsch C (2018) The role of particle size, ballast, temperature, and oxygen in the sinking flux to the deep sea. *Global Biogeochemical Cycles* 32: 858–876.
- Cram JA, Fuchsman CA, Duffy ME, Pretty JL, Lekanoff RM, Neibauer JA, Leung SW, Huebert KB, Weber TS, Bianchi D, Evans N, Devol AH, Keil RG, and McDonnell AMP (2022) Slow particle remineralization, rather than suppressed disaggregation, drives efficient flux transfer through the Eastern Tropical North Pacific oxygen deficient zone. *Global Biogeochemical Cycles* 36: e2021GB007080.
- Cruz BN and Neuer S (2019) Heterotrophic bacteria enhance the aggregation of the marine picocyanobacteria prochlorococcus and synechococcus. *Frontiers in Microbiology* 10.
- Cunliffe M, Engel A, Frka S, Gašparović B, Guitart C, Murrell JC, Salter M, Stolle C, Upstill-Goddard R, and Wurl O (2013) Sea surface microlayers: A unified physicochemical and biological perspective of the air–ocean interface. *Progress in Oceanography* 109: 104–116.
- Dall'olmo G and Mork KA (2014) Carbon export by small particles in the Norwegian Sea. *Geophysical Research Letters* 41: 2921–2927.
- Dam HG and Baumann H (2017) Climate change, zooplankton and fisheries. In: Phillips BF and Pérez-Ramírez M (eds.) *Climate Change Impacts on Fisheries and Aquaculture*. Wiley. <https://doi.org/10.1002/9781119154051.ch25>.
- Davis J and Benner R (2007) Quantitative estimates of labile and semi-labile dissolved organic carbon in the western Arctic Ocean: A molecular approach. *Limnology and Oceanography* 52: 2434–2444.
- Davison PC, Checkley DM, Koslow JA, and Barlow J (2013) Carbon export mediated by mesopelagic fishes in the northeast Pacific Ocean. *Progress in Oceanography* 116: 14–30.
- De Baar HJW, Boyd PW, Coale KH, Landry MR, Atsushi Tsuda PA, Bakker DCE, Bozec Y, Barber RT, Brzezinski MA, Buesseler KO, Boyé M, Croot PL, Gervais F, Gorbunov MY, Harrison PJ, Hiscock WT, Laan P, Lancelot C, Law CS, Levasseur M, Marchetti A, Millero FJ, Nishioka J, Nojiri Y, Tim Van Oijen ULF, Riebesell MJA, Rijkenberg HS, Takeda S, Timmermans KR, Veldhuis MJW, Waite AM, and Wong C-S (2005) Synthesis of iron fertilization experiments: From the iron age in the age of enlightenment. *Journal of Geophysical Research* 110: C09S16.
- De Haas H, Van Weering TCE, and De Stigter H (2002) Organic carbon in shelf seas: Sinks or sources, processes and products. *Continental Shelf Research* 22: 691–717.
- De La Rocha C and Passow U (2007) Factors influencing the sinking of POC and the efficiency of the biological carbon pump. *Deep-Sea Research Part II* 54: 639–658.
- de Martini F, Neuer S, Hamill D, Robidart J, and Lomas MW (2018) Clade and strain specific contributions of Synechococcus and Prochlorococcus to carbon export in the Sargasso Sea. *Limnology and Oceanography* 63: S448–S457.
- Deangelis M, Barkov NI, and Petrov VN (1987) Aerosol concentrations over the last climatic cycle (160 Kyr) from an Antarctic ice core. *Nature* 325: 318–321.
- Deb S and Mandal B (2021) Soils and sediments of coastal ecology: A global carbon sink. *Ocean and Coastal Management* 214.
- Deng W, Cruz BN, and Neuer S (2016) Effects of nutrient limitation on cell growth, TEP production and aggregate formation of marine Synechococcus. *Aquatic Microbial Ecology* 78: 39–49.
- Deuser WG, Brewer PG, Jickells TD, and Commeau RF (1983) Biological control of the removal of abiogenic particles from the surface ocean. *Science* 219: 388–391.
- Deutsch C, Sarmiento JL, Sigman DM, Gruber N, and Dunne JP (2007) Spatial coupling of nitrogen inputs and losses in the ocean. *Nature* 445: 163–167.
- Devol AH and Hartnett HE (2001) Role of the oxygen-deficient zone in transfer of organic carbon to the deep ocean. *Limnology and Oceanography* 46: 1684–1690.
- Devries T and Holzer M (2019) Radiocarbon and helium isotope constraints on deep ocean ventilation and mantle-<sup>3</sup>He sources. *Journal of Geophysical Research: Oceans* 124: 3036–3057.
- Devries T and Primeau F (2011) Dynamically and observationally constrained estimates of water-mass distributions and ages in the global ocean. *Journal of Physical Oceanography* 41: 2381–2401.
- Devries T and Weber T (2017) The export and fate of organic matter in the ocean: New constraints from combining satellite and oceanographic tracer observations. *Global Biogeochemical Cycles* 31: 535–555.
- Devries T, Primeau F, and Deutsch C (2012) The sequestration efficiency of the biological pump. *Geophysical Research Letters* 39: 1–5.
- Dilling L and Allredge AL (2000) Fragmentation of marine snow by swimming macrozooplankton: A new process impacting carbon cycling in the sea. *Deep-Sea Research Part I* 47: 1227–1245.
- Doney SC, Ruckelshaus M, Emmett Duffy J, Barry JP, Chan F, English CA, Galindo HM, Grebmeier JM, Hollowed AB, Knowlton N, Polovina J, Rabalais NN, Sydeman WJ, and Talley LD (2012) Climate change impacts on marine ecosystems. *Annual Review of Marine Science* 4: 11–37.
- Duarte CM, Bruhn A, and Krause-Jensen D (2022) A seaweed aquaculture imperative to meet global sustainability targets. *Nature Sustainability* 5: 185–193.
- Dugdale RC and Goering JJ (1967) Uptake of new and regenerated forms of nitrogen in primary productivity. *Limnology and Oceanography* 12: 196–206.
- Dunne JP, Armstrong RA, Gnanadesikan A, and Sarmiento JL (2005) Empirical and mechanistic models for the particle export ratio. *Global Biogeochemical Cycles* 19: 1–16.
- Durkin CA, Estapa ML, and Buesseler KO (2015) Observations of carbon export by small sinking particles in the upper mesopelagic. *Marine Chemistry* 175: 72–81.
- Dutreuil S, Bopp L, and Tagliabue A (2009) Impact of enhanced vertical mixing on marine biogeochemistry: Lessons for geo-engineering and natural variability. *Biogeosciences* 6: 901–912.
- Dybwad C, Assmy P, Olsen LM, Peeken I, Nikolopoulos A, Krumpfen T, Randelhoff A, Tatarek A, Wiktor JM, and Reigstad M (2021) Carbon export in the seasonal sea ice zone north of Svalbard from winter to late summer. *Frontiers in Marine Science* 7.
- Ebersbach F and Trull TW (2007) Sinking particle properties from polyacrylamide gels during KEOPS: Zooplankton controls on carbon export in an area of persistent natural iron inputs in the Southern Ocean. *Limnology and Oceanography* 53: 212–224.
- Elderfield H and Rickaby R (2000) Oceanic Cd/P ratio and nutrient utilization in the glacial Southern Ocean. *Nature* 405: 305–310.
- Emerson S (2014) Annual net community production and the biological carbon flux in the ocean. *Global Biogeochemical Cycles* 28: 14–28.
- Engel A and Passow U (2001) Carbon and nitrogen content of transparent exopolymer particles (TEP) in relation to their Alcian Blue adsorption. *Marine Ecology-Progress Series* 219: 1–10.
- Engel A and Schartau M (1999) Influence of transparent exopolymer particles (TEP) on sinking velocity of Nitzschia closterium aggregates. *Marine Ecology-Progress Series* 182: 69–76.
- Eppley RW and Peterson BJ (1979) Particulate organic matter flux and planktonic new production in the deep ocean. *Nature* 282: 677–680.
- Estapa M, Valdes J, Tradd K, Sugar J, Omand M, and Buesseler K (2020) The neutrally buoyant sediment trap: Two decades of progress. *Journal of Atmospheric and Oceanic Technology* 37: 957–973.
- Fabry VJ (2008) Marine calcifiers in a high CO<sub>2</sub> Ocean. *Science* 320: 1020–1022.
- Fagerbakke K, Norland S, and Heldal M (1999) The inorganic ion content of native aquatic bacteria. *Canadian Journal of Microbiology* 45: 304–311.
- Falkowski PG and Raven J (2007) *Aquatic Photosynthesis*. Princeton, Nj: Princeton University Press.
- Fenaux R (1985) Rhythm of secretion of oikopleurid's houses. *Bulletin of Marine Science* 37: 498–503.
- Feng Y, Hare C, Leblanc K, Rose J, Zhang Y, Ditullio G, Lee P, Wilhelm S, Rowe J, Sun J, Nemcek N, Gueguen C, Passow U, Benner I, Brown C, and Hutchins D (2009) Effects of increased pCO<sub>2</sub> and temperature on the North Atlantic spring bloom. I. The phytoplankton community and biogeochemical response. *Marine Ecology Progress Series* 388: 13–25.
- Field CB, Behrenfeld MJ, Randerson JT, and Falkowski PG (1998) Primary production of the biosphere: Integrating terrestrial and oceanic components. *Science* 281: 237–240.
- Fischer G and Karakaş G (2009) Sinking rates and ballast composition of particles in the Atlantic Ocean: implications for the organic carbon fluxes to the deep ocean. *Biogeosciences* 6: 85–102.
- Francois R, Altabet MA, Yu E-FF, Sigman DM, Bacon MP, Frank M, Bohrmann G, Boreille G, Labeyrie LD, Frankk M, and Geosciences M (1997) Contribution of Southern Ocean surface-water stratification to low atmospheric CO<sub>2</sub> concentrations during the last glacial period. *Nature* 389: 929–935.



- Francois R, Honjo S, Krishfield R, and Manganini S (2002) Factors controlling the flux of organic carbon to the bathypelagic zone of the ocean. *Global Biogeochemical Cycles* 16: 34–1–34–20.
- Frangoulis C, Christou E, and Hecq J (2004) Comparison of marine copepod outfluxes: Nature, rate, fate and role in the carbon and nitrogen cycles. *Advances in Marine Biology* 47: 253–309.
- Gaerdes A, Iversen MH, Grossart H-P, Passow U, and Ullrich M (2011) Diatom associated bacteria are required for aggregation of *Thalassiosira weissflogii*. *ISME Journal* 5: 436–445.
- Gattuso J-P, Williamson P, Duarte CM, and Magnan AK (2021) The potential for ocean-based climate action: Negative emissions technologies and beyond. *Frontiers in Climate* 2.
- Geider R and La Roche J (2002) Redfield revisited: Variability of C: N: P in marine microalgae and its biochemical basis. *European Journal of Phycology* 37: 1–17.
- Giering SLC, Sanders R, Martin AP, Lindemann C, Möller KO, Daniels CJ, Mayor DJ, and St. John, M. A. (2016) High export via small particles before the onset of the North Atlantic spring bloom. *Journal of Geophysical Research: Oceans* 121: 6929–6945.
- Giordano M, Beardall J, and Raven JA (2005) CO<sub>2</sub> concentrating mechanisms in algae: Mechanisms, environmental modulation, and evolution. *Annual Review of Plant Biology* 56: 99–131.
- Giovanoni S, Chan F, Davis E, Deutsch C, and Wolf S (2021) Biochemical barriers on the path to ocean anoxia? *MBio* 12.
- Goldthwait SA, Carlson CA, Henderson GK, and Alldredge AL (2005) Effects of physical fragmentation on remineralization of marine snow. *Marine Ecology-Progress Series* 305: 59–65.
- Gregoire M, Garçon V, Garcia H, Breitburg D, Isensee K, Oschlies A, Telszewski M, Barth A, Bittig HC, Carstensen J, Carval T, Chai F, Chavez F, Conley D, Coppola L, Crowe S, Currie K, Dai MH, Deflandre B, Dewitte B, Diaz R, Garcia-Robledo E, Gilbert D, Giorgetti A, Glud R, Gutierrez D, Hosoda S, Ishii M, Jacinto G, Langdon C, Lauvset SK, Levin LA, Limburg KE, Mehrtens H, Montes I, Naqvi W, Paulmier A, Pfeil B, Pitcher G, Pouliquen S, Rabalais N, Rabouille C, Recape V, Roman M, Rose K, Rudnick D, Rummer J, Schmechtig C, Schmidtko S, Seibel B, Slomp C, Sumalia UR, Tanhua T, Thierry V, Uchida H, Wanninkhof R, and Yasuhara M (2021) A global ocean oxygen database and atlas for assessing and predicting deoxygenation and ocean health in the open and coastal ocean. *Frontiers in Marine Science* 8.
- Grossart HP, Engel A, Arnosti C, De La Rocha CL, Murray AE, and Passow U (2007) Microbial dynamics in autotrophic and heterotrophic seawater mesocosms. III. Organic matter fluxes. *Aquatic Microbial Ecology* 49: 143–156.
- Gruber N and Galloway JN (2008) An Earth-system perspective of the global nitrogen cycle. *Nature* 451: 293–296. <https://doi.org/10.1038/nature06592>.
- Guidi L, Jackson GA, Stemmann L, Miquel JC, Picheral M, and Gorsky G (2008) Relationship between particle size distribution and flux in the mesopelagic zone. *Deep Sea Research Part I: Oceanographic Research Papers* 55: 1364–1374.
- Guidi L, Stemmann L, Jackson GA, Ibanez F, Claustre H, Legendre L, Picheral M, and Gorsky G (2009) Effects of phytoplankton community on production, size and export of large aggregates: A world-ocean analysis. *Limnology and Oceanography* 54: 1951–1963.
- Guidi L, Legendre L, Reygondeau G, Uitz J, Stemmann L, and Henson SA (2015) A new look at ocean carbon remineralization for estimating deepwater sequestration. *Global Biogeochemical Cycles*: 1–16.
- Hale B and Dilling L (2011) Geoengineering, ocean fertilization, and the problem of permissible pollution. *Science, Technology & Human Values* 36: 190–212.
- Hamm CE (2002) Interactive aggregation and sedimentation of diatoms and clay-sized lithogenic material. *Limnology and Oceanography* 47: 1790–1795.
- Hamm C, Reigstad M, Riser CW, Muhlebach A, and Wassmann P (2001) On the trophic fate of Phaeocystis pouchetii. VII. Sterols and fatty acids reveal sedimentation of P. pouchetii-derived organic matter via krill fecal strings. *Marine Ecology Progress Series* 209: 55–69.
- Hansell D, Carlson CA, Repeta DJ, and Schlitzer R (2009) Dissolved organic matter in the ocean. *Oceanography* 22: 202–211.
- Harrison DP (2017) Global negative emissions capacity of ocean macronutrient fertilization. *Environmental Research Letters* 12: 035001.
- Harrison PJ, Thompson PA, and Calderwood GS (1990) Effects of nutrient and light limitation on the biochemical composition of phytoplankton. *Journal of Applied Phycology* 2: 45–56.
- Hartmann J, West AJ, Renforth P, Köhler P, De La Rocha CL, Wolf-Gladrow DA, Dürr HH, and Scheffran J (2013) Enhanced chemical weathering as a geoengineering strategy to reduce atmospheric carbon dioxide, supply nutrients, and mitigate ocean acidification. *Reviews of Geophysics* 51: 113–149.
- Hedges JL and Keil RG (1995) Sedimentary organic matter preservation: An assessment and speculative synthesis. *Marine Chemistry* 49: 81–115.
- Heinrich AK (1962) The life histories of plankton animals and seasonal cycles of plankton communities in the oceans. *ICES Journal of Marine Science* 27: 15–24.
- Henson SA, Sanders R, Madsen E, Morris PJ, Le Moigne F, and Quartly GD (2011) A reduced estimate of the strength of the ocean's biological carbon pump. *Geophysical Research Letters* 38: 10–14.
- Henson SA, Sanders R, and Madsen E (2012) Global patterns in efficiency of particulate organic carbon export and transfer to the deep ocean. *Global Biogeochemical Cycles* 26: 1–14.
- Henson SA, Laufkötter C, Leung S, Giering SLC, Palevsky HI, and Cavan EL (2022) Uncertain response of ocean biological carbon export in a changing world. *Nature Geoscience* 15: 248–254.
- Hidaka K, Kawaguchi K, Murakami M, and Takahashi M (2001) Downward transport of organic carbon by diel migratory micronekton in the western equatorial Pacific: Its quantitative and qualitative importance. *Deep Sea Research Part I: Oceanographic Research Papers* 48: 1923–1939.
- Hoffmann LJ, Peeken I, and Lochte K (2007) Effects of iron on the elemental stoichiometry during EIFEX and in the diatoms *Fragilariopsis kerguelensis* and *Chaetoceros dichroaeta*. *Biogeosciences Discussions* 4: 249–275.
- Honjo S, Manganini SJ, Krishfield RA, and Francois R (2008) Particulate organic carbon fluxes to the ocean interior and factors controlling the biological pump: A synthesis of global sediment trap programs since 1983. *Progress in Oceanography* 76: 217–285.
- Hutchins DA (2011) Forecasting the rain ratio. *Nature* 476: 41–42.
- Hutchins DA, Fu F-X, Webb EA, Walworth N, and Tagliabue A (2013) Taxon-specific response of marine nitrogen fixers to elevated carbon dioxide concentrations. *Nature Geoscience* 6: 790–795.
- Iglesias-Rodríguez MD, Brown CW, Doney SC, Kleypas J, Kolber D, Kolber Z, Hayes PK, and Falkowski PG (2002) Representing key phytoplankton functional groups in ocean carbon cycle models: Coccolithophorids. *Global Biogeochemical Cycles* 16: 47–1–47–20.
- Iglesias-Rodríguez MD, Halloran PR, Rickaby REM, Hall IR, Colmenero-Hidalgo E, Gittins JR, Green DRH, Tyrrell T, Gibbs SJ, Von Dassow P, Rehm E, Armbrust EV, and Boessenkool KP (2008) Phytoplankton calcification in a high-CO<sub>2</sub> world. *Science* 320: 336–340.
- Ito T and Follows MJ (2003) Upper ocean control on the solubility pump of CO<sub>2</sub>. *Journal of Marine Research* 61: 465–489.
- Ito T and Follows MJ (2005) Preformed phosphate, soft tissue pump and atmospheric carbon dioxide. *Journal of Marine Research* 63: 813–839.
- Ito T, Follows MJ, and Boyle EA (2004) Is AOU a good measure of respiration in the oceans? *Geophysical Research Letters* 31.
- Iversen MH and Lampitt RS (2020) Size does not matter after all: No evidence for a size-sinking relationship for marine snow. *Progress in Oceanography* 189: 102445.
- Iversen MH and Ploug H (2010) Ballast minerals and the sinking carbon flux in the ocean: Carbon-specific respiration rates and sinking velocity of marine snow aggregates. *Biogeosciences* 7: 2613–2624.
- Iversen MH and Robert ML (2015) Ballasting effects of smectite on aggregate formation and export from a natural plankton community. *Marine Chemistry* 175: 18–27.
- Jackson GA (1990) A model of the formation of marine algal flocks by physical coagulation processes. *Deep-Sea Research* 37: 1197–1211.
- Jackson GA (1995) TEP and coagulation during a mesocosm experiment. *Deep-Sea Research Part II* 42: 215–222.
- James AK, Passow U, Brzezinski MA, Parsons RJ, Trapani JN, and Carlson CA (2017) Elevated pCO<sub>2</sub> enhances bacterioplankton removal of organic carbon. *PLoS One* 12: e0173145.
- Jenkins WJ (1982) Oxygen utilization rates in North-Atlantic sub-tropical gyre and primary production in oligotrophic systems. *Nature* 300: 246–248.
- Jenkins WJ (1987) H-3 and He-3 in the beta-triangle - observations of gyre ventilation and oxygen utilization rates. *Journal of Physical Oceanography* 17: 763–783.
- Jiao N and Azam F (2011) Microbial carbon pump and its significance for carbon sequestration in the ocean. In: Jiao N, Azam F, and Sanders S (eds.) *Microbial Carbon Pump in the Ocean*. Washington DC: Science/AAAS Business Office.
- Jiao N, Cai R, Zheng Q, Tang K, Liu J, Jiao F, Wallace D, Chen F, Li C, Amann R, Benner R, and Azam F (2018) Unveiling the enigma of refractory carbon in the ocean. *National Science Review* 5: 459–463.

- Jickells TD, An ZS, Andersen KK, Baker AR, Bergametti G, Brooks N, Cao JJ, Boyd PW, Duce RA, Hunter KA, Kawahata H, Kubilay N, Laroche J, Liss PS, Mahowald N, Prospero JM, Ridgwell AJ, Tegen I, and Torres R (2005) Global iron connections between desert dust, ocean biogeochemistry, and climate. *Science* 308: 67–71.
- Johnson KS, Chavez FP, and Friedrich GE (1999) Continental-shelf sediment as a primary source of iron for coastal phytoplankton. *Nature* 398: 697–700.
- Jónasdóttir SH, Visser AW, Richardson K, and Heath MR (2015) Seasonal copepod lipid pump promotes carbon sequestration in the deep North Atlantic. *Proceedings of the National Academy of Sciences of the United States of America* 112: 12122–12126.
- Jørgensen BB, Wenzhöfer F, Egger M, and Glud RN (2022) Sediment oxygen consumption: Role in the global marine carbon cycle. *Earth-Science Reviews* 228.
- Jürchott M, Oschlies A, and Koeve W (2023) Artificial Upwelling – A New Narrative. *Earth and Space Science* Open Archive 20.
- Kadko D (2009) Rapid oxygen utilization in the ocean twilight zone assessed with the cosmogenic isotope  $^{10}\text{Be}$ . *Global Biogeochemical Cycles* 23: GB4010.
- Keeling RF, Körtzinger A, and Gruber N (2010) Ocean deoxygenation in a warming world. *Annual Review of Marine Science* 2: 199–229.
- Keil RG, Neibauer JA, Biladeau C, Van Der Elst K, and Devol AH (2016) A multiproxy approach to understanding the “enhanced” flux of organic matter through the oxygen-deficient waters of the Arabian Sea. *Biogeosciences* 13: 2077–2092.
- Kepkay PE (1994) Particle aggregation and the biological reactivity of colloids. *Marine Ecology Progress Series* 109: 293–304.
- Kiko R, Picheral M, Antoine D, Babin M, Berline L, Biard T, Boss E, Brandt P, Carlotti F, Christiansen S, Coppola L, De La Cruz L, Diamond-Riquier E, De Madron XD, Elineau A, Gorsky G, Guidi L, Hauss H, Irissou JO, Karp-Boss L, Karstensen J, Kim DG, Lekanoff RM, Lombard F, Lopes RM, Marec C, McDonnell AMP, Niemeyer D, Noyon M, O’daly SH, Ohman MD, Pretty JL, Rogge A, Searson S, Shibata M, Tanaka Y, Tanhua T, Taucher J, Trudnowska E, Turner JS, Waite A, and Stemmann L (2022) A global marine particle size distribution dataset obtained with the Underwater Vision Profiler 5. *Earth System Science Data* 14: 4315–4337.
- Kjørboe T (2000) Colonization of marine snow aggregates by invertebrate zooplankton: Abundance, scaling, and possible role. *Limnology and Oceanography* 45: 479–484.
- Kjørboe T (2011) How zooplankton feed: Mechanisms, traits and trade-offs. *Biological Reviews* 86: 311–339.
- Kjørboe T and Jackson GA (2001) Marine snow, organic solute plumes, and optimal chemosensory behavior of bacteria. *Limnology and Oceanography* 46: 1309–1318.
- Kjørboe T, Grossart HP, Ploug H, Tang K, and Auer B (2004) Particle-associated flagellates: Swimming patterns, colonization rates, and grazing on attached bacteria. *Aquatic Microbial Ecology* 35: 141–152.
- Klaas C and Archer DE (2002) Association of sinking organic matter with various types of mineral ballast in the deep sea: Implications for the rain ratio. *Global Biogeochemical Cycles* 16: 1116.
- Koch BP, Kattner G, Witt M, and Passow U (2014) Molecular insights into the microbial formation of marine dissolved organic matter: Recalcitrant or labile? *Biogeosciences* 11: 4173–4190.
- Koeve W and Kahler P (2016) Oxygen utilization rate (OUR) underestimates ocean respiration: A model study. *Global Biogeochemical Cycles* 30: 1166–1182.
- Köhler P, Abrams JF, Völker C, Hauck J, and Wolf-Gladrow DA (2013) Geoengineering impact of open ocean dissolution of olivine on atmospheric  $\text{CO}_2$ , surface ocean pH and marine biology. *Environmental Research Letters* 8: 014009.
- Koski M, Møller EF, Maar M, and Visser AW (2007) The fate of discarded appendicularian houses: degradation by the copepod, *Microsetella norvegica*, and other agents. *Journal of Plankton Research* 29: 641–654.
- Kranz SA, Levitan O, Richter K-U, Prášil O, Berman-Frank I, and Rost B (2010) Combined effects of  $\text{CO}_2$  and light on the  $\text{N}_2$ -fixing cyanobacterium *Trichodesmium* IMS101: Physiological responses. *Plant Physiology* 154: 334–345.
- Kriest I and Oschlies A (2008) On the treatment of particulate organic matter sinking in large-scale models of marine biogeochemical cycles. *Biogeosciences* 5: 55–72.
- Kwiatkowski L, Torres O, Bopp L, Aumont O, Chamberlain M, Christian JR, Dunne JP, Gehlen M, Ilyina T, John JG, Lenton A, Li H, Lovenduski NS, Orr JC, Palmieri J, Santana-Falcón Y, Schwinger J, Séférian R, Stock CA, Tagliabue A, Takano Y, Tjiputra J, Toyama K, Tsujino H, Watanabe M, Yamamoto A, Yool A, and Ziehn T (2020) Twenty-first century ocean warming, acidification, deoxygenation, and upper-ocean nutrient and primary production decline from CMIP6 model projections. *Biogeosciences* 17: 3439–3470.
- Kwon EY, Primeau F, and Sarmiento JL (2009) The impact of remineralization depth on the air-sea carbon balance. *Nature Geoscience* 2: 630–635.
- Lam P and Kuypers MMM (2011) Microbial nitrogen cycling processes in oxygen minimum zones. *Annual Review of Marine Science* 3: 317–345.
- Lam PJ, Doney SC, and Bishop JKB (2011) The dynamic ocean biological pump: Insights from a global compilation of particulate organic carbon,  $\text{CaCO}_3$ , and opal concentration profiles from the mesopelagic. *Global Biogeochemical Cycles* 25: GB3009.
- Lampitt RS, Wishner KF, Turley CM, and Angel MV (1993) Marine snow studies in the Northeast Atlantic ocean - distribution, composition and role as a food source for migrating plankton. *Marine Biology* 116: 689–702.
- Lampitt RS, Achterberg EP, Anderson TR, Hughes JA, Iglesias-Rodríguez MD, Kelly-Gerreyn BA, Lucas M, Popova EE, Sanders R, Shepherd JG, Smythe-Wright D, and Yool A (2008) Ocean fertilization: a potential means of geoengineering? *Philosophical Transactions of the Royal Society A: Mathematical, Physical and Engineering Sciences* 366: 3919–3945.
- LaRowe DE, Arndt S, Bradley JA, Estes ER, Hoarfrost A, Lang SQ, Lloyd KG, Mahmoudi N, Orsi WD, Shah Walter SR, Steen AD, and Zhao R (2020) The fate of organic carbon in marine sediments - New insights from recent data and analysis. *Earth-Science Reviews* 204.
- Laufkötter C, John JG, Stock CA, and Dunne JP (2017) Temperature and oxygen dependence of the remineralization of organic matter. *Global Biogeochemical Cycles* 31: 1038–1050.
- Laws EA and Maiti K (2019) The relationship between primary production and export production in the ocean: Effects of time lags and temporal variability. *Deep Sea Research Part I: Oceanographic Research Papers* 148: 100–107.
- Laws EA, Falkowski PG, Smith WO, Ducklow H, and Mccarthy JJ (2000) Temperature effects on export production in the open ocean. *Global Biogeochemical Cycles* 14: 1231–1246.
- Laws EA, D’Sa E, and Naik P (2011) Simple equations to estimate ratios of new or export production to total production from satellite-derived estimates of sea surface temperature and primary production. *Limnology and Oceanography: Methods* 9: 593–601.
- Le Quéré C, Harrison SP, Prentice IC, Buitenhuis ET, Aumont O, Bopp L, Claustre H, Cotrim Da Cunha L, Geider R, Giraud X, Klaas C, Kohfeld KE, Legendre L, Manizza M, Platt T, Rivkin RB, Sathyendranath S, Uitz J, Watson AJ, and Wolf-Gladrow D (2005) Ecosystem dynamics based on plankton functional types for global ocean biogeochemistry models. *Global Change Biology* 11: 2016–2040.
- Lee C, Peterson ML, Wakeham SG, Armstrong RA, Cochran JK, Miquel JC, Fowler SW, Hirschberg D, Beck A, and Xue J (2009) Particulate organic matter and ballast fluxes measured using time-series and settling velocity sediment traps in the northwestern Mediterranean Sea. *Deep Sea Research Part II: Topical Studies in Oceanography* 56: 1420–1436.
- Legendre L, Rivkin RB, Weinbauer MG, Guidi L, and Uitz J (2015) The microbial carbon pump concept: Potential biogeochemical significance in the globally changing ocean. *Progress in Oceanography* 134: 432–450.
- Leung SW, Weber T, Cram JA, and Deutsch C (2021) Variable particle size distributions reduce the sensitivity of global export flux to climate change. *Biogeosciences* 18: 229–250.
- Levy M, Bopp L, Karleskind P, Resplandy L, Ethe C, and Pinsard F (2013) Physical pathways for carbon transfers between the surface mixed layer and the ocean interior. *Global Biogeochemical Cycles* 27: 1001–1012.
- Lin H, Rauschenberg S, Hexel CR, Shaw TJ, and Twining BS (2011) Free-drifting icebergs as sources of iron to the Weddell Sea. *Deep Sea Research Part II: Topical Studies in Oceanography* 58: 1392–1406.
- Litchman E, Klausmeier CA, Schofield OM, and Falkowski PG (2007) The role of functional traits and trade-offs in structuring phytoplankton communities: Scaling from cellular to ecosystem level. *Ecology Letters* 10: 1170–1181.
- Liu H, Landry MR, Vulot D, and Campbell L (1999) Prochlorococcus growth rates in the central equatorial Pacific: An application of the fmax approach. *Journal of Geophysical Research: Oceans* 104: 3391–3399.
- Liu GP, Bracco A, and Passow U (2018) The influence of mesoscale and submesoscale circulation on sinking particles in the northern Gulf of Mexico. *Elementa: Science of the Anthropocene* 6.
- Logan BE, Passow U, Alldredge AL, Grossart H-P, and Simon M (1995) Rapid formation and sedimentation of large aggregates is predictable from coagulation rates (half-lives) of transparent exopolymer particles (TEP). *Deep-Sea Research Part II* 42: 203–214.

- Lohbeck KT, Riebesell U, and Reusch TBH (2012) Adaptive evolution of a key phytoplankton species to ocean acidification. *Nature Geoscience* 5: 346–351.
- Lombard F and Kjørboe T (2010) Marine snow originating from appendicularian houses: Age-dependent settling characteristics. *Deep Sea Research Part I: Oceanographic Research Papers* 57: 1304–1313.
- Long RA and Azam F (1996) Abundant protein-containing particles in the sea. *Aquatic Microbial Ecology* 10: 213–221.
- Longhurst AR, Bedo AW, Harrison WG, Head EJH, and Sameoto DD (1990) Vertical flux of respiratory carbon by oceanic diel migrant biota. *Deep Sea Research Part A. Oceanographic Research Papers* 37: 685–694.
- Lutz MJ, Caldeira K, Dunbar RB, and Behrenfeld MJ (2007) Seasonal rhythms of net primary production and particulate organic carbon flux to depth describe the efficiency of biological pump in the global ocean. *Journal of Geophysical Research-Oceans* 112: 26.
- Mahowald NM, Muhs DR, Levis S, Rasch PJ, Yoshioka M, Zender CS, and Luo C (2006) Change in atmospheric mineral aerosols in response to climate: Last glacial period, preindustrial, modern, and doubled carbon dioxide climates. *Journal of Geophysical Research: Atmospheres* 111.
- Mari X, Passow U, Migon C, Burd AB, and Legendre L (2017) Transparent Exopolymer Particles: Effects on carbon cycling in the ocean. *Progress in Oceanography* 151: 13–37.
- Marsay CM, Sanders RJ, Henson SA, Pabortsava K, Achterberg EP, and Lampitt RS (2015) Attenuation of sinking particulate organic carbon flux through the mesopelagic ocean. *Proceedings of the National Academy of Sciences* 112: 1089–1094.
- Martin JH (1990) Glacial-interglacial CO<sub>2</sub> change: The iron hypothesis. *Paleoceanography* 5: 1–13.
- Martin JH and Fitzwater SE (1988) Iron deficiency limits phytoplankton growth in the northeast Pacific subarctic. *Nature* 331: 341–343.
- Martin JH, Knauer GA, Karl DM, and Broenkow WW (1987) Vertex: Carbon cycling in the northeast Pacific. *Deep Sea Research* 34: 267–285.
- Martin JH, Fitzwater SE, and Gordon RM (1991) We still say iron deficiency limits phytoplankton growth in the subarctic Pacific. *Journal of Geophysical Research* 96: 20699–20700.
- Martinez-Garcia A, Sigman DM, Ren H, Anderson RF, Straub M, Hodell DA, Jaccard SL, Eglinton TI, and Haug GH (2014) Iron fertilization of the Subantarctic ocean during the last ice age. *Science* 343: 1347–1350.
- Martiny AC, Pham CTA, Primeau FW, Vrugt JA, Moore JK, Levin SA, and Lomas MW (2013) Strong latitudinal patterns in the elemental ratios of marine plankton and organic matter. *Nature Geoscience* 6: 279–283.
- McCave IN (1984) Size spectra and aggregation of suspended particles in the deep ocean. *Deep-Sea Research Part I* 31: 329–352.
- McDonnell A, Boyd P, and Buesseler K (2015) Effects of sinking velocities and microbial respiration rates on the attenuation of particulate carbon fluxes through the mesopelagic zone. *Global Biogeochemical Cycles* 29: 175–193.
- Millero FJ, Woosley R, Ditrolo B, and Waters J (2009) Effect of ocean acidification on the speciation of metals in seawater. *Oceanography* 22: 72–85.
- Moore JK and Doney SC (2006) Remote sensing observations of ocean physical and biological properties in the region of the Southern Ocean Iron Experiment (SOFEX). *Journal of Geophysical Research-Oceans* 111.
- Moore M, Hickman A, Poulton AJ, and Seeyave S (2007) Iron-light interactions during the CROZet Experiment (CROZEX) II: taxonomic responses and elemental stoichiometry. *Deep-Sea Research Part II* 54: 2066–2084.
- Moore JK, Fu WW, Primeau F, Britten GL, Lindsay K, Long M, Doney SC, Mahowald N, Hoffman F, and Randerson JT (2018) Sustained climate warming drives declining marine biological productivity. *Science* 359: 1139–1142.
- Mopper K, Schultz C, Chevrolot L, Germain C, Revuelta R, and Dawson R (1991) Determination of sugars in unconcentrated seawater and other natural waters by liquid chromatography and pulsed amperometric detection. *Environmental Science and Technology* 26: 133–138.
- Moran XAG, Lopez-Urrutia A, Calvo-Diaz A, and Li WKW (2010) Increasing importance of small phytoplankton in a warmer ocean. *Global Change Biology* 16: 1137–1144.
- Mustaffa NIH, Latif MT, and Wurl O (2021) The role of extracellular carbonic anhydrase in biogeochemical cycling: Recent advances and climate change responses. *International Journal of Molecular Sciences* 22: 7413.
- Myklestad SM (1995) Release of extracellular products by phytoplankton with special emphasis on polysaccharides. *Science of the Total Environment* 165: 155–164.
- N'Yeurt AD, Chynoweth DP, Capron ME, Stewart JR, and Hasan MA (2012) Negative carbon via Ocean Afforestation. *Process Safety and Environmental Protection* 90: 467–474.
- Nagata T, Yamada Y, and Fukuda H (2021) Transparent exopolymer particles in deep oceans: Synthesis and future challenges. *Gels* 7.
- Nagelkerken I and Connell SD (2015) Global alteration of ocean ecosystem functioning due to increasing human CO<sub>2</sub> emissions. *Proceedings of the National Academy of Sciences* 112: 13272–13277.
- Nelson DM, Treguer P, Brzezinski MA, Leynaert A, and Queguiner B (1995) Production and dissolution of biogenic silica in the ocean: Revised global estimates, comparison with regional data, and relationship to biogenic sedimentation. *Global Biogeochemical Cycles* 9: 359–372.
- Nishioka J and Takeda S (1997) Literature surveys on the role of micro-nutrients, such as iron, in the carbon cycle of open ocean ecosystem. *Dennyoku Chuo Kenkyusho Hokoku* 0: 1–25.
- Noji TT (1991) The influence of macrozooplankton on vertical particulate flux. *Sarsia* 76: 1–9.
- Nowicki M, Devries T, and Siegel DA (2022) Quantifying the carbon export and sequestration pathways of the ocean's biological carbon pump. *Global Biogeochemical Cycles* 36.
- Ogawa H, Amagai Y, Koike I, Kaiser K, and Benner R (2001) Production of refractory dissolved organic matter by bacteria. *Science* 292: 917–920.
- Omand MM, D'Asaro EA, Lee CM, Perry MJ, Briggs N, Cetinic I, and Mahadevan A (2015) Eddy-driven subduction exports particulate organic carbon from the spring bloom. *Science* 348: 222–225.
- Oschlies A, Pahlow M, Yool A, and Matear RJ (2010) Climate engineering by artificial ocean upwelling: Channelling the sorcerer's apprentice. *Geophysical Research Letters* 37.
- Paasche E (1999) Reduced coccolith calcite production under light-limited growth: A comparative study of three clones of *Emiliania huxleyi* (Prymnesiophyceae). *Phycologia* 38: 508–516.
- Pan Y, Fan W, Zhang D, Chen J, Huang H, Liu S, Jiang Z, Di Y, Tong M, and Chen Y (2016) Research progress in artificial upwelling and its potential environmental effects. *Science China Earth Sciences* 59: 236–248.
- Pan Y, You L, Li Y, Fan W, Chen C-TA, Wang B-J, and Chen Y (2018) Achieving highly efficient atmospheric CO<sub>2</sub> uptake by artificial upwelling. *Sustainability* 10: 664.
- Passos TU (2018) *Biological Response to Ocean Macronutrient Fertilisation*. BSc, The University of Sydney.
- Passow U (1991) Vertical migration of *Gonyaulax catenata* and *Mesodinium rubrum*. *Marine Biology* 110: 455–463.
- Passow U (2000) Formation of Transparent Exopolymer Particles, Tep, from dissolved precursor material. *Marine Ecology Progress Series* 192: 1–11.
- Passow U (2002) Transparent exopolymer particles (TEP) in aquatic environments. *Progress in Oceanography* 55: 287–333.
- Passow U (2004) Switching perspectives: Do mineral fluxes determine particulate organic carbon fluxes or vice versa. *Geochemistry, Geophysics, Geosystems* 5: 1–5.
- Passow U and Alldredge AL (1995) Aggregation of a diatom bloom in a mesocosm: The role of transparent exopolymer particles (TEP). *Deep-Sea Research Part II* 42: 99–109.
- Passow U and Carlson C (2012) The biological pump in a high CO<sub>2</sub> world. *Marine Ecology Progress Series* 470: 249–271.
- Passow U and De La Rocha CL (2006) Accumulation of mineral ballast on organic aggregates. *Global Biogeochemical Cycles* 20: 7.
- Passow U and Laws EA (2015) Ocean acidification as one of multiple stressors: Response of *Thalassiosira weissflogii* (diatom). *Marine Ecology Progress Series* 541: 75–90.
- Passow U and Wassman P (1994) On the trophic fate of *Phaeocystis pouchetti* (Hariot): IV The formation of marine snow by *P. pouchetti*. *Marine Ecology Progress Series* 104: 153–161.
- Passow U, Shipe RF, Murray A, Pak DK, Brzezinski MA, and Alldredge AL (2001) Origin of transparent exopolymer particles (TEP) and their role in the sedimentation of particulate matter. *Continental Shelf Research* 21: 327–346.
- Pavia FJ, Anderson RF, Lam PJ, Cael BB, Vivancos SM, Fleisher MQ, Lu Y, Zhang P, Cheng H, and Edwards RL (2019) Shallow particulate organic carbon regeneration in the South Pacific Ocean. *Proceedings of the National Academy of Sciences* 116: 9753.
- Pavia FJ, Anderson RF, Winckler G, and Fleisher MQ (2020) Atmospheric dust inputs, iron cycling, and biogeochemical connections in the south Pacific ocean from thorium isotopes. *Global Biogeochemical Cycles* 34.



- Paytan A and Mclaughlin K (2007) The oceanic phosphorus cycle. *Chemical Reviews* 107: 563–576.
- Pfannkuche O and Lochte K (1993) Open ocean pelagic-benthic coupling: Cyanobacteria as tracers of sedimenting salp faeces. *Deep-Sea Research* 40: 727–737.
- Phillips B, Kremer P, and Madin L (2009) Defecation by *Salpa thompsoni*, and its contribution to vertical flux in the Southern Ocean. *Marine Biology* 156: 455–467.
- Picheral M, Guidi L, Stemmann L, Karl DM, Iddaoud G, and Gorsky G (2010) The Underwater Vision Profiler 5: An advanced instrument for high spatial resolution studies of particle size spectra and zooplankton. *Limnology and Oceanography: Methods* 8: 462–473.
- Plattner G-K, Gruber N, Frenzel H, and McWilliams JC (2005) Decoupling marine export production from new production. *Geophysical Research Letters* 32: L11612.
- Ploug H (2001) Small-scale oxygen fluxes and remineralization in sinking aggregates. *Limnology and Oceanography* 46: 1624–1631.
- Ploug H and Grossart H-P (2000) Bacterial growth and grazing on diatom aggregates: Respiratory carbon turnover as a function of aggregate size and sinking velocity. *Limnology and Oceanography* 45: 1467–1475.
- Ploug H, Iversen MH, and Fischer G (2008a) Ballast, sinking velocity and apparent diffusivity within marine snow and fecal pellets: Implications and substrate turnover by attached bacteria. *Limnology and Oceanography* 53: 1878–1886.
- Ploug H, Iversen MK, Koski M, and Buitenhuis ET (2008b) Production, oxygen respirations rates and sinking velocity of copepod fecal pellets: Direct measurements of ballasting by opal and calcite. *Limnology and Oceanography* 53: 469–476.
- Poulsen L and Iversen M (2008) Degradation of copepod fecal pellets: Key role of protozooplankton. *Marine Ecology Progress Series* 367: 1–13.
- Primeau F (2005) Characterizing transport between the surface mixed layer and the ocean interior with a forward and adjoint global ocean transport model. *Journal of Physical Oceanography* 35: 545–564.
- Redfield AC, Ketchum BM, Richards FA, and Hill MN (1963) The influence of organism on the composition of sea-water. In: Hill MN (ed.) *The Sea*. New York: Wiley.
- Regaudie-De-Gioux A and Duarte CM (2012) Temperature dependence of planktonic metabolism in the ocean. *Global Biogeochemical Cycles* 26.
- Repeata DJ and Aluwihare LJ (2006) Radiocarbon analysis of neutral sugars in high-molecular-weight dissolved organic carbon: Implications for organic carbon cycling. *Limnology and Oceanography* 51: 1045–1053.
- Ricart AM, Krause-Jensen D, Hancke K, Price NN, Masqué P, and Duarte CM (2022) Sinking seaweed in the deep ocean for carbon neutrality is ahead of science and beyond the ethics. *Environmental Research Letters* 17: 081003.
- Richardson TL (2019) Mechanisms and pathways of small-phytoplankton export from the surface ocean. *Annual Review of Marine Science* 11: 57–74.
- Richardson TL and Jackson GA (2007) Small phytoplankton and carbon export from the surface ocean. *Science* 315: 838–840.
- Riebesell U, Zondervan I, and Morel FMM (2000) Reduced calcification of marine plankton in response to increased atmospheric CO<sub>2</sub>. *Nature* 407: 364–367.
- Riebesell U, Schulz KG, Bellerby RGJ, Botros M, Fritsche P, Meyerhöfer M, Neill C, Nondal G, Oschlies A, Wohlers J, and Zöllner E (2007) Enhanced biological carbon consumption in a high CO<sub>2</sub> ocean. *Nature* 450: 545–548.
- Riebesell U, Bellerby RGJ, Grossart HP, and Thingstad TF (2008) Mesocosm CO<sub>2</sub> perturbation studies: From organism to community level. *Biogeosciences* 5: 1157–1164.
- Riley JS, Sanders R, Marsay C, Le Moigne FAC, Achterberg EP, and Poulton AJ (2012) The relative contribution of fast and slow sinking particles to ocean carbon export. *Global Biogeochemical Cycles* 26.
- Robinson C, Steinberg DK, Anderson TR, Aristegui J, Carlson CA, Frost JR, Ghiglione J-F, Hernández-León S, Jackson GA, Koppelman R, Quéguiner B, Ragueneau O, Rassoulzadegan F, Robison BH, Tamburini C, Tanaka T, Wishner KF, and Zhang J (2010) Mesopelagic zone ecology and biogeochemistry – A synthesis. *Deep Sea Research Part II: Topical Studies in Oceanography* 57: 1504–1518.
- Roshan S and Devries T (2017) Efficient dissolved organic carbon production and export in the oligotrophic ocean. *Nature Communications* 8: 2036.
- Rost B and Riebesell U (2004) Coccolithophores and the biological pump: Responses to environmental changes. In: Thierstein H and Young J (eds.) *Coccolithophores: From Molecular Processes to Global Impact*. Berlin: Springer.
- Rost B, Zondervan I, and Wolf-Gladrow DA (2008) Sensitivity of phytoplankton to future changes in ocean carbonate chemistry: Current knowledge, contradictions and research direction. *Marine Ecology Progress Series* 373: 227–237.
- Saba GK, Steinberg DK, and Bronk DA (2011) The relative importance of sloppy feeding, excretion, and fecal pellet leaching in the release of dissolved carbon and nitrogen by *Acartia tonsa* copepods. *Journal of Experimental Marine Biology and Ecology* 404: 47–56.
- Saba GK, Burd AB, Dunne JP, Hernández-León S, Martin AH, Rose KA, Salisbury J, Steinberg DK, Trueman CN, Wilson RW, and Wilson SE (2021) Toward a better understanding of fish-based contribution to ocean carbon flux. *Limnology and Oceanography* 66: 1639–1664.
- Sanders R, Morris PJ, Poulton AJ, Stinchcombe MC, Charalampopoulou A, Lucas MI, and Thomalla SJ (2010) Does a ballast effect occur in the surface ocean? *Geophysical Research Letters* 37.
- Sato R, Tanaka Y, and Ishimaru T (2001) House production by *Oikopleura dioica* (Tunicata, Appendicularia) under laboratory conditions. *Journal of Plankton Research* 23: 415–423.
- Schneider B, Schlitzer R, Fischer G, and Nothig EM (2003) Depth-dependent elemental compositions of particulate organic matter (POM) in the ocean. *Global Biogeochemical Cycles* 17: 1. <https://doi.org/10.1029/2002GB001871>.
- Schneider B, Engel A, and Schlitzer R (2004) Effects of depth- and CO<sub>2</sub> dependent C: N ratios of particulate organic matter (POM) on the marine carbon cycle. *Global Biogeochemical Cycles* 18: GB2015.
- Schoemann V, Becquevort S, Stefels J, Rousseau V, and Lancelot C (2005) Phaeocystis blooms in the global ocean and their controlling mechanisms: A review. *Journal of Sea Research* 53: 43–66.
- Seebah S, Fairfield C, Ullrich MS, and Passow U (2014) Aggregation and sedimentation of *Thalassiosira weissflogii* (diatom) in a warmer and more acidified future ocean. *PLoS One* 9: e112379.
- Seferian R, Berthet S, Yool A, Palmieri J, Bopp L, Tagliabue A, Kwiatkowski L, Aumont O, Christian J, Dunne J, Gehlen M, Ilyina T, John JG, Li HM, Long MC, Luo JY, Nakano H, Romanou A, Schwinger J, Stock C, Santana-Falcon Y, Takano Y, Tjiputra J, Tsujino H, Watanabe M, Wu TW, Wu FH, and Yamamoto A (2020) Tracking improvement in simulated marine biogeochemistry between CMIP5 and CMIP6. *Current Climate Change Reports* 6: 95–119.
- Seiter K, Hensen C, and Zabel M (2005) Benthic carbon mineralization on a global scale. *Global Biogeochemical Cycles* 19.
- Shi D, Kranz SA, Kim JM, and Morel FM (2012) Ocean acidification slows nitrogen fixation and growth in the dominant diazotroph *Trichodesmium* under low-iron conditions. *Proceedings of the National Academy of Sciences of the United States of America* 109: E3094–E3100.
- Siegel DA, Fields E, and Buesseler KO (2008) A bottom-up view of the biological pump: Modeling source funnels above ocean sediment traps. *Deep Sea Research Part I: Oceanographic Research Papers* 55: 108–127.
- Siegel DA, Buesseler KO, Doney SC, Sailley SF, Behrenfeld MJ, and Boyd PW (2014) Global assessment of ocean carbon export by combining satellite observations and food-web models. *Global Biogeochemical Cycles* 28: 181–196.
- Siegel DA, Devries T, Doney SC, and Bell T (2021) Assessing the sequestration time scales of some ocean-based carbon dioxide reduction strategies. *Environmental Research Letters* 16: 104003.
- Siegel DA, Devries T, Cetinić I, and Bisson KM (2022) Quantifying the ocean's biological pump and its carbon cycle impacts on global scales. *Annual Review of Marine Science*.
- Sigman DM, Fripiat F, Studer AS, Kemery PC, Martinez-Garcia A, Hain MP, Ai X, Wang X, Ren H, and Haug GH (2021) The Southern Ocean during the ice ages: A review of the Antarctic surface isolation hypothesis, with comparison to the North Pacific. *Quaternary Science Reviews* 254: 106732. <https://doi.org/10.1016/j.quascirev.2020.106732>.
- Silsbe GM, Behrenfeld MJ, Halsey KH, Milligan AJ, and Westberry TK (2016) The CAFE model: A net production model for global ocean phytoplankton. *Global Biogeochemical Cycles* 30: 1756–1777.
- Silver M (2015) Marine snow: A brief historical sketch. *Limnology and Oceanography Bulletin* 24: 5–10.
- Silver MW, Coale SL, Pilskaln CH, and Steinberg DR (1998) Giant aggregates: Importance as microbial centers and agents of material flux in the mesopelagic zone. *American Society of Limnology and Oceanography* 43: 498–507.

- Simon M, Grossart HP, Schweitzer B, and Ploug H (2002) Microbial ecology of organic aggregates in aquatic ecosystems. *Aquatic Microbial Ecology* 28: 175–211.
- Smayda T (1971) Normal and accelerated sinking of phytoplankton in the sea. *Marine Geology* 11: 105–122.
- Smetacek VS (1985) Role of sinking in diatom life-history cycles: Ecological, evolutionary, and geological significance. *Marine Biology* 84: 239–251.
- Smetacek V and Passow U (1990) Spring bloom initiation and Sverdrup's critical depth model. *Limnology and Oceanography* 35: 228–234.
- Smetacek V, Von Bodungen B, Knoppers B, Peinert R, Pollehne F, Stegmann P, and Zeitzschel B (1984) Seasonal stages characterizing the annual cycle of an inshore pelagic system. *Rapports et Procès-Verbaux des Réunions Conseil International pour l'Exploration de la Mer* 183: 126–135.
- Smith DC, Simon M, Aldredge AL, and Azam F (1992) Intense hydrolytic enzyme activity on marine aggregates and implications for rapid particle dissolution. *Nature* 359: 139–141.
- Smith DC, Steward GF, Long RA, and Azam F (1995) Bacterial mediation of carbon fluxes during a diatom bloom in a mesocosm. *Deep-Sea Research Part II* 42: 75–97.
- Sondergaard M, Williams PJL, Cauwet G, Riemann B, Robinson C, Terzic S, Woodward EMS, and Worm J (2000) Net accumulation and flux of dissolved organic carbon and dissolved organic nitrogen in marine plankton communities. *Limnology and Oceanography* 45: 1097–1111.
- Stamieszkin K, Pershing A, Record N, Pilskal NC, Dam H, and Feinber GLR (2015) Size as the master trait in modeled copepod fecal pellet carbon flux. *Marine Ecology Progress Series* 60: 2090–2107.
- Stange P, Taucher J, Bach LT, Algueró-Muñiz M, Horn HG, Krebs L, Boxhammer T, Nauendorf AK, and Riebesell U (2018) Ocean acidification-induced restructuring of the plankton food web can influence the degradation of sinking particles. *Frontiers in Marine Science* 5.
- Steinacher M, Joos F, Frolicher TL, Bopp L, Cadule P, Cocco V, Doney SC, Gehlen M, Lindsay K, Moore JK, Schneider B, and Segsneider J (2010) Projected 21st century decrease in marine productivity: A multi-model analysis. *Biogeosciences* 7: 979–1005.
- Steinberg DK and Landry MR (2017) Zooplankton and the ocean carbon cycle. *Annual Review of Marine Science* 9: 413–444.
- Steinberg DK, Carlson CA, Bates NR, Johnson RJ, Michaels AF, and Knap AH (2001) Overview of the US JGOFS Bermuda Atlantic Time-series Study (BATS): A decade-scale look at ocean biology and biogeochemistry. *Deep Sea Research Part II: Topical Studies in Oceanography* 48: 1405–1447.
- Steinberg DK, Mooy BASV, Buesseler KO, Boyd PW, Kobari T, and Karl DM (2008) Bacterial vs. zooplankton control of sinking particle flux in the ocean's twilight zone. *Limnology and Oceanography* 53: 1327–1338.
- Steinberg DK, Stamieszkin K, Maas AE, Durkin CA, Passow U, Estapa ML, Omand MM, McDonnell AMP, Karp-Boss L, Galbraith M, and Siegel DA (2023) The outsized role of salps in carbon export in the Subarctic Northeast Pacific Ocean. *Global Biogeochemical Cycles* 37: e2022GB007523.
- Stemmmann L and Boss E (2012) Plankton and particle size and packaging: From determining optical properties to driving the biological pump. *Annual Review of Marine Science* 4: 263–290.
- Stone J and Steinberg DK (2016) Salp contributions to vertical carbon flux in the Sargasso Sea. *Deep-Sea Research Part I* 3: 90–100.
- Strom LS, Benner R, Ziegler S, and Dagg MJ (1997) Planktonic grazers are a potentially important source of marine dissolved organic carbon. *Limnology and Oceanography* 42: 1364–1374.
- Studer AS, Sigman DM, Martiez-García A, Benz V, Winckler G, Kuhn G, Esper O, Lamy F, Jaccard SL, Wacker L, Oleynik S, Gersonde R, and Haug GH (2015) Antarctic Zone nutrient conditions during the last two glacial cycles. *Paleoceanography* 30(7): 845–862. <https://doi.org/10.1002/2014pa002745>.
- Suttle CA (2007) Marine viruses — Major players in the global ecosystem. *Nature Reviews Microbiology* 5: 801–812.
- Tagliabue A, Kwiatkowski L, Bopp L, Butenschön M, Cheung W, Lengaigne M, and Vialard J (2021) Persistent uncertainties in ocean net primary production climate change projections at regional scales raise challenges for assessing impacts on ecosystem services. *Frontiers in Climate* 3.
- Tanioka T and Matsumoto K (2020) Stability of marine organic matter respiration stoichiometry. *Geophysical Research Letters* 47.
- Taucher J, Bach LT, Riebesell U, and Oeschles A (2014) The viscosity effect on marine particle flux: A climate relevant feedback mechanism. *Global Biogeochemical Cycles* 28: 415–422.
- Taucher J, Jones J, James A, Brzezinski MA, Carlson CA, Riebesell U, and Passow U (2015) Combined effects of CO<sub>2</sub> and temperature on carbon uptake and partitioning by the marine diatoms *Thalassiosira weissflogii* and *Dactylosolen fragilissimus*. *Limnology and Oceanography* 60: 901–919.
- Taucher J, Stange P, Algueró-Muñiz M, Bach LT, Nauendorf A, Kolzenburg R, Büdenbender J, and Riebesell U (2018) In situ camera observations reveal major role of zooplankton in modulating marine snow formation during an upwelling-induced plankton bloom. *Progress in Oceanography* 164: 75–88.
- Taucher J, Bach LT, Prowe AEF, Boxhammer T, Kvale K, and Riebesell U (2022) Enhanced silica export in a future ocean triggers global diatom decline. *Nature* 605: 696–700.
- Teira E, Pazo MJ, Serret P, and Fernandez E (2001) Dissolved organic carbon production by microbial populations in the Atlantic Ocean. *Limnology and Oceanography* 46: 1370–1377.
- Toggweiler JR (1999) Variation of atmospheric CO<sub>2</sub> by ventilation of the ocean's deepest water. *Paleoceanography* 14: 571–588.
- Toggweiler JR (2003) Representation of the carbon cycle in box models and GCMs: 2. Organic pump. *Global Biogeochemical Cycles* 17.
- Toggweiler JR, Russell JL, and Carson SR (2006) Midlatitude westerlies, atmospheric CO<sub>2</sub>, and climate change during the ice ages. *Paleoceanography* 21: 1–15.
- Torres-Valdés S, Roussenov VM, Sanders R, Reynolds S, Pan X, Mather R, Landolfi A, Wolff GA, Achterberg EP, and Williams RG (2009) Distribution of dissolved organic nutrients and their effect on export production over the Atlantic Ocean. *Global Biogeochemical Cycles* 23: 1–16.
- Tortell PD and Morel FMM (2002) Sources of inorganic carbon the phytoplankton in the eastern Subtropical and Equatorial Pacific Ocean. *Limnology and Oceanography* 47: 1012–1022.
- Tortell PD, Payne CD, Li Y, Trimbom S, Rost B, Smith WO, Riesselman C, Dunbar RB, Sedwick P, and Ditullio GR (2008) CO<sub>2</sub> sensitivity of Southern Ocean phytoplankton. *Geophysical Research Letters* 35: L04605.
- Trimbom S, Wolf-Gladrow D, Richter K-U, and Rost B (2009) The effect of pCO<sub>2</sub> on carbon acquisition and intracellular assimilation in four marine diatoms. *Journal of Experimental Marine Biology and Ecology* 376: 26–36.
- Turner JT (2002) Zooplankton fecal pellets, marine snow and sinking phytoplankton blooms. *Aquatic Microbial Ecology* 27: 57–102.
- Turner JT (2015) Zooplankton fecal pellets, marine snow, phytodetritus and the ocean's biological pump. *Progress in Oceanography* 130: 205–248.
- Turner A and Holmes LA (2015) Adsorption of trace metals by microplastic pellets in fresh water. *Environmental Chemistry* 12: 600–610.
- Tyrrell T (1999) The relative influences of nitrogen and phosphorus on oceanic primary production. *Nature* 400: 525–531.
- Van De Waal DB and Litchman E (2020) Multiple global change stressor effects on phytoplankton nutrient acquisition in a future ocean. *Philosophical Transactions of the Royal Society, B: Biological Sciences* 375: 20190706.
- Van De Waal D, Brandenburg K, Keuskamp J, Trimbom S, Rokitta S, Kranz S, and Rost B (2019) Highest plasticity of carbon-concentrating mechanisms in earliest evolved phytoplankton: Plasticity of carbon-concentrating mechanisms. *Limnology and Oceanography Letters* 4: 37–43.
- Verdugo P (2012) Marine microgels. *Annual Review of Marine Science* 4: 375–400.
- Voss M, Bange HW, Dippner JW, Middelburg JJ, Montoya JP, and Ward B (2013) The marine nitrogen cycle: recent discoveries, uncertainties and the potential relevance of climate change. *Philosophical Transactions of the Royal Society, B: Biological Sciences* 368: 20130121.
- Wang B and Fennel K (2022) Biogeochemical-Argo data suggest significant contributions of small particles to the vertical carbon flux in the subpolar North Atlantic. *Limnology and Oceanography* 67: 2405–2417.
- Wassmann P (1998) Retention versus export food chains: Processes controlling sinking loss from marine pelagic systems. *Hydrobiologia* 363: 29–57.
- Weber T and Bianchi D (2020) Efficient particle transfer to depth in oxygen minimum zones of the Pacific and Indian oceans. *Frontiers in Earth Science* 8: 376.
- Weber TS and Deutsch C (2010) Ocean nutrient ratios governed by plankton biogeography. *Nature* 467: 550–554.
- Weber T, Cram JA, Leung SW, Devries T, and Deutsch C (2016) Deep ocean nutrients imply large latitudinal variation in particle transfer efficiency. *Proceedings of the National Academy of Sciences* 113: 8606–8611.
- Westberry TK and Siegel DA (2006) Spatial and temporal distribution of Trichodesmium blooms in the world's oceans. *Global Biogeochemical Cycles* 20.

- Westberry T, Behrenfeld MJ, Siegel DA, and Boss E (2008) Carbon-based primary productivity modeling with vertically resolved photoacclimation. *Global Biogeochemical Cycles* 22.
- Williamson P, Wallace DWR, Law CS, Boyd PW, Collos Y, Croot P, Denman K, Riebesell U, Takeda S, and Vivian C (2012) Ocean fertilization for geoengineering: A review of effectiveness, environmental impacts and emerging governance. *Process Safety and Environmental Protection* 90: 475–488.
- Wilson JD, Andrews O, Katavouta A, De Melo Virissimo F, Death RM, Adloff M, Baker CA, Blackledge B, Goldsworth FW, Kennedy-Asser AT, Liu Q, Sieradzan KR, Vosper E, and Ying R (2022) The biological carbon pump in CMIP6 models: 21st century trends and uncertainties. *Proceedings of the National Academy of Sciences* 119: e2204369119.
- Wohlers J, Engel A, Zoellner E, Breithaupt P, Juergens K, Hoppe H-G, Sommer U, and Riebesell U (2009) Changes in biogenic carbon flow in response to sea surface warming. *Proceedings of the National Academy of Sciences* 106: 7067–7072.
- Wolf-Gladrow A and Zeebe RE (2001) *CO<sub>2</sub> in seawater: equilibrium, kinetics and isotopes*. Amsterdam: Elsevier.
- Yool A, Martin AP, Fernández C, and Clark DR (2007) The significance of nitrification for oceanic new production. *Nature* 447: 999–1002.
- Yoon WB and Rosson RA (1991) Improved method of enumeration of attached bacteria for study of fluctuation in the abundance of attached and free-living bacteria in response to diel variation in seawater turbidity. *Applied and Environmental Biology* 56: 595–600.
- Yoon JE, Yoo KC, Macdonald AM, Yoon HI, Park KT, Yang EJ, Kim HC, Lee Ji, Lee MK, Jung J, Park J, Lee J, Kim S, Kim SS, Kim K, and Kim IN (2018) Reviews and syntheses: Ocean iron fertilization experiments – past, present, and future looking to a future Korean Iron Fertilization Experiment in the Southern Ocean (KIFES) project. *Biogeosciences* 15: 5847–5889.
- Zhou J, Mopper K, and Passow U (1998) The role of surface-active carbohydrates in the formation of transparent exopolymer particles by bubble adsorption of seawater. *Limnology and Oceanography* 43: 1860–1871.
- Ziervogel K, Steen AD, and Arnosti C (2010) Changes in the spectrum and rates of extracellular enzyme activities in seawater following aggregate formation. *Biogeosciences* 7: 1007–1015.



# Correlating microbial community profiles with geochemical data in highly stratified sediments from the Arctic Mid-Ocean Ridge

Steffen Leth Jorgensen<sup>a,1</sup>, Bjarne Hannisdal<sup>b</sup>, Anders Lanzén<sup>a,c</sup>, Tamara Baumberger<sup>b,d</sup>, Kristin Flesland<sup>b</sup>, Rita Fonseca<sup>e,f</sup>, Lise Øvreås<sup>a</sup>, Ida H. Steen<sup>a</sup>, Ingunn H. Thorseth<sup>b</sup>, Rolf B. Pedersen<sup>b</sup>, and Christa Schleper<sup>a,g,1</sup>

<sup>a</sup>Centre for Geobiology, Department of Biology, and <sup>b</sup>Centre for Geobiology, Department of Earth Science, University of Bergen, 5007 Bergen, Norway; <sup>c</sup>Computational Biology Unit, Uni Computing, Uni Research, 5007 Bergen, Norway; <sup>d</sup>Institute for Geochemistry and Petrology, Eidgenössische Technische Hochschule Zürich, 8092 Zurich, Switzerland; <sup>e</sup>Department of Geosciences, University of Évora, 7000 Évora, Portugal; <sup>f</sup>Cremer Laboratory of Robotics and Systems in Engineering Science (LARSys), Faculty of Sciences, University of Lisbon, 1749-016 Lisboa, Portugal; and <sup>g</sup>Department of Genetics in Ecology, University of Vienna, A-1090 Vienna, Austria

Edited by David M. Karl, University of Hawaii, Honolulu, HI, and approved September 5, 2012 (received for review May 4, 2012)

**Microbial communities and their associated metabolic activity in marine sediments have a profound impact on global biogeochemical cycles. Their composition and structure are attributed to geochemical and physical factors, but finding direct correlations has remained a challenge. Here we show a significant statistical relationship between variation in geochemical composition and prokaryotic community structure within deep-sea sediments. We obtained comprehensive geochemical data from two gravity cores near the hydrothermal vent field Loki's Castle at the Arctic Mid-Ocean Ridge, in the Norwegian-Greenland Sea. Geochemical properties in the rift valley sediments exhibited strong centimeter-scale stratigraphic variability. Microbial populations were profiled by pyrosequencing from 15 sediment horizons (59,364 16S rRNA gene tags), quantitatively assessed by qPCR, and phylogenetically analyzed. Although the same taxa were generally present in all samples, their relative abundances varied substantially among horizons and fluctuated between Bacteria- and Archaea-dominated communities. By independently summarizing covariance structures of the relative abundance data and geochemical data, using principal components analysis, we found a significant correlation between changes in geochemical composition and changes in community structure. Differences in organic carbon and mineralogy shaped the relative abundance of microbial taxa. We used correlations to build hypotheses about energy metabolisms, particularly of the Deep Sea Archaeal Group, specific Deltaproteobacteria, and sediment lineages of potentially anaerobic Marine Group I Archaea. We demonstrate that total prokaryotic community structure can be directly correlated to geochemistry within these sediments, thus enhancing our understanding of biogeochemical cycling and our ability to predict metabolisms of uncultured microbes in deep-sea sediments.**

taxonomic profiling | ultraslow-spreading ridge | amplicon sequencing

**M**arine sediments host the largest reservoir of organic carbon in the world and outnumber any other environment with respect to microbial cell abundance (1, 2). The microbial activity in this habitat has a profound impact on the global carbon cycle through the remineralization of sedimentary organic carbon, thus ultimately regulating the oxygen level of the atmosphere (3). Extensive sampling and drilling efforts during the past decade have changed our perception of microbial life in the inaccessible deep seafloor fundamentally (4–17). This pioneering work has led to novel insights into the composition and abundance of potentially active groups of Archaea and Bacteria in deep-sea sediments.

The density of prokaryotic cells in coastal and continental margin sediments typically is  $10^8$ – $10^9$  cells/cm<sup>3</sup> in the top sediment layers and declines with increasing depth in a logarithmic fashion (2). Even though cell abundance in organic-poor open-ocean sites can be several orders of magnitude lower, it may still exceed  $10^5$  cells/cm<sup>3</sup> at depths close to 1,000 m below the seafloor (mbsf)

(12). This omnipresence of prokaryotic cells was demonstrated recently by Roussel et al. (16) who detected viable cells at a sediment depth of 1,626 mbsf, supporting the idea that temperature is the ultimate limit for microbial survival at depth (18). In general, marine sediment communities appear to be dominated by a restricted number of bacterial and archaeal phyla, including Chloroflexi, Planctomycetes, Japanese Sea division 1 (JS-1), a diverse spectrum of Proteobacteria, the Deep Sea Archaeal Group (DSAG), Marine Group I (MG-I), the Miscellaneous Crenarchaeotic Group (MCG), and the South African Goldmine Euryarchaeotal Group (SAGMEG) (reviewed in refs. 13, 19, and 20). These groups have been found in a variety of different marine sediments, including coastal and open-ocean sites, based on 16S rDNA clone libraries (6, 9, 21, 22), 16S rRNA clone libraries (15), and metagenomic shotgun sequencing (23, 24). The vast majority of these communities seem to be alive and active, although the fractions of dead and dormant cells vary substantially among locations (15, 25, 26).

Geochemical pore water profiles in marine sediments show distinct redox zones (27), suggesting that each of these zones are shaped by organisms with specific metabolic traits. In agreement with this notion, several studies have demonstrated down-core stratification of microbial community composition (28–31). Furthermore, a few specific microbial groups, such as anaerobic methane oxidizers (ANME) (32, 33) and anaerobic ammonium oxidizers (anammox) (34) have been associated consistently with specific redox zones. In addition, samples obtained from markedly different sedimentary settings (e.g., high or low temperature, presence or absence of methane, high or low carbon load) have been found to show distinct microbial community compositions (7, 35, 36). Nonetheless, an explicit, quantitative correlation

Author contributions: S.L.J., L.Ø., I.H.S., I.H.T., R.B.P., and C.S. designed research; S.L.J., T.B., K.F., R.F., and I.H.T. performed research; S.L.J., B.H., A.L., and I.H.T. analyzed data; and S.L.J., B.H., I.H.T., and C.S. wrote the paper.

The authors declare no conflict of interest.

This article is a PNAS Direct Submission.

Freely available online through the PNAS open access option.

Data deposition: 16S rRNA gene sequences are deposited in the National Center for Biotechnology Information Sequence Read Archive (accession no. [SRP009131](https://doi.org/10.1093/bioinformatics/btt013)). A comma-separated text file listing the taxonomic affiliations of all operational taxonomic units and their distribution across datasets can be downloaded from <http://services.cbu.uib.no/supplementary/jorgensen2012>. Data have been deposited in the Pangaea database ([doi:10.1594/PANGAEA.786687](https://doi.org/10.1594/PANGAEA.786687)).

See Commentary on page 16756.

<sup>1</sup>To whom correspondence may be addressed. E-mail: [steffen.jorgensen@bio.uib.no](mailto:steffen.jorgensen@bio.uib.no) or [Christa.Schleper@univie.ac.at](mailto:Christa.Schleper@univie.ac.at).

See Author Summary on page 16764 (volume 109, number 42).

This article contains supporting information online at [www.pnas.org/lookup/suppl/doi:10.1073/pnas.1207574109/-DCSupplemental](http://www.pnas.org/lookup/suppl/doi:10.1073/pnas.1207574109/-DCSupplemental).



between stratigraphic variability in geochemical properties and concomitant changes in the structure of the total microbial community or the relative abundance of individual taxa has remained elusive. This lack of correlation could be explained in part by limited datasets, low spatial resolution, and insufficient depth of the taxonomic profiling. Here we address these challenges and quantitatively explore the relationship between microbial community structure and multivariate geochemistry in highly stratified deep-sea sediments.

We investigated two 3-m-long sediment cores from the ultraslow-spreading Arctic Mid-Ocean Ridge system, one of the few places where substantial amounts of sediment accumulate in the mid-ocean rift valley. The cores were retrieved from two sites, one 15 km southwest (SW) and one 15 km northeast (NE) of the Loki's Castle Vent Field (37). In addition to the hemipelagic and glaciomarine sediments derived from the Bear Island Fan system, the rift valley also receives episodic input of volcanogenic and metallogenic hydrothermal material. The resulting stratification of the cored sediments allowed us to study the influence of changes in sediment geochemistry on the microbial subsurface communities on a compact depth scale. We used deep sequencing of 16S rRNA gene amplicon tags, covering both the archaeal and bacterial domains, to obtain a detailed qualitative and quantitative taxonomic inventory from selected sediment horizons in both cores. We linked estimates of the relative abundance distribution of the entire prokaryotic community to copy numbers of marker genes from both domains as well as to 16 different geochemical and geophysical parameters of sedimentary solids and solutes. We found that stratigraphic variation in the structure of the microbial community as well as in the relative abundance of individual taxa can be correlated directly to stratigraphic variation in geochemical properties across both cores.

## Results

**Core Descriptions.** Core GC6, retrieved SW of the vent field, consisted of highly stratified hemipelagic-glaciomarine sediments with layers of different colors varying on a centimeter scale from light to darker brown and gray (Fig. 1A). Distinct coarser layers of detrital pyrite, likely of hydrothermal origin [71 and 95 cm below sea floor (cmbsf)], and of altered volcanoclastic material (65 and 232 cmbsf) generally were reflected by Fe enrichments in X-ray fluorescence (XRF) core scanner profiles (Fig. 1A) and by elevated  $\text{Fe}_2\text{O}_3$  and S concentrations in quantitative geochemical sediment analyses (Table 1). The XRF profiles also revealed five distinct Mn-enriched layers, the uppermost of which (22 cmbsf) was interpreted as the lower boundary of the oxic layer (Table 1). Overall, the reduction potential (Eh) profile in GC6 (Table 1) covaries with the color changes, with higher values in the brown sections and lower but still positive values in the gray sections.

Core GC12, retrieved NE of the vent field, consisted of hemipelagic-glaciomarine sediments in the upper half and glaciogenic debris flows in the lower half. The oxic/anoxic transition zone was marked by a single Mn-enriched layer at 38 cmbsf, and the Eh profile again covaried with the sediment color (Table 1).

Total organic carbon (TOC) content varied between 0.1–1.2% of weight in GC6 (Table 1, Fig. 1A) and 0.2–1.3% of weight in GC12 (Table 1 and Fig. 1B). These values were slightly higher than commonly reported for open-ocean sediments and likely reflect input from the Bear Island Fan and the high productivity of the Arctic Ocean. However, these sediments still are considered a low organic carbon system (<1%) compared with continental margin sites.

We recognized four to five chemical redox zones as defined by Canfield and Thamdrup (38) based on pore water depth profiles of dissolved nitrate, ammonium, manganese, iron, and sulfate (Table 1 and Fig. 1). These profiles include an oxic, nitrogenous, manganous, ferruginous, and sulfidic zone (Fig. 1, *Left*), the last deduced from sulfate depletion in GC12. Despite their proximity,

the two cores showed clear differences: Although dissolved  $\text{Mn}^{2+}$  followed a typical diagenetic profile in both cores, the concentration in GC6 was higher than usually reported for deep-sea sites (up to 200  $\mu\text{M}$  at 156 cmbsf) even in metal-rich deep-sea sediments (39). An increase in  $\text{NH}_4^+$  coincided with the detection of dissolved  $\text{Mn}^{2+}$  in both cores, likely as a result of oxygen depletion. However, the down-core increase was less pronounced for GC6 and even decreased in the two volcanoclastic horizons. In GC6 dissolved  $\text{Fe}^{2+}$  increased in the deepest horizon as  $\text{Mn}^{2+}$  decreased, probably defining the shift from the manganous to the ferruginous zone. In GC12, on the other hand,  $\text{Fe}^{2+}$  already was elevated in the manganous zone and increased with depth in an irregular manner. A decrease in  $\text{SO}_4^{2-}$  to 23 mM in the lower part of GC12 indicates microbial sulfate reduction. In contrast, no indication of sulfate reduction was observed in GC6. However, traces of  $\text{H}_2\text{S}$  were detected at 88 cmbsf, between the two detrital pyrite layers. This horizon also showed traces of dissolved  $\text{Fe}^{2+}$  and a significant pH increase and  $\text{NH}_4^+$  decrease.

$\text{NO}_3^-$  was depleted from the interstitial phase below the oxic layers. Interestingly, however,  $\text{NO}_3^-$  could be extracted from the solid phase of all horizons in both cores (Table 1), suggesting that it was adsorbed to mineral phases, as observed in soils (40).

**Composition and Diversity of the Microbial Community.** For each of the 15 sampled sediment horizons, we generated a 16S rRNA gene amplicon library, with one primer set covering the V5–V8 region of both bacterial and archaeal taxa (*Materials and Methods*). Pyrosequencing yielded a total of 59,364 high-quality sequence reads after extensive filtering. In total, 4,790 reads were unique, with an average length of 231 bp.

From the nine horizons in core GC6, 1,668 different operational taxonomic units (OTUs) (cutoff, 97% sequence identity) were divided into 50 classes (39 bacterial and 11 archaeal) representing 33 different phyla. For the six horizons in core GC12, 1,135 OTUs were identified within 48 different classes (36 bacterial and 12 archaeal) distributed among 38 phyla (for a complete list of represented taxa and their abundance on phylum and class level, see Table S1). A comma-separated text file listing the taxonomic affiliations of all OTUs and their distribution across datasets can be downloaded from <http://services.cbu.uib.no/supplementary/jorgensen2012>. At the class rank, more than 85% of all observed taxa were present in both cores, but their abundance varied greatly between cores and among horizons within each core (Fig. 1 and Table S1). Approximately 50% of the OTUs present in core GC12 were shared with GC6. It is noteworthy that none of the 2,277 unique OTUs was represented in all 15 horizons.

**Determination of Bacterial and Archaeal Abundance.** Quantitative PCR (qPCR) was used to estimate total numbers of bacterial and archaeal small subunit (SSU) rRNA genes separately (Table 1). The total numbers in GC12 (Archaea plus Bacteria) varied between  $5.1 \times 10^5$  and  $5.2 \times 10^6$  16S rRNA gene copies/g sediment (wet weight), comparable to the abundance in other open-ocean sediments (41, 42). GC6, on the other hand, exhibited stronger variability between horizons, with both Bacteria and Archaea up to 100-fold more abundant in the horizon where  $\text{H}_2\text{S}$  and  $\text{Fe}^{2+}$  were detected in the pore water ( $3 \times 10^8$  16S rRNA gene copies/g sediment in total at 88 cmbsf). In contrast, abundances were barely above the detection limit in the volcanoclastic layers.

The archaeal 16S rRNA gene copy numbers made up 3–89% of the total number of SSU rRNA gene copies in core GC6 and 31–75% in core GC12 (Fig. S1). Thus, the microbial population fluctuates between a bacterial- and an archaeal-dominated community even within these relatively short cores. The ratio between bacterial and archaeal SSU rRNA gene copies as determined by qPCR supported the relative amount of Bacteria versus Archaea as estimated from the amplicon library (Fig. S1), indicating that

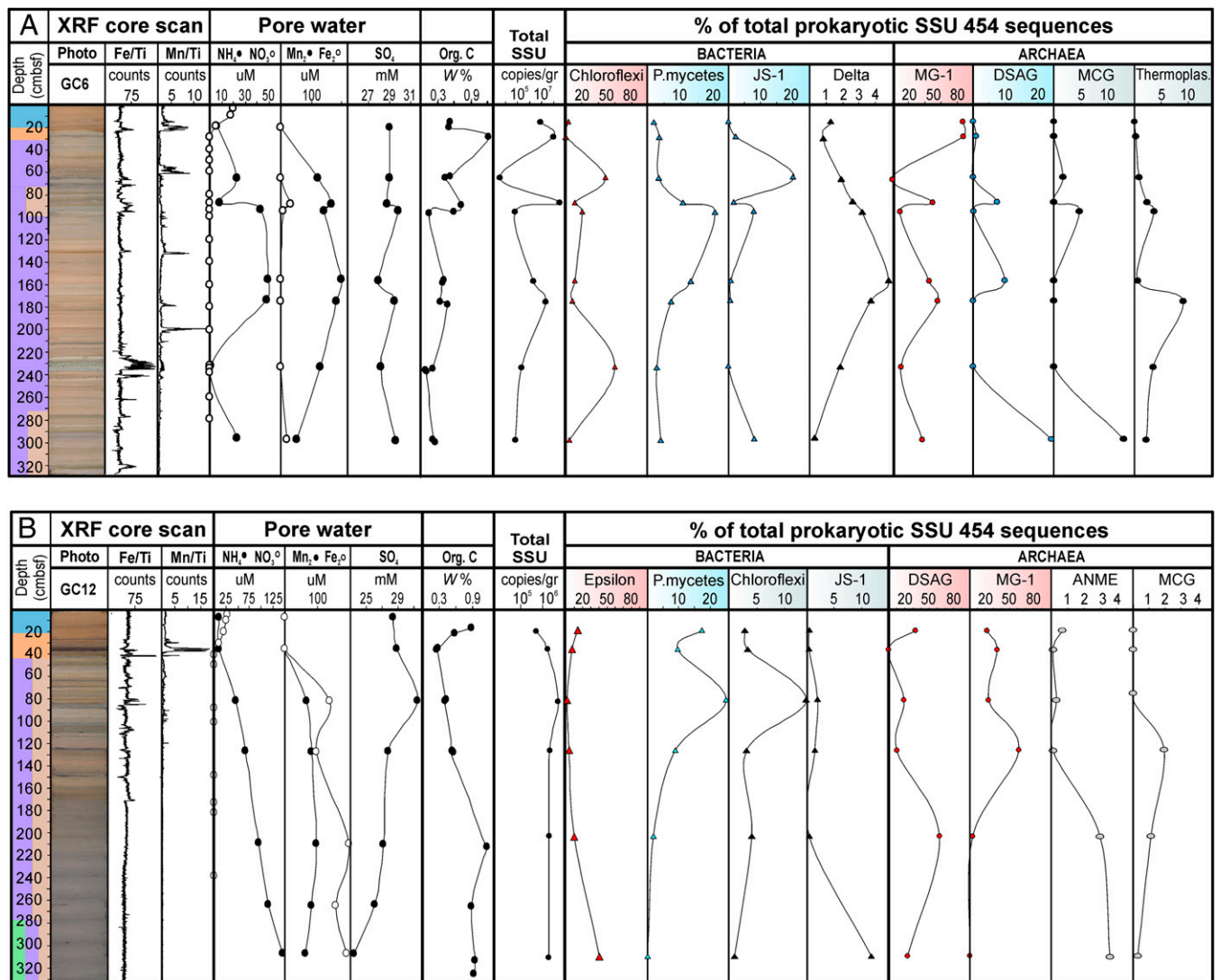


**Fig. 1.** Characteristics of gravity cores GC6 (A) and GC12 (B) including geochemical data and relative abundances of the four most dominant bacterial and archaeal taxa/phyla. (Left to Right) Photograph of the archive half core; XRF core scanner maps of normalized iron and manganese content; pore water concentrations of ammonium, nitrate, manganese, iron and sulfate; organic carbon content in the sediment (weight %); total number of 16S rRNA gene copies/g sediment (wet weight) as measured by qPCR; percent of total SSU reads obtained from the given taxa in the amplicon library in each horizon. Note that different scales on the x-axis are color coded to indicate the different respiration processes, based on pore water geochemistry: blue, aerobic oxidation; red, nitrate reduction; purple, manganese reduction; brown, iron reduction; green, sulfate reduction. Delta, Deltaproteobacteria; Epsilon, Epsilonproteobacteria; P.mycetes, Planctomycetes; Thermoplas, Thermoplasmata.

the primers used for the amplification for deep sequencing allowed a high rate of coverage and amplified with relatively little bias under the applied conditions.

**Principal Components and Correlation Analyses.** Principal component analysis (PCA) was performed independently on the relative abundance data (Table S1) and on the geochemical data excluding all gene copy numbers, but including depth (Table 1). Sample scores on the first principal component (PC1) of the two datasets showed a significant rank-order correlation at the class level ( $\rho = 0.671, P = 0.02$ ) (Fig. S2A), and the strength of this relationship increased substantially when oxic layers were removed ( $\rho = -0.883, P = 0.003$ ) (Fig. S2B). This result demonstrates that changes in the geochemical structure of the sediments, especially below the oxic zone (PC1 explained 41% of the variance), covary with changes in the overall community structure (PC1 explained 33% of the variance at class level).

Next, we plotted the original data for each individual geochemical parameter against PC1 scores of the relative abundance data and found the strongest correlations with TOC ( $\rho = 0.621, P = 0.016$ ) (Fig. 2A), dissolved  $\text{SO}_4^{2-}$  in the pore water ( $\rho = 0.691, P = 0.006$ ) (Fig. 2B), and the relative content of iron and manganese in the solid phase [ $\rho = -0.821, P < 0.000$  (Fig. 2C) and  $\rho = 0.582, P = 0.025$  (Fig. 2D), respectively].

Finally, pairwise comparisons uncovered several strong linkages between the relative abundance of individual taxonomic groups and specific geochemical parameters (Fig. S3) as well as striking patterns of co-occurrence among microbial groups at different taxonomic levels (Fig. S2 C–F). The most important results are discussed in more detail below.

**Distribution of the Most Abundant Bacterial Phyla.** Expressing the relative abundance of taxa as the proportion of total SSU rRNA gene tags allows the depth variation of the most abundant bac-

Table 1. Context data

| Depth (cmbfsf) | Solid phase                         |                       |               |        |                     |         |         |                |                |                | Interstitial phase |                                    |                                   |                                    |                       |                       | Gene copies/g sediment      |                             |                             |  |
|----------------|-------------------------------------|-----------------------|---------------|--------|---------------------|---------|---------|----------------|----------------|----------------|--------------------|------------------------------------|-----------------------------------|------------------------------------|-----------------------|-----------------------|-----------------------------|-----------------------------|-----------------------------|--|
|                | Fe <sub>2</sub> O <sub>3</sub> (W%) | MnO <sub>2</sub> (W%) | Nitrate (ppm) | S (W%) | E <sub>h</sub> (mV) | TIC (%) | TOC (%) | Fe/Ti (counts) | Mn/Ti (counts) | A <sub>T</sub> | pH                 | *NO <sub>3</sub> <sup>-</sup> (μM) | NH <sub>4</sub> <sup>+</sup> (μM) | SO <sub>4</sub> <sup>2-</sup> (mM) | Mn <sup>2+</sup> (μM) | Fe <sup>2+</sup> (μM) | Archaea (SSU)               | Bacterial (SSU)             | Archaea (amoA)              |  |
| GC6            |                                     |                       |               |        |                     |         |         |                |                |                |                    |                                    |                                   |                                    |                       |                       |                             |                             |                             |  |
| 16             | 3.2                                 | 0.6                   | 50.4          | 0.6    | 320                 | —       | 0.5     | 46.0           | 1.3            | 3.0            | 7.6                | 4.9                                | 6                                 | 29.0                               | 0.0                   | 0.0                   | 7.5 × 10 <sup>6</sup> ± 2.5 | 1.3 × 10 <sup>6</sup> ± 0.3 | 2.0 × 10 <sup>6</sup> ± 0.5 |  |
| 29             | 7.1                                 | 0.1                   | 75.6          | 0.3    | 90                  | —       | 1.2     | 41.4           | 0.4            | —              | —                  | 0                                  | —                                 | —                                  | —                     | —                     | 8.3 × 10 <sup>7</sup> ± 0.9 | 1.0 × 10 <sup>7</sup> ± 0.0 | 2.4 × 10 <sup>6</sup> ± 0.5 |  |
| 65             | 6.6                                 | 0.1                   | 39.0          | 0.6    | 45                  | 0.3     | 0.4     | 58.6           | 0.8            | 3.2            | 7.8                | 0                                  | 23                                | 29.0                               | 123.1                 | 0.0                   | BD                          | 3.4 × 10 <sup>3</sup> ± 0.1 | BD                          |  |
| 88             | 11.4                                | 0.2                   | —             | —      | 40                  | 1.51    | 0.7     | 63.8           | 0.8            | 3.0            | 8.3                | 0                                  | 8                                 | 28.9                               | 166.4                 | 34.0                  | 2.0 × 10 <sup>8</sup> ± 0.5 | 1.0 × 10 <sup>8</sup> ± 1.0 | 1.6 × 10 <sup>6</sup> ± 0.5 |  |
| 95             | 12.4                                | 0.2                   | 21.3          | 3.7    | —                   | 2.53    | 0.1     | 62.8           | 1.0            | 3.1            | 7.9                | 0                                  | 43                                | 29.8                               | 143.2                 | 9.0                   | 1.9 × 10 <sup>4</sup> ± 1.3 | 4.3 × 10 <sup>4</sup> ± 1.0 | 2.5 × 10 <sup>3</sup> ± 1.0 |  |
| 156            | 6.1                                 | 0.1                   | 42.4          | 0.5    | 155                 | 0.4     | 0.4     | 43.2           | 0.6            | 3.2            | 7.7                | 0                                  | 49                                | 28.0                               | 201.5                 | 0.0                   | 1.1 × 10 <sup>6</sup> ± 0.0 | 1.1 × 10 <sup>6</sup> ± 0.3 | 2.4 × 10 <sup>4</sup> ± 0.0 |  |
| 174            | 3.0                                 | 0.1                   | 44.5          | 1.1    | 215                 | 0.6     | 0.4     | 46.8           | 0.8            | 3.1            | 7.7                | 0                                  | 48                                | 29.5                               | 184.9                 | 0.0                   | 1.7 × 10 <sup>7</sup> ± 0.8 | 5.5 × 10 <sup>6</sup> ± 0.2 | 3.9 × 10 <sup>4</sup> ± 0.0 |  |
| 232            | 20.2                                | 0.2                   | 25.1          | 0.6    | 120                 | 0.05    | 0.2     | 99.3           | 1.1            | 3.1            | 7.6                | 0                                  | 1                                 | 28.2                               | 129.8                 | 0.0                   | 3.0 × 10 <sup>4</sup> ± 0.4 | 1.8 × 10 <sup>5</sup> ± 0.2 | 1.5 × 10 <sup>5</sup> ± 0.9 |  |
| 296            | 5.9                                 | 0.1                   | 33.7          | 0.7    | -7                  | 0.5     | 0.3     | 38.7           | 0.3            | 3.0            | 7.9                | 0                                  | 23                                | 29.6                               | 54.4                  | 22.4                  | 5.1 × 10 <sup>4</sup> ± 1.3 | 1.8 × 10 <sup>4</sup> ± 0.5 | 4.7 × 10 <sup>3</sup> ± 4.0 |  |
| GC12           |                                     |                       |               |        |                     |         |         |                |                |                |                    |                                    |                                   |                                    |                       |                       |                             |                             |                             |  |
| 19             | 6.4                                 | 0.2                   | 42.3          | 0.7    | 286                 | 0.7     | 0.6     | 46.0           | 1.3            | 2.4            | 7.6                | 21.4                               | 9                                 | 28.4                               | 0.0                   | 0.0                   | 3.2 × 10 <sup>5</sup> ± 0.5 | 1.9 × 10 <sup>5</sup> ± 0.0 | 3.0 × 10 <sup>4</sup> ± 1.1 |  |
| 35             | 4.1                                 | 0.9                   | 16.9          | 0.4    | 350                 | 0.02    | 0.2     | 41.4           | 0.4            | 2.9            | 7.5                | 9.4                                | 9                                 | 28.8                               | 0.0                   | 0.0                   | 6.4 × 10 <sup>5</sup> ± 0.9 | 1.0 × 10 <sup>6</sup> ± 0.1 | 2.9 × 10 <sup>6</sup> ± 1.9 |  |
| 81             | 6.7                                 | 0.1                   | 32.6          | 0.5    | -118                | 0.3     | 0.4     | 58.6           | 0.8            | 3.5            | 7.3                | 0                                  | 45                                | 31.3                               | 66.4                  | 136.1                 | 2.2 × 10 <sup>6</sup> ± 0.2 | 3.0 × 10 <sup>6</sup> ± 0.7 | 1.5 × 10 <sup>4</sup> ± 1.4 |  |
| 126            | 5.0                                 | 0.1                   | 23.7          | 0.5    | -165                | 0.1     | 0.6     | 63.8           | 0.8            | 3.1            | 7.3                | 0                                  | 65                                | 27.8                               | 80.0                  | 94.9                  | 1.7 × 10 <sup>6</sup> ± 0.5 | 4.0 × 10 <sup>5</sup> ± 0.9 | 2.8 × 10 <sup>5</sup> ± 0.3 |  |
| 207            | 7.0                                 | 0.1                   | 36.3          | 1.7    | -110                | 0.3     | 1.3     | 99.3           | 1.1            | 3.4            | 7.3                | 0                                  | 94                                | 27.1                               | 94.8                  | 195.2                 | 1.4 × 10 <sup>6</sup> ± 0.2 | 5.2 × 10 <sup>5</sup> ± 0.6 | 1.7 × 10 <sup>4</sup> ± 0.3 |  |
| 310            | 5.4                                 | 0.1                   | 25.2          | 0.7    | -155                | 0.3     | 1.0     | 38.7           | 0.3            | 3.5            | 7.3                | 0                                  | 146                               | 23.4                               | 64.1                  | 188.0                 | 5.1 × 10 <sup>5</sup> ± 1.5 | 1.4 × 10 <sup>6</sup> ± 0.0 | 5.3 × 10 <sup>4</sup> ± 0.0 |  |

Context data for gravity core GC6 and GC12. See *Materials and Methods* for details on each measured parameter. All gene copy numbers are given per gram of wet weight sediment. Values marked with an asterisk were measured in gravity cores retrieved at the same position in year 2010. —, missing value; BD, below detection; \*, W%, percent by weight; %C, percent of carbon.

terial phyla to be compared with down-core variation in selected context data (Fig. 1).

Planctomycetes exhibited a high diversity in SSU rRNA gene sequences, represented by 461 different OTUs in GC6 and 311 in GC12 (97% cutoff). The great majority of these sequences could be assigned to the family of Planctomycetaceae, with little similarity to characterized relatives. We found a significant positive correlation between the abundance of this group and the SO<sub>4</sub><sup>2-</sup> concentration in pore water in core GC12 ( $r = 0.861$ ,  $P = 0.028$ ) (Fig. S3H). On the other hand, their relative abundance correlated positively with total inorganic carbon content in GC6 ( $r = 0.815$ ,  $P = 0.026$ ) (Fig. S3A). Although the former result suggests a link to the sulfur cycle, the latter is difficult to interpret. We detected low abundances of the *Candidatus Scalindua* group in the uppermost two horizons of GC12 (0.2 and 0.9% of the total SSU rRNA gene pool). This group is represented by members able to oxidize ammonium under anaerobic conditions (anammox) using nitrite as the electron acceptor (43). Interestingly, their appearance, albeit at very low numbers, in deeper layers of GC6 (156 and 174 cmbfsf) coincided with relatively high numbers of reads affiliated with *Nitrospina*, *Nitrosococcus*, and MG-1 (all potentially involved in the nitrogen cycle). Chloroflexi were among the most dominant bacterial groups in both cores, with the majority of reads affiliating within the class of Dehalococcoides, but representatives from SAR202, Ktedonobacteria, Caldilineae, and Anaerolineae were present also. None of the 56 different Chloroflexi OTUs (97% cutoff) from the two cores showed close sequence similarity to any of the few cultured species (maximum similarity was 90% to *Dehalococcoides ethanogenes*). Members of the candidate division JS-1 often co-occur with Chloroflexi in anoxic sediment zones (13). This co-occurrence also was observed in our cores. No inferences can be drawn about potential physiologies of either group, but, notably, the relative abundance of JS-1 in GC6 had a significant positive correlation with that of the family Desulfobacteraceae ( $r = 0.912$ ,  $P = 0.011$ ) (Fig. S2C) within the class of Deltaproteobacteria. Epsilonproteobacteria represented up to 39.5% of total reads in GC12 horizons and exhibited a unique depth profile. All reads that could be assigned to genus level affiliated with phylogenies involved in the sulfur cycle, including genera within the Helicobacteraceae (*Sulfurimonas* and *Sulfofervum*) and to a lesser extent within Campylobacteraceae (*Arcobacter* and *Sulfospirillum*). A high proportion of reads could be resolved only to the family of Helicobacteraceae but displayed a depth distribution similar to that of the above-mentioned groups. Interestingly, the same OTUs are present in high numbers in both the uppermost (oxic) and lowermost (anoxic) horizons, indicating organisms with a facultative mode of energy metabolism (either reducing or oxidizing sulfur compounds), as has been shown for some cultured representatives (44, 45). In GC12 a significant negative correlation was found between the abundance of this group and SO<sub>4</sub><sup>2-</sup> concentration in the pore water ( $r = -0.896$ ,  $P = 0.015$ ) (Fig. S3G), indicating involvement in the sulfur cycle. In GC6, on the other hand, Epsilonproteobacteria were virtually absent, indicating minor importance of the sulfur cycle, in agreement with the geochemical data.

The presence of Epsilonproteobacteria in the deeper layers of GC12 could indicate elevated temperatures at depth. However, high abundances of the same bacterial OTUs in the uppermost and lowermost layers and the lack of any overall depth trends suggest a moderate temperature gradient, if any. Deltaproteobacteria was the most abundant class of proteobacteria in GC6, with a strong positive correlation with Mn<sup>2+</sup> concentration in the pore water ( $r = 0.895$ ,  $P = 0.003$ ) (Fig. S3B). This correlation could be attributed to the abundance of *Nitrospina* and Sh765\_TZT\_29, an uncultured group within the Deltaproteobacteria (Silva taxonomy), pointing to their likely involvement in the manganese cycle.



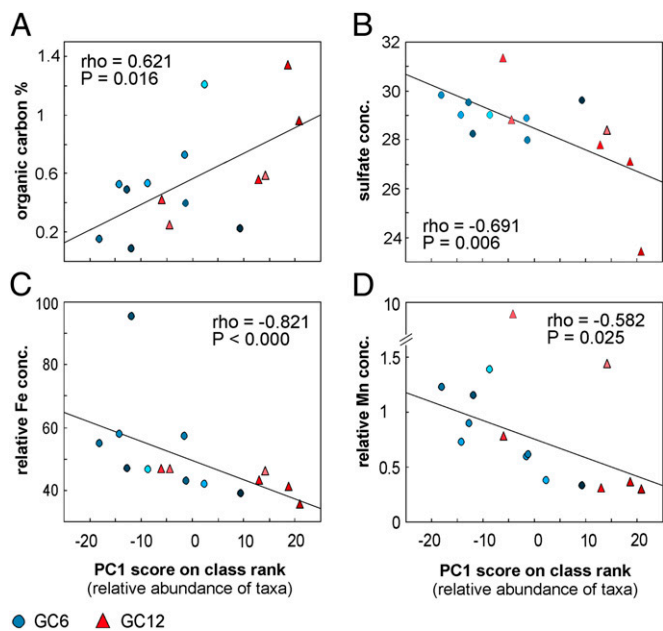


**Fig. 2.** Significant correlations ( $\alpha = 0.05$ ) between variation in microbial community structure and context data. Microbial community variation is measured by PC1 scores on relative abundance data at the class level. (A) Organic carbon content (% C). (B) Pore water sulfate concentration (mM). (C) Relative iron content in solid-phase Iron values as measured by XRF and normalized to Ti counts. (D) Relative content of manganese measured in the solid phase. Manganese values are measured as counts by XRF and normalized to titanium (Ti) counts. Correlations are given as Spearman's rank-order correlation ( $\rho$ ). Blue circles indicate values from gravity core GC6; red triangles indicate values from gravity core GC12. Color shading indicates depth in sediment (light, shallow; dark, deep).

**Distribution of the Most Abundant Archaeal Phyla.** As observed for the Bacteria, most archaeal taxa were present (at the class level) in both cores, but the relative abundance varied greatly between and within cores (Fig. 1).

MG-I, also named “Marine Group I.1a,” now assigned to the Thaumarchaeota phylum (46, 47), was the most abundant in six of the nine horizons in GC6. This group contributed as much as  $\geq 87\%$  of the total number of SSU rRNA gene-sequence reads in the two top layers (16 and 29 cmbsf). They also dominated in GC12 except for the two deepest horizons (203 and 310 cmbsf). These Archaea not only constitute one of the most abundant microbial planktonic groups in the oceans (48, 49) but also are a highly abundant component in marine sediments (29, 50, 51). Although only aerobic growth has been reported for Thaumarchaeota thus far (52–55), we found MG-I-related organisms in anoxic horizons in our study. Their presence was particularly evident at 126 cmbsf in GC12 (61% of total reads) and at 88, 156, and 174 cmbsf in GC6 (45–56% of total reads), giving an absolute estimate of  $4.2 \times 10^5$  to  $1.5 \times 10^8$  MG-I-affiliated 16S rRNA gene copies/g sediment (wet weight) in these horizons. Phylogenetic analysis (Fig. 3) of all published full-length sequences of MG-I for which the habitat origin was assigned unambiguously in the database entry (*Materials and Methods*) demonstrated a separation of planktonic (gamma, delta), sponge-associated (beta), and terrestrial (lambda I, II) taxa from those found predominantly in the sediment (upsilon, eta, iota, theta, epsilon, zeta, and mu clusters; no sequences related to cluster kappa fulfilled the requirements mentioned in *Materials and Methods*) (Fig. 3A). With the exception of sequences affiliated with cluster alpha 1 (9%), all MG-I-related sequences in GC6 and GC12 were affiliated with the lineages that are found predominately in sediments (Fig. 3 B and C). This finding augments the earlier

observations by Durbin and Teske (50), who stated that novel clusters distinct from planktonic MG-I organisms can be discovered in marine sediments. A similar habitat-specific clustering has been shown for the archaeal ammonia monooxygenase (*amoA*) (56, 57). To explore the potential of sedimentary MG-I archaea to oxidize ammonia, we quantified the archaeal *amoA* gene, which is used as a genetic marker for this metabolism. Copy numbers ranged from  $1.5 \times 10^3$  to  $2.4 \times 10^6$  and from  $1.5 \times 10^4$  to  $2.9 \times 10^6$ /g sediment (wet weight) for GC6 and GC12, respectively (Table 1). We found a significant correlation of archaeal *amoA* gene copy numbers with the abundance of group MG-I ( $r = 0.929$ ,  $P < 0.000$ ) (Fig. 4C and Fig. S3E) and total numbers of archaeal 16S rRNA genes ( $r = 0.861$ ,  $P = 0.003$ ) (Figs. 4B and Fig. S3F) in GC6. Both marker genes (*amoA* and 16S rDNA) were found in the same order of magnitude in all samples. More intriguingly, the MG-I abundances also correlated with total  $\text{NO}_3^-$  concentration ( $r = 0.827$ ,  $P = 0.011$ ) (Fig. 4A and Fig. S3D) and, to a lesser but still significant extent, with TOC content ( $r = 0.692$ ,  $P = 0.039$ ) (Fig. S3C).

The DSAG, also referred to as “Marine benthic group B,” is the most abundant single group of organisms in deep-sea sediments, along with the MCG (20). They were a dominant archaeal constituent in both cores. The relative abundance of DSAG in GC12 ( $\sim 25\%$  of total reads) correlated significantly with both TOC and  $\text{Fe}_2\text{O}_3$  concentration ( $r = 0.869$ ,  $P = 0.025$ , and  $r = 0.819$ ,  $P = 0.046$ , respectively) (Fig. 5 A and B and Fig. S3 I and J). This observation is consistent with a heterotrophic lifestyle (14) possibly coupled to the reduction of iron oxides rather than to sulfur compounds, as previously proposed (7).

SSU rDNA signatures of the MCG often are found in high numbers in clone libraries from deep-sea sediments [reviewed by Teske and Sørensen (19)]. In our samples they constitute up to  $\sim 10\%$  of all prokaryotic SSU rRNA genes in certain layers. This group, like the DSAG, has been proposed to be anaerobic heterotrophs (14) and has no cultured representatives. Unlike the DSAG, however, they populate a wide variety of habitats and exhibit larger diversity at the 16S rDNA level. No correlation for this group with any of the measured geochemical parameters was found within our dataset.

Methanomicrobia SSU rDNA signatures were among the four most dominant of the archaeal classes in GC12. The obtained sequences affiliated with ANME groups 1, 2a, 2b, and 2c, all of which are thought to be involved in anaerobic oxidation of methane (AOM) (58). Both their relative and total abundance increased with depth, reaching a maximum of 3.6% of all reads at the deepest horizon (310 cmbsf).

Notably, we found a tight correlation of ANME-1 phylotypes with both Methylococcales and Campylobacterales (Fig. S2 D–F), suggesting a common metabolism or a syntrophic partnership.

## Discussion

The proximity of the two investigated sediment cores to hydrothermal active sites combined with sediment input from the Bear Island Fan has resulted in a compact redox zonation profile and high concentrations of dissolved metals in both cores. These properties make the sediments interesting model sites to study the variation of subsurface microorganisms in the context of geochemical changes. There were substantial differences between the two cores. For example, the GC12 core is distinguished from GC6 by a clear signature of shallow sulfate reduction and much higher concentrations of dissolved iron (Table 1). Despite such differences, the PCA analysis (Fig. S2 A and B) shows that the samples from both cores share a major axis of variation that links changes in the overall composition of the microbial community to changes in the overall geochemical composition. More specifically, the structure of the prokaryotic communities is coupled to variation in the iron and manganese content of the minerals, TOC, and pore water  $\text{SO}_4^{2-}$  concentration (Fig. 2).

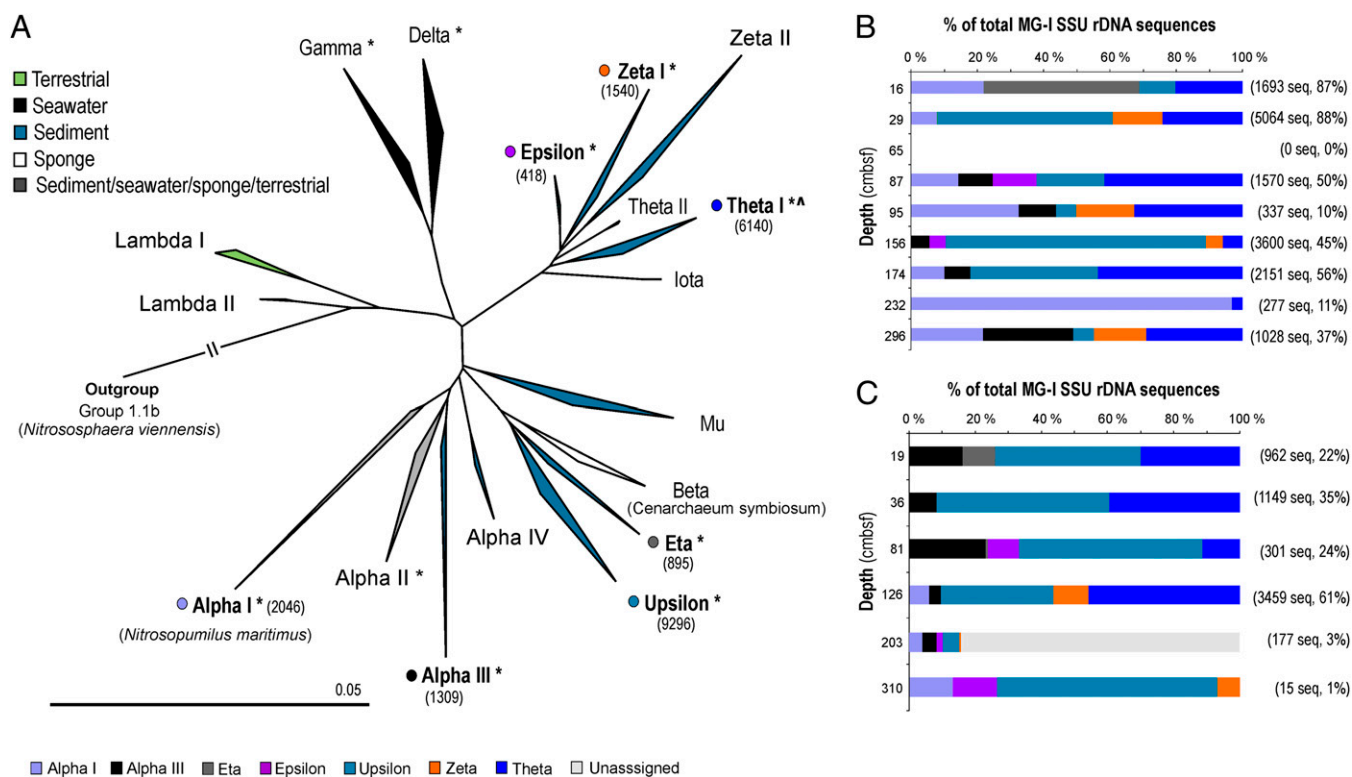


**Fig. 3.** Phylogenetic analysis and depth distribution of MG-I. (A) Phylogeny based on SSU rRNA gene information from all published sequences available in the Silva database (release 104). The nomenclature follows that used by Durbin and Teske (50), but the additional group names lambda I, lambda II, and mu are given. The tree is reconstructed by NJ using the Felsenstein correction. Topology and clusters are supported by RaxML and PhyML reconstructions on the same dataset. Clusters marked with an asterisk contain sequences retrieved from marine hydrothermal environments. The sediment cluster marked with a dot contains a subcluster of freshwater/terrestrial sequences. Numbers in parentheses indicate the total number of reads from our study that affiliated with that particular group. (B and C) Depth distribution of MG-I 16S rDNA gene sequences affiliating with each cluster obtained in this study from core GC6 (B) and core GC12 (C). Numbers in parentheses indicate the number of reads from that horizon assigned to MG-I and the percentage of the total. Color codes correspond to the groups in A.

Our results provide quantitative evidence for the common assumption that organic carbon is one of the fundamental factors shaping microbial communities, supporting the argument that heterotrophic organisms play an important role in deep-sea sediments (14, 20). The content of iron and manganese within the sediments is strongly related to microbial community structure, and, although the causal relationships are highly complex, our results suggest that mineralogy is a key determinant. Finally, we attribute the correlation between abundance and sulfate concentration to the effect of microbial sulfur metabolisms on pore water chemistry, rather than vice versa.

By directly correlating the abundance of each individual taxonomic group to the individual context data, we were able to make predictions about the metabolism of the most dominating organisms in the deep-sea sediments, in particular MG-I, DSAG, and Epsilon- and Deltaproteobacteria. In addition, strong correlations in the relative abundances of different taxa (Fig. S2 C–F) might help elucidate syntrophic partnerships and/or common metabolic preferences.

The archaeal class MG-I belongs to the newly defined phylum Thaumarchaeota, represented by two pure cultures and a few enrichments (59) that were shown to gain energy from aerobic oxidation of  $\text{NH}_4^+$  to  $\text{NO}_2^-$ . Their main carbon source is  $\text{CO}_2$ , but coassimilation of organic carbon has been reported for this group (52). The majority of MG-I sequences retrieved in our study (21,644 reads) clustered in phylogenetic groups mainly associated with marine sediments, suggesting the presence of a specialized sediment population (Fig. 3).

None of these groups has any characterized members, but at least four observations support their ability to oxidize ammonia

to nitrite in the sediments from GC6: (i) the tight correlation between the abundance of this group and *amoA* gene copy numbers (Fig. 4C and Fig. S3E); (ii) a high positive correlation of the MG-I with nitrate concentration (Fig. 4A and Fig. S3D); (iii) their co-occurrence with several other phylotypes normally linked to the nitrogen cycle, such as members related to anammox and nitrite-oxidizing *Nitrospina*; and (iv) the fact that the increase in ammonium concentration below the oxic zone is less pronounced than would be expected otherwise (Fig. 1). The presence of an active group of ammonia-oxidizing archaea is surprising, because the sediments are considered to be anoxic below the two uppermost sampling depths. However, MG-I-related sequences have been reported previously from supposedly anoxic environments, although the metabolic implications of these findings have not been addressed (7, 29, 39, 60). Their presence in anoxic horizons can have several explanations: (i) sediment-specific phylogenetic groups of MG-I may have the ability to oxidize ammonium with an alternative electron acceptor; (ii) oxygen could be produced intracellularly, as recently described for the methane-oxidizing group NC10 (50); or (iii) *amo* genes present in the organisms could have some other function, as suggested by Mussmann and colleagues (61). In summary, our data strongly support ammonia oxidation, but the electron acceptor remains unknown. In this context it is noteworthy that members of Methylococcales, another group assumed to be comprised exclusively of aerobes, also occur in highly reduced horizons in this study.

The DSAG is proposed to represent heterotrophic organisms based on indirect evidence from stable carbon isotopes in archaeal lipids (14). A strong correlation between the relative abundance of DSAG and organic carbon content in our study (Fig. 5A and

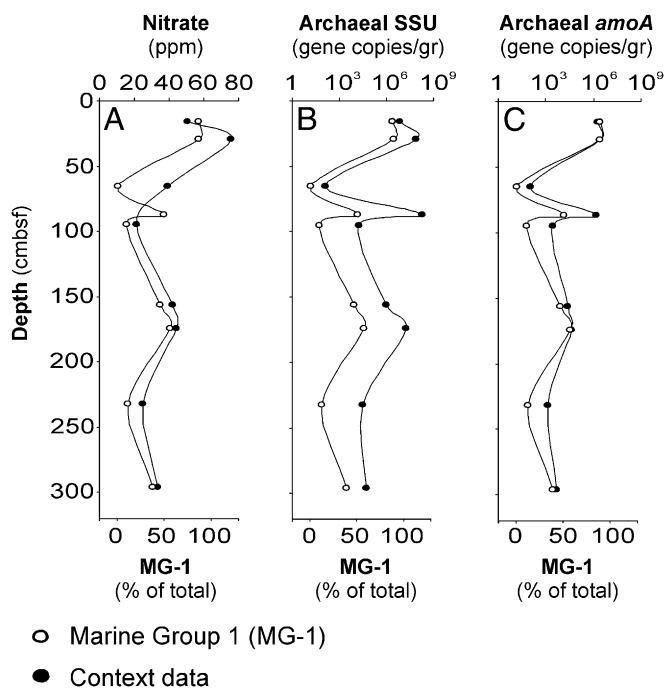


**Fig. 4.** Covariance between relative abundance of MG-1 and context data. The depth distribution of the relative abundance of MG-1 in core GC6 strongly covaries with (A) nitrate concentration (ppm) extracted from the solid phase (Pearson's  $r = 0.827$ ,  $P = 0.011$ ); (B) archaeal SSU rDNA ( $r = 0.827$ ,  $P = 0.011$ ); and (C) archaeal *amoA* gene copies ( $r = 0.929$ ,  $P < 0.000$ ). Gene copy numbers are estimated by qPCR and given per gram of sediment (wet weight). See also Fig. S3.

Fig. S3J) supports this suggestion. Their energy-yielding metabolism is a subject of debate, and several studies have proposed direct or indirect coupling to methane oxidation (7, 14, 62) as well as possible sulfate reduction (7). Here we argue that labile iron oxides serve as the terminal electron acceptor either in the direct oxidation of organic carbon or as an energy-yielding metabolism coupled to another electron donor, such as  $\text{CH}_4$ ,  $\text{NH}_4^+$ , or sulfur compounds. We base this proposal on the significant correlation between iron oxide and the relative abundance of DSAG in core GC12 (Fig. S3J). The correlation between DSAG and dissolved  $\text{Fe}^{2+}$  in the pore water was positive but not significant (Fig. S3K). (GC6 showed a similar relationship but was omitted from statistical analysis because of the low number of observations.)

It is well known that the iron and sulfur cycles are tightly linked; hence  $\text{Fe}^{2+}$  in the pore water also could result from sulfate reduction to sulfide and the subsequent reaction with iron oxide (63). However, our sulfate profiles do not suggest any significant sulfate reduction except at the deepest horizon in GC12. Thus, iron oxide is the most likely electron acceptor, and the results discussed above, as well as theoretical energy yield, point to organic carbon as the most likely donor. Alternatively, this pathway could involve AOM coupled to iron oxide reduction, a process that potentially yields more energy than AOM coupled to sulfate reduction. Such a metabolism has been demonstrated recently based on geochemical data by Beal and colleagues (64).

In summary, these highly stratified sediments offered a unique possibility to correlate stratigraphic variation in geochemical properties directly to stratigraphic variation in the structure of the microbial community as well as to the relative abundance of individual taxa. We combined deep sequencing of bacterial and archaeal SSU rRNA genes, using a single primer set with broad target coverage, with an extensive set of environmental context data, including nitrate from the solid phase. We used PCA to

distill the covariance structures of the prokaryotic community and the geochemical data separately, thereby revealing a significant correlation between overall changes in geochemistry and overall changes in community composition. Four geochemical components were linked closely to the taxonomic distribution of microorganisms: the total organic carbon, iron, and manganese content in the minerals and the sulfate concentration in pore water. Our findings yield testable predictions about the metabolisms of the most typical and abundant microbial lineages found in the deep subsurface, including the DSAG and sediment lineages of potentially anaerobic MG-1.

### Materials and Methods

**Site Location and Shipboard Sampling.** After retrieval, the cores immediately were cut in sections and split into archive and working halves. Sampling of pore water and sediment for geochemical and microbial analyses from the working halves was conducted onboard the ship as quickly as possible. The two gravity cores, GC6 ~15 km SE of the vent field ( $73^\circ 21.39' \text{N}$ ,  $7^\circ 33.90' \text{E}$ , 3,280 mbsl), and GC12 ~15 km NE of the vent field ( $73^\circ 45.80' \text{N}$ ,  $8^\circ 27.83' \text{E}$ , 3,250 mbsl), were selected for microbiological studies. The in situ bottom water temperature was  $-0.2^\circ \text{C}$  when cores were retrieved. Samples were collected at depths of 16, 29, 65, 87, 95, 156, 174, 232, and 296 cm in GC6 and 19, 36, 81, 126, 203 and 301 cm in GC12. All samples were collected with sterile 10-mL syringes and were processed immediately or snap-frozen in liquid nitrogen before storage at  $-80^\circ \text{C}$ . Pore water was extracted with Rhizon samplers from approximately the same depths as the microbiological samples and was analyzed immediately onboard for pH, alkalinity, sulfide, and ammonium or was stored at  $4^\circ \text{C}$  until later onshore analysis of dissolved ions. Eh measurements of the sediment were carried out onboard. After sampling was completed, the sediment cores were stored in plastic boxes at  $4-6^\circ \text{C}$  on the ship and later at the University of Bergen core repository.

**DNA Extraction.** DNA was extracted from ~0.5 g of sediment in each sample using a FastDNA spin for soil kit in conjunction with the FastPrep-24 in-

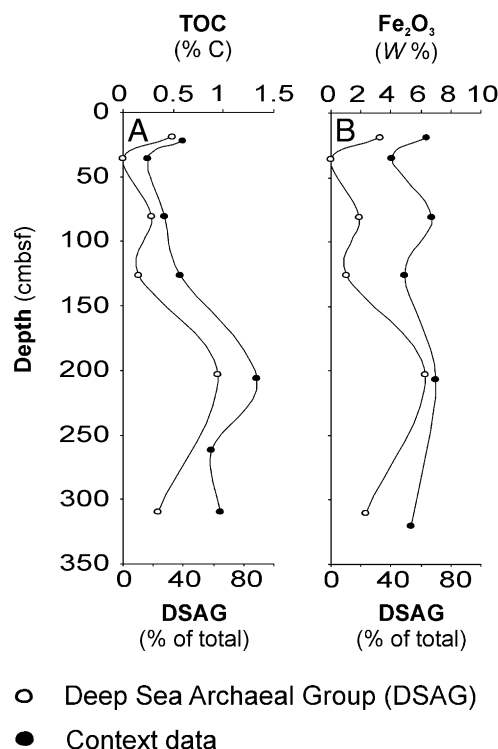


**Fig. 5.** Covariance between relative abundance of DSAG and context data. The depth distribution of the relative abundance of DSAG in core GC12 strongly covaries with (A) TOC (Pearson's  $r = 0.869$ ,  $P = 0.025$ ) and (B)  $\text{Fe}_2\text{O}_3$  concentrations in the sediment (Pearson's  $r = 0.819$ ,  $P = 0.046$ ). See also Fig. S3.



strument (MP Biomedicals) following the manufacturer's protocol applying the poly(A) modification described by Hugenholz et al. (65).

**DNA Amplification for the 16S rRNA Gene Library.** Different primer combinations were evaluated *in silico* before final selection using the Ribosomal Database Project (RDP) (66), to select the lowest possible degeneracy while maintaining high overall prokaryotic target coverage. In addition, the 454 GS (454 Life Sciences, Roche) FLX technology requires that the length of the amplified product be within 300–800 bp. The optimal primer combination was found to be Uni787F (5'-ATTAGATACCCNGGTAG-3') (67) and Uni1391R (5'-ACGGGCGGTGWGTRC-3'), modified from ref. 68. These primers target the V5–V8 region on the 16S rRNA gene and cover 87% and 94%, respectively, of all prokaryotes in the RDP without mismatch (as of May, 2011). The stringency of the performed PCR was kept at a minimum to obtain as much taxonomic diversity as possible, with one mismatch increasing the coverage of both primers to 98%. Furthermore, the chosen primer combination had the least bias toward any one specific taxonomic group ("universal" prokaryotic primers often are problematic, in that they tend to have mismatches against specific taxonomic groups such as Verrucomicrobia, Planctomycetes, and Chloroflexi). DNA from each horizon was PCR amplified in triplicate using the above-mentioned primer combination under the following thermal conditions: 95 °C for 15 min, then 25–30 cycles of 94 °C for 45 s, 53 °C for 45 s, 72 °C for 1 min followed by 72 °C for 7 min before cooling at 4 °C. Each reaction (25  $\mu$ L) contained 1 $\times$  HotStar Taq Master Mix (Qiagen), template DNA, and 1.2  $\mu$ M of each primer. To ensure correct amplicon length, the PCR product was evaluated by gel electrophoresis. The triplicate PCR products then were pooled to minimize PCR drifting and were purified using GenElute PCR Clean-Up kit (Sigma). A new round of PCR was performed using the same specific primers and thermal conditions but linked to the 454 Life Sciences A and B pyrosequencing adaptor sequence. In addition, the forward primer was labeled with a unique barcode (one for each analyzed sediment horizon) as described by Hamady et al. (69). To minimize PCR bias, the number of cycles was held to a minimum (25–30 in the first PCR and five in the second). Amplicons were purified again, and the concentration and quality were controlled by gel inspection, spectrometry (Cary-300 Bio UV-vis; Varian), and BIO-analyzer (Agilent Technologies). All amplicons (a total of 15 unique samples) then were pooled in a 1:1 ratio based on DNA concentration (~20 ng/ $\mu$ L from each sample) and sequenced using multiplex GS FLX pyrosequencing (without titanium chemistry) at the Norwegian High-Throughput Sequencing Centre in Oslo, Norway.

Pyrosequencing flowgrams (SSF files) have been deposited in the National Center for Biotechnology Information (NCBI) Sequence Read Archive under the accession number SRP009131.

**Filtering and Removal of Noise from Amplicon Sequence Data.** The dataset (84,580 reads) was filtered and cleaned from noise by using AmpliconNoise (70) software. In short, this method includes four steps: filtering, flowgram clustering, sequence clustering, and chimera removal. In the filtering step, reads were truncated at 600 flows, and those with fewer than 360 flows or a noisy signal (flow intensity 0.5–0.7, equivalent to a degenerate base) before this position were removed. In addition, all reads not matching the barcode and primer sequences were removed. In the sequence-clustering step, reads were truncated at 240 bp. AmpliconNoise generated a set of de-noised and chimera-filtered sequences, each with a set of reads most likely to be derived from it. Barcode and primer sequences were removed before further analysis such as taxonomic classification and linkage clustering.

**Taxonomic Evaluation.** To assign the filtered, de-noised, and chimera-filtered sequences to taxa, we modified and updated the Silva SSUref database release 100 (71) with respect to taxonomy, based on the most recent literature. This database (available at <http://services.cbu.uib.no/supplementary/community-profiling/>) is described in Lanzén et al. (72).

The sequences were aligned to this database using Blastn (NCBI), and the results were analyzed and assigned to specific taxa using the software MEGAN version 3.7 (73) by applying a lowest common ancestor algorithm [for details see Lanzén et al. (72)].

**OTU Clustering.** All unique de-noised sequences were clustered into OTUs using maximum linkage clustering of pairwise distances. The distance matrix was generated using the Needleman–Wunsch algorithm as implemented in NDist, and clustering was carried out using FDist (both programs are distributed with AmpliconNoise) (70). A 3% distance cutoff was used to define OTUs.

**Phylogenetic Analysis of MG-1.** The phylogenetic relationship within the MG-1 was evaluated to find habitat-specific groups and to calculate the affiliation

of MG-1 sequences from this study. The tree was calculated based on all published full-length (>900 bp) sequences available in the Silva database release 104 (71), applying the archaeal positional filter and removing highly variable positions (if a sequence was described as "unpublished" in the ARB entry field "journal," it was excluded from the calculation). Length was truncated to ARB position 1773–31131 leaving 784 valid columns for calculation. After calculation, sequences were removed if the ARB entry field "Isolation source" contained one of the following words: mangrove, marsh, or estuary (to avoid uncertainties in the habitat type), leaving 659 sequences. Clusters containing one or more sequences obtained from hydrothermal environments are marked with an asterisk. We do not label these clusters as hydrothermal in Fig. 3, because sequences obtained from marine hydrothermal settings are inherently difficult to assign unambiguously to a specific habitat (e.g., seawater, sediment, chimney, microbial mat). The phylogenetic tree (Fig. 3A) was calculated by Neighbor Joining (NJ) using the Felsenstein correction (74). To verify the tree topology, RaxML (75) and PhyML (76) algorithms likewise were applied on the same dataset; both supported the displayed clustering and grouping. The nomenclature follows that reviewed by Durbin and Teske (50). In addition, we have identified and named three clusters: lambda I and II (exclusively from terrestrial habitats) and mu (exclusively from marine sediments).

All unique sequences from each sediment horizon that could be assigned to MG-1 from our dataset (123 sequences from a total of 21,644) were added to the tree using the parsimony tool in the ARB package. Adding this many short sequences distorts the branch length; hence they are not included in the displayed tree. To confirm the affiliation of our sequences, an NJ tree was calculated based on the above-mentioned database sequences and our sequences but with all truncated to a length of 230 bp. All affiliations were confirmed, with a few exceptions for which the sequences could not be phylogenetically resolved. The depth distributions of our sequences and cluster to which they affiliate are displayed for both gravity core GC6 (Fig. 3B) and gravity core GC12 (Fig. 3C).

**Real-Time qPCR.** Archaeal 16S rRNA genes were quantified using the prokaryotic primer Uni519F (5'-CAGCMGCCGCGGTAA-3') (77) and the archaeal-specific primer Arc908R (5'-CCC GCCAATTCCTTAAGTT-3') [modified from Jurgens et al. (78)]. Each reaction (25  $\mu$ L) contained 1 $\times$  QuantiTech Sybr Green PCR master mixture (Qiagen), 0.8  $\mu$ M of each primer, and 1  $\mu$ L template DNA. The thermal cycling program was 15 min at 95 °C, then 40 cycles of 95 °C for 30 s, 60 °C for 30 s, and 72 °C for 45 s. The quantification standard consisted of a dilution series of a known amount of linearized fosmid 54d9 (79) and a copy number of archaeal 16S rRNA genes between 10 and 10<sup>7</sup> copies/ $\mu$ L [calculated as described by Leininger et al. (80)]. Genomic DNA from *Escherichia coli* was used as a negative control. The  $R^2$  value for the standard curve was 0.99, and the slope value was –3.26, giving an estimated amplification efficiency of 102%.

Bacterial 16S rRNA genes were quantified using the bacterial-specific primer bac341f (5'-CCTACGGGWWGGCWGCA-3') [modified from Ishii and Fukui (81)] and the prokaryotic 519r (5'-TTACCGGCKGCTG-3') (77). The quantification standard consisted of a dilution series (between 1  $\times$  10<sup>2</sup> and 1  $\times$  10<sup>7</sup> copies/ $\mu$ L) of a known amount of purified PCR product obtained from genomic *E. coli* DNA by using the bacterial 16S rRNA gene-specific primers 8F/1392R (68, 82). *Sulfolobus solfataricus* genomic DNA was used as negative control. The  $R^2$  value for the standard curve was 0.99, and the slope value was –3.06, giving an estimated amplification efficiency of 112%. The thermal cycle program was 15 min at 95 °C, then 35 cycles of 95 °C for 15 s, 58 °C for 30 s, and 72 °C for 30 s.

Archaeal *amoA* genes were quantified using the archaeal *amoA*-specific primers CrenamoA23f (5'-ATGGTCTGGCTWAGACG-3') (80) and CrenamoA61r (5'-GCCATCCABCKRTANGTCCA-3') (83). Each reaction (25  $\mu$ L) contained 1 $\times$  QuantiTech Sybr Green PCR master mixture (Qiagen), 1.2  $\mu$ M of each primer, and 1  $\mu$ L template DNA. The thermal cycling program was 15 min at 95 °C, then 40 cycles of 95 °C for 30 s, 50 °C for 45 s, and 72 °C for 45 s. The quantification standard was the same as used in archaeal and crenarchaeal 16S rRNA gene quantification. Genomic DNA from *E. coli* was used as a negative control. The  $R^2$  value for the standard curve was 0.99, and the slope value –3.51, giving an estimated amplification efficiency of 93%. All qPCR experiments were performed with the Step-OnePlus real-time PCR system (Applied Biosystems) using SYBRGreen1 as the fluorescent dye. To confirm product specificity, melting curve analyses were performed after each run for all experiments, and each qPCR setup contained samples, standard series, negative controls, and blanks, all in triplicate.

**XRF Core Scanning.** The archived core halves were scanned using the non-destructive ITRAX XRF core scanner system at Bergen Geoscientific Facility,



University of Bergen. Samples were irradiated with 3 kW Mo. Step size was 0.5 mm for XRF analysis with a count time of 10 s. Manganese and iron were normalized to titanium counts.

**Organic and Inorganic Carbon Measurements.** Coulometric titration (CM5012 CO<sub>2</sub> Coulometer; IUC, Inc.) was used to determinate the total inorganic carbon (TIC) and the total carbon (TC) contents in 12 of the 15 samples. Analytical precision determined by analysis of replicate standards for TIC and TC was  $\pm 0.02\%$  C and  $\pm 0.03\%$  C, respectively. The TOC contents were calculated by subtracting TIC contents from the TC contents, leading to an error of  $\pm 0.05\%$  C for TOC contents. The remaining three samples were measured applying the method described for nitrogen in the *Solid-Phase Geochemistry* section below.

**Pore Water Chemistry.** Pore water was extracted using Rhizon samplers, and aliquots were analyzed onboard for pH by using a mobile pH meter, for alkalinity by an autotitrator, and for sulfide and ammonium by spectrophotometric methods (84). Onshore analysis of sulfate was performed by ion chromatography, and dissolved iron and manganese were analyzed by inductively coupled plasma optical emission spectrometry.

**Solid-Phase Geochemistry.** Eh was measured in all layers directly by electrodes (SP 50x; Consort) inserted into undisturbed sediment as soon as cores were split.

Nitrates were measured in an aqueous solution of (NH<sub>4</sub>)<sub>2</sub>SO<sub>4</sub> (2 M) and sediment (5:1 ratio) through an ion-selective electrode (nitrate ion combination epoxy electrode no. 31503; Phoenix). Nitrogen and sulfur were determined using an elemental analyzer for CHNS-O based on the principle of dynamic flush combustion coupled with gas chromatography. Nitrogen was measured using a GC packed column for CHNS polytetrafluoroethylene, 2 m (Eurovector), and sulfur was measured using a GC packed column for sulfur, 1 m, 6 × 5 mm (Eurovector). Each sample was dried and powdered before analysis. Iron oxide and manganese oxide contents were determined by atomic absorption spectrometry after digestion of samples by microwave, using H<sub>2</sub>O<sub>2</sub>+HCl, HNO<sub>3</sub>, and HF.

**Statistical Analyses.** PCA was used to summarize the community structure (relative abundance data) and the geochemical structure (context data) of the sediments quantitatively. Each sample was standardized to zero mean and unit SD. The relative abundance data also were subjected to a centered log-ratio transformation with multiplicative zero replacement (85, 86) to remove any forced correlations imposed by the constant-sum constraint. PCA uses the covariance structure to rotate the original data onto a new set of orthogonal (independent) axes oriented in the direction of maximal remaining variance. By projecting the samples onto the first axis (PC1), we effectively reduced the community (or geochemical) structure to a single variable accounting for the greatest proportion of variance. If the overall community structure were causally related to the overall geochemical structure of the sediment, then we would expect a significant, monotonic (if not strictly linear), arbitrarily signed relationship between the PC1 scores of the relative abundance and geochemical datasets. We tested this hypothesis using the Spearman rank-order correlation ( $\rho$ ).

The community–geochemistry relationship was dissected further by correlating the relative abundance PC1 scores against the original geochemical measurements, again using Spearman's  $\rho$ . Finally, we mined the relative abundance data directly to explore linkages among individual taxa and linkages between individual taxa and geochemical variables, using Pearson's product–moment correlation.

**ACKNOWLEDGMENTS.** We thank S. Mosen and all the onboard scientific members and crew members of the research vessel *G.O. Sars* during the 2008 H2Deep expedition. We thank H. Hafliðasson for help with the core scanning and T. Ulrich for fruitful discussions. The Norwegian High-throughput sequencing Centre at the University of Oslo performed the sequencing (<http://www.sequencing.uio.no>). The project was funded by the H2Deep project through the European Science Foundation program (EuroMARC). Additional funding was provided by Norwegian Research Council through the Centre for Geobiology.

- Whitman WB, Coleman DC, Wiebe WJ (1998) Prokaryotes: The unseen majority. *Proc Natl Acad Sci USA* 95:6578–6583.
- Parkes RJ, Cragg BA, Wellsbury P (2000) Recent studies on bacterial populations and processes in subseafloor sediments: A review. *Hydrogeol J* 8(1):11–28.
- Berner RA (1982) Burial of organic carbon and pyrite sulfur in the modern ocean; its geochemical and environmental significance. *Am J Sci* 282(4):451–473.
- Rochelle PA, Fry JC, Parkes RJ, Weightman AJ (1992) DNA extraction for 16S ribosomal-RNA gene analysis to determine genetic diversity in deep sediment communities. *FEMS Microbiol Lett* 100(1–3):59–65.
- Marchesi JR, Weightman AJ, Cragg BA, Parkes RJ, Fry JC (2001) Methanogen and bacterial diversity and distribution in deep gas hydrate sediments from the Cascadia Margin as revealed by 16S rRNA molecular analysis. *FEMS Microbiol Ecol* 34(3):221–228.
- Reed DW, et al. (2002) Microbial communities from methane hydrate-bearing deep marine sediments in a forearc basin. *Appl Environ Microbiol* 68(8):3759–3770.
- Inagaki F, et al. (2006) Biogeographical distribution and diversity of microbes in methane hydrate-bearing deep marine sediments on the Pacific Ocean Margin. *Proc Natl Acad Sci USA* 103:2815–2820.
- Inagaki F, et al. (2003) Microbial communities associated with geological horizons in coastal subseafloor sediments from the sea of Okhotsk. *Appl Environ Microbiol* 69:7224–7235.
- Kormas KA, Smith DC, Edgcomb V, Teske A (2003) Molecular analysis of deep subsurface microbial communities in Nankai Trough sediments (ODP Leg 190, Site 1176). *FEMS Microbiol Ecol* 45:115–125.
- Newberry CJ, et al. (2004) Diversity of prokaryotes and methanogenesis in deep subsurface sediments from the Nankai Trough, Ocean Drilling Program Leg 190. *Environ Microbiol* 6:274–287.
- Parkes RJ, et al. (2005) Deep sub-seafloor prokaryotes stimulated at interfaces over geological time. *Nature* 436:390–394.
- Parkes RJ, et al. (1994) Deep bacterial biosphere in Pacific Ocean sediments. *Nature* 371:410–413.
- Fry JC, Parkes RJ, Cragg BA, Weightman AJ, Webster G (2008) Prokaryotic biodiversity and activity in the deep subseafloor biosphere. *FEMS Microbiol Ecol* 66:181–196.
- Biddle JF, et al. (2006) Heterotrophic Archaea dominate sedimentary subsurface ecosystems off Peru. *Proc Natl Acad Sci USA* 103:3846–3851.
- Sørensen KB, Teske A (2006) Stratified communities of active Archaea in deep marine subsurface sediments. *Appl Environ Microbiol* 72:4596–4603.
- Roussel EG, et al. (2008) Extending the sub-sea-floor biosphere. *Science* 320:1046.
- D'Hondt S, et al. (2009) Subseafloor sedimentary life in the South Pacific Gyre. *Proc Natl Acad Sci USA* 106:11651–11656.
- Jørgensen BB, Boetius A (2007) Feast and famine—microbial life in the deep-sea bed. *Nat Rev Microbiol* 5:770–781.
- Teske A, Sørensen KB (2008) Uncultured archaea in deep marine subsurface sediments: Have we caught them all? *ISME J* 2:3–18.
- Orcutt BN, Sylvan JB, Knab NJ, Edwards KJ (2011) Microbial ecology of the dark ocean above, at, and below the seafloor. *Microbiol Mol Biol Rev* 75:361–422.
- Wang P, et al. (2010) Community structure of archaea from deep-sea sediments of the South China Sea. *Microb Ecol* 60:796–806.
- Webster G, et al. (2006) Prokaryotic community composition and biogeochemical processes in deep subseafloor sediments from the Peru Margin. *FEMS Microbiol Ecol* 58:65–85.
- Biddle JF, Fitz-Gibbon S, Schuster SC, Brenchley JE, House CH (2008) Metagenomic signatures of the Peru Margin subseafloor biosphere show a genetically distinct environment. *Proc Natl Acad Sci USA* 105:10583–10588.
- Biddle JF, White JR, Teske AP, House CH (2011) Metagenomics of the subsurface Brazos-Trinity Basin (IODP site 1320): Comparison with other sediment and pyrosequenced metagenomes. *ISME J* 5:1038–1047.
- Schippers A, et al. (2005) Prokaryotic cells of the deep sub-sea-floor biosphere identified as living bacteria. *Nature* 433:861–864.
- D'Hondt S, Rutherford S, Spivack AJ (2002) Metabolic activity of subsurface life in deep-sea sediments. *Science* 295:2067–2070.
- Froelich PN, et al. (1979) Early oxidation of organic matter in pelagic sediments of the eastern equatorial Atlantic: Sboxic diagenesis. *Geochim Cosmochim Acta* 43(7):1075–1090.
- Durbin AM, Teske A (2011) Microbial diversity and stratification of South Pacific abyssal marine sediments. *Environ Microbiol* 13:3219–3234.
- Roussel EG, et al. (2009) Archaeal communities associated with shallow to deep subseafloor sediments of the New Caledonia Basin. *Environ Microbiol* 11:2446–2462.
- Fry JC, Webster G, Cragg BA, Weightman AJ, Parkes RJ (2006) Analysis of DGGE profiles to explore the relationship between prokaryotic community composition and biogeochemical processes in deep subseafloor sediments from the Peru Margin. *FEMS Microbiol Ecol* 58:86–98.
- Webster G, et al. (2007) Distribution of candidate division JS1 and other Bacteria in tidal sediments of the German Wadden Sea using targeted 16S rRNA gene PCR-DGGE. *FEMS Microbiol Ecol* 62:78–89.
- Hoehler TM, Alperin MJ, Albert DB, Martens CS (1994) Field and laboratory studies of methane oxidation in an anoxic marine sediment: Evidence for a methanogen-sulfate reducer consortium. *Global Biogeochem Cycles* 8(4):451–463.
- Boetius A, et al. (2000) A marine microbial consortium apparently mediating anaerobic oxidation of methane. *Nature* 407:623–626.
- Strous M, et al. (1999) Missing lithotroph identified as new planctomycete. *Nature* 400:446–449.
- Nunoura T, et al. (2010) Archaeal diversity and distribution along thermal and geochemical gradients in hydrothermal sediments at the Yonaguni Knoll IV hydrothermal field in the Southern Okinawa trough. *Appl Environ Microbiol* 76:1198–1211.
- Durbin AM, Teske A (2012) Archaea in organic-lean and organic-rich marine subsurface sediments: An environmental gradient reflected in distinct phylogenetic lineages. *Front Microbiol*, 10.1038/ncomms1124.

37. Pedersen RB, et al. (2010) Discovery of a black smoker vent field and vent fauna at the Arctic Mid-Ocean Ridge. *Nat Commun* 1:126.
38. Canfield DE, Thamdrup B (2009) Towards a consistent classification scheme for geochemical environments, or, why we wish the term 'suboxic' would go away. *Geobiology* 7:385–392.
39. Sørensen KB, Lauer A, Teske A (2004) Archaeal phylotypes in a metal-rich and low-activity deep subsurface sediment of the Peru Basin, ODP Leg 201, Site 1231. *Geobiology* 2(3):151–161.
40. Harmand J-M, Ávila H, Oliver R, Saint-André L, Dambrine E (2010) The impact of kaolinite and oxi-hydroxides on nitrate adsorption in deep layers of a Costarican Acrisol under coffee cultivation. *Geoderma* 158(3–4):216–224.
41. Schippers A, Neretin LN (2006) Quantification of microbial communities in near-surface and deeply buried marine sediments on the Peru continental margin using real-time PCR. *Environ Microbiol* 8:1251–1260.
42. D'hondt SL, Jorgensen BB, Miller DJ, et al. (2003) .
43. Schmid M, et al. (2003) Candidatus "Scalindua brodae", sp. nov., Candidatus "Scalindua wagneri", sp. nov., two new species of anaerobic ammonium oxidizing bacteria. *Syst Appl Microbiol* 26:529–538.
44. Yamamoto M, Nakagawa S, Shimamura S, Takai K, Horikoshi K (2010) Molecular characterization of inorganic sulfur-compound metabolism in the deep-sea epsilonproteobacterium *Sulfurovum* sp. NBC37-1. *Environ Microbiol* 12:1144–1153.
45. Sievert SM, et al.; USF Genomics Class (2008) Genome of the epsilonproteobacterial chemolithoautotroph *Sulfurimonas denitrificans*. *Appl Environ Microbiol* 74:1145–1156.
46. Brochier-Armanet C, Boussau B, Gribaldo S, Forterre P (2008) Mesophilic Crenarchaeota: Proposal for a third archaeal phylum, the Thaumarchaeota. *Nat Rev Microbiol* 6:245–252.
47. Spang A, et al. (2010) Distinct gene set in two different lineages of ammonia-oxidizing archaea supports the phylum Thaumarchaeota. *Trends Microbiol* 18:331–340.
48. DeLong EF (1992) Archaea in coastal marine environments. *Proc Natl Acad Sci USA* 89:5685–5689.
49. Bano N, Ruffin S, Ransom B, Hollibaugh JT (2004) Phylogenetic composition of Arctic Ocean archaeal assemblages and comparison with Antarctic assemblages. *Appl Environ Microbiol* 70:781–789.
50. Durbin AM, Teske A (2010) Sediment-associated microdiversity within the Marine Group I Crenarchaeota. *Environmental Microbiology Reports* 2(5):693–703.
51. Wuchter C, et al. (2006) Archaeal nitrification in the ocean. *Proc Natl Acad Sci USA* 103:12317–12322.
52. Tourna M, et al. (2011) Nitrosoarchaea, an ammonia oxidizing archaeon from soil. *Proc Natl Acad Sci USA* 108:8420–8425.
53. Lehtovirta-Morley LE, Stoecker K, Vilcinskas A, Prosser JI, Nicol GW (2011) Cultivation of an obligate acidophilic ammonia oxidizer from a nitrifying acid soil. *Proc Natl Acad Sci USA* 108:15892–15897.
54. Hatzepichler R, et al. (2008) A moderately thermophilic ammonia-oxidizing crenarchaeote from a hot spring. *Proc Natl Acad Sci USA* 105:2134–2139.
55. Könneke M, et al. (2005) Isolation of an autotrophic ammonia-oxidizing marine archaeon. *Nature* 437:543–546.
56. Dang H, et al. (2009) Diversity and spatial distribution of amoA-encoding archaea in the deep-sea sediments of the tropical West Pacific Continental Margin. *J Appl Microbiol* 106:1482–1493.
57. Pester M, et al. (2012) amoA-based consensus phylogeny of ammonia-oxidizing archaea and deep sequencing of amoA genes from soils of four different geographic regions. *Environ Microbiol* 14:525–539.
58. Knittel K, Boetius A (2009) Anaerobic oxidation of methane: Progress with an unknown process. *Annu Rev Microbiol* 63:311–334.
59. Pester M, Schleper C, Wagner M (2011) The Thaumarchaeota: An emerging view of their phylogeny and ecophysiology. *Curr Opin Microbiol* 14:300–306.
60. Jiang H, et al. (2008) Dominance of putative marine benthic Archaea in Qinghai Lake, north-western China. *Environ Microbiol* 10:2355–2367.
61. Musmann M, et al. (2011) Thaumarchaeotes abundant in refinery nitrifying sludges express amoA but are not obligate autotrophic ammonia oxidizers. *Proc Natl Acad Sci USA* 108:16771–16776.
62. Teske AP (2006) Microbial communities of deep marine subsurface sediments: Molecular and cultivation surveys. *Geomicrobiol J* 23(6):357–368.
63. Canfield DE (1989) Reactive iron in marine sediments. *Geochim Cosmochim Acta* 53:619–632.
64. Beal EJ, House CH, Orphan VJ (2009) Manganese- and iron-dependent marine methane oxidation. *Science* 325:184–187.
65. Hugenholtz P, Pitulle C, Hershberger KL, Pace NR (1998) Novel division level bacterial diversity in a Yellowstone hot spring. *J Bacteriol* 180:366–376.
66. Cole JR, et al. (2009) The Ribosomal Database Project: Improved alignments and new tools for rRNA analysis. *Nucleic Acids Res* 37(Database issue):D141–D145.
67. Roesch LFW, et al. (2007) Pyrosequencing enumerates and contrasts soil microbial diversity. *ISME J* 1:283–290.
68. Lane DJ, et al. (1985) Rapid determination of 16S ribosomal RNA sequences for phylogenetic analyses. *Proc Natl Acad Sci USA* 82:6955–6959.
69. Hamady M, Walker JJ, Harris JK, Gold NJ, Knight R (2008) Error-correcting barcoded primers for pyrosequencing hundreds of samples in multiplex. *Nat Methods* 5:235–237.
70. Quince C, Lanzen A, Davenport RJ, Turnbaugh PJ (2011) Removing noise from pyrosequenced amplicons. *BMC Bioinformatics* 12:38.
71. Pruesse E, et al. (2007) SILVA: A comprehensive online resource for quality checked and aligned ribosomal RNA sequence data compatible with ARB. *Nucleic Acids Res* 35:7188–7196.
72. Lanzén A, et al. (2011) Exploring the composition and diversity of microbial communities at the Jan Mayen hydrothermal vent field using RNA and DNA. *FEMS Microbiol Ecol* 77:577–589.
73. Huson DH, Auch AF, Qi J, Schuster SC (2007) MEGAN analysis of metagenomic data. *Genome Res* 17:377–386.
74. Felsenstein J (1985) Phylogenies and the comparative method. *Am Nat* 125(1):1–15.
75. Stamatakis A, Ludwig T, Meier H (2005) RAxML-III: A fast program for maximum likelihood-based inference of large phylogenetic trees. *Bioinformatics* 21:456–463.
76. Guindon S, Gascuel O (2003) A simple, fast, and accurate algorithm to estimate large phylogenies by maximum likelihood. *Syst Biol* 52:696–704.
77. Ovreås L, Forney L, Daae FL, Torsvik V (1997) Distribution of bacterioplankton in meromictic Lake Saelenvannet, as determined by denaturing gradient gel electrophoresis of PCR-amplified gene fragments coding for 16S rRNA. *Appl Environ Microbiol* 63:3367–3373.
78. Jurgens G, Lindström K, Saano A (1997) Novel group within the kingdom Crenarchaeota from boreal forest soil. *Appl Environ Microbiol* 63:803–805.
79. Treusch AH, et al. (2005) Novel genes for nitrite reductase and Amo-related proteins indicate a role of uncultivated mesophilic crenarchaeota in nitrogen cycling. *Environ Microbiol* 7:1985–1995.
80. Leininger S, et al. (2006) Archaea predominate among ammonia-oxidizing prokaryotes in soils. *Nature* 442:806–809.
81. Ishii K, Fukui M (2001) Optimization of annealing temperature to reduce bias caused by a primer mismatch in multitemplate PCR. *Appl Environ Microbiol* 67:3753–3755.
82. Edwards U, Rogall T, Blöcker H, Emde M, Böttger EC (1989) Isolation and direct complete nucleotide determination of entire genes. Characterization of a gene coding for 16S ribosomal RNA. *Nucleic Acids Res* 17:7843–7853.
83. Nicol GW, Leininger S, Schleper C, Prosser JI (2008) The influence of soil pH on the diversity, abundance and transcriptional activity of ammonia oxidizing archaea and bacteria. *Environ Microbiol* 10:2966–2978.
84. Grasshoff K, Kremling K, Ehrhardt M (1999) *Methods of Seawater Analysis* (Wiley-VCH, Weinheim, NY), 2nd Ed.
85. Aitchison J (1986) *The Statistical Analysis of Compositional Data. Monographs on Statistics and Applied Probability* (Chapman and Hall, London), p 416.
86. Martín-Fernández J, Barceló-Vidal C, Pawłowsky-Glahn V (2003) Dealing with Zeros and Missing Values in Compositional Data Sets Using Nonparametric Imputation. *Math Geol* 35(3):253–278.

## History

Scientific drillships allow scientists access to some of Earth's most challenging environments, collecting data and samples of sediment, rock, fluids, and living organisms from below the seafloor. A long running international collaboration in scientific ocean drilling has transformed human understanding of our planet, addressing fundamental questions about Earth's dynamic history, processes, and structure. The growth of scientific ocean drilling as a research technique has led to the development of new tools and methodologies and has fostered enduring international collaborations in research, education, and public engagement.

### 1940: Advancement in Piston Coring

Advances in piston coring in the 1940s allowed research ships to routinely recover long sediment sections from the seafloor. These ocean bottom sediments, accumulating slowly over geologic time, contain microscopic fossils whose chemistry is a proxy for ancient ocean conditions. Piston coring was used on expeditions such as the worldwide cruise of the Swedish research vessel *Albatross* to begin studying the rich and varied planetary history captured at the bottom of the world's oceans.

### 1961: Project MoHole

In 1961 when dynamic positioning was successfully used to keep the drilling platform *CUSS I* on target in strong current, scientific drilling took root as a feasible technology to study Earth's subseafloor geology. **Project Mohole** (<http://www.nasonline.org/about-nas/history/archives/milestones-in-NAS-history/project-mohole.html>), a concept proposed to the U.S. National Science Foundation, considered the feasibility of drilling through the geological boundary identified by an abrupt change in rock physical parameters (Mohorovičić discontinuity) that marks the transition from thin oceanic crust to the mantle, Earth's main interior layer.

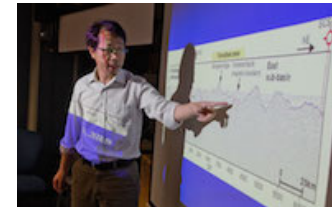
### 1966-1983: Deep Sea Drilling Project (DSDP)

The next phase of scientific ocean drilling, the **Deep Sea Drilling Project (DSDP 1966-1983)** ([http://www.iodp.tamu.edu/publicinfo/glomar\\_challenger.html](http://www.iodp.tamu.edu/publicinfo/glomar_challenger.html)), began in 1966 using the Drilling Vessel *Glomar Challenger*. This pioneering vessel conducted drilling and coring operations in the Atlantic, Pacific, and Indian Oceans as well as the Mediterranean and Red Seas. The *Glomar Challenger* also advanced the technology of deep-ocean drilling.

### 1983-2003: Ocean Drilling Program (ODP)

In 1985, the *JOIDES Resolution* replaced the *Glomar Challenger* at the start of the **Ocean Drilling Program (ODP 1983-2003)** (<http://www-odp.tamu.edu/index.html>). ODP was truly an international cooperative effort to explore and study the composition and structure of the Earth's subseafloors. The *JOIDES Resolution* conducted 110 expeditions for ODP at 2000 drill holes located throughout the world's ocean basins.

### 2003-2013: Integrated Ocean Drilling Program (IODP)



The **Integrated Ocean Drilling Program (IODP 2003-2013)** ([/iodp-legacy/iodp-2003-2013-documents](#)) built upon the international partnerships and scientific success of the DSDP and ODP by employing multiple drilling platforms financed by the contributions from 26 participating nations. These platforms - a refurbished *JOIDES Resolution*, the new marine-riser equipped Japanese Deep Sea Drilling Vessel *Chikyu*, and specialized Mission-Specific-Platforms - were used to reach new areas of the global subsurface during **52 expeditions** ([/expeditions/completed-integrated-ocean-drilling-program-expeditions](#)). The **IODP 2003-2013 Legacy Document Archive** ([/iodp-legacy/iodp-2003-2013-documents](#)) contains reports, minutes, and other documents from the program's panels and advisory bodies.

#### **2013-2024: International Ocean Discovery Program (IODP)**

Since in October 2013, the IODP partners have continued their collaboration via the International Ocean Discovery Program (IODP). Read more about the science, operations, and structure of the current IODP throughout [iodp.org](#).

---

IODP website maintenance will be performed every Thursday, from 16:30-17:30 Pacific Time

Copyright © 2024 Science Support Office at Scripps Institution of Oceanography | [Webmaster \(mailto:webmaster@iodp.org?\)](mailto:webmaster@iodp.org)  
Subject=IODP%20Website%20Question | [Contact Us \(/program-organization/science-support-office\)](#)

[Back to Top](#)